AD-A119 661 PALISADES INST FOR RESEARCH SERVICES INC NEW YORK F/G 9/5
IEEE CONFERENCE RECORD OF 1976 TWELFTH MODULATOR SYMPOSIUM, NEW--ETC(U)
1976
UNCLASSIFIED 76-CH-1045-4-ED NL

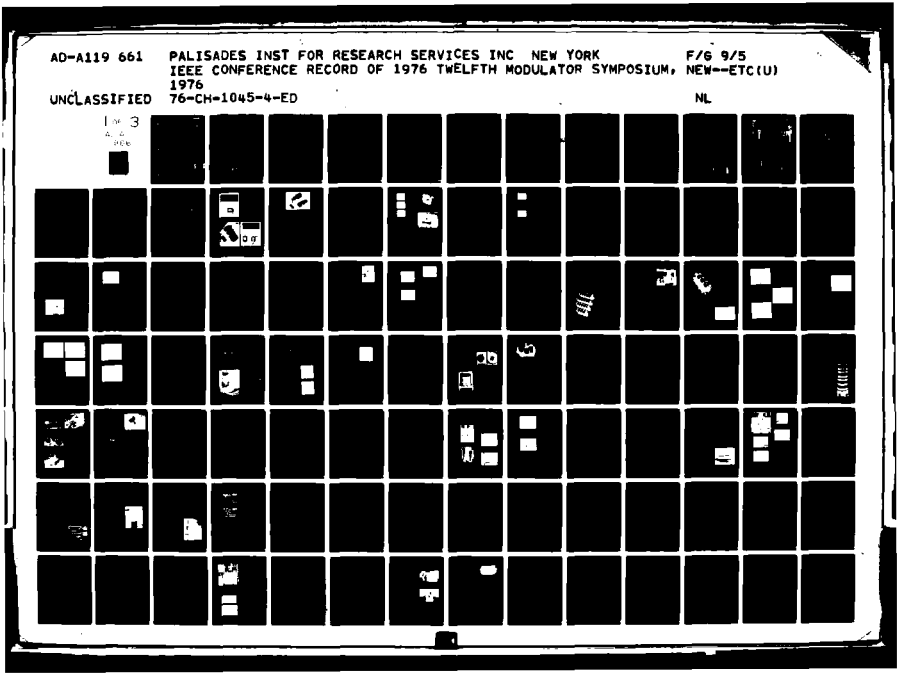

76 CH 1045-4 ED

IEEE

CONFERENCE RECORD OF

1976 TWELFTH MODULATOR SYMPOSIUM

February 4-5, 1976

Sponsored by the
IEEE Electron Devices Society
and
Advisory Group on Electron Devices
in conjunction with
Palisades Institute for Research Services, Inc.

76 CH 1045-4 ED

IEEE

CONFERENCE RECORD OF

1976 TWELFTH MODULATOR SYMPOSIUM

Papers presented at the
Statler Hilton - New York City
February 4-5, 1976

Sponsored by the
IEEE Electron Devices Society
and
Advisory Group on Electron Devices
in conjunction with
Palisades Institute for Research Services, Inc.

Printed in USA

FORWARD

The 1976 Twelfth Modulator Symposium was the latest in a series beginning with the Hydrogen Thyratron Symposium in 1950. The movement of technology can be deduced readily from examination of the proceedings and records of these conferences.

There were eight sessions which covered: Switches; High Power Switches for Intermittent Operation; High Power Modulators for Intermittent Operation; Charging Systems; Circuit Techniques; Line Type Modulators; SCR Line Type Modulators; Protective Devices and Circuits.

1976 CONFERENCE COMMITTEE

Sol Schneider, Chairman
U.S. Army Electronics Command

John E. Creedon, Co-Chairman
U.S. Army Electronics Command

Robert Feinberg
AVCO Everett

Richard A. Fitch
Maxwell Laboratories

Bobby R. Gray
U.S. Air Force Rome Air Development Center

Leonard H. Klein
Palisades Institute for Research Services, Inc.

Hugh Menown
The English Electric Valve Company, U.K.

Nigel S. Nicholls
Royal Radar Establishment, U.K.

David L. Pruitt
RCA

David V. Turnquist
EG&G Inc.

Richard L. Verga
U.S. Air Force Aero Propulsion Laboratory

Thomas A. Weil
Raytheon

TABLE OF CONTENTS

PAGE

TABLE OF CONTENTS

PAGE

TABLE OF CONTENTS PAGE

HIGH VOLTAGE SWITCH TUBES FOR NEUTRAL BEAM INJECTORS - A NEW DESIGN APPROACH

D.H.Preist

EIMAC Division of Varian
301 Industrial Way
San Carlos, Calif.
94070

SUMMARY

A conventional tetrode with grids cooled by radiation is an excellent choice for many applications. As a high voltage switch where current may be required for many seconds it is very unattractive because of excessive size due to the low power dissipation capability of the grids and the unfavorable voltage breakdown properties of a thin wire screen grid. The new approach would use a combination of microwave linear beam and gridded tetrode technologies to achieve a result unobtainable with either one. Well defined and separated strip beams are focussed through slot apertures in a thick screen electrode and travel some distance toward the anode without intermingling. Theoretical analysis and computer modelling indicate substantial improvement in performance: for the same electrode voltages and spacing as a conventional tetrode the current density at the anode may be nearly 2.5 times as great, or for the same current density, the spacing may be nearly 1.6 times. Also the screen electrode, being of large cross sectional area, may be water cooled, and has a much larger minimum radius of curvature than a wire grid, allowing higher voltage for a given spacing.

INTRODUCTION

A major advance in research on Controlled Thermonuclear Fusion has been the injection of neutral beams of uncharged particles which can penetrate the magnetic field containing the hot plasma and heat it much more. These neutral beams start as ion beams of low energy, subsequently accelerated to potentials of tens to hundreds of KV, after which neutralization is brought about. In the acceleration process the system arcs over frequently, making necessary a protective current limiting device. It is also necessary to start and stop the beam in a precise and repeatable manner. The most suitable device for this is a high vacuum electron tube, capable in the foreseeable future of holding off 250KV when the ion beam is cut off, passing tens to hundreds of amperes when turned on, for periods as long as 30 seconds, and equipped with a means of turning off the current in microseconds. It is also desirable that in the event of a short-circuited load, the current can be limited to a value not much higher than the normal load current. These requirements broadly suggest the classical gridded tetrode tube as a solution, and combinations of available high power tubes in series and in parallel can be and are being used in present installations. These tubes were designed and optimized for RF communications service, however, where the operating conditions are very different. It will be shown that a tube designed expressly for optimum performance and lowest cost as a switch under the conditions mentioned will tend to be quite different structurally and in its electronic behaviour from the classical tubes.

EVOLUTION OF DESIGN CONCEPT

First, the tube must hold off the applied voltage reliably. This determines the distance, or spacing, between the anode and the next electrode to it, taking into consideration the material, geometry and temperature of the electrodes. Second, the cross sectional area of the electrodes must be determined. Here, the limitation is a thermal one. The quantities of heat involved are governed by the behaviour of the electrons and in particular by space charge effects. It will be assumed throughout that the tube size should be minimized or current density maximized, since increased size inevitably means increased manufacturing cost. However, it is also necessary to minimize the power dissipated at the electrodes during conduction, since this involves cost of a different kind, in power consumption and cooling systems. In the classical tube the way these factors are related can be summarized by a few well-known equations. For simplicity and ease of understanding, we shall first assume a tetrode operated with the screen grid and anode at the same potential during conduction (the "ON" condition).

For this condition, the equation connecting these variables is as follows:

$$\frac{J_{A\ (max.)}\ d^2}{V^{3/2}} = k$$

Where $J_{A\ max.}$ is the "saturated" anode current density in amps per cm^2
Where V is the anode and screen grid voltage
Where d is the screen grid to anode distance in cm
K, a constant, will be 9.33×10^{-6} for parallel plane electrodes
or 7.0×10^{-6} for cylindrical electrodes having a ratio of diameters of 2.3.

The reason for this upper limit to current density is that a potential minimum is produced between the two electrodes by the presence of the electrons. At the maximum current density this minimum falls to zero and if more current is injected through the screen grid it will not reach the anode but will arrive at the grid wires causing heating.

This equation means that if d is fixed, then an increase in anode current density (required to minimize tube size) can be obtained only by raising the voltages.

The efficiency of a tube as a switch in

the "ON" position, neglecting for the moment screen grid dissipation, is given by:

$$\eta = \frac{V_B - V_A}{V_B}$$

Where V_B is the power supply voltage

Where V_A is the tube anode to cathode voltage when maximum current flows.

Clearly then, as a first approximation, it is desirable to use the lowest voltage for highest efficiency and the highest voltage to minimize the tube cost. A compromise is, therefore, required.

Disregarding efficiency for the moment, if the voltages are raised there will eventually be limitations on the dissipation of both screen grid and anode. In a conventional tube with grids made of wire meshes, the screen grid dissipation limit will occur first. This is because a wire grid of the size needed will be cooled essentially by radiation. This is a function of temperature. At the upper limit, set usually by primary electron emission or by continuous evolution of vapour, and for the best available materials, such a grid will radiate on the order of ten watts per cm^2 of surface area. On the other hand, the anode if water cooled can dissipate on the order of 1000 watts per cm^2. Clearly, the screen grid limitation will occur first if the current to the screen grid exceeds about one percent of the anode current, if the anode and screen grid are at the same potential. But in a typical tetrode, operated at the maximum, or saturated, anode current, the screen grid current will be on the order of ten percent of the anode current. In RF service this condition exists only at the time when the sinusoidal control grid voltage is at its peak value; the average screen grid current may be only a few percent of the average anode current. Also the average screen grid voltage may be only five to ten percent of the average anode voltage. In switching service the situation is entirely different.

Some relief may be obtained by raising the anode voltage above the screen voltage as in most tubes this will decrease the screen grid to anode current ratio, but this is obtained of course at the expense of efficiency. It would be more attractive to use a more powerful method of cooling the screen grid, such as thermal conduction or liquid cooling, or to find ways of reducing the current intercepted by the screen grid or a combination of both.

Fortunately, high power microwave tube technology has already solved a similar problem. A typical klystron tube includes an electron gun with an insulated, or "modulating", anode which may intercept less than one percent of the beam current when the anode and the rest of the tube (cavities and collector) are at the same potential. This result can be obtained in an electrostatically focussed tube or in a magnetically focussed tube using Brillouin flow where no magnetic field is present in the electron gun to help focus the beam. Also, the gun anode is typically a thick rugged member which may be liquid cooled if desired. It is reasonable to expect that strip beams obtained from gridded electron guns can be made to perform in the same way.

It is logical, then, to conceive a switch tube in which a number of strip beams are deployed in a symmetrical fashion about a central axis, each beam being generated by an electron gun preferably equipped with a control grid, the whole assemblage being mounted within or around a concentric anode. The output region of such a structure could be as shown in Figure 1. It will be of

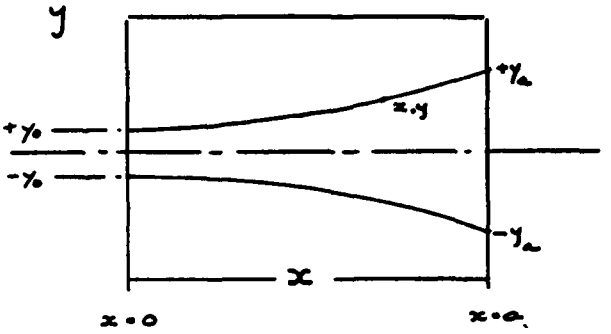

Electron strip beam of unit depth (into paper) injected into box with potential V, velocity $\sqrt{2\eta V}$, and current density J_w.

Figure 1

interest to calculate the electron trajectories and potential distribution in this structure, assuming first that laminar and parallel electron beams are injected between the screen grid bars without interception and that these beams are free to expand without intermingling before they reach the anode.

SPACE CHARGE LIMITED ELECTRON FLOW IN FREELY EXPANDING STRIP BEAMS

Analytical

Consider a strip beam injected through a plane perpendicular to direction of motion into a region of zero electric field, such as a closed metal box. We shall assume the beam is undirectional (no components of velocity perpendicular to direction of motion) and has uniform current density. See Figure 2. This beam will expand due to space charge forces, and will satisfy Poisson's equation:

$$\frac{d^2V}{dx^2} + \frac{d^2V}{dy^2} + \frac{d^2V}{dz^2} = -\frac{\rho}{\epsilon}$$

Where ρ is electronic charge density

Where ϵ is permittivity of free space

Where V is potential

If the beam is assumed to be infinitely wide in the Z direction, this reduces to

$$\frac{d^2V}{dx^2} + \frac{d^2V}{dy^2} = -\frac{\rho}{\epsilon}$$

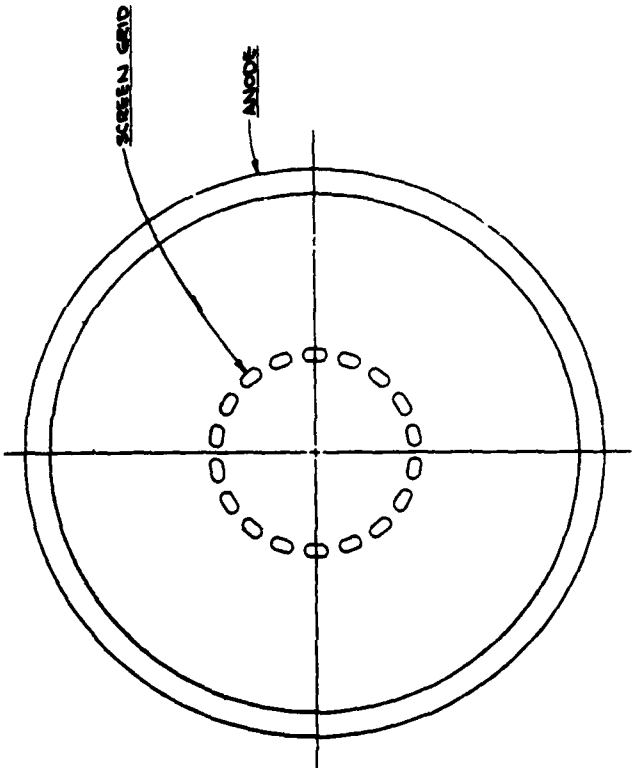

Figure 2

Since there is no potential gradient in the x direction of motion,

$$\frac{d^2V}{dy^2} = -\frac{\rho}{\epsilon}$$

following Pierce [1]

$$\frac{y}{y_o} = 1 + 2.34 \times 10^4 \frac{I}{V^{3/2}} \frac{x^2}{y_o}$$

In terms of current density at the beam waist J_w,

$$\frac{y}{y_o} = \frac{1 + 2.34 \times 10^4 J_w \, 2 \, y_o \, x^2}{V^{3/2} \, y_o}$$

$$= \frac{1 + 4.68 \times 10^4 J_w x^2}{V^{3/2}}$$

In terms of current density J_a at the plane x = a, which may be thought of as an anode,

$$J_a = J_w \frac{y_o}{y_a}$$

$$= \frac{J_w \, V^{3/2}}{1 + 4.68 \times 10^4 J_w x^2}$$

If $4.68 \times 10^4 J_w x^2 \gg 1$, then, very nearly,

$$\frac{J_a x^2}{V^{3/2}} = \frac{1}{4.68 \times 10^4} = 21.4 \times 10^{-6}$$

For a conventional tetrode with $V_{g_2} = V_a$ and a distance x between screen grid and anode, and parallel plane electrodes,

$$\frac{J_a x^2}{V^{3/2}} = 9.34 \times 10^{-6}$$

The ratio of the parameters $\frac{J_a x^2}{V^{3/2}}$ for the two cases

will therefore approach $\frac{21.4}{9.34} = 2.29$

in the limiting case of a beam with a very large injected current density and/or a very large spread, or expansion ratio,

$$\frac{y_a}{y_o}$$

For less current density and less expansion, the ratio will be less than 2.29.

The situation analyzed, a beam expanding in a metal box, does not of course, correspond closely to the situation in a tetrode. In the tetrode, the injection plane and the anode plane are electrically conductive but the side walls of the box are missing. This situation is too complex to permit analytical solution, and, therefore, a digital computer has been programmed with this problem. The side walls can now be planes of symmetry, assumed to lie between adjacent beams which would be used in an actual multiple beam tube.

Digital Computer Calculations

Simple case of expanding beam in a metal box

To check the validity of the above calculation, the run shown as Plot 1 was made. The agreement is within about 1%.

This plot shows the potential depression which amounts to less than 15% of the injection potential.

Laminar beams injected into realistic model with planes of symmetry

Plot 2 shows an example. Electron trajectories and equipotentials are plotted. If anode current density is taken as the injected beam current divided by the beam cross-sectional area at the anode, it is found that the anode current density is 1.83 times the saturated current density assuming infinite parallel planes and uniform current density.

It is also found that the minimum potential in the freely expanding beam is two-thirds of the potential at the entrance and exit planes, instead of zero as it would be for uniform flow at saturation.

Proceeding further towards a realistic model of an actual tube, the computer was programmed with three beams so that the effects of intermingling could be studied. Plot 3 shows a typical result without

intermingling, Plot 4 shows what happens when the injected current density is slightly increased and in Plot 5 there is a further increase. The beam spread is greatly increased and the potential minima inside the beams have fallen close to zero. A still further increase in injected current produces virtual cathodes and electrons are returned to the entrance plane. The limiting current is nearly twice the saturation current for uniform flow.

As another step towards a realistic model concentric cylindrical electrodes were programmed. It seemed reasonable to expect that with separated freely expanding beams the maximum anode current density would not be a strong function of the angle between beam axes, in which case an extra bonus would be obtained, since in a conventional cylindrical tube the anode current density falls off as the ratio of radii of the electrodes increases. (See constant K in equation (1) for illustration).

Plot 6 shows a typical result. Analysis shows the current density to be 0.9 times that for parallel planes. For the ratio of radii chosen the conventional tube would have a reduction of about 0.7.

Further work is planned to discover how these improvements in performance depend on the ratio of beam separation to beam entrance width, and to beam non-linearity and initial divergence.

CONCLUSIONS

The major limitation in performance of a tetrode tube of conventional construction, in very long pulse service, the screen grid heating, can be removed if liquid or conduction cooling can be used instead of radiation cooling. This requires screen grid elements of unusually large cross-sectional area. It is probable that electron guns can be developed to inject beams through the apertures in such a screen grid with acceptably small beam interception.

Mathematical analysis has indicated that tetrode tubes using separated, laminar, well collimated strip beams injected through slots in the screen grid should provide an increase in the parameter:

$$\frac{J_A \cdot x^2}{V^{3/2}}$$

Where J_A is anode current density

Where x is screen grid to anode spacing

Where V is anode and screen grid potential

compared to the value obtainable for conventional uniform electron flow

In examples calculated numerically, the increase has been found to be 1.83 for parallel plane geometry and 2.32 for cylindrical geometry with a radius ratio of 2.3 This means that for given voltage and spacing the current density can be increased by these amounts, or for a given current density the spacing can be increased by the square root of these amounts, or for a given current density and spacing the voltages and the anode dissipation can be reduced by the two-thirds power of these amounts.

More study is needed to find out how this parameter varies with beam separation to beam width ratio and beam non-laminarity and initial divergence.

It is to be expected that the improved performance will be obtained only with beams of high electron optical quality.

It is, of course, necessary to build experimental tubes to find out if this improvement can be realized in practical devices.

REF: 1.J. R. Pierce, "Theory & Design of Electron Beams", 2nd Edition, 1954, P.151.

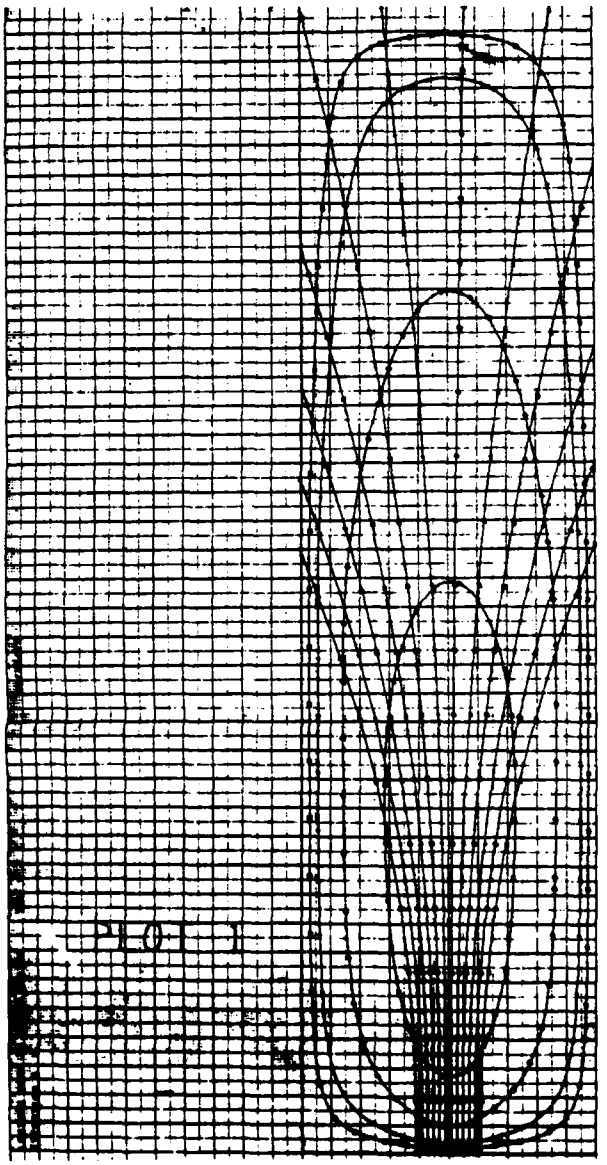

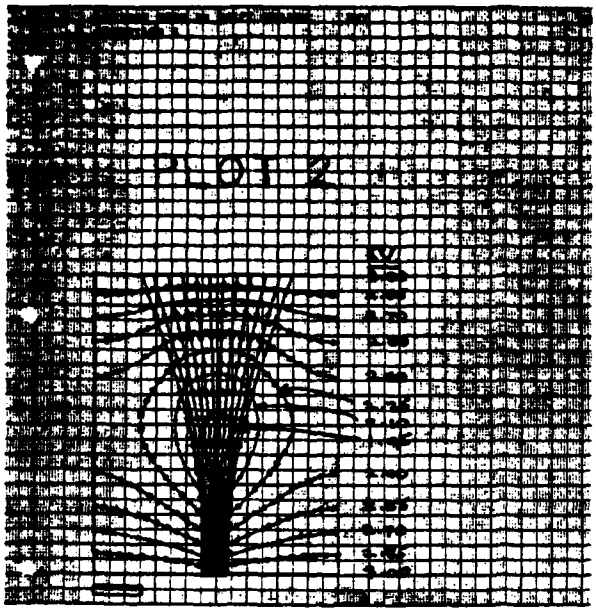
PLOT 2

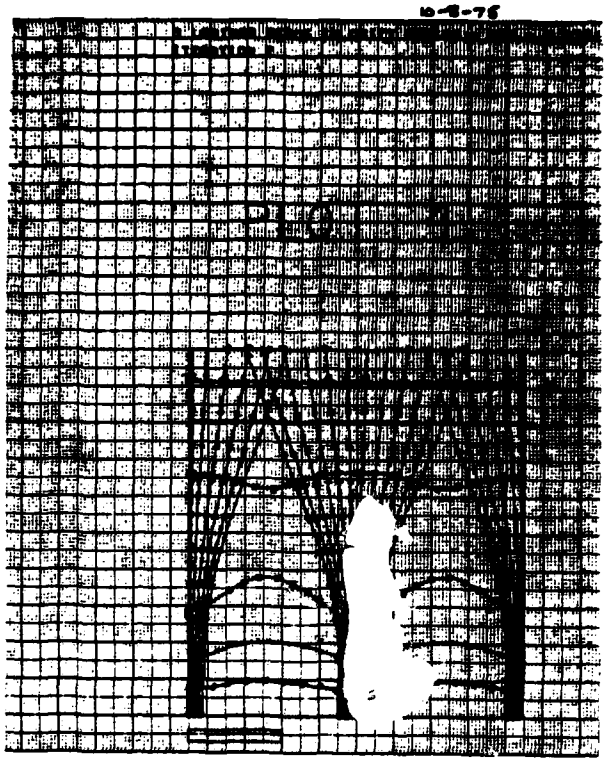

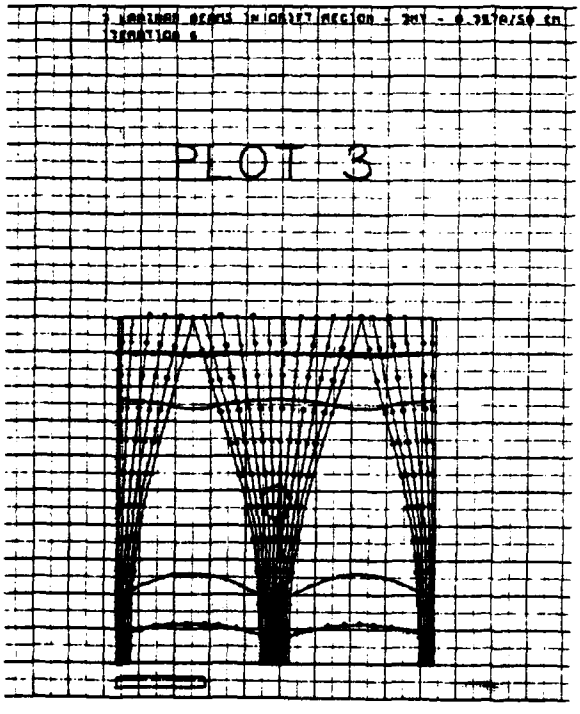
PLOT 3

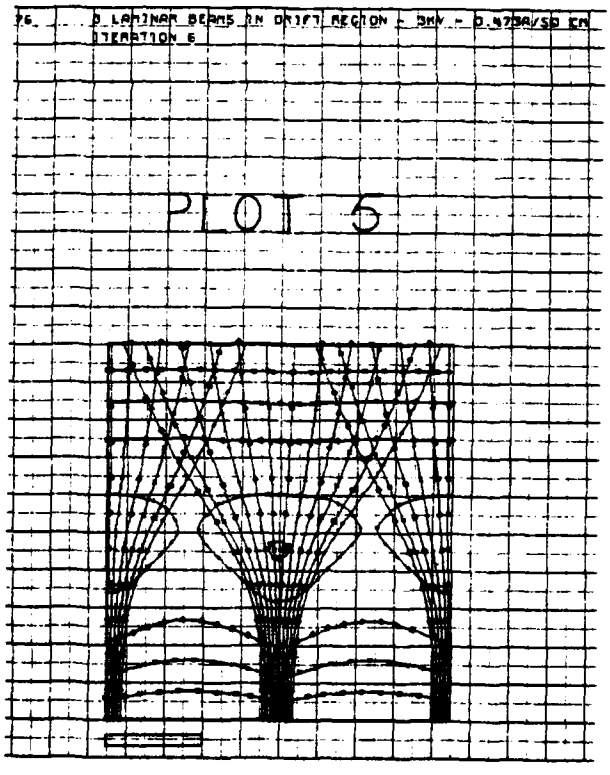
PLOT 5

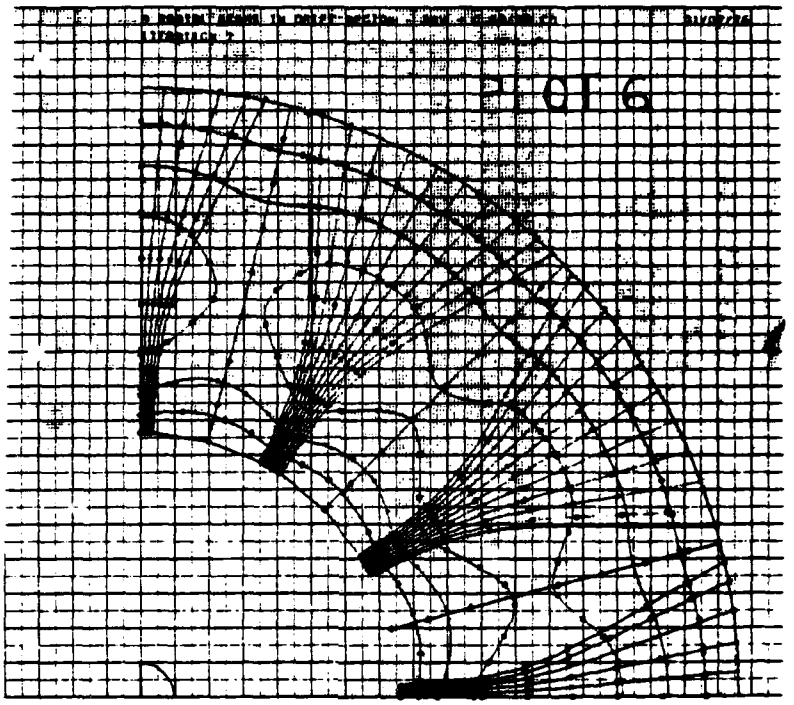
PLOT6

AN EBS MODULATOR FOR HIGH POWER TRAVELING-WAVE TUBES

J. V. Stover and M. J. Westby
Hughes Aircraft Company
Fullerton, California

and

B. W. Bell and R. I. Knight
Watkins-Johnson Company
Palo Alto, California

Abstract

Switching EBS's (Electron Bombarded Semiconductors) provide high voltage, high output current capability for use in fast risetime, short time delay pulse generation. These devices have been used in the development of a versatile, high performance grid modulator for power traveling-wave tubes.

The first section of this paper describes the characteristics of the EBS which consist of a high transconductance gridded electron gun which focuses a low current (10-50 mA peak), high voltage (10 kV) electron beam onto a reverse biased semiconductor diode. The electron beam produces a current amplification of approximately 2,000 in the diode, resulting in an output pulse of several amperes. Existing switching EBS's require input pulses of 10-25 V and can provide over 7 kW peak output power.

The output risetime is controlled by the load capacitance and the peak current capability. Risetimes into a 100 pF load of 8.5 nanoseconds have been achieved at 750 V and 19 nanoseconds at 1000 V. The transit time delay through the EBS, excluding the output risetime is typically less than 2 nanoseconds.

The second section of this paper describes the practical design and implementation of the EBS switch into a grid modulated TWT pulse amplifier. The EBS modulator provides up to 900 V peak grid voltage swings over pulse width ranges of 0.1 to 1.8 microseconds. The performance, size and weight of the EBS modulator is presented and compared with an all transistor modulator.

The projected effect of improved EBS performance on the overall modulator performance will be described.

Introduction

The switching EBS offers advantages over the use of other switching devices such as transistors or hard tubes, specifically in the areas of pulse risetime, internal delay, high PRF operation, and reliability. The EBS can switch voltages up to 1000 V with risetimes between 3 and 30 nanoseconds depending on the load impedance and capacitance, while the delay through the tube is typically only 2 nanoseconds. Switching EBS's have demonstrated operation at duty cycles as high as 60% and PRF's as high as 2.5 MHz. Switching EBS's can also be designed with arc protection circuitry which results in no damage to the switching EBS due to arcs by the TWT being modulated. In addition, EBS devices have demonstrated MTTF's in excess of 100,000 hours. Switching EBS's which have previously been built at Watkins-Johnson have included the WJ-3652, a high current device capable of switching 100 V with 100 A of peak current in 3 nanoseconds; the WJ-3653 and WJ-3684, both 400 V, 4 A devices; the WJ-3683, a dual output 400 V pulse amplifier; and the WJ-3680, a 750 V, 7 A device.

Theory of Operation

The switching EBS consists of a high transconductance gridded electron gun and a reverse biased silicon diode, as shown in Fig. 1. The grid is normally biased in cut-off and the only current flowing in the external circuit is a small diode leakage current, typically less than 1 mA. When a positive pulse is applied to the grid, the diode is illuminated by a beam of high voltage electrons. These 10-15 kV electrons penetrate the thin surface contact of the semiconductor diode and create a large number of electron-hole pairs by impact ionization. Formation of a single electron-hole pair requires 3.6 eV; the current gain in the semiconductor diode is given by

$$a = \frac{V_k - V_l}{3.6\ eV}$$

V_k - Cathode voltage

V_l - Junction penetration loss (Typically 3-5 kV)

Typical values for the diode current gain range from 1500 to 3000. As a result, relatively small electron beam currents can control large currents in the output circuit.

Static operating characteristics for a typical EBS are shown in Fig. 2. This curve shows the diode current as a function of diode bias for a number of control grid voltages. The characteristic curve may be divided into three regions. Above voltage V_a the diode is in avalanche breakdown. To avoid damage the EBS must never be allowed to operate in this region. Region II is the active region in which the EBS acts as a high impedance current source. When operated in this region, the EBS behaves as a broadband video amplifier. Carrier transport within the diode is entirely by drift at high velocity rather than by diffusion, as in many semiconductor devices. As a result, there is no carrier storage time other than the extremely short transit time. For this reason an EBS operating in the active region may be turned "on" or "off" with equal rapidity.

Region III is the saturation region in which substantial storage time may arise due to the injection of excess beam current into the diode. This excess current will stretch the pulse width and increase the fall time. However, operation in this mode presents two primary advantages; first, the load impedance is typically greater than 1000 ohms, as opposed to the 100 ohm or lower load impedance when operating in the active region. This higher load impedance greatly reduces the power dissipated in the diode, allowing operation at very high duty cycles. The second advantage is that by operating in saturation, the sensitivity of the output voltage with respect to variations in the grid drive or cathode voltages is greatly reduced. For these reasons, the switching EBS's are operated in the saturation region in the EBS modulator. However, special steps are taken to eliminate the stored charge and to achieve a fast fall time. These

techniques, which will be discussed in greater detail in the second section of the paper, involve the use of clamp circuitry to prevent the accumulation of stored charge and the use of a second EBS device to act as a "tail-biter" to achieve the fast fall time.

Tube Design

The original design of the 1000 V switching EBS used two parallel diode strings of 3 diodes each, with the diodes of the type originally used in the WJ-3653 400 V switching EBS. However, during testing of the prototype models, it was found that the diodes would stabilize with breakdown voltages between 300 and 350 V. Hence, the tube was redesigned to utilize four diodes in series; because of the length of the array and the large number of diodes, only one string of diodes was used. A photograph of a completed target is shown in Fig. 3. Note that tabs are provided for electrical connection to each point in the diode array. With this design it was possible to consistently fabricate arrays with stable breakdown voltages greater than 1200 V. In addition, the use of the fourth diode provided an extra reliability factor in that if one of the diodes were to fail, the unit would still be capable of operation at 900 V peak output, the maximum voltage swing required to drive the TWT's.

The mechanical design of the 1000 V switching EBS was based on the design of the WJ-3653, with the target holder modified to accept the larger target. A photograph of the completed tube is shown in Fig. 4. The five bias pins allow the use of an external voltage division network to equalize the voltages across the four diodes.

Device Performance

The device performance and electrical characteristics are summarized in Table I. The performance values are given for operation into a 5 k-ohm load shunted by 100 pF capacitance. The risetime of the device will be limited by the 3.5 A of peak current available to charge the load capacitance; Fig. 5 graphs the output risetime versus load capacitance measured for WJ-3680-3 S/N 16. When operating into a primarily capacitive load, the major amount of power dissipation in the diode is caused by the charging and discharging of the load capacitance at high PRF's. The power dissipation under these conditions is given by the following formula:

$$P = 1/2\ (C_{diode} + C_L) \times V^2 \times PRF$$

C_d - Diode capacitance

C_l - Load capacitance

V - Peak voltage swing

Thus with a diode plus load capacitance of 150 pF, an output pulse voltage of 1000 V, and a PRF of 200 kHz, the diode power dissipation would be 15 W.

Testing of the original units revealed that the cathode current would shift downward with increasing PRF even when the grid voltage was held constant. This change in cathode current, which is discussed in more detail in the second part of the paper, made it difficult to adjust the EBS modulator to operate over a wide range of PRF's. The cause of this decrease was traced to partial poisoning of the cathode, most likely caused by the diode target. To correct the problem, a new activation schedule in conjunction with a higher temperature bake-out was instituted. These techniques resulted in a marked improvement in the performance of the remaining devices delivered.

Due to the processing complexity involved in achieving satisfactory performance from the oxide cathodes used in the switching EBS's, testing has been done on the use of impregnated cathodes. This has resulted in the design and testing of switching EBS's which show no variation in cathode current, while the better oxide cathode would show 5% change from 100 Hz to 20 kHz. Dispenser cathodes are now being used in the WJ-3684 switching EBS, and will be used in the 1000 V switching EBS's provided for the EBS modulator. The use of the dispenser cathode has had an additional advantage; because of the reduced processing required and because of the reusability of the cathodes, it has been possible to significantly reduce the cost of the devices.

Testing of the switching EBS's in the EBS modulator has led to a second modification in the design of the switching EBS. During operation of the devices in the EBS modulator, it was found that after the units had been allowed to sit for several weeks without operating, an arc would occur between grid and target during initial application of high voltage. The arcing was apparently occurring along the ceramic insulating surface. Any arcing across the ceramic surface would most likely be caused by contaminants deposited on the ceramic during outgassing of the tube. To solve this problem, the outgassing path was modified so that the ceramic was shielded from most contaminants, particularly those resulting from cathode activation.

Further Device Development

The 1000 V switching EBS's supplied for the EBS modulator contain the four diode series configuration. As was mentioned earlier, this design was selected based upon the achievable stable breakdown voltages of the diodes. Since that time, Watkins-Johnson Company has developed their own capability to design and fabricate the EBS diodes. The facility, in operation since April of 1975, has resulted in the fabrication of diodes of the type used in the EBS modulator with initial breakdown voltages of 600 to 650 V. The stabilized breakdown voltage, after exposure to the electron beam, is typically 550 to 600 V.

The diode fabrication capability has led to the feasibility of fabricating switching EBS's with the six diode target originally proposed for the EBS modulator. The use of this device would result in a 50% improvement in the risetime and fall time capability of the EBS modulator, as well as the ability to operate with narrower pulse widths.

A second type of device currently being fabricated by Watkins-Johnson Company utilizes a single high-voltage diode target. The initial breakdown voltage for the high-voltage diodes is typically 1100 to 1200 V. Upon stabilization after exposure to the electron beam, these diodes have breakdown voltages of typically 800 to 900 V. The single diode target has several advantages: first, the diode can be fabricated with a relatively large area, resulting in high output currents. The diodes used in the four diode series target have an active area of 2 mm^2, whereas the high-voltage diodes have an area of 19 mm^2. A photograph comparing the two diode targets is shown in Fig. 6. The larger area results in an output current capability of greater than 12 A. The use of a switching EBS of this type in the EBS modulator would reduce the rise and fall times to about 10 nanoseconds. A second advantage of the high-voltage diode is the power dissipation capability. Due to the large area, the power dissipation rating of the tube could be doubled while maintaining the same power dissipation capability per

unit area. A third advantage of the diode is that due to the fabrication of the diode in a circular geometry, the part of the beam actually striking the diode is 60%, whereas for the four diode series configuration the ratio of current striking the diode to total beam current is less than 10%. Not only would this simplify power supply requirements, it would also mean that the EBS would require less grid drive voltage. As mentioned in Part II of the paper, the present EBS modulator uses a spiked grid pulse with a maximum amplitude of +40 V. With the new diode, this could be reduced to +5 V. A fourth advantage is, since the single diode has a smaller effective radius than the present target, it is possible to design it into a tube with smaller overall dimensions. A photograph of the two units is shown in Fig. 7. Both the size and weight of the single diode unit, the WJ-3681 have been reduced 50%.

As mentioned previously, the present limitation on output voltage of the WJ-3681 is approximately 750 V. Work is progressing on fabrication of the higher voltage diodes. Three approaches are currently being pursued; the first is the use of less highly doped material. This has recently resulted in the fabrication of diodes with 1400 V breakdown voltages. The second approach is the continued use of the planar diode geometry but with different guard ring depths and multiple guard rings. The third and most promising approach is the use of mesa diodes. This technique has led to the development of diodes with greater than 1500 V breakdown, although these diodes would not have been suitable for use in vacuum due to the lack of any passivation. However, techniques are currently being developed to fabricate passivated EBS mesa geometry diodes which are expected to result in diodes with greater than 1500 V breakdown voltages. With an initial breakdown voltage of 1500 V, the stabilized breakdown voltages of these diodes would be on the order of 1300 V, fully suitable for use in the EBS modulator. Table II gives a comparison of the performance specifications of the WJ-3680-3 switching EBS presently used in the EBS modulator and the WJ-3681 utilizing the single diode target.

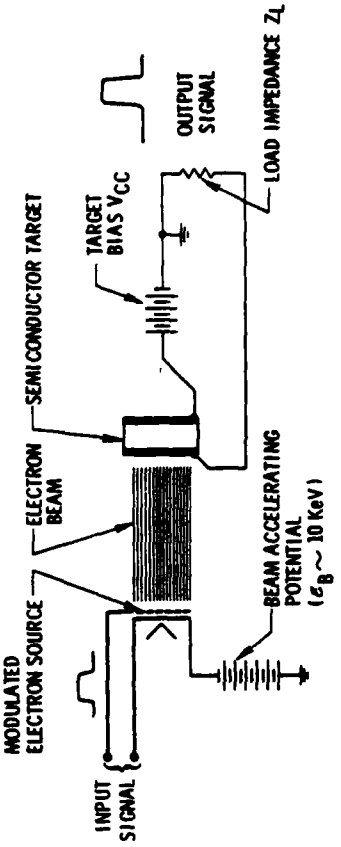

as 22324B

Fig. I-1 Schematic showing internal components of switching EBS.

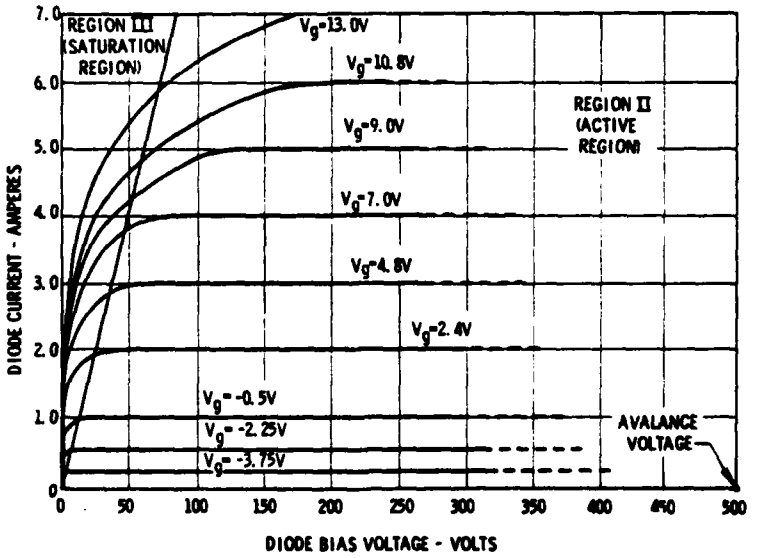

Fig. I-2 Static operating characteristic showing output current versus diode voltage for different grid pulse voltages.

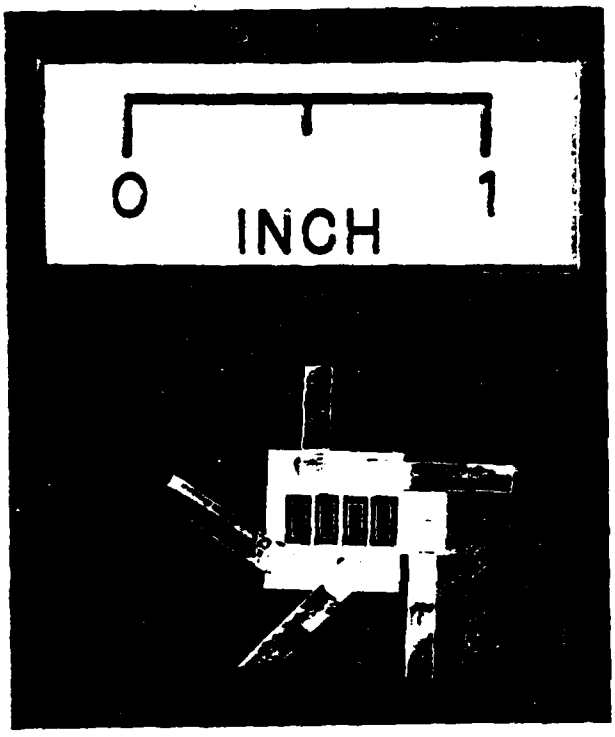

Fig. I-3 Photograph showing completed four diode series target.

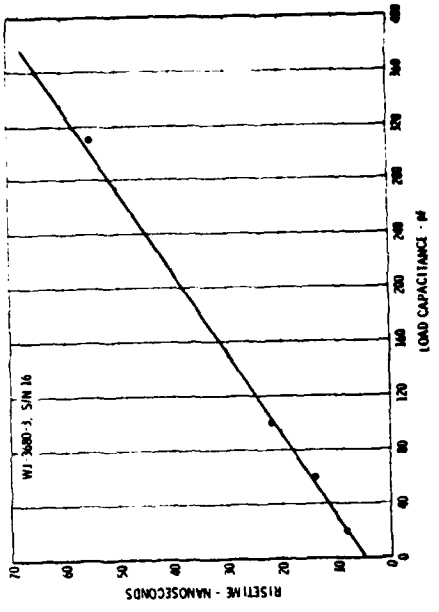

Fig. I-5 Measured risetime versus load capacitance for WJ-3680-3 S/N 16.

Fig. I-4 Photograph showing 1000 V switching EBS.

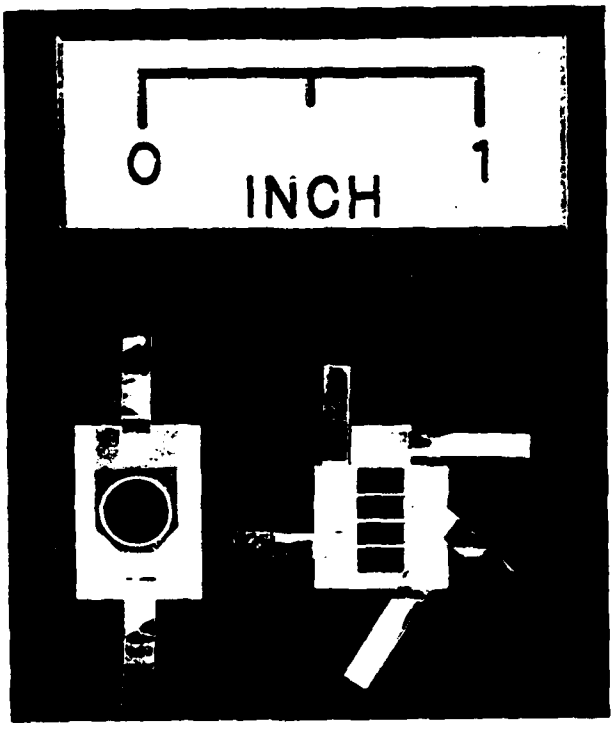

Fig. I-6 Photograph comparing the four diode series target with the high voltage single diode target.

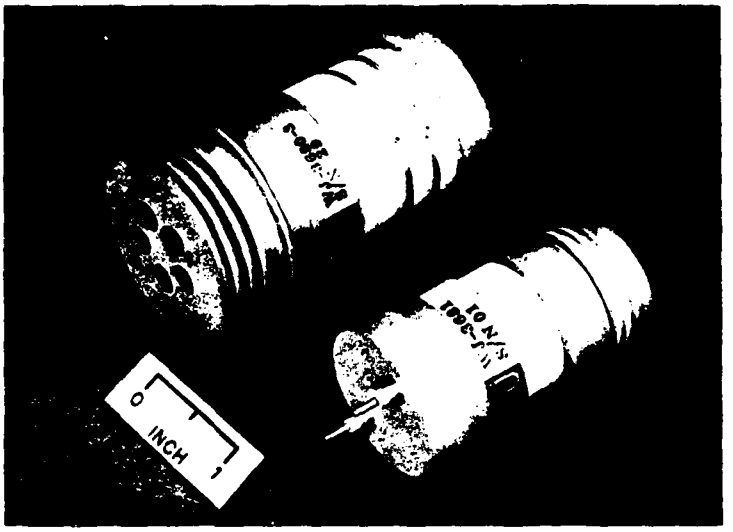

Fig. I-7 Photograph comparing the size of the WJ-3680-3 presently used in the EBS Modulator with the reduced size WJ-3681.

TABLE I

WJ-3680-3
ELECTRON BOMBARDED SEMICONDUCTOR (EBS)
1000 VOLT SWITCH

PERFORMANCE CHARACTERISTICS	VALUES
2.5K ohm, 100pF LOAD	
PEAK OUTPUT VOLTAGE	1000V
PEAK OUTPUT CURRENT	3.5A
OUTPUT RISETIME	25 ns
DELAY (10% input - 10% output)	2 ns
DIODE POWER DISSIPATION	15W, max.
PULSE REPETITION FREQUENCY	200 KHz, max.
PULSE DURATION	50usec, max.
DUTY CYCLE	10%, max.

TABLE II

COMPARISON OF SINGLE DIODE VS. 4 DIODE PERFORMANCE

PERFORMANCE CHARACTERISTICS	VALUES	
2.5K ohm, 100 pF LOAD	WJ-3680-3	WJ-3681
PEAK OUTPUT VOLTAGE	1000 V	750 V
PEAK OUTPUT CURRENT	3.5A	12A
OUTPUT RISETIME	25 ns	10 ns
DELAY (10% input - 10% output)	2 ns	2 ns
DICDE POWER DISSIPATION	15W	25W
PULSE REPETITION FREQUENCY	200 KHz	350 KHz
PULSE DURATION	50usec	50usec
DUTY CYCLE	10%	10%

Part II

Part II of this paper describes a floating deck modulator configuration which uses two electron-bombarded semiconductor (EBS) tubes as switching devices to control the grid of a high power pulsed traveling-wave tube (TWT) amplifier which operates at -34.5 kVDC. This modulator provides 780 V peak, 900 V maximum grid voltage swings over a pulse width range of 35 ns to 2.0 μs with a rise time of 33 ns.

The initial design goals for this modulator are shown in the first column of Table II-I while the actual performance achieved is shown in the second column. Figure II-1 contains the block diagram for the EBS modulator.

TABLE II-I. EBS PULSE MODULATOR PARAMETERS

Output Pulse Parameters	Values	
	Objective	Achieved
Rise Time (10 to 90%)	25 ns	33 ns
Fall Time (90 to 10%)	25 ns	40 ns
Duty Cycle, Percent		100*
Min. Pulse Width (50%)	25 ns	35 ns
Max. Pulse Width (50%)	2.0 μs	2.0 μs**
Pulse Amplitude	1000 V	920 V
Pulse Repetition Freq., Max.		200 kHz
Load Capacitance	100 pF	100 pF

*Calculated maximum duty cycle based upon rated EBS diode power dissipated of approximately 25 W.
**Limited by drive circuitry, not EBS.

Theory of Operation

During the interpulse period the TWT grid is biased beyond cutoff by the negative grid-to-cathode voltage from power supply PS1 applied through resistor R1. To pulse the TWT, a 40 V peak amplitude voltage spike is applied from grid to cathode of EBS V1. Within its operating range, the EBS acts like a current source in that the diode (internal to EBS) output current is proportional to EBS beam current, the EBS beam current being a function of the EBS grid-to-cathode voltage. As a result of the 40 V grid-to-cathode voltage spike applied to EBS V1, a large current spike of approximately 5 A peak is produced by the EBS diode. This current pulse rapidly charges the TWT grid capacitance and drives the TWT grid-to-cathode voltage from its negative bias level to its positive ON state bias level. Once the TWT grid capacitance is fully charged, the grid-to-cathode voltage of EBS V1 is reduced to a value sufficient to maintain the TWT grid-to-cathode voltage at its positive ON state bias level. This requires EBS V1 to furnish approximately 0.8 A peak output to maintain the positive ON state bias level to the TWT grid due to TWT grid current requirements and loading of the EBS output due to resistor R1 and the EBS clamp circuit.

To end the TWT grid pulse, the grid-to-cathode voltage of EBS V1 is allowed to revert to its OFF state bias voltage level. After a short delay of approximately 15 ns, which is provided to ensure sufficient time for EBS V1 to turn off, a large momentary voltage spike of approximately 50 V peak for approximately 75 ns is applied across the grid to cathode of EBS V2. This causes the TWT positive grid-to-cathode voltage to be discharged rapidly to the OFF bias voltage level through the low ON state impedance of the diodes in EBS V2.

The modulator performance measured into a simulated TWT grid load of 10,000 Ω shunted by 100 pF is shown in Figure II-2. The packaging of the modulator is shown in Figure II-3.

AC filament and DC bias power for the TWT and EBS switches is provided by regulators which reduce the number of components required on the floating deck by regulating the AC at ground level with phase-controlled triac circuitry. A typical block diagram of this type of regu-

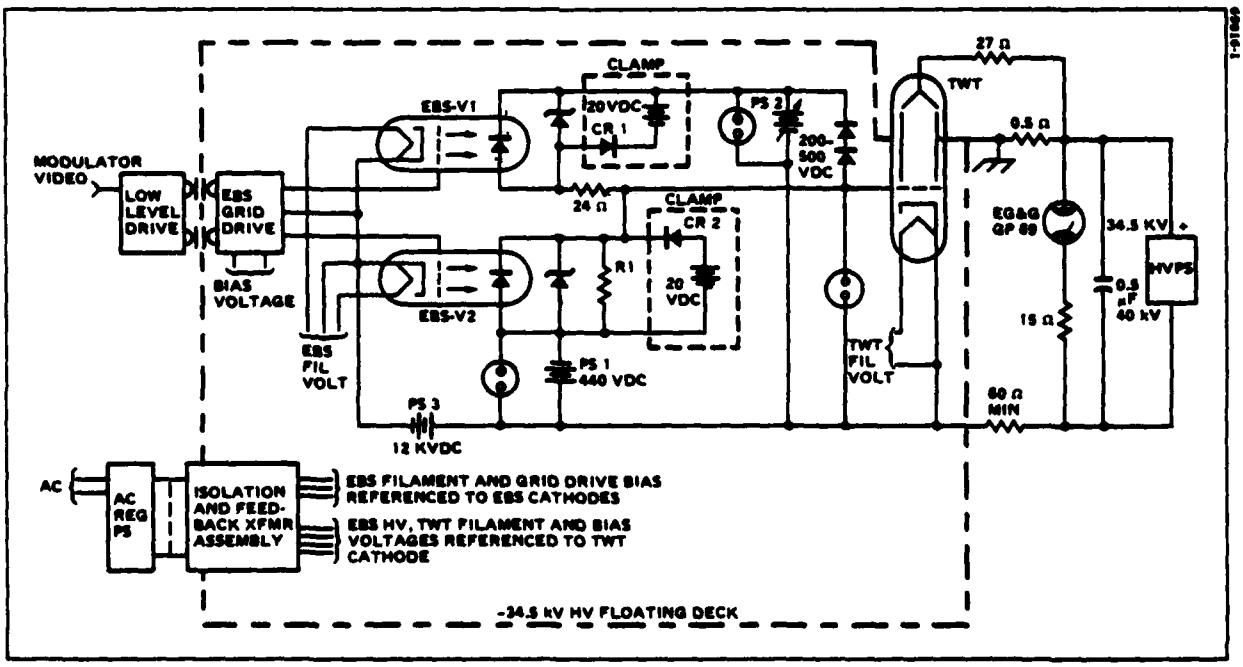

Figure II-1. Block Diagram of the EBS Modulator

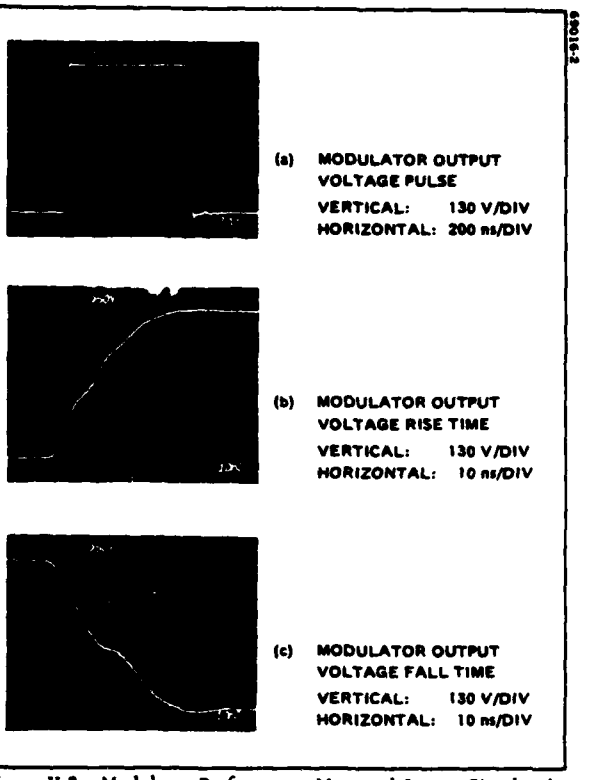

Figure II-2. Modulator Performance Measured Into a Simulated TWT Grid Load of 10,000 Ω Shunted by 100 pF

lator is shown in simplified form in Figure II-4. Voltage transformers monitor the output voltage of the power transformer secondaries on the floating deck and feed back the information to circuitry at ground level to produce the error signals. These error signals are then used to regulate the various power supplies. A total of three regulators are used and these are:

- Positive TWT bias supply, variable from 200 to 500 VDC.
- Negative TWT bias, EBS HVDC and EBS grid bias power supply using a common power transformer.
- TWT and EBS filament supply.

Modulator triggers are generated at ground level by the low level drive circuitry which accepts logic level signals of -0.90 V and -1.6 V from standard MECL III logic outputs. The MECL III logic drives an input differential amplifier in the low level drive circuitry. Both outputs of the differential amplifier are differentiated and drive separate pulse amplifiers for the formation of the ON and OFF trigger pulses to the floating deck circuitry. Each ON and each OFF trigger pulse is coupled by its individual ferrite core pulse current transformer to the floating deck circuitry operating at -47 kVDC. In the low level drive circuitry a positive differential change in input logic level has been arbitrarily chosen to generate an ON trigger pulse.

A modulator inhibit signal also is provided to the low level drive circuitry to prevent the generation of modulator ON and OFF trigger pulses.

The outputs of the individual ON and OFF trigger pulse current transformers drive separate ON and OFF EBS grid drive circuitry in the EBS grid drive unit on the floating deck. This EBS grid drive unit is shown in block diagram form in Figure II-5.

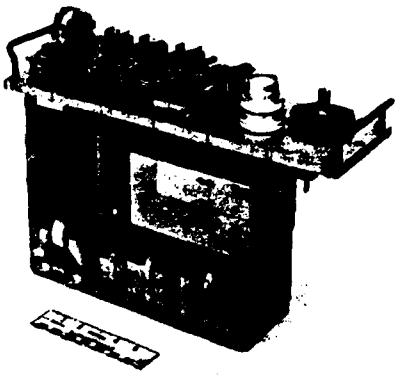

Figure II-3A. Mechanical Package of the EBS Modulator with Shields in Place. The modulator operates in fluorochemical liquid FC 78.

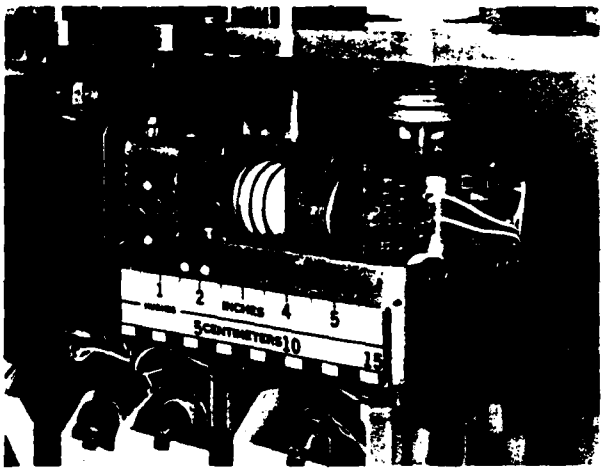

Figure II-3B. Close Up View of EBS Modulator with Shields Removed Showing the Placement of the EBS Switches

As shown in Figure II-5, the ON trigger pulse from the low level drive unit at ground level is used to trigger on a resettable monostable multivibrator, and is itself further amplified by transistor and FET circuitry to provide a fixed amplitude, fixed pulse width pulse. This fixed amplitude, fixed pulse width pulse is combined through diodes with a variable amplitude, variable pulse width pulse which is the amplified output of the resettable monostable multivibrator. The variable pulse width output of the resettable monostable multivibrator is obtained from the time spacing between ON and OFF triggers from the low level drive circuitry. The variable amplitude pulse output of the resettable monostable multivibrator is obtained by a "top-of-the-pulse clipper" incorporated within the amplifier circuitry at the output of the resettable monostable multivibrator.

The combined output obtained by diode combining forms the grid drive for EBS V1, and its typical pulse shape is as shown in Figure II-6. This shape of the EBS grid drive pulse is necessary to achieve a fast TWT grid voltage rise time, but minimize EBS diode saturation from EBS grid overdrive after the TWT grid is charged.

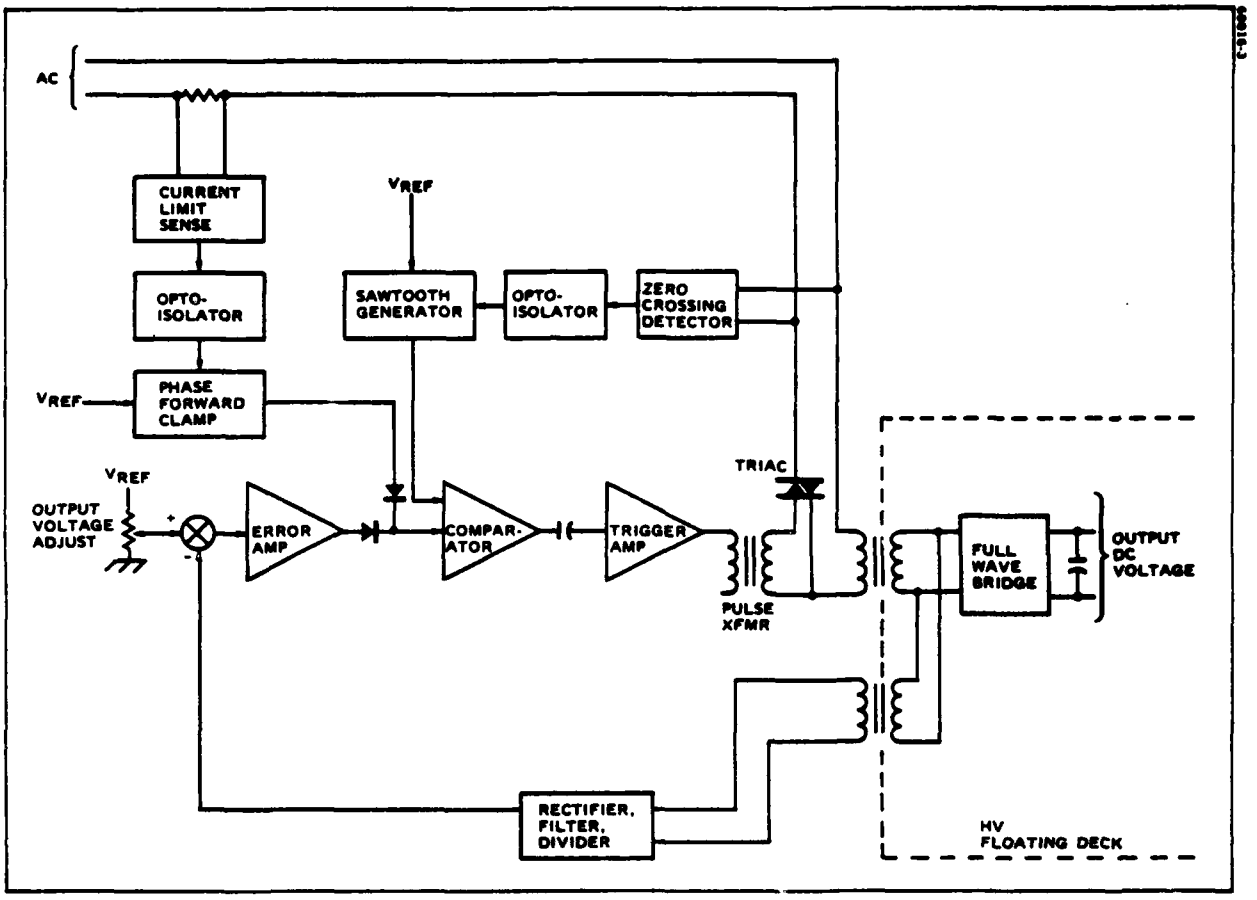

Figure II-4. Simplified Block Diagram of a Typical Bias Power Supply

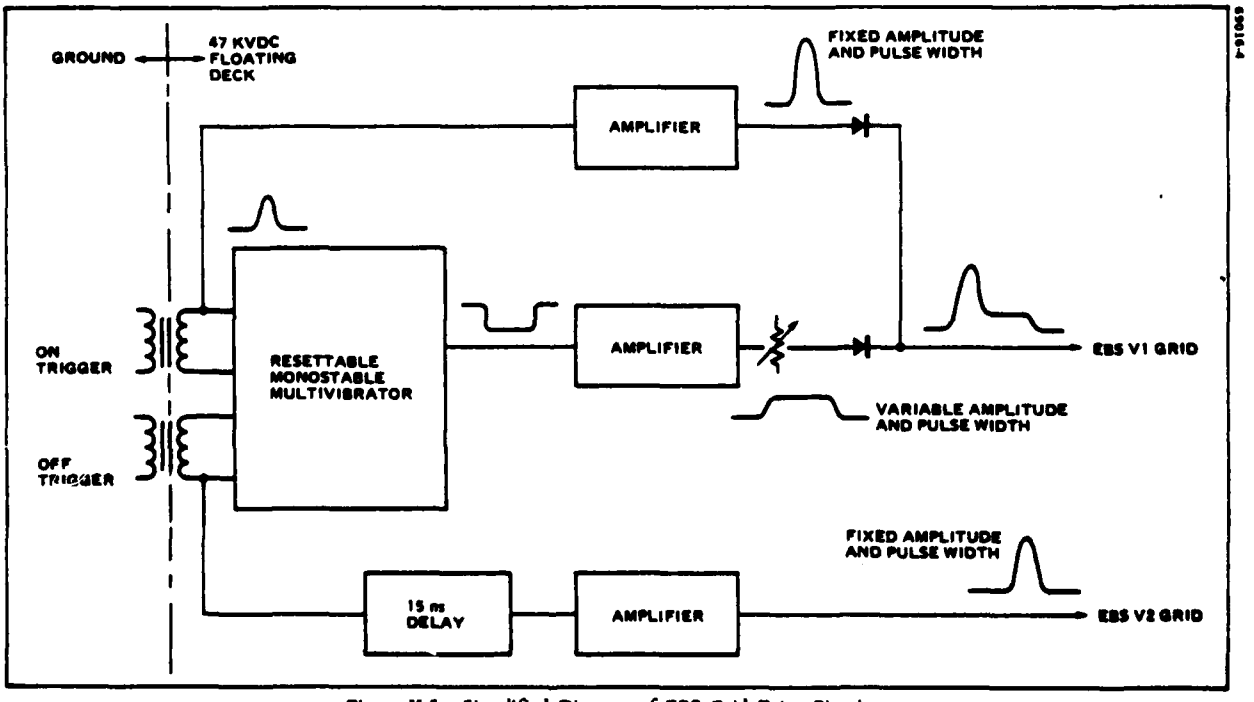

Figure II-5. Simplified Diagram of EBS Grid Drive Circuitry

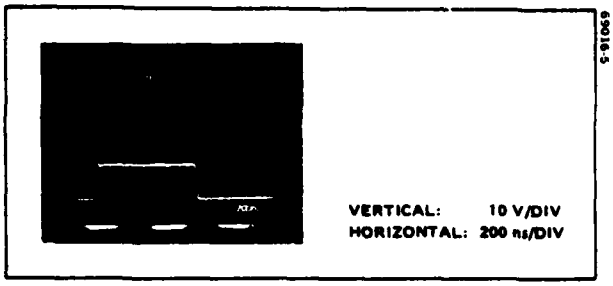

Figure II-6. EBS-V1 Grid Drive Voltage

The OFF trigger pulse from the low level drive circuitry not only serves to trigger off the resettable monostable multivibrator, but, after a delay of 15 ns, is amplified to form a fixed amplitude, fixed pulse width pulse to the grid of EBS V2. The typical pulse shape of the grid-to-cathode voltage applied to EBS V2 is shown in Figure II-7.

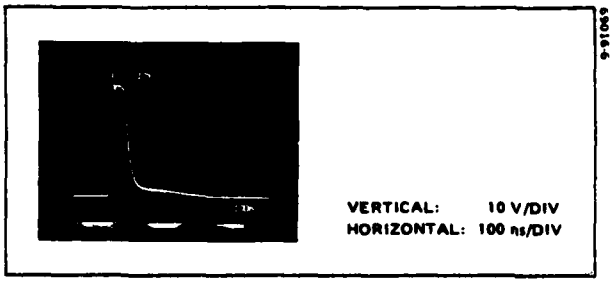

Figure II-7. EBS-V2 Grid Drive Voltage

Special Design Considerations

Three major design considerations must occur in the design of an EBS modulator. These are:

- Shaped grid drive to EBS-V1, the EBS ON or pull up switch tube.
- Clamp circuitry to prevent EBS diode saturation.
- High energy transient suppression.

Grid Drive

The requirements for shaped grid drive to the EBS ON switch are dictated by the rise time requirements of the TWT grid voltage, the TWT effective grid capacitance, and the normal ON state TWT grid interception current requirements. For this application the TWT grid and associated circuitry represents an equivalent load of approximately 150 pF in parallel with 3000 Ω. To achieve a fast grid rise time, a higher current must be provided during the leading edge of the pulse to charge up the effective grid capacitance than is required by the grid interception current to maintain the top of the pulse. A peak diode current in excess of 5 A peak for the EBS ON switch is required to achieve a 35 ns rise time while only 0.3 A peak is necessary during the pulse top to supply the TWT grid interception current requirements. Since the EBS diode or output current is a function of the EBS beam current, the output or diode current is a function of the EBS grid drive. Thus a heavily spiked EBS grid-to-cathode voltage must be applied during the leading edge of the pulse to charge the TWT effective grid capacitance, but must be reduced to a low value during the top of the pulse to prevent EBS diode saturation. If the EBS diode saturation is not prevented, then the TWT grid voltage waveform will suffer from pulse width stretching and fall time degradation.

Also, the EBS grid-to-cathode voltage required to produce a specific diode output current varies from EBS to EBS. A variable level control must be provided to make a one-time adjustment upon installation of a new EBS ON switch. Empirically speaking, the Δ Io/ΔEg-K sensitivity of the EBS is greatest at the lower EBS diode output currents, making it possible to provide only a variable level control for that portion of the EBS grid voltage associated with the top of the pulse and allowing the leading edge voltage spike to have a fixed amplitude. For the design presented herein, a fixed amplitude EBS grid-to-cathode voltage spike of typically +40 V is required on the leading edge, while an adjustable -4.0 to +12.0 V amplitude is provided during the top of the pulse. The fixed OFF bias on the EBS grid is -8.2 V.

EBS Diode Clamp Circuitry

Even with the provisions for shaped EBS grid drive, some grid overdrive is necessary to allow for variations in TWT grid interception current with TWT aging, variations in EBS parameters with aging, and EBS pulse repetition frequency sensitivity characteristics which are described elsewhere. To limit the degree of saturation of the EBS diodes it is necessary to provide the EBS switches with the clamp circuitry. This clamp circuitry is shown in Figure II-8 in a simplified form.

Each EBS switch used is similar to the Watkins-Johnson Part No. 3680-3 and has three to four diode junctions electrically connected in series to form, as termed by this paper, the EBS diode. The output current from the EBS diode is a function of the energy level of the impinging electrons upon the diode target and the quantity of electrons impinging per unit of time (EBS beam current) upon the diode target.[1] Since the electron energy level is fixed by the EBS cathode-to-diode target voltage which is constant in value and the EBS beam current is fixed by the EBS grid-to-cathode voltage, the EBS diode current is a constant value over a wide operating range of load impedance. If, in the application of the EBS switch, variations occur in the current level in the diode output circuitry, then the voltage across the EBS diode will vary directly for a fixed EBS grid-to-cathode voltage. When the EBS diode is saturated the EBS diode voltage should approach zero limited only by the diode ohmic resistance. To prevent EBS diode saturation from occurring, a portion of the EBS diode bias voltage (the + TWT bias power supply) is zener diode regulated by resistor R1 in series with zener diode VR1 in Figure II-8 for EBS V1. Capacitor C1 provides the necessary energy storage and the clamp circuit is connected in parallel across the EBS diode through a fast recovery switching diode CR1.

In the nonconducting state of EBS V1 a high voltage appears across the EBS diode, causing diode CR1 to be reverse biased. As the conduction of the EBS diode is initiated by the application of EBS grid drive, the voltage across the EBS diode drops. As the EBS diode voltage drops below the level set by the zener diode VR1 and the forward voltage of diode CR1, diode CR1 begins to conduct and current flows out of capacitor C1, through diode CR1 and the EBS diode. This additional current cannot be supplied by the EBS diode for the level of EBS grid drive available and the EBS diode voltage rises, causing the EBS diode to be pulled out of saturation.

The clamp circuitry associated with EBS V2 operates in a similar manner. In typical operation the EBS diode clamp circuitry associated with both EBS V1 and V2 operates with a clamp current (as measured through diode CR1) of approximately 0.5 A during the top of the pulse. This arbitrary value allows for changes in diode output current due to variations in EBS beam voltage, EBS grid drive, temperature, pulse repetition rate and TWT grid loading.

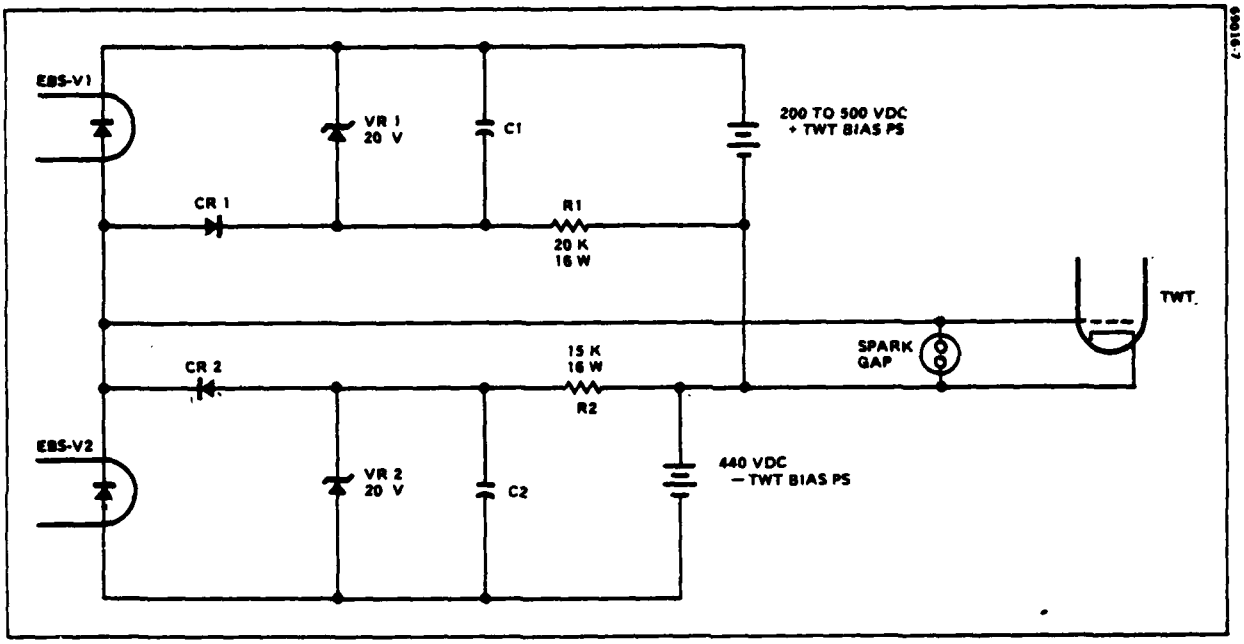

Figure II-8. Simplified Diagram of EBS Output Circuitry Showing Clamp Circuitry

High Energy Transient Suppression

As shown in Figure II-1 the primary fault protection for the TWT is a crowbar using an EG & G No. GP69 triggered spark gap.

Modulator protection is provided by a spark gap placed across the TWT grid to cathode in the event of a direct TWT arc to the grid or in the event that any transient voltages are induced during crowbar operation.

Additional spark gaps are located at the outputs of power supplies PS1 and PS2 to protect against EBS diode overvoltage due to power supply regulator failures.

Primary EBS protection is achieved by the placement of a high surge-rated zener diode across each diode junction in the EBS. Two EBS diode failures were experienced during early modulator development. Since the implementation of zener diode protection across each EBS diode junction, no additional EBS diode failures have occurred.

Areas Requiring Further Improvement

The present EBS switches have diode targets which consist of four diode junctions which are electrically connected in series. Access to each diode junction is provided to enable the addition of voltage equalizing networks across each diode. However, in some cases only three of these diode junctions are used, posing mechanical implementation problems when these EBS switches are utilized in mechanically interchangeable assemblies. This is because the voltage equalizing networks consist of voltage equalizing resistors which compensate for unequal diode leakage current and zener diode overvoltage protection of the individual diode junctions. In the case where only three diodes are used, a short must be added across the unused terminals and zener diode values changed to achieve the same overall EBS diode voltage rating, e.g. three 330 V zener versus four 250 V zeners.

A more serious problem exists in the electron beam gun portion of the EBS. It was found on the initial devices delivered by Watkins-Johnson that the beam current, and consequently diode current, varied significantly with pulse repetition frequency. Increases in the pulse repetition frequency would produce a decrease in beam current for a constant EBS peak grid drive voltage. The percentage in the steady state EBS beam current as a result of increasing the pulse repetition frequency from 100 Hz to 20 kHz is shown in Table II-II. To obtain this data, the EBS tubes were operated using the shaped EBS grid drive waveform of Figure II-6, with the steady state EBS grid voltage amplitude adjusted to produce a steady state EBS beam current during the top of the pulse of approximately 20 ma. Due to the use of the clamp circuit mentioned earlier, changes in the steady state EBS beam current of less than 10 percent have little effect on overall modulator performance. However, changes of more than 10% require increased EBS grid drive voltage at high pulse repetition frequencies, which produces undesirable higher diode currents at low pulse repetition frequencies. As mentioned in the first part of the paper, research at Watkins-Johnson indicated that the problem was caused by poisoning of the cathode. Modifications to the cathode processing improved the performance of most of the remaining units delivered; however, the switch from oxide to dispenser cathodes appears to offer a much more satisfactory solution.

TABLE II-II. STEADY STATE EBS BEAM CURRENT CHANGE DURING THE TOP OF THE PULSE AS A FUNCTION OF A 100 Hz TO 20 kHz PULSE REPETITION FREQUENCY CHANGE

EBS Serial No.	EBS Beam Current Decrease in Percent
14	-71
17	-13
18	-17
19	-29
20	- 5

A problem area which was not anticipated was the internal arcing of the EBS switch to its grid. This arcing typically occurs only after the EBS switch has not been

used for several weeks and usually occurs immediately upon the application of EBS beam voltage only with no EBS grid pulsing. The EBS switch appears to clean itself up as a result of the arc, and normal operation may be obtained after repairing the damaged grid drive circuitry. Transient protection of the EBS grid circuitry has not proven practical due to high transient energy available during an EBS switch arc. Also, such suppression circuitry has been found to cause severe pulse performance degradation. Instead, transient protection must be incorporated into the EBS target-to-cathode voltage power supply to limit filter capacitor discharge energy.

EBS Modulator Versus the Transistor Modulator

The objective of the EBS modulator development was to obtain a significantly improved pulse performance and a reduced size over the transistor floating deck modulator reported upon earlier.[2] A comparison of the pulse performance and size of these two modulators is shown in Table II-III. It will be noted that the EBS modulator is superior in the areas of pulse fall time, minimum pulse width, maximum pulse repetition frequency, and size. The rise times of the two units are nearly equal, because as was mentioned earlier, Watkins-Johnson found it necessary to use the four diode series target instead of the originally conceived target consisting of two parallel strings of three series-connected diodes.

The EBS modulator has demonstrated an overall performance and size advantage when compared with the transistor modulator. However, there are several areas specifically relating to device improvement where further development work is required to produce a modulator superior in all respects to the transistor modulator. These areas are as follows:

- Develop the EBS switch using a single 1000 V diode junction
- Eliminate the EBS switch output sensitivity to pulse repetition frequency.
- Markedly improve the EBS switch arcing problem.

Development is taking place which is expected to result in a device meeting the above characteristics. The device will be used in later versions of the EBS modulator.

TABLE II-III. COMPARISON OF EBS MODULATOR AND PREDECESSOR TRANSISTOR MODULATOR PERFORMANCE

Output Pulse Parameters	EBS Modulator Performance Achieved	Transistor Modulator Performance Achieved
Rise Time (10 to 90%)	33 ns	30 ns
Fall Time (90 to 10%)	40 ns	147 ns
Duty Cycle, Percent	100*	100
Min. Pulse Width (50%)	35 ns	143 ns
Max. Pulse Width (50%)	2.0 μs**	DC
Pulse Amplitude	920 V	960V
Pulse Repetition Freq., Max.	200 kHz	50 kHz
Load Capacitance	100 pF	100 pF
Volume, in^3	861	1034

*Calculated maximum duty cycle based upon rated diode power dissipation of approximately 25 W.
**Limited by drive circuitry, not EBS.

Acknowledgements

The authors of this section of the paper wish to acknowledge the support of the U.S. Navy, for without their support this paper would not have been possible.

References

1. R. I. Knight and D. J. Bates, "Characteristics and Capabilities of the Modulator EBS," Proceedings of the *Eleventh Modulator Symposium, September 1973*, pages 17-22.
2. J. V. Stover and M. J. Westby, "A Versatile Transistor Modulator For TWT Grid Modulator Application," Proceedings of the Tenth Modulator Symposium, May 1968, pages 164-176.

SOLID STATE MODULATOR SWITCH LOSS PERFORMANCE CHARACTERIZATION

J. B. Brewster
Westinghouse Research Laboratories
Pittsburgh, Pennsylvania

R. A. Hill
Westinghouse Electric Corporation
Baltimore, Maryland

Summary

The work described in this paper verifies that standard rating techniques, similar to those used for thyristors, may be applied to the Reverse Switching Rectifier (RSR) if appropriate loss information is available. For a sample group of T62R RSR's, loss measurements were made using a flow calorimetric technique. Energy loss per pulse was measured for RSR's switching peak currents up to 5000 amperes at a pulse width of 20 microseconds. These measurements suggest that RSR switching devices may be classified by considering the relationship between loss per pulse and peak current switched. As an example, a derating curve using such data is described which can be used to predict maximum allowable peak pulse current for a given pulse repetition rate. Rating information such as this will make possible reliable RSR applications which realize the long life normally associated with solid state devices.

1. Introduction

The Reverse Switching Rectifier (RSR) is a four-layer semiconductor switching device with very short turn-on time. Because of this, it serves well as a radar modulator switch where a high value of di/dt must be tolerated at turn-on. Because the structure of the RSR resembles that of a thyristor in many ways, thyristor characterization and rating techniques were used initially to characterize the RSR. Typical of the parameters defined and measured were turn-on time, dynamic forward drop and maximum allowable turn-on di/dt. However, as modulator circuit designers attempted to use these parameters and ratings to design practical circuits, they found them to be inadequate for the determination of permissible operating conditions.

In order to satisfy the need for characterization and rating information suitable for use by modulator circuit designers, a new approach to RSR characterization has been adopted. The approach, described in this paper, involves the determination of RSR losses using a flow calorimeter, and the subsequent use of this information to determine device junction temperature for any set of operating conditions.

Whereas the characterization of a thyristor for phase controlled rectification service is indeed simple, that for use of the device in a chopper application with trapezoidal current waveforms becomes more difficult because of the complexity of specifying the current waveform. RSR current pulse waveforms are similarly complex. Pulse current waveform parameters to be specified include width, rise time, peak current and repetition rate.

The work described in this paper was done using a T62R RSR which is the largest switch of this type available. The T62R, which is about one inch in diameter, was used to switch a current pulse of 5000A peak, 2 microseconds risetime, and 20 microseconds width at a repetition rate of 250 Hz. Although the test conditions used covered a reasonably broad range, it is recognized that the results are insufficient to provide complete across-the-board characterization for all possible RSR operating conditions. Nevertheless, since any other RSR application must proceed with a similar approach to rating, and since this approach, so similar to that used for thyristor high frequency rating, has never before been applied to RSR devices, it is important to demonstrate the applicability of this technique which is the purpose of this paper.

2. The Test System

A. Electrical Test System

The important components of the RSR electrical test system are shown in Figure 1. The pulse forming networks are resonantly charged as is commonly done in modulator circuits. The two-terminal nature of the RSR requires two hold-off diodes, D-1 and D-2, which isolate the pulse forming network from the high voltage trigger pulse needed to turn-on the two RSR's in series. Similarly, diodes D-5 and D-6 ensure that the pulse forming network does not discharge through RSR trigger pulse transformer, TR-1. The peak RSR pulse current is determined by the value of the power supply voltage used, and by the number of PFN's connected.

To operate the system, the parallel-connected PFN's are charged from the charging power supply, after which trigger capacitor C_T is resonantly charged. The RSR's are triggered when capacitor C_T is discharged through the primary of transformer TR-1 by triggering thyratron T_A. A thyratron is used in the trigger circuit only to achieve a broad range of triggering conditions, necessary to the determination of optimum trigger requirements. The results obtained show that optimum RSR triggering requirements can easily be met using circuits which are exclusively solid-state.

B. The Power Measuring System

The RSR's under test are mounted between heat exchangers as shown in Figure 2. Heat exchangers are mounted above, below, and between RSR's so that all of the energy dissipated causes a rise in the temperature of the cooling water. Power losses of pairs of devices are determined because one device alone cannot hold off sufficient voltage to produce the desired maximum peak load current of 5000 amperes even with many paralleled PFN's and loads. One T62R RSR can hold off only 1000 volts, however, as many as five devices have been operated in series, yielding a combined hold-off voltage of greater than 5000 volts, and no limitation is seen to increasing the number of series connected devices to achieve even higher hold-off voltages. Therefore, all data presented is the average loss for a single device, i.e., losses are determined for two devices and divided by two.

The flow colorimeter used is shown functionally in Figure 3. The flow rate of the water used to cool the RSR pair is carefully monitored, as is water temperature before and after passage through the heat exchangers. Short connecting hoses are used to minimize heat losses from the cooling water. By measuring the heat sink cooling water inlet and outlet temperatures, and the flow rate, the power loss of two devices can be computed using Equation (1).

$$\text{Power} = .07 \times \text{Flow}\left(\frac{cc}{min}\right) \times \Delta T(^{o}C) \times \rho\left(\frac{cal}{cc\text{-}^{o}C}\right) \text{ watts} \quad (1)$$

where

$\Delta_T = T_2 - T_1$ (^{o}C)

T_1 = Inlet water temperature (^{o}C)

T_2 = Outlet water temperature (^{o}C)

Measurement accuracy is limited by errors in temperature measurement, errors in flow measurement, and most importantly, heat losses in connecting hoses. By measuring the power losses of a pair of rectifiers carrying direct current, the flow calorimeter can be shown to read true power to within 5% of that determined by a simple current-voltage measurement. Even with this error, the flow calorimetric technique is desirable because of the speed and convenience with which measurements can be made when the RSR is subject to a host of different pulse current waveforms and switching conditions.

3. Test Results

The purpose of the test was to determine the energy loss per pulse per device in a fashion similar to that used for high frequency thyristor characterization. A typical current pulse switched by a pair of RSR's is shown in Figure 4. Pulses with the shape of the one shown were applied at various pulse repetition rates and peak currents. Through the use of the power measuring system, losses for many pairs of devices were determined using Equation (1). In Figure 5, loss per pulse is shown plotted as a function of pulse repetition rate to specifically demonstrate that watt-second per pulse losses are well behaved, and are nearly independent of pulse repetition rate as expected. For this reason, all further testing was performed at a constant pulse repetition rate of 150 Hertz.

The increase in loss per pulse with peak current is better shown in Figure 6, where the characteristics of several pairs of devices are shown to illustrate the spread of measurements. For the particular pulse conditions used, the losses center about one joule per pulse at a peak current of 4000 amperes. At higher peak currents, losses increase rapidly, almost doubling at 5000 amperes. One pair of devices failed to operate at 5000A peak, but were not destroyed. This result could be anticipated from the high losses of device pair 33-6A and 35-6A in the vicinity of 4000A peak current. Device pair 25-5A and 43-5A showed exceptionally low losses, suggesting superior switching ability. The spread of performance data suggests that devices can be classified using results from as little as two loss measurements at different peak currents.

4. Sample Rating

The purpose of the device rating procedure described is to determine the relationship between maximum permissible peak pulse current and pulse repetition rate for a given pulse waveform. The rationale' underlying the procedure is the same as that used for high frequency thyristor ratings. A current pulse, no matter how complex in form, results in an average power dissipation which can be determined for the peak current and pulse repetition frequency used. The average power dissipation, P_{AV}, can then be used with conventional device thermal analysis to relate average junction temperature to case temperature to cooling water or air temperature using case-to-ambient thermal resistance.

The accuracy of this approach depends strongly on the uniformity of pulse current conduction across the area of the RSR fusion. Experimental evidence obtained using equipment which senses recombination radiation supports the assumption of uniform current conduction across the fusion surface. Also, because of the broad-area turn-on mechanism operative in the RSR structure, the types of hot spots occurring in thyristors at high levels of di/dt are not expected. Therefore, the treatment of junction temperature on an average basis seems justified.

The relationship between average junction temperature and ambient temperature is shown by Equation (2).

$$T_j = P_{AV}\theta_{JC} + (P_{AV}\theta_{CA} + T_A) \quad (2)$$

where

T_J = RSR average junction temperature (^{o}C)

T_A = Cooling water or ambient air temperature (^{o}C)

P_{AV} = RSR average power loss (watts)

θ_{JC} = RSR junction-to-case thermal resistance ($^{o}C/W$)

θ_{CA} = Heat sink thermal resistance, case-to-ambient ($^{o}C/W$)

The first term on the right side of Equation (2), $P_{AV}\theta_{JC}$, is the difference in temperature between the RSR junction and case. Because RSR junction-to-case thermal resistance, θ_{JC}, is determined by device construction, it is a constant and for the T62R is 0.08°C/W. In any given application, then, RSR junction-to-case temperature difference is proportional to average power dissipation.

The second term on the right side of Equation (2) is the RSR case temperature. It is arrived at by adding the case-to-ambient temperature drop, $P_{AV}\theta_{CA}$, to the temperature of the ambient air or water, T_A. Both the case-to-ambient thermal resistance, θ_{CA}, and the ambient temperature, T_A, can be specified by the circuit designer.

As an illustration of the use of this technique, Equation (2) will be solved graphically to determine RSR junction temperature, T_J, for a number of combinations of peak pulse current and pulse repetition frequency.

The second term on the right side of Equation (2) is shown plotted in Figure 7 as a function of pulse repetition frequency with peak current as a parameter. The experimental conditions used to obtain the data plotted are shown in the figure.

Similar data for the first term on the right side of Equation (2) can be generated analytically using Equation (3).

$$P_{AV}\theta_{JC} = \text{Loss/Pulse} \times f \times \theta_{JC} \quad (3)$$

where

f = pulse repetition frequency

The experimental loss/pulse data shown in Figure 5 can be substituted into Equation (3) and the results added graphically to the data shown in Figure 7 to obtain the results shown in Figure 8 for junction temperature as a function of pulse repetition frequency with peak current as a parameter.

It can be seen from the data presented in Figure 8, that although T_J increases linearly with pulse repetition rate, it increases more than linearly with peak pulse current. A horizontal line can be drawn to indicate the effect on performance of different maximum junction temperature limits. If $T_{J(max)}$ is 100°C, the intersection of the horizontal line drawn at 100°C with the plots of junction temperature vs. pulse repetition frequency determine the maximum permissible pulse repetition frequency for each value of peak pulse current. For example, at a peak pulse current of 5000A, the maximum permissible pulse repetition frequency is 250 Hz, and at 2000A, it is 1350 Hz for the case of $T_{J(max)}$ = 100°C and T_A = 18°C.

The result of increasing the temperature of the cooling water can be determined graphically in a similar fashion. The case of increasing the temperature of the coolant by 20°C is illustrated in Figure 8 by the horizontal line drawn 20°C below the original maximum permissible junction temperature line at 100°C. The new set of maximum permissible pulse repetition frequency values for the peak pulse currents used are determined by the intersections of the new effective maximum permissible junction temperature line at 80°C with the lines relating junction temperature to pulse repetition frequency. The data determined by the intersection of the horizontal lines at junction temperatures of 80°C and 100°C with the junction temperature vs. pulse repetition frequency lines are shown plotted in Figure 9. The permissible area of operation is that existing below the curve for the cooling water temperature chosen.

5. Summary and Conclusions

It has been shown that standard rating techniques, similar to those used for fast thyristors, may be applied to the RSR if appropriate loss information is available. For a sample group of T62R's, loss measurements were made using a flow calorimetric technique. Losses were measured for RSR's switching peak currents up to 5000A with a pulse width of 20 microseconds. The results suggest that RSR switching devices may be classified using losses measured at several different peak currents. As an example, a derating curve was determined, using measured loss data, which may be used to predict the maximum permissible pulse current for a given pulse repetition rate. Rating information such as this will make possible RSR applications which will realize the long life normally associated with solid-state devices.

6. Acknowledgements

This work was performed on Contract Number F 29601-74-C-0021 under the sponsorship of the Air Force Weapons Laboratory at Kirtland Air Force Base, and under the direction of Major F. S. Zimmerman.

7. References

1. Westinghouse, "SCR Designers Handbook", pp. 4-5 to 4-10.

2. P. F. Pittman and J. B. Brewster, "A New Solid State Switch for Power Pulse Modulator Applications; The Reverse Switching Rectifier", 11th Modulator Symposium, September 18-19, 1973.

3. R. A. Gardenghi, "A Super Power RSR", International Electron Devices Meeting, Washington, D. C., December, 1975.

4. R. A. Gardenghi and E. H. Hooper, "A New High Power RSR Solid State Switch", Power Electronics Specialists Conference, June, 1975.

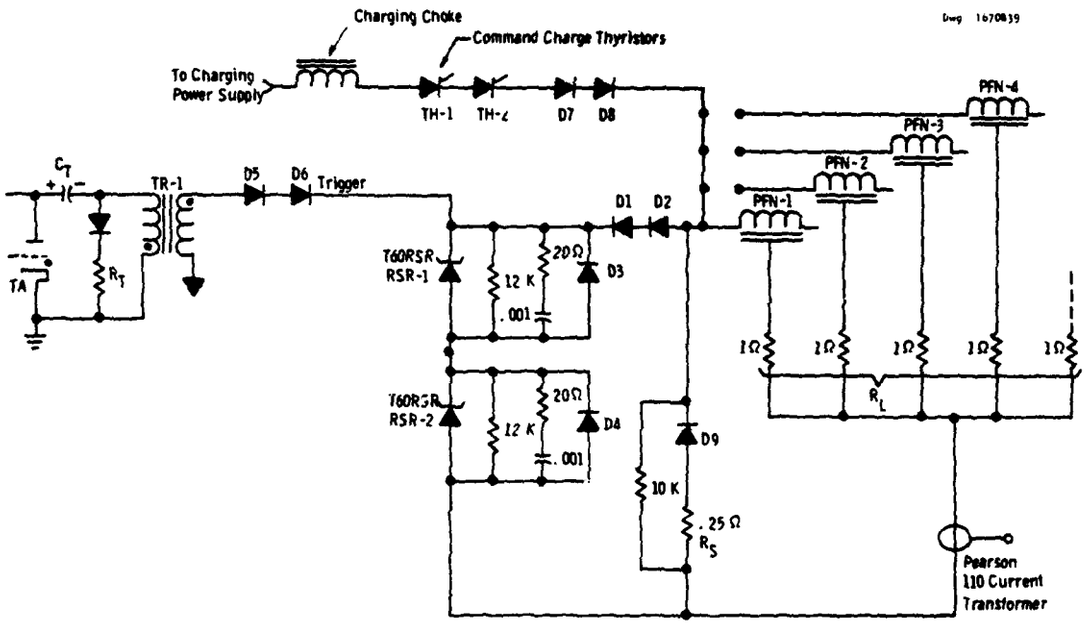

Fig. 1 - Electrical Test Circuit

Fig. 2 - Heat Exchanger Assembly

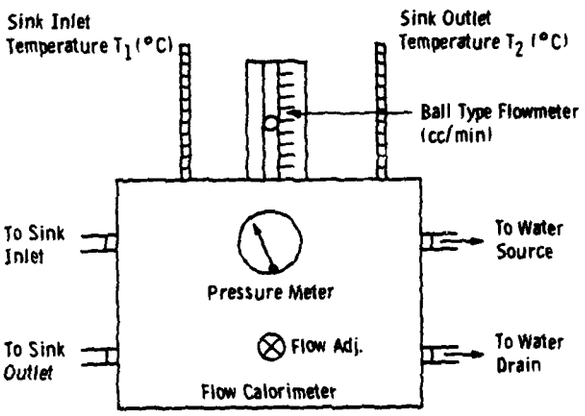

Fig. 3 - Flow Calorimeter Power Measuring System

Fig. 4 - Sample Load Current Pulse
Horiz. 5 Microsecond/Div.
Vert. 1000 Amperes/Div.

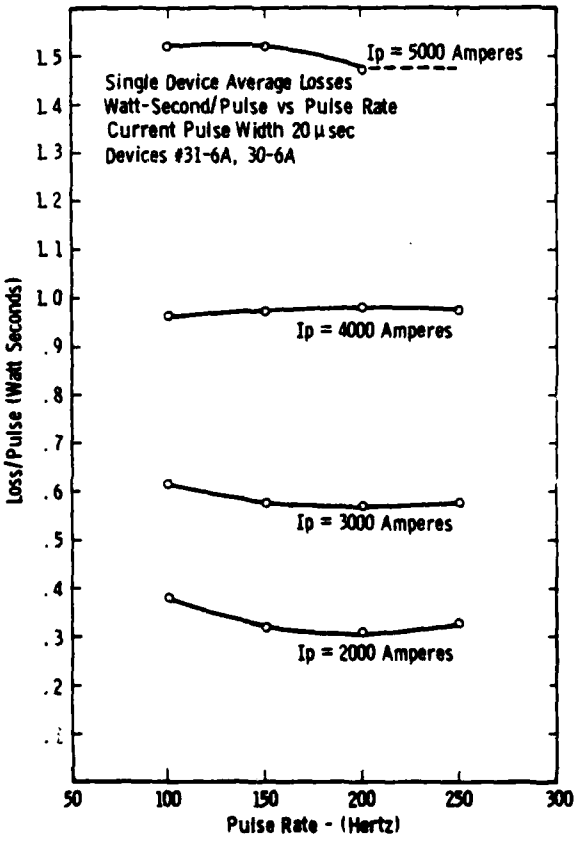

Fig. 5 - Watt-Second Loss/Pulse Vs. Pulse Rate

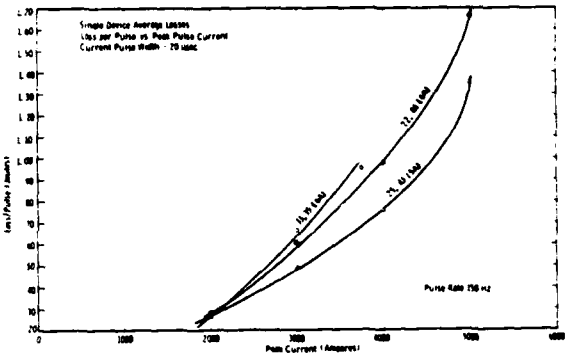

Fig. 6 - Watt-Second Loss/Pulse Vs. Peak Current

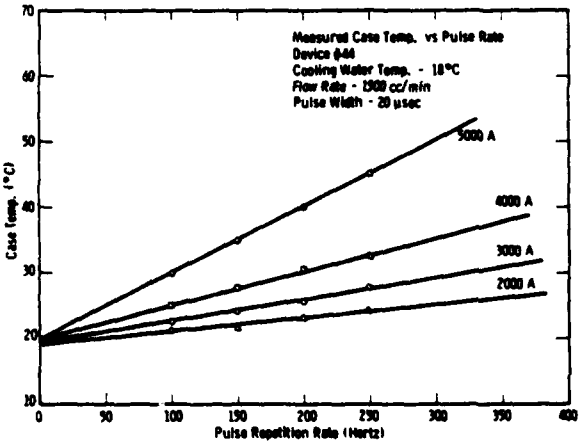

Fig. 7 - Measured Case Temperature Vs. Pulse Rate

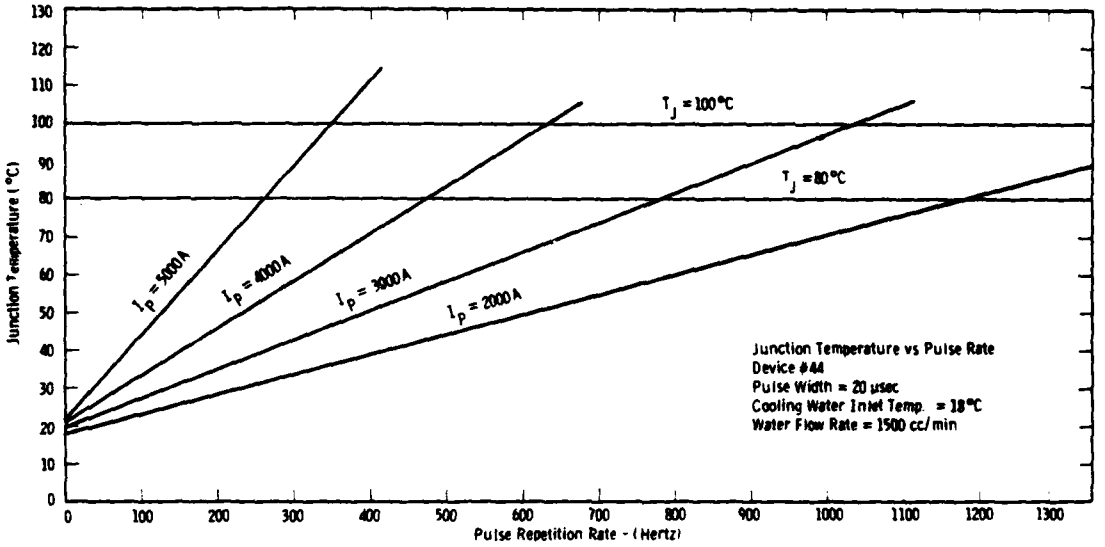

Fig. 8 - Junction Temperature Vs. Pulse Rate

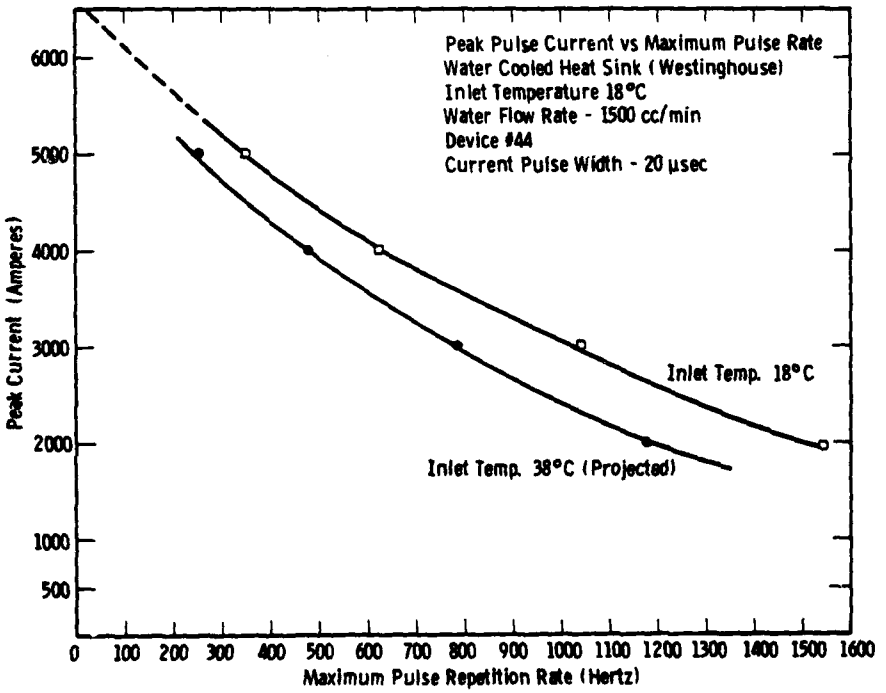

Fig. 9 - Peak Pulse Current Derating Vs. Pulse Rate

A FLOWING GAS PLASMA SWITCH FOR EXTRACTING PULSES FROM A SUPERCONDUCTING ENERGY STORAGE COIL

Edward J. Lucas, Paul M. G. Margosian, William F. B. Punchard
Magnetic Corporation of America
179 Bear Hill Road
Waltham, Massachusetts 02154

Richard L. Verga, Jerrell M. Turner
Wright-Patterson Air Force Base
Dayton, Ohio 45433

Summary

A two electrode flowing gas switch has been tested which is capable of operation at a repetition rate of at least 500 hertz and at an average power level of at least one megawatt. In the experiments performed, the energy stored in a superconducting coil was extracted as a string of pulses by forming a relaxation oscillator from the charged coil which acted as the current source, a capacitor, a load resistor, and the flowing gas switch with suitable arc quench circuitry. A string of three kilojoule pulses was obtained at a voltage of two kilovolts, peak currents of approximately 8 kiloamps, and an initial repetition rate of 250 hertz.

Introduction

Pulsed Energy Storage System Comparisons

Superconducting energy storage coils have been undergoing development[1-4] for a number of years because of potential advantages in size and weight over capacitors for pulsed power systems. A comparison of capacitors, inductors, and batteries as energy storage devices is given in Figure 1. Batteries have the lowest specific weight because the energy is stored chemically; however, they cannot be discharged rapidly. Capacitors are heaviest because of limitations on the dielectric strength of available insulating materials; however, they can be discharged very rapidly by closing a switch. Superconducting coils are much lighter than capacitors because of the high available current densities; their specific weight is limited by the maximum allowable stress in the conductor material. They are discharged by opening a switch, hence output pulse rise times and voltage levels are limited by the recovery characteristics of the switch. Further, the total weight of a superconducting coil system must include the refrigeration equipment (Figure 2) needed to remove the power dissipated in the coil during complete charge/discharge cycles. A calculation of system power efficiency must include the required refrigerator power (Figure 3). These penalties in weight and efficiency can be minimized for limited duration applications by using stored cryogens instead of a refrigerator. However, an ideal superconducting energy storage coil system should consist of a coil with very low losses and a fast, reliable, high voltage opening switch.

Switches for Inductive Systems

The most commonly used switch for inductive energy storage systems is a vacuum interrupter equipped with an arc quench circuit (Figure 4) which forces the switch current to zero for a sufficiently long time to allow switch recovery. Conventional linearly actuated vacuum interrupters exhibit recovery times of 20 to 30 microseconds, current capacities up to 10 kiloamps, and voltage limits of about 50 kilovolts, and are limited by mechanical considerations to repetition rates of five to ten cycles per second. Designs have been worked out for a rotating vacuum switch[5] and for a two-stage

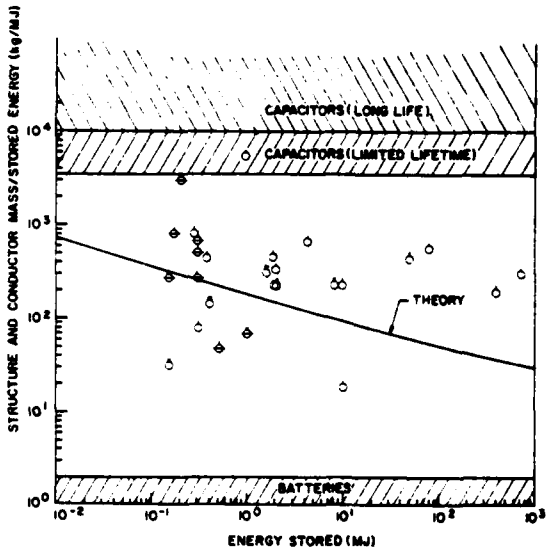

Figure 1: Weight of conductor plus structure for existing superconducting solenoids as a function of energy stored. Approximate ranges for capacitors and batteries are shown for comparison.

torsional with flowing gas/plasma interrupter tube switch[6], both of which would be capable of higher repetition rates. However, no definitive tests have been conducted for either type of switch to date.

Other Constraints on a Pulsed Inductive System

In a conventional application a superconducting energy storage coil is completely charged and completely discharged for each output pulse. This means that the charging power supply must operate stably into a widely varying load which can fluctuate up to several times per second and must be capable of supplying the peak charging power for the coil. Further, the switching system must open once every cycle at maximum coil current; the rate of rise and the amplitude of the output pulse are limited by this switch. Finally, the hysteretic losses in the coil (e.g. Figure 5), which are typically 0.1 to 0.2 percent of the coil stored energy, are at a maximum when the coil is fully charged and discharged each cycle. These coil losses require installed cooling capacity, either a refrigerator (Figures 2, 3) or stored cryogens (2500 joules/liter heat capacity for liquid helium), which increase the weight of the system.

Partial Discharge Inductive System

The coil losses could be reduced considerably if the coil were not completely charged and discharged each cycle because only a small fraction of the hysteresis loop would be traversed during each pulse.

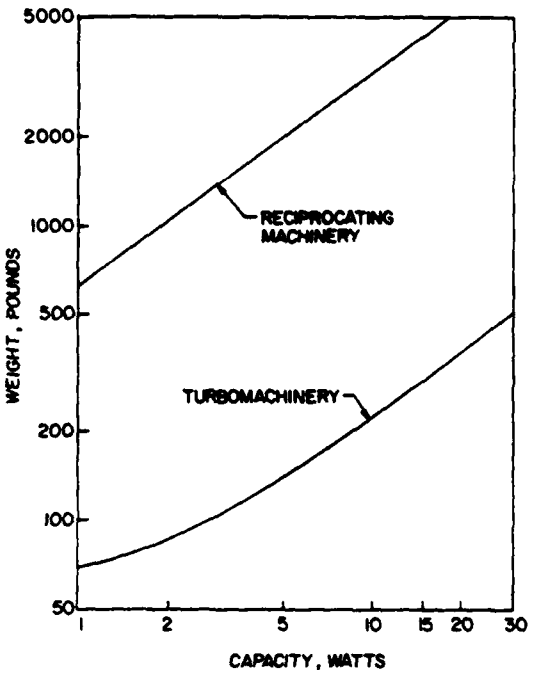

Figure 2: Refrigerator weight versus capacity at 4.2 K.

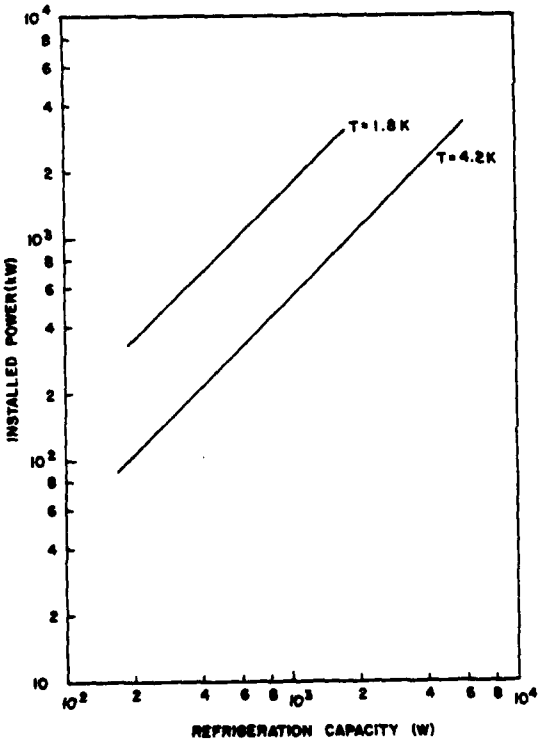

Figure 3: Installed refrigeration power required as a function of heat load.

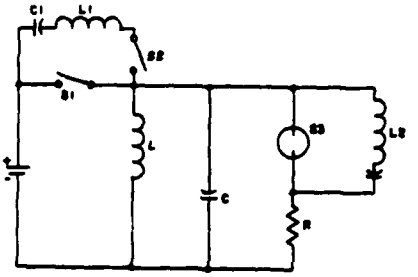

Figure 4: Electric circuit for operating energy storage coil, L, in a pulsed mode. The charging circuit consists of a battery and a vacuum interrupter, S_1, with an arc quench circuit, C., L., and S. (spark gap). The helium switch is S_3, its arc quench is L_2 and C_2; the buffer capacitor is C, the load is R.

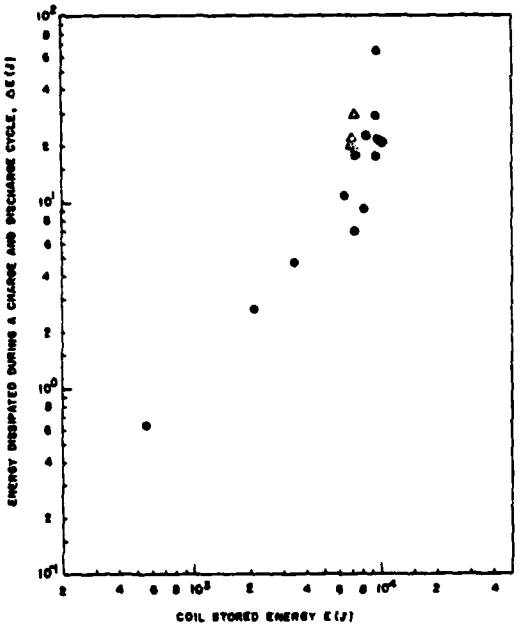

Figure 5: Energy dissipated in a charge/discharge cycle versus coil stored energy for a ten kilojoule superconducting energy storage coil.

For an application requiring an occasional burst of fast pulses, the overall system would be simplified if the coil were sized to store enough energy for the entire pulse train. The coil would be charged slowly during a relatively long period by a small power supply and the opening switch would break the maximum coil current once for each train of pulses instead of once for each pulse. Because the specific weight of a superconducting coil decreases with increasing stored energy (Figure 1), a trade of increased coil size for reduced power supply weight, reduced switching problems, and reduced cooling requirements would probably be favorable up to a total stored energy of a few hundred megajoules.

The simplest practical partial discharge inductive system is a relaxation oscillator consisting of the charged coil which acts as a current source, a capacitor which stores the energy for a single pulse, and a closing switch which connects the capacitor to the load when the desired voltage is reached and then opens rapidly enough to permit the capacitor to charge for the next pulse. For the components available to us it was determined that the switching system should be capable of supplying three to five kilojoule pulses at rates up to 800 per second. A survey of commercially available switches indicated that our requirements were beyond the present state of the art. Hence, we decided to try the flowing gas plasma switch.

Design of Switch

Available Materials

The materials available for these experiments consisted of a 100 kilojoule superconducting energy storage coil (L = 51.5 millihenries, Imax = 2000 amps) with charging power supply and vacuum interrupter switch (Figure 4); an energy storage capacitor rated at 3 KV and 1125 microfarads, and various smaller capacitors (up to 100 microfarads) with comparable voltage ratings. The storage capacitor voltage limit of 3 KV dictates a maximum energy per pulse of 5 kilojoules. For safety reasons we chose to design for a maximum voltage of 2 KV and hence an energy of 2.25 kilojoules per pulse. Use of the straightforward design equations[3] shows that the maximum coil current (2000 amps) can charge the capacitor (1125 microfarads) to operating voltage (2000 volts) in 1.2 milliseconds. In order to conduct a partial discharge experiment for a fully charged coil we require a switch that will fire at 2 KV and recover fast enough to permit a repetition rate of 800 hertz while passing 2 coulombs per shot.

The Switch

A gas discharge design was selected because no other available type can approach the required repetition rates. Helium gas was chosen because electrical breakdown occurs at the desired voltage (2000 volts) at easily controllable electrode spacings (of order one centimeter). Carbon electrodes were selected to carry the required currents (10 kiloamps peak). To minimize recovery time the helium gas is passed through the switch at high velocity in order to cool the arc and the electrodes. A sketch of the switch that was constructed is given in Figure 6. The simply constructed version of this switch that was tested is given in Figure 7. The helium bottle, charged to 2000 psi, provided the required high velocity gas flow.

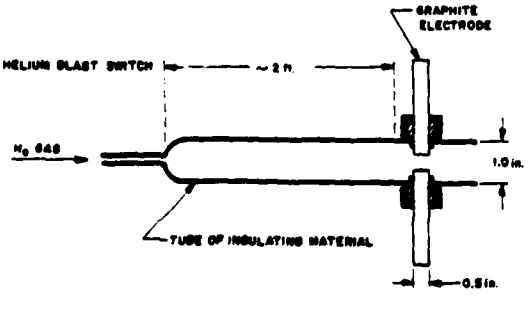

Figure 6: Schematic of Flowing Gas Plasma Switch.

Figure 7: Photograph of the Plasma Switch.

Electric Circuit

For the helium blast to be effective in removing the ions from the arc region it is essential to halt ion production by forcing the switch current to zero for a reasonable length of time by means of a suitable arc quench circuit. We used a simple L-C circuit across the switch to force a current zero after 3/4 of a cycle of the arc quench circuit. For this to be effective the recovery time of the switch must be less than 1/4 of a cycle and an output pulse must be completed in 3/4 cycle of the arc quench circuit. The ohmic resistance of the arc quench circuit must be several times less than the characteristic impedance, stray circuit inductance must be low enough (a few microhenries) to permit a rapid output pulse, and the interpulse time should be long enough (3 or 4 arc quench cycles) to permit proper recharge of this circuit. A balance between these considerations[3] and available components led to the circuit shown in Figure 8. It was designed for a repetition rate of 800 hertz; for proper operation the switch must recover in 100 microseconds or less.

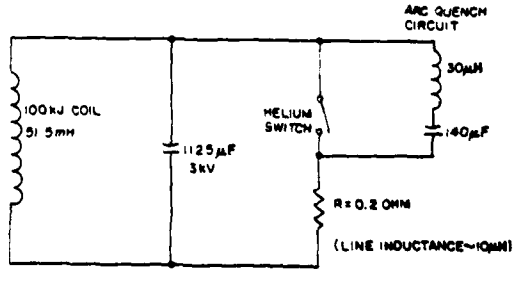

Figure 8: Circuit used to extract train of pulses from a 100 KJ superconducting coil.

Experiments

Preliminaries

Initially, single pulse tests were conducted in order to determine the proper electrode spacing of the switch for operation near 2 KV, to check the operation of the arc quench circuit, and to determine the effect

of various gas flow rates. For low gas flow rates the switch did not recover in the allotted 100 microseconds; for high flow rates it did. Switch current and load current waveforms obtained with high gas flow rates are given in Figures 9 and 10. Quantitative measurements of gas flow velocity were not made.

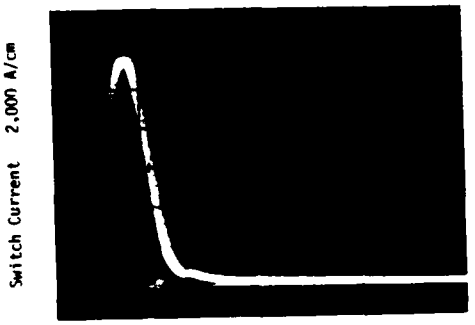

Figure 9: Single pulse of current through the switch (includes load current and first half cycle of the arc quench current). Load resistance, 0.2Ω; firing voltage, 2000V.

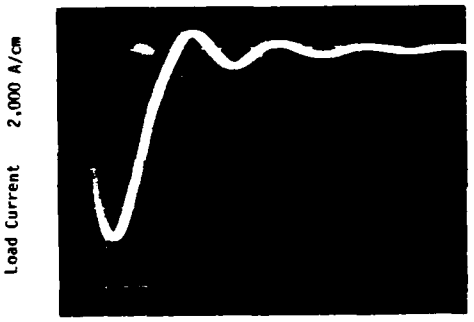

Figure 10: Single pulse of current to 0.2Ω load delivered by switch. Firing voltage, 2000V. Oscillations after main pulse are decay of arc quench circuit.

Coil Tests

The final test consisted of charging the coil to 960 amps (24 kilojoules), opening the vacuum interrupter, and using the circuit of Figure 8 to test the switch at maximum helium flow velocity. The resulting string of pulses (Figure 11), which was accompanied by a roar and a burst of flame shows that the switch worked as designed up to a repetition rate of about 250 per second. The exponential increase in the pulse spacing is a reflection of the exponential decay of current in the coil. The large amplitude of the first pulse shows that the initial breakdown voltage is higher than for succeeding pulses, indicating a residual ionization in the switch. The observed amplitude fluctuations could be removed by adding a trigger electrode to the switch and taking active control of the breakdown potential.

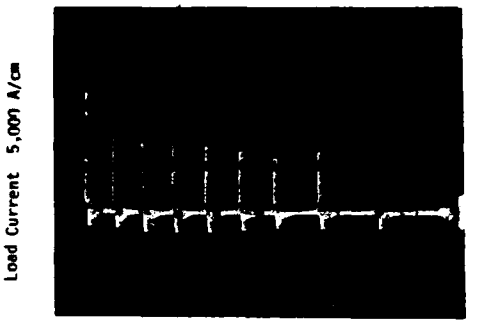

Figure 11: Pulses extracted from coil with switch. Total energy - 24 KJ; average pulse energy - 2.67 KJ.

Discussion

The idea of using a flowing gas to speed the quenching of an arc is not new[7]. The traditional application has been in high power circuit breakers. Although the physical processes taking place in a flowing gas arc are not simple, sufficient literature is available to establish approximate design guidelines.

Basic Physics--No Gas Flow

Considerable work has been done with arcs of intensity up to a few thousand amps at atmospheric pressure and above in a variety of gases. It has been observed[8] that electron densities in the gas remain high for more than 100 microseconds after the arc; for an intense arc (kiloamps) electron densities and temperatures are not strongly dependent on the gas used. In a more detailed study[9] with noble gases, it was shown that the observed temperature profiles can be predicted for moderate current (up to 300 amps) arcs by means of a classical diffusion model providing that the (unequal) electron and gas atom temperatures are properly calculated. This model leads to estimates of relaxation times of hundreds of microseconds. In another set of experiments[10] in which arc recovery times were measured directly for low current (20-40 amp) arcs in air, recovery times of order 100 microseconds were again observed. It is only when a nonclassical energy transport mechanism is introduced[11] that energy transport times of less than 100 microseconds are found. The simplest method of speeding energy transport from the arc region is to flow the gas, thus providing the possibility of convection cooling and of turbulent mixing.

Arc Cooling With Gas Flow

The addition of gas flow to the arc quenching problem brings up the questions of optimum electrode geometry, gas flow direction and velocity, and cooling mechanisms. For the case of both arc and gas flowing in the same direction, an empirical study[12] of nozzle geometrics has shown that for SF_6 at sonic velocity, arc recovery times near 20 microseconds from current zero can be achieved for a 1000 amp arc; recovery is to 40 kilovolts. An analysis of this type of flow[13] indicates that an arc radius of about 3 mm for a current of 1000 amperes is consistent with time scales of order 20 microseconds provided that the heat transfer is partly radial (turbulence and radiation) and partly axial (enthalpy flow); the radial heat transfer rate is about twice the axial rate.

The improvement in heat transfer with increased turbulence has led to the double nozzle design in which the electrodes are hollow cylindrical tubes; the gas enters radially from the sides and exits axially through the electrodes. An experimental study[14] of this geometry indicates that best performance is obtained for a separation to diameter ratio (of the electrodes) of 0.5 in SF_6 and of 0.7 in air. For these experiments the electrode diameter was one centimeter, pressure was about 2.5 atmospheres, the recovery rate was 1.3 KV per microsecond (to 20 KV) from maximum arc currents of 6 kiloamps (air) and 8 kiloamps (SF_6). An analysis[15] shows that very strong turbulence, and hence excellent heat transfer, occurs for an electrode separation to diameter ratio of 0.7 for the double nozzle design. The turbulence effects diminish rapidly as electrode separation is increased until the heat transfer becomes dominated by enthalpy flow, as in axial flow nozzle designs. The selection of electrode separation for a given gas is a trade between dielectric strength, which sets a lower limit on the gap size, and heat transfer properties, which set an upper limit. Electrode diameter should be greater than the arc diameter which is approximately[15] 0.7 cm for an 11 kiloamp arc under turbulent flow conditions.

Differences Among Gases

At moderate gas temperatures and no gas flow[16], the recovery times of various gases vary markedly. The recovery rate for helium falls between[7] those for air and for hydrogen. In a blown arc where recovery rates depend primarily on heat transfer, differences among gases are reduced[14], especially when the flow is turbulent.

Flowing Gas (Helium) Plasma Switch

The switch reported here can be considered a specialized application of the flowing gas circuit breaker technology cited[12-16]. The helium flow through our switch can be analyzed approximately if the flow channel is modeled as a 1/4-inch diameter by 7.5-inch long pipe attached to a 1-inch diameter by 24-inch long pipe with an inlet pressure (at the small end) of 136 atmospheres (2000 psi) at room temperature. The analysis indicates a flow velocity of about Mach 0.42 (1400 feet per second) at a pressure of 6.5 atmospheres and a temperature of 226°K near the electrodes, assuming that the exit shock is attached to the end of the tube. For these flow conditions the Reynolds number is approximately one million, indicating a strongly turbulent flow. A more realistic analysis would have to include the fact that the electrodes protrude into the flow near the end of the tube. One or more shocks must attach to them, increasing the flow velocity to near sonic at the electrodes. The experiments (Figure 11) were conducted for electrode diameter and separation both approximately equal to one centimeter with an arc current near 10 kiloamps and hence an approximate arc diameter[15] of 0.7 centimeter. The literature cited[12-16] indicates that we should expect recovery times in the range of 20-50 microseconds under these conditions. A more accurate prediction is not available because our geometry and gas do not match the arrangements found in the literature.

In the experiments reported here the dielectric strength of the gap was set for 2000 volts. The most severe test of gap recovery time was provided by the arc quench circuit (Figure 8) which applied approximately 1000 volts within 100 microseconds following current zero without the occurrence of restrikes. Some additional single pulse experiments with faster arc quench circuits showed occasional restrikes when the residual arc quench voltage (1000 volts) was reapplied within 50 microseconds of current zero.

Conclusions

A flowing gas plasma switch has been used to obtain 3 kilojoule pulses from an energy storage coil at a repetition rate of 250 hertz. An examination of arc recovery data in the literature indicates that this type of switch might be capable of operation at repetition rates greater than 1 kH_z. Successful operation of this switch in DC pulse generating circuits is dependent upon an external circuit which forces a current zero for a few microseconds, then allows reapplication of the gap voltage in times in the range of 20 to 50 microseconds while a high velocity turbulent gas flow is directed through the interelectrode region. The literature indicates that these recovery times can be achieved at tens of kilovolts and tens of kiloamps if a gas with superior dielectric properties (SF_6) is used at a pressure near 10 atmospheres and at sonic velocity. If a third (trigger) electrode were added to this switch it might be possible to obtain accurately controlled bursts of high energy (several kilojoule) pulses at high repetition rates with a single, lightweight device. Some preliminary work of this type has been reported[17].

Acknowledgment

We express our gratitude to Mr. Alan Forbes of MIT for his assistance in the calculation of the approximate gas flow pattern in the switch.

References

1. Lucas, E.J., Punchard, W.F.B., Thome, R.J. Development of Pulsed High Energy Inductive Storage System, Technical Report AFAPL-TR-72-38. Vol I (December, 1972).

2. Stekly, Z.J.J., Lucas, E.J., Thome, R.J., deWinter, T.A., Inductive Energy Storage System Study, Technical Report AFAPL-TR-69-101 (December, 1969).

3. Lucas, E.M., Punchard, W.F.B., Margosian, P.M.G. Design, Construction, and Testing of a Pulsed High Energy Inductive Superconducting Energy Storage System, Technical Report AFAPL-TR-75-60 (September, 1975).

4. Punchard, W.F.B., A 300 KJ Pulsed Superconducting Energy Storage Coil, IEEE Transactions on Magnetics Vol MAG-11, No. 2, March, 1975, p508.

5. Thome, R.J., Short Pulse Switches for Airborne High Power Supplies, Technical Report AFAPL-TR-74-88 (January, 1975).

6. Lutz, M.A., Short Pulse Switches for Airborne Power Supplies, Technical Report AFAPL-TR-73-99 (October, 1973).

7. Cobine, J.D., Gaseous Conductors, Dover Publications New York, 1958, p395.

8. Ito, Y., Jeda, Y., Komura, H., Nitta, T., Spectroscopic Study of High Current Discharges, Proceedings of the IEEE, V59, n4, April, 1971, p573.

9. Uhlenbusch, J., Fischer, E., Influence of Diffusion

and Nonequilibrium Populations on Noble-Gas Plasmas in Electric Arcs, Proceedings of the IEEE, V59, n4, April, 1971, p578.

10. Evans, K., Strachan, D., Elels, H., Refractory Electrode Region Recovery Following Arc Interruption, Proceedings of the IEEE, V59, n4, April, 1971, p525.

11. Phillips, R., Induced Radial Velocity in Nonstationary Electric Arcs, Proceedings of the IEEE, V59, n4, April, 1971, p466.

12. Perkins, J.F., Frost, L.S., Effect of Nozzle Parameters on SF_6 Arc Interruption Paper T72 529-6 at IEEE PES Summer Meeting, San Francisco, Calif., July 9-14, 1972.

13. Swanson, B.W., Roidt, R.M., Some Numerical Solutions of the Boundary Layer Equations for an SF_6 Arc, Proceedings of the IEEE, V59, n4, April, 1971, p493.

14. Kopplin, H., Rolff, K., Zuckler, K., Study of the Effects of Gas Flow on the Performance of Gas Blast Circuit Breakers, Proceedings of the IEEE, V59, n4, April, 1971, p518.

15. Thiel H., Turbulence Controlled High Power Arcs With Different Electron and Gas Temperatures, Proceedings of the IEEE, V59, n4, April, 1971, p508.

16. Hertz, W., Motschmann, H., Wittel, H., Investigation of the Properties of SF_6 as an Arc Quenching Medium, Proceedings of the IEEE, V59, n4, April, 1971, p485.

17. Clark, W., High Power Spark Gap Switch Development Technical Report AFAPL-TR-75-41, May, 1975.

SYMMETRICAL DOUBLE-ENDED THYRATRONS IN PULSE MODULATORS

R.B. Molyneux-Berry
Marconi Research Laboratories, Chelmsford, U.K.

Summary

A new variant of the hydrogen thyratron has recently entered the market; this is the double-ended ceramic tube which is already available in a range of sizes both single-gap and multiple-gap. Experimental work described here has demonstrated, at moderate power level, the characteristics and capabilities of these tubes in a variety of modulator circuits.

Brief descriptions are given of the tubes and their characteristics, trigger circuits, and the line-type modulator used for the tests. Tube performance in main-switch, tailbiter and inverse-diode service is reported and commented on; alternative circuit arrangements are compared.

Tube performance is satisfactory in simple circuits; modulator arrangements are derived in which the special features of double-ended thyratrons may be used to ensure reliable pulsing into ill-defined or unstable loads.

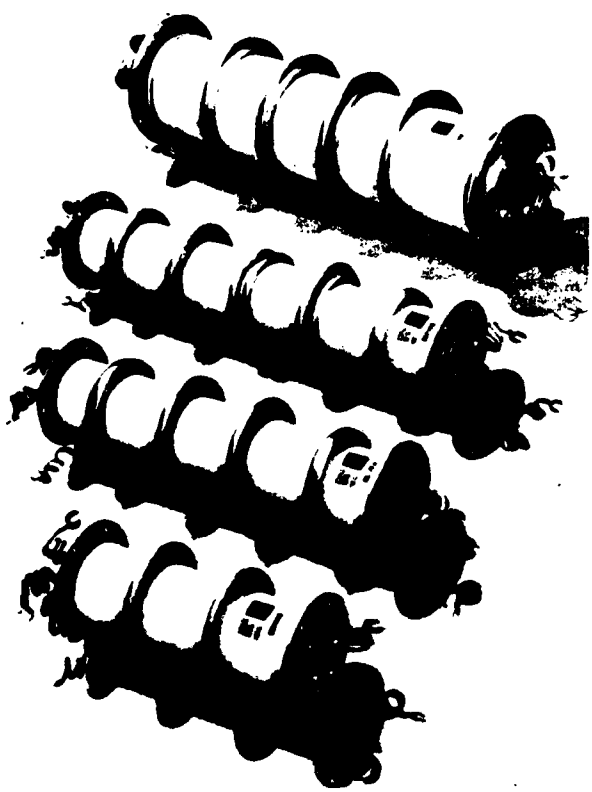

Figure 1. Double-Ended Thyratrons

Introduction

Description of Tubes

Double-ended thyratrons (Figure 1) have been described in papers read to the last Modulator Symposium, and elsewhere, [1, 2, 3]. The tubes are symmetrical, having a cathode structure complete with heater, gas reservoir and grids (usually tetrode) at each end (Figure 2). Opposite g_2's face each other across the high-voltage gap, which may be subdivided by gradient-grid structures to hold off voltages up to about 150 kV for a four-gap tube. As there is no separate anode, the current flows to the positive cathode structure. The deck design must prevent the occurrence of damaging voltages between grids and cathode under these conditions.

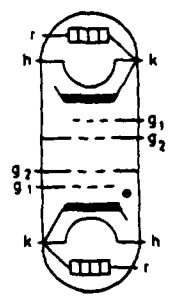

Figure 2. Single-Gap Double-Ended Thyratron

Special Features

Double-ended thyratrons have been used to replace conventional tubes in high-energy crowbar applications where inductive overswing after conduction had led to reverse-arc damage. With suitable deck design, double-ended tubes are immune to such damage up to their rated peak current in either direction. A second feature of these tubes is the gas reservoir within the positive end structure. This reduces the tendency to quench during long-duration, high-current pulses, and has been used to good effect in certain low p.r.f. modulators at CERN.[2]

A third feature is the ability of these tubes to switch in either direction, much as a triac does. In circuits where this is required, one double-ended tube might replace a pair of conventional tubes, or eliminate the need for a reverse diode stack. Even in single-tube circuits it has been argued that the cost of the extra deck is offset by a saving in protection circuitry and the increased tube cost is returned in improved life.

Outline of Test Programme

With these advantages in mind, a programme of study and experiment has begun in order to determine the characteristics of these tubes and their optimum relationship to pulse modulator circuits. This paper reports on initial work.

It was apparent from the first that tube turn-off and recovery was a crucial area for investigation: the tube protects itself by reverse conduction; it cannot therefore be force-commutated off by reverse voltage immediately following a forward pulse. Most traditional modulator circuits operate with the load nearly matched to the pulse forming network (p.f.n.) and rely on the pulse transformer overswing to commutate the switch. A double-ended tube will conduct backwards and will not start to recover until the resultant damped oscillation has fallen to the level of the tube's holding current. Delayed recovery may be acceptable in crowbar or low p.r.f. applications but not in radar and similar modulators. The experimental work reported here began with the investigation of common circuits and led on to arrangements which make better use of the special characteristics of double-ended thyratrons.

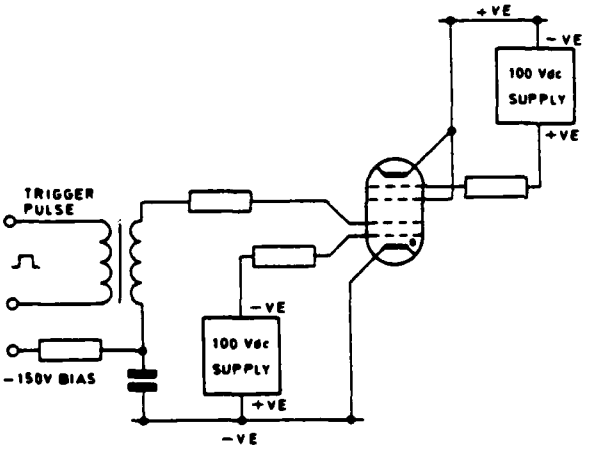

Figure 3. Manufacturer's Recommended Trigger Circuit

Trigger Circuits

The tube manufacturers recommend a basic deck and trigger arrangement (Figure 3) which has proved satisfactory in crowbar applications and at C.E.R.N. The tube is triggered by pulsing g_2 at the negative end. The other g_2, connected to its cathode, forms the 'anode'. A modest positive bias (about 25 mA at 20 volts) is continuously applied to each g_1 to protect the cathodes from fast ions, reduce delay and jitter, and promote smooth current reversal. The 'negative' g_2 is given negative bias to maintain voltage hold-off and reduce dark current. All waveforms presented below were taken using decks of this type.

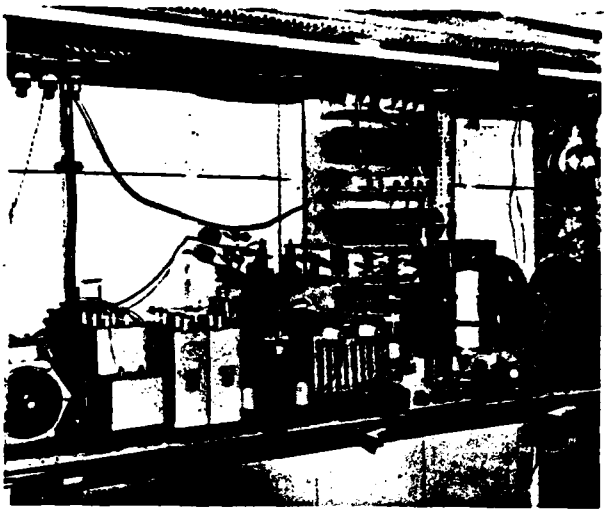

Figure 4. Test Modulator

Test Arrangements

Description of Modulator

Since double-ended thyratrons seem most likely to be used in high-energy, long-pulse p.f.n. modulators, at up to a few hundred p.p.s., they are being tested under these conditions. As a preliminary exercise, a versatile experimental modulator (Figure 4) has been built which can be adapted to model, with calculable scale factors, many circuit arrangements and a wide range of running conditions. Running levels on this test modulator were chosen for safe working conditions and the convenience of using standard components and measurement equipment, while using small double-ended tubes at a reasonable fraction of their maximum ratings. Experience already gained has proved invaluable to the design of high power equipment.

Main Parameters

For convenience in comparing results, all tests reported here were taken under the following conditions unless otherwise stated.

p.f.n.	1 μF, 94 μS, 47Ω
H.T.	2.7 kV, 0.25A
Resonant charge	5.0 kV peak, 0.55A peak, 14 mS base
p.r.f.	50 Hz

A direct-coupled resistive load was used, which was padded with lumped capacitance or inductance when required.

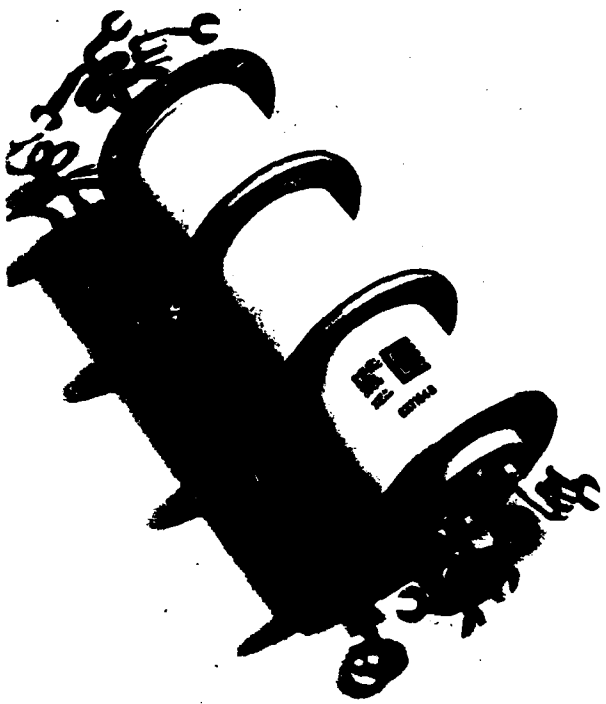

Figure 5. Small Double-Ended Tube Type CX1154B

Tubes Tested

Results presented were taken with type CX1154B single gap ceramic tubes rated at 35 kV, 3000A peak, 3A mean. Full data[3] is available from the manufacturer. Where comparisons with conventional tubes are made, or hybrid circuit arrangements with single and double-ended tubes are mentioned, tests have been made with types 8503 (glass triode) CX1140 (glass tetrode) and CX1154 (ceramic tetrode). All tubes tested were manufactured by the English Electric Valve Company Limited, Chelmsford, England.

Holding Current

CX1154B tubes were tested for holding current (i.e. the lowest current at which steady conduction can be maintained). There was some variation between different tubes and substantial variation if the bias levels were altered. Under manufacturer's recommended bias conditions the mean holding current was about 100 mA d.c. This may not be representative of other double-ended thyratrons, as the manufacturers do not normally quote holding current.

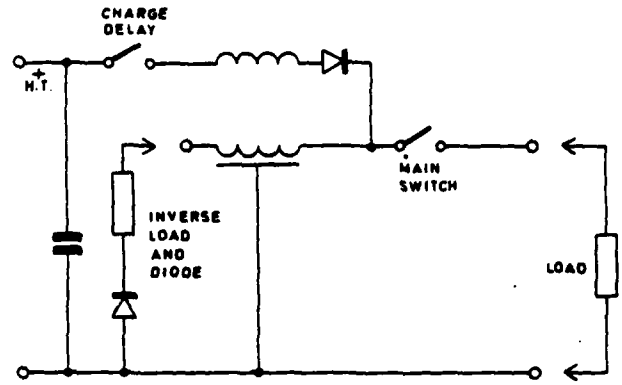

Figure 6. Simple P.F.N. Modulator Circuit

Operation in the Main Switch Position

Match

A CX1154B tube was used as the discharge switch in a simple p.f.n. modulator circuit (Figure 6). The tube operated satisfactorily into resistive load (Figure 7) without needing an inverse circuit or delayed charging because the slow rate-of-rise of charge current (150 mA/mS) allowed at least 0.5 mS for tube recovery before the holding current was exceeded. In Figure 7, the current stops immediately after the pulse and the tube withholds subsequent p.f.n. oscillations of a few hundred volts amplitude. This occurred reliably only for a narrow range of load resistance, about 44 to 48 ohms, the mean Zo of the p.f.n. being 47 ohms. Outside this range, tube current continued for one or more additional pulse lengths, although early tube recovery sometimes occurred with certain critical settings at which some point of inflection on the oscillatory current waveform maintained the tube below holding current for a few microseconds.

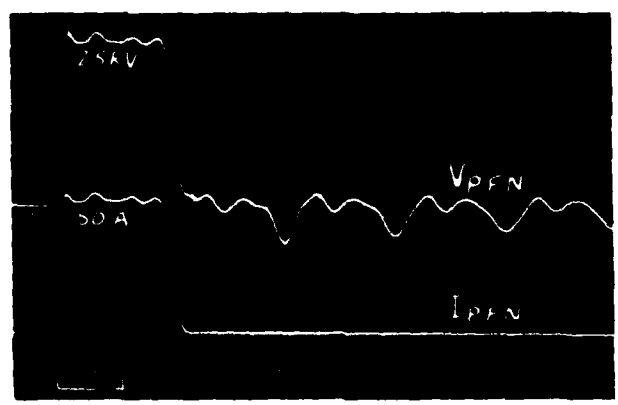

Figure 7. Simple Modulator with Matched Load

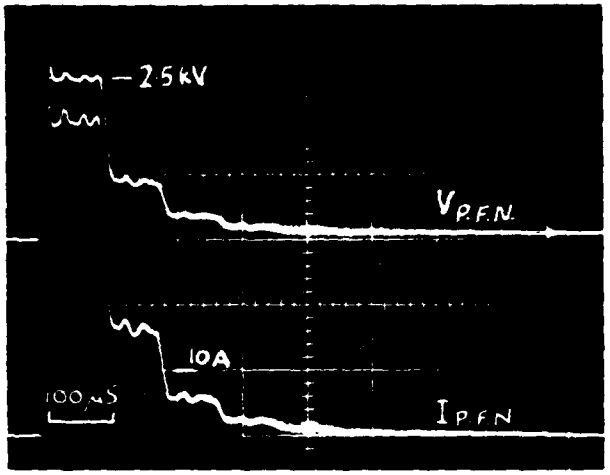

Figure 8. Simple Modulator with $R_L = 2Z_0$.

Overmatch

Where $R_L > Z_0$, operation was unsatisfactory, exactly as with a conventional thyratron. Figure 8 (taken with $R_L = 2Z_0$) shows typical waveforms in which the discharge current continues for hundreds of microseconds, while the p.f.n. voltage never quite reaches zero. This picture was taken at reduced voltage and with considerable charge delay, without which the modulator would not run at all. Careful examination of the lower trace shows that stray coupling from the charge switch, triggered at $t = 770$ μS. provides the momentary current zero at which the discharge switch turns off.

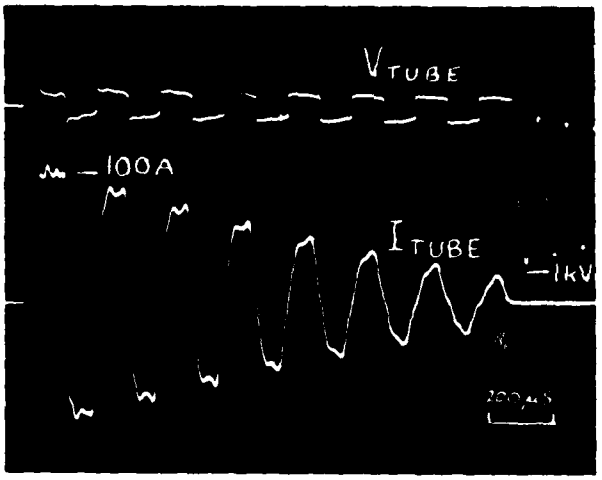

Figure 9. Simple Modulator with $R_L = 0$.

Undermatch into Bidirectional Loads

Severe undermatch causes high-amplitude oscillations (Figure 9, $R_L = 0$) but the modulator runs satisfactorily. The double-ended thyratron accepts the current reversals smoothly with a constant ± 55 volt tube drop until the oscillation has been damped and degraded to a level at which some small inflection helps to maintain the tube below holding current for a few microseconds for recovery to begin. This may occur on either positive or negative-going current reversals. Figure 9 was taken with the charge triggered 700 μS before recovery, without ill effect.

Undermatch into Unidirectional (diode) loads

Where a unidirectional load is seriously under-matched, the double-ended discharge switch conducts backwards after each pulse to charge the load capacitance to the p.f.n. inverse voltage which is then held off across the load. Apart from this, the circuit behaves as though it had a conventional switch: the p.f.n. climbs rapidly to breakdown voltage and satisfactory running is impossible.

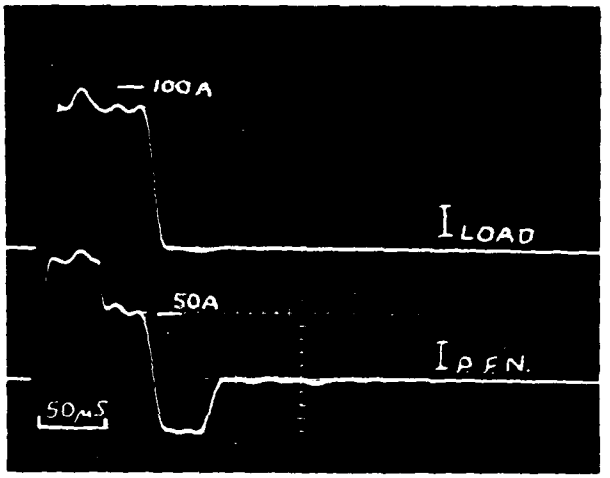

Figure 10. $R_L = 0$ With Inverse Diode and Load

Matched Inverse Load with Diode

The provision of a matched load, with series inverse diode, across the p.f.n. at the end remote from the discharge switch is well known as an effective means of preventing p.f.n. inverse voltage and subsequent charge to an overvoltage. It is equally effective with a double-ended discharge switch and eliminates the oscillatory output which otherwise occurs (Figure 9) with undermatched bidirectional loads; early switch recovery is thereby obtained. This is shown in Figure 10, which was taken under similar conditions to Figure 9, but with a matched inverse circuit. If the inverse load is not matched to the p.f.n. one or more current reversals may occur. The test modulator still ran satisfactorily under

these conditions. The adjustment of the inverse load to prevent current reversal was not too critical (± 20%) and appeared stable over the useful range of running conditions.

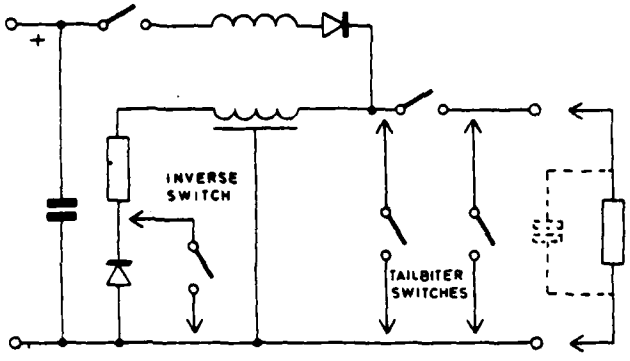

Figure 11. Alternative Dump Switch Positions

Operation in 'Dump-Switch' Circuits

The double-ended thyratron has been found to work satisfactorily with matched and undermatched loads, as do conventional thyratrons. It is where the load is overmatched, ill-defined or erratic that the self-protecting properties of double-ended tubes are most desirable. With such loads, unused p.f.n. energy must be quickly dissipated, or returned to the supply, so the p.f.n. can be re-charged to its normal level. Conventionally, this may be achieved by adding a 'dump switch' tube (Figure 11) either across the output terminals (the 'tailbiter switch' position), or in series with the inverse load (across the inverse diode - the 'inverse switch' position). Either of these arrangements is also effective where the main switch is double-ended; the dump switch may be double-ended or conventional. However, the use of a double-ended tube offers some new possibilities.

Tailbiter Switch Circuits

A conventional main switch tube must be protected from full instantaneous reverse voltage immediately after forward conduction. The tailbiter switch must therefore be placed after the main switch (Figure 11) so that it discharges the load capacitance directly. In this position the dump tube short-circuits the p.f.n. through the main switch, with consequent risk of quenching. Under load-arc conditions, the dump tube can offer no crowbar protection to the main switch, and little to the load, as the fault arc drop may be less than the tube drop. The better position for the dump switch is across the p.f.n. before the discharge switch which requires a protective inverse diode across it. With silicon diodes, a very robust stack may be needed to withstand the duty. Use of a double-ended discharge switch removes this difficulty completely. Load capacitance current is discharged through it in the reverse direction. Quenching is most unlikely and, provided the tailbiter tube is assisted by suitable trigger circuits to conduct from a low initial anode voltage, it can offer crowbar protection to the discharge switch and load, if the latter arcs, since the voltage drops across the two tubes offset one another. If the tailbiter tube is also double-ended it can act as a front-end inverse diode, if needed. Tailbiter circuits are also useful, of course, for shaping or shortening the modulator output pulse.

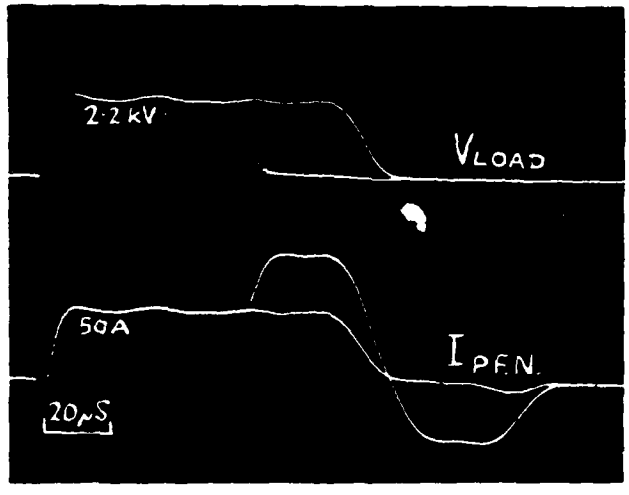

Figure 12. Pulse Shortening with Tailbiter Switch

A tailbiter circuit of this type was tested in combination with a double-ended discharge tube and a conventional matched inverse load and diode. Figure 12 illustrates the use of this circuit for pulse shortening with a matched load. Pulse voltage and p.f.n. current are shown with the pulse unshortened and, by double exposure, with the tailbiter switch triggered at $t = 60\ \mu S$. The modulator ran satisfactorily over the range $0 < R_L < 10\ Z_0$, and also with a number of unusual load arrangements. Waveforms obtained with one such load, a 1 μF paper capacitor, are shown (Figure 13) because they illustrate well the chief characteristics of this circuit. It was found necessary to use a small series load resistor (18Ω) to reduce the dissipation within the capacitor to a safe value for the duration of the test. In Figure 13, the p.f.n. is shown discharging into the capacitor for 50 μS until the tailbiter tube is triggered. The discharge tube current then reverses to 100 amps as the capacitor is discharged, ending the output voltage pulse. The recovered energy is reflected along the p.f.n. and dissipated in the inverse load.

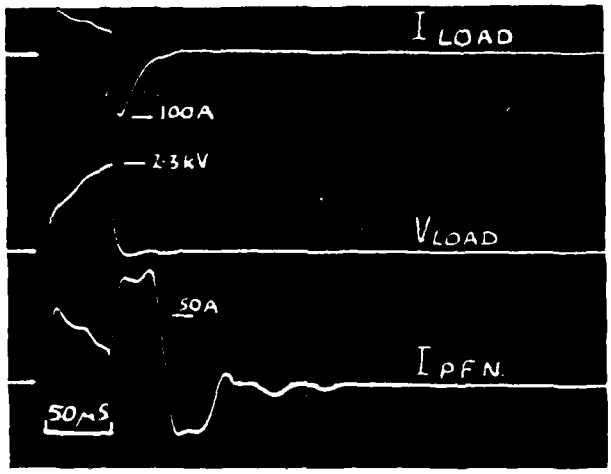

Figure 13. Tailbiter Switch Circuit with Capacitor Load

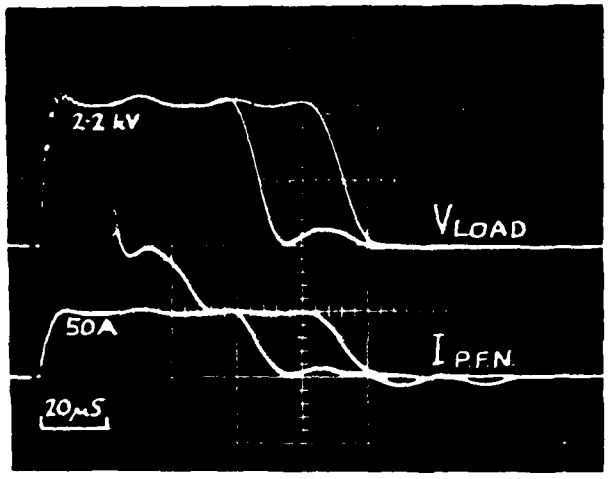

Figure 15. Pulse Shortening with Inverse Switch

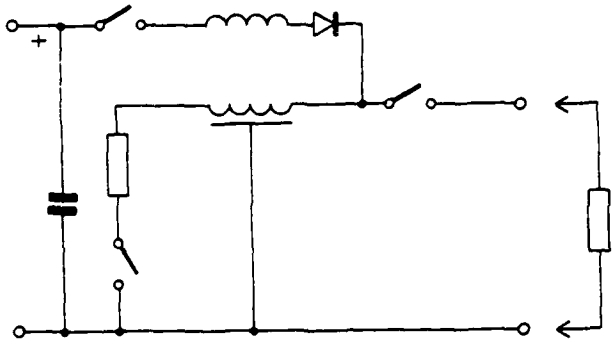

Figure 14. Double-Ended Inverse Switch Circuit

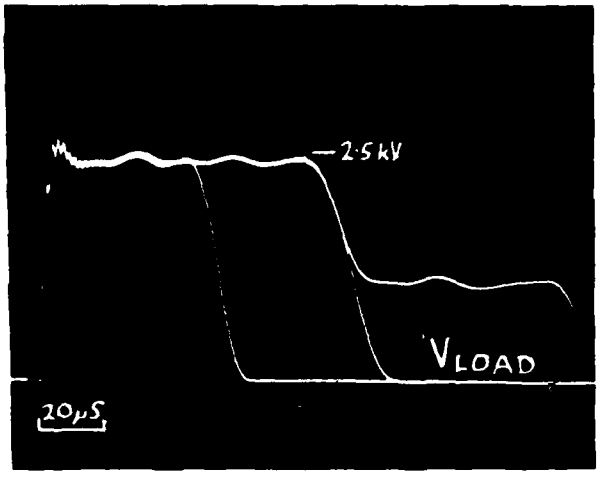

Figure 16. $R_L = 3Z_0$ with Inverse Switch

Inverse Switch Circuits

The use of a forward conducting dump switch across the inverse diode is fairly well known. and may be used where the main switch is either double-ended or conventional although, in the latter case, reverse-arc protection may be required for the reasons given above. If the inverse dump switch itself is a double-ended thyratron, it can additionally perform the inverse diode function, giving a compact and economical circuit (Figure 14) which has been successfully tested over a wide load range.

Figure 15 illustrates the use of a double-ended thyratron in the inverse switch position for pulse shortening, with a matched load. Pulse voltage and p.f.n. current were recorded by double exposure to show waveforms with the inverse switch triggered at t = 21 μS, and untriggered. Of course, this method cannot shorten the pulse to less than half its natural length unless the inverse switch is triggered before the main switch.

Figure 16 shows waveforms obtained with the same modulator arrangement pulsing into an over-matched load ($R_L = 3Z_0$). The triple exposure of output pulse voltage shows the inverse switch triggered at t = 0, t = 47 μS (half pulse width) and t = 120 μS. Operation was smooth even with high resistance loads.

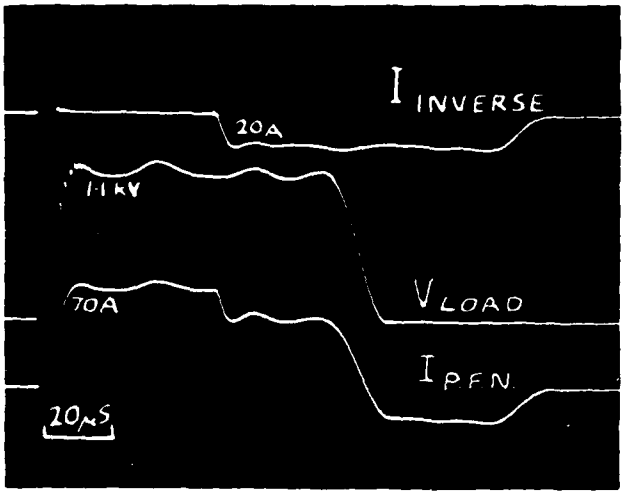

Figure 17. $R_L = \frac{1}{3}Z_0$ with Inverse Switch

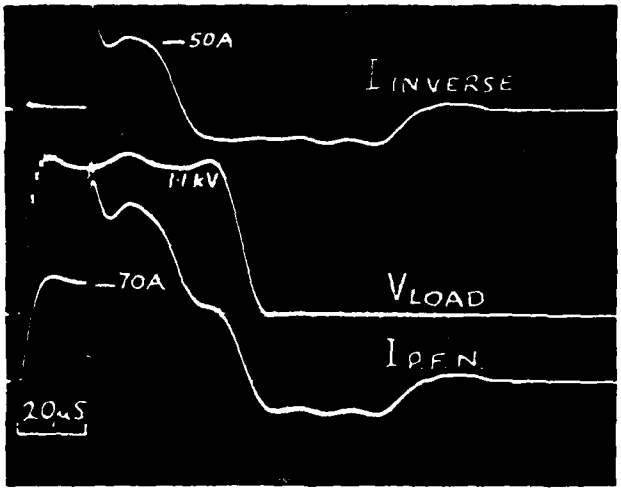

Figure 18. Inverse Switch Pulse Shortening with $R_L = \frac{1}{3}Z_0$

Figure 17 illustrates the same circuit with an undermatched load ($R_L = \frac{1}{3}Z_0$) where the inverse switch is acting as an inverse diode. The tube is triggered at t = 47 μS, just as the p.f.n. voltage is starting to reverse. The circuit performed satisfactorily at all undermatched load values tested. Figure 18 was taken under identical conditions to Figure 17, except that the inverse thyratron was triggered at t = 20 μS to demonstrate pulse shortening with undermatched load. Current reversal in the inverse switch tube is clearly seen.

This modulator circuit performed efficiently in all tests. It is, however, much less effective as a protective crowbar than the tailbiter circuit described above because its effect is delayed by the transmission time of the p.f.n.

Alternative Trigger Circuits

All results reported above were taken using the valve manufacturer's recommended bias and trigger circuit (Figure 3). It became clear early in the test programme that better results (e.g. earlier turn-off and recovery) could be obtained in certain modulator circuits by varying the trigger and bias arrangements. An alternative system which has been devised and tested is the subject of patent applications.

Other Work on Double-Ended Thyratrons

Associated work includes the extension of the tests reported here to cover multi-gap tubes, and the determination of the quenching characteristics of single and multi-gap tubes under high current, long pulse conditions.

Conclusions

The results presented point the way to the successful use of double-ended thyratrons in high power pulse modulators.

Acknowledgements

The author wishes to thank the Ministry of Defence (Procurement Executive) and the Technical Director, GEC-Marconi Electronics Ltd., for permission to publish this paper. He also wishes to acknowledge the contribution to this work of his colleagues in the High Power Systems Research Group.

References

1. H. Menown and B.P. Newton
'A Multi-gap, Double-ended Hydrogen Thyratron'.
Proceedings, Eleventh Modulator Symposium, 1973.

2. P.E. Faugeras, H. Kuhn, J.P. Zanasco,
'Generation of High Current, Long Duration Rectangular Pulses'.
Proceedings, Eleventh Modulator Symposium, 1973.

3. English Electric Valve Co.Ltd.,
CX1154B Data Sheet.

A TRIPLE GRID THYRATRON

L. J. Kettle & R. J. Wheldon
English Electric Valve Company Limited
Chelmsford, Essex.

Summary

In a conventional thyratron with a single control grid a large fraction of the discharge boundary is negatively biassed although for recovery purposes the biassed region is only effective at the grid aperture.

To improve this situation three closely spaced grids have been substituted for the single control grid. The outer pair shield the central control grid (G2) from the slowly decaying grid-cathode plasma and leave it exposed only to the rapidly decaying plasma in the grid aperture. This allows large bias voltages to be applied to the control grid whilst there is still considerable ionisation in the tube. Low impedance bias supplies can be used without the power becoming excessive.

A triple grid ceramic thyratron type CX1535 is described which will operate at 100 kHz and switch 12.5 MW.

A novel method of triggering such a pentode thyratron and certain tetrode thyratrons is also described. This makes use of the cathode-G1-G2 space of the main switch tube as the output stage of the normal trigger generator. The method also provides a large negative voltage pulse to aid recovery without the need of a separate bias supply.

The Use of Multiple Grids in Hydrogen Thyratrons

It is difficult to operate conventional triode or tetrode thyratrons in circuits where the recovery time of the thyratron is the governing factor. In practice this means that there is an upper limit of recurrence frequency at which each type of thyratron can be operated. By giving special attention to the design of the grid structure, this recovery time can be reduced dramatically and operation at extremely high recurrence frequencies becomes possible. Basically this involves reducing the volume of plasma surrounding the effective control grid. This paper describes a triple-grid configuration and also how the criterion is met resulting in a most effective type of high-frequency thyratron. The triple-grid arrangement enables the grid nearest to the anode to be connected to the cathode and, when this is done, almost perfect anode/G2 screening is obtained. This has a number of advantages, especially in circuits where rapid changes of anode/cathode potential occur.

The close inter-electrode spacings of a triple-grid structure enable higher voltages to be applied to the intermediate grid of the three and, as this grid is normally used as the control electrode, it permits the use of larger amplitude triggering pulses and also higher negative bias levels. The thyratron will operate at a higher gas pressure than is normally possible, which enables short, steep-fronted pulses to be switched.

The CX1535 Triple-Grid Thyratron

This is the first of a new EEV range of triple-grid thyratrons, intended for operation at high recurrence frequencies. As well as providing close inter-grid spacings, the design is such that heat dissipated at any electrode will be rapidly conducted to the exterior. As the thyratrons are intended for liquid immersion, this serves to extract the heat from the metal parts in contact with it. The ceramic insulation between the anode and the other electrodes is well removed from the path of the discharge and this means that any deposition of metal on its inner surface by sputtering is minimised. A special cathode structure is used which provides the instantaneous emission necessary for high p.r.f. operation over a long working life. It is also suitable for switching relatively long pulses at reduced p.r.f. However, the rated anode heating factor is very high for a thyratron of this size because of its rapid switching ability and this enables it to be used as a means of switching short pulses at very high recurrence frequencies. Fig. 1 shows diagrammatically the triple-grid structure and Fig. 2 a photograph of CX1535. Fig. 3 shows that the rate of grid current decay is much faster than that of an existing more widely spaced, two-grid structure CX1180 whilst Fig. 4 compares the

rapid recovery characteristics of the new tube again with the CX1180.

The CX1535 has the target ratings as shown in Table I.

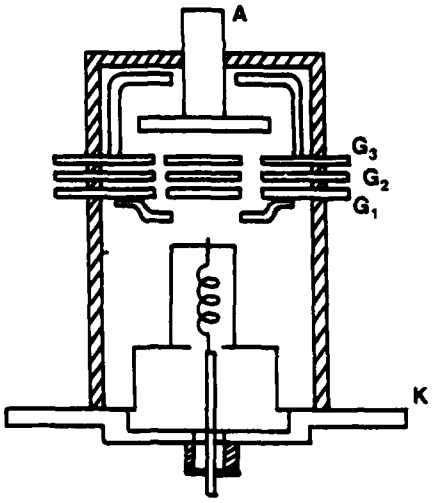

Fig.1
Diagram of Triple Grid Thyratron

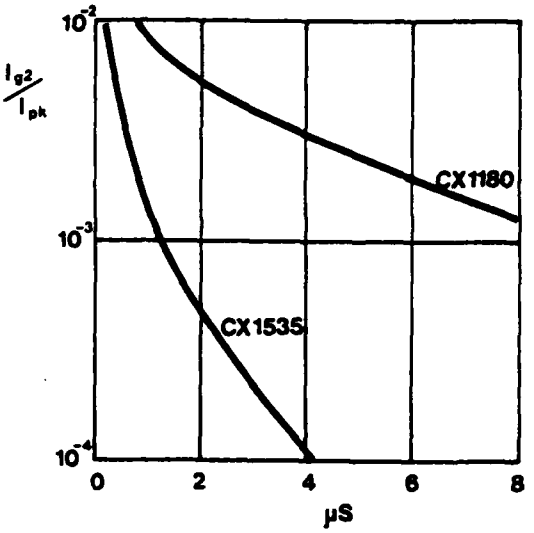

Fig. 3 Grid current during recovery for triple grid and normal thyratrons

Fig. 2

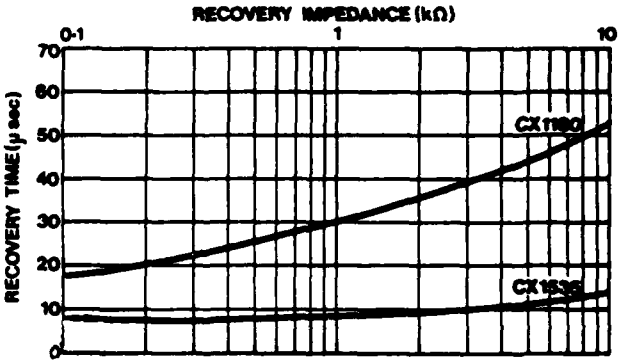

Fig. 4 Recovery Characteristics

English Electric Valve Co. Ltd. - CX1535 Triple-Grid Thyratron	
Peak forward anode voltage	25 kV
Peak anode current	1000 A
Average anode current	1.25 A
Peak output power	12.5 MW
Anode heating factor	500×10^9
Anode to grid 2 capacitance	1 pF

Table I

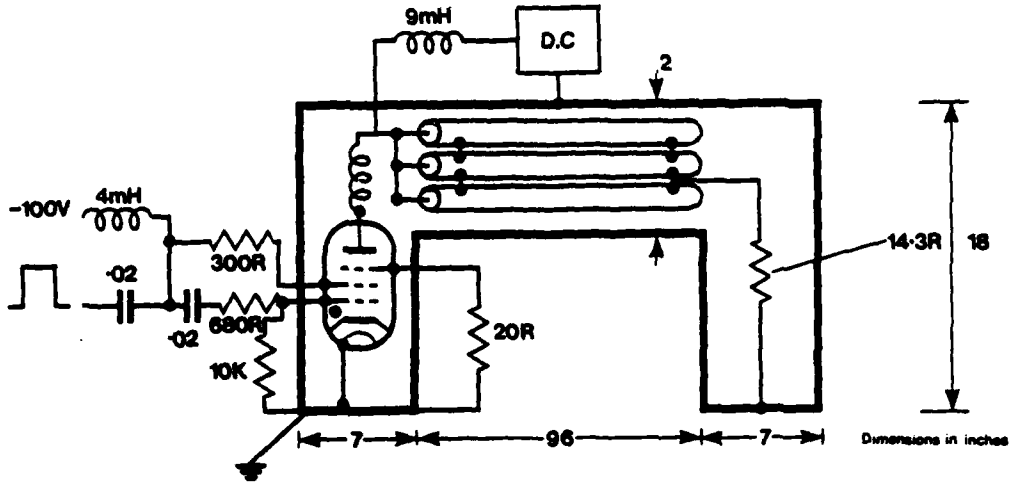

High frequency Modulator with the CX1535 Fig.5

Experimental Operation at High PRF

Fig. 5 shows an experimental assembly which has been used to demonstrate the ability of the CX1535 to switch pulses at high recurrence frequencies. The thick lines represent an oil-filled tank (here shown in plan) with its more important dimensions indicated on the diagram. The pulse forming network consists of three 50 ohm, high voltage cables in parallel, the complete assembly being equivalent to a 16.7 ohm network whose pulse length is 25 nsec. A matching load (of carbon composition discs) is housed in the right-hand "horn" of the tank; the thyratron under test occupies a corresponding space in the other horn. The pulse generator is energised from a d.c. source via inductance, chosen to give a charge time slightly shorter than that corresponding to resonance.[1][2] This means that the network charges to a voltage slightly greater than twice that of the supply falling to twice the supply voltage level when the tube is fired (Fig. 6). At the instant of firing a reverse current flows via the charging inductor causing the anode voltage to go negative immediately after conduction. This avoids any risk of the thyratron "firing through" due to insufficient delay before re-application of positive anode voltage. The CX1535 operates reliably in the above circuit at a p.r.f. of 80 kHz when switching an anode voltage of 13.5 kV. In this regime the anode becomes positive approximately 4 μsec after each pulse and, with the particular grid circuit employed, the control grid recovered after 3 μsec. Waveforms from this circuit with a CX1535 are shown in Figs. 6, 7, 8 and 9. The maximum power levels so far achieved have been limited by the power supply.

From the grid circuit shown in Fig. 5 it will be seen that the fast recovery capability of the CX1535 allows a conventional arrangement to be used at this high pulse repetition frequency.

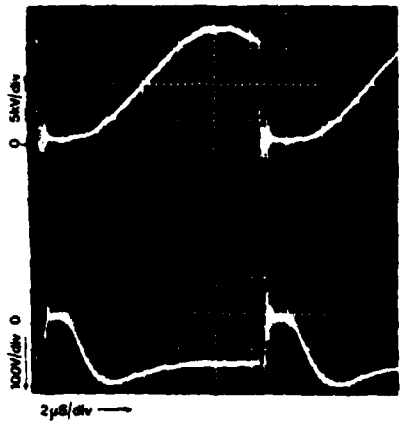

Fig.6 Anode Voltage Waveform

Fig.7 G2 Waveform

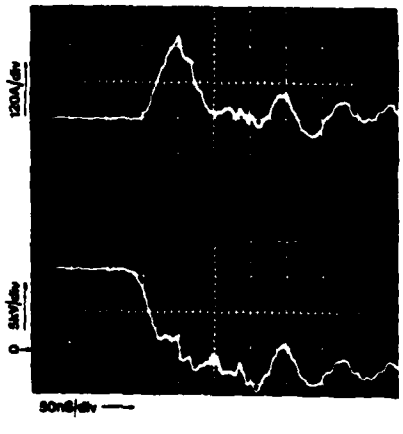

Fig.8 Anode Current Waveform

Fig.9 Anode Voltage Waveform

A Novel Triggering Method for Multigrid Thyratrons

It is normal practice to trigger a tetrode hydrogen thyratron by applying overlapping trigger pulses to the two grids, or alternatively by applying a d.c. priming current to the grid nearest the cathode (G1) whilst supplying a trigger pulse to the control grid (G2). Both techniques are satisfactory, but when large tubes are being operated both methods require a relatively high power trigger source. For tubes where G1 provides a screen between the cathode and the control grid G2 a novel form of triggering has been devised.

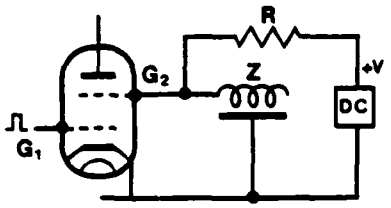

Fig. 10a. For Tetrodes e.g. CX1157 CX1529/GHT9 CX1528/GHT8

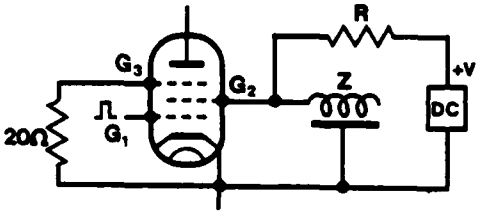

Fig. 10b. For Pentodes e.g. CX1535

Fig. 10 illustrates this method of triggering for a tetrode and pentode (triple grid) thyratron. A positively precharged p.f.n. is connected to G2, whilst G1 has either zero voltage or a negative bias depending on the degree of screening that G1 provides in any particular tube. Under these conditions the tube anode holds off HT voltage. The application of a low power trigger pulse to G1 ionises both grids and the p.f.n. connected to G2 discharges under short circuit conditions, generating a high power current pulse ideal for switching on the main tube discharge very rapidly. Since the p.f.n. is discharged into a short circuit it is left negatively charged. A powerful source of negative bias therefore exists to assist the rapid clean up of plasma associated with G2. The p.f.n. connected to G2 must produce a pulse of duration greater than that of the main tube pulse so that the negative voltage swing is produced during the recovery period of the tube.

This circuit has been used to trigger a number of tetrode and pentode thyratrons including the CX1535 up to frequencies of the order of 20 kHz. The maximum frequency is limited by the recovery characteristics of G1 which in most tubes is that of a triode. Fig. 11 shows typical G2 waveforms for the circuit of Fig. 10 (b).

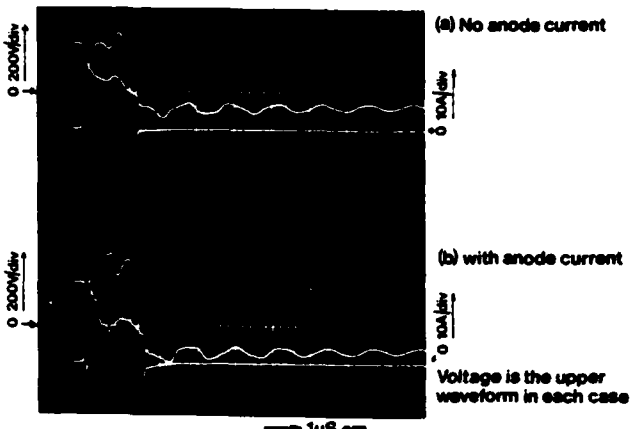

Fig 11. Grid 2 voltage & current waveforms for circuit in Fig 10(b).

References

(1) Very High Frequency Pulse Generators Using Hydrogen Thyratrons. (Eleventh Modulator Symposium 1973). (EEV Reprint).

(2) Handbook of Electronic Circuits, Section 29-3. G. J. Scoles (John Wiley).

Acknowledgements

The authors wish to thank the Directors of English Electric Valve Company Limited for permission to publish this paper.

Acknowledgements are also given to the Ministry of Defence (Procurement Executive) who have given support for this work.

GROUNDED GRID THYRATRONS

D. Turnquist, S. Merz, and R. Plante
EG&G, Inc.
Salem, Massachusetts 01970

Summary

This paper describes the development of grounded grid thyratrons and the observed characteristics of these tubes.

Grounded grid thyratrons are modified versions of hydrogen thyratrons used in low impedance systems. These tubes are operated with the control grid as the negative electrode and with the hot cathode as the trigger electrode. The main current pulse is carried by a metal vapor arc between grid and anode. This mode of operation gives the tube a peak current capability of several tens of thousands of amperes, with an inductance of the order of 15 nanohenries.

The principal uses of these tubes have been in spark chambers and in pulsed nitrogen UV lasers.

Introduction

Recent developments, particularly of large spark chambers and of high power gas lasers, have created new switching requirements not well met by conventional devices. These are typically:

1) Load impedance less than 1 ohm
2) Operating voltage 10 to 35 kV
3) 0.001 to 0.005 coulomb per pulse
4) di/dt 100 to 1000 kiloamp/microsec
5) Peak currents of several kiloamps to tens of kiloamps.

For spark chambers a total switching time, delay plus load voltage rise time, of 50 to 100 ns or less is needed, and time jitter may be critical. Delay time has not, so far, been very important in high-power laser circuits. Repetition rates have been less than 100 pps in most operational systems, but there is interest in laser operation at much higher rates.

Spark gaps have been widely used in these circuits, particularly in laboratory models, but have several serious drawbacks. High pressure gaps of the type used in low impedance systems have an operating voltage range of about 3 to 1, and an upper limit on repetition rate of a few hundred pps. For some systems, the high trigger voltage requirement, 5 to 20 kV, is particularly undesirable. The life time of a sealed spark gap, under optimum conditions, is presently on the order of 20,000 coulombs of total conducted charge.

A number of successful circuits, particularly at somewhat higher impedance levels, have used standard hydrogen thyratrons. Spark chambers at CERN[1,2] and at Brookhaven[3] use tetrode thyratrons at up to several thousand amperes peak with 20 ns rise times. Similarly, a number of high power nitrogen lasers have been built using conventional thyratrons[4]. If the circuit conditions do not force the thyratron into an arc, the thyratron generally has several advantages over a spark gap.

Of the various gaseous switching devices, the thyratron has the most stable shot-to-shot characteristics (time and impedance jitter). It has been shown[4,5] that a laser's electrical discharge conditions may be somewhat independent of switch and capacitor inductance. The transmission lines near the channel are usually more critical. Even so, variations in switch tube impedance, which are important to most systems, are often critical to lasers. In gas lasers, variations of a few percent in the switch tube impedance may produce large amplitude fluctuations in laser output. The thyratron's relatively low, stable shot-to-shot impedance minimizes output fluctuations due to impedance jitter.

Other advantages of the thyratron are lower trigger voltage requirements, very much higher repetition rate capability, and a far longer life.

The requirements of low-impedance circuits, however, frequently exceed the capabilities of conventional thyratrons. Figure 1 shows typical circuit arrangements. A spark chamber circuit similar to Figure 1A is described by K. Foley et al[3]. In that

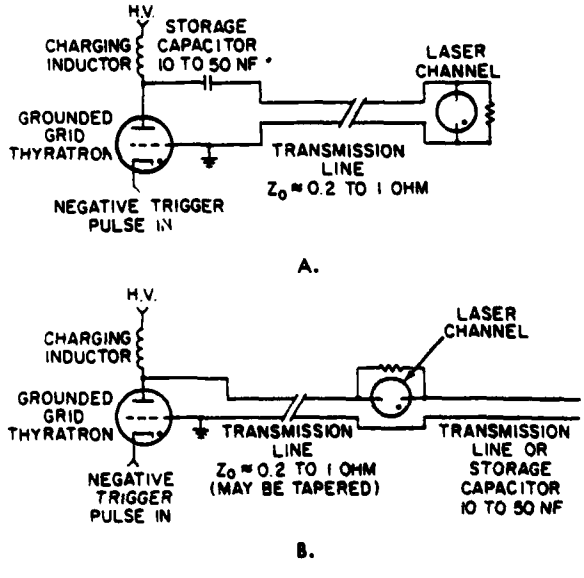

Figure 1. Typical Laser Discharge Circuits.

particular system, the energy storage was provided by eight parallel 4-ohm strip lines, with a peak current of 15 kA. Under such conditions, a conventional thyratron would be quickly destroyed by arc damage to the cathode and clean-up of the gas fill.

It is possible, however, to obtain the necessary peak current and rise-time capabilities, while preserving most of the advantages of the thyratron, by operating the tube in the grounded grid mode. In this mode, the grid is used as the negative electrode for the main discharge, while the normal cathode is used only for triggering. In this way, some of the desirable triggering and operating range characteristics of thyratrons can be combined with the high peak current capability of spark gaps, in a fairly small, low-inductance structure.

Originally, standard thyratrons were tried for operation in the grounded grid mode, with some success, but short life. At EG&G, we have developed a number of tubes specifically for use in grounded grid circuits, and we are now engaged in an evaluation and improvement program.

Design and Construction of Grounded Grid Thyratrons

Figure 2 shows a cross section of one of the tubes now being produced by EG&G, the HY-1102. The internal spacings are basically the same as a standard thyratron. The major structural differences are in the treatment of the grid and anode structures, which are made of refractory materials. Also, the mounting flange is attached at the grid seal.

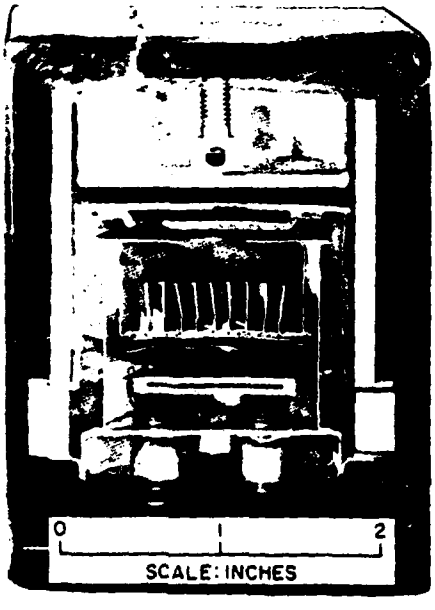

Figure 2. Cross Section of HY-1102 Grounded Grid Thyratron.

In use, the hot cathode is pulsed negative, to form a low density plasma in the grid-cathode region, just as in a standard thyratron. This plasma supplies electrons to the anode field penetrating the grid slots, and thus initiates anode-grid breakdown. The arrangement of the external circuit then forces transition to a grid-anode metal vapor arc. Examination of tube parts after some operation shows arc erosion on the grid baffle and on the side of the grid facing the hot cathode. Evidently the negative arc spot is formed on the cathode side of the grid.

Figure 3 shows the grid of a tube after about 10^8 shots in a laser system. The arc has favored one position, and has eroded a round channel through the grid structure. The discharge was 0.00125 coulomb per shot at 10 to 30 kiloamps peak. The corresponding anode damage was minimal.

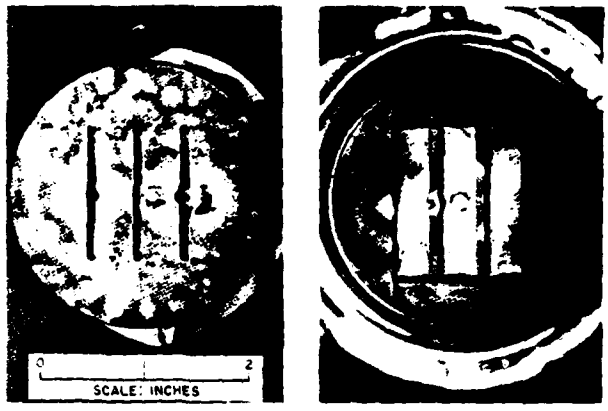

Figure 3. Arc Damage to Grid.

The hydrogen reservoirs used in these tubes are essentially the same structures used in standard thyratrons, but of greater capacity.

The hot cathodes used are identical with the standard tubes. Since in this case the cathode is used only as a trigger element, it could probably be greatly reduced in size. At the present time, however, the cathode is used during processing, since these tubes are first run in as standard thyratrons at full power.

Figure 4 shows the three types of thyratrons currently manufactured. The largest of these, the HY-3202, based on the 7322 configuration, is rated at 35 kV. The 20 kV HY-1102 is more compact to allow a lower inductance mounting arrangement. The third tube, the HY-13, is similar to the HY-1102, but is a tetrode structure for short delay time. This tube is intended for spark chamber applications with delays of the order of 50 ns. The open baffling in this tube somewhat compromises the high voltage hold-off reliability.

Characteristics

Switch Impedance

Figure 5 shows one experimental apparatus used at EG&G to measure tube characteristics. Figure 6 shows the circuit diagram. In this array, for example, we have been able to operate at up to 7500 amps peak, with di/dt = 275 kiloamp/μsecond, into a 0.45-ohm load, at 20 kV.

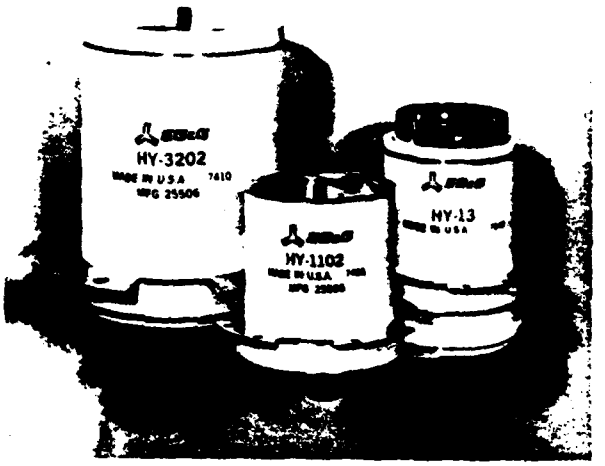

Figure 4. Grounded Grid Thyratrons.

In this sort of an apparatus we generally find switch inductance 10 to 15 nhy, effective switch resistance on the order of 0.2 ± 0.1 ohm, and load current rise time 20 ns ± 20% (10 to 90%) with the circuit underdamped. We also find that the switch resistance is dependent on tube pressure, varying by about 0.07 ohm with a reservoir voltage swing of one volt (or a pressure swing of about 0.15 torr).

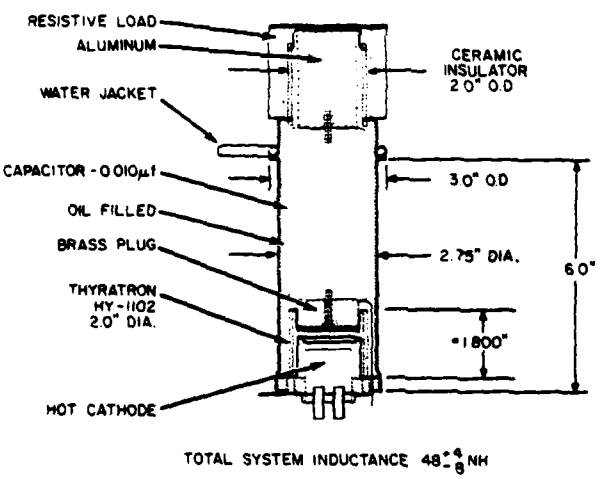

Figure 5. Experimental Apparatus - HY-1102.

We do not find a corresponding change in inductance or rise time. In fact, the 20 ns rise time seems to be a constant for these devices, this rise time having been found in the Brookhaven spark chamber[3], in our experiments, and in some laser systems which we have measured. Using the apparatus shown in Figure 5, a load current wave form, with a typical rise time and also a typical knee at the beginning of the pulse, was found. This current wave form is shown in Figure 7.

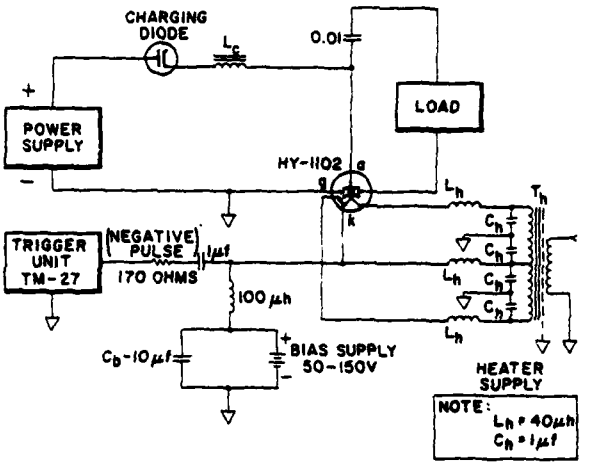

Figure 6. Experimental Testing Circuit.

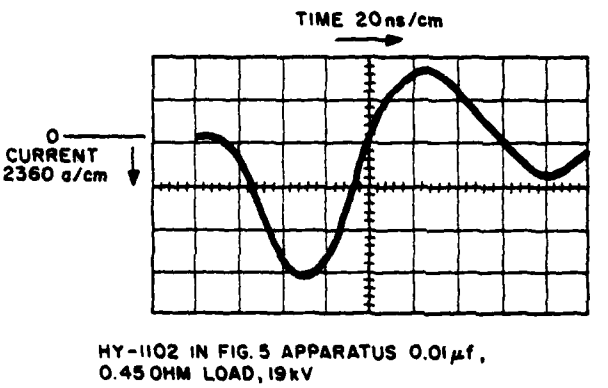

Figure 7. Current Pulse with Resistive Load.

Figure 8 shows a current waveform in a high energy nitrogen laser near threshold. Again we have the 20 ns initial rise. The circuit here was of the type of Figure 1B, and the time between the two peaks is, at least in part, due to time delay in the laser channel discharge formation. At full power, the current values shown here are about doubled. This current waveform was of particular interest because the circuit itself is very tightly coupled, leading to the original supposition that the peak current was much higher, and the pulse width much shorter, than was actually the case. This has been our general experience so far with pulsed lasers, where current measurements are very difficult and often nearly impossible.

A comparison between a grounded grid thyratron and its corresponding standard thyratron version is shown in Figure 9. The apparatus of Figures 5 and 6 was used. Load resistance was 0.45 ohm, and

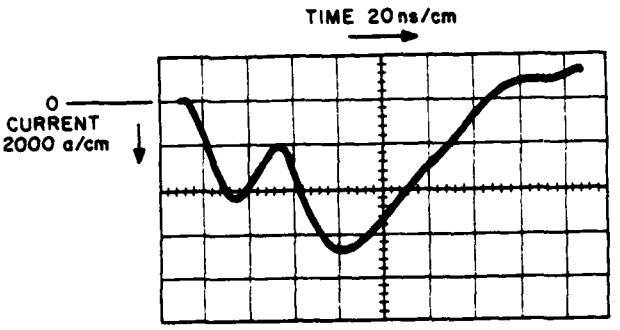

CURRENT THROUGH SWITCH TUBE NEAR LASER THRESHOLD

Figure 8. Current Pulse in Laser.

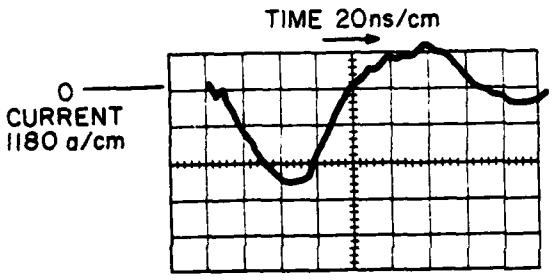

GROUNDED CATHODE, STANDARD HY-11, 3000 a peak

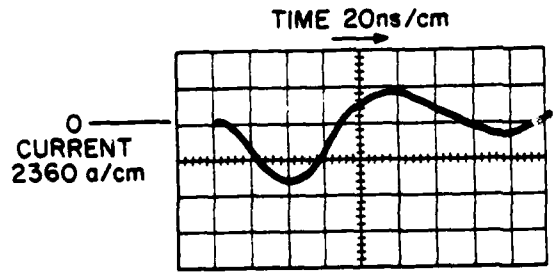

GROUNDED GRID HY-1102, 3800 a peak

Figure 9. Current Pulses of Standard and Grounded Grid Thyratrons (0.45-ohm load, 10 kV, 0.01 μf).

charging voltage was 10 kV. The grounded grid tube gives 3800 amperes peak current with a 20 ns rise time. The standard tube, capable of 2000 amperes peak in a short pulse, is here driven past its limits and gives only 3000 amperes peak and a 30 ns rise time.

The grounded grid tube, on the other hand, has an important low-current limitation. Because conduction current is supplied by an arc from the grid, rather than by the freely emitting hot cathode, it is necessary to use peak currents high enough to form a low-impedance discharge. At currents of less than 600 to 1000 amperes, a high-impedance, unstable arc condition occurs, causing large current fluctuations from pulse to pulse, or during a pulse. In circuits of a few ohms, this has been seen as steps and slope discontinuities on both leading and trailing edges of the load voltage (or current). In a series of tests at 500 to 1500 amperes, in a 2-1/2 microsecond line type modulator, and at about 1/2 ampere average, this behavior was shown dramatically by 150°C fluctuations in the tube envelope temperature. These changes corresponded to fluctuations in tube dissipation of one to several hundred watts. From a number of experiments, it appears that, for best results, the present generation of grounded grid tubes should be operated at peak currents greater than 1-1/2 kiloamperes.

Another limitation is found in average heating effects. From several experiments under diverse conditions, it is found that we encounter severe grid heating, or hot spot problems, at average currents of about one ampere, and sometimes less. The usual symptom is forward hold-off failure, which may persist for several seconds or even minutes. This effect is approximately the same for all of the present generation of tubes, which are not reliable at greater than 1/2 ampere average.

Repetition Rate

Most of the actual operational results so far are at less than 100 pps, with some tests at up to a few hundred pps. At EG&G we have recently conducted a series of experiments with a 2500 pps charging rate, and an actual pulse rate of 2000 pps. No forward hold-off or recovery problem was found. A conventional charging inductor and diode arrangement was used. Bias was applied (in this case, positive cathode bias) and the bias supply current was found to be higher than expected, about 20 milliamperes. It was also found that we needed a fairly low drive impedance to avoid missing pulses. A drive impedance of 125 ohms, at 400 volts (open circuit voltage) gave reliable triggering.

The actual upper limits of pulse rates are not yet known, and while these tubes will probably not achieve the 10-microsecond recovery times of standard thyratrons, the short spacings and low pressures should give at least several kilohertz.

Triggering

In general, the trigger requirements are basically the same as the similar conventional thyratron. Some problems with arc stability, missing pulses, and recovery, however, have been found to be related to the trigger generator characteristics. It is found to be desirable to keep the driver impedance relatively low, 50 to 125 ohms, if possible. Ideally, the driver pulse should be matched, or at least rapidly damped. Resistive, not inductive, isolation should be used between

the tube and the driver.

In spite of the apparent physical isolation of the trigger element (the hot cathode) from the main arc, a positive spike is produced on the trigger when the tube fires. This spike may be several kilovolts, and needs to be clamped. A GE MOV varistor or an NL silicon carbide varistor mounted close to the tube, between grid and cathode, can provide the necessary spike protection. A spark gap across the driver often produces worse problems than the original spike, and should be avoided.

Life

Not very many life test results are available yet, and therefore it is difficult to predict life in particular applications. In laser systems, we have had life times of 10^7 to 10^8 pulses, with failure due to gas clean-up. These numbers correspond to 20,000 to 100,000 coulombs of total conducted charge. In spark chamber systems, the results have not been as good, with life times of 10^6 to 10^7 shots, often ending in hold-off failure, which again may be related to damage caused by gas clean-up. Life time is clearly capable of considerable improvement, and is the object of current work at EG&G, but it is already clear that thyratrons specifically designed for grounded grid service in fact do combine the best features of spark gaps and conventional thyratrons as switch tubes for low impedance systems.

References

1. B. Friend, "A Ceramic Thyratron Wire Spark Chamber Pulser", Nuclear Instruments and Methods G5 (1968) 311-313.

2. R. Cappi, "A High Repetition Rate Pulse Generator Using a Hydrogen Ceramic Thyratron," CERN/MPS/CO 69-17 (1969).

3. K.J. Foley, W.A. Love, S. Ozaki, E.D. Platner, A.C. Saulys, and E.H. Willen, "The Brookhaven Double Vee Magnetic Spectrometer," Nuclear Instruments and Methods 108, 33-60 (1973).

4. B.W. Woodard, V.J. Ehlers, and W.C. Lineberger, "A Reliable, Repetitively Pulsed, High-Power Nitrogen Laser," Rev. Sci. Instrum., 44, 882-887 (1973).

5. M. Geller, D.E. Altman, and T.A. DeTemple, Appl. Opt. 7, 2232 (1968).

ADIABATIC MODE OPERATION OF THYRATRONS FOR MEGAWATT AVERAGE POWER APPLICATIONS

John E. Creedon, Joseph W. McGowan, Anthony J. Buffa
US Army Electronics Technology and Devices Laboratory (ECOM)
Fort Monmouth, New Jersey 07703

Summary. Significant impact on the size, weight, and cost of high energy pulse systems having short on times can be obtained by designing components to operate in the adiabatic mode. In the specific case of the thyratron switch the mass of the cathode and grid elements can be used as internal heat sinks. This allows its average current capability and thus its power handling ability to be increased several times over its normal steady state value for short operating times. Several other thyratron design concepts for short term, high peak and average power switching applications have also been studied and will be discussed. They include cavity grid designs for high voltage reliability, grid baffling designs to improve anode take over times, and plasma cathode designs to eliminate standby filament power. Effect and advantages of unbaffled grid structures on the anode take over time of the cavity grid structure was investigated. Average and peak current capabilities of several cathode sizes have been experimentally studied at a pulse width of 20 microseconds. Using these concepts several thyratron designs have fabricated and evaluated at average powers approaching one megawatt. In addition our evaluation of an off the shelf HY-5, operating in the adiabatic mode, was conducted. It was found that by modifying the cathode structure the device was capable of being operated reliably at 22.5 amperes of average current at a peak voltage of 15 kilovolts.

DISCUSSION

Adiabatic Mode of Operation

Recently, there has been interest in developing modulators that operate for short-on periods of one minute or less at peak and average powers substantially above those controllable with a single state-of-the-art switching device. Off-times, however, are relatively long and may be from several minutes to several hours. Since significant heat losses by convection,conduction,and radiation will not occur until a substantial temperature rise in the specific element occurs, the device can be considered to be operating in the adiabatic mode. For this type of an operating mode, the temperature rise of the internal elements are proportional to the total energy dissipated and the mass of the element and inversely proportional to the heat capacity. If the pulse width is long, that is, greater than a few microseconds, anode and grid heating effects associated with the P_b factor, will not be significant. For this condition, the internal dissipation of the thyratron will be directly proportional to the average current.

High Average Power Thyratron Design

Figure 1 shows a high average power switch design which differs in several ways from devices designed for radar applications. One is that high voltage hold-off capability is obtained by using a multiple cavity-grid structure rather than a stack of parallel plate grids. The problem with the latter approach is that in practice it is limited to two gaps when operation in air is desired. The limitation occurs because the external voltage stress must be less than 10 kilovolts/inch to prevent flashovers across the insulators while the internal spacing is adjusted to give a voltage stress in hydrogen or deuterium of nearly 200 kilovolts/inch. The disproportionate differences in the internal and external spacing requirements results in the use of deep cup electrodes which are not suitable for unlimited stacking of grids, the gradient grids must have the same physical configuration which permits easy construction and results in equal capacitance distribution and short paths for good electrical and heat conduction. All of the above design characteristics can be obtained by using wide spaced cavities between the high voltage grids.

In operation the cavities are made nearly field free except for a small value required to ensure complete internal breakdown and plasma propagation. One disadvantage of the wide spaced, low voltage hold-off cavities is that recovery times are long. To increase the speed of cavity deionization, which is predominaantly governed by ambipolar diffusion mechanisms, inverted metal cups are placed in the cavity to increase the surface to volume ratio.

Another departure from conventional thyratron design is the incorporation of the virtual anode. This design concept offers two advantages. One is that it provides a defocusing region for high voltage electrons formed during the breakdown or commutation period prior to their collection by the annode. Substantial numbers of electrons are accelerated up to full anode potential during commutation, and in the conventional geometry the beam waist caused by the focusing action of the high field occurs at a distance approximately equal to the grid anode spacing. The high electron energy is then dissipated in a small area resulting in hole drilling and localized anode heating. The resulting sputtering of metal atoms degrades both inverse hold-off and recovery characteristics. Another advantage of the virtual anode design is that it provides a large reservoir of gas molecules behind the anode. During high peak current operation pronounced ion pumping as well as transient clean-up may take place which deplete the anode grid region of neutral gas. Gas diffusion from the upstream virtual anode cavity temporarily compensates for these losses until circulating gas flow and reservoir replenishment actions are established.

A potential problem with the multi-cavity-grid design involves the commutation time for each gap and cavity to break down and commute. If the upper gaps break down too slowly, then high voltages appear across the insulation causing external spark-over. This problem has been found to occur frequently and several ways of eliminating it are presently being evaluated.

Another departure from conventional thyratron usage is in the large peak and average current requirements that are being considered for the cathode. For example, in one high average power modulator currently of interest, switching of peak current up to 250 kiloamperes at average currents of up to 300 amperes are being considered. Cathodes designed to operate in the adiabatic mode of operation, are felt to be the most practical approach to achieve current densities of these magnitudes.

Megawatt Average Power Switches (MAPS)

Three MAPS type switches are being developed by ECOM. The electrical and mechanical objectives and characteristics are summarized in Table 1. Also shown are the characteristics for the HY 5001 and the HY 5002, which are being developed to meet a short on-time requirement for Air Force Weapons Laboratory (AFWL). The development of the MAPS 70, shown in Figure 2, has been partially supported by Wright-Patterson Air Force Base (WPAFB) who initiated and are continuing to sponsor the ECOM technology studies associated with the MAPS program. This device is a three gap two cavity deutrium filled device having a 5000 cm^2 cathode. Internal water cooling is provided to all of the grid elements. Approximately five of the devices have been fabricated by EG&G to date. In general, leaks in the seals for the cooling channels have limited the performance of this design. One MAPS 70 operated at 700 kilowatts of average power at a peak voltage of 56 kilovolts. Operation was terminated by a seal leak.

The MAPS 250, shown in Figure 3, is being developed for use in the Blumlein Modulator. This modulator is described in a symposium paper by Wright and Schneider, entitled, "A Blumlein Modulator for a Time-Varying Load."[1] The MAPS 250 has 10 gaps and 9 cavities and a 2000 cm^2 oxide coated cathode. The cathode is mounted in a steel housing, 6 inches in diameter and the convoluted ceramic high voltage super structure is 4 inches in diameter. The cavity spacers are graduated in length and are longer at the top of the tube because of the external spark over probability during commutation. Four MAPS 250 devices have been fabricated by EG&G. One is presently being used in the MICOM modulator and the other three are being processed and evaluated at ECOM. To date the tubes have operated in the Blumlein modulator at 200 kilovolts under single shot pulsing and at 175 kilovolts at 50 hertz. In addition, the tube has been operated at a peak current of 9 kiloamperes and at an average current of 15 amperes at 40 kilovolts peak forward voltage in a line type modulator.

Figure 4 shows the HY 5001 on the right and HY 5002 on the left. These tubes are modifications of the standard EG&G HY 5. The HY 5 was evaluated at 22.5 amperes average current with a 30 second on-time and a 4 1/2 minute off-time. After approximately 50 on-off cycles, the devices exhibited a missing pulse characteristic which was found to be due to severe distortion of the cathode baffle. An 0.060 mils molybdenum baffle was substituted for the 0.040 mils copper. Over 1000 fault free cycles at 22.5 amperes have been demonstrated for the 5002. The 5001 had 3 pre-firings in a similar number of on-off cycles.

The MAPS 40 is to be developed on an external contract. Several preliminary devices, dependent of the contract effort, have been designed and are being fabricated by EG&G. These pre-MAPS 40 devices will be tested and evaluated at ECOM and the results will be used to implement the contractual development particularly with respect to cathode and grid current characteristics near full power. The MAPS 40 work is being sponsored by MICOM.

The test facilities being used to evaluate devices are shown in Figures 5 and 6. Figure 5 shows the 250 kilovolt - 2.5 microsecond Blumlein modulator which is described in detail in the paper of Wright, Schneider and Buffa.[1] An essential element of the modulator, from the viewpoint of the MAPS 250 thyratron is the front end clipper diode which in the photograph is in front of and partially blocks the thyratron from view. The clipper diode shunts the thyratron during the time that inverse voltage is present. At the peak current of interest the thyratron conducts easily in the reverse direction and this limits recovery characteristics. The modulator is charged by a 250 kilovolt 4 ampere dc power supply. Figure 6 shows the facility being set up for testing either the HY 5001/5002 or the MAPS 40 devices. Each PFN is 2 ohm in impedance and has a pulse width of 20 microseconds. One line is used for the AFWL tests at 15 kilovolts, 281 hertz. For the MAPS 40 testing all four networks are connected in parallel but with the number of sections reduced to give a 10 microsecond pulse width. The large box in front of the PFNS houses 4 banks of ohmweave resistors which can be arranged to give a load impedance of 0.25, 0.5, 1.0, and 2.0 ohms with a continuous dissipation of 500 kilowatts. For short term operation it is anticipated that the load will be capable of dissipating nearly one megawatt.

The modulator is charged from a 40 kilovolt - 30 ampere dc power supply which can be run at 40 amperes at somewhat reduced voltage. Two charging inductors of 0.75 henries each are available and they can be connected in either series, parallel or used individually to give the resonance frequencies of interest. Two 40 kilovolt - 20 amperes charging diodes are also in the facility and they allow the modulator to be run at frequencies lower than resonance.

Table 2 summarizes the maximum operating levels obtained to date. Both the HY 5001 and the HY 5002 meet the original objectives of AFWL. The 5002 has demonstrated a peak current capability of 75 percent higher than originally needed. The 5002 also operated for over 50 cycles at a 30 ampere average current level with a 10 second on-time. It has also demonstrated a capability to run at 35 amperes provided the current did not exceed 8 kiloamperes. There was not difficulty experienced with a 3 second on, 3 second off, operating cycle, obtained by snapping the grid on and off at full peak and average powers. Both types were capable of being snapped on after a 15 minute warm up and during stand-by.

The MAPS 70 has demonstrated operation at 80 percent of the voltage and at 87 percent of the average current objectives. The MAPS 250 has operated at 80 percent of the objective voltage level on single shot and70 percent of the objective at 50 hertz.

Figure 7 shows an earlier 8 gap version of the MAPS 250 with the gap-cavity geometry outlined on the photograph. Nominally, a series resistance divider is used to assure equal voltage division across the gaps. The value of resistance per gap depends on the distributed capacitance and anode recharging time. Generally, values between 10 and 40 megohms are used. A smaller resistor, usually 100-200 kilohms, is used across the cavity. The cavity can be negatively biased by placing the gap resistor from gradient anode to gradient anode and this has been found in some instances to give higher peak voltage operation. At the high values of peak and average current of interest

for the adiabatic thyratron development, the peak forward voltage hold-off obtainable per gap is reduced from 30 -40 kilovolts to 15 - 20 kilovolts. The reduction in hold-off is mainly due to recovery limitations. It has been observed that the thyratron conducts in the inverse direction when the peak forward current exceeds approximately 3 kiloamperes. As a result, matched end of line clipper circuits and front and clippers have been found necessary to prevent or limit the inverse arc from forming. Use of the virtual anode has been observed to minimize glow discharges in the grid anode region during recharging the network.

Commutation of the multiple cavity-grid structure takes time and this has caused external spark-over. Ordinarily the breakdown proceeds from the bottom of the structure up and on each gap breakdown, the anode voltage is capacitively divided among the remaining caps and cavities. Since the distributive capacitances of the gaps and cavities are about equal, high voltage can appear across the upper ceramics. Probability of an external breakdown in air thus assumes a non-vanishing value and spark-over can occur. Although the device subsequently breaks down internally and commutes the deionization of the external discharge, thus limits the rate at which recharge voltage can be applied.

The problem can be effectively eliminated by (a) increasing the internal spacing of the upper elements; (b) using a high dielectric strength medium; and (c) decreasing the breakdown time of the gaps. All three approaches have been tried with some success. Decreasing the breakdown time was achieved by eliminating the grid baffling in the upper structure. Although the hold-off capability was reduced to approximately 13 kilovolts per gap, the firing time (TAD) was for a 3 gap structure from 0.75 to 0.3 microseconds.

Considerable interest has been expressed by the Air Force in reducing heater power requirements. Towards this end we are investigating the feasibility of using a plasma cathode. Figure 8 shows a photograph of an experimental device fabricated by IT&T in which peak currents of 70 amperes at 8-10 kilovolts were switched using a plasma cathode. The electron source was a cold cathode arc from which electroncs were extracted through apertures in a cathode plate. The anode-cathode separation and pressure are similar to those used in conventional thyratrons. This cathode arc current must be comparable to the circuit current. The approsch appears to be quite promising with respect to achieving an instant turn-on device.

ACKNOWLEDGMENT

The work reported here has been supported and encouraged by R. Verga of WPAFB. D. Turnquist of EG&G contributed to the design of the MAPS and his efforts are gratefully appreciated. IT&T's contribution on fabricating the plasma cathode is acknowledged and finally the authors wish to express their appreciation to S. Schneider of ECOM for many technical discussions and suggestions particularly with respect to the unbaffled structure.

REFERENCE

1. W. Wright, S. Schneider, "A Blumlein Modulator for a Time Varying Load."

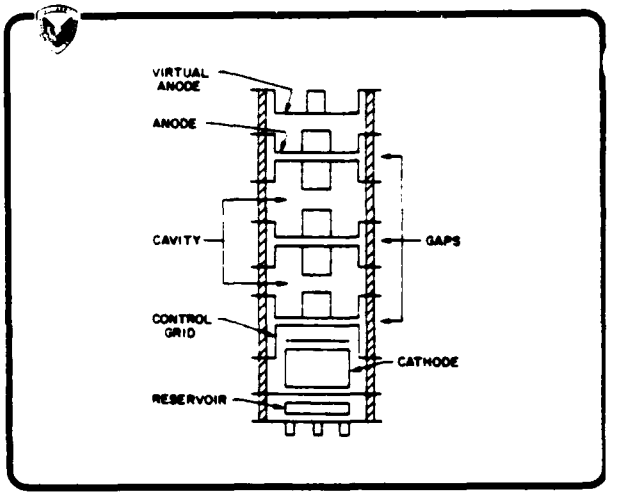

Figure 1. Cavity Grid Design

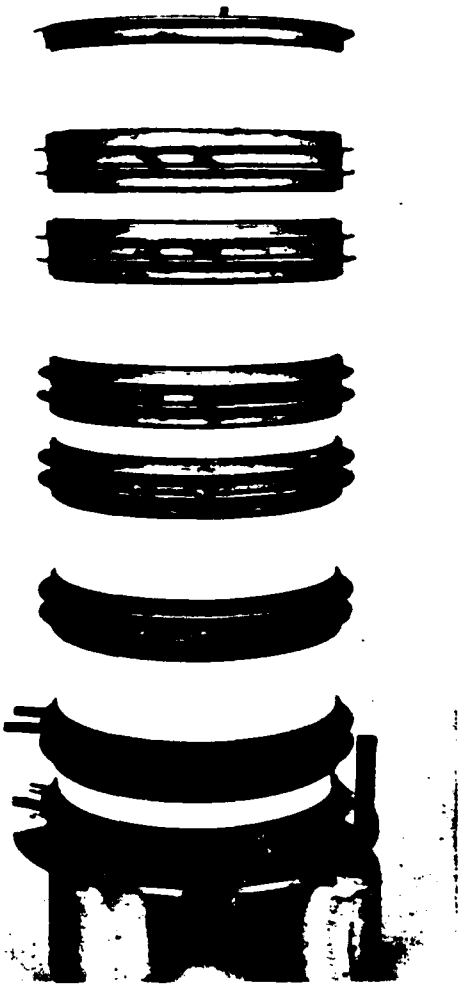

Figure 2. MAPS 70

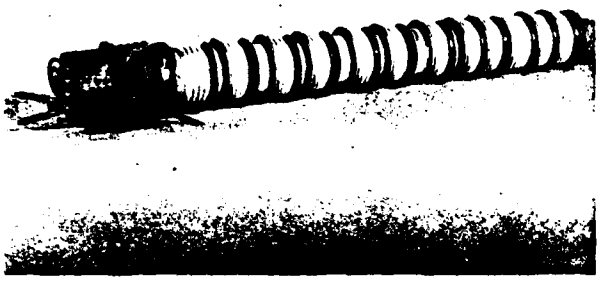

Figure 3. MAPS 250

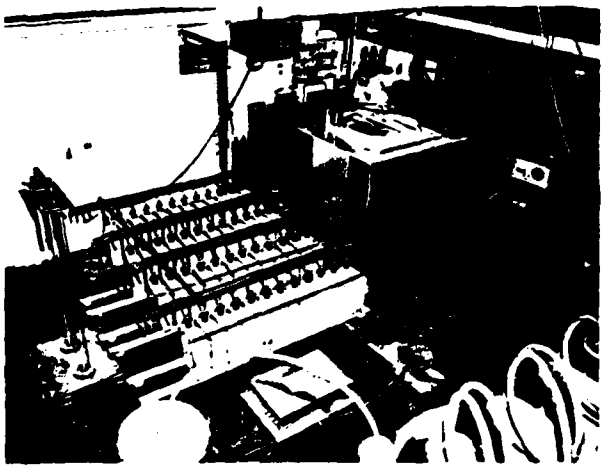

Figure 6. AFWL and MAPS 40 Test Facility

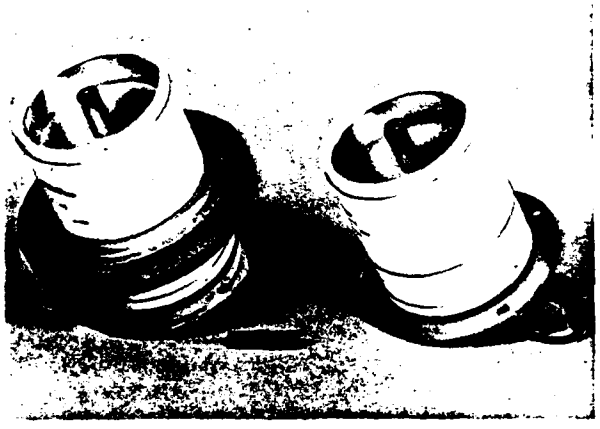

Figure 4. HY 5001 and HY 5002

TABLE I

MAPS ELECTRICAL AND MECHANICAL OBJECTIVES

TYPE	PEAK VOLTAGE kV	PEAK CURRENT kA	AVERAGE CURRENT A	DIAMETER INCHES	HEIGHT INCHES	WEIGHT POUNDS
MAPS 70	70	5	30	8	27	85
MAPS 250	250	20	4	4	54	45
HY 5001/5002	15	5	22.5	4.5	5	7/12
MAPS 40	40	40	50	--	--	25

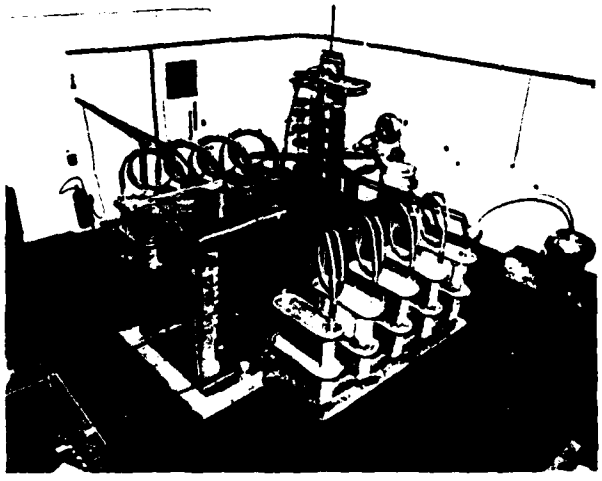

Figure 5. 250 kilovolt Blumlein Test Set-Up

TABLE II

SUMMARY OF RESULTS

TYPE	PEAK VOLTAGE kV	PEAK CURRENT kA	AVERAGE CURRENT A	PULSE WIDTH s
HY 5001	15	4	22.5	20
HY 5002	15	8.4	30	20
MAPS 70	56	4	26	20
MAPS 250	200	13	15*	2.5-5

*OBTAINED AT 40 kV AND 10 -s

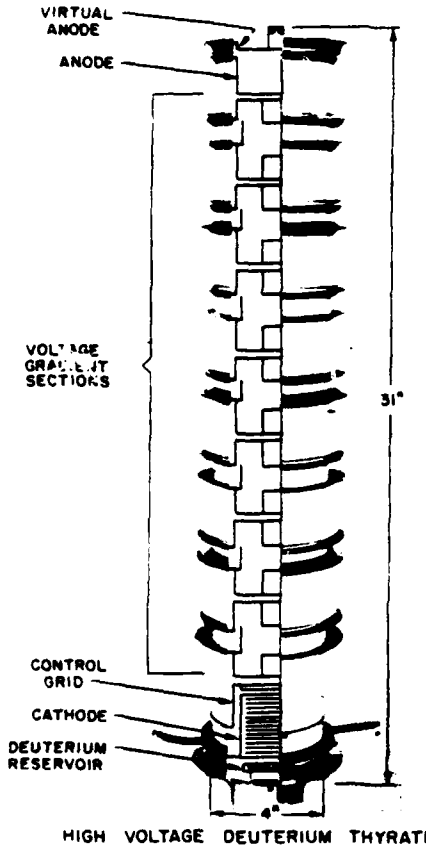

Figure 7. 8 Gap Cavity Grid Thyratron

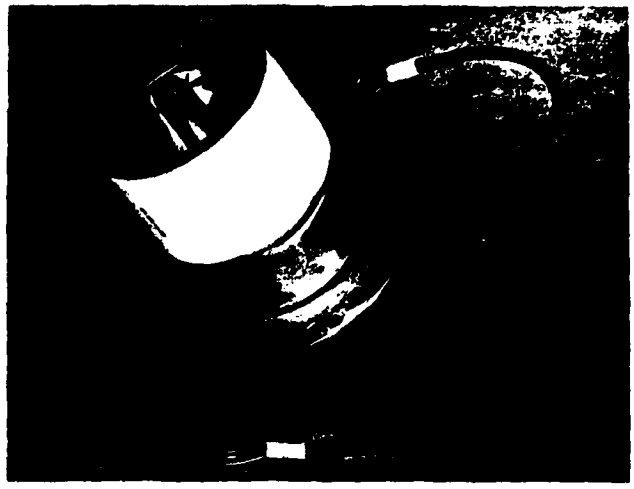

Figure 8. Plasma Cathode Switch

HIGH ENERGY SWITCH DEVICE STUDY AT RADC

Bobby R. Gray
High Power Component & Effects Section
Techniques Branch
Surveillance Division
Griffiss Air Force Base, New York

Summary

This paper gives a brief comparison of some features or characteristics of three types of closing switches, namely the thyratron, SCR, and the spark gaps. It does not cover completely all features of the devices but describes mostly those areas where the spark gap device has some particularly good points that can be exploited. A spark gap design based on some earlier work is reported on, giving some construction details and operating features. Certain precautions and problem areas are pointed out for future work. While a spark gap is not the answer to every line pulser designer problems, it does have some features that can be exploited. The writer feels that the spark gap has been overlooked for many applications where it would have been well suited and it should be investigated further.

It is the intent of this paper to point out some of the features of a spark gap that could have some bearing on one's choice for a switch.

Introduction

When the need for a switch for high energy/high power arises, the experimentor or systems designer is often in time in a quandry as to whether to use a spark gap, thyratron, or solid state device. Other times he may have a built-in bias either for or against a particular approach based on past experiences. Again, in other cases, there seems to be only one approach worth pursuing because of nothing else being available. The arrangement of this particular session of the Symposium compares the thyratron, spark gap and solid state devices. A brief comparison of the three types of devices is in order to point out some pertinent features of the three device types. It may provide some additional consideration for selecting a switch in some critical application.

a. Voltage and Current Limitations

For all three types of devices, performance during the main body of the pulse is essentially the same except for impedance. The blocking voltage and load currents of the three device types of course, vary widely. SCR's and thyratrons have a more severe current problem than do spark gaps because eventually the allowable current is limited by available current carriers within any particular device. The spark gap can more easily accept increased current levels, but at the expense of more electrode erosion, because the arc channel will simply increase in size to meet increased current demands until the so-called pinch effect begins to try to reduce the conducting area. Likewise, voltage limitations exist on the three type devices that tend to favor the spark gap. SCR's have a upper limit 100-2000 volts per device and thyratrons tend to have a limit of about 25-30 KV per section with the maximum to date of 250 KV across eight gaps for an experimental device. The spark gap can be made to have a greater voltage across a single gap by careful design practices.

b. Rate of Rise of Current

The problems of turning on the devices and the pulse circuit conditions for the devices differ. Rate of rise of current for the SCR is critical and must be held below some upper limit until the junction is completely turned on. Various techniques have been used to alleviate those problems. A similar problem exists in the thyratron but the effects are usually not catastrophic although excessive dissipation can occur in the thyratron if the current rate of rise is too great. In theory, the spark gap can be more immune to this problem if one ignores the limiting rise time imposed by the self inductance of the spark itself and associated circuit leads.

c. Jitter

Here the SCR and the thyratron can have an advantage on the spark gap because these devices are sealed and more consisten in nature. Spark gaps can be affected by electrode conditions, external ionizing sources, dust, and residual ionization. Also where SCR's trigger with a few volts and thyratrons trigger with about one kilovolt, spark gaps generally require a much larger voltage. Without going to great extremes, it is usually easier to construct a pulser with very fast rise times for the few volts needed to trigger the SCRs and thyratrons. Where very accurate control of the exact point of turn-on is essential one would possibly prefer the scr or thyratron assuming other factors were equal. However, there are many experiemntal situations where this is not the case and jitter can be tolerated better.

d. Post Pulse Conditions

This portion of the sequence of events in a line switch operation more clearly differentiates the three type of switches. Thyratrons and SCRs are, by design, unidirectional switches if satisfactory operation is to occur. Excessive inverse voltage appearing on the anode while the thyratron is still in an ionized condition or before the SCR is able to block reverse voltage will cause failure of the device. A forward voltage appearing during this period is absolutely intolerable, unless a delayed recharge of the PFN is employed. As the peak and average currents through the thyratron become larger, the inverse voltage effects become even more severe. A reversal of current in the thyratron during the inverse voltage period usually will insure that the tube will "hang up" shortly, or will be short lived at best. In some cases, these post pulse inverse conditions are difficult to control because the reversal of voltage is caused not by the PFN-load impedance match per se, but by distributed components in the discharge circuits and it is difficult sometimes to control these extraneous circuits. Most types of spark gaps however, can take post-pulse inverse voltage quite well. If

for no other reason, spark gaps are often used in cases where an oscillatory discharge is expected. Since the gap can conduct both directions, all energy in the current PFN is dissipated at every pulse usually. The PFN always starts recharging from a zero voltage level. This prevents a build-up of the PFN voltage after a series of faulted load pulses as a unidirectional switch would do in event of a shorted load if one did not use a diode clipper. However, it tends to limit the protection offered to the faulted load, particularly if the PFN has a large charge remaining when the load faults because the faulted load usually represents a large decrease in impedance which leads to an underdumped discharge of the PFN. With essentially zero ohms, impedance in both the load and switch in comparison to the PFN, the system is now underdumped and will oscillate for many pulse lengths in an exponential decaying fashion ensuring that much of the remaining energy in the PFN will be deposited into the faulted load. An inverse diode with a dampening resistor is of no value in this case to help dampen out the oscillation because the spark gap cannot block a reversing voltage unless it becomes de-ionized.

The above brief description of some of pertinent parameters of the thyratron tube, SCR's and spark gaps makes the rather gross assumption that all devices of the same type have similar characteristics and physical design. Manufacturer's of course, have their own particular techniques to make the switch work but, in general, the basic physics of the process of ionization of a gas or generation of current carriers in a solid state device pretty much makes these types of devices similar.

Spark Gap Design

The rest of this paper deals with a spark gap design that has been worked on at RADC specifically for line pulsers. It has been demonstrated in one version at hold-off voltages as high as 250 KV at a PRF of 180 pps switching a peak power of 180 megawatts and 1 megawatt average[1]. Figure 1 is a photograph of the gap array. More recently, a new model has been made to reduce the overall size of the device and make it more adaptable for very high peak power pulse applications in a laboratory environment. It is shown in Figure 2.

The basic concept of the multigap design goes back to the 1950's and a University of California development whereby increased voltage operating range is achieved by putting a large number of gaps in series. It can be shown that this method makes possible a 100% range of voltage control if sufficient trigger energy with fast rise time is available to trigger all gaps. Although the original design was based on use as a line switch for PFN discharge, it apparently was not used in serious practice, probably because the development of the thyratron negated any need for it. It has found the greatest use as a multigap crowbar and has been reported on by a number of authors.[2,3,4,5,6,7,8]

In a attempt to use this type of spark gap as a line switch in the 250 KV modulator at RADC, it was found that the normal sequential or mid-gap triggering was unsatisfactory. The gap array, when mid-point triggered, was sensitive to the polarity of the trigger pulse with respect to the level and polarity of the voltage on the PFN. It appeared that the presence of the DC voltage across a gap with polarity opposite the trigger voltage tended to inhibit the gap breakdown. Since the sequential scheme requires the gaps to break down in sequence, one whole section, either the top or bottom, of the series of gaps could be biased off so that triggering of that section was not possible. It is uncertain whether this was a result of insufficient triggering energy or of too slow rise time of the trigger pulse. In addition to the apparent biasing effect of the DC voltage across the gaps, the presence of the trigger coupling capacitor, in the sequential triggering method, causes unbalanced voltage distribution of the line voltage across the gap array, particularly at an increased PRF is this a problem. A solution was developed for that design which used parallel triggering of the gap array. The parallel triggering scheme is discussed in more detail in the referenced proceedings, but a simplified schematic of the arrangement is shown in Figure 3

Theoretical Study

Since the previously described spark gap performed exceptionally well, it was decided to expand the series spark gap design to pulse a much higher peak current in a low impedance circuit of about one ohm. The peak hold-off voltage would be reduced to be compatible to some of today's pulser requirements such as lasers and flash lamp type loads which require high peak currents. A goal was therefore set to construct a switch that could pulse a PFN and load of one ohm each and do it efficiently.

Several questions needed to be considered in this program. It was not exactly clear that the same triggering schemes would work for spark gaps operating in low impedance systems because of some of the following potential problem areas:

1. Efficiency
2. Effects of increased peak currents.
3. Electrode erosion.
4. Noise - (Audible).
5. By-products.
6. Cooling.
7. Radiation effects.

A brief discussion of these points is presented here and some results of investigations performed to date presented later. The evaluation program of the gap is still being pursued and a clearer picture of these problem areas will be presented at a later date.

a. Efficiency

As the impedance in the load and PFN are decreased, other circuit component losses become more important from an efficiency standpoint. A one ohm resistance in a 100 ohm system represents a 1 percent loss in efficiency but the same switch resistance in a one ohm system represents 50% loss in efficiency. The resistance of a thyratron or spark gap is difficult to measure, but one value often quoted for the voltage drop across a spark gap in air is about 30 volts. It is uncertain

whether this is a fixed value regardless of current through the gap or whether it behaves in a more linear fashion. In any event, the cascading tends to lower the maximum efficiency of the discharge system. It is therefore necessary to determine to just what extent this disadvantage outweighs any possible advantages to switch very high peak and average powers.

b. Noise (Audible)

A spark gap type discharge, particularly an open air gap, produces a very sharp noise pulse when triggered. The sound level is proportional to the total energy switched or total coulombs transferred. Certain modifying effects such as the length of the gap, background noise, sound enclosing shield, etc., determine just how the ear responds to the absolute sound level produced by the gap. If the spark gap is pulsed at some high PRF, the ear becomes unable to separate the pulsed sound and it then senses an average level. A sound level meter would read an average or RMS level but in reality there would be high peaks at each pulse.

c. Radiation from Spark Gaps

It is a fairly common misconception that spark gaps in themselves radiate electrical signals, as if within the arc itself a generator is formed. This is of course not true no more than it exists for SCR's or thyratrons. It is true that there are certain frequencies generated during the turn on and turn off of the various switches but these are partly result of circuit effects and the rise time. The thyratron generates certain signals as a result of ion or electron resonances within the tube itself and usually radiate some RF during the grid-cathode ionization period and the anode take over period. These effects are of much lower order than the signals generated in the main pulse itself or from stray circuits.

The main radiation effects from spark gaps would have to be in the form of sound and light. Particularly in an atmospheric pressure gap is this true. These forms of radiation inevitably affect the overall efficiency of a spark gap pulser but it is usually of little consequence in comparison to the total power switched. It does mean that some method of controlling them must be provided though.

d. Electrode Cooling and Erosion

Heat dissipation in a spark gap is a fairly complicated process. Just how much of the arc drop appears on the electrode material depends on several factors. With a flowing gas system, much of the heat of the spark itself will be pulled away before it can radiate to the electrode. A certain amount is deposited directly at the anode and cathode surfaces itself. Finally, the flow of current within the electrode body itself develops a certain amount of heat.

For erosion of the electrode to occur, the material must be raised to the point of melting. Other effects such as ion bombardment of the electrode surface or shock waves may occur but these can do little damage unless the material melts first. If the spark moved about randomly on a large surface of the electrode no one spot would rise rapidly enough in temperature to erode. This hardly ever happens however, for the arc channel tends to favor the point of highest electrical stress across the gap. The arc will be anchored at one point primarily and will rapidly erode this one point.

Different materials withstand the erosion better than others. Tungsten and tungsten-copper alloys make good electrode materials because of the higher melting temperatures. Ideally the best design for an electrode would have a surface that could withstand the temperature rise from one spark and then before the next spark occurred, dissipate this heat away. This is one reason the tungsten-copper alloy works well. With good heat sinking this could be accomplished. We are presently working on a design that will employ water cooling of a copper block to which tungsten arcing surface is silver soldered.

Design Criteria

Some of the objectives we were attempting to reach in the design stage were:

1. Be expandable.
2. Small as possible.
3. Utilize available materials.
4. Be constructable in a normal model shop.

Reviewing the previous designs for crowbars showed them to be fairly large devices and should be reduced in size. We felt the gap array should be flexible enough that different electrode mounting arrangements could be tried. We also felt that a new design was needed for the trigger coupling capacitors used to trigger the gaps with.

The approach followed is discussed in the next sections.

a. Gap Design

All of the multigap crowbars designed over the years have arranged the gaps so that ultra-violet radiation from an early triggering gap would help trigger a delayed gap. This arrangement, however, tends to make the overall assembly larger than necessary. Therefore, one of the options used in this program was to simply place the electrodes in a straight line array which effectively blocked the UV triggering effects between adjacent gaps. There has been no apparent effect on the triggering of the gap however. Physical design of the array is shown in Figure 2 and Figure 6 is a sketch of the electrode assembly and the trigger coupling capacitor.

Since we have not noted any bad effects from arranging the electrode in a straight line array the next approach will be to shorten the electrodes themselves. All that is really necessary is some form of a holder for the electrode and some manner of heat sinking. With a reduced mass in the electrode, additional cooling will be necessary for long running periods. Possibly a special designed air foil could both hold the electrode and provide a heat sink.

The present design uses a 3/4 x 2" long pure tungsten electrode. The arcing surfaces are on the gently rounded ends of the electrode which are held in position by aluminum bars bolted to the side of the air box along a slot which passes from top to bottom of the box. The purpose of the slots is to allow adjustment of the electrode spacing and also serve as a viewing part for the arc itself.

b. Trigger Coupling Capacitors

As in all the other multigap devices, this spark gap requires a trigger coupling capacitor for each electrode. A scheme using a coaxial oil filled capacitor arrangement has been developed. Each electrode is connected to a short section of 4 inch aluminum pipe in the middle of 9 inch brass pipe thus forming a coaxial capacitor. It is shown schematically and photographically in Figures 2 and 3. Successful operation up to 60 KV has been achieved at pulse rates up to 300 pps with this design. This is the level of the PFN voltage and the top capacitor has to charge up to this level between pulses. All the capacitors, subsequently, lower down on the array, take proportionally less voltage. All the gaps have to divide the PFN voltage equally for proper operation.

c. Gas Supply

Spark gaps have to have some gaseous media to ionize in order for current to flow. Different gases have effects on such properties as recombination, arc drop, maximum voltage hold-off, trigger levels, etc. In addition the pressure and gas density are important. The source of the gas may be in a free state in a sealed environment, be combined in some metal hydride, or be produced as a cloud of metal atoms in a high vacuum. It may be in a open flowing system where exchange of the gas is possible. If it is an open flowing system a sufficient reserve of gas must be maintained for long running periods. For this reason in this experiment we used air as the gas. It is easy to flow past the arc area and there is no build-up of arc products to change the gas composition within the gap area. The oxygen in the air helps the recovery of the gap but adds considerably to the erosion rates probably. While other gases may have certain desirable features the large volume and the high velocity required to properly cool the electrode and thoroughly flush the gap area make normal air the best choice if the resultant byproducts are disposed of properly.

Experimental Results

The following table gives some data points taken on the limited testing to date:

PRF	P.S. Volt	P.S. Current AV	Peak I	Load Voltage
200	10	10	12.180	9400
120	20	5	17000	14000
191	15	10	14000	12000

Figure 4 thru 5 are scope photographs of switch voltages and currents taken for the spark gap and a Chatham-CH1222 thyratron. Pulse length of the PFN is a nominal 6 microseconds at the 50% point.

a. Discussion of Experimental Results

As in all experimental programs there are some problem areas and this one is no exception. The encouraging thing is that at this point the problems we were expecting are not as severe as expected. We were expecting the impedance of the gap to be too great to have an efficiently operating device. This does not seem to be the case. Another problem we expected which did not occur was the in-line placement of the electrodes tending to block the UV radiation between adjacent gaps and causing triggering problems. This did not seem to be a problem however. We also were uncertain about clearing the gap between pulses so that continuous conduction does not occur. At this point it appears this is no major problem but we have had some "hang-ups." Exact cause of these is uncertain for it takes several minutes for this to occur. This indicates a heating problem rather than a failure to deionize on a regular basis.

b. Thermal Effects

Thus far, cooling of the electrodes is one of the main problem areas of the present gap design. After about 10 minutes of operation the tungsten electrode and aluminum holder become too hot to touch. Temperature of the electrode rises to 263 C^{o} from 22^{o}C after about 8 minutes of running time with the spark gap switching 120 kilowatts of average power from the supply. RMS current through the gap was approximately 316 amperes. The electrodes changed from a normal metallic gray color to bright blue. It is interesting that only those electrodes in which the pulse current flow the full length of the electrode changed color and were also the hottest. This indicates that the heating load on the electrode is a bulk resistance effect in the electrode material itself from I^2R losses rather than the anode and cathode sheath losses being absorbed by the electrodes.

With extended running times, the electrode holders expand and allow the electrodes to slip and change gap spacing. The electrode holders get so hot the glass laminate material the box is made from begins to burn or change in dimensions so that the holder slips. These problems are being resolved by designing a new box that will not burn and by designing a new electrode holder which is smaller and is water cooled.

c. Radiation Effects (Acoustical and Light)

Another aspect of efficiency for a spark gap is in the radiative losses other than in the form of heat. The acoustical power and light radiated by the gap can become appreciable at the high peak currents. There is an apparently high ultra violet radiation from the gap in addition to the visible light. It was noticed that a nearby high voltage thyratron developed a darkened pattern on the surface of the ceramic after the gap had been operated for a short while. Areas of the ceramic lying in the shadow of objects lying in a straight line between the arc centers and the tube were not changed. A group of 2 x 2 inch alumina substrate material

was placed near the gap for a further check of this phenomena. Portions of some of the test pieces were covered with paper and others were covered with tape. In all tests, those areas left uncovered were darkened after about 5 minutes in the light radiating from the gap. A control sample left uncovered and separated from the test area remained as white as those covered ones left in the vicinity of the gap. These effects are still being studied but it is believed to be the result of strong ultra violet radiation coming from the gap and causing chemical change of the surface material of the test piece.

The acoustical power generated by the gap has to be dealt with yet. Sound level measurements taken about 10 feet away from the gap with no extra shielding material indicated a level of approximately 116 decibel above a quiet room. Background level before the spark gap was turned on was 90 decibels. This level is mostly caused by the electrode cooling air supply. The frequency content of the sound level indicate a preponderance of higher frequency components. At 16 KHz, the level was about 110 decibels.

d. "Hang up" - or Self Fire

On several occasions the gap has either self fired or failed to recover after a pulse. There is no indication however that these failures are due to the basic theory of the gap design. In all cases failure occurred after the gap had been pulsing for several minutes and the electrodes were very hot. The electrode geometry itself had not changed but several electrodes had slipped in the holders shorting out some gaps and making others very long. This apparently unbalances the series arrangement enough to cause self-triggering.

e. Radiation (RF)

Another form of radiation that occurs with this particular design is in a RF signal caused by the discharge of the energy stored in the trigger coupling capacitors. This signal is in addition to the normal amount of "hash" that would accompany the breakdown of the gaps from trigger voltage alone. It is fairly proportional to level of voltage on the main PFN because the trigger coupling capacitors have impressed across them proportionate amounts of the PFN voltage. The signal is likely to be in the 1-2 MHz range and can be somewhat prevented from radiating by inserting a non-inductive resistance in the connecting lead between the coupling capacitor and each electrode.

f. Pulse Rise Time Degradation

A totally unexpected result was the effect on the pulse rise time. We had assumed the formative time of the arc to about the same as in a thyratron. It was also assumed that the tail end of the pulse should decay at about the same rate. This was not the case however. Comparing the pulse shape obtained for a thyratron and from the spark gap we see in Figure 4 and 5 the rise time, pulse length 50% point and the fall time have all increased. Other than a larger circuiting inductance in connecting the spark gap at essentially the same electrical point in the pulser, the only difference is in the switches. Since the gap current is measured at the same location in the circuit, the measurement techniques should not make the difference we saw. Also since all the gaps must close for any current to flow problems in commutation of the closing action of individual gaps should not be involved. To check the effect of the spark gap inductance itself, fifteen of the gaps were shorted out so that only 5 gaps were carrying the pulse current. There appears to be no change in the rise time or pulse length but the gap did pulse at a lower voltage.

It appears that the change in pulse conditions with the spark gap is caused by the extra inductance of the circuit itself and not the gap. This is to be investigated further with a new test stand that will minimize all possible inductances.

Conclusions and Recommendations

This paper has attempted to describe some of the basic characteristics of three types of closing switches; the thyratron, the SCR and the spark gap. One version of the spark gap, operating at RADC, was described for the purpose of showing what can be achieved for limited application in a laboratory environment.

One particular application the spark gap might fill is switching in an underdumped discharge circuit. Non linear loads such as flash lamps and certain lasers would be ideal situations for this type switch. It has high pulse repetition rate capabilities, can take the voltage reversals from the underdumped situation and, could recover in event the load failed in event the load itself failed to conduct.

Although we have operated one of the gap devices for many hours without electrode replacement and problems normally associated with spark gaps have been eliminated for our particular situation, there are obviously some applications for which this type spark gaps are unsuitable. These might be airborne applications requiring tight spaces or where an adequate air supply is not available.

References

1. "250 KV Multigap Spark Line Switch for Line Modulators", B. Gray, Ninth Modulator Symposium, (1966).

2. "Triggering Mode Study of a Spark Gap Array", S. Schneider and A. Buffa, Ninth Modulator Symposium, (1966).

3. "Improved Multigap Electronic Crowbar", W. Schraeder, Eleventh Modulator Symposium, (1973).

4. "Multigap Crowbar Triggering Study", T. Weil, Eleventh Modulator Symposium, (1973).

5. "Oil Immersed High Voltage Crowbar", C. K. Hooper and B. Drummond, Ninth Modulator Symposium, (1968).

6. "A Versatile Electronic Crowbar System", S. Schneider, M. Zinn and A. Buffa, Seventh Symposium on Hydrogen Thyratrons and Modulators, (1962).

7. "A 300 KV Multigap Crowbar", G. Grotz, Seventh Symposium on Hydrogen Thyratrons and Modulators, (1962).

8. "Electronic Energy Diverter Application and Design", M. Dranchak, Eighth Symposium on Hyrdrogen Thyratrons and Modulators", (1964)

Figure 1. Photo of Electrodes and Air Plenum Chamber in Earlier Gap Design.

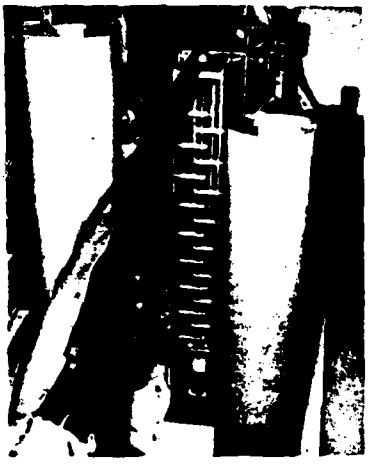

Figure 2. Photo of Experimental Re-Designed Gap Showing Electrode as Coupling Capacitor.

PARALLEL METHOD OF TRIGGERING MULTIPLE NUMBERS OF GAPS

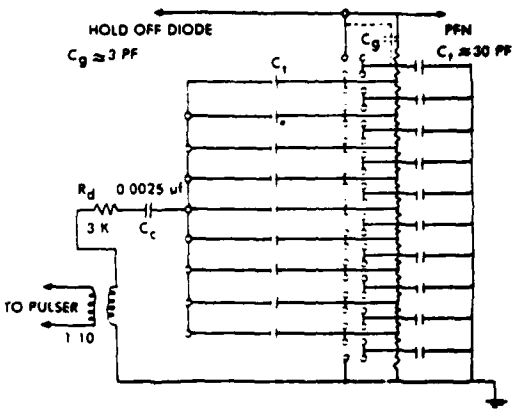

Figure 3

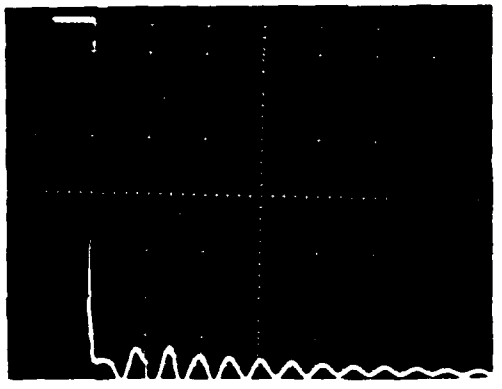

Figure 4 (a) Thyratron Pulse
Vert - 10V/cmx470
Horiz - 10 usec/cm
Epower supply - 15 KVDC

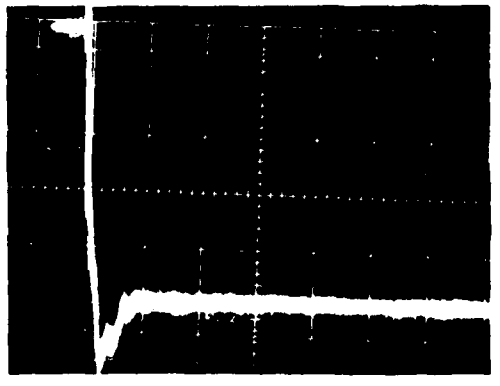

Figure 4 (b). Spark Gap Pulse
Vert - 10V/cmx470
Horiz - 20 usec/cm
Epower supply - 12 KV @ 10 AMP DC

Comparison photographs of voltage across a CH1222 Thyratron and the Spark Gap.

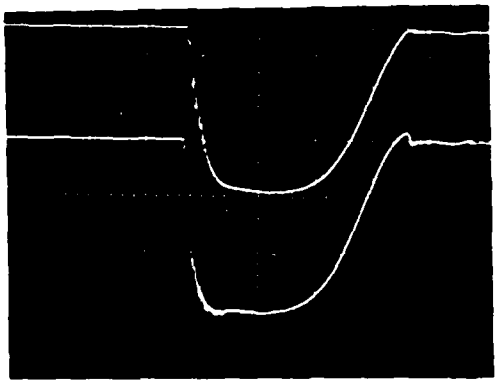

Figure 5 (a). Thyratron Pulses
Vert - 10V/cm
Horiz - 2 usec/cm
Top Pulse-Load Current-4300V/cm
Bot Pulse-Load Voltage-4700V/cm

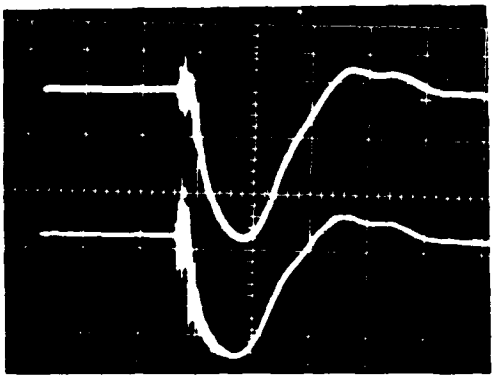

Figure 5 (b) Spark Gap Pulse
Vert - 10V/cm
Horiz - 5 usec/cm
Top Pulse-Load Current-4300V/cm
Bot Pulse-Load Voltage-4700V/cm

Comparison Photographs of Load Voltage and Current Pulses for CH1222 Thyratron and Spark Gap Switches.

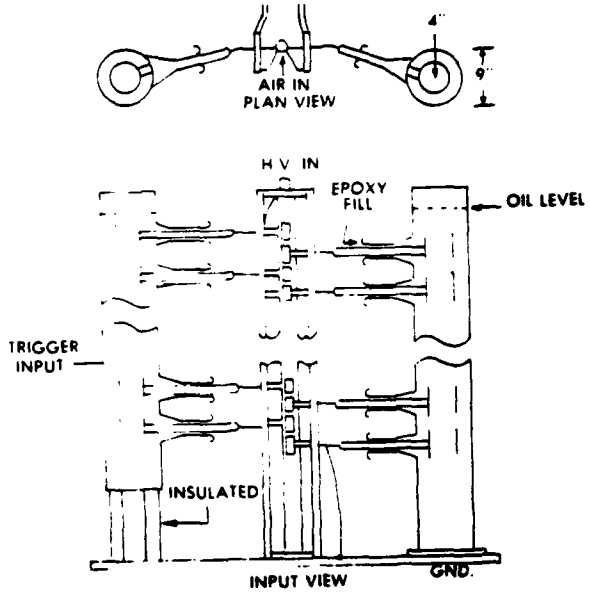

Figure 6. Simplified Sketch of Spark Gap Array and Trigger Capacitors

A 12.5 MEGAWATT MODULE FOR HIGH ENERGY PULSERS

Robert A. Gardenghi
Edward H. Hooper
Westinghouse Electric Corporation
Baltimore, Maryland 21203

Major Frank S. Zimmermann
Air Force Weapons Laboratory
Kirtland AFB, New Mexico

SUMMARY

A solid state line type pulser module capable of producing pulses of 12.5 megawatts peak and 62.5 kW average has been developed, breadboarded, and demonstrated. The switch element consists of six Westinghouse T60R RSR's stacked in series. The RSR is a two terminal, four layer semi-conductor switch triggered by dv/dt. It is well suited for high power applications and is easily seriesed for stack operation.

Circuitry, physical characteristics, triggering characteristics and test results are presented.

The module was developed for high energy laser pulser applications. It is ideal for this application since it has the advantage of "instant-on" due to the RSR switch element. In comparison to thyratrons or ignitrons, it requires no auxiliary power supplies and no filament warm-up or standby. In comparison to SCR switched modules it has the advantage of small size and simple trigger circuitry due to the RSR's inherent high di/dt capability and two terminal triggering operation. The module was also single shot tested with a short circuited load to simulate load fault conditions. The module successfully passed this test. The fault current was nominally 10,000 amperes.

This paper is based on studies performed for the U.S. Air Force under contract no. F29601-74-C-0021, Air Force Weapons Laboratory, Kirtland Air Force Base, Albuquerque, New Mexico.

INTRODUCTION

A basic high power 5,000 volt, 5000 amp pulser module was developed to permit eventual realization of pulsers capable of multi-megawatts of average power. Large numbers of these modules can be combined to produce virtually any desired power.

The parameters of the module were evolved by simultaneously considering the constraints of high power, light weight, and existing alternator designs. It was reasoned that the interface between the pulser and alternator could be optimized by eliminating the traditional transformers and DC power supply. This could be done if AC resonant charging directly from the alternator was used. Hence, the 5 kV voltage rating. It was also reasoned that an existing high capability solid state switch, the T40R RSR, could be scaled up from its 1000 ampere rating to 5000 amperes by changing the fusion diameter. Hence, the 5000 ampere current rating.

Proof of performance of the module was demonstrated with a breadboard model. The module consists of a solid state switch to discharge the PFN. Figure 1 shows a functional block diagram of the module and peripheral circuitry.

The basic element of the switch is the Westinghouse T60R RSR. The RSR is a two terminal, four layer, PNPN semi-conductor switch. It is designed to be triggered by a rate of increase in anode-cathode voltage (dv/dt triggered). The device can conduct very high currents and also accomodate a very high rate of rise of current (di/dt).

The T60R RSR was developed and optimized especially for high energy laser pulsers under the sponsorship of the U.S. Air Force. Its characteristics are as follows:

Breakover Voltage	1200 Volts nominal
Pulse Current	5000 A in 20 µSec Pulses at 250 PPS
Forward Voltage Drop	10 V at 5000 A
Turn-On Time	100 nanoseconds
Recovery Time	200 µSec
Rate of Current Rise (dI/dt)	2500 A per µSec to 5000 A
Required Trigger dV/dt	5000 V per µSec

The T60R RSR is packaged in the Westinghouse R62 POW-R-DISC (sometimes referred to as "hockey-puck") cases, shown in Figure 2. External electrical connection is through pressure contact to the two opposing faces of the package.

MODULE DESIGN

Figure 3 shows the module breadboard circuit. It should be noted here that although the module was conceived for AC charging, DC resonant charging was used for test purposes. With the proper peripheral circuitry the module can be charged by either AC or DC methods.

The T60R RSR, which is the unit building block for the stack assembly, has a hold-off voltage capability of at least 1,100 volts. In switch applications, however, the actual per device operation voltage should not exceed 80% of this voltage, or about 880 V, to allow a margin against untriggered breakover. Hence, a 5,000 volt stack consists of six RSR's in series as shown in Figure 3.

Auxiliary components in parallel with each RSR support operation of the stack. The resistor across each RSR ensures proper low frequency voltage division across the stack. The resistor-capacitor circuit is a switching aide which provides energy to the individual RSR's upon triggering as well as dividing the trigger impulse among the RSR's in the series string. The reverse diode conducts reflected or reverse current around the RSR to protect the device from severe recovery transients which accompany high dI/dt pulses.

The T60R devices are packaged into a stack configuration by sandwiching them between heat sinks as shown in Figure 4. In the device and stack tests,

water cooled heat sinks were used to permit calorimetric heat loss measurements to be made. For use with the intended application, more sophisticated packaging and cooling can be employed to minimize switch size and weight.

STACK DESIGN CONSIDERATIONS

A. Circuit

The basic RSR stack assembly circuit as employed in the test pulser circuit configuration is shown in Figure 3. In addition to the RSR switch, this circuit consists of:

- Trigger blocking diode assembly D1
- Reverse diode assembly D2
- Reverse damping resistor R1
- Trigger coupling diode assembly D3
- A pulse forming network configuration Z1

The operating cycle for the circuit begins with the resonant charging of PFN Z1. The PFN voltage, which reaches 5,000 volts as a result of resonant charging, is supported by the RSR switch until the stack is switched on. Diodes D2 and D3 block this voltage and prevent a bleed-off through the trigger or backswing circuits. Turn-on of the RSR stack results from application of a very high dV/dt impulse through the trigger transformer and diode D3 to the top of the RSR stack. In response to this, the RSR's switch to the "on" state and discharge the PFN through the load resistor and diode D1. At the end of the pulse, reflections from the load are blocked from the RSR's by diode D1 and diverted through damping resistor R1 and backswing diode D2.

The individual diodes across the RSR's in the switch assembly are, unlike the high power diodes D1 and D2, small medium current diodes which reverse bypass the RSR's during switch transients and provide a voltage limiting path around the RSR's for the resetting current after device recovery.

B. Trigger

Triggering or turn on of the stack assembly occurs when a very high dv/dt impulse of sufficient amplitude is applied across the RSR's. In the circuit in Figure 3, this impulse is applied at the top of the RSR string and is divided among the six RSR's in the string by RC transient divider circuits. The more sensitive RSR's turn-on first leaving the available trigger voltage to divide among the fewer less sensitive devices. This increased trigger speeds up the turn on of these slower devices and completes the total stack turn on.

Switching of the RSR stack requires energy. The trigger circuit for a stack assembly must not only supply the required voltage but also to do so while supplying current or charge displacement necessary for the RSR device and circuit capacitance to follow this voltage. This factor means that the RSR switch has an inherent immunity to spurious noise triggering. Measurements on T60R devices have established 5 kV per microsecond as a minimum trigger dv/dt for high current operation. Under these conditions, the trigger circuit supplied 20 A for about 100 nanoseconds for a total energy of 0.002 Joules per pulse per device.

These requirements were established as being necessary for the RSR to turn on over its full junction area to switch 5,000 A pulses. Sufficient conditions to trigger the stack to partial junction area turn on may be much less but do not prepare the RSR for full current conductions and must be avoided.

BREADBOARD MODULE OPERATION

Figure 5 shows the lab breadboard test set-up. The breadboard module consisted of an RSR switch stack, PFN, air cooled non-inductive load resistor plus power supplies, timing, and trigger generators.

Module PFN characteristics were as follows:

- Pulse Width ..... 20 µSec
- PFN Characteristic Impedance ..... 0.5 Ω
- Load Resistance ..... 0.5 Ω
- Maximum PFN Storage Voltage ..... 6000 V
- Maximum Repetitive Pulse Current ..... 6000 A
- Pulse Rise Time ..... 2 µSec
- Pulse Fall Time ..... 3 µSec
- Maximum PRF ..... 300 PPS

Full power testing was carried out on three different RSR stack assemblies under both continuous full-load and single-shot shorted load conditions summarized in Table 1. The three stack assemblies operated successfully for repeated 30 second periods at full power of 5,000 A and 5,000 V at 250 PPS without the loss of a single RSR. The stack assemblies were also single-shot discharged into a short circuit repeatedly without RSR failure. Figure 6 shows the typical 20 microsecond pulse current through the T60R RSR's under both conditions.

Turn on time of the six device switch was 0.07 µsec to 0.12 µsec. All RSR's in the stack triggered nearly simultaneously. The turn on time for the stack of six devices was less than 20 nanoseconds greater than that for a single RSR.

The voltage on the RSR stack assembly was evenly distributed across all RSR's in the stack. Figure 7 shows the voltage from the top of each RSR to ground plus the bottom sweep showing ground noise on a stack of six RSR's. Figure 7a is a photograph taken between the times T_1 and T_2 on Figure 7b with time scale expanded 5,000 times and the voltage scale halved. The time T_0 is the beginning of the resonant charge of the PFN and T_3 is when the switch triggers.

CONCLUSION

A solid-state module was demonstrated to respectively switch 5,000 volts at 5,000 amps at a duty of 0.005, switching and average power of 62.5 kW at a peak of 12.5 megawatts. This module is well suited for the basic building block of a high energy laser pulser.

The technique is flexible since the switch may be constructed to hold-off virtually any voltage since this is a function of the number of RSR's used in the stack.

The RSR switch stack is particularly useful for switching high power at relatively low voltages as opposed to hydrogen thyratrons. It also has the advantage of "instant-on" with no warm-up time or standby power along with shock and vibration immunity.

ACKNOWLEDGEMENT

This paper was based on studies performed for the U.S. Air Force under contract number F29601-74-C-0021, Air Force Weapons Laboratory, Kirtland Air Force Base, Albuquerque, New Mexico.

REFERENCES

1. E. H. Hooper and B. L. Jordan, "Advanced Reverse Switching Rectifier (RSR) Modulator," Final Technical Report, Air Force Weapons Laboratory, Kirtland Air Force Base, New Mexico.

2. J. B. Brewster and P. F. Pittman, "A New-Solid State Switch for Power Pulse Modulator Applications, the Reverse Switching Rectifier, "IEEE Conference Record of 1973 Eleventh Modulator Symposium, September, 1973, New York, p. 6-9.

3. R. A. Gardenghi, E. H. Hooper and F. S. Zimmermann, "A New High Power RSR Solid State Switch", IEEE Conference Record of 1975 Power Electronic Specialists Conference, June 1975, Culver City, California, pp. 313-317.

4. R. A. Gardenghi, "A Super Power RSR", 1975 International Electron Devices Meeting Technical Digest, December, 1975, Washington, D.C., pp. 367-370.

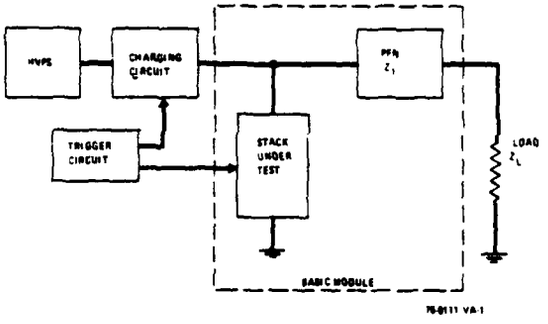

Figure 1. Block Diagram

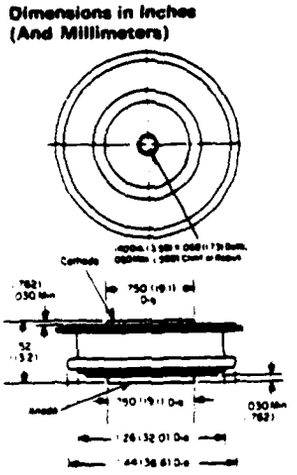

Figure 2. T62 Case Outline

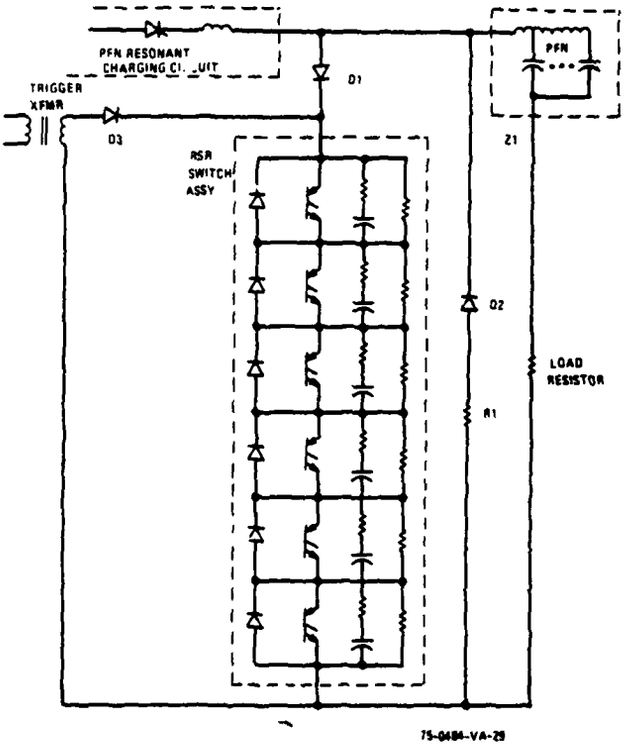

Figure 3. Module Breadboard Circuit

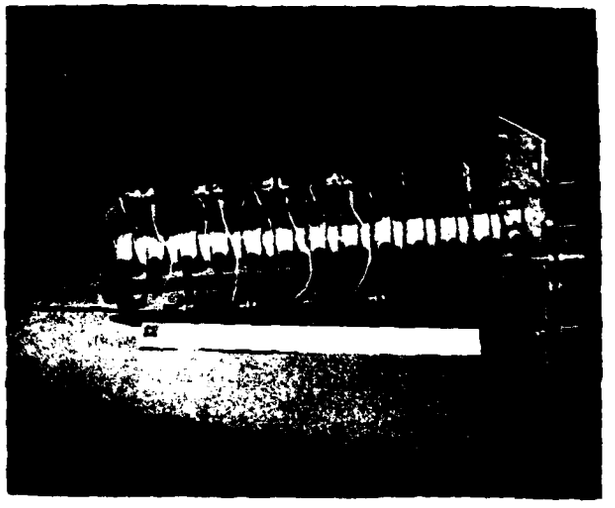

Figure 4. RSR Stack Assembly

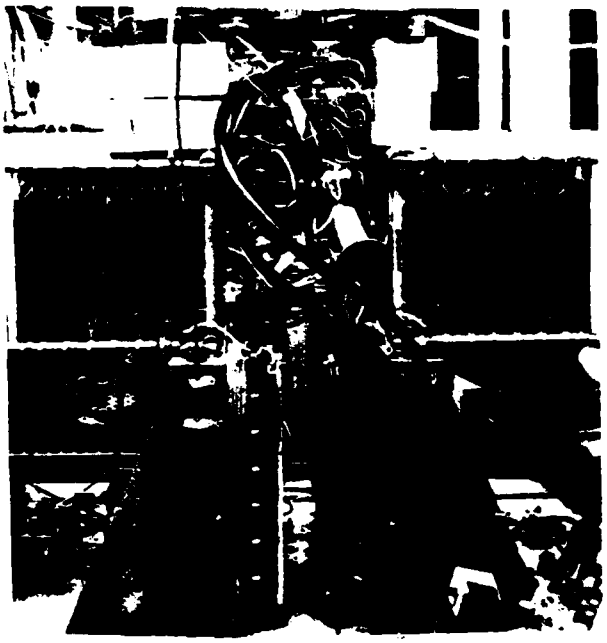

Figure 5. Module Breadboard

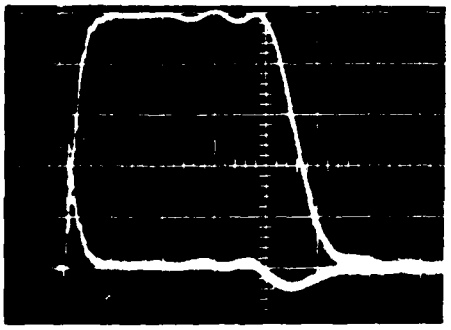

(a) Full Load Pulse Current (1000 A/Div Vert, 5 uSec/Div Horiz)

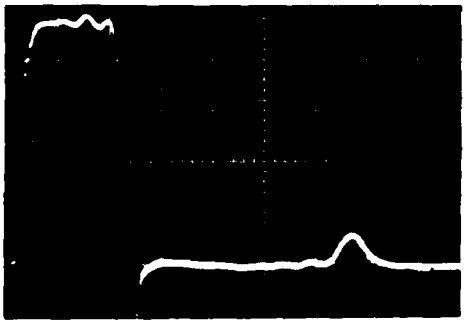

(b) RSR Stack Current Under Shorted Load Operation (2000 A/Div Vert, 10 uSec/Div Horiz)

Figure 6. Pulse Current Waveforms

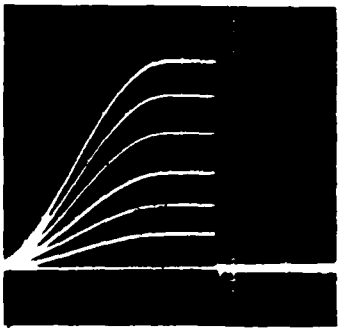

(a) PFN Charging: Vertical, 1000 Volts/Div, Horizontal 500 Microseconds/Div

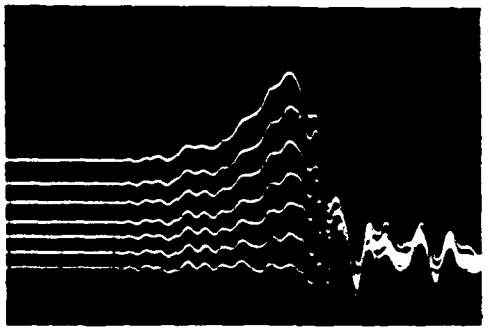

(b) Trigger Voltage: Vertical, 2000 Volts/Div, Horizontal, 0.1 Microsecond/Div

Figure 7. Six-Device Stack Voltage Distribution

TABLE I

Module Test Conditions

CHARACTERISTIC	CONTINUOUS FULL POWER OPERATION	SINGLE-SHOT SHORTED LOAD OPERATION	UNITS
PFN STORAGE VOLTAGE	5.0	5.0	kV
PEAK CURRENT	5.0	10.0	kA
AVERAGE CURRENT	26.0	-	A
PULSEWIDTH	20.0	20.0	μsec
REPETITION RATE	250.0	-	PPS
PFN CAPACITANCE	21.0	21.0	μF
LOAD IMPEDANCE	0.5	0.0	Ohm

76-0111-TA-2

MULTI-MEGAWATT SOLID-STATE SWITCH

Duard L. Pruitt
RCA Government and Commercial Systems
Missile and Surface Radar Division
Moorestown, New Jersey

Introduction

High-power pulsed radar or laser systems are projected to require input pulse power up to several gigawatts peak at relatively high duty cycles (up to 1/2%). Such heroic power levels require a combination of the outputs from a multiplicity of the largest known devices.

Since life, reliability, size, and weight are always important considerations, the application of solid-state devices is a preferable approach. Typical requirements are for 20 microsecond wide pulses, with 2 microsecond rise time, at 200 to 300 pulses per second. Continuous or intermittent duty may be required, depending on the application.

This paper gives the results of work at RCA which established the feasibility of using a multiplicity of small, commercially available thyristors to produce the required pulse power.

Background

In February 1973, the RCA Missile and Surface Radar Division was awarded a study contract by the Rome Air Development Center for a "High-Energy High-Duty Pulser." This contract was for a one-year, in-depth study on methods of achieving a high peak energy and high average-power pulser. Design objectives were for a 2.5 gigawatt peak and 10 megawatt average power continuous-duty pulser. Use of "off-the-shelf or near-state-of-the-art" components was a design requirement.

Emphasis was placed on selection of the type of switching device (hydrogen thyratrons versus spark gaps versus mercury pool devices versus solid-state devices, etc.) and on selection of a particular device of the chosen type. Hydrogen thyratrons were chosen over competing types of switches because suitable types were available off-the-shelf, whereas all of the competing types of devices required development work to meet the requirements.

During the switch survey, the potential advantage of solid-state switches became clear: flexibility, reliability, compactness, no standby power, and competitive economically. Correspondence with investigators at RCA's David Sarnoff Research Laboratories led to a more detailed analysis of solid-state possibilities with the RCA Solid State Division.

As a result of these analyses, solid-state switch development was pursued on internal RCA projects during late 1973 and early 1974. Results of these projects were encouraging, leading to Air Force interest and a development contract from RADC. A major objective of this RADC contract was to develop a 30 megawatt peak-power, 150 kilowatt average-power switch, suitable for generating 20 microsecond pulses at 250 pulses per second with 2 microsecond (maximum) rise time.

Preliminary Solid-State Investigations

General Comments

Power transistors are generally inappropriate for use as switches in super-power short-pulse modulators, mainly because the peak capability of a power transistor is little higher than its DC capability. This characteristic leads to an inefficient use of silicon, resulting in a large and unreasonably expensive switch. Also, transistors are more susceptible to damage from fault current than are thyristors.

Power thyristors tend to be limited by rms current rather than peak current, and are thus more appropriate for design of a relatively small, low cost pulse switch. Power thyristors are limited in pulse current rise time because of slow spread of current across the silicon chip after the gate is triggered. This characteristic (slow rate of current spreading) can cause localized chip overheat for rapidly rising current pulses -- the well known *di/dt limit*. Large power thyristors are more susceptible to di/dt limitations than are small, low-power thyristors. A variety of interdigitated and regenerative gate designs have been developed to enhance high frequency performance. However, at the present state of the art, it appears that relatively small chips (up to 0.2 inch diameter and 35 amperes rms rating) have a definite performance edge over larger devices for pulses with rise times up to 2 microseconds.

RCA Solid-State Devices

The initial interest was centered on the RCA S3700M/ RCA S3703SF family of TV deflection thyristors. These are 5 ampere rms thyristors in a TO-66 case with voltage ratings up to 750 volts (absolute maximum). In the initial investigation, type RCA S6431M was also considered. The S6431M is a TO-48 stud mounted, pulse rated SCR: up to 900 amperes peak and 35 amperes rms with 600 volts DC blocking voltage. However, the S6431M is a low volume, high cost device, so attention was turned to its "parent" device, the high volume 2N3899 family. The 2N3899 (or its press fit equivalent, the 2N3873) is priced at less than $5 each in large quantities. A dark horse candidate, the RCA S2600M (a 600 volt, 7 ampere rms, thyristor in a TO-5 can) was also considered.

Pulse dissipation tests were run on these three types, with results given in the next section of this paper.

Device Selection

Arrangements were made with the RCA Solid State Division to make pulse dissipation tests on the device families noted: RCA S3700M, RCA S2600M, and 2N3899. From these tests, tentative ratings were derived, thus allowing cost and size tradeoffs to be made in order to select the best device for further work. The tests were made using 20 microsecond pulses, with rise time up to 2 microseconds, and a low repetition rate.

A short summary of the results is given in Tables I and II.

TABLE I. 20 MICROSECOND DISSIPATION/PULSE

Peak Current (Amps)	Energy Dissipation (millijoules/pulse) (2N3899)	(S3700M)	(S2600M)
200	20	55	--
400	100	--	112
600	150	--	--

TABLE II. SINGLE-PULSE BURNOUT (20 MICROSECOND PULSE)

Device Type	Single Pulse Burnout (amps)
2N3899	≥ 2000
S3700M	≥ 1000
S2600M	≥ 1000

The "Single Pulse" data from Tables I and II were translated into tentative ratings for a 20 microsecond pulse, 250 pulses/second operation as follows:

TABLE III. TENTATIVE DEVICE RATINGS

Device Type	Amperes Peak	Amperes rms	Power Dissipation Watts	θJS °C/W	Temp. Rise °C
S3700M	150	10.6	7.5*	7	52
S2600M	200	14.1	7.5	5	38
2N3899	600	42.4	37.5	1.4	52

*Extrapolated

Note that, since dissipation is roughly proportional to the current squared, the tentative ratings in Table III cannot be increased significantly. For example, extrapolating the S2600M data to 300 amperes peak gives an uncomfortable temperature rise of 80°C.

Examining the data, it is seen that one 2N3899 can replace four S3700M's or three S2600M's. The significantly higher parts count with the smaller devices seems certain to make a S3700M or a S2600M modulator more expensive than a 2N3899 modulator. Further, relative package sizes would indicate that a 2N3899 modulator would be smaller in overall size. Therefore, the 2N3899 (stud mount)/2N3873 (press fit) family was selected for further work.

Sub-Module Design

After much deliberation it was decided to build up a switch "module" in two steps:

1. Construct a "sub-module" by paralleling a number of individual devices on a common anode plate.

2. Connect a number of "sub-modules" in series to obtain the desired voltage capability.

Figure 1 is a schematic of the sub-module as it was developed after an evolutionary period of many months. Ten type 2N3873 thyristors are pressed into a common anode heat sink (ten is an arbitrary number; any convenient number up to probably several dozen may be paralleled). A pilot thyristor, SCR1, provides gate drive to the ten main thyristors by switching the voltage on C1 onto the common gate bus. C1 is charged to the sub-module anode-cathode voltage. Gate isolating resistors R2 through R11 ensure a proper overdrive (2 amperes peak at the nominal 500 volt operating level) into each of the main thyristor gates. Diodes D2 through D11 provide further gate isolation, preventing feedback from a leaky or shorted thyristor to the gate bus. Inductors L1 through L10 are straight No. 18 bus wires, each approximately 4 centimeters long, which connect the ten main cathodes to the next anode plate for a series stack. Fuses F1 to F10 provide automatic disconnect of an individual failed thyristor.

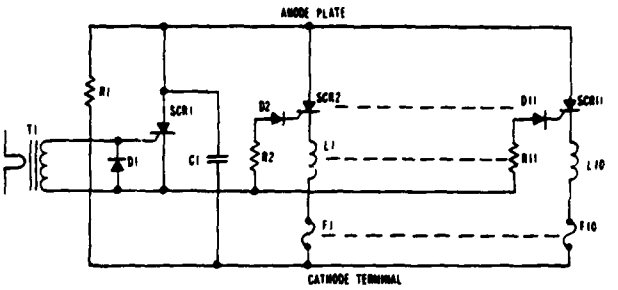

Figure 1. Parallel SCR Switch

The pilot thyristor SCR1, an RCA S2600M, is normally triggered by a nominal 1 ampere peak, 5 microsecond pulse from current transformer T1. The secondary of T1 has 50 turns of magnet wire on a small (CF111-Q1) ferrite toroid. In a series stack of sub-modules, a 50 ampere (peak) primary pulse is conducted through a single turn primary which links all of the toroids in series. The primary turn is a silicon rubber-insulated high-voltage wire.

Early versions of the sub-module were constructed using the stud mounted 2N3899 thyristors on a water-cooled copper plate. Later versions were constructed using press-fit 2N3873 thyristors on a water-cooled aluminum plate. Figure 2 is a photograph of this latter version.

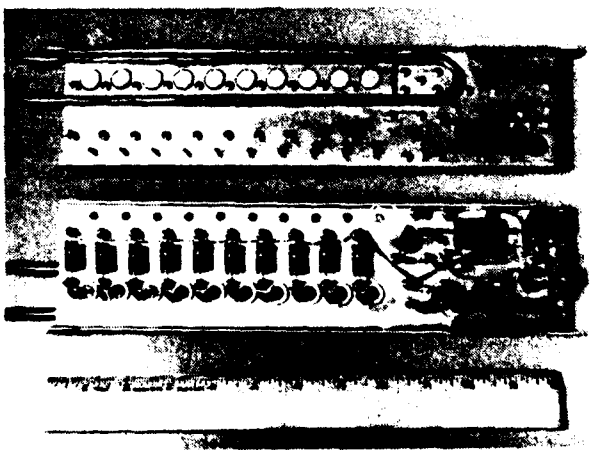

Figure 2. Parallel SCR Switch

These sub-modules have been extensively tested[1] in a conventional artificial line type modulator circuit with the following characteristics:

Pulse width	20 microseconds
Current rise time	2 microseconds
Peak pulse voltage	600 volts
Peak pulse current	6000 amperes
Load resistance	0.05 ohms
Peak power	1.8 megawatts
Repetition rate	250 pulses per second
Average power	9 kilowatts

Using RCA 2N3873 thyristors selected at random from a lot of 1000 units containing two different date codes, current sharing among ten paralleled thyristors typically fell within ±20% of the average value. Two continuous runs of 8 hours each were made at the given conditions. In destructive tests, the devices exhibited remarkable toughness: at least four, and sometimes five of the ten devices had to be removed (by clipping the cathode leads) before failure occurred among the remainder in a 5 minute test. Typically, soft solder melted at the cathode connection before device failure occurred in these destructive tests.

Series Switch Tests

6 Megawatt Switch

Four sub-modules, constructed as described above, were arranged in series to form a switch rated at 2000 volts peak, 6000 amperes peak, 6 megawatts peak power, 30 kilowatts average power. This switch was tested for brief periods with satisfactory results.

12 Megawatt Switch

Four additional sub-modules were constructed and added in series with the previous four units to make a 4 kV switch. This switch is rated at 4 kV, 6 kA, 12 MW peak, and 60 kW average. An artificial line type modulator test set was constructed. Measured pulse parameters were: 17 microseconds width at 1/2 power points; 1 microsecond rise time (10% to 90%); and 5 microsecond fall time (90% to 10%). Normal PRF was 250 pulses per second, giving a duty cycle of 0.00425. "Full power" operation was 6 kA peak, 12 MW peak, 25 A average, and 50 kW average (average was limited by power supply rating.)

This test set (and the 4 kV switch) was tested extensively in the first half of 1974. Heating of the PFN capacitors limited continuous runs to about 45 minutes. The thyristor switch operation was very encouraging.

Since the switch in a line type pulse modulator must be capable of conducting twice normal current during load fault (short), a series of "shorted load" tests was made. The fault sensing circuit detects a load fault in a few microseconds and inhibits the following charging switch pulse. The triggers could be reset manually at any time after a one second delay. In a series of tests the 4 kV switch was capable of withstanding the double current pulses and the resulting high peak inverse voltage without failure. The test was made by shorting out the coaxial load with a short (≈ 2 cm) copper strap during an otherwise normal operation. Repeated shorting tests were made at full power. Upon manual reset, normal operation was resumed. Since the power supply regulation is approximately 10%, reset at full power is initially at a 10% over voltage.

30 Megawatt Switch

In 1974 the Air Force awarded RCA a contract[1] to construct and test a 30 megawatt switch.

Twenty sub-modules were constructed, using ten type 2N3873 press-fit thyristors in parallel in each sub-module; the 20 units were connected in series to form a 10 kV peak voltage, 6 kA peak current switch (Figure 3). A modulator was constructed, similar to that used in the previous test sets, to permit testing this switch to 30 megawatts peak power and 150 kilowatts average power (see Figure 4). This test set was not suitable for full power arcing load tests because of the limited voltage rating (9.6 kV absolute maximum) of the thyristor charging switch, but was otherwise capable of full 150 kW average power operation.

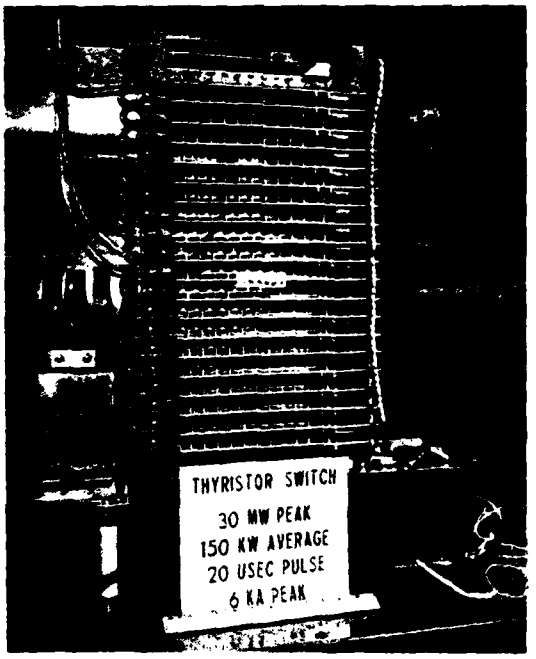

Figure 3. Thirty Megawatt Switch

This switch has been operated for short periods (up to 5 minutes) at the full design power levels (the thermal time constant of the thyristor switch is short compared to 5 minutes). With water cooling provided, the switch heat sink temperature rise was only a few degrees Centigrade. Longer operational periods were precluded by the danger of overheating test set components, particularly the pulse forming network capacitors.

Levels achieved were:

Peak switch voltage	10 kilovolts
Peak switch current	7000 amperes
Peak load power	32 megawatts
Average load power	160 kilowatts
Pulse width	20 microseconds

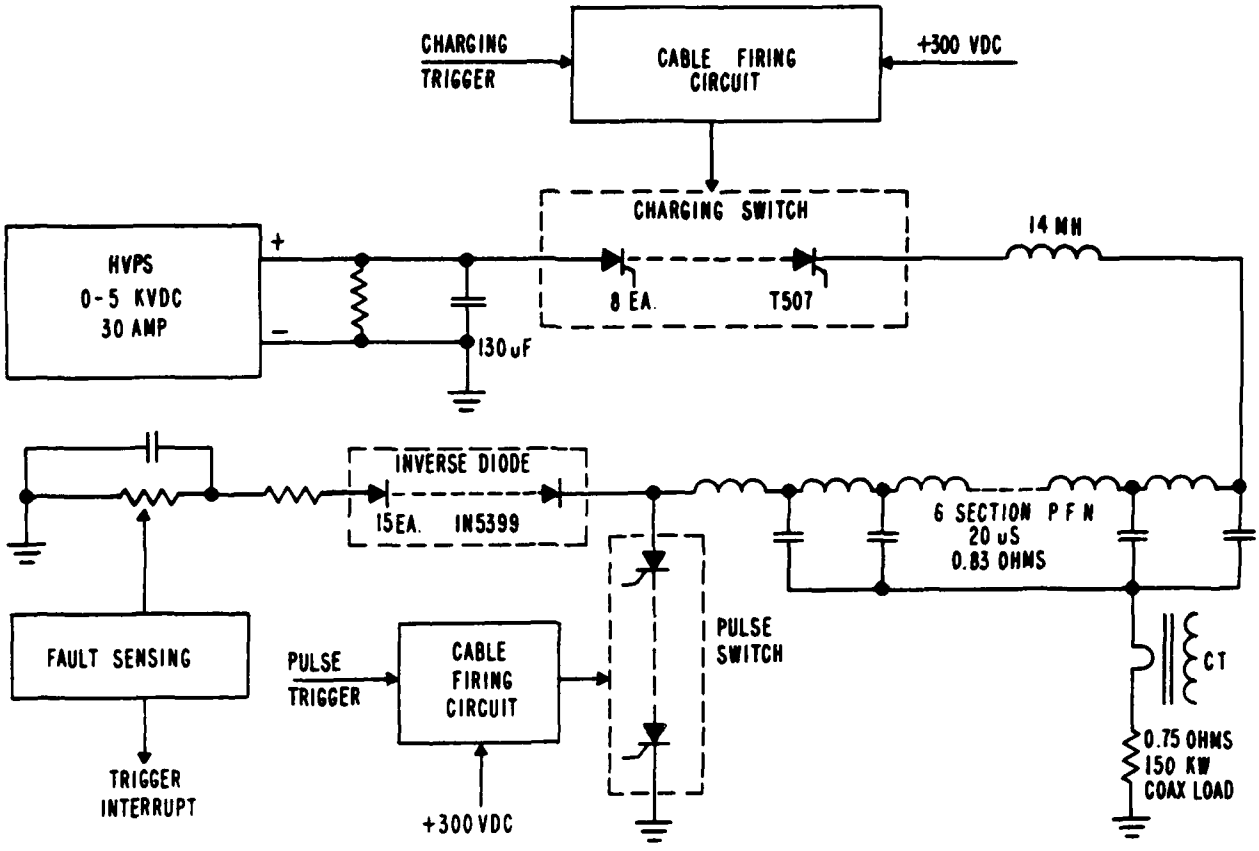

Figure 4. Thirty Megawatt Test Modulator

Current rise time (10% to 90%)	1.7 microseconds
Repetition rate	250 pulses per second

15 Kilovolt Switch

Under a contract extension from RADC[1], the 10 kV switch described above was extended to a 15 kV switch by adding 10 additional sub-modules in series to give a total of 30 series sub-modules. A photograph of this 15 kV switch is shown in Figure 5.

Because of test set limitations, this switch could not be tested to its full inherent capabilities of 45 megawatts peak and 225 kilowatts average power. Using a modification of the test set of Figure 4, the 15 kV switch was tested to the following parameters:

Pulse width	10 microseconds
Current rise time	0.8 microsecond
Peak PFN voltage	15 kilovolts
Peak load current	4700 amperes
Peak load power	30.9 megawatts
Repetition rate	285 pulses per second
Average load power	88.1 kilowatts

The switch was repeatedly snapped on and off at full power, demonstrating instant full power availability without

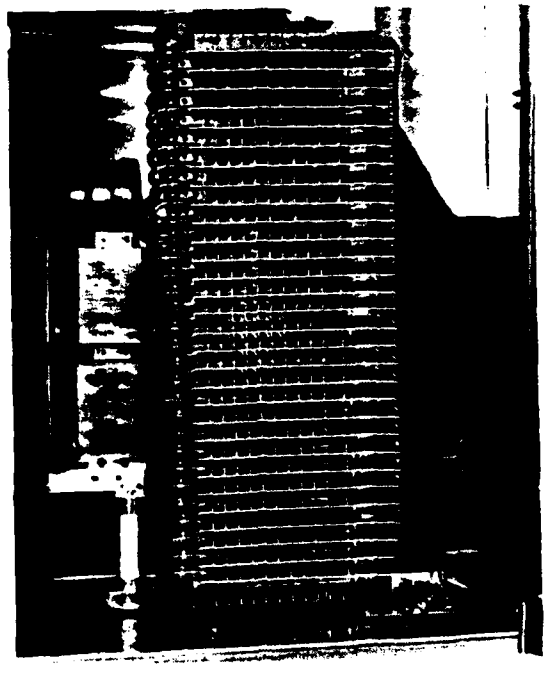

Figure 5. Fifteen Kilovolt Switch

warmup. Continuous runs were again limited to about 5 minutes by component (PFN capacitor) heating. Figure 6 shows switch current and voltage waveforms during the pulse.

Switch Current: 1 kA/Division
Switch Voltage: 5 kV/Division
Horizontal: 2 μsec/Division

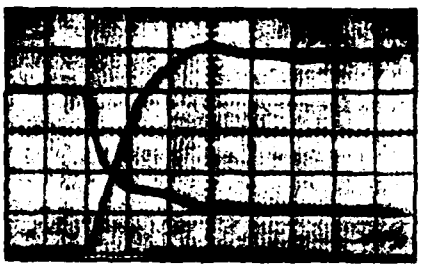

Expanded Time Scale:
Switch Current: 1 kA/Division
Switch Voltage: 5 kV/Division
Horizontal: 0.5 μsec/Division

Figure 6. Switch Current and Voltage Waveforms

Conclusions

The work described herein proves that the 2N3899/2N3873 family of thyristors can be operated in series/parallel arrangements to obtain very high peak pulse power with pulse rise times of up to 2 microsecond. A 30 megawatt peak, 150 kilowatt average power operation was demonstrated using 200 thyristors in a 10 parallel/20 series combination. Cost of the thyristors in the 30 megawatt switch is under $1000, which is competitive with other pulse switch costs (hydrogen thyratrons, tetrodes), even after a generous allowance for other parts and fabrication.

Acknowledgments

The following people at RCA contributed significantly to this program:

E. O. Johnson (David Sarnoff Research Laboratories)
E. M. Leyton (David Sarnoff Research Laboratories)
G. Albrecht (Solid State Division)

[1]This work sponsored by the Air Force Systems Command's Rome Air Development Center, Griffiss AFB, N.Y.

A SYSTEMS APPROACH TO LIGHTWEIGHT MODULATOR DESIGN FOR AIRBORNE APPLICATIONS

Major F. S. Zimmermann
Capt J. D. Miller
Mr. J. P. O'Loughlin
Air Force Weapons Laboratory
Kirtland Air Force Base, New Mexico

Dr. T. R. Burkes
Texas Tech University
Lubbock, Texas

A preliminary design of an airborne modulator has been performed to achieve the least overall system weight for an airborne pulse power source for high power gas discharge studies. The modulator is modular in design to allow for direct AC resonant charging from a dedicated synchronous alternator. This eliminates the need for intermediate power conditioning or rectification. Extra modules are used to load the alternator during pulse output to eliminate pulse repetition rate load transients on the alternator. This scheme requires a special purpose alternator specifically designed to drive a leading power factor load. The alternator weight is decreased due to the reduction in excitation required for aiding armature reaction loads. The modulator is basically an "artificial line" type modulator which uses a pulse transformer to increase voltage and combine the output of the multiple modules. The pulse transformer geometry is optimized to minimize weight and take the gas discharge into account in the design of the pulse forming network and transformer reactances.

Introduction

A great deal of information has been written about the importance of the systems approach in designing optimal systems. The heart of the matter, of course, lies in the fact that a system which consists of optimal components does not necessarily represent the optimal system. On the contrary an optimal system will more than likely contain components which are not optimum in the sense that they are not the most efficient devices for accomplishing the functions which they are most commonly used for. Innovation and creativity are called for in the design of optimum systems. Such inventiveness abounds in the realm of mass produced electronics but is less prevalent in one-of-a-kind systems. The reason for this lies in the trade off of cost versus requirements. In fact economics tends to drive designers of one-of-a-kind systems to the use of common components in their most traditional application as long as minimum requirements can be met with such an approach.

System Engineering

The topic of this paper is the design of a one-of-a-kind system which has severe weight and volume requirements due to the fact that it is for an airborne application. The use of common components in a traditional fashion is unacceptable in this application because the weight and volume associated with such designs would exceed maximum weight and volume requirements many times over. The overall system to be optimized for weight and volume is some combination which will provide pulsed high power at relatively high voltage (60 Kv) for a short duration (30 to 60 seconds). There are many ways to accomplish this, the following power sources were considered; MHD, superconducting and conventional alternators, direct drive alternators, and electrochemical devices such as lightweight batteries and fuel cells. Source selection criteria was based on several factors:

1. Good power to weight ratio (KW/LB).
2. Technology required to develop the candidate sources to a reliable source ($).
3. Integration of candidate source into the pulsed system (interface requirements).
4. Operational aspects of the candidate source in the system as a whole (voltage of the candidate source, start characteristics, etc.).

The combination considered for the paper will be the conventional alternator, power conditioning, and load as shown in Figure 1.

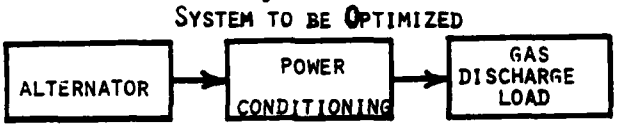

FIGURE 1

Overall system optimization included the rotational input necessary to propel the alternator. A detailed discussion of the selection of this energy source has not been presented here as it is considered to be beyond the scope of this paper. Briefly, however, the prime mover for this system is assumed to be a monopropellant rocket turbine with a drive gear box which allows latitude in the selection of the alternator speed.

Direct Application of System Engineering

The key ideas in the following discussion are the use of a special purpose alternator specifically designed to drive a leading power factor load, and the use of extra pulse forming networks (PFN's) to load the generator in a manner which avoids pulse repetition rate (PRR) transients on the alternator. A lighter system weight results from the incorporation of these ideas into the system.

Alternator Design

The voltage output of the alternator was determined by load requirements, pulse transformer characteristics, and EMI considerations. The generation of power at the load voltage which is in excess of 50 Kv was found to be impractical. It was therefore necessary to consider pulse transformers or voltage multiplication techniques. Low source voltage implies very high switching currents on the primary side of the pulse transformer and thus stringent magnetic shielding requirements. High source voltage implies spacing and/or excessive pressurization within the confines and high altitude operation of an aircraft. For these reasons a charge voltage of 15 Kv was chosen as a compromise. Heat sinking of the alternator was found to be the optimum method of cooling the alternator. If the run times are expected to be greater than about two minutes with high power levels, forced cooled alternators must be considered. The exact choice of other alternator parameters depends on the pulses repetition rate and pulse energy. Several independent studies indicated that a rather broad minimum in

alternator weight of classical design occurs in the vicinity of 1000 Hz. Operating in the vicinity of 1000 Hz does not effect the power conditioning weight or volume greatly as the alternator weight difference tradeoff overrides the other system component weight.

Power Conditioning

Power conditioning provides the interface between the alternator and the load. The power conditioning must provide a load for the alternator as well as shape of the pulse. A classical "artificial line" type modulator with an output pulse transformer was considered initially and later compared to voltage multiplication circuits such as Blumleins and Marx generators. The pulse transformer method was still favored after the comparison. Alternator loading may either be done directly thereby charging by A.C. or indirectly by using diodes and charging by D.C. Pulse shaping is handled by a standard PFN. To match the load requirement the PFN feeds a pulse transformer.

Charging Scheme

The choice of PFN charging scheme was determined by several factors:

1. Interface Complexity
2. Pulser Repetition Rate
3. Alternator Impact
4. Fault Control

Because of the nature of the load, command charge control is necessary. This part of the interface is therefore a fixed constraint of the design. Obviously, resonate charging must be used for minimum weight.

D.C. Resonate Charging A D.C. charging scheme requires rectifiers, filter, and command charge or simply a rectifier with phase control and charging reactor. The latter scheme represents a simpler choice if ripple can be tolerated. However, this scheme would introduce a strong torque harmonic into the alternator drive system at the PRR. Also, an alternator designed for a rectifier should have a very low internal impedance to efficiently drive the resulting lagging power factor load.

A.C. Resonate Charging An attractive alternative to the D.C. charging scheme is a A.C. resonate charging scheme. This method is discussed in detail in the Massachusetts Institute of Technology Radiation Laboratory series. By using several PFN's per phase a relatively smooth loading of the alternator could be achieved. Also, by loading each phase separately (line to neutral) the internal inductance of the alternator forms part of the resonate circuit. Thus, if the internal inductance of the alternator can be utilized for part or all of the charging reactor, a system simplification can be achieved with the possibility of weight reduction. This method has been proven under USAF Contract #F29601-74-C-0055 with Garrett/AiResearch Corporation. The weight reduction is due to a tradeoff within the alternator. Since, the object is to put more inductance in the alternator rather than keep it at a minimum, a very favorable track between iron and copper results so that an A.C. resonate alternator is significantly lighter in weight than the required D.C. alternator. Other system benefits occur as a result. Alternator fault currents are not significantly different from load currents and the resulting fault torques reflected into the drive train are minimized. As an example, by using 5 PFN's per phase with 3 phases and an alternator frequency of 1000 Hz, a repetition rate of 500 Hz could be obtained by discharging only 12 PFN's at a time. The alternator shaft load is relatively smooth due to continuous loading by 15 PFN's and the discharge of 12 while the remaining 3 are being charged. The individual capacitance to be charged is compatible with realizable alternator inductance. The switches required to discharge the PFN's are within the state-of-the-art as well.

Timing

Precise timing and execution is required for the A.C. resonant charging method. The control system must be capable of knowing precisely the shaft location or displacement to control the charging switches. If phase control is to be applied to limit surges or voltage overshoots an even more precise controller will be required. The discharge window must be monitored by the controller as well; to ensure the power conditioning is not charging and discharging the same PFN.

Charging Every positive and negative half cycle of each phase is loaded by a PFN. For maximum voltage (and power) transfer charging would start at the 0 volt cross-over points. During operation it may be desirable to regulate the peak charging voltage and this may be done by using phase control on the charging switches. Initiation of charging later in the half cycle rather than at cross-over would provide a lower absolute peak charging voltage. For this reason initiation of charging must be precise to ensure proper PFN voltage. As the number of electrical phases of the alternator increases the possibilities of freedom in design also increases. For simplicity, we have chosen a 3 phase machine for this paper. The timing required is within the state-of-the-art for a 3 phase machine and the power delivered from such a unit is adequate. Figure 2 shows a timing circuit of 6 PFN's. Using a total of 6 PFN's, two PFN's per phase and 3 phases, requires a total of 6 charging switches. Each individual PFN is charged sequentially on each half cycle. Figure 3 shows a charging diagram for 39 PFN's for 3 phases. Figure 4 shows the timing required for a 6 phase machine with 42 PFN's for comparison. As can been seen the timing requirements are significantly increased. The number of PFN's required depends on the several requirements: power, discharge repetition rate, weight, and alternator frequency. See Table 1 for these tradeoffs.

TABLE I

PRR VS PFN FOR A 3 PHASE ALTERNATOR

Possible PRR	Number of PFN's
$2x$	6
$2x, x$	9
$2x, x, \frac{x}{2}$	15
$2x, x, \frac{x}{2}, \frac{x}{3}$	21
$2x, x, \frac{x}{2}, \frac{x}{3}, \frac{x}{4}$	27
.	.
.	.
.	.
$2x, x, \frac{x}{2}, \frac{x}{3}, \frac{x}{4} \cdots \frac{x}{N}$	$6N + 3$

WHERE: X = Alternator Frequency
N = An Integer

CHARGING DIAGRAM FOR 6 PFN'S
WITH 3 PHASES

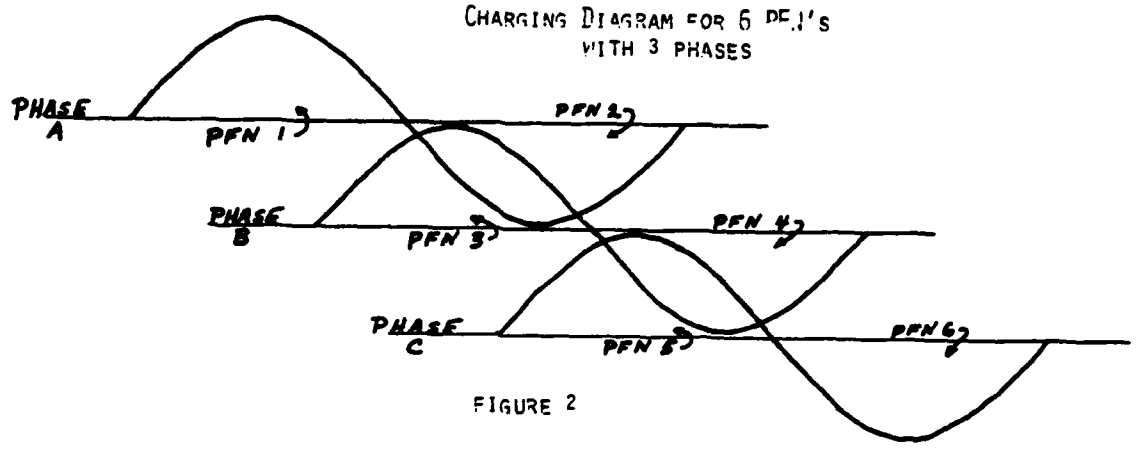

FIGURE 2

CHARGING DIAGRAM FOR 39 PFN'S WITH 3 PHASES

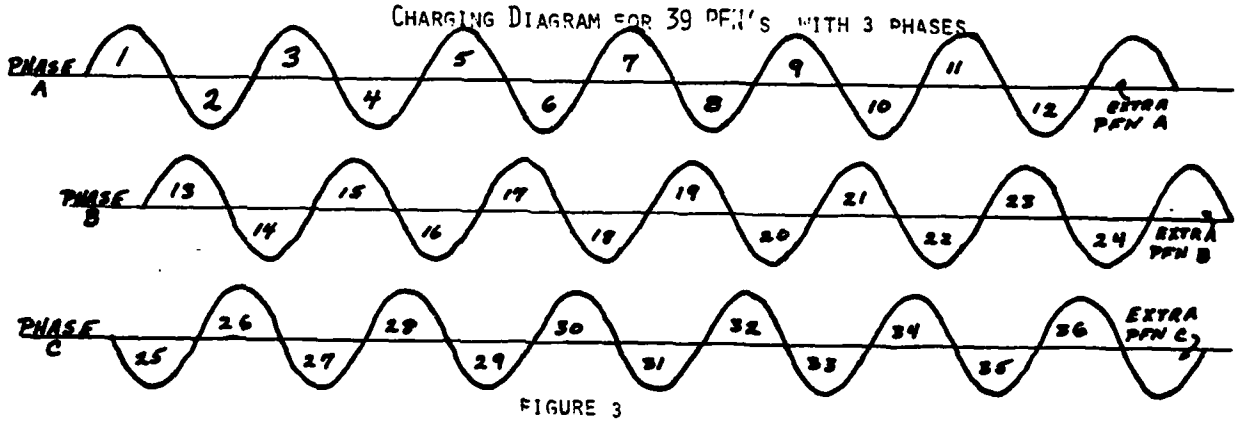

FIGURE 3

CHARGING DIAGRAM FOR 42 PFN'S WITH 6 PHASES

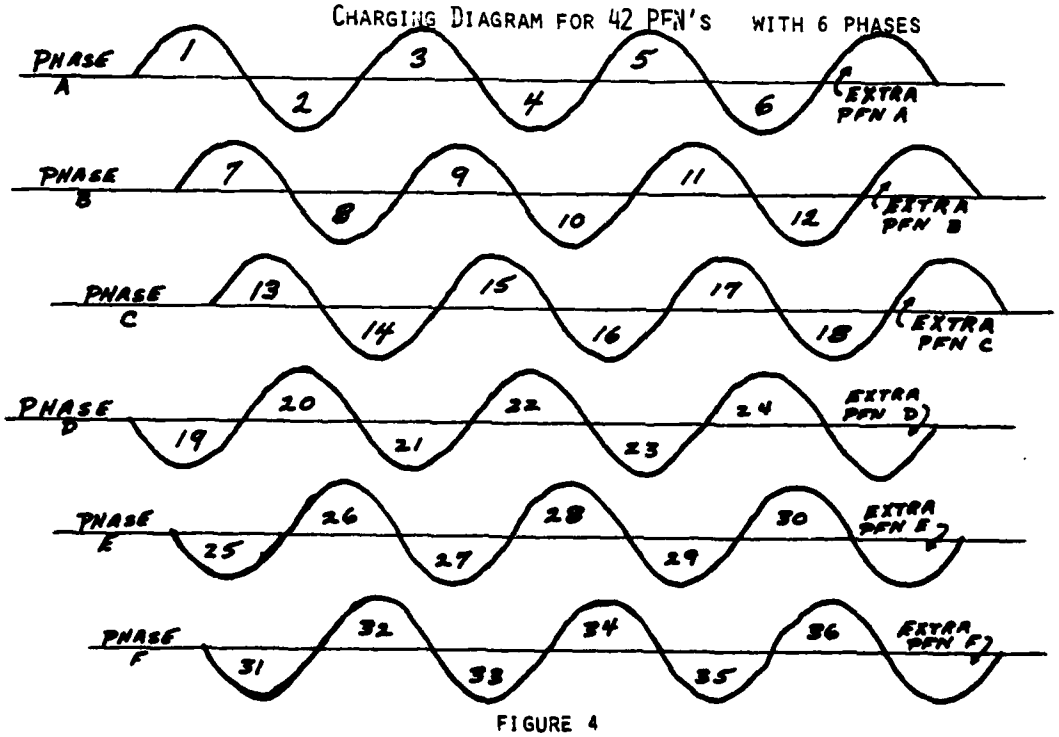

FIGURE 4

Controls Sensing of 0 volt crossover points is required in order to control precise charging times. This will require a sensing coil in the alternator as the actual voltage and current output signals will not be well formed. There may be some differences between the terminal phase and the sensing coil phase, this difference would have to be preprogrammed in the controller circuitry. During a start the phase displacement would be zero, but then shift after full speed was obtained. Monitoring of the final output could be used also as a feedback item to control the charging voltage if phase control is used (this would imply a substantially more complex system). The control system must detect faulted PFN's and may change the charging sequence accordingly. Furthermore, after a load fault the system must be reinitialized as the PFN's may have reverse charge, thereby making the controls the most complex portion of the pulser. After charging the charging switch will be off (non-conducting) until after its PFN is discharged and the switch has been commanded by the controller to again charge at the appropriate time. In this manner the alternator may be loaded at all times. Before the charged PFN may be recharged a discharge cycle must have occurred. This paper considers a 3 phase system, however if a 6 phase system were used, for instance, with the same alternator frequency the discharge window would be cut in half. The controller must also ensure that the correct PFN's are discharge at the proper time. The entire high power system should not have need of external electrical power, however the controller will require auxillary power. This typically could be a few kilowatts of 400 cycle aircraft power.

Discharging Charging 3 PFN's per phase and discharging 2 PFN's per phase allows the alternator to remain loaded at all times. If 3 were charged and 3 discharged the discharge rate would be reflected back into the mechanical system, which may lead to a early mechanical failure. The extra PFN per phase allows charging while the rest are discharging when at the higher repetition rate. Figure 5 shows a timing diagram both charging and discharging for this system. As in Table 1, the maximum energy storage per pound while using 3 phases occurs when the PRR = $\frac{X}{N}$ and the number of PFN's = $3(2N + 1)$. More than one extra PFN per phase while discharging decreases the energy storage per pound. Generalized to the multi-phase case these equations become PRR = $\frac{X}{N}$ as before, and the number of PFN's = $\emptyset\ (2N + 1)$ where $\emptyset$ becomes the number of phases in the alternator, in some applications, such as electric discharge lasers, several separate loads are required. This adds another complexity to the control system to ensure that the PFN's for both loads have been charged. Discharging must be timed precisely, particularly in the case of multiple loads.

Components

The power conditioning contains several critical components; charging switches, discharging switches, and the PFN's. A schematic of a 9 PFN pulser with 2 loads is shown in Figure 6.

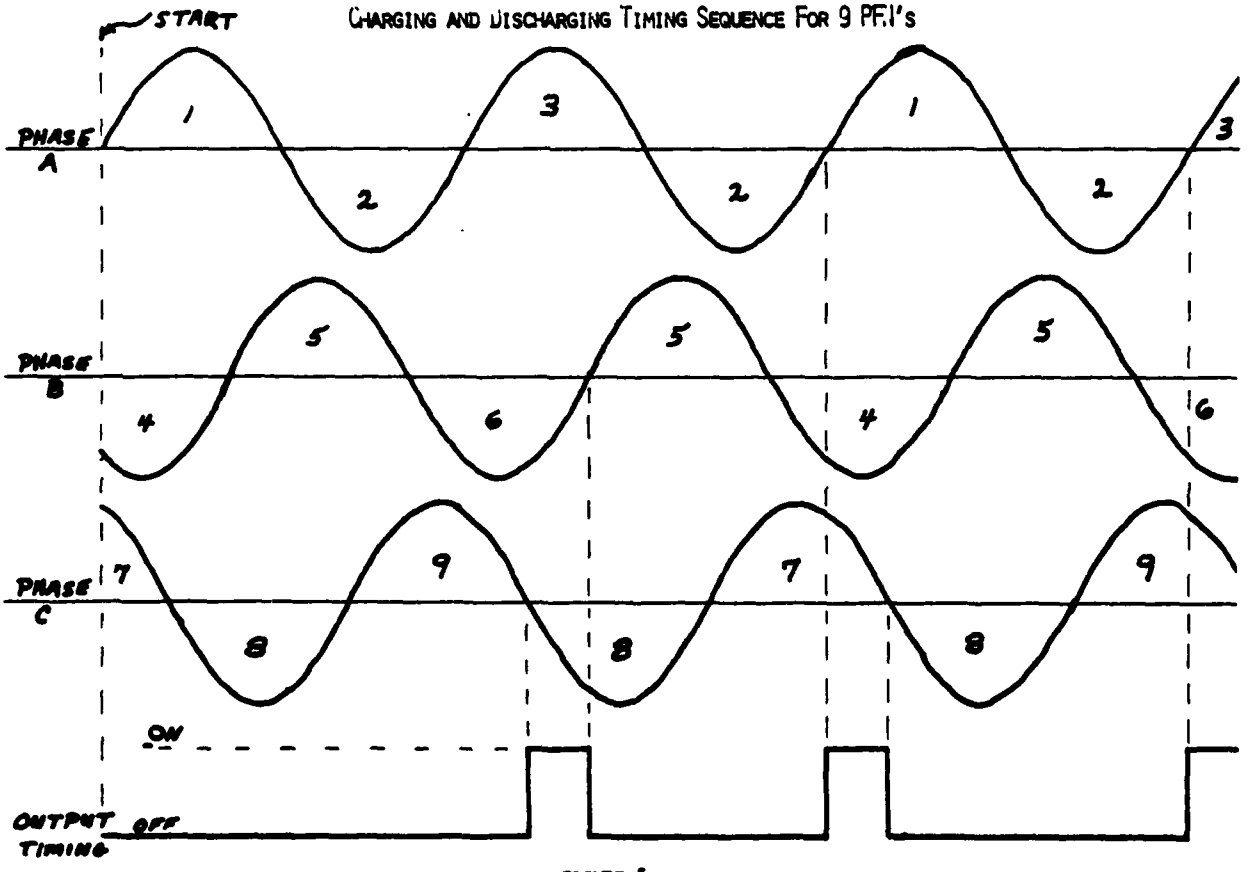

FIGURE 5

Charging Switch

The charging switch is the direct link between the alternator output and one of the PFN's. For this reason it must be capable of safely isolating the alternator and provide a high current rating to charge the PFN. The reverse hold-off voltage must be twice the charging voltage due to the condition of a fully positively charged PFN being on one side of the switch when the alternator swings fully negative on the other. An additional rating should be provided for fault conditions and safety. Peak charging currents of several hundred amps will be necessary to provide ample power transfer in reasonable times for a typical megawatt application. As discussed earlier, control of the switch is also important, being able to turn on-and-off the switch when required. This switch must be capable of substantial average current as the system may have a PRR of up to a few kilohertz. Heat dissipation must also be considered as well as volume and weight. No actual "off the shelf" switch can fulfill all these requirements, but a silicon control rectifier (SCR) is an attractive option. The desire to have the ability of instant turnoff is not possible with SCR's as they must go through a zero crossing. However, this does not appear to be a real problem as the alternator would operate at around 1000 Hz. In order to obtain reasonable voltage stand-off stacks of SCR's would be required. A typical number would be 60 per stack. A rather elaborate method of stacking would be required in order to maintain a good voltage gradient under all conditions as well as to provide a trigger to each of the SCR's. In order to carry the peak current loads, several SCR's can be paralleled on each layer of the stack. Stacking of the SCR's is complex, however laboratory versions of this method have been built and tested with satisfactory results from an Air Force Contract #F30602-74-C-0195 with RCA. A lightweight version of these assemblies would be desirable and indications are that this can be done rather easily. The SCR assembly is compatible with phase control as they may be turned-on later in the cycle. The lightweight version of this switch assembly would weigh typically about 2.9 kilograms (6.5 pounds) as each SCR would require about 20 grams of heat sink plus 4 grams of structure and triggering circuit. The remaining weight consists of the devices themselves. A typical volume for this lightweight switch assembly would be $4.9 \times 10^3 cm^3$ ($300 in^3$). These lightweight assemblies do not require any technology programs but rather just repackaging.

PFN

Typical applications require a rather square pulse. Since rectangular pulse generation is common, detailed analysis will not be presented. Rise times of 2 microseconds and fall times of 4 microseconds may be expected on a 20 microsecond power pulse. Within this section, PFN requirements and consideration will be discussed first, followed by a discussion of a PFN which has been built.

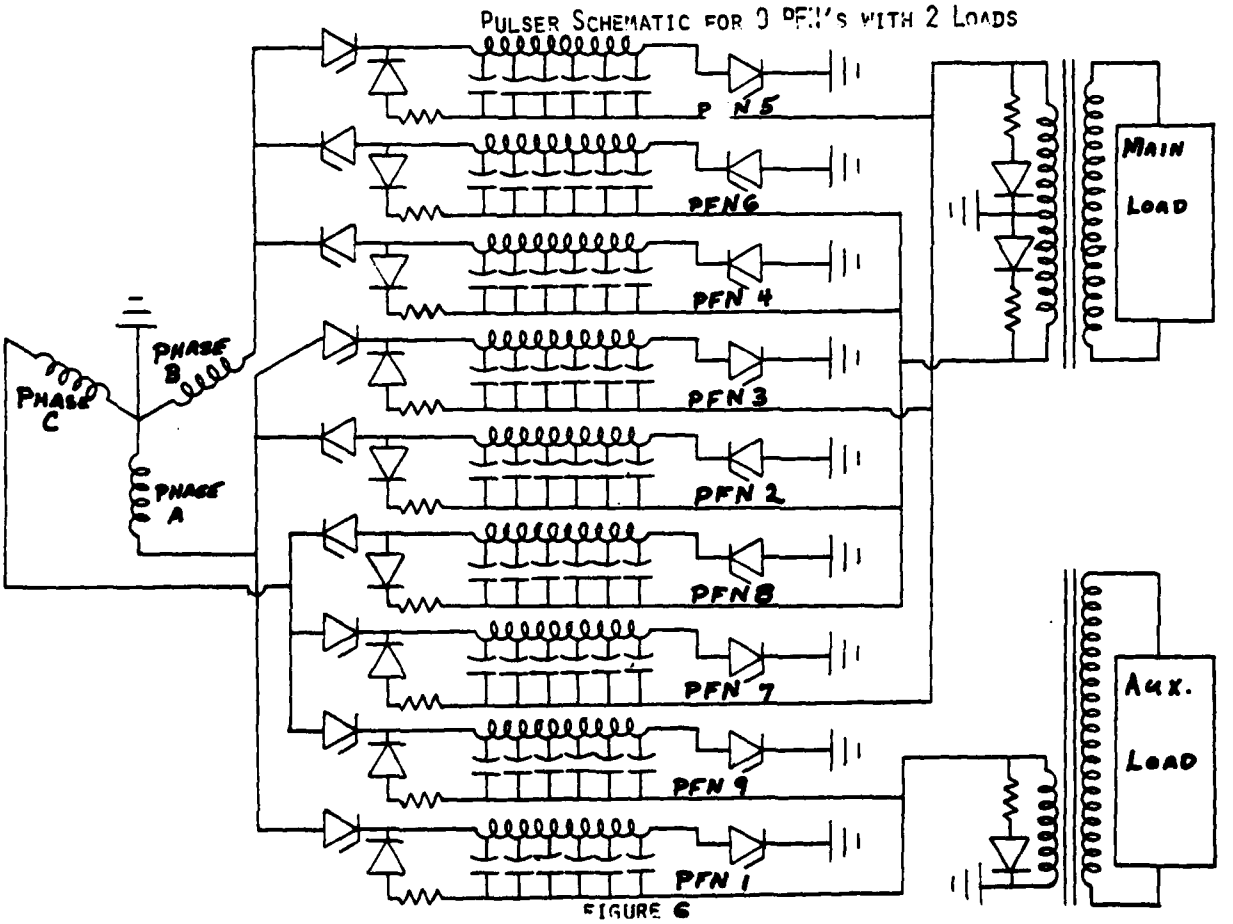

FIGURE 6

Requirements and Considerations In order to have a flat-topped pulse a compromise was made with respect to weight and a six section PFN was chosen. The last coil should be left off as external circuit inductance would be sufficient. Heat sinking as well as minimum weight suggests the use of a multiconductor rather than single. Capacitors must be capable of temperature extremes which are felt in the operational environment. Self-induced heating within the capacitor should not be a problem for short run times, say 40 seconds at 300 Hz. High dielectric strengths as well as low dissipation factors must also be considered. Life and weight must be considered as there is a compromise between these two factors when the dielectric is selected. A life of 1×10^6 pulses would be reasonable for mylar and consistent with heat generation. In order to be used in an airborne environment (high altitude) or on a mobile unit (dust) the entire PFN assembly should be sealed in a unit to prevent breakdown due to corona. Once the unit is sealed, it is conducive to modularization and tight packaging may be obtained. As the PFN is connected directly to the alternator through the charge switch, and the output is connected directly to the pulse transformer through the discharge switch, the PFN assembly should also contain the necessary fault protection. An end-of-line clipper and its associated resistor are the only additional components that should be added to make a complete PFN assembly. The capacitors, inductors, diodes, and resistor must be considered in order to obtain the proper heat sink capacity within the sealed unit. An aluminium case should be ideal for weight, strength, and shielding considerations. Coaxial connectors should be used on either end of the PFN box to allow charging from one end and discharging from the other. A PFN assembly of this type should be capable of 25 to 30 joules per pound.

Previously Built PFN Under Air Force Contract F33615-75-C-2003 through TRW to CSI several PFN's were developed. These PFN's were then tested at the USA High Power Facility at Camp Evans, NJ. The PFN's had values typical of those required of high energy systems as each PFN stored 600 joules. Not an ultimate in the state-of-the-art PFN's, as they did not contain the end-of-line clipper, however there appeared to be no technology problem by putting it into the unit. Several definite improvements can be made on future PFN's within the state-of-the-art. The case of the CSI PFN's were stainless steel; due to the high inductive coupling, the inductive heating was untolerable. For this reason, a shield was required around the coils, thereby driving up the weight unnecessarily. Future cases could be aluminium, thereby avoiding this problem. The inductor was made of uniform litz rope wire. The rope could be tappered, according to discharge current to further reduce the weight. These PFN's had a life of over 10^6 pulses with full energy storage and a capability of running for 30 seconds continuous in an adiabatic mode. Further treatment of these PFN's and projection of improvements to these self-contained PFN's will be made by another paper, "Development of Integral Light-Weight High Pulse Rate PFN." The advanced state-of-the-art PFN should be capable of even a greater range.

Discharge Switch

Although not as simple as the charging switch, the discharge switch is still within the state-of-the-art. Each charging switch, PFN and discharging switch may be considered a module. This design, therefore, allows increased output power without requiring new switches; just increase the module number. Several switches have been developed and tested to values which would be typical of a high power modulator. Switch requirements will be discussed first followed by a brief comment on the state-of-the-art switch.

Requirements In order for the discharge switch to operate satisfactory many considerations must be made, as in the case of the charging switch. Adiabatic operation is desired, this eliminates the need for plumbing and makes installation, modification, repair, and operation simpler. If the added complexity of cooling was not objectionable, even higher power levels could be obtained. Going along with the adiabatic operation is the "instant-on" capability. Some programs make use of the fast start concept and therefore it is desirable for the components, as well as the system, to start working as soon as a start button is pushed. Airborne applications impose other environmental factors such as G loading, vibration, altitude, temperature extremes, etc. Although the switch itself may not be sensitive to many of these factors the mounting may require some engineering. Turn-on jitter becomes rather important as well since multiple PFN's are discharging simultanously. Although not terribly important below 400 Hz, recovery time is a factor to consider. Self-containment of the switch must be considered as some switches require a substantial amount of auxiliary triggering circuitry, additional stand-by power, et al. In a final analysis it is doubtful that the best of all considerations will be made by one switch. Solid state switches are excellent for fast start and do have good weight and volume for an airborne application. Heat generation and removal, environmental factors, as well as mounting do present problems. Tubes can handle adiabatic operation and airborne environmental conditions. They do require warm-up time (additional stand-by power) and have turn-on jitter.

Switch Development Due to the harsh considerations on the discharge switch, it was considered a critical item. Switch development continues and the progress within the field is growing continually. The present state-of-the-art in high power switches is adequate for airborne high power modulators. As examples, the RCA-SCR switched high power multi-megawatt modulator, from AF Contract #F30602-74-C-0195, the Westinghouse 12.5 Megawatt Module (as presented in this symposium), from AF Contract #F29601-74-C-0021, and the Thyratron testing done by the USA (as presented in this symposium). The EG&G HY 5001 and HY 5002 are excellent tubes for this application as the basic HY 5 tube was flight qualified; the HY 5001 and HY 5002 are simply modifications of the HY 5. A smaller neater package could be obtained with the 2N3897 SCR package of RCA, it it were made into a heat sunk design, Presently, this unit is water cooled but can be operated continuously at a power level typical of these requirements.

Pulse Transformer

As the output load voltage requirements of a pulse modulator system increase there exists a voltage level above which the weight, cost and size penalties associated with generating and conditioning the power at high voltage offset the addition of a transformer which permits the generator and conditioning components of the system to operate at an optimum voltage level and results in an overall system optimization. In the A.C. resonant charging type system, under consideration, the use of a pulse transformer becomes advantageous when the output voltage level exceeds about 20 Kv at average power

levels of several megawatts. An A.C. resonant charging system using 6 PFN's and a pulse transformer is shown in Figure 7. The system may operate with either 1, 2 or 3 PFN's discharging at a time so the PRR will be respectively 6, 3 or 2 times the alternator frequency. When unequal numbers of PFN's are discharged through each half of the primary there is a small utilization penalty in the transformer primary. The case shown with 1 PFN discharging at a time amounts to a 41% increase in primary RMS current over the ideal case which is an equivalent power rating increase in the overall transformer of 21%, since the secondary is fully utilized. With 2 PFN's discharging at a time there is no penalty and with 3 PFN's discharging at a time the penalty is only 2.7% for the overall transformer rating. Therefore, for 3 or more network systems the effect is negligible.

Advantages

An inherent advantage in this system is the fact that the constant loading of the alternator takes place through the transformer primary in such a manner as to provide effective full flux resetting of the transformer core. Forced flux resetting is a great advantage in high power pulse transfomers but it usually requires an additional reset power supply and isolation inductor; but, in this system, the reset is inherent and no additional components are required. There is, however, a point which requires attention and that is if the load is a high impedance during the interpulse period, as is the case with gaseous discharges, then the reset current flowing in the primary will cause a high inverse voltage spike to develop during the rest period of the core. This can be avoided by the addition of a diode and resistor across the primary (See Figure 7) to provide a path for the reset current in parallel with the transformer open circuit primary inductance. The value of resistance must be high enough to develop an inverse volt-second product sufficient to reset the core during the interpulse period. The diodes are used to block unnecessary power dissipation during the output pulse. In addition to the flux reset, the pulse transformer itself can be further optimized by geometrical considerations,[1] the use of special high performance core material (Vanadum Permendur)[2] and high temperature coil materials.

Applications

In some applications it is necessary to provide two pulse outputs, for example, one to an auxiliary electron gun and the other to a main discharge. In this case with the multiple PFN A.C. resonant charged modulator it is convenient to use one of the PFN's and a pulse transformer to drive the auxiliary load and the remaining PFN's for the main load as shown in Figure 8. Of course when two outputs are used the total number of PFN's and the possible operating PRR's are different than for the single output case.

Load Characteristics

The interaction of the load characteristics with the pulse transformer and power conditioning is an important factor in system optimization. These effects have been analyzed in the literature quite well for the cases of resistive and diode loads[3] and are familiar to modulator designers. In the case of electron beam sustained gaseous discharge pulsed loads however, the interaction is somewhat different. This is due to the fact that the discharge impedance changes considerably both as a function of time and other parameters. Generally an atmospheric 3:2:1 mixture of He, N_2, CO_2 will undergo a rapid impedance drop of about 3 to 1 during the first two to three microseconds after application of a voltage pulse and then continues to fall at a much slower rate as shown in Figure 9.

A simplified explanation of this behavior but adequate for system interfacing and optimization is as follows.

The current density in the discharge is given in equation (1).

$$j = e*Ne*Vd = \sigma*E \qquad (1)$$

where j = current density, amps/cm^2
e = electronic charge, 1.602E-19 coulomb
Ne = electron number density, cm^{-3}
Vd = drift velocity, cm/sec
E = voltage gradient, volts/cm

In order to determine the number density Ne, one must solve equation (2).

$$\frac{dNe}{dt} = Sje - \alpha Ne^2 \qquad (2)$$

where S = constant
je = electron beam current density, ma/cm^2
α = .54E-7+.6E-5/((.011*E)**2.5+1)
(α as a function of E/N and mix, value given is for 3.2.1 atmospheric)

The drift velocity Vd as a function of E/N is given in Table II (N = 2.69E19).

TABLE II

E	Vd *
0	1
500	1.2E6
1000	2.2E6
1000	2.9E6
2000	3.2E6
3000	3.7E6
5000	4.9E6
7000	5.8E6

From equation (2) if the je is constant and the applied voltage is approximately constant it is clear that Ne and thus the conductivity (or impedance) will settle down to a constant value with a time constant determined by S, je and α; thus, explaining the rapid impedance change in the first few microseconds. The slower change which continues is due to the fact that the electron beam current density (je) is not uniform over the discharge but falls off considerably from the center of the discharge to the edges. This fall-off results not only a lower steady state conductivity but also a much longer time to reach steady state. Thus as these lower je density regions slowly come to steady state, the effect on the overall discharge impedance is to drop slowly after the initial rapid drop of the center region until the entire discharge reaches steady state; thus, explaining the overall result as shown in Figure 9. This impedance characteristic presents two important system optimization considerations. First, if the slow impedance change over the pulse for a particular case is large it is advantageous to design the PFN with an impedance taper; also, to improve the match, inverse power

A.C. Resonant Charging System Operating PRF's 2X, 3X, or 6X Alternator Frequency

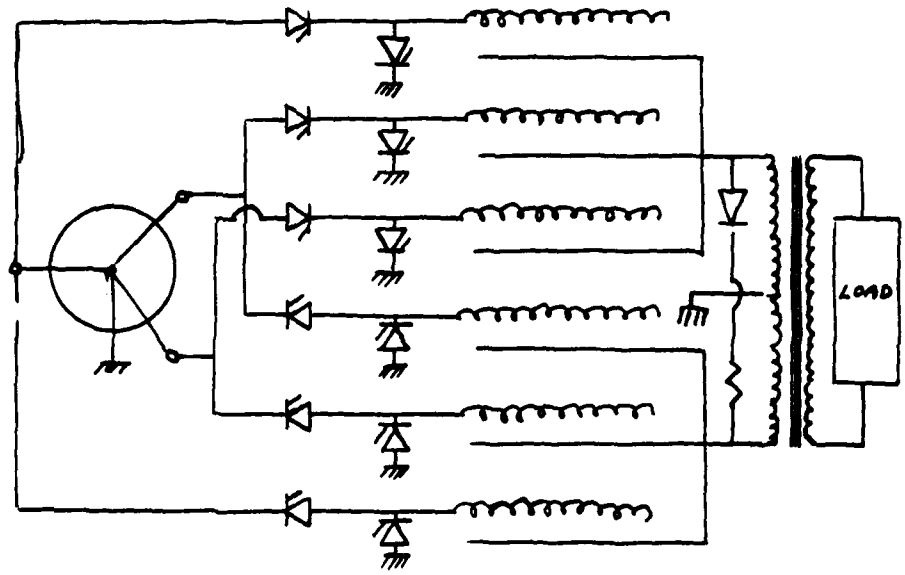

FIGURE 7

A.C. Resonant Charging System with Two Loads Operating PRF 2X Alternator Frequency

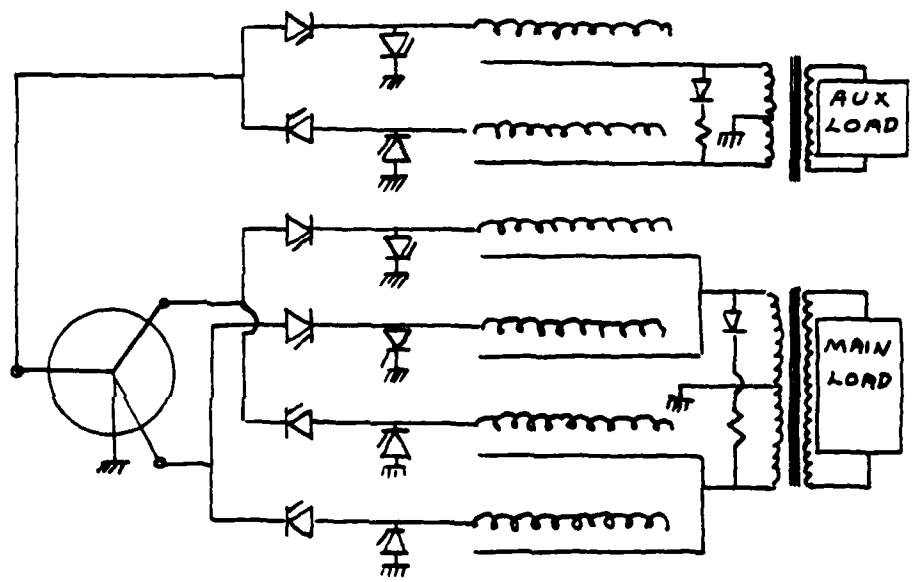

FIGURE 8

Pulsed Gaseous Load Characteristics Pulse Width Time Scale Approximately 25 Microseconds

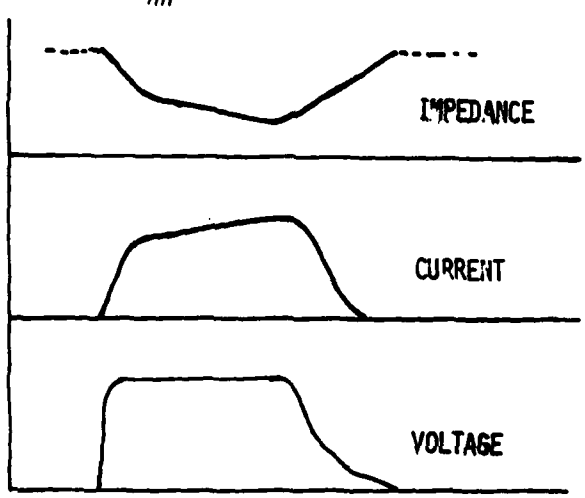

FIGURE 9

transfer and efficiency. Second, both computer analysis and experimental data show that the PFN and transformer rise can be designed for a value two to three times slower than that required on the basis of a resistive load matched to the settled impedance of the load. That is the high initial impedance characteristic of the gaseous load speeds up the voltage rise time by a factor of two to three over a resistive load. To take maximum advantage of this in the systems design, the leakage inductance of the transformer is used as the major portion of the inductance for the first section of the PFN. Furthermore, the load character as explained allows this leakage to be two to three times higher than that required for a resistive load thus a much less demanding rise time requirement for the pulse transformer and thus a lighter and easier to build transformer.

REFERENCES

[1] J. P. O'Loughlin, "Minimum weight, high power, high energy adiabatic pulse transformers," 12th IEEE Modulator Symposium, Feb. 1976.

[2] R. Lee, "Properties of reset cores in radar pulse transformers," J. Appl. Phys. Suppl., vol. 33, Mar. 1962.

[3] Massachusetts Institute of Technology Radiation Laboratories Series, vol. 5, Chapter 14 "Effect of pulse-transformer parameters on circuit behavior," 1948.

POLYPHASE AC CHARGED LINE-TYPE PULSER

Edward H. Hooper
Westinghouse Electric Corporation
Baltimore, Maryland

SUMMARY

Lighter weight and smaller size are advantages of AC charging in line-type modulators, a technique that eliminates the entire DC conversion and storage portion of the power system. In addition, the advent of lower voltage circuitry resulting from solid-state switching techniques makes modulator operating voltages compatible with the voltage available from AC generators without high voltage transformation.

With the advent of very high-power modulator systems, in which a dedicated generator is necessary, there is no longer a need to isolate generator frequency from PRF. Instead, generator frequency can be made synchronous with PRF and provision even made for pulse stagger.

This paper describes a novel application of polyphase AC charging in a line-type modulator system. A number of PFN's are charged in phase sequence directly from the generator in a manner which keeps nearly continuous loading on the generator. No high voltage transformer, rectifier banks, or filter chokes and capacitors are used. A discharge window permits a significant degree of stagger in the discharge pulse. The load imposed on the generator is no more severe than that imposed by the input to a conventional DC supply.

INTRODUCTION

Westinghouse recently completed, as part of an Advanced RSR Modulator program for the Air Force Weapons Laboratory under contract F29601-74-C-0021, preliminary investigation on AC resonant charging.[1] This work culminated in the construction of a demonstration model of a three phase, six module system. This paper presents some results of this program and extends these results to a generalized polyphase concept.

AC charging in a line-type pulser is a technique in which the pulse forming networks (PFN) are charged directly from the AC source. In comparison with conventional DC resonant charging, this technique minimizes both the number of energy transformation stages and the number of places where energy is stored. Its use can result in a significant reduction in equipment size and weight.

Figure 1 is a diagram that identifies the various operations in a conventional DC charged line-type pulser. Primary AC power is transformed to a higher voltage, rectified and the resulting DC stored in a filter capacitor. Periodically, a quantity of energy is taken from the filter by the charging circuit and placed on the PFN in preparation for pulse discharge. In the ensuing discharge of the PFN through the discharge switch, a pulse transformer matches the load to the PFN. Two voltage transformations are usually necessary to permit the discharge switch to function at its most efficient operating point, i.e., at a voltage level somewhere between that available from the power source and that required by the load.

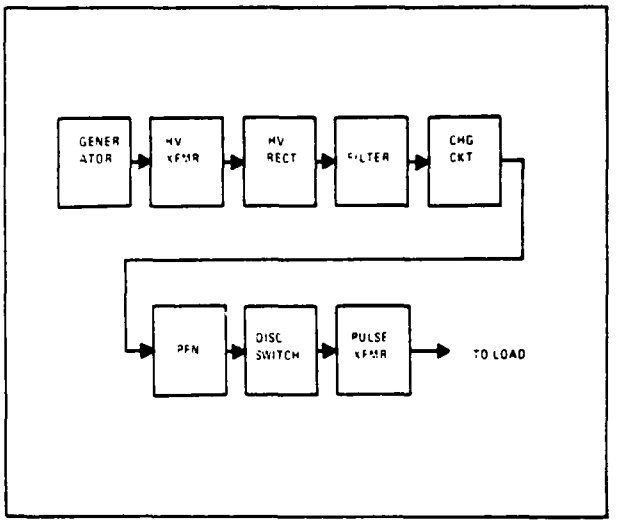

Figure 1. Conventional Pulse Modulator

As a comparison, figure 2 is a block diagram of a pulser using AC charging. The most striking property of this system is the elimination of the entire first transformer, DC conversion, and filtering or storage functions. The single stage of voltage transformation that is present follows the discharge switch. This fixing of the switch voltage by the AC source voltage is of no consequence since modern solid-state switches can be made to operate at the full power potential over a wide range of voltage.

AC RESONANT CHARGING

AC resonant charging, illustrated in figure 3, is a particular method of PFN capacitance charging from an AC source in which a series inductance resonates with the capacitance at the AC source frequency. The circuit in figure 3a consists of an AC voltage source, an SCR, a charging inductance, and the PFN capacitance to be charged represented by a capacitor. The charging cycle for full resonant charging begins with triggering of the charging switch as the source voltage passes through zero in a positive going direction. The waveforms in figure 3b illustrates the resulting charging response. The charging cycle ends as the capacitor voltage reaches its peak. Discharge of the capacitor back into a AC source is blocked by the charging switch.

The waveforms for AC resonant charging in figure 3b show current flowing for 180 deg to charge the

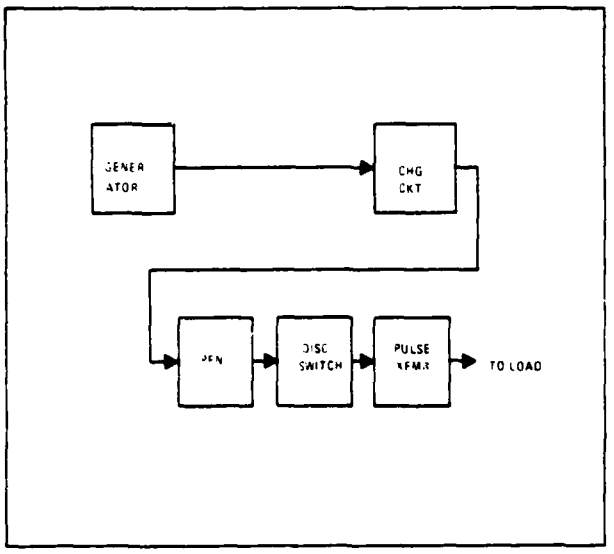

Figure 2. AC Charge Pulse Modulator

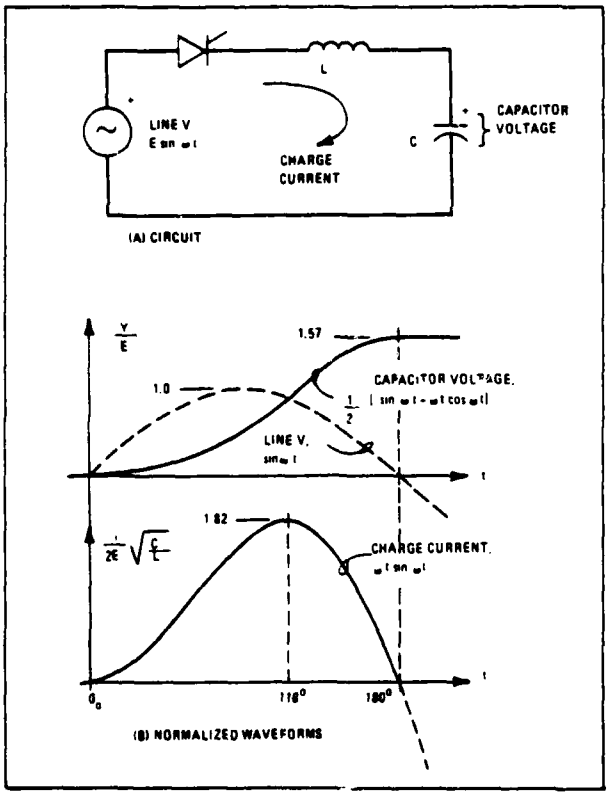

Figure 3. AC Resonant Charging

capacitor to $\pi/2$ times the peak value of the source voltage. The expressions for charge voltage and current are:

$$v(t) = \frac{E}{2} (\sin \omega t - \omega t \cos \omega t)$$

$$i(t) = \frac{E}{2\sqrt{\frac{L}{C}}} \omega t \sin \omega t$$

respectively, where E is the peak voltage of the source sinewave and ω is the line frequency and circuit resonant frequency in radians per second.

Deviation in line frequency from circuit resonance (or deviation in circuit resonant frequency from line frequency) results in the PFN capacitance charging to a voltage other than $\pi/2$. Figure 4 is a plot of peak capacitor voltage as a function of the ratio of generator or source frequency f to circuit resonant frequency f_o The curve is a plot of the maximum value of v(t) in the more general expression for capacitor voltage,

$$v(t) = \frac{E}{1 - \frac{\omega^2}{\omega_o^2}} \left(\sin \omega t - \frac{\omega}{\omega_o} \sin \omega_o t\right) \quad \omega \neq \omega_o$$

where ω is the angular frequency of the AC source, and $\omega_o = 1/\sqrt{LC}$ is the circuit resonant angular frequency. The voltage v(t) is maximum for $t = t_1$ so that the charging current

$$i(t_1) = \frac{\omega CE}{1 - \frac{\omega^2}{\omega_o^2}} \left(\cos \omega t_1 - \cos \omega_o t_1\right)$$

is zero for the first time since t = 0.

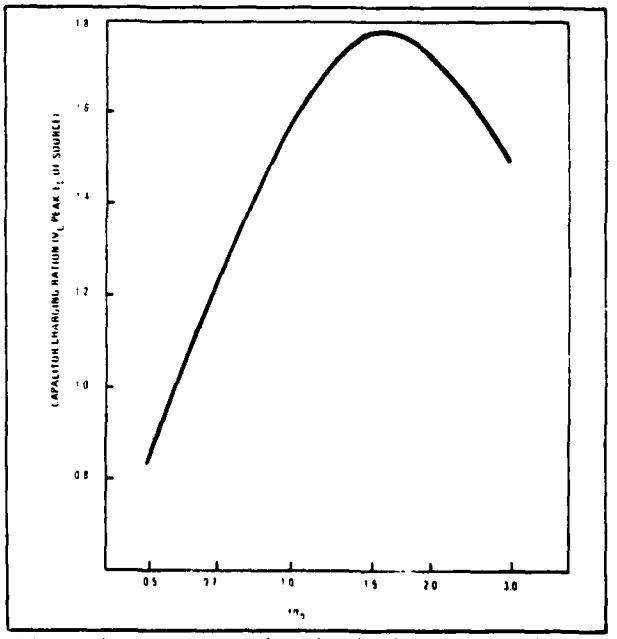

Figure 4. Capacitor Charging Ratio as a Function of the Ratio of Line Frequency f to Circuit Resonant Frequency f_o.

Figure 4 shows that the maximum voltage to be obtained on the PFN capacitance is 1.77, occurring at $f/f_o = 1.6$, which is significantly removed from resonance. However, consideration has been restricted to resonance or $f = f_o$ in the interest of spreading generator loading over the full half cycle and maintaining a current waveform that as closely as possible represents a waveform that would flow from the generator to a resistive load. The desirability of this becomes more apparent as the AC charging concept is expanded to full wave operation.

Figure 5 illustrates a two-step charging sequence in which a full generator cycle is used to charge two PFN capacitances. This results in a balanced load on the AC source generator, but at the expense of two capacitances charged to opposing polarities. This means that the combining pulse transformer through which the capacitances (representing PFN's) discharge must be wound to accommodate opposing primary pulse polarities.

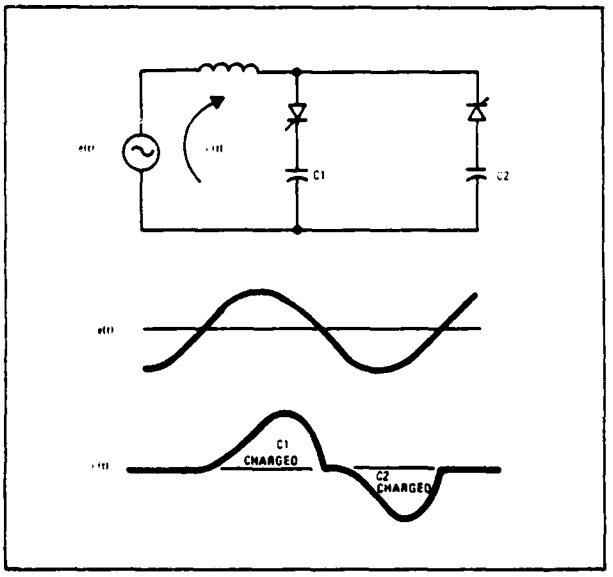

Figure 5. Full Wave or Two-Step Charging Sequence

Figure 6 is a simplified circuit of a basic full wave AC resonant charged modulator. The SCR symbols represent the SCR switch assemblies which would most likely be used as charging switches. The discharge switch assemblies are represented by Reverse Switching Rectifier (RSR) symbols representing switching devices uniquely suited to this application.[1,2] The simultaneous discharge of the two PFN's into the load is through a center tapped primary pulse transformer that combines the two pulses in adding polarity and matches the PFN's to the load.

A further extension from full wave AC resonant charging to sequential charging of a number of PFN is illustrated in figure 7. Eight PFN's are used as an example. In this case, the generator current waveform in figure 7b is nearly a sinewave over a charging period of four cycles. Charging is interrupted for one full cycle as a window for pulse discharge of the PFN's and then charging resumes.

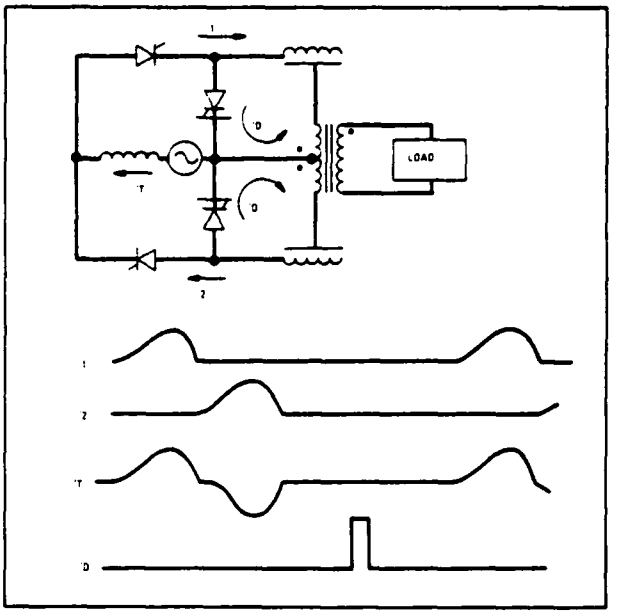

Figure 6. Basic Full Wave AC Resonant Charged Pulser

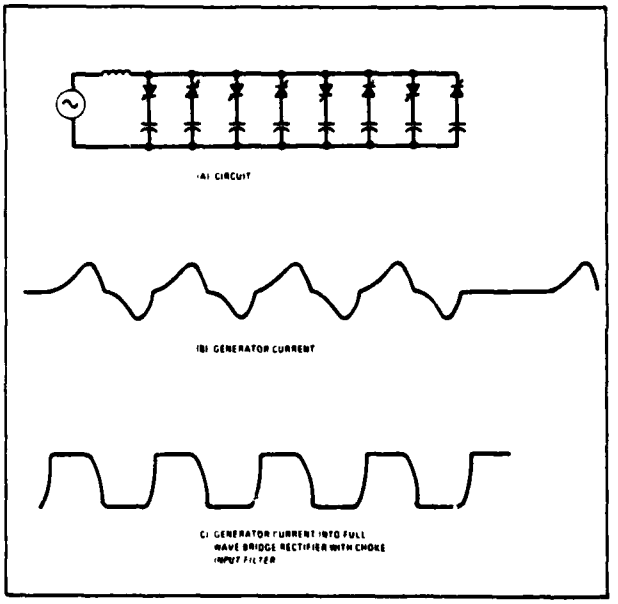

Figure 7. Sequential Resonant Charging of Capacitors

A second current waveform, figure 7c, is the square waveform of the current that would flow from a single phase AC generator to a bridge rectifier if a DC conversion step were employed with a choke input filter. It is quite obvious that the harmonic content of generator current would be much higher for the DC charging case than for AC resonant charging. This

would increase generator heating and make a larger heavier primary power source necessary.

The interruption for pulse discharge introduces a moderate subharmonic, which if objectionable can be eliminated by stagger sequence charging. In the example illustrated in figure 7, two extra modules can be added to continue AC source loading during the discharge window for modules one through eight. The sequence then proceeds with a discharge window occurring on every fourth cycle and a different selection of PFN's being discharged for each pulse.

POLYPHASE AC RESONANT CHARGING

A generalized polyphase AC resonant charging concept follows quite readily from the single phase basis presented thus far. The Westinghouse program for the Air Force Weapons Laboratory was centered around a three-phase, six section pulse modulator. Figure 8 is a simplified schematic and waveform diagram for this system that illustrates the essentials of polyphase charging.

The basic circuit includes a three-phase generator as prime electrical power source and six PFN-switch modules, one for each polarity of each phase of the generator. The outputs of the six modules are combined and transformed to the required voltage by the output pulse transformer.

The time sequence of PFN charging and pulse discharge is illustrated by the waveforms in figure 8b. The time t_c indicates the beginning of the PFN charg- sequence. In the basic circuit, SCR's act as controlled charging diodes for the PFN's. The charging sequence begins with the triggering of SCR A1 at t_c. In sequence, SCR C2 is triggered 60 deg later followed by B1, A2 and so on. The charging cycle ends upon completion of charging of PFN B2.

Discharge of the six PFN's through the pulse transformer to the load occurs when the six RSR switches are triggered simultaneously. Because PFN charging occurs during both positive and negative half cycles of line voltage, three of the six PFN's are charged positively and three negatively. Therefore, the output pulse transformer is center tapped and connected in a manner to combine all module outputs in the proper polarity.

The output of the basic pulser circuit is a repetitive pulse sequence whose pulse repetition frequency (PRF) is a submultiple of the generator frequency. In the basic example in figure 8, a second charging sequence can begin at time t_c' which follows t_c by two cycles. Therefore, if the generator is a 400 Hz generator the highest output PRF is 200 pulses per second (pps), that is one pulse every two cycles of line frequency. Time t_c' can be delayed for three cycles after t_c' in which case the PRF is 133 pps. Longer delays result in lower PRF.

Figure 9 is a photograph of the breadboard model of this system. Waveform photographs of the charging current and voltage between the charging inductor and switch obtained with this system are shown in figure 10.

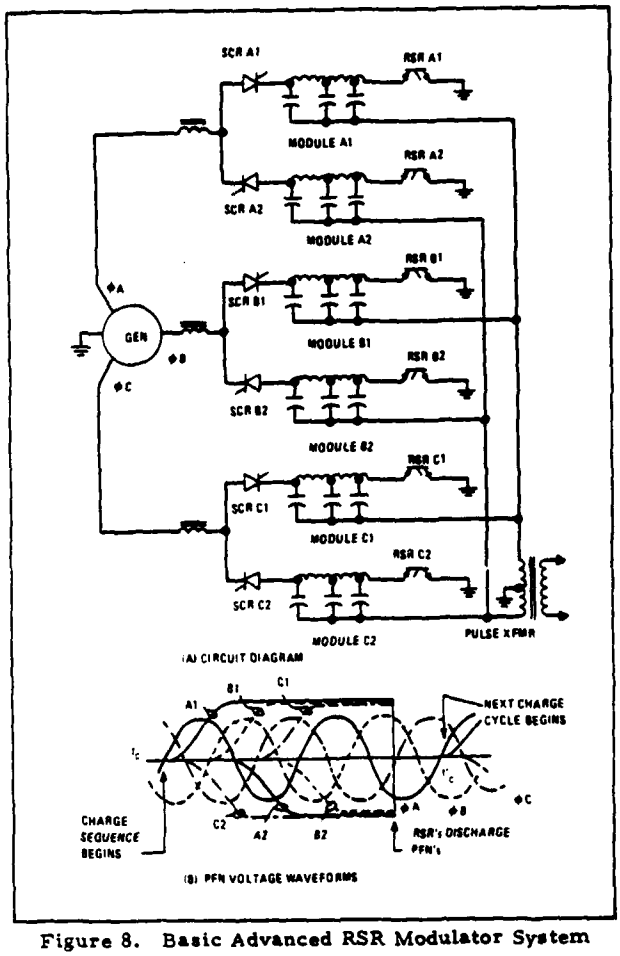

Figure 8. Basic Advanced RSR Modulator System

MULTIMODE SYSTEM

The expansion of the basic six-module system into a multimodule system is illustrated in figure 11. This system uses three phases and N modules per phase; therefore, the total number of modules is 3N. If η phases were used, the number of modules would then be ηN.

The charging sequence is programmed so that one module at a time is charged from each line. Therefore, the entire charging sequence requires a number of operating cycles of the generator. A typical charging sequence and waveforms from one phase are illustrated in figure 12. The total per pulse energy out of this three-phase system is 3N times the stored energy per module. Storage voltage per module is $\pi/2$ times the peak line-neutral voltage of the AC source.

A key consideration in this approach is the relationship between PRF and the generator frequency f_g. For the six-module system, maximum PRF is $f_g/2$. For the multimodule system, with each module charged in sequence, the maximum PRF is $2 f_g/(N + 2)$, where

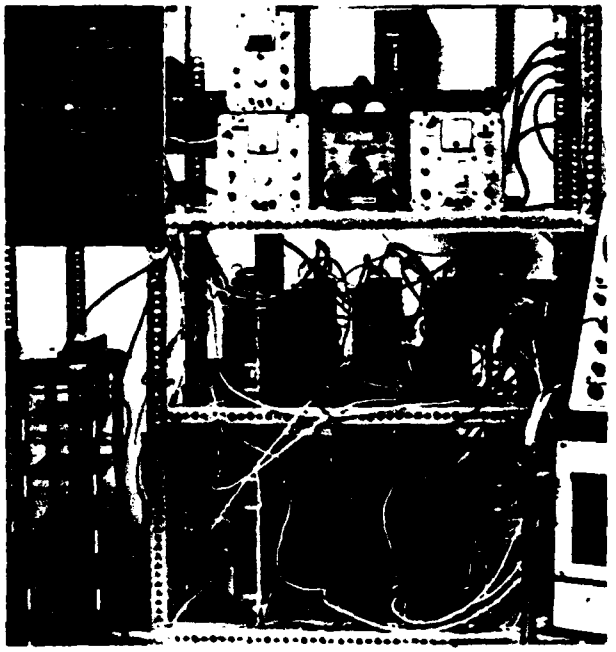

Figure 9. 3ϕAC Resonant Charging Pulse Modulator Breadboard

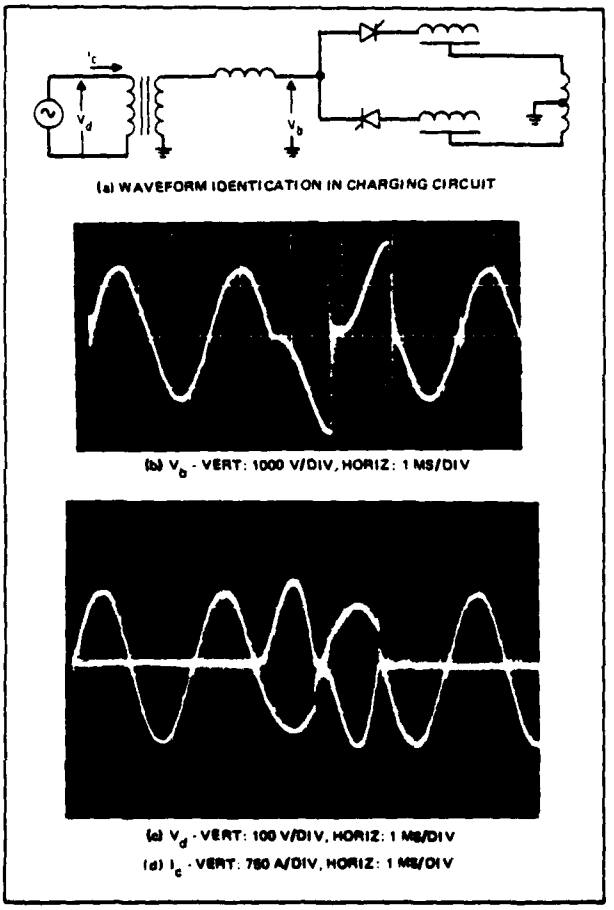

Figure 10. Breadboard PFN Charging Waveforms

N is the number of sequentially charged modules per phase. This frequency can be increased by charging more than one module at a time. It is important to note that with this approach, the PRF of the pulser is related to the generator frequency.

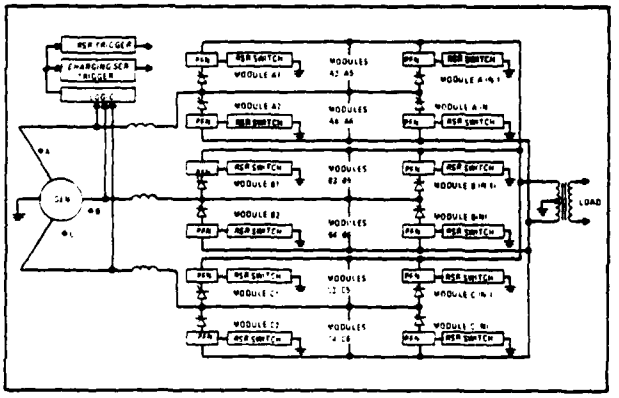

Figure 11. Multimodule, Three-Phase AC Resonant Charging

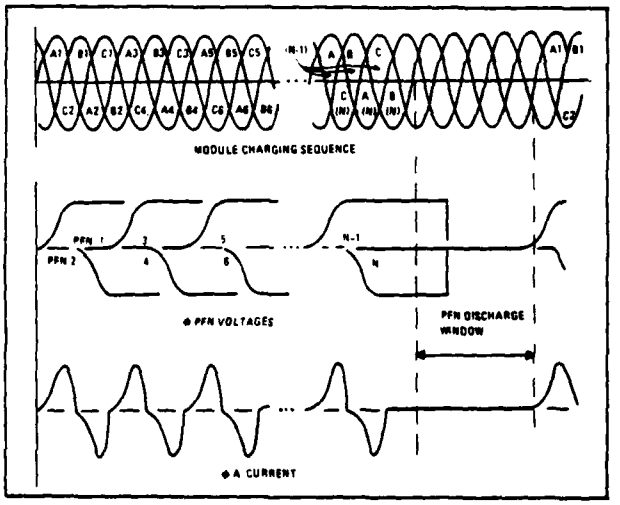

Figure 12. Multimodule, Three-Phase AC Resonant Charging Waveforms

Figure 13 illustrates a phase charging sequence that may be used in expanding the simple three-phase, six section pulser to a η-phase pulser containing two sections or PFN's per phase (one charged on a positive half cycle, the other on a negative). The timing sequence shown is for minimum time to charge all PFN's. From an examination of figure 13, the time τ, in seconds, required to charge all networks in a given system is given by

$$\tau = \begin{cases} T_c \left(1 + \frac{\frac{\eta}{2} - 1}{\phi}\right) = \frac{3\eta - 2}{2\eta} T_c & \text{for } \eta \text{ even} \\ T_c \left(1 + \frac{\frac{\eta - 1}{2} - 1}{\eta}\right) = \frac{3\eta - 1}{2\eta} T_c & \text{for } \eta \text{ odd} \end{cases}$$

where T_c is the full cycle period in seconds and η is the number of phases in the system. Note that as η increases without bounds τ approaches 1.5 T_c as a limit.

Sequential charging of PFN's within each phase of this polyphase system will spread out the loading on the generator and improve efficiency as in the three-phase case. Generalizing the system to contain 2N sections or PFN's per phase modifies the expression for total charging time to

$$\tau_{2N} = \begin{cases} \frac{3\eta-2}{2\eta} T_c + (N-1)\, T_c & \text{for } \eta \text{ even} \\ \frac{3\eta-1}{2\eta} T_c + (N-1)\, T_c & \text{for } \eta \text{ odd} \end{cases}$$

The addition of sections uniformly to all phases increases the charging time by the period of one cycle per added section.

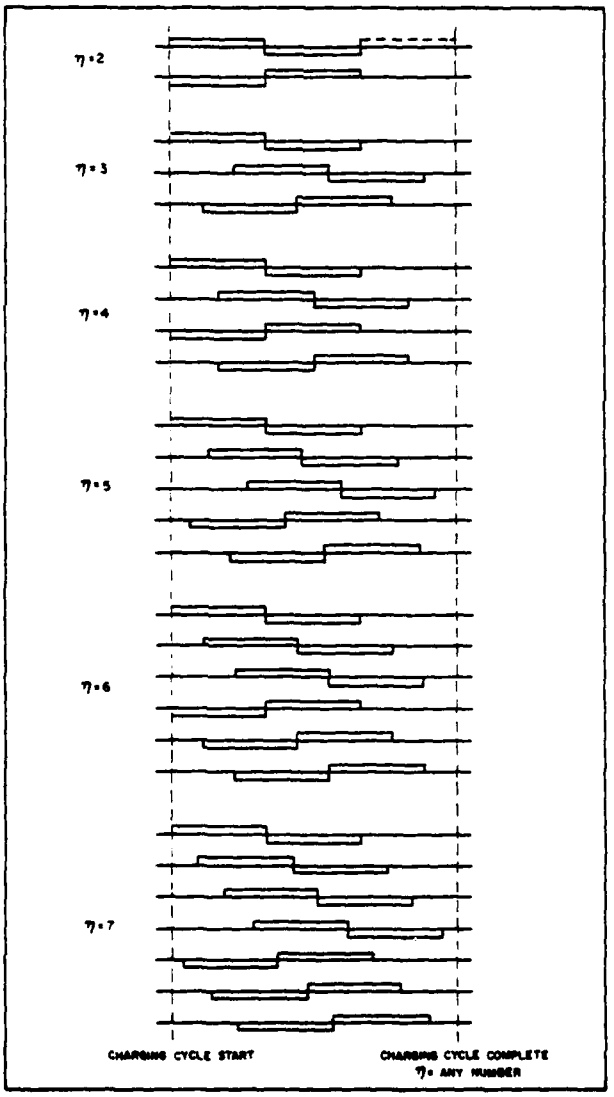

Figure 13. Charging Sequence for Various Numbers of Phases

Other relationships for the generalized case follow logically. The minimum time between adjacent charging starts or interpulse period is $(N + 1)\, T_c$. The discharge window T_D which is the time permitted for pulse discharge between the completion of one charging sequence and the next is given by

$$T_D = (N+1)\, T_c - \begin{cases} \frac{3\eta-2}{2\eta} T_c + (N-1)\, T_c & \text{for } \eta \text{ even} \\ \frac{3\eta-1}{2\eta} T_c + (N-1)\, T_c & \text{for } \eta \text{ odd} \end{cases}$$

$$\geq 0.5\, T_c$$

The maximum PRF obtainable from such a system is

$$PRF = \frac{1}{(N+1)T_c} = \frac{f_g}{N+1} \quad \text{pps}$$

where f_g is the AC source frequency in Hz.

All of the avove expressions are independent of the number of phases η. A nomograph in figure 14 based on the above analysis describes the performance of a polyphase AC charged system. The total number of sequential sections per phase is the essential parameter in determining the relationship between generator frequency and PRF. The number of phases employed becomes a question of convenience.

CONCLUSION

The polyphase AC charged line-type pulser concept is an innovative approach to very high power pulse modulation. It offers the advantages of:

1. Size and weight savings through elimination of the DC conversion steps.

2. Further size and weight savings through charging choke elimination if it is possible to utilize generator leakage reactance as the charging inductance.

3. More efficient generator loading through harmonic reduction.

All of which tend to offset some of the size and weight growth which increasing power levels in conventional line-type modulators necessitate.

The universal applicability of this approach must be tempered somewhat by its drawbacks. These are:

1. Inherent correlation between PRF and generator frequency.

2. The complexity of the charging logic and switch system.

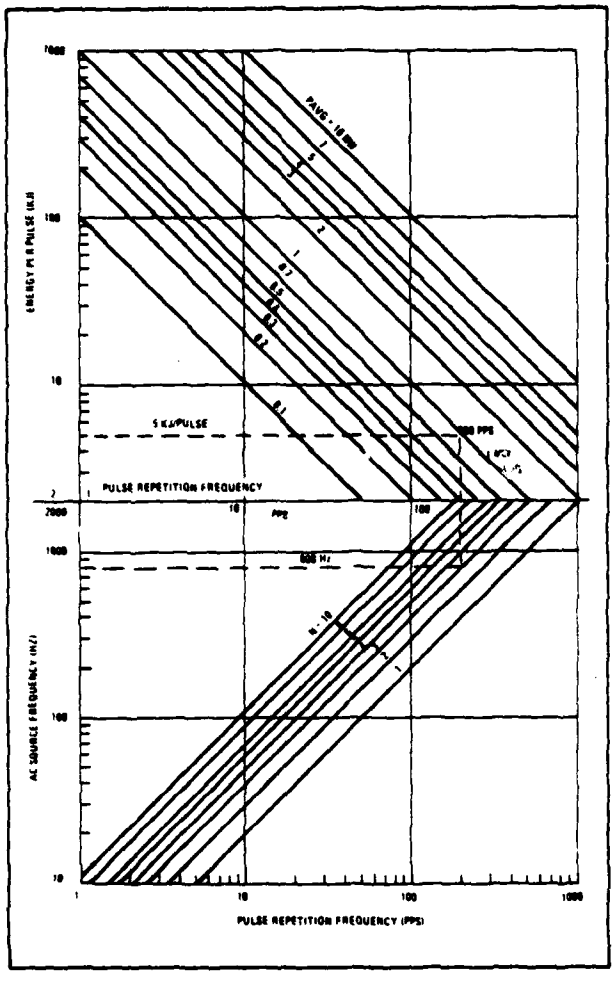

Figure 14. Polyphase AC Charge System Performance

In a system having uniform PRF requirements and a dedicated generator, the first is of no consequence. The second must be weighed against size and weight savings in other areas, and is a consideration that must be applied to each system individually.

The number of phases appears to have little impact on the modulator. This is more a function of generator technology, and it appears that three-phase systems are and will continue to be the most common.

In conclusion, AC charging of a line-type pulser is a technique that offers savings in equipment size and weight when PRF can be related to primary power frequency.

ACKNOWLEDGEMENT

Portions of this paper are based on studies performed for the U.S. Air Force under contract F29601-74-C-0021, Air Force Weapons Laboratory, Kirtland Air Force Base, New Mexico.

REFERENCES

1. E.H. Hooper and B.L. Jordan, "Advanced Reverse Switching Rectifier (RSR) Modulator," Contract F29601-74-C-0021, Final Technical Report, Air Force Weapons Laboratory, Kirtland Air Force Base, New Mexico.

2. R.A. Gardenghi, "A Super Power RSR," International Electron Devices Meeting 1975, Washington, D.C., December, 1975.

DEVELOPMENT OF AN INTEGRAL LIGHTWEIGHT HIGH PULSE RATE PFN

C. L. Dailey
TRW Systems Group
Redondo Beach, California

C. W. White
Capacitor Specialists Inc.
Escondido, California

J. P. O'Loughlin and Capt. J. Miller
Air Force Weapons Laboratory
Albuquerque, New Mexico

Summary

The feasibility of an integral, high temperature, pulse forming network (PFN) operating at a high pulse rate for a short duration burst has been demonstrated. The dielectric construction of the capacitors consisted of Kapton film and paper impregnated with Monsanto Chemical Co. MS 1489 oil. Litz wire coils were wound on a high temperature foam core and the entire assembly was placed in a stainless steel enclosure. A U-shaped aluminum shield was used between the coils and the case to reduce eddy current heating. An overall weight of approximately 20 pounds for an energy storage density of 600 joules (30 joules per pound) was achieved in a design that operated for 1.5×10^5 shots at a pulse rate of 280 shots per second in 18-second bursts. The burst duration was limited by heating of the stainless steel enclosure due to eddy currents induced by the coil magnetic field. An aluminum case construction would greatly reduce this effect.

This program was supported by the Air Force Aeropropulsion Laboratory*, with Mr. Jerrell M. Turner Program Monitor. Technical support was provided by Major Frank Zimmerman, Capt. James Miller and James P. O'Loughlin of AFWL. The coils were designed and constructed by TRW Systems, the capacitors and cases were designed and built by Capacitor Specialists Inc. (CSI), testing of the PFNs was conducted by John Creedon in the high power test facility in the Evans Area of the Army Electronics Command at Fort Monmouth and the program was managed by TRW Systems.

Discussion

Two designs were developed. One was a lightweight unit having three series-connected capacitor pads. The other was a more conservative design using four larger, series-connected pads. The same coil was used for both designs. Figures 1 and 2 are photographs of the completed units, showing one of the lightweight designs and two of the conservative designs. A charging bushing is seen at one end of the line with the heavier discharge bushing located at the other end.

The six-section PFNs stored 600 joules at 15 kv, delivering 4000 amperes at 280 pulses per second for a pulse duration of 20 microseconds (90% to 90% amplitude). The current pulse had a rise time of 2 microseconds (10% to 90% amplitude) and a fall time of 4 microseconds (90% to 10% amplitude). The nominal six-section capacitance and inductance values were 5.3 microfarads and 18.8 μH, respectively, corresponding to a source impedance of 1.9 Ω; the corresponding power transferred through the PFN was 169 kw. The ambient operating temperature was 160°F.

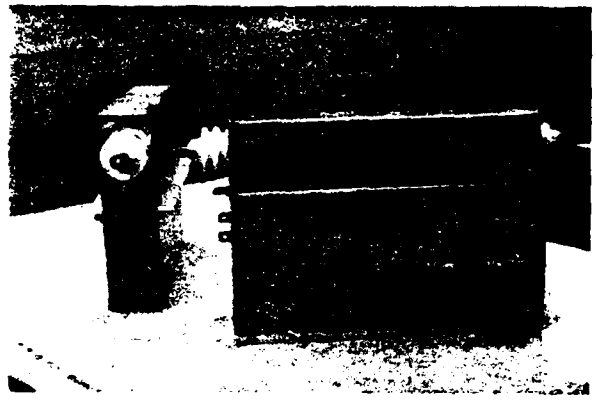

Figure 1. Comparison of Lightweight and Conservative PFN Assemblies Showing Charge and Discharge Bushings

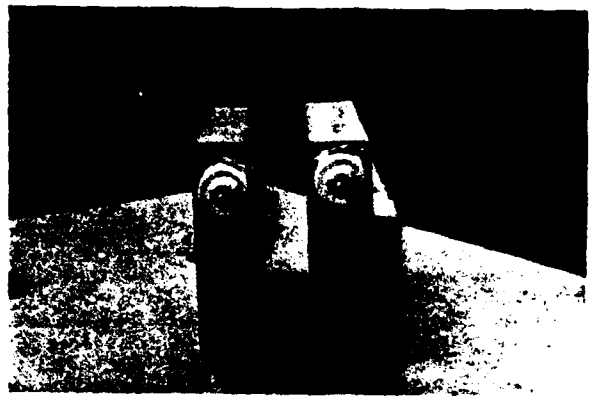

Figure 2. Side View of PFNs Showing Discharge Bushings

The completed lightweight PFN weighed 20 pounds after impregnation while the four-pad units weighed 29 pounds. These weights correspond to overall energy storage densities of 30 and 21 joules per pound, respectively. The PFN volumes were 321 and 474 cubic inches. These represent volumetric energy densities of 1.9 and 1.3 joules per cubic inch for the lightweight and conservative designs, respectively.

Capacitor Design

Kapton film capacitors were used to meet the high ambient temperature requirement. Some variation in Kapton properties was found for three different film lots used in this program. Optimum performance

*Contract No. F33615-75-C-2003

would require a screening procedure to select only the high strength film. An alternate film could be used if somewhat lower ambient temperatures were acceptable.

The capacitor pads used three-layer, extended foil constructions of paper and Kapton film. For the four-pad capacitors, this construction is represented as 50/30/50, which designates a 30-gauge layer of paper between two 50-gauge Kapton film layers. The paper serves to wick the impregnant into the space between the films; the metal foil to film region impregnates well without requiring paper. For the three-pad capacitors, the construction was 50/40/50 to increase the useful pad voltage slightly. MS 1489 oil was used to impregnate all of the PFN capacitor pads and to fill the PFN cases. The active film length of the pads (in the axial direction of the wrap) was 5.5 inches. An edge margin of 1/4 inch was used at each end and solid solder end connections, about 1/16 inch thick, were used to collect the foil current. A radial gap of 1/8 inch was left in the solder end caps to ensure complete impregnation. Copper straps were soldered to the end connections to connect the pads in series and to connect the low voltage end of each capacitor to the stainless steel case to complete the current return path. The high voltage end of each capacitor was connected to a copper "T" fitting that was provided between each of the individual coil segments. The completed capacitors were individually wrapped in a double sheeting consisting of a 5-mil paper sheet and a 5-mil Kapton sheet, with the film placed adjacent to the capacitors.

No significant heating of the PFN was attributable to capacitor losses. It was due almost entirely to ohmic losses in the coil and in eddy currents induced by the coil fields in the enclosure. The coil losses were shown to be unacceptably high for solid conductor coils mounted externally. This problem was eliminated by using a continuous winding of Litz rope, manufactured by the New England Electric Wire Corporation, Lisbon, New Hampshire. The particular Litz rope used here is designated as AS 833 cable having single armored polythermaleze coating (SAPT) and a glass braid jacket. It is 0.22 inch in diameter and has a total copper area of 20,825 circular mils. The individual wires in this rope are 5 mils in diameter with an 0.0045-inch thick coating of polythermaleze. A Hi-Pot test showed a dry wire-to-wire breakdown voltage of 5 kv. This was increased to 8 kv by impregnation. The coil was wound on a high temperature epoxy foam, formed by curing hollow epoxy spheres. The open volume between the spheres was thoroughly impregnated with oil. The dry foam had a specific gravity of 0.23. After impregnation, the specific gravity was 0.72. This foam, known as ECCO Foam EFF-14, is a product of the Emerson and Cummings Company. It can be used continuously at 170°C and for short periods at 200°C. A thermal vacuum test was performed on a coil core to determine whether high temperature outgassing would occur. After two hours at 200°C, a total weight loss of only 0.7% had occurred. In a 24-hour test at 125°C, performed for an earlier spacecraft application, the condensible fraction of the total weight loss was 0.025. Assuming the same fraction of condensibles exists at 200°C, this would indicate a condensible weight loss of 0.018% after 2 hours at 200°C. The foam was also tested by sudden immersion of one end of the coil form in 200°C oil; no thermal shock effect was observed. Samples of Litz rope and foam were left in 200°C oil for 30 minutes and no physical changes were noted.

As shown in Figure 3, each PFN coil consisted of five sections having eight turns which were wound

Figure 3. Litz Wire Coil Attached to Four-Pad PFN During Assembly

on a 2-inch diameter core. Copper "T" fittings were used at all connection points. The polythermaleze insulation was removed from each of the individual wires of the Litz rope for a distance of approximately 1/4 inch, using a special wire stripper manufactured by Ideal Industries, Inc., Sycamore, Illinois. The clean copper ends were then tinned by dipping in a solder pot, after which the tinned rope ends were sweated into the copper fittings. Examination of the wires after stripping showed complete removal of the insulation with no broken or abraded wires, so that a good solder contact was made to each of the wires in the rope. Resistance and inductance values were measured with a Marconi 1/4% Universal Bridge. The measured end-to-end resistance of each of the three coils was 0.013 Ω. The end-to-end inductance was 18.9 μH. The inductance of each coil section was 2.9 μH and the mutual inductance was 0.48 μH.

A full power run was made on a two-section sample of the coil to check the thermal design of the coils and of a typical "T" connection. At 300 amps rms for 30 seconds, the temperature of the dry rope (without oil impregnation) rose from 70° to 172°C. A maximum power run for the available supply was made to examine the high temperature behavior of the rope. The current started at 431 amps rms and decreased to 315 amps rms after 30 seconds as the wire temperature increased from 35° to 205°C. No change in the appearance of the rope was apparent.

Case Design

The PFN case consisted of welded, nonmagnetic, 0.020-inch thick stainless steel. The cases were rectangular with flat sides to permit side-by-side stacking. Charging bushings were located at one end of the cases with discharge bushings at the other. Rugged 1/4-inch diameter stud bushings were used for charging, to minimize the risk of damage in handling, while 3/8-inch diameter discharge bushings were used to handle the large discharge current of 300 amps rms. The convoluted bushings provide adequate surface area for epoxy encapsulation of external circuit connections that can be used to meet environmental requirements. However, the bushings can also work without encapsulation if a pressurized container is used for the PFNs in a flight installation. Steel tabs were welded to the cases to locate bolts that could be used with angle brackets to clamp a group of PFNs together and provide a means of attachment to aircraft support structure.

Full power operation of the PFNs in the steel enclosures resulted in high case temperatures in the

coil region after a few seconds of operation. Tests conducted at AFWL by Capt. Miller and J. P. O'Loughlin showed substantial reduction in case heating could be achieved by placing a U-shaped aluminum shield over the coils (i.e., between the coils and the case). The PFNs were modified accordingly. An 0.040-inch thick aluminum shield was separated 0.050-inch from the coil by paper spools wound around the coil segments. The skirt of the shield extended 1/4 inch below the bottom of the coil and about 1/2 inch beyond each end of the coil. With this modification the four-section PFN was able to run 30 seconds at full power while the three-section PFN could run 18 seconds at full power without overheating. Further reduction in case heating through the use of an aluminum case would be desirable.

Test Summary

The lightweight PFN was tested for 6000 shots in the original steel enclosure before testing was terminated because of excessive case heating. A total of 20,000 shots was accumulated for one of the conservative four-pad PFNs before its test was terminated. In both cases, the highest case temperature occurred adjacent to the coil segment at the discharge end. A strip of solder, laid on the coil cover, melted after 6 seconds of running and the case became red hot after 8 seconds. The steel cases were then removed from all three PFNs and replaced with new cases after inserting the 0.040-inch thick aluminum shields. The heating was found to have produced charring of some of the paper sheets that had been used with Kapton sheets to insulate the capacitors and coils from the cases. The capacitors were unaffected by the heating and the oil near them was clean. In spite of darkening of the film due to the paper charring, the insulation strength of the Kapton film was essentially unaffected.

After the PFNs had been reassembled, life testing was resumed. The four-pad design was able to run for the full 30-second, full power, burst duration, but testing had to be limited to 18 second bursts for the lightweight design. After a total of 2×10^5 shots for the four-pad unit, and 1×10^5 shots for the lightweight unit, the solder melted at the discharge bushing and testing was terminated. These two units were disassembled, inspected, rewrapped with paper and Kapton, enclosed in new steel cases with the same aluminum shields and returned to the ECOM test facility. The lightweight design failed while being brought up to full power. The four-pad PFN ran for one full power burst before failure. Subsequent failure analysis showed extensive charring in the four-pad unit. One of its capacitor pads was found to have experienced a normal edge margin failure at the negative foil edge. This is the usual type of failure encountered in a film capacitor. It appears as a puncture through the dielectric of the edge margin and close to the negative foil edge. It is not a "flashover" that can occur when inadequate edge margin is used to support the operating voltage. The lightweight PFN experienced a similar edge margin failure, but it was located at the positive edge. Extensive damage occurred in the failure zone because of power dissipated locally after the initial puncture.

Conclusions

Lightweight and compact PFN construction is feasible for short duration, high power operation by enclosing the capacitors and coils within a single case. An energy density of 30 joules per pound (1.9 joules per cubic inch) was achieved in a design that operated for 1.5×10^5 shots. Substantial case heating was observed in the stainless steel enclosures adjacent to the PFN coils. This was greatly reduced by the use of an aluminum shield between the coil and case and would be further reduced to a satisfactory level by an aluminum case construction.

MINIMUM WEIGHT HIGH POWER HIGH ENERGY ADIABATIC PULSE TRANSFORMERS

James P. O'Loughlin
Air Force Weapons Laboratory
Kirtland Air Force Base, New Mexico

SUMMARY

Analysis of high power high energy adibadic pulse transformers is made for the purpose of obtaining a minimum weight geometrical configuration for a given rise time and power. The analysis is restricted to low impedance loads and neglects the effects of capacitance and magnetizing current. A transformer configuration and winding arrangement is selected and described in terms of geometrical ratios. The effect of these ratios on the weight and performance is analyized and presented in graphs such that an optimum design configuration may be determined given the required performance characteristics. The effect on weight and performance of aluminium windings is also considered. It is found that the weight versus geometrical parameters is a rather broad function and departures from the optimum geometrical parameters in the order of 50% result in a weight penalty in the order of 5 to 15%. Rise time improvements at the expense of weight are in the order of ten to one for a weight penalty of two to one. There is a slight weight advantage if aluminium windings are used, however faster rise times in the order to two are possible with copper windings for transformers of the same power rating. A model transformer was designed, built and tested and found to be in agreement with the analysis as presented.

METHOD OF ANALYSIS

The method of analysis is to define a core and coil configuration and a winding configuration as shown in Figure 1 and Figure 2 with the dimensions and dimension ratios as shown. The core dimensions and dimension ratios are self-explanatory. The coil insulation dimension ES corresponds to the insulation thickness in centimeters at the point of maximum voltage and all other insulation thicknesses in the coil are related to ES via the voltage distribution defined by the winding configuration as in Figure 2. A listing of the parameters and definitions used in the analysis is given in Table 1.

To describe the characteristics of the transformer two terms are defined,

$$PO = EO*IO*T_p*\sqrt{du}, \text{ which is defined as the power characteristic and} \quad (1)$$

$$TO = T_{RL}\sqrt{du}/T_p, \text{ which is defined as the rise time characteristic.} \quad (2)$$

These two characteristics are evaluated in terms of the dimensions (V, W, X, Y) or dimension ratios (A, B, C, K), the material characteristics (σ, δ, ρ), the flux density (Bm), the thermal rate or rise ($\dot{T}$), the insulation thickness (ES), and the space factors (SFC, SFW).

Since the temperature varies considerably over a run interval, consideration must be given to the variation of material characteristics. The specific heat and density variations are small enough to neglect, however the resistivity variation is not. Therefore, in using the equations or using the graphs, the values of resistivity (ρ) and of thermal rate of rise ($\dot{T}$) are to be interpreted as the average values over the run which leads to a small inaccuracy but greatly simplifies the work. Whenever possible, in the graphs of the results, $\dot{T}$ and Bm have been factored and normalized.

Also this analysis assumes that the limiting thermal consideration is the rate of temperature rise in the conductors and not the core. In some cases, this may not be true where high flux densities, narrow pulses at high pulse repetitive rates exist, in which case it will be appropriate to evaluate the core loss and rate of rise and if necessary select a value of Bm which will correspond to an acceptable value of core rate of thermal rise. The value of Bm used in the calculations is 38,000 gausses. This high flux swing is based on using forced core reset and Vanadium Permendur material. [1]

Also this analysis is based on a specific winding configuration, Figure 2, which may not be optimum in all cases; however, it is a good compromise over the ranges of ES and PO considered. Although it does not appear in the analysis, a high turns ratio can be troublesome in that it implies a very low primary impedance and this will require a great deal of attention in arrangement of the primary conductors and leads.

The calculations of voltage, current and inductance are all referred to one turn and are given by:

$$IO = SFW*(V*W/2-2*V*ES+12*ES^2)*(\dot{T}*\sigma*\delta*4.16/(\rho*du))^{1/2} \quad (3)$$

$$EO = X*Y*SFC*Bm*10^{-8}/T_p \quad (4)$$

$$LO = \pi*10^{-9}*(2*X+2*Y+V*\pi/2)*(5*V/192+81*ES/288)/(W-4*ES) \quad (5)$$

RO is defined as,

$$RO = EO/IO \quad (6)$$

and the rise time constant, not to be confused with the rise time parameter TO, is defined as,

$$T_{RL} = LO/RO \quad (7)$$

The weight of the transformer is made up of three components, the coil, the core and the insulation and is related to the geometry and other factors as:

$$WT = W_w+W_c+W_i$$

$$W_w = SFW*(W*V/2+12*ES^2-3*W*ES-2*V*ES)*(4*X+4*Y+V*\pi)*\delta_w$$

$$W_c = X*Y*(2*V+2*W+\pi*X)*SFC*\delta_c$$

$$W_i = [(W*V/2*(1-SFW)+(3*W*ES+2*V*ES-12*ES^2)*SFW*(4*X+4*Y+V*\pi)]*\delta_i \quad (8)$$

TABLE I

Nomenclature and Definitions (See Figures 1 & 2)

A = core strip width/core build = Y/X
B = core window length/core window width = W/V
C = core build/core window width = X/V
K = XYVW
V = core window width
W = core window length
X = core build
Y = core strip width
EO = peak volts per turn (Equation (4))
IO = total peak current of both coils referred to one turn (Equation (3))
RO = EO/IO
LO = total leakage inductance of both coils (in parallel) referred to one turn (Equation (5))
T_{RL} = rise time constant = LO/RO
T_p = pulse width
Bm = peak flux swing (gauss)
WT = total core and coil weight (grams) = $W_w+W_i+W_c$
W_w = winding weight (grams)
W_i = insulation weight (grams)
W_c = core weight (grams)
SFW = winding space factor
SFC = core space factor
T = winding rate of thermal rise (°C/sec)
σ = specific heat of the conductor (CU = .092) (AL = .215)
ρ = resistivity of the conductor (CU = 1.72 micro-ohm-cm) (AL = 2.83 micro-ohm-cm)
δ_c = density of core material (7.38 g/cc)
δ_i = density of insulation (2.0 g/cc)
δ_w = density of conductor (CU = 8.9 g/cc, AL = 2.7 g/cc)
du = duty cycle = PRF*T_p
PO = power rating parameter = EO*IO*$T_p\sqrt{du}$
TO = rise time rating parameter = $(T_{RL}/T_p)*\sqrt{du}$
ES = insulation thickness at point of maximum voltage
PRF = pulse repetition frequency
TO^n = normalized rise time parameter
PO^n = normalized power parameter
WT^n = normalized weight

NOTE: Normalized terms are normalized with respect to the design which has been optimized for a maximum PO/WT ratio.

RESULTS

The first analysis carried out was done with a computer program which determined the maximum PO (power characteristic) for a set of constant weight transformers, and various insulation thicknesses by varying the geometry parameters A, B, C and K. This analysis was done over a range of weights from 1000 grams to 900,000 grams. Other parameters were a thermal rate of rise of 3°C/sec, a flux swing of 38,000 gausses, a core space factor of .9, a winding space factor of .5 and copper conductors. The winding space factor (SFW) applies only to that portion of the window area allotted to the winding and does not include the space taken for the major insulation and margins which is accounted for by the ES term. The resulting optimized values of PO and the corresponding values of A, B, C, K and TO are plotted in Figures 3-8. The values of TO correspond to a design which has been optimized for PO and, of course, for many applications the rise time is not fast enough. If a faster rise time is required presumably it can be had at a cost in weight. It was determined that the greatest improvement in rise time for the least increase in weight is to be had by increasing the C parameter from the value determined by optimizing PO for minimum weight. The sensitivity of the geometrical parameters in effecting rise time is shown in Figure 9 and effecting weight in Figure 10. Both Figures 9 and 10 are plots with PO held constant.

In order to further evaluate the effect of requiring a faster TO than that given by the optimized PO case, a computer program was used to start with a given PO optimized design and hold PO constant while the geometry is varied in such a way that TO decreases (rise time speeds up) at a maximum rate with a minimum rate of increase in weight. That is, the partial derivative of TO, with respect to WT are continually evaluated along the A, B and C axis with PO being held constant and the geometry is modified along whichever axis gives the greatest improvement in TO for the least increase in WT. The results show in Figure 11 that it is always the C parameter which gives optimum improvement. It was determined that the effects of PO (not shown for Figure 11) and ES are quite small over the ranges considered. In general an improvement in rise time of about ten can be obtained with a weight penalty of about two and a corresponding increase in the C parameter above the PO optimized value of about four.

Larger improvements in rise time become diminishingly advantageous in terms of weight as shown by the saturation of the curve in Figure 11. If greater rise time improvements are required, it would probably be best to investigate different winding configurations rather than further increases in the C parameter much above about 4 times the PO optimized value.

The effect of using aluminium windings rather than copper was evaluated by comparing the PO optimized design of each material. The results are plotted in Figure 12 and Figure 13. The results show that for low values of PO and high values of ES the copper and aluminium designs are close in both weight and rise time. For high values of PO the aluminium design is significantly lighter but has a rise time in the order of 1.5 to 2.0 times slower than the copper design. Thus the requirements of each individual application will determine which material is best.

A model transformer was designed and built based on the configuration analyzed in this paper. The design and construction was done before the analysis presented was complete, thus the geometry is not precisely optimum but is close. The performance specification of the model is given in Table II.

TABLE II

Model Transformer Specification

Turns Ratio, PY:SY:BIAS	1:3:0.5
Primary Voltage	20 kv, 20 usec
Secondary Voltage	60 kv, 5 ohms
Secondary Leakage Inductance	15 microhenries max
Core Bias Current	80 ADC
Duty Cycle	30 seconds on @ .0056

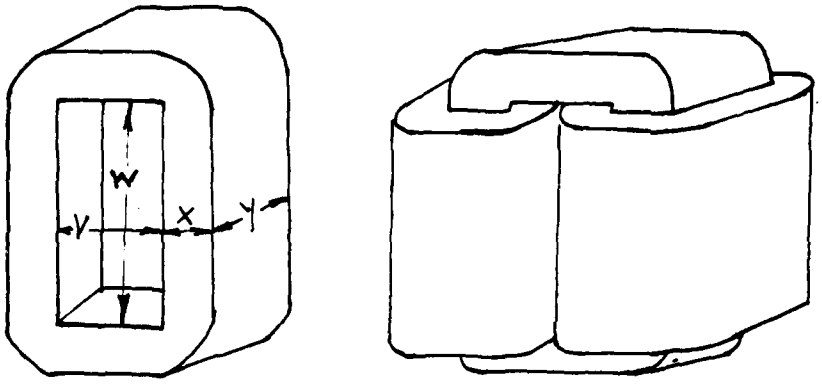

FIG.1

PULSE TRANSFORMER CONFIGURATION

DIMENSION RATIOS	DIMENSION PARAMETERS
A = Y/X	V = (K/A*B**2))**.25
B = W/V	W = (K*B**3/(A*C**2))**.25
C = X/V	X = (K*C**2/(A*B))**.25
K = V*W*X*Y	Y = (K*A**3/B)**.25

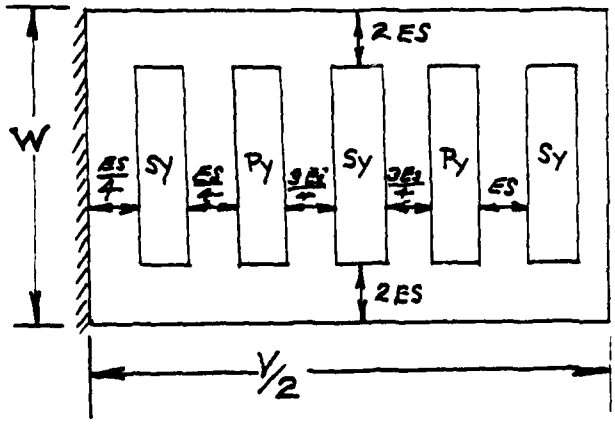

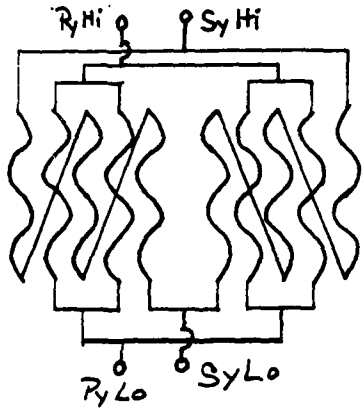

FIG.2

COIL CROSSECTION AND WINDING CONFIGURATION

LO = TT*1E-9*(2*X+2*Y+TT*V/2)*(5*V/192+81*ES/288)/(W-4*ES) HENRIES LEAKAGE RE ONE TURN

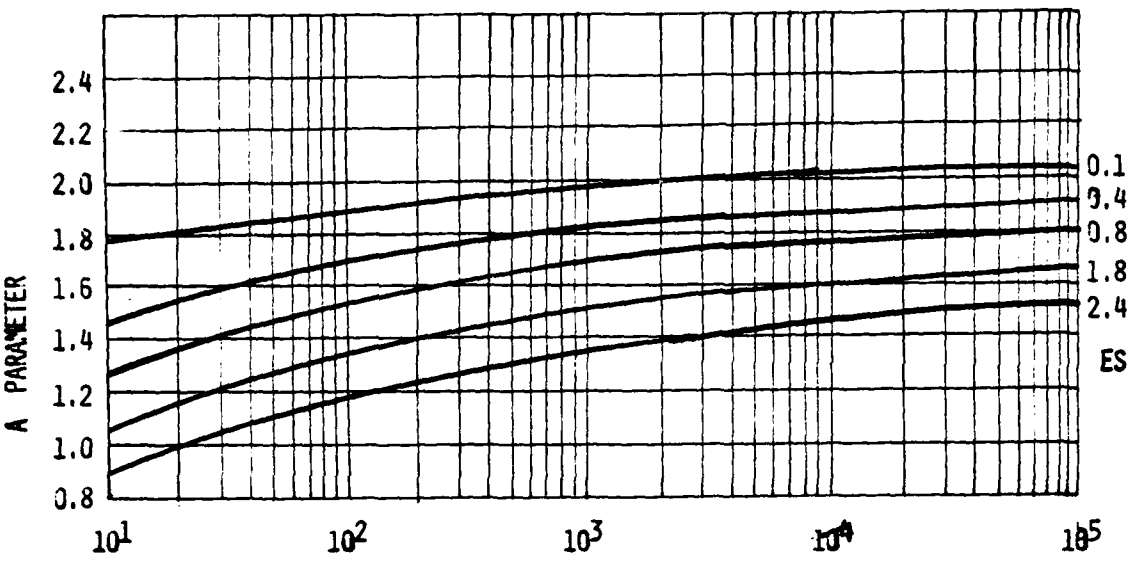

FIG.3

A PARAMETER VS POWER CHARACTERISTIC

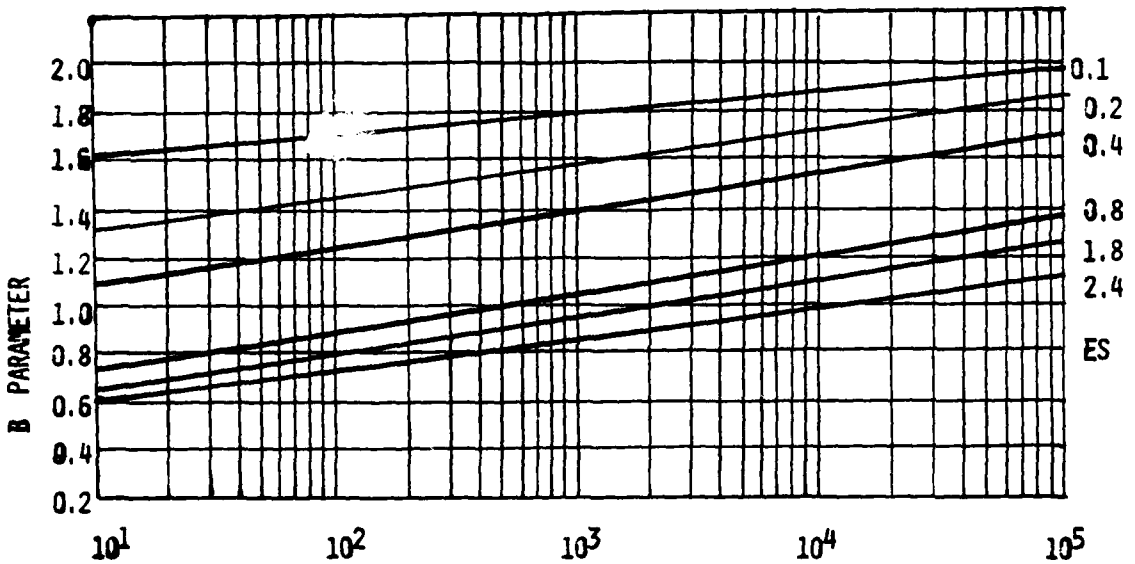

FIG.4

B PARAMETER VS POWER CHARACTERISTIC

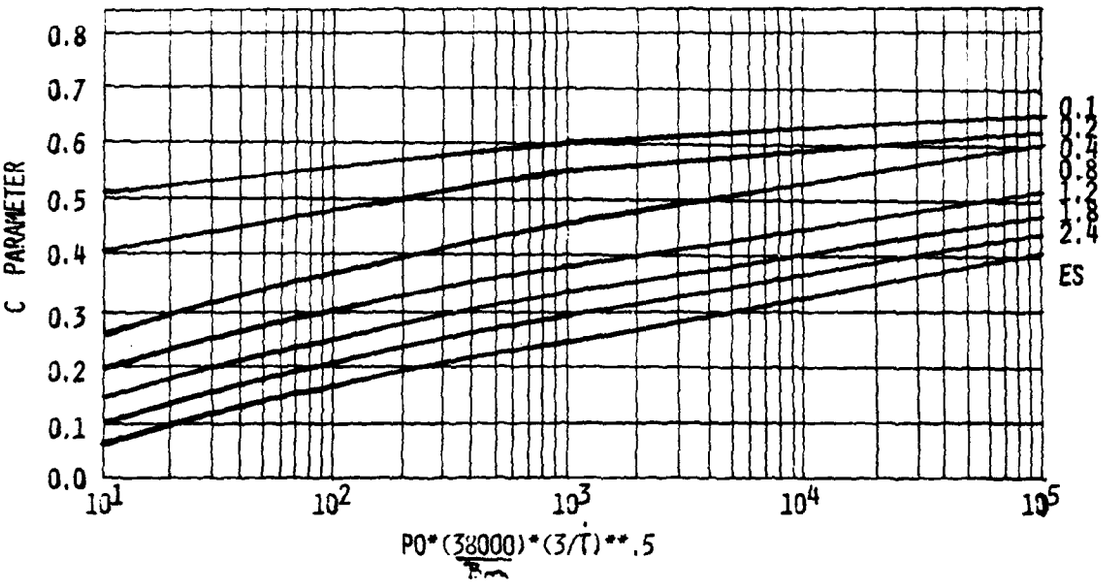

FIG.5 C PARAMETER VS POWER CHARACTERISTIC

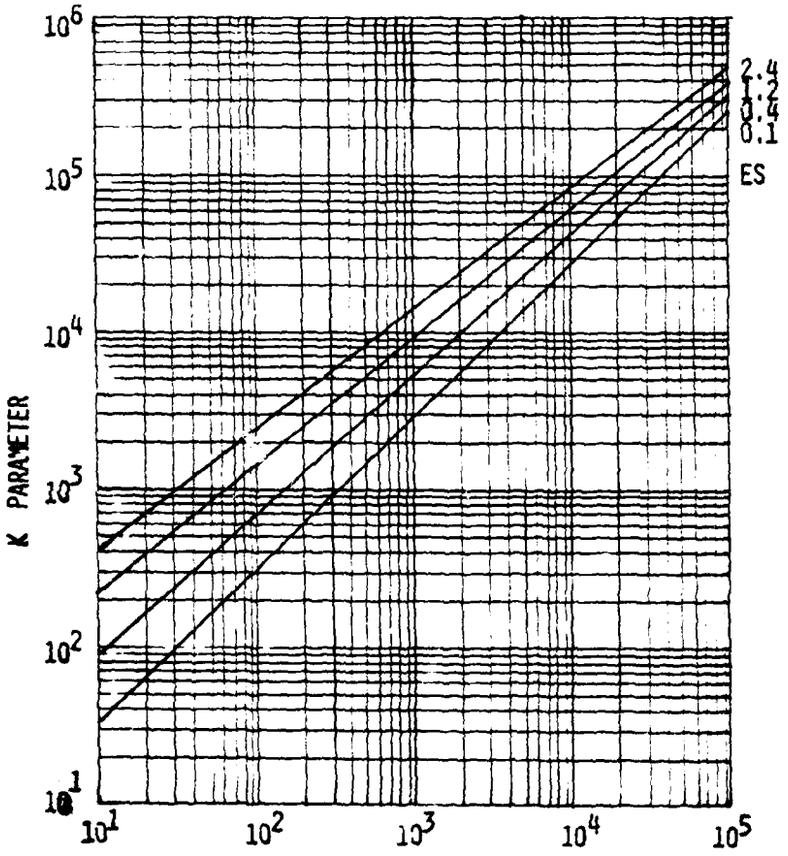

FIG.6 PO*(38000)*(3/T)**.5
Bm

K PARAMETER VS POWER CHARACTERISTIC

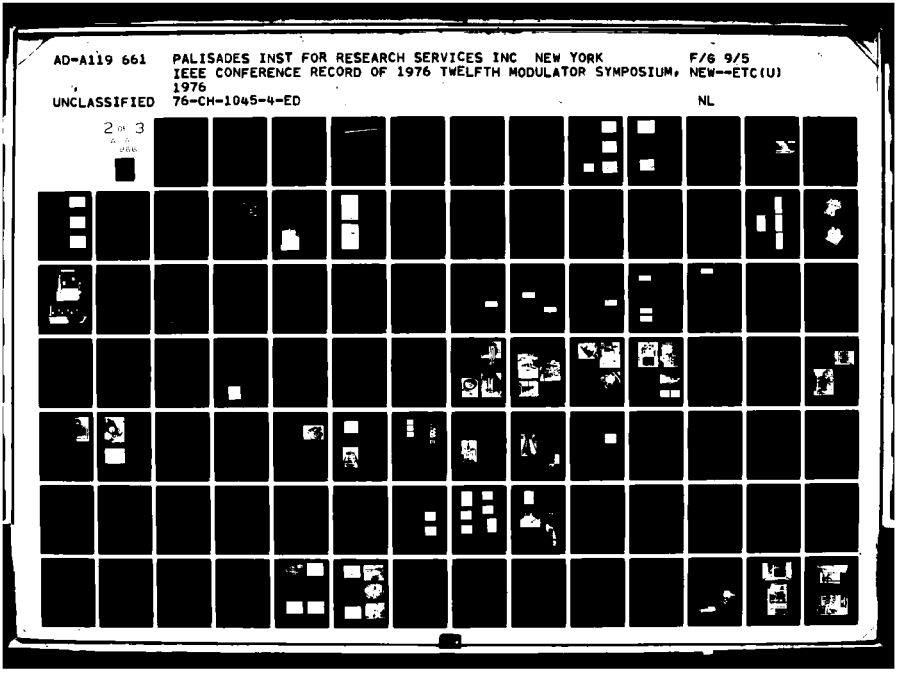
AD-A119 661
PALISADES INST FOR RESEARCH SERVICES INC NEW YORK
IEEE CONFERENCE RECORD OF 1976 TWELFTH MODULATOR SYMPOSIUM, NEW--ETC(U)
1976
UNCLASSIFIED
76-CH-1045-4-ED
F/G 9/5
NL
2 OF 3

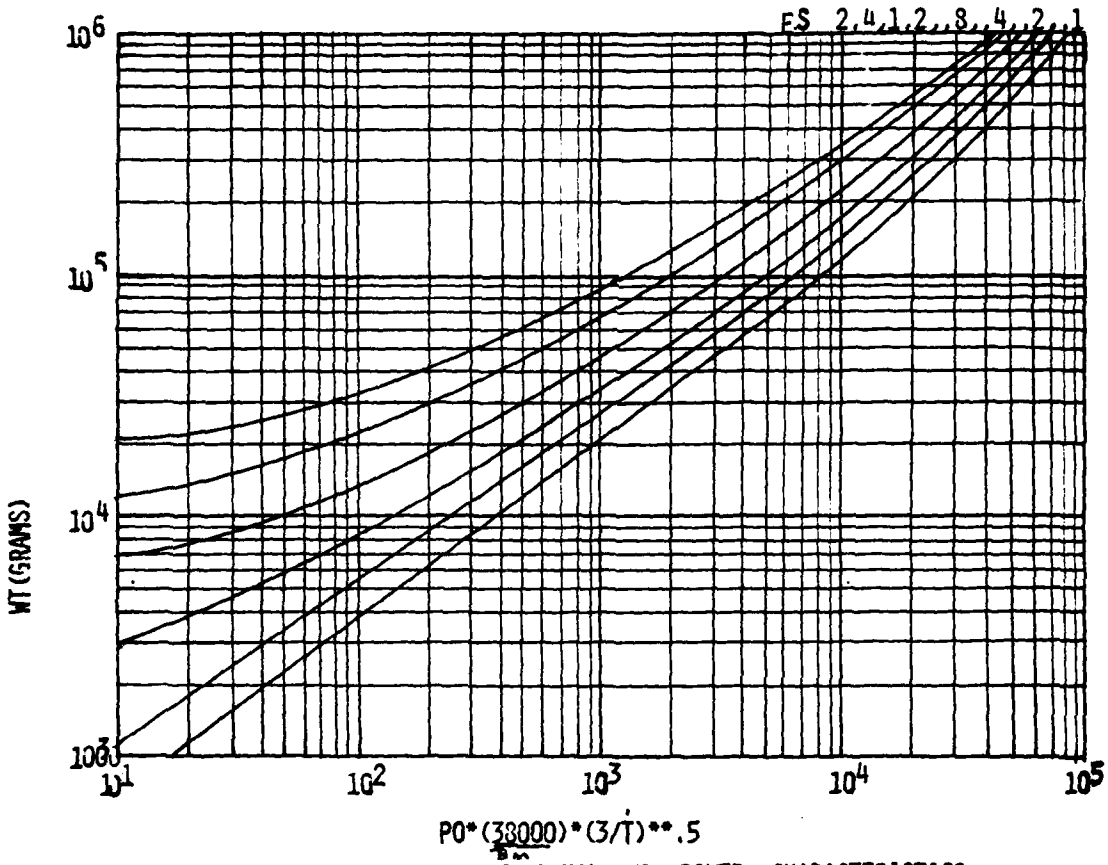

FIG.7 WT(GRAMS) VS POWER CHARACTERISTICS

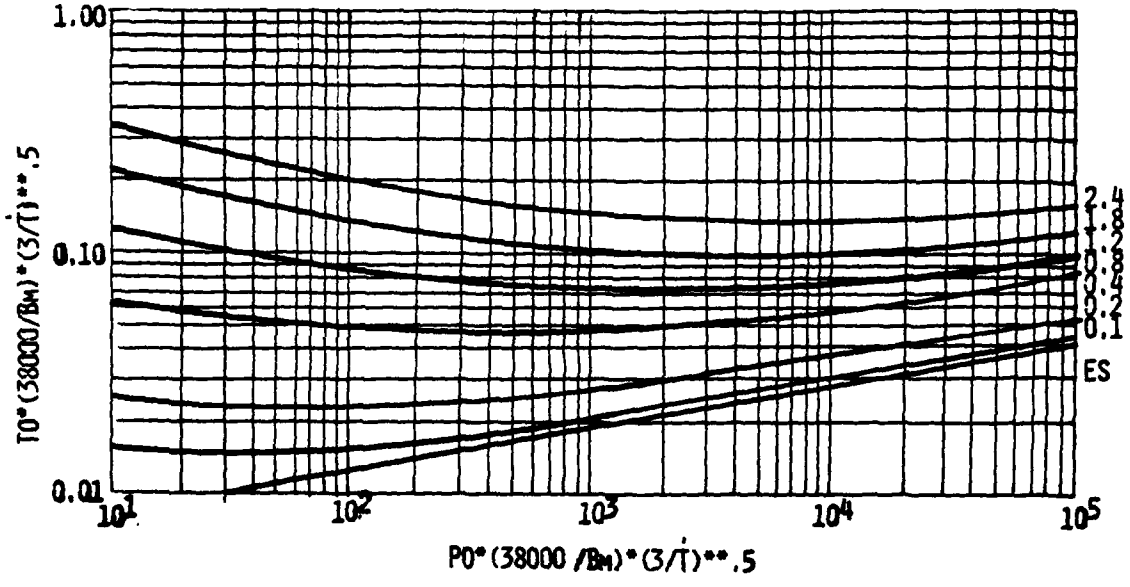

FIG.8
TO (RISE TIME PARAMETER) VS POWER CHARACTERISTIC

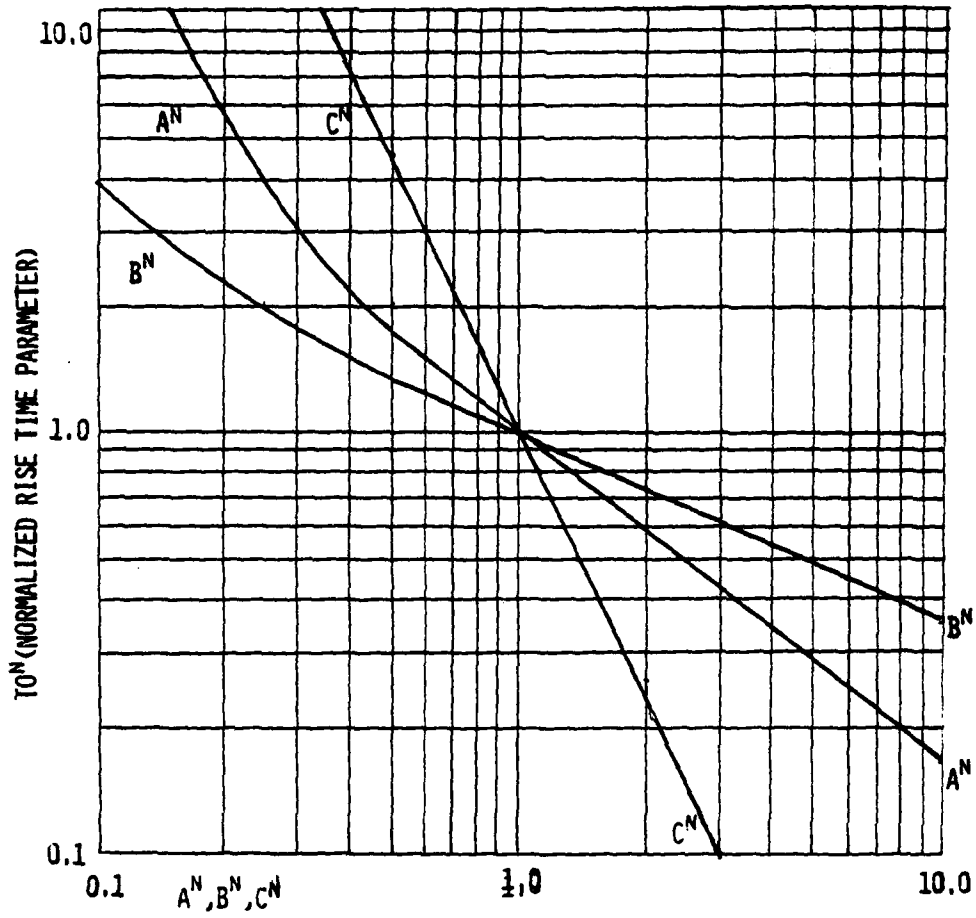

FIG.9 TO^N VS NORMALIZED DIMENSION PARAMETERS

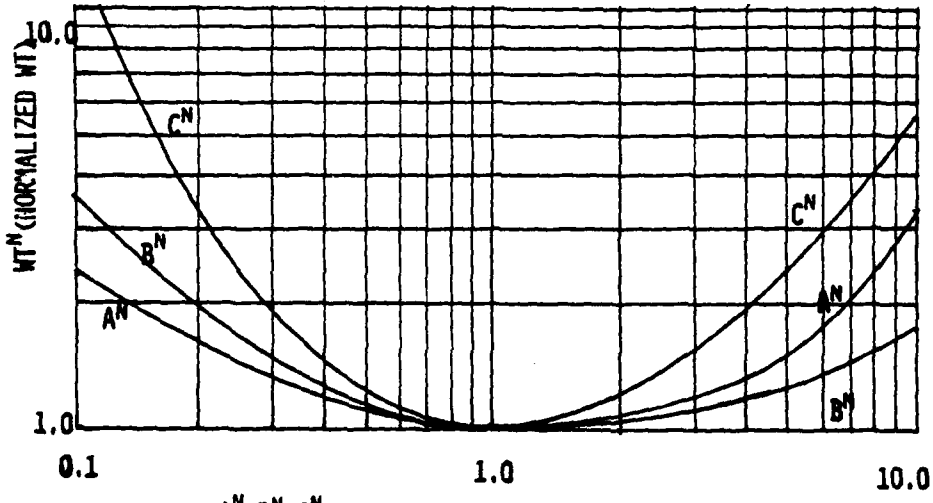

FIG.10

WT^N(NORMALIZED WT) VS NORMALIZED DIMENSION RATIOS

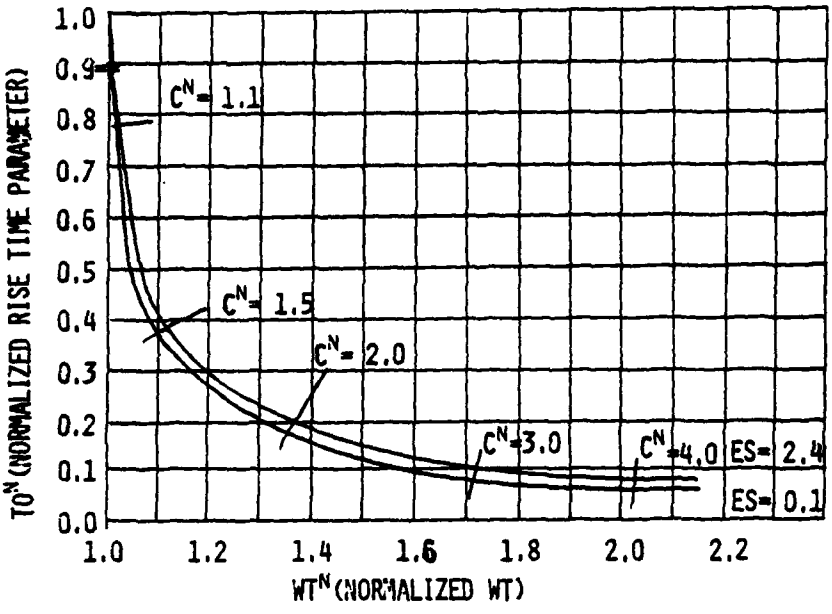

FIG.11
TO^N (NORMALIZED RISE TIME PARAMETER) VS NORMALIZED WT

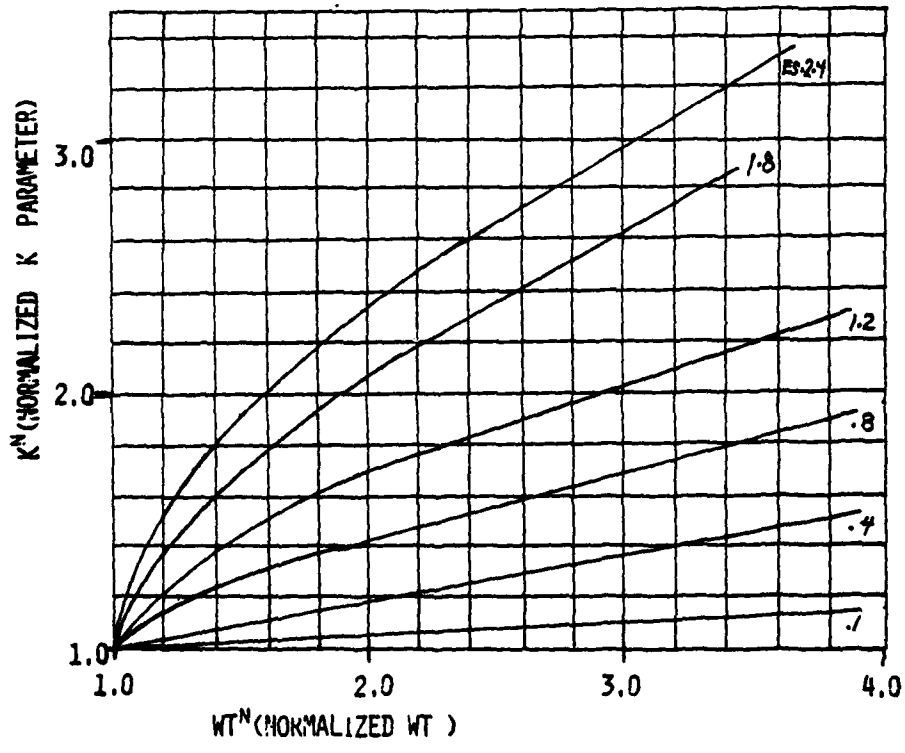

FIG.12
K^N (NORMALIZED K PARAMETER) VS NORMALIZED WT

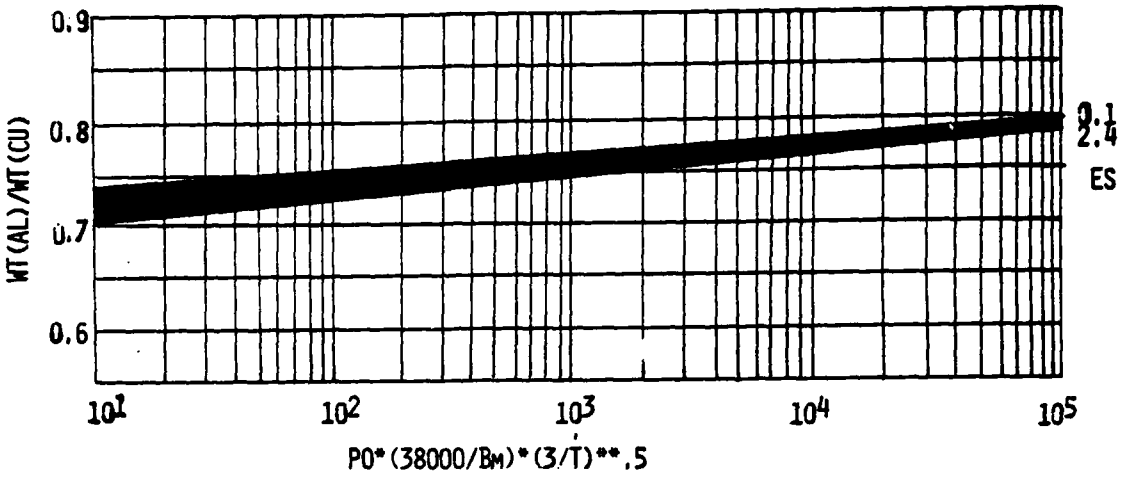

FIG.13

WT OF AL COIL TRANSFORMER/WT OF CU COIL TRANSFORMER VS POWER CHARACTERISTIC

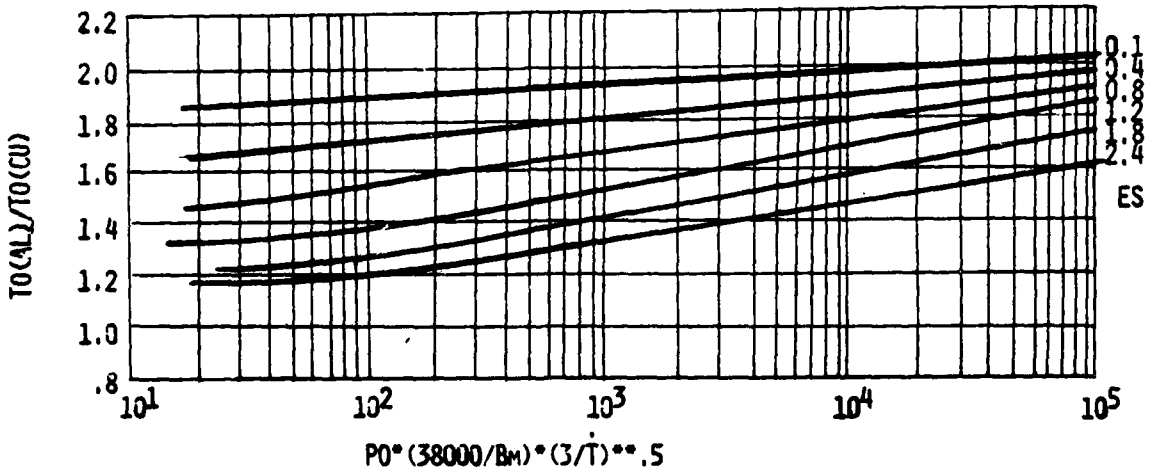

FIG.14

RISE TIME CHARACTERISTIC AL/RISE TIME CHARACTERISTIC CU VS POWER CHARACTERISTIC

The PO and TO parameters for this specification by equations (1) and (2) are:

$$PO = 20\times10^{-6}\frac{(60\times10^{3})^{2}}{5}\sqrt{.0056} = 1066$$

$$TO = 15\times10^{-6}/(5\times20\times10^{-6})\sqrt{.0056} = .0112$$

Complete full power testing of the model was not possible because of modulator power limitations. The leakage inductance specification of 15 microhenries was not quite met, the model measured 17 microhenries but it is felt that this could be brought into specification with minor coil modifications, particularly in the lead breakout. The core reset characteristics and permeability were evaluated and found to be satisfactory. The core material, .004 (mil) Vanadium Permendur, operated satisfactorily up to 40,000 gauss (total reset flux swing). The measured pulse incremented permeability was 1500. The measured reset characteristic, flux swing versus core bias ampere turns, is shown in Figure 15.

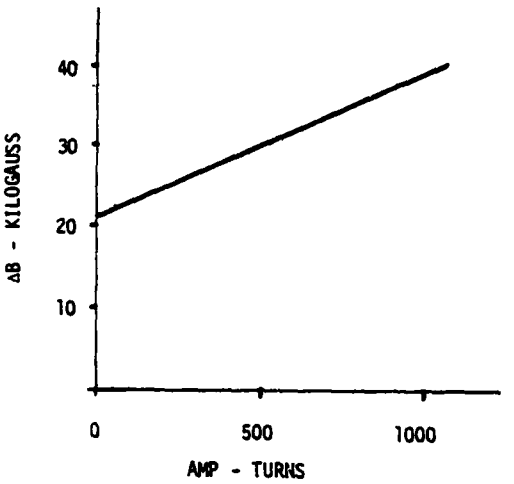

Fig. 15. Flux Reset Characteristic of Model Transformer

From Figures 3, 4, 5, 6, 7 and 8 the characteristics of the design optimal for PO = 1066 are: A = 1.75, B = 1.2, C = .42, K = 8000, TO = .047, WT = 40 kg. Since this design gives a TO = .047, and a TO = .0112 is required, the C ratio must be increased by 1.9 to give a rise time improvement of 4.2 with a weight penalty of 1.35 as determined in Figures 11 and 12.

In Table III the optimized design parameters as determined from the charts are compared to the actual parameters used in the model design which was constructed. The 58 kg weight given for the model is the coil, core and insulation weight and does not include the case, terminals and fill. In the design and construction of the case for the model no particular effort was made for a low weight. The total cased weight of the model is 103 kg. With an optimum weight case design this could be reduced to about 80 kg.

TABLE III

Parameter	Opt Design	Model
A	1.75	1.6
B	1.2	1.75
C	.798	.625
K	9600	11654
V	9.2 cm	10.16 cm
W	11.87 cm	17.78 cm
X	6.83 cm	6.35 cm
Y	11.95 cm	10.16 cm
WT	54 kg	58 kg

CONCLUSIONS

It is concluded that the geometrical proportions are an important consideration in optimizing a pulse transformer design, however, the sensitivity of optimization to geometry is such to permit moderate departures from the true optimum geometry sufficient to accommodate the use of standard wire size and core size increments with penalties of only a few percent. Also some weight advantage is possible by using aluminium windings in designs with slow risetime requirements. It is also concluded that the use of Vanadium Permendur core material with d.c. reset is feasible up to 40,000 gauss.

REFERENCE

[1] R. Lee, "Properties of reset cores in radar pulse transformers," J. Appl. Phys. Suppl., vol. 33, Mar. 1962.

CONSTANT CURRENT CHARGING CIRCUITS FOR HIGH ENERGY MODULATORS

John L. Carter
US Army Electronics Technology and Devices Laboratory (ECOM)
Fort Monmouth, NJ 07703

ABSTRACT. In the design of power conditioning systems for high energy systems for short term operation, the interface between the prime power and the pulser requires careful consideration. In the majority of cases the prime power source considered is a battery or conventional alternator with rectified output. The considerations of transient operation of the prime power source and allowable peak values of voltage and current supplied by the prime power source has profound effects on the design of the prime power source. For the case of an alternator feeding into a rectifier and resonant charging of a PFN the fact that the current on the dc side of the rectifier is time variable adds not only additional transients and heat loading to the alternator but also generates mechanical stress problems because the torque loading of the generator varies with the output power. In the case of a battery prime power source, resonant charging leads to the requirement for a battery bank with larger peak values of voltage and current than would normally be required to supply the same average power into a constant load.

A technique has been investigated to achieve square wave charging of the pulse forming networks in line type pulsers. The proposed circuit uses parallel PFNs with charging inductors connected between the PFNs. The value of the charging inductors is chosen so that when combined with the total capacitance of the PFNs, the charging network pulse width equals the interpulse period.

Experimental and computer data will be presented for the constant current charging circuit and compared with resonant charging circuits.

INTRODUCTION

The conventional resonant charging circuit for high energy pulsers is shown in Figure 1. The pulser consists of multiple PFNs and switches. Multiple PFNs are used in order to achieve the low PFN impedance required to match the load through the pulse transformer. There is a lower limit to the PFN impedance determined by capacitor inductance. Therefore, the most practical approach is to parallel a number of PFNs to achieve the low impedance value. Multiple switches are used in order to maintain the current ratings of the switch within realistic values. Thyratrons are used as the switch element in the circuit shown in Figure 1. The capacitors are charged from the dc power supply through a charging inductor. The charging inductor is designed to resonate the total capacitance of the networks at the specified pulser repetition rate. The charging inductance of the network is given by the equation:

$$L = \frac{T^2}{\pi^2 4C} \qquad (1)$$

Where L = charging inductance
T = charging period
C = total PFN capacitance

The charging current for this type of circuit is given by:

$$I = \left(\frac{E}{Zo}\right) \sin \omega t \qquad (2)$$

$$\text{Where } Zo = \left(\frac{L}{C}\right)^{1/2}$$

$$\omega = (LC)^{-1/2}$$

E = dc power supply voltage

The charging current wave form for this circuit is a half sine wave with a maximum value of E/Zo, with a period equal to 1/PRF.

The proposed constant current charging circuit is shown in Figure 2. Charging inductors are connected to each of the pulse forming network terminals. The inductance of each section is chosen so that charging inductors and the total capacity of the networks comprise a pulse forming network which will allow constant current and voltage charging. The inductance of the individual networks is small enough to be ignored in comparison with the charging inductance. Each PFN section requires its own discharge switch. A single discharge switch cannot be used since the PFNs would then have to be connected to a common point which would short out all but the first charging inductor section. A single discharge switch can be used if diodes are inserted to prevent charging from the switch end of the PFNs.

Experimental Test Circuit

A low voltage test circuit was used to verify the concept. The low voltage circuit makes it possible to make accurate measurements at various points in the circuit without encountering high voltage measurement problems. Fabrication cost and time are also greatly reduced.

The test circuit is shown in Figure 3. Four PFNs and four switches are connected in parallel. The switches are 1258 thyratrons. The individual 25 ohm PFNs have a pulse width of 5 μs. The capacitance of each network is 0.1 μf and the inductance is 62.5 μH. These values were used in the design of a charging network for a pulser operating at a pulse discharge repetition frequency of 250 Hz, or a charging period of 4×10^{-3} seconds. The charging period and the total capacitance of the discharge pulse forming network is used to calculate the inductance required for the charging pulse forming network using the following equation:

$$L = \frac{T^2}{4C} = \frac{(4 \times 10^{-3})}{16 \times 10^{-7}} = 10 \text{ henrys} \qquad (3)$$

The inductance value for each of the adjustable inductors is therefore 2.5 henrys. The calculated discharge load impedance is 6.25 Ω since four 25 ohm networks are connected in parallel through the thyratron switches. Since operation was at low dc voltage (100 volts) the thyratron impedance had to be considered. It was determined experimentally that a load impedance of 1.3 ohms gave the best impedance match. The charging voltage and current for the circuit is shown in Figure 4. The charging voltage is 100 volts, the top horizontal line of the lower voltage curve represents the 100 volt calibration line. The charging sequence for the PFNs is shown in the voltage

curves in Figure 4 to Figure 7. The last PFN #4 charges directly to twice the power supply voltage after a delay of about 1 millisecond, the third and second charge in steps after a time delay. The charging current pulse width in Figure 4 is very close to the design value of 4 milliseconds at the half amplitude point. The rise time is 0.5 millisecond and the fall time approximately 0.8 millisecond. The amplitude of the pulse is 22 milliamps compared to the calculated value of 20 milliamps. The discharge current through the 1.3 ohm load is shown in Figure 8. Measurement of the current through the switches indicates that the current is shared equally by the switches.

The experimental circuit was modified for resonant charging in order to obtain comparison data. The resonant charging circuit is shown in Figure 9. The charging current waveform and the PFN voltages for resonant charging are shown in Figure 10 for a charging potential of 100 volts and 250 Hz discharge rate. The charging current is a half sine wave with a measured amplitude of 36 milliamps. The value calculated using equation (2) is 32 milliamps.

The circuit was also analyzed by computer using the ECAP circuit analysis program. The current wave form for the experiment circuits shown in Figure 3 and Figure 9 obtained using computer analysis is shown in Figure 11. Good agreement was obtained between the two techniques.

Preliminary Design of a Multi-Megawatt Average Power Pulser

The circuit for a proposed pulser for multi-megawatt applications is similar to that shown in Figure 2, except that thyratron switches are used, and each thyratron switches a group of PFNs connected in parallel. The charging network consists of charging inductors connected between the groups of PFNs. The design procedure described above for the experimental circuit was used to calculate the inductance values. In order to achieve a better pulse shape the value of the first and last inductor was increased by 20% and 15% respectively. The current wave form for the six section charging network obtained by computer analysis is plotted in Figure 12. The wave form obtained using resonant charging is also plotted. The constant current charging circuit draws 35% less current than the resonant charging circuit.

The trade-off between resonance charging and constant current charging is peak current vs. weight. In order to gain some insight on the weight of the two circuits, a weight analysis of both circuits was made for the case of charging 60 μf to a peak voltage of 40 kv at a repetition rate of 125 Hz.

The results of this analysis is given in Table I. A current density of 14,000 amps per in^2 was used in calculating wire size. The best available information indicates that this is the maximum current density that can be used for aluminum wire and still satisfy thermal operating requirements. The RMS current for each section of the charging inductor was calculated and the wire size selected to maintain a constant current density. The power dissipated is calculated in the same manner.

The weight of the constant current inductor is 127 pounds while the weight of the resonant charging inductor is 64 pounds. This is wire weight only, and does not include insulation, form, and bushing weight.

Another factor that must be considered is the amount of power dissipated in the charging inductor. The power dissipated in the inductor must be supplied by the prime power supply, therefore, adding additional weight to the supply and the overall system. In order to obtain a realistic comparison of the two different types of charging circuits, a power supply weight penalty must be added to the actual charging circuit weight. The power supply weight penalty will vary for different types of supplies, and the dissipation is a function of the type of conductor material and the current density in the material. The total weight of the charging inductor for the 6 MW modulator described above has been calculated as a function of wire current density assuming power supply penalties ranging from 0.4 pounds - 1.8 pounds per kW of inductor dissipation. The results for resonant charging is plotted in Figure 13 and constant current charging in Figure 14. Preliminary prime power studies indicate that the prime power penalty will be in the range of 0.8 pound to 1.2 pounds per kW of power dissipated. If we consider this penalty range the minimum weight for both the resonant charging and the constant current charging circuits falls in a current density range of 10,000 to 14,000 amps per square inch for aluminum wire. The current density selected using thermal considerations was 14,000 amps per in^2.

It should be noted that the weight of the constant current circuit is about twice the weight of the resonant charging circuit at the same current density and prime power penalty.

CONCLUSIONS

The results of the investigation described above show that a circuit to achieve constant current charging is feasible. The major disadvantage is the increased weight and dissipation of the components. The constant current charging circuit is desirable only if the lower peak current demands, and reduced mechanical requirements result in a weight savings in the prime power supply that exceeds the increased weight of the constant current charging inductor.

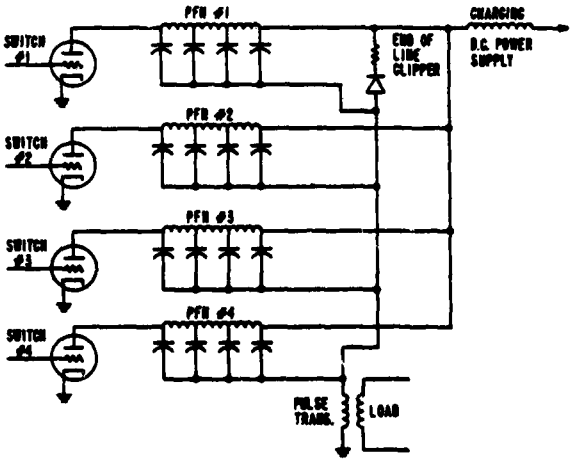

D.C. RESONANCE CHARGING PULSER

Figure 1

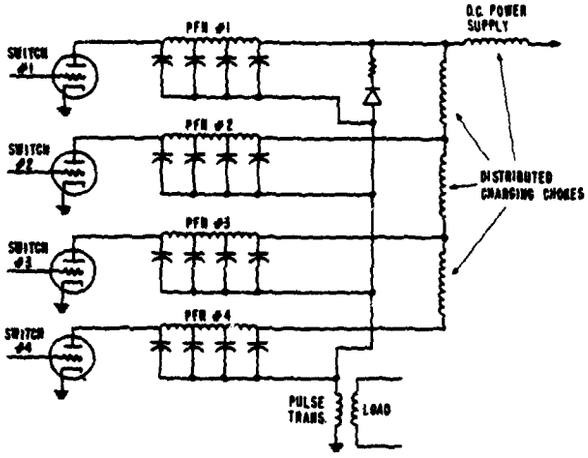

CONSTANT CURRENT D.C. CHARGING PULSER
Figure 2

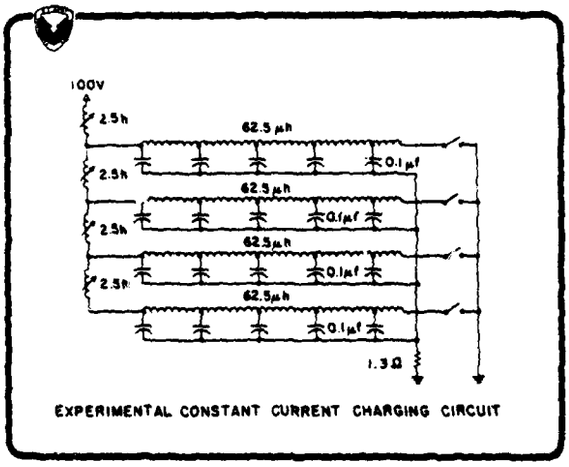

Figure 3

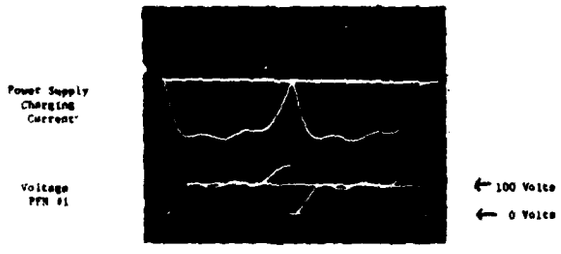

Figure 4
Constant Current Charging
Upper Trace Vertical 10 MA/div
Lower Trace Vertical 100 V/div
Horizontal 1 Millisecond/div

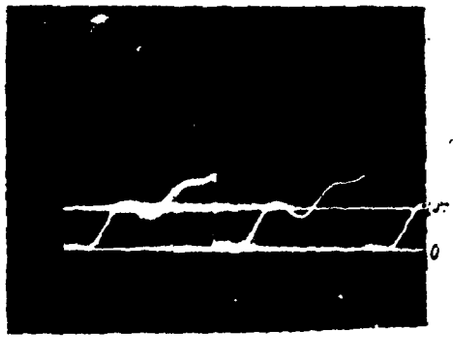

Figure 5
Charging Voltage PFN #2
Vertical 200 volts/div
Horizontal 1 millisecond/div

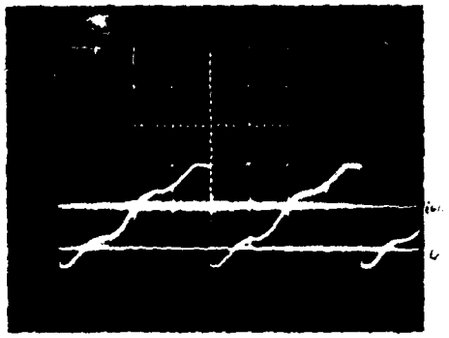

Figure 6
Charging Voltage PFN #3
Vertical 100 V/div
Horizontal 1 millisecond/div

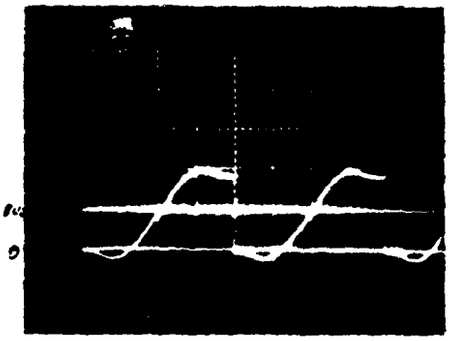

Figure 7
Charging Voltage PFN #4
Vertical 100 V/div
Horizontal 1 millisecond/div

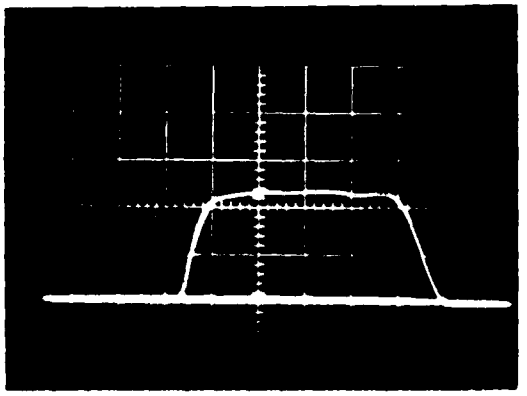

Figure 8

Discharge Load Current
Vertical 2.5 Amp/div
Horizontal 1 usec/div

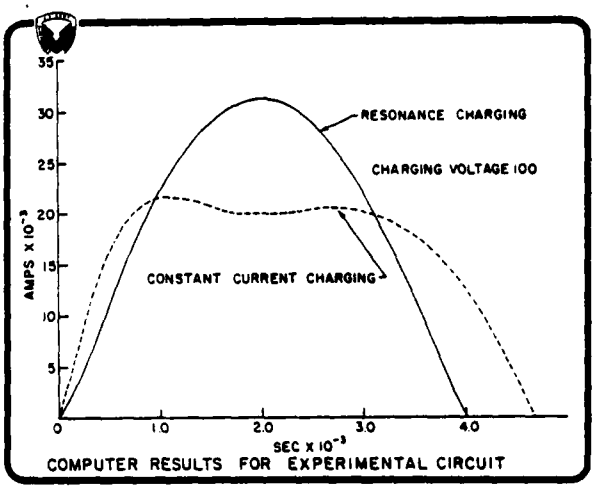

Figure 11

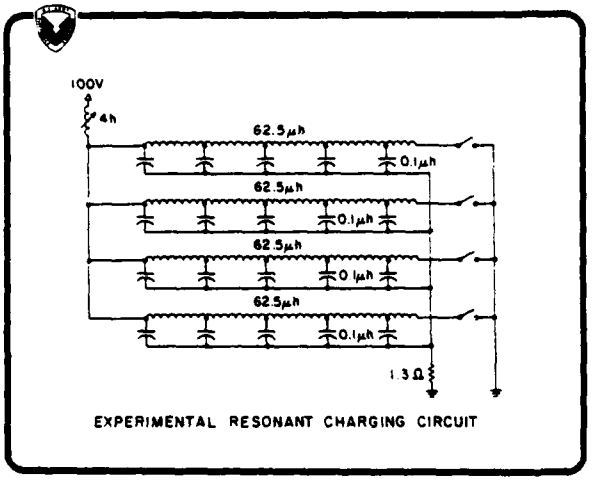

Figure 9

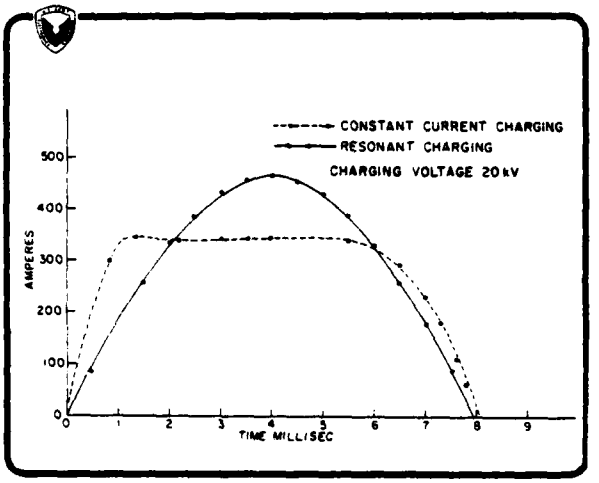

Figure 12

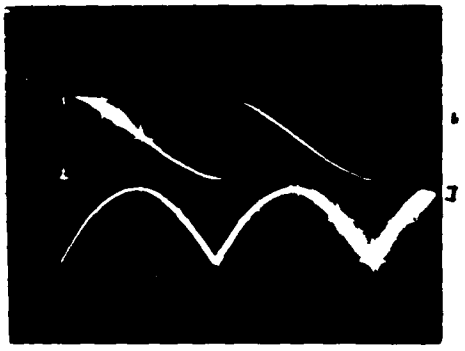

Figure 10

Resonant Charging Voltage
and Current
Upper Trace 100 V/div
Lower Trace 20 MA/div
Horizontal Sweep Speed 1 MS/div

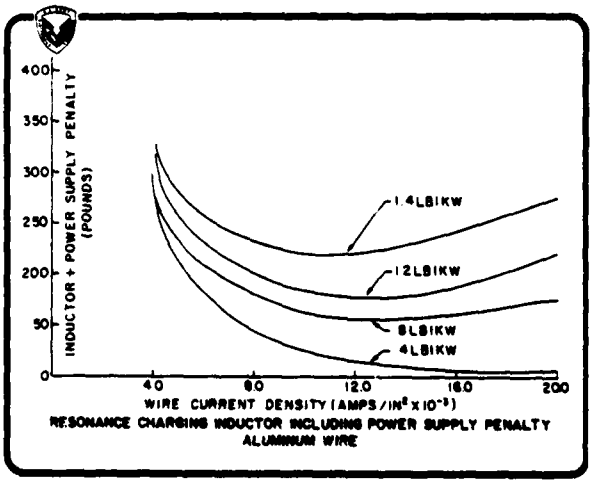

Figure 13

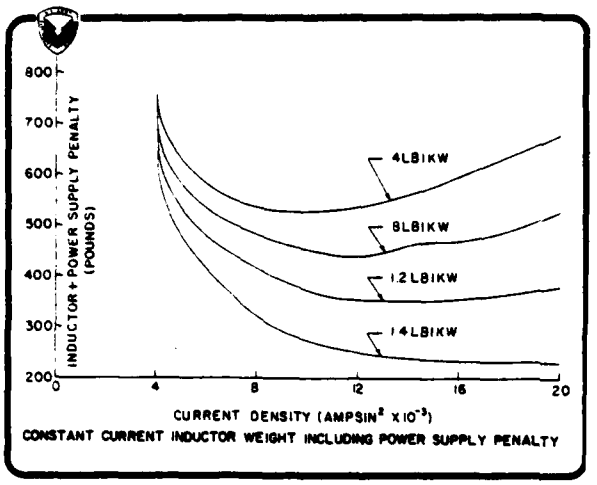

Figure 14

TABLE I. PARAMETERS FOR CHARGING INDUCTORS

CONSTANT CURRENT CHARGING INDUCTOR

COIL INDUCTANCE		CURRENT	WIRE DIAMETER	WIRE NO.	WIRE LENGTH	COIL WEIGHT	COIL RESISTANCE	COIL DISSIPATION
Units	Millihenrys	Amps RMS	Inches		Feet	Pounds	Ohms	Kilowatts
#1	40.8	327	0.102	#5	1,172	35.71	0.504	63.5
#2	34.2	302	0.102	#6	1,026	24.73	0.655	59.7
#3	34.2	277	0.102	#6	1,026	24.73	0.655	50.7
#4	34.2	243	0.144	#7	979	18.76	0.888	46.6
#5	34.2	181	0.129	#8	934	14.28	0.952	31.1
#6	39.1	114	0.102	#10	923	8.83	1.498	19.4
TOTAL						126.96		300.0

RESONANT CHARGING INDUCTOR

TOTAL	100	326	0.102	#5	2,103	64.1	1.067	115

MODULATOR PERFORMANCE PREDICTION BY SIMULATION

T. H. Powell, Jr., L. A. Kerr, J. Basel
The Bendix Corporation
Communications Division
Towson, Maryland 21204

Summary

Advances in digital signal processing made during the last several years have led to an improved target detection in clutter capability for MTI (Moving Target Indicator) radar. In attempting to incorporate the improved receiver processing circuitry into existing radars, the transmitter often presents a problem because of the requirement for short term variation of the PRF of a line-type modulator. Voltage variations at the modulator output cause phase and amplitude modulation of the transmitted waveform. This degrades the MTI performance by imparting apparent motion onto stationary clutter.

The task for the design engineer is to determine what modifications should be made to the existing transmitter so that the transmitter stability does not degrade the capability of the improved processing circuitry. Accomplishing this by trial and error experimentation is not very desirable since modifications can be expensive and the experiments are tedious (due to the high voltage). The more desirable method is to obtain a transient solution of the linear circuit equations using the Laplace transform. This is nearly untractable however, because of the algebra involved, non-linear elements, and the need to re-initialize the capacitors and inductors each pulse period.

The purpose of this paper is to demonstrate that a well documented, available, and easily used computer program termed ECAP (Electronic Circuit Analysis Program) can accurately predict the modulator transient waveforms. The paper discusses simplification and linearization of the power supply and modulator circuit model, and compares graphic predictions of the power supply ripple and the output pulse amplitude (modulating pulse to the Klystron) with photographs of an actual modulator under the same varying PRF conditions. The options for solving the problem are discussed briefly.

Introduction

The specific task being addressed here is to determine the change in amplitude of the modulator output pulse when a 10-percent alternating block variation of 10 pulses, as illustrated in Figure 1, is applied to the line-type modulator of a modified AN/FPS-20A radar. A model of this radar is located at the Bendix plant in Towson, Maryland. A photograph of the installation is shown in Figure 2. It is an L-band (1250 MHz–1350 MHz) air search radar, designed for a constant PRF of 360 PPS, with a pulse width of 6 μs and is equipped with MTI processing circuitry.

A schematic of the line-type modulator is shown in Figure 3. It is basically a series tuned LC circuit resonant at one-half the PRF frequency. The modulator has been modified by inserting a hold-off diode. The principles and operation of the line-type modulator are discussed thoroughly in the literature[1,2] since it is widely used in conventional radar.

Circuit Model

The circuit model to be analyzed is shown in Figure 4. Several simplifications were made.

The PFN network was eliminated since only the change in pulse amplitude rather than its exact amplitude or shape is important.

The power source, which consists of three full wave rectifiers (six tubes), was replaced with a Thevenin equivalent voltage source.

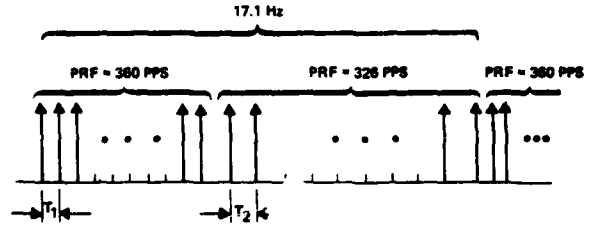

F 1.
10 PULSE BLOCK PRF VARIATION PERIOD = $10(T_1+T_2)$ = 58.45 MS)

FIGURE 2.
MODIFIED AN/FPS-20A TEST BED RADAR INSTALLATION

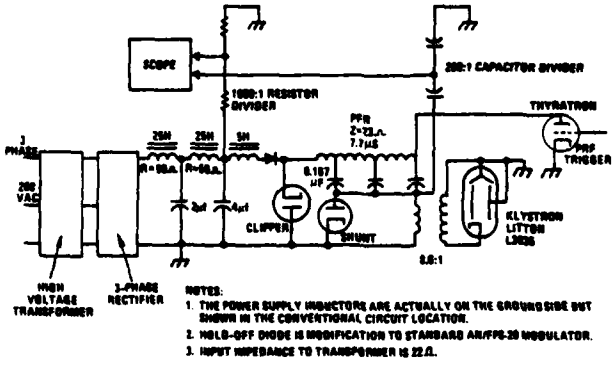

FIGURE 3.
POWER SUPPLY AND MODULATOR CIRCUIT FOR MODIFIED AN/FPS-20 RADAR SYSTEM

The circuit model is prepared for ECAP by associating each element with a branch number B1, B2, . . . , BN. Nodes are identified as V1, V2, . . . , VM. Switched loads and diodes are two valued branches identified as (R1, R2), having resistance value R1 in one state and R2 in the other state.

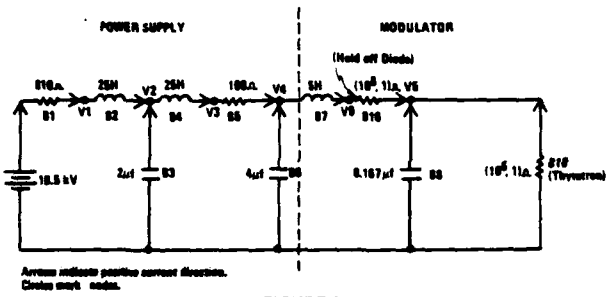

FIGURE 4.
ECAP POWER SUPPLY AND MODULATOR MODEL

The actual rules for encoding will not be discussed, but are straightforward and covered in the ECAP manual.[3] ECAP, itself, is an IBM routine. It requires a computer with a Fortran compiler, a disk, card reader, punch (optional), and at least 8K of core storage. The algorithm approximates the differentials and integrals with finite differences and sums. Starting with the initial conditions, the circuit currents and voltage are computed in discrete time steps. The final values for the given time step then become the initial conditions for computation in the next time interval. This approach allows piecewise modeling of non-linear elements, although errors will accumulate due to the recursive type calculation.

Results of ECAP Program

The ECAP program was run for the case of (1) a constant PRF of of 360 PPS and (2) a 10 percent block variation of the PRF as shown in Figure 1. The modulator is assumed to operate under full power which corresponds to a voltage supply source of 16.5 kV.

Constant PRF of 360 PPS

Since the ECAP program is performing a DC transient solution it expedites the running time to compute the steady state voltage values and use them as initial conditions at the starting time.

The predicted waveform at the power supply output is plotted in Figure 5A. It shows a sinewave modulation of 220 volts peak-to-peak synchronized with the PRF on a DC voltage of 14.66 kV.

The predicted pulse amplitude of 13.5 kV is plotted in Figure 5B. This amplitude is computed from the ratio of the PFN characteristic impedance (23Ω) to the load resistance of 22Ω based on the voltage across the 0.167 μF capacitor (V5) at the instant prior to the Thyratron trigger.

Variation of the PRF

Figure 6A plots the expected voltage at the power supply output for the case of the PRF variation shown in Figure 1. The results show a peak-to-peak change of 350 volts synchronized with the PRF superimposed on a peak-to-peak change of 971 volts during one full cycle of the PRF variation (58.45 ms). The average DC level at the power supply output is 15.1 kV.

Figure 6B plots the expected pulse output amplitude for the given PRF variation. The envelope of the pulse train follows an exponential increase and decrease with a peak-to-peak change of 614 volts.

Experimental Measurements

Photographs were taken of the waveforms at the output of the power supply and of the pulse on the primary of the transformer driving the Klystron. These measurements were made on the modified AN/FPS-20 system discussed earlier using the resistive and capacitive dividers shown in Figure 3. Tests were made with both a constant and varied PRF.

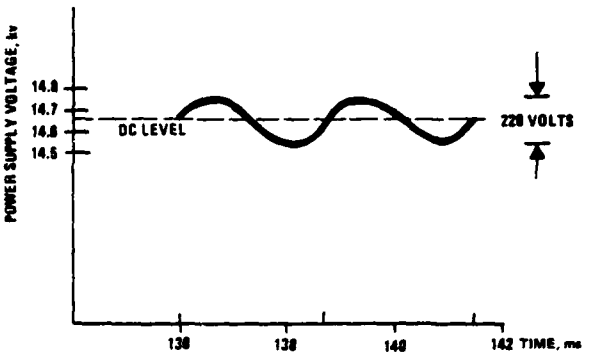

FIGURE 5A.
ECAP PREDICTED VOLTAGE VARIATION OF POWER SUPPLY AT CONSTANT PRF OF 360 PPS

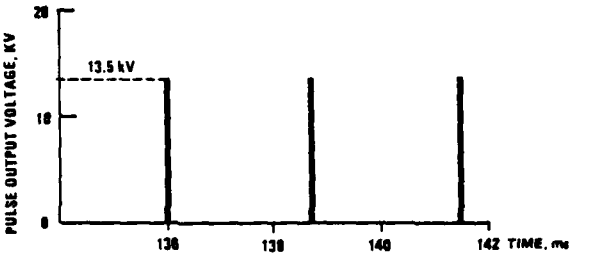

FIGURE 5B.
ECAP PREDICTED OUTPUT PULSE AMPLITUDE AT CONSTANT PRF OF 360 PPS

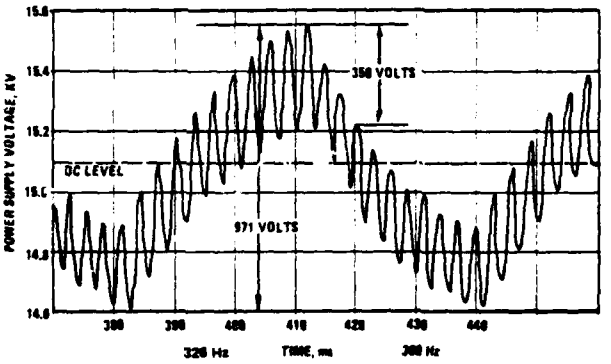

FIGURE 6A.
ECAP PREDICTION OF POWER SUPPLY OUTPUT VOLTAGE UNDER PRF VARIATION

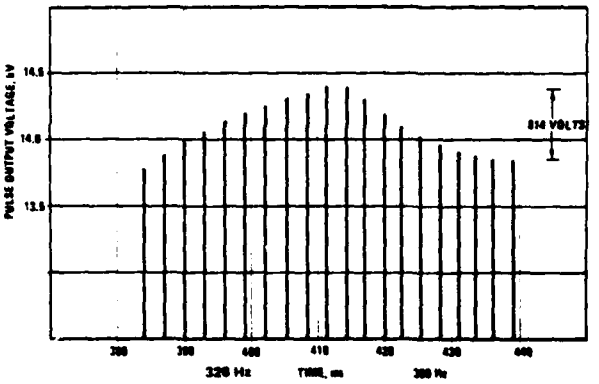

FIGURE 6B.
ECAP PREDICTION OF PULSE AMPLITUDE OUTPUT UNDER PRF VARIATION

Constant PRF of 360 PPS

Due to a temporary problem with the Thyratron the power supply output was held to 8.8 kV instead of the full power supply output voltage of approximately 14.66 kV.

Figure 7 shows the waveform on the power supply output. It consists of a sinewave synchronized with the PRF having a peak-to-peak amplitude of 150 volts. Superimposed on the photograph is the pulse output with an amplitude of approximately 9.4 kV.

To compare these results with the ECAP simulation the previous values must be scaled by the ratio of the power supply voltages. The predicted sinewave peak-to-peak variation therefore is 132.6 volts (220 x 8.8/14.66), and the predicted pulse amplitude is 8.10 kV. Although the magnitudes are in error by approximately 11 and 13 percent, respectively, the power supply waveform corresponds precisely with the ECAP result.

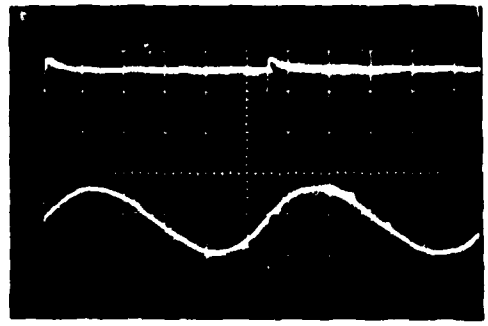

FIGURE 7.
POWER SUPPLY OUTPUT AND PULSE AMPLITUDE OUTPUT WITH CONSTANT PRF OF 360 PPS

POWER SUPPLY	VERTICAL: 100V/cm HORIZONTAL: 0.5 ms/cm
PULSE AMPLITUDE	VERTICAL: 2 kV/cm HORIZONTAL: 0.5 ms/cm

Variation of the PRF

Figures 8A and 8B plot the power supply output and the output pulse amplitude for a PRF variation between 326 PPS and 360 PPS in the format illustrated in Figure 1.

The waveform at the power supply output (Figure 8A) consists of a peak-to-peak sinewave fluctuation of 221 volts (at top of cycle) synchronized with the PRF superimposed on a peak-to-peak change of 610 volts during one full cycle of the PRF variation (58.45ms). This corresponds closely to the ECAP prediction (after scaling to a power supply voltage of 15.1 kV) of 204 volts and 566 volts respectively. These results represent errors of 7.6 and 7.2 percent.

The pulse amplitude output waveform (Figure 8B) shows a peak-to-peak change of approximately 315 volts. This compares with an ECAP prediction of 358 volts (614 x 8.8/15.1) and represents an error of 13 percent. Although the amplitude variation appears sinusoidal, the positive and negative slopes are slightly different suggesting that the exponential prediction for the waveform is correct.

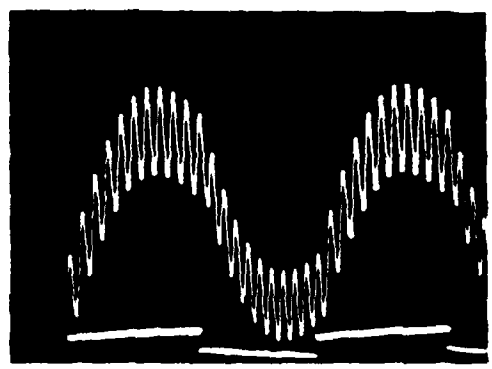

FIGURE 8A.
POWER SUPPLY OUTPUT WITH PRF VARIATION OF 10 PULSES AT 326 PPS FOLLOWED BY 10 PULSES AT 360 PPS

SCALE
VERTICAL: 100 V/cm
HORIZONTAL: (Uncalibrated)

Proposed Approaches

The amount of amplitude change that can be tolerated on the output pulse will be determined by the specifics of the MTI system. The degradation in performance results primarily from phase modulation of the Klystron and secondarily from the amplitude modulation itself. Additional factors include the spectrum of the phase modulation (sinusoidal in this case) and the type of receiver processing.

The phase variation to the Klystron is:

$$\Delta\phi = K_\phi N \Delta A$$

where
- K_ϕ = Klystron pushing figure ≈ 3.85 degrees/kV for L3035
- N = transformer turns ratio ≈ 8.61
- ΔA = amplitude change in kV across transformer primary

Once the required amplitude change has been determined, the first step is to add a hold-off diode (the standard AN/FPS-20 modulator does not have a diode in the circuit). Increasing the power supply capacitance is undesirable because of the increased energy that must be dissipated in case the Thyraton "hang-fires."

Series or shunt regulation is another alternative. Shunt regulation was simulated by switching an 83.77K resistor across the power supply during the lower PRF. This value was computed from the average resistance seen at 360 PPS and 326 PPS assuming a 7.7 μs pulse width and a 22Ω load:

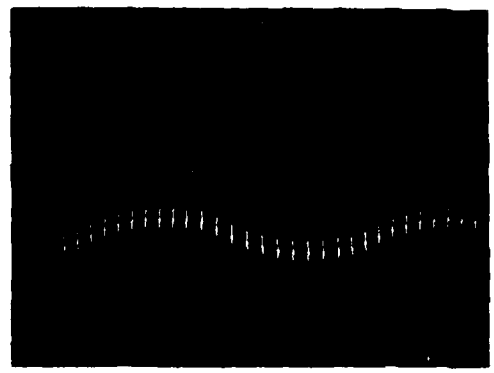

FIGURE 8B.
PULSE AMPLITUDE OUTPUT WITH PRF VARIATION OF 10 PULSES AT 326 PPS FOLLOWED BY 10 PULSES AT 360 PPS

SCALE
VERTICAL: 400 V/cm
HORIZONTAL: (Uncalibrated)

$$R = \frac{2777}{7.7} \times 22\Omega = 7.934K\Omega \quad PRF = 360\ PPS$$

$$R = \frac{3067}{7.7} \times 22\Omega = 8.764K\Omega \quad PRF = 326\ PPS$$

The 83.77K resistor in parallel with the 8.764K resistor at 326 PPS produces a constant average resistance of 7.934K. The peak-to-peak amplitude change was reduced to 98 volts on the output pulse.

Conclusions

The results demonstrate that ECAP is capable of predicting the form of the voltage change on the power supply and of the amplitude change of the output pulse very accurately for a line-type modulator under constant and varying PRF conditions. The predicted magnitude of the peak-to-peak fluctuations and the pulse amplitude were found to be in error, however, by about 12 percent.

The error in computing the voltage magnitudes is reasonable considering the uncertainties involved in modeling. The values were taken from the schematic and not measured at the operating point. The power supply resistance and power supply inductance were linearized, whereas both are known to be functions of the current drawn. A Thevenin equivalent voltage source was used and the pulse forming network eliminated. In addition, the ECAP computation itself has some inaccuracy. Although the calculations are made to 7 place decimal accuracy, the algorithm is recursive. As a result, errors can accumulate, particularly in circuits with several switches where the current changes orders of magnitude with the change in resistance.

Despite the errors involved, which can be reduced with a more accurate circuit model, ECAP is clearly a valuable tool for analyzing the transmitter power supply and modulator under varying PRF conditions.

A specific example of a 10-percent block variation of the PRF (shown in Figure 1) applied to a circuit model of a modified AN/FPS-20 transmitter was analyzed with ECAP. The results predict that at full power, the output pulse amplitude will change 614 volts, which represents a peak-to-peak phase modulation of 20.35 degrees (614 x 8.61 x 3.85) over a full cycle of the PRF variations (58.45 ms). The impact on the MTI system performance will depend on the specific processing.

References

1. Glasoe, G. N., and Lebacqz, J. B. (eds): "Pulse Generators," MIT Rad. Lab. Series, Volume 5, McGraw-Hill Book Co., N.Y., 1948.

2. Skolnik, M.: "Radar Handbook," McGraw-Hill Book Co., N.Y., 1970, Section 7.1.

3. Users Manual: "1620 Electronic Circuit Analysis Program, (ECAP) (1620 – EE – 02X), IBM Applications Program, H20-0170-1," IBM, 1965.

A CLASS D MODULATOR-REGULATOR FOR THE HIGH POWER RF SYSTEM OF A SYNCHROCYCLOTRON *

F. G. Tinta
Columbia University, New York, N.Y. 10027

Abstract

The frequency-modulated RF voltage in modern synchrocyclotrons has to meet relatively critical requirements in order to produce a time-stretched extractable beam of high intensity and low energy spread. A novel class D modulator-regulator was designed to control the power oscillator of the Nevis 550 MeV proton synchrocyclotron. The device provides voltage regulation of RF oscillations over a frequency sweep from 28 to 19 MHz and provides a programmable turnoff decay in the region where $d\omega/dt$ approaches zero. The RF power level is about 300 kW at 50% macroscopic duty factor. Feedback signals coming from RF and plate supply probes are compared with adjustable and programmable time-varying voltages in a low level control unit which generates pulses of constant amplitude but of variable width and repetition rate. These control pulses are applied to a switching type modulator-amplifier which, with suitable low pass filtering, supplies the RF power stage (in series). The total supply voltage is 14 kV. The final stage of the modulator employs tubes (pre-existing hardware), but the use of solid state switching devices is contemplated. Some pertinent problems of high level class D modulators for use in various applications are discussed. This use of class D modulator-regulator represents a new and so far unique approach in synchrocyclotrons. It has been in reliable operation for several months.

Introduction

Modern synchrocyclotron conversion projects aim for a substantial increase of the accelerated particle beam intensity. Details of such projects as well as the general framework can be found elsewhere.[1,2,3] The demand for high beam intensity implies, among other things, much higher RF accelerating voltages and a much higher RF power to be handled (well over one order of magnitude as compared with the previous situations).

Even the power carried by the beam of accelerated particles becomes important, for instance, a 20 μA beam of 550 MeV protons (typical design parameters) represents an average power of 11 kW and the instantaneous beam loading of the RF resonator is no longer negligible.

Figure 1 indicates the general layout of the Columbia University Nevis Synchrocyclotron which uses a particular configuration of "floating" magnetic sectors for strong focusing. Everything is enclosed in the vacuum tank (the pressure is in the mPa range, 1 mPa = 7.5 x 10^{-6} Torr.).

The RF voltage across the accelerating gap reaches peak values up to 40 kV. The delivered RF power exceeds 300 kW during the accelerating cycle and it is provided by a self-excited grounded grid RF oscillator using an ITT F 7560VN power triode. The oscillator is supplied via a series modulator regulator whose task is to turn on and off the high voltage at the beginning and at the end of the accelerating and to maintain a certain level of accelerating voltage over the FM cycle. During the FM cycle, one must compensate for the effects of beam loading, protect against sparking, and provide a turnoff voltage vs time curve for stretching the beam in a parking orbit before extraction.

Power Class D Modulation

Class D operation represents the use of switching capabilities of electron tubes or semiconductor devices for getting results which were previously obtained with exclusively analog techniques. It is in some way an extension of the class C mode used in tuned RF amplifiers.

The use of only on- and off-states brings an important reduction in the internally dissipated power (actually most dissipation is confined to switching time intervals) and may significantly increase stage efficiency. Class D operation has been investigated and used both in RF and LF applications and offers good promises for high power AM broadcasting transmitters[4,5] as well as for smaller audio amplifiers.[6] Pulse duration modulation is generally used and for LF applications, the output is smoothed out with low pass filters.

Efficiency computations can be found in the quoted literature. The present work represents the first use of class D techniques in particle accelerators and, to the best knowledge of the author, at the highest level of handled RF power.

For the present application, we have some particular constraints which benefit from the use of a class D modulator. The pulsing rate of our synchrocyclotron has a maximum value of 300 pps, but the machine has also to work well at very low pulse rate and even with non-recurrent pulses. This leads to the necessity of a direct coupled amplifier. The only analog alternative for the regulating function would be a class A direct coupled modulator. The power dissipation of the final modulator tubes (pre-existing hardware) would become prohibitive in true class A operation at full power).

In addition, for minimizing the energy wasted during "off time", the DC current has to be completely turned off. That requirement leads to the necessity of "floating" some low level control stages at a relatively high DC level, which again, poses some problems for the transmission of a regulating analog signal. In our configuration, the series modulator is on the high voltage (+14 kV) side and the filament of the power RF tube is DC grounded. We solved this problem by transmitting the on-off low level control signals via an optical coupler. On the other hand, the synchrocyclotron inherent phase stability provides rather large tolerance to small RF voltage level variations - such as

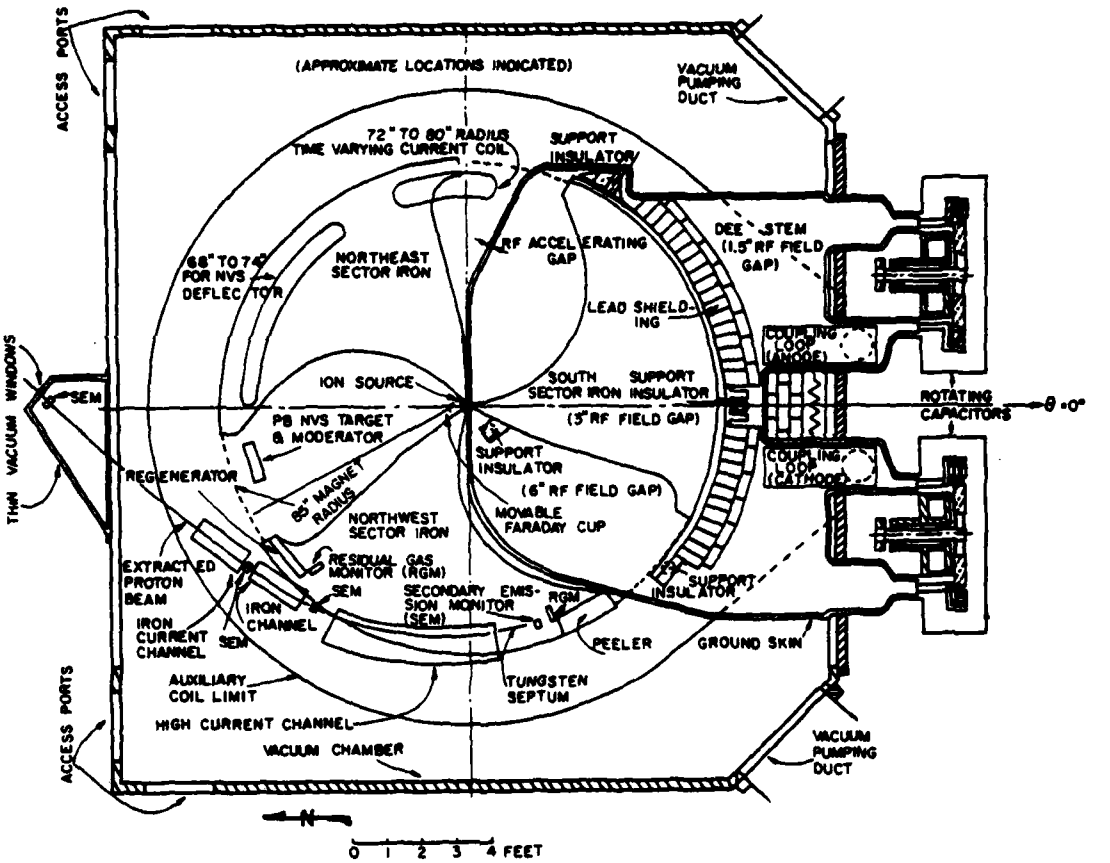
ACCESS PORTS
(APPROXIMATE LOCATIONS INDICATED)
VACUUM PUMPING DUCT
72" TO 80" RADIUS TIME VARYING CURRENT COIL
SUPPORT INSULATOR
DEE STEM (1.5" RF FIELD GAP)
68" TO 74" FOR NVS DEFLECTOR
NORTHEAST SECTOR IRON
RF ACCELERATING GAP
LEAD SHIELDING
COUPLING LOOP (ANODE)
THIN VACUUM WINDOWS
SEM
ION SOURCE
SOUTH SECTOR IRON
SUPPORT INSULATOR (5" RF FIELD GAP)
ROTATING CAPACITORS
θ = 0°
Pd NVS TARGET & MODERATOR
REGENERATOR
85" MAGNET RADIUS
SUPPORT INSULATOR (6" RF FIELD GAP)
COUPLING LOOP (CATHODE)
NORTHWEST SECTOR IRON
MOVABLE FARADAY CUP
EXTRACTED PROTON BEAM
RESIDUAL GAS MONITOR (RGM)
SEM
SECONDARY EMISSION MONITOR (SEM)
RGM
SUPPORT INSULATOR
IRON CHANNEL
IRON CURRENT CHANNEL
SEM
PEELER
GROUND SKIN
AUXILIARY COIL LIMIT
TUNGSTEN SEPTUM
HIGH CURRENT CHANNEL
VACUUM CHAMBER
ACCESS PORTS
VACUUM PUMPING DUCT
N
0 1 2 3 4 FEET

FIG. 1

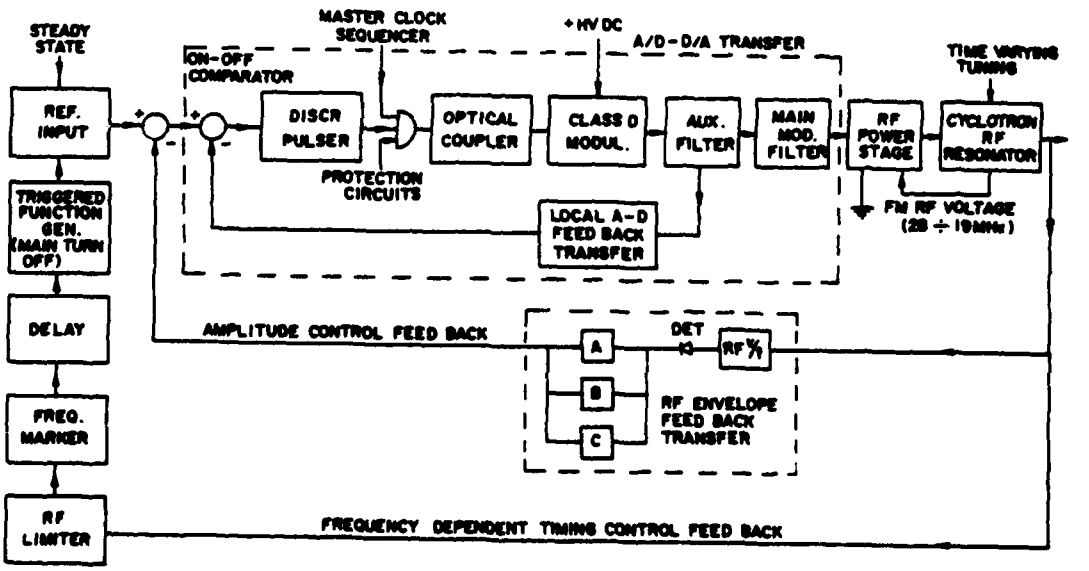
STEADY STATE
MASTER CLOCK SEQUENCER
+HV DC
A/D-D/A TRANSFER
TIME VARYING TUNING
ON-OFF COMPARATOR
REF. INPUT
DISCR PULSER
OPTICAL COUPLER
CLASS D MODUL.
AUX. FILTER
MAIN MOD. FILTER
RF POWER STAGE
CYCLOTRON RF RESONATOR
PROTECTION CIRCUITS
LOCAL A-D FEED BACK TRANSFER
FM RF VOLTAGE (2B ÷ 19MHz)
TRIGGERED FUNCTION GEN. (MAIN TURN OFF)
DELAY
AMPLITUDE CONTROL FEED BACK
DET
RF %
A
B
C
RF ENVELOPE FEED BACK TRANSFER
FREQ. MARKER
RF LIMITER
FREQUENCY DEPENDENT TIMING CONTROL FEED BACK

FIG. 2

residual ripple at the filtered output.

This situation eased somewhat the filtering requirements and gave the possibility of using a combined pulse duration and pulse rate modulation. The pulse rate is self-adjusting to the lowest rate required by the system. In comparison with class D modulators, which operate at a fixed pulse rate (the highest required rate), this feature saves unnecessary on and off switching and the associated power losses.

Synchrocyclotron Modulator-Regulator System

The overall block diagram of the modulator-regulator system is indicated in Fig. 2. The main direct transfer chain involves as a sub-unit an A/D-D/A transfer bloc which includes the class D modulator and a self-adjusting pulser. The combined pulse-width and pulse-rate modulation are obtained with the help of a local A-D feedback transfer loop and a go/no-go comparator-discriminator combination. The analog comparison between the reference input and a pre-filtered signal yields a logical T^2L signal. This signal is conditionally transmitted (validation by the master clock sequencer and protection interlock) to the series switching type modulator via the optical coupler.

Pre-filtering eliminates the need of a hysteresis comparator (which was initially employed at this point). The stability of class D amplifiers with fast and delayed feedback has been analyzed[7,8] and we had no trouble in obtaining dynamic stabilization. The main modulator filter reduces the high voltage ripple to a tolerable amount (a few percent in our case). Figure 3 shows the photograph of an air core inductor used in the construction of the modulator filter.

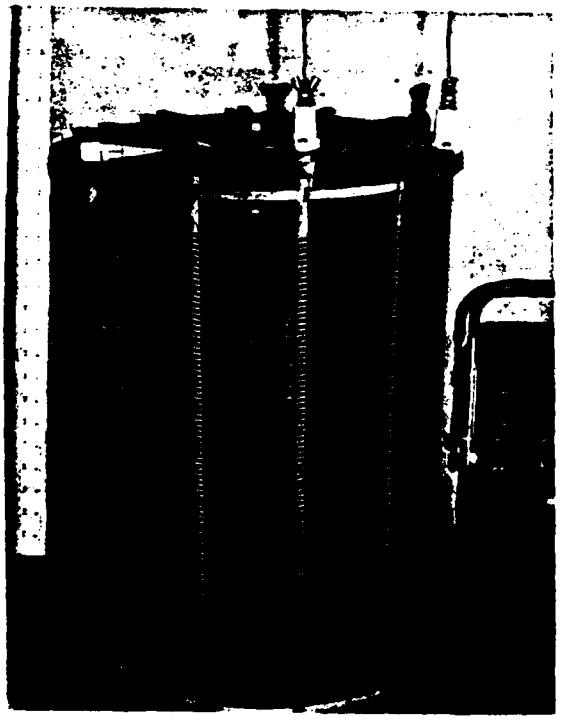

FIG. 3

It has an inductance of 15 mH and no bothersome electrical or mechanical resonances. It can carry an average current of 30 A. The DC high voltage is now 14 kV; we plan to go up to 18 kV. For class D modulator applications, core losses tend to become rather important and we experienced prohibitive heating with our previous thin laminated iron core chokes. RF filtering is provided by special filters.

For the rest, the synchrocyclotron modulator-regulator behaves very much like a conventional feedback control system, having nevertheless several distinctive particularities. The time varying turning of the RF resonator over an extended frequency range introduces a periodic perturbation of the output RF voltage. The accelerating cycle begins at a frequency of about 28 MHz, which decreases monotonically toward 19 MHz in about 1.6 ms. During this cycle, system parameters, such as Q factor and coupling efficiency, change. In addition, the RF voltage requirements may be frequency dependent.

The feedback control signal originates in an RF probe coupled with the resonator and is transmitted via an adjustable RF transfer network to produce a desirable voltage vs frequency response. Afterwards, the RF signal is rectified, filtered and sent to the first analog comparator through a LF feedback compensation network, represented in Fig. 2 by the blocks marked A, B and C. The amplitude control feedback loop is thus closed. Some adjustments in the RF envelope feedback transfer bloc were necessary to obtain optimum load stabilization. The amplitude feedback signal is compared with a reference signal which is a combination of a steady reference level and the output of a triggered wave form generator. This last signal was intended to be used mainly for achieving a slow turnoff at the end of the accelerating cycle when a simple frequency dependent control would be rather inefficient, since in the turnoff region df/dt - 0. The timing feedback control uses the delayed signal of a frequency marker. This feature also has been used for other useful level adjustments. The two sets of four oscilloscope traces in Fig. 4 represent in descending order:

1) the switching pulses before the optical coupler in the A/D-D/A transfer bloc,
2) the prefiltered current output,
3) the main modulator filter output voltage on a constant load (no time varying RF effects),
4) the reference input.

Figure 5 shows the operation of the system with the RF envelope feedback loop closed. In this case, the RF pattern on the trace #4 represents the resonator probe signal over the entire RF sweep (28 to 19 MHz). The frequency response of the probe is not uniform (goes down with the frequency). The actual accelerating voltage is obtained using a calibration curve.

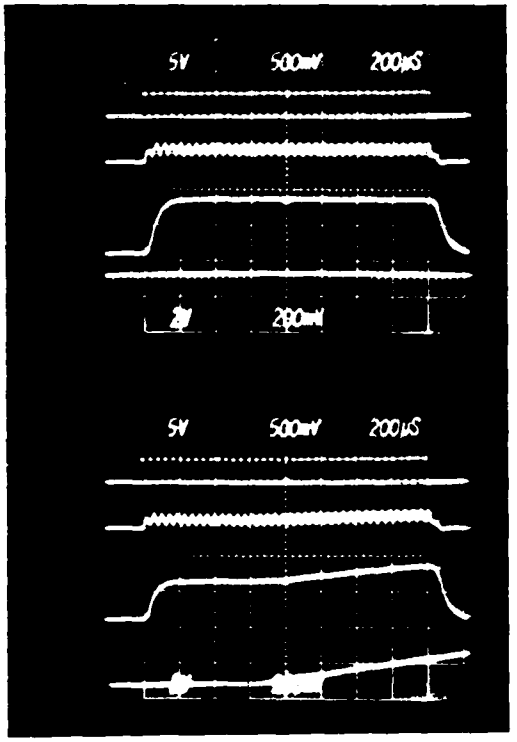

FIG. 4

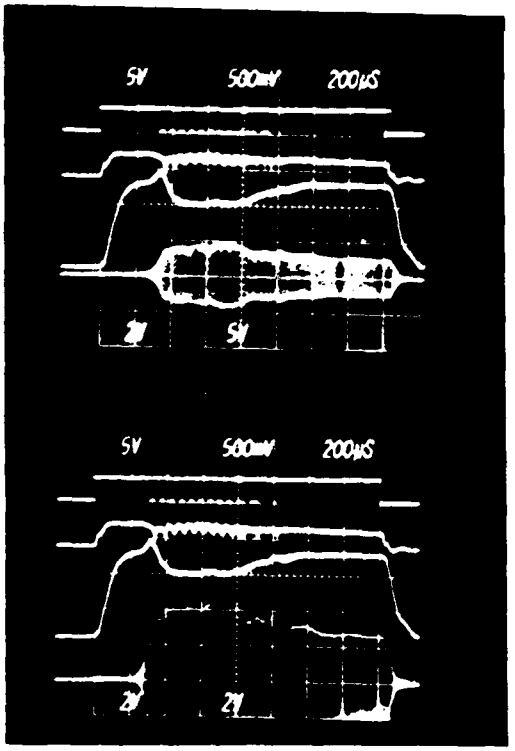

FIG. 5

Concluding Remarks and Future Prospects

The system presented may be considered as an example of a programmable switching regulator power supply and has all the inherent advantages. The use of switching power supplies represents a growing trend in industrial electronics due to their improved efficiency and smaller size when compared with other kinds of power supplies.[9]

The series switching function in our case is still performed by power triodes (three EIMAC 3CW30000 in parallel) but the use of modern semiconductor switching devices is being now considered in conjunction with increased voltage and power requirements. Cost evaluation using present available data (and substantial progress has been made lately in the area of high power solid state devices) indicates that a solid state modulator-regulator could be built at less than one-third the expense of vacuum tube equipment. There would be no more need in our case for high voltage DC insulated filament transformers and high level DC amplification. In addition, the entire modulator-regulator units would be far more compact. Our switching modulator-regulator has been in reliable operation for more than nine months. It has provided a good deal of flexibility in adjusting the level of the RF voltage for the operation of the synchrocyclotron. (Beam extraction studies are presently being conducted.) Class D modulator regulators operated in association with an RF power stage could find ready application in the area of dielectric heating. The power supplies for the vacuum tube oscillators, operating in the 1 to 50 MHz range are expected to reach the 2000 to 2500 kW range.[9]

High power AM broadcasting transmitters which are now reaching RF power levels up to 2 MW may also benefit from the use of solid state series switching modulators.

References

* Research supported by the National Science Foundation.

[1] E.G. Michaelis, "Review of Meson Factories" IEEE Trans. Nucl. Sci. NS-22(3),1385(1975).

[2] D.W. Storm et al, "Nevis Synchrocyclotron Beam Status Report", IEEE Trans. Nucl. Sci. NS-22(3),1408(1975).

[3] J. Rainwater, "Status of the Nevis Synchrocyclotron Modification", Proc. VIth Int. Conf. on Cyclotrons, AIP Conf. Proc. 9, p. 165 (Vancouver 1972).

[4] A. Gschwindt, "Considerations Regarding Future Design of AM Broadcasting Transmitters" Rundfunktech. Mittl. 15(5),201(1971).

[5] H. Swanson, "The Pulse Duration Modulator: A New Method of High Level Modulation in Broadcast Transmitters", IEEE Trans. Broadcast BC 17(4),89(1971).

[6] W.V. Subbarao, "Boost Audio-Amplifier Efficiencies", Electronic Design 22(8),96 (1974).

[7] K.P. Polov, "Stability Conditions of a Class D Amplifier with Feedback", Telecommun. & Radio Engineering 25(6),109(1971).
[8] "Investigation of the Stability of an Amplifier Operating in Class D with Feedback", Ibid. 28-29(1),119(1974).
[9] G. Kaplan, "Industrial Electronics", IEEE Spectrum 13(1),87(1976).

A THYRISTOR SWITCHED HIGH FREQUENCY INVERTER FOR DIRECTLY CHARGING A LINE TYPE MODULATOR

P.J. Fitz and T.H. Robinson
Marconi Research Laboratories, Chelmsford, U.K.

Summary

This inverter system is used to charge the pulse forming network of a high power TWT pulse modulator. It performs the functions of a smoothly controlled power supply, charging circuit and output voltage stabiliser. Comprising three self-contained modules, step-up transformer and control unit, the inverter uses specially developed thyristors operated at 40 kHz. Stabilisation against wide variations in input and load is achieved by stopping the charge within half an inverter cycle, stabilising the output to within 0.16% r.m.s. and with simple clamping to 0.03% r.m.s. Because the line modulator is totally discharged for each output pulse, repetitive operation into short-circuit is required; the rating for this condition is 30 kW at over 80% efficiency. For pulsed reservoir charging, the rating is approximately 60 kW. Full fault indication and protection is included. Without specific development for low weight and volume, other than that intrinsically available from the h.f. inverter technique itself, the system has a total volume of 24 cu.ft. and a weight of 880 lb: less than half that of a comparable 50/60 Hz conventional system.

Introduction

The inverter system is a complete energy conversion unit connected directly between 415/440V, 50/60 Hz, 3 phase supply and a pulse forming network, without additional filtering, transformers or charging and charge control circuits (Figure 1). The stability criteria are maintained through input supply changes of +10%, -20% and an output is maintained through input supply changes of +50%, -20%. An input filter, designed to reject modulator p.r.f. components, reduces the level of high voltage transients on the input supply and the system is protected by 'drop-out' from under and over-voltage. The pulse forming network voltage is controlled by the inverter and can be both manually and remotely varied between 5 kV and the full output of 40 kV. The overall long term stability is better than $\pm$ 1% and the pulse-to-pulse output stability is held under normal operation to 0. 16% r.m.s. for random variations in modulator pulse repetition frequency of $\pm$ 10% at 300 Hz. The inverter system, which operates at a fixed-switching rate of 40 kHz is protected against both internal and external faults. It incorporates a central control unit, three power modules feeding the step-up transformer and a high-speed rectifier unit. Provision is made for operation with a different number of modules.

Inverter Power System

Each power module is self-contained, requiring only 3-phase input and timing pulses. An auxiliary inverter provides power for all the control functions and, when all the auxiliaries are correctly established, triac switches are triggered to power the inverter. A block diagram, Figure 2, shows the separate units contained in each module.

There are two low voltage filters in the system; the one nearest the inverter is designed to remove inverter switching frequencies and the other, isolated under fault conditions by the d.c. switch, is arranged to attenuate both current variations at the modulator p.r.f. and input transients.

The d.c. switch consists of series thyristors which, under fault conditions, hold-off the supply by the removal of triggers and the switching of a pre-charged pulse forming network by a thyristor, producing a circulating commutation current.

The control circuit for the system is centred on a master timing unit. This provides digital timing for all units. Operation is modified in a pre-selected programme by inputs from fault and stabilisation units. The fault unit processes and identifies fault signals from each module and the output. To aid fault location, timing information for the display is decoded by a multiplex board.

Inverter Circuit

An inverter to charge a p.f.n. must be able to operate into a capacitive load (i.e. a capacitor large enough to require many inverter cycles to charge), with an output voltage starting from zero to the maximum voltage required. When the capacitor is discharged at the start of each p.f.n. re-charge cycle it presents an equivalent to the inverter of operation into a short-circuit. The most suitable inverter circuit for this mode is the series commutated, thyristor switched type. However, the difficulties of clamping a series inverter require a modification which changes normal operation by removal of the clamping circuit and adding 'free-wheeling' diodes in reverse polarity across the thyristors. It is characteristic of this variant of the series inverter that it produces a train of current pulses, the mean value of which is constant irrespective of loading. It is therefore immune to external short circuits and can be switched-on at full voltage into the uncharged capacitive load without producing damaging overcurrents or exciting filter resonances. Although the inverter may be switched-on directly without the need for a gradual run-up, both a run-up and the facility of running at reduced voltage are incorporated. The basic circuit is shown in Figure 3.

Operation of the inverter is initiated when THY_1 is triggered. C is charged in cosinusoidal form via the capacitive load C_L and L_1 to a voltage above V_S, current then reverses and C discharges via C_L, L_1 and D_1 to a voltage less than V_S. During the discharge, THY_1 is reverse biassed by the forward volt-drop of D_1, and THY_1 recovers. When current ceases in D_1, THY_2 can be triggered and a cycle, the inverse of that

above, takes place in THY_2 and D_2. Diodes D_1 and D_2 return the capacitor voltage to between zero and V_S on every cycle: for any load condition, the system voltages do not increase in a regenerative manner. The limit of load voltage is reached when the output voltage is equal to half the supply voltage.

The advantages of this circuit are that circuit voltages are reduced, recovery time for the thyristors is increased and no clamping transformer is required. The major disadvantage is that under some load conditions high dV/dt, at low voltage, is impressed across the thyristors.

Since the inverter charges the p.f.n. to a condition where it is 'matched' and then is switched-off for stabilisation purposes until the p.f.n. has been discharged, the initial conditions within the inverter are not correct for the short-circuit operation at the start of the next charge cycle and a high dV/dt can occur. A special circuit is included to clamp excess voltages and restore levels for correct initial conditions.

Method of Stabilisation
(see references 1 and 2)

During each interpulse interval of the modulator, every switching cycle of the inverter introduces charge into the network. By operating the inverter at high frequency the increment of voltage for each switching cycle can be made small. Over the final period of charge, each increment defines the variation in final voltage. Provided the sensing and inhibiting of triggers is of adequate accuracy, the stability is set by the charge content of the final inverter half cycle. For network charging, where the voltage excursion is 100% on each load pulse, a high switching rate must be used to reduce the magnitude of each inverter cycle or 'quantum'. The principle of operation is shown in Figure 4. Typical waveforms are shown in Figure 5; the p.f.n. charging voltage (a), and (b, c & d) the output current at different times during the charge.

For additional stabilisation beyond that set by the main inverter, a simple clamp switch operating within the inverter cycle can give a 5:1 improvement, allowing 1 μS for delay in drive and current build-up time. Other solutions are to use one module alone, or a lower power, smaller module, switched-in to provide the final higher stability charge at the end of the main charge period, i.e. a 'topping-up' inverter.

Module and System Layout

The cabinet shown in Figure 8 contains the complete inverter system. Each module can be withdrawn and replaced by simple quick-release connections at the rear of the water cooling circuit and the low voltage bus-bars. The control and indicator unit is located in the top section. The transformer and rectifier tank is fixed at the bottom, with the 40 kV peak charge output lead coming from the rear.

In each inverter module, shown in Figure 6, the sub-units are arranged separately for ease of assembly and servicing.

The main switch thyristors, diodes and ceramic insulating washers, are clamped to a common water-cooled heat sink, for which the commutating inductors form part of the cooling water circuit. Because of the high switching frequency, both the thyristors and diodes were specially developed for this application.[3] The VX26002 thyristor manufactured by Westinghouse, U.K., has a forward blocking rating of 600V, transient 700V; a recovery time of 3 μS at T_j = 100°C for a dV/dt of 1kV/μS up to 150V, with reverse gate drive, and 150V/μS to blocking voltage; I (peak) of 400A, I (mean) 30A and I (r.m.s) 80A, and the forward voltage drop on a 100A peak 5 μS half-sine current is 2.5V. The VX4520-SUB diode manufactured by AEI Semiconductors has the following characteristics: reverse blocking 800V (125°C); recovery 250 nS from a 150A peak 1 μS half-sine current, and I (mean) 30A.

Careful layout is used to reduce stray inductance and to enable the sharing, commutation and recovery circuits to be placed near to the main switches - at full power the r.m.s. current per module is 200A, 400A peak. Full screening and decoupling is required to remove interference from the low level driver circuits, fault sensing and protection circuits, and the auxiliary supply circuit.

The transformer, ratio 1:200, and the fast recovery rectifiers are contained in an oil-filled tank. The core of the transformer is made up of 12 ferrite blocks arranged to give a 4 inch square window. No air gap is needed, but there are incidental gaps at the butt-joints of the blocks. To shield sharp edges from the high voltage windings, core screens are used. Each limb of the core has 2 single turn primaries, a separate earth screen and a 100 turn secondary winding. Each secondary winding is connected to a separate diode stack and the outputs connected in series: this reduces the a.c. capacitance of the secondary from 30 to 15 pF, an important saving on the level of primary circulating current required to cycle this referred capacitance - 0.6 μF. High voltage terminals are mounted on the side of the tank and all other components are mounted on the lid, including the water-cooled heat exchanger. Figure 7 illustrates this arrangement.

Over-voltage detection is externally mounted and the stabiliser unit, comprising compensated potentiometer, variable reference and comparator, is enclosed in a screened unit with the pulse forming network.

Conclusions

Although considerable development of the series commutated inverter was essential for this application, the size and weight compared with equivalent 50/60 Hz circuits has been reduced, for the following more fundamental reasons:

(i) reducing the number of energy conversion cycles;

(ii) using high frequency voltage transformation;

(iii) simple stabilisation of output voltage with changes in the supply voltage and output load (without incurring the problem, in closed-loop

control, of disturbances only being sampled at the chopping frequency; which can produce instability at sub-harmonics of this sampling rate), and

(iv) reduced filtering requirements - at low voltage.

For use with a reservoir capacitor and beam switched load, e.g. gridded TWT or r.f. triggered CFA, while the inverter must be able to operate into a short-circuit during the initial switch-on conditions or into a fault, the repetitive operation required for line modulator charging is unnecessary. Because the inverter is rated for twice the mean power delivered, since the inverter current is fixed but the network voltage is twice the mean voltage, the line modulator load is disadvantageous (the size of some of the largest components in the inverter, such as the filter and commutating capacitors are proportional to peak power). The rating of the inverter described is therefore approximately 60 kW for the reservoir capacitor and beam switched load condition. In addition, because the reservoir capacitor voltage droop is unlikely to be more than 10% , the reservoir voltage will normally be stable to within 0.016% r.m.s. The relationship between droop and stability will hold until limitations in sensing and control occur.

Acknowledgements

The authors wish to thank the Ministry of Defence (Procurement Executive) and the Technical Director, GEC-Marconi Electronics Ltd. for permission to publish this paper. They also wish to acknowledge the contribution to this project of M.J. Gamage and their other colleagues in the High Power Systems Research Group.

References

(1) British Patent No. 1384283 and U.S. Patent No. 3860864.

(2) T.P. Crowfoot and G.W. Whalley, 'Charging and Stabilising System for a Pulsed CFA'. Proceedings, Eleventh Modulator Symposium, 1973.

(3) CVD Development of VX 26002 and VX 4520, Ministry of Defence (Procurement Executive).

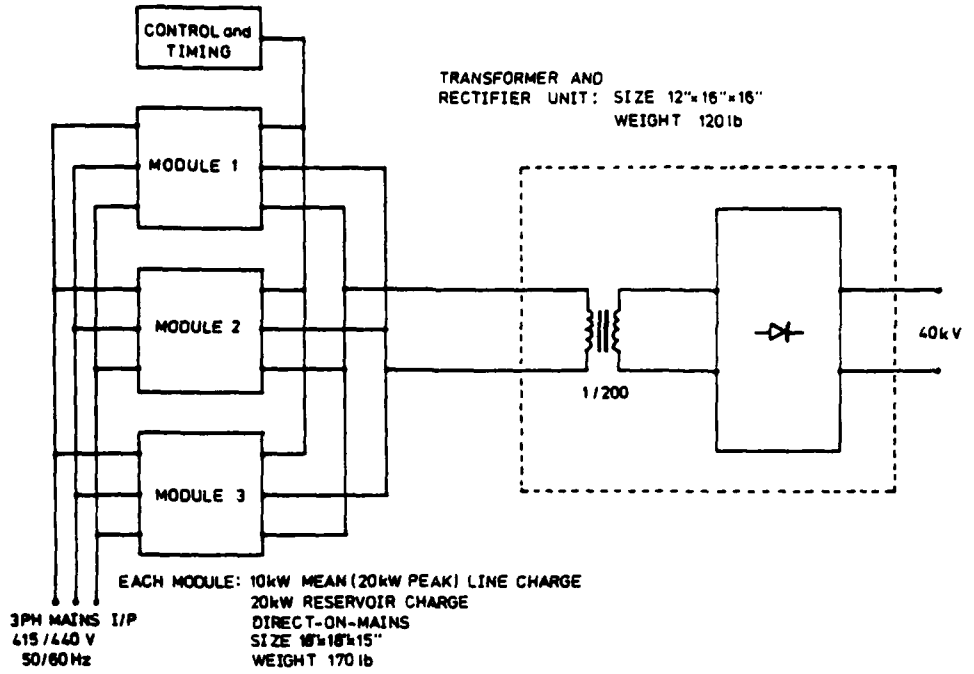

40kHz INVERTER SYSTEM BLOCK DIAGRAM

FIG.1

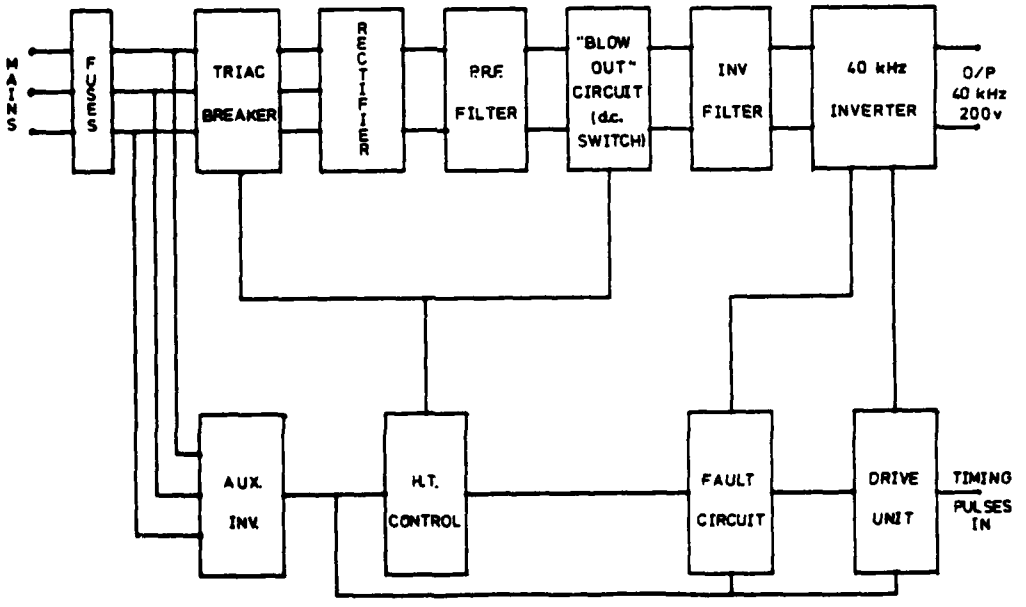

40 kHz INVERTER MODULE BLOCK DIAGRAM

FIG.2

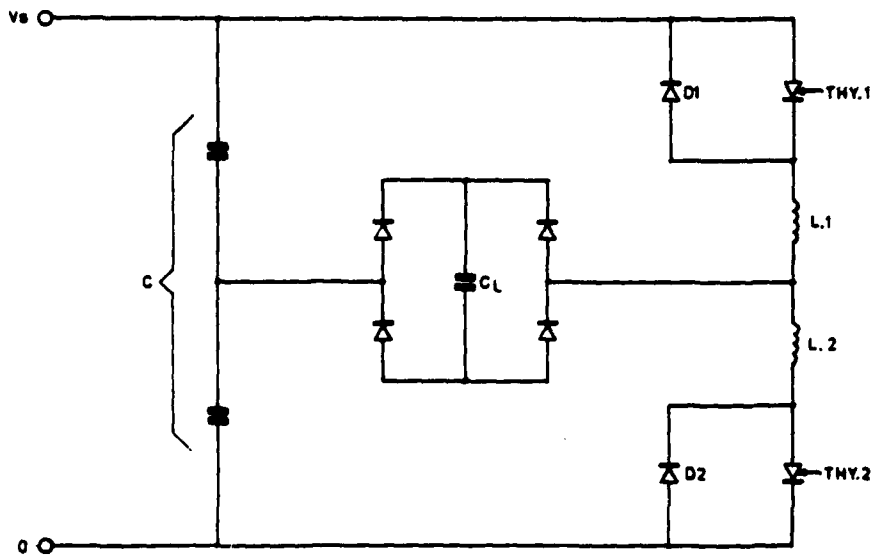

BASIC INVERTER CIRCUIT

FIG.3

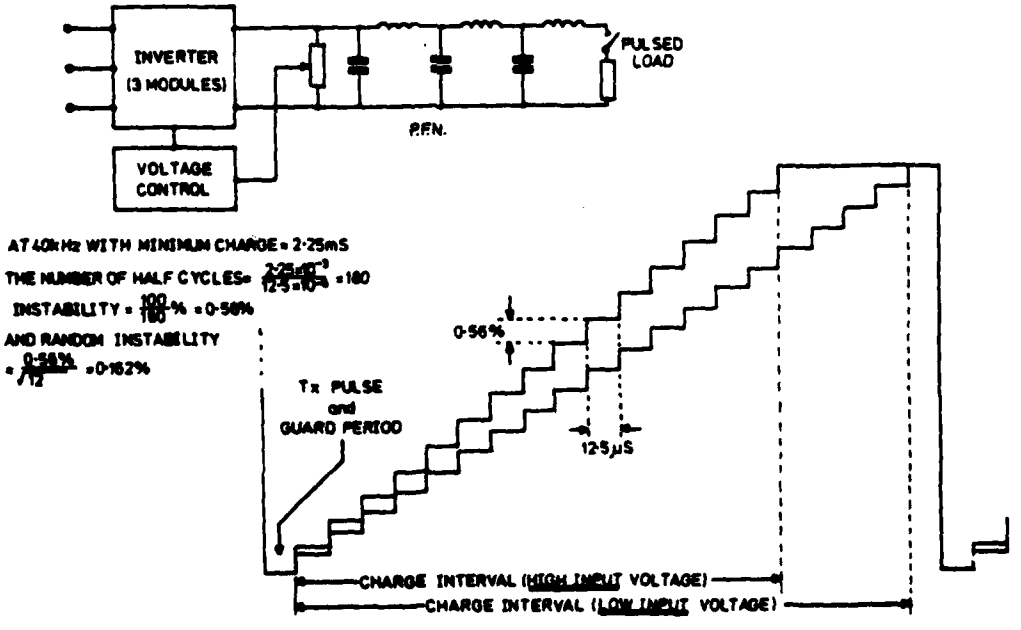

PRINCIPLE OF OPERATION

FIG.4

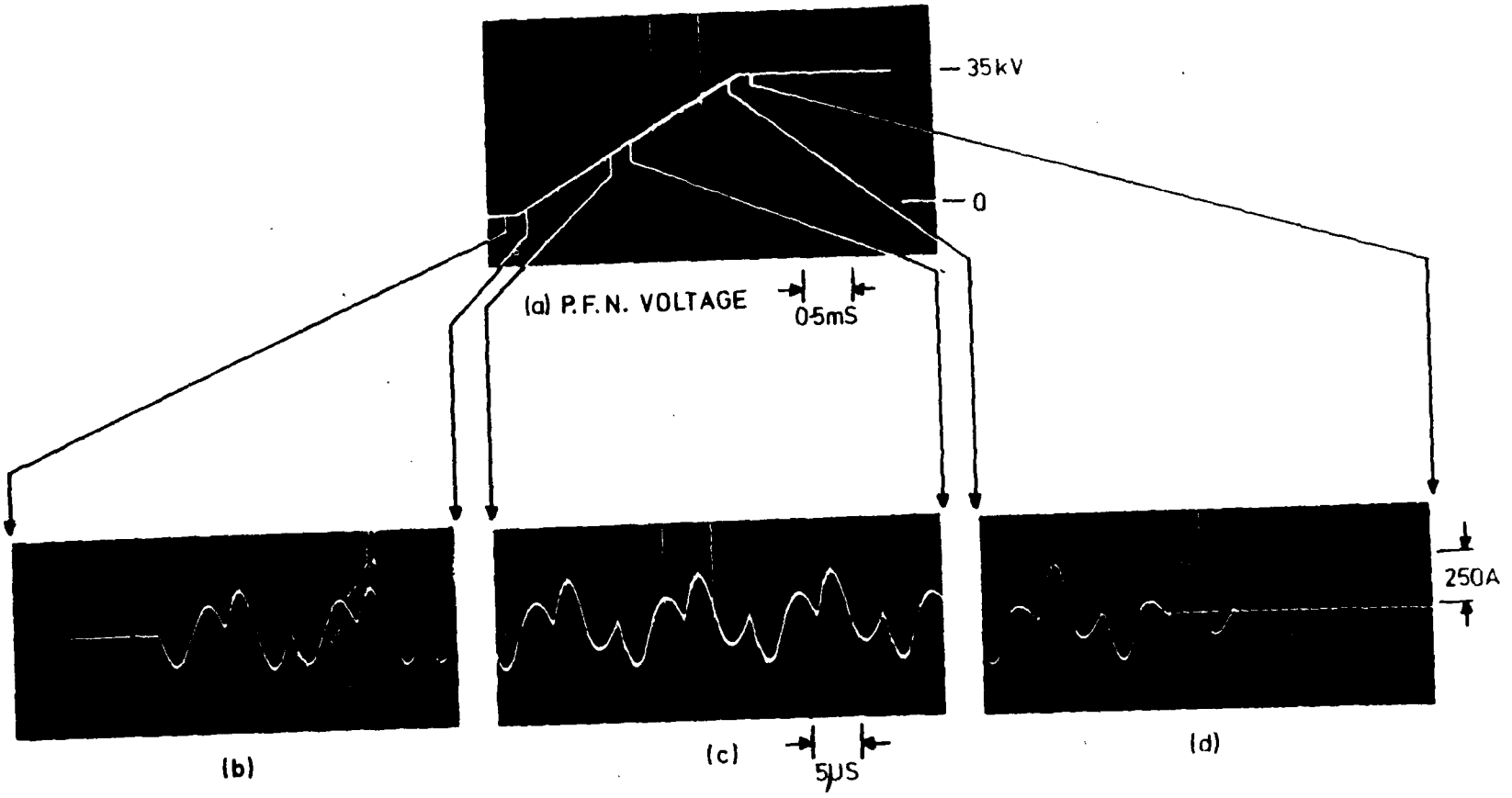

INVERTER PRIMARY CURRENT AT DIFFERENT STAGES IN CHARGE SEQUENCE

INVERTER SYSTEM WAVEFORMS

FIG.5

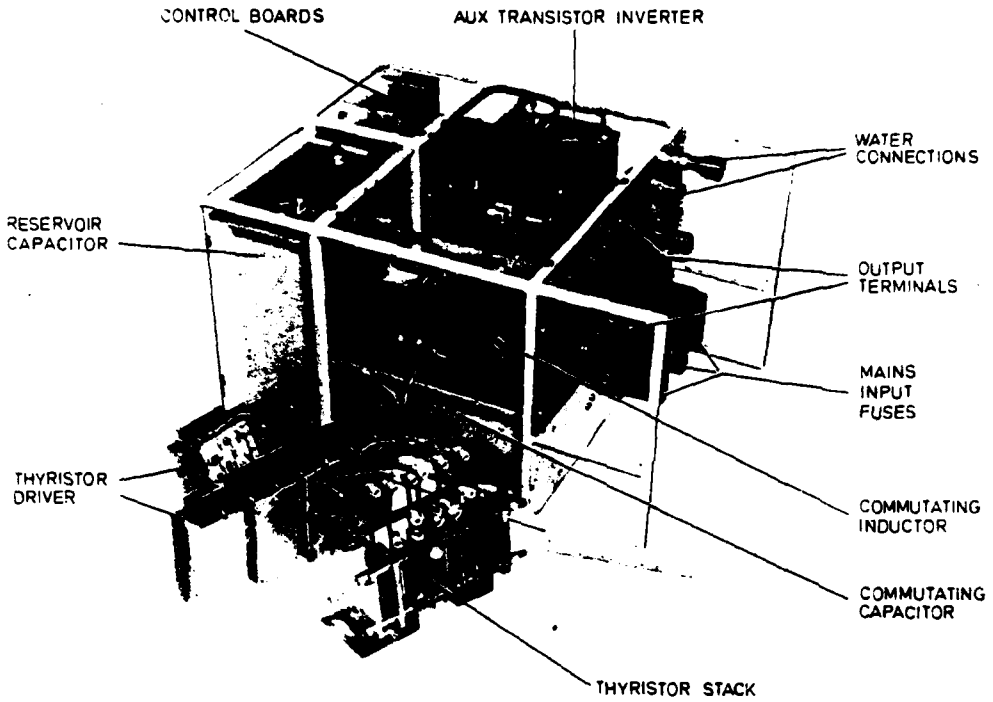

INVERTER MODULE FIG. 6

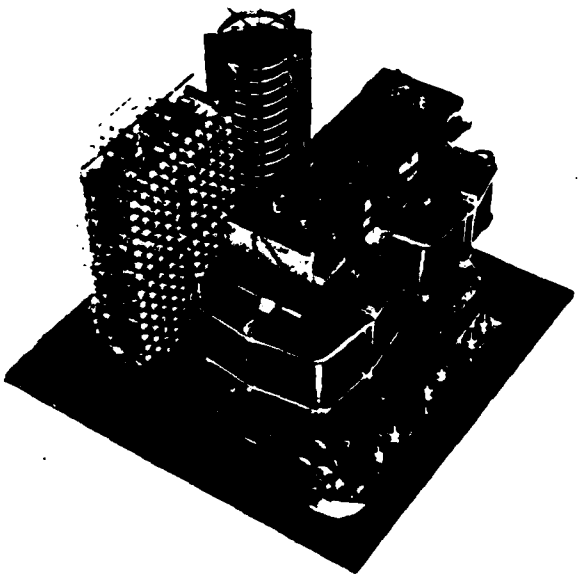

OUTPUT TRANSFORMER and RECTIFIER FIG. 7

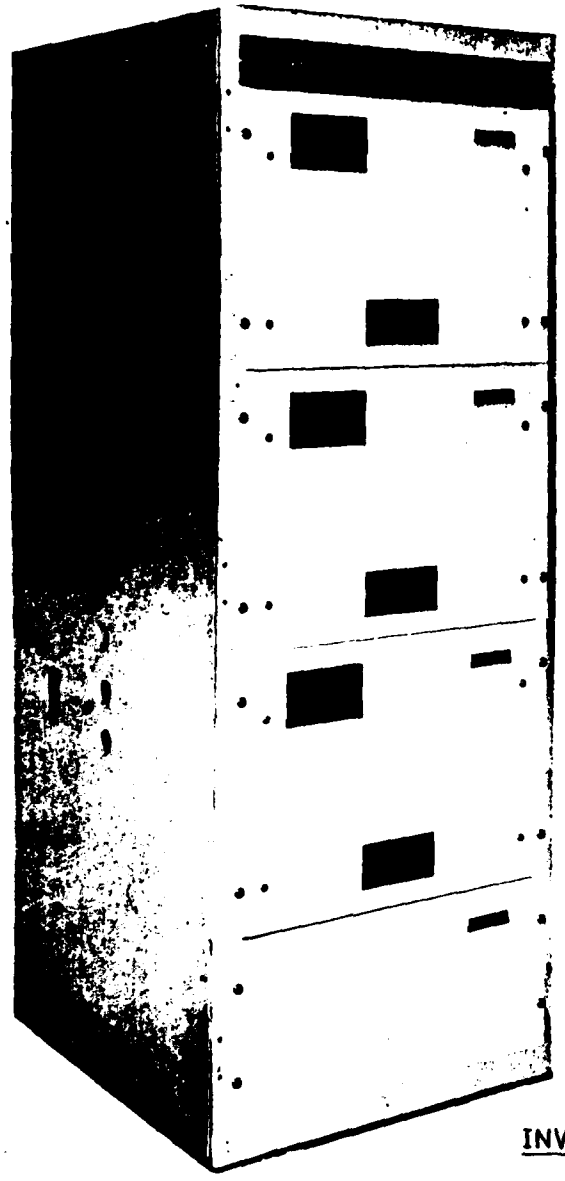

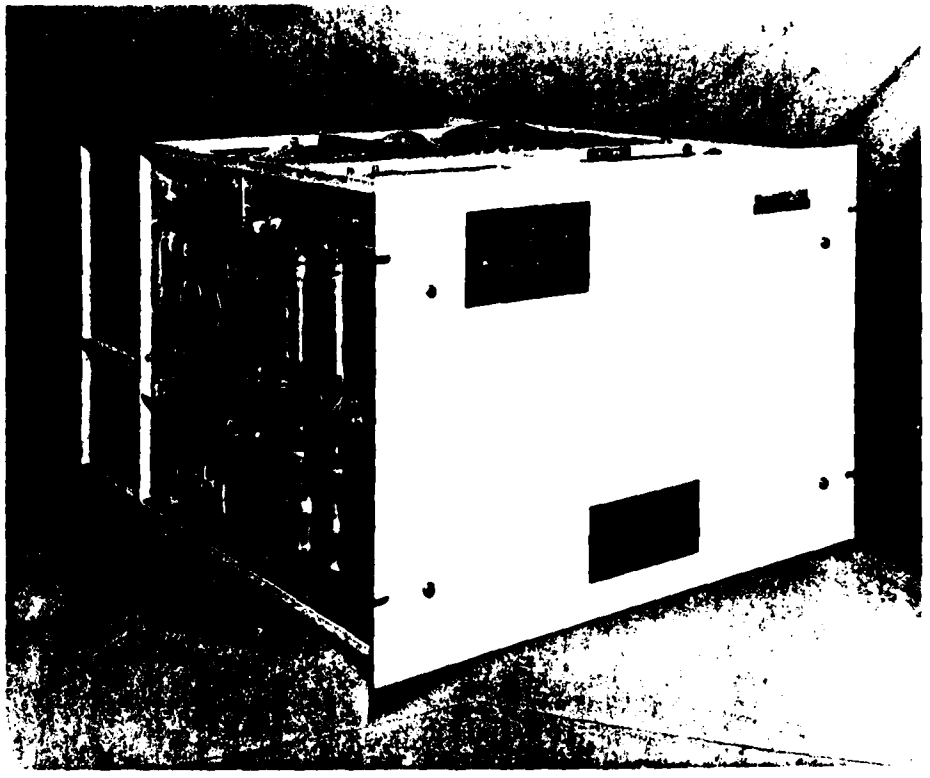

INVERTER SYSTEM and a SINGLE MODULE

FIG. 8

TECHNIQUES FOR VARYING THE VOLTAGE OBTAINABLE FROM PULSE GENERATING CIRCUITS

G. J. Scoles & B. P. Newton
English Electric Valve Company Limited
Chelmsford, Essex.

Summary

In these days of economic difficulties it is felt that practical advantage can be gained by the discussion of methods whereby the output of existing pulse generators can be readily altered without extensive re-engineering or wholesale replacement of components. The paper is therefore concerned with means whereby this can be achieved, even though no existing means of adjustment are provided.

Two techniques are considered. One involves variation of the actual output of the d.c. power supply to the pulse generator[1] by means of minor circuit alterations or additions. The other uses a clipping mechanism in which an additional low-power source causes the actual voltage to which the network is charged to be varied. This second method is such that as the voltage of the extra source becomes greater that of the network becomes less. No power loss is involved, as all the output of the lower voltage source is used to reduce the current drawn from the original, high voltage source.

A number of simple methods of varying the output of conventional single-phase and three-phase rectifier circuits are described and, in addition, two different ways of using the clipping technique.

It is assumed that all the rectifier circuits are associated with a "choke-input" (or LC) filter circuit and some indication of the critical inductance value is therefore given where relevant.

The second technique is unaffected by the type of power supply, so long as the adjustment is manual, rather than automatic.

Single-Phase Power Supplies

Voltage Increasing Circuits

Only those circuits in which the whole of a secondary winding is utilised in a full-wave manner are considered here since alternative arrangements are wasteful of materials and liable to cause transients dangerous to the rectifiers. In all cases modified circuits are compared with the unmodified form and a factor by which the output voltage is altered is given.

For most applications the bridge rectifier circuit is simplest and best. This, together with "choke-input" filter, is shown in Fig. 1. Adding a very large reservoir capacitor C as in Fig. 2 converts this into a "condenser-input" filter[2], in which case the output voltage increases from $2/\pi$ times the peak transformer voltage to almost the peak value. Ignoring ripple, this corresponds to an increase in voltage of 57%.

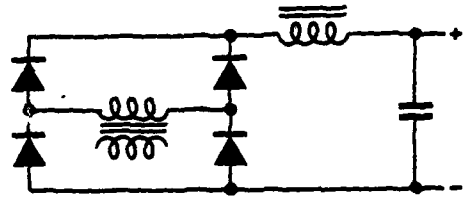

Fig.1

If, instead of making C very large, it is chosen such that the time constant CR equals the duration of one half cycle of the supply frequency (f), then an increase in voltage of around 5% is obtained. (R is the effective resistance of the load.) This small value of C, however, is found to halve the total output ripple (compared with choke-input) at little cost and the 5% voltage increase is often all that is needed. This addition of C adds only slightly to the currents flowing through the rectifiers and the transformer. It also automatically helps to protect the rectifiers against damage by transients[3]. The critical inductance is reduced by a factor of about 2 if C is used as stated.

If rather more than 5% output voltage is required, then an extra capacitor C may be added to the centre tap of the transformer in a bridge circuit. (See Fig. 3.) Here C charges twice per cycle to the peak voltage of half the winding and the basic ripple waveform applied to the filter is a

combination of a rectified full-wave (due to half the transformer voltage), superimposed on a ripple (slightly less than I/2fC due to the discharging of C via the load). The average output voltage (ignoring ripple) increases from $2/\pi$ times the peak voltage of the transformer winding to 0.82 of the peak, an increase of 28%. However, voltage ripple at supply frequency (f) reduces this by approximately I/4fC. The critical inductance for a simple rectifier bridge is R/19f henrys and with C added it becomes about R/49f for large values of C. Increasing C reduces the transformer utilisation factor which, in practice, increases its copper loss but not the iron loss. The total heating must therefore increase as a result of adding C.

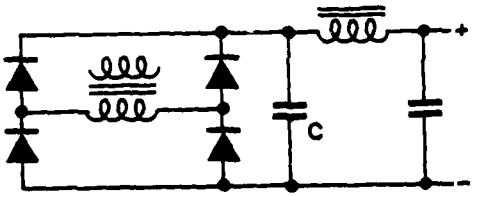

Fig.2

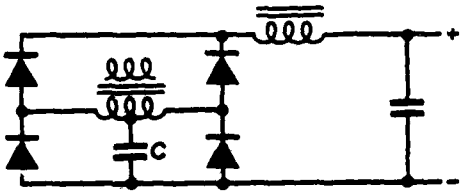

Fig.3

If more than 28% increase of voltage is required, then a second capacitor C can be used as in Fig. 4. This is in many ways similar in performance to the capacitor-input circuit of Fig. 2 but it trades two half-voltage capacitors for one rated at the full voltage of the circuit. The critical inductance for the circuit of Fig. 4 now becomes about $I/40f^2C$ henrys as above and the input ripple voltage about I/fC. The utilisation factor is similar to that of a capacitor-input circuit and Terman[4] quotes this as being "rather poor".

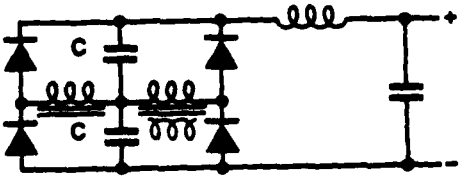

Fig.4

Fig. 5 shows an arrangement in which one rectifier of a bridge circuit is replaced by a capacitor. This circuit is about half way between one half of the circuit of Fig. 3 and a conventional "voltage-doubler"[5]. In practice it superimposes a half-wave rectified waveform (equal to the peak voltage of the transformer) on top of a steady voltage of the same value. This is equivalent to 1.32 times the peak voltage. If C is large the output waveform demands a critical inductance of about R/15f henrys.

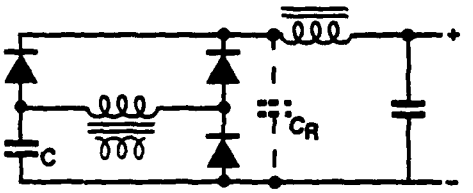

Fig.5

Reducing C introduces a ripple of I/fC volts but, as this is interlaced with the rectified sine waveform, its overall effect on critical inductance and output voltage will be small. The transformer passes a steady current when its right hand (Fig. 5) terminal is positive and a short-duration current flow (to recharge C) when it is negative. Its utilisation factor thus lies roughly midway between that for choke-input and capacitor-input filters[4].

If a relatively large reservoir capacitor C_R is added (shown dotted) then the output voltage is approximately $(2\hat{V} - I/fC_R)$ and the critical inductance $1/10f^2C$ henrys.

Voltage Reducing Circuits

Single-phase bridge rectifier circuits can be designed which, in association with choke-input filters, can give output voltages which are substantially half of those obtained from the conventional bridge. Whereas a normal bridge gives $2/\pi$ of the peak transformer voltage via a choke-input filter, these "halving" circuits give approximately $1/\pi$. Fig. 6 shows the basic "halving" circuit and Fig. 7 a bridge variant which gives a full-wave output of half the voltage and output current close to twice that supplied by the transformer. Reference to Fig. 6 shows that whenever the transformer voltage exceeds that of the reservoir capacitor, energy is stored in L via the rectifier X. When the transformer voltage is less than that of the reservoir capacitor the stored energy causes current to flow via rectifier Y and, if the inductance of L is

greater than the critical value, this current will persist throughout the period when X is non-conducting. This tends to double the current and to halve the voltage relative to the transformer. (It should be noted that it is not possible to use a half-wave rectifier with a choke-input filter. This combination simply does not work because the diode conducts during both half cycles.) The critical inductance of the Fig. 6 arrangement is nominally equal to R/3.63f henrys.

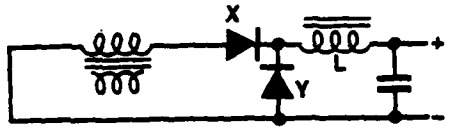

Fig.6

The bridge circuit of Fig. 7 gives the waveform of the Fig. 6 circuit, twice per cycle and interlaced and, so long as the two outputs are separated as shown, it is a true full-wave "voltage halver". Each inductor must have at least twice the value of R/3.63f henrys as quoted above and this is a possible disadvantage of the circuit. Fig. 8 shows how a single inductor can be used in association with a centre tapped auto-transformer. The critical inductance is now only R/19f henrys but the auto-transformer must handle the same voltage as the main transformer. It has only one winding and thus should be relatively small and cheap, so that the combination of an auto-transformer plus a single inductor may well be preferable to the pair of inductors of Fig. 7.

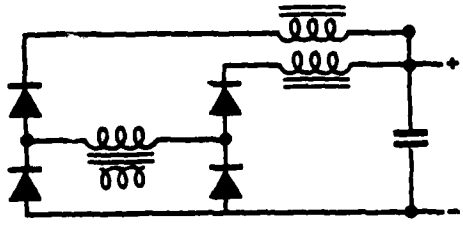

Fig.7

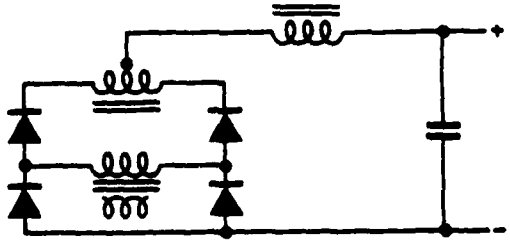

Fig.8

Three-Phase Power Supplies

Voltage Increasing Circuits

The equivalents of Figs. 3 and 4 are considered and these are shown in Figs. 9 and 10 respectively. The critical inductance of a three-phase bridge with choke-input filter is R/664f henrys. A single large capacitor at the star-point increases the d.c. output by about 10% and two capacitors of the same value by just over 20%. If C is the value of each capacitor, then a voltage regulation (due to ripple) of I/3fC should be allowed for.

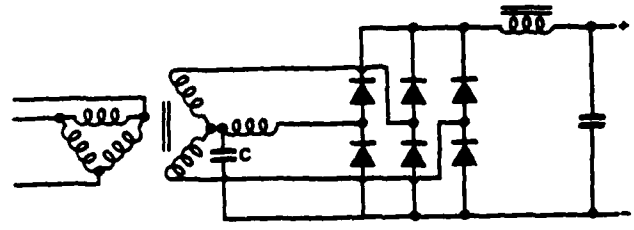

Fig.9

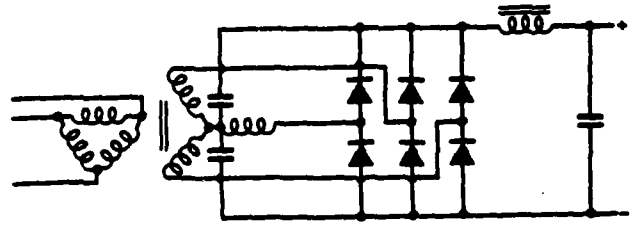

Fig. 10

Voltage Reducing Circuits

There are also a number of possible three-phase voltage reducing circuits which can be half-wave, full-wave or bridge. Two of these are shown by way of example.

Fig. 11 shows a three-phase, half-wave circuit (based on the single-phase circuit of Fig. 6) and three smoothing inductors are shown. By using a star-connected auto-transformer winding on a three-phase core as in Fig. 12, a single inductor can be used instead. The three inductors of Fig. 11 each correspond to a critical inductance of R/1.2f henrys (i.e. 3 times that of the single-phase circuit) whilst that of Fig. 12 need only exceed a value of R/76f henrys.

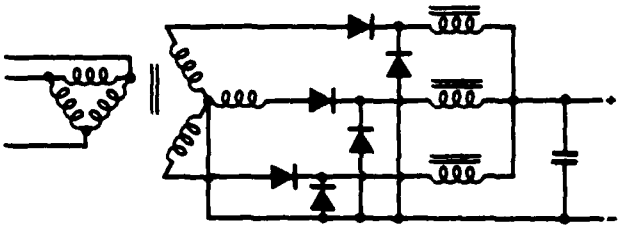

Fig.11

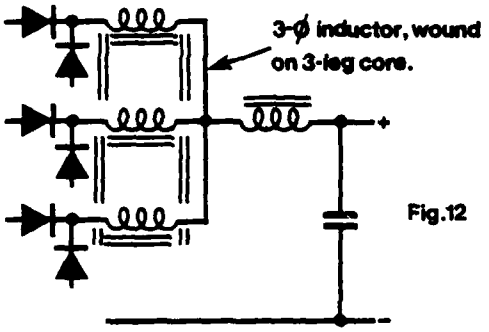

Fig.12

Fig. 13 shows a three-phase voltage reducing bridge and, if an equalizing transformer is used then the critical inductance becomes approximately R/664f henrys. This particular three-phase bridge gives an output voltage which is about half that of a normal bridge circuit. Note - If the equalizing transformer includes a delta winding then the interwinding coupling is much improved.

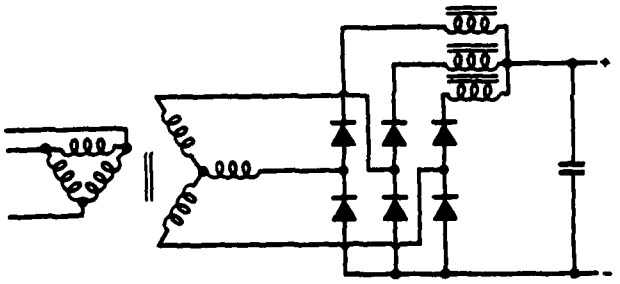

Fig.13

Critical Inductance

It may be helpful at this stage to define what is meant by the term critical inductance. The critical inductance is that value which just permits the current in the circuit to fall to zero but not to reverse. In practice at least twice the critical inductance should be used, partly because it gives a factor of safety and partly because it makes the ripple filtering more effective. It is also desirable that with a smoothing capacitor of C farads, the term ω^2LC should have a value of at least 2. This avoids any possibility of voltage build-up at supply frequency due to resonance. (For 50 Hz the LC product - in microfarad henrys - should exceed 20 and for 60 Hz it should exceed 14.)

The Estimation of Ripple Voltages

The circuit techniques described so far require some knowledge of the amount of ripple appearing across the added capacitors. Exact calculation (with sinusoidal input voltages) is most complex but, in practice, it is normally sufficiently accurate to assume that the ripple waveforms are all of sawtooth shape. Using this approximation tends to give an error such that the ripple amplitudes are over-estimated, thus equipment designed using calculations based on this assumption should always operate in a safe mode.

Clipping Techniques for Voltage Control (Line Type Modulators)

The principle for clipping techniques is quite different from those already discussed; a second power supply is introduced, which is then used to control the voltage at which a rectifier conducts in order to bypass charging current back to the original high voltage supply. This mechanism prevents any further charging of the pulse forming network in the pulse generator and thereby enables the voltage to which it is charged to be adjusted by altering the output of a low voltage (and consequently low power) auxiliary supply. Any power drawn from the latter is automatically returned to the main supply, thus reducing the current drawn from it and avoiding any need for power dissipating components.

Fig. 14 shows a circuit which operates in the above manner. Consider firstly the circuit without P_2. Capacitors C_1 and C_2 couple inductors L_1 and L_2 in such a way that the a.c. component of the charging current is shared equally between the electrically equivalent circuits L_1C_1 and L_2C_2. (Note - When designing the choke L_1 it must be remembered that all the d.c. current flows through it.) The voltage waveform at point C rises from approximately zero to about twice the applied d.c. voltage V in a cosinusoidal manner[1]. Point D

follows the same wave shape, with zero datum, rather than that of the d.c. supply. When the voltage at point D exceeds that of V, the rectifier D_1 conducts and thus prevents further voltage rise. Energy stored in both inductors then causes current to flow through rectifier D_1 charging capacitors C_1 and C_2, rather than flowing through D_2 to increase the voltage across the PFN. This mechanism is that of a voltage limiter[6].

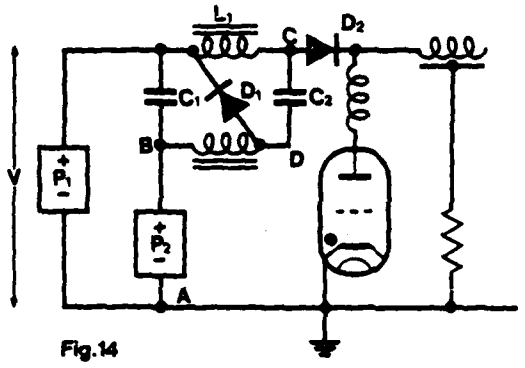

Fig.14

Now consider the circuit with P_2 as shown in Fig. 14. This will shift the datum of the waveform at point D from the zero datum already considered to a new positive value. This will cause D_1 to conduct sooner and it will be seen that the greater the voltage of P_2, the lower will be the voltage to which the PFN is charged. Any current flowing through D_1 as a result of this must charge C_1 and C_2. This can only mean that power supply P_1 will have to supply less current than previously.

The average current I drawn from P_1 must be $I = V_N C_N f$ amperes, where V_N is the voltage to which a PFN of capacitance C_N is charged f times per second. I decreases with V_N, the reduction in current required from P_1 being supplied by feedback from P_2.

With manual adjustment of P_2 the system is stable but it may become unstable if automatic control is attempted. Stability can be achieved in most cases without too much difficulty[7].

Fig. 14 shows inductors L_1 and L_2 as separate items coupled only by C_1 and C_2. In practice it is advantageous if they are magnetically coupled as well. This can readily be achieved on the two legs of a "core-type" core, in which case only a single core is required, the size is less and so are the total losses. In such a case it is obvious that the two windings must each be wound with exactly the same number of turns. (The r.m.s. current carried by L_1, however, is more than that carried by L_2.)

Fig. 15 shows another method of achieving the same result. Here the charging inductor L is centre tapped and the diode-pump involving C, X and Y[8] acts to limit the voltage at point A whenever the peak-to-peak voltage excursion at that point exceeds the supply voltage V. L behaves as an auto-transformer and in this way the diode-pump limits the voltage to which the PFN is charged. Adding the power supply P_2 in series with the diodes must cause the rectifiers to conduct earlier in the cycle, thus restricting the voltage on the PFN. As with the alternative arrangement of Fig. 14, any power flowing through X and Y must (a) also flow through P_2 and (b) serve to reduce the total current supplied from P_1.

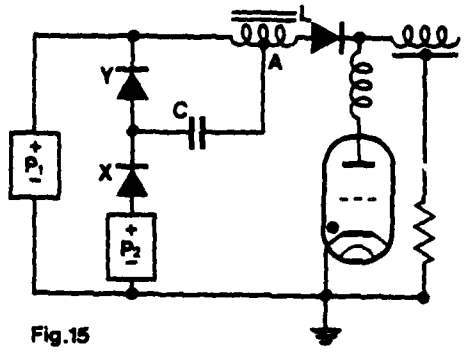

Fig.15

Thus the two clipping circuits, though quite different in detail, basically behave in the same manner and achieve the same result.

References

(1) Handbook of Electronic Circuits,
Section 29-2.
G. J. Scoles (John Wiley).

(2) Handbook of Electronic Circuits,
Section 25-1.
G. J. Scoles (John Wiley).

(3) Handbook of Electronic Circuits,
Section 25-2.
G. J. Scoles (John Wiley).

(4) Radio Engineering, third edition,
Chapter 11, pp 544-576.
F. E. Terman (McGraw Hill).

(5) Handbook of Electronic Circuits,
Section 21-1.
G. J. Scoles (John Wiley).

(6) The Reduction of Excessive Forward and
Inverse Voltages in Line-Type Pulse
Generating Circuits.
(Paper Twelfth Modulator Symposium).

(7) E.E.V. Co. Preamble (Hydrogen
Thyratrons),
P 49, Fig. 36.
(English Electric Valve).

(8) Handbook of Electronic Circuits,
Sections 13-2, 21-1.
G. J. Scoles (John Wiley).

Acknowledgements

The authors wish to thank the Directors of English Electric Valve Company Limited for permission to publish this paper.

THE REDUCTION OF UNWANTED OSCILLATIONS (RINGING) IN CHARGING INDUCTORS AND POWER TRANSFORMERS

G. J. Scoles
English Electric Valve Company Limited
Chelmsford, England.

Summary

Voltage oscillations are often present across the charging inductor of a pulse modulator and can cause unnecessary stress both to itself and to adjacent circuit elements. They should therefore be reduced in amplitude as much as possible.

Two methods of doing this are described; one uses conventional damping techniques whilst the other depends upon charge-sharing. Of the two methods the former is more simple, whilst the latter is considerably less lossy and can be adapted to function as an inverse diode.

It is not generally appreciated that iron cored inductors are liable to internal self-oscillations of large amplitude which do not normally appear at the output terminals. This can often lead to internal breakdown. Damping techniques can also be applied to these but it has been found that with suitably chosen capacitance added, the oscillations can be prevented from happening at all. This depends upon forming a capacitive potential divider and, once the correct value of capacitance has been found, this method is extremely effective.

Inductors which are wound in two halves upon the two legs of a "core-type" core are particularly liable to such oscillations owing to the large physical separation between the two halves of the winding. A form of double auto-connection is described which considerably tightens the coupling and simultaneously permits adjustment of the inductance without introducing any overhung windings.

This last technique is also described as a means for improving the design of power transformers and it also makes possible the construction of multi-ratio pulse transformers.

Oscillations Across the Inductor

At the instant when current ceases to flow in a charging inductor a voltage approximately equal to the d.c. supply will exist across its terminals. As the series rectifier will prevent any return flow of current, any charge stored in the stray capacitance existing across the inductor must result in a train of damped oscillations whose frequency is determined by that stray capacitance in association with the self-inductance of the charging inductor L. Fig. 1 shows the basic circuit of such a pulse generator[1] and Fig. 2 an oscillogram of the type of waveform to be expected at the point A.

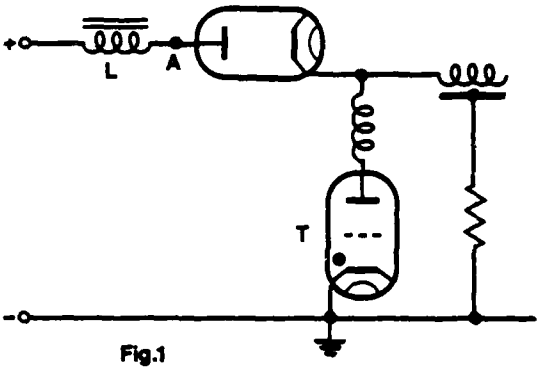

Fig.1

Fig. 2

Reduction by Damping. Fig. 3 shows how conventional damping can be applied to the inductor of Fig. 1, the resistor R providing the necessary damping whilst capacitor C minimises the flow of current through R at times other than when actually damping the oscillations. This capacitor has the dual effect of reducing the amount of heat dissipated in R and of keeping the effective "Q" of the circuit as high as possible. Ideally C should be at least 8 times the total stray capacitance but, in practice, a value of 4 times is normally quite satisfactory; this lower value further reduces the power dissipation and hence the ratings of R and C. The exact calculation of R is complex but in practice it is

sufficiently accurate to use the normal "critical shunt damping" formula such that $R = \frac{1}{2}\sqrt{\frac{L}{C_s}}$, where L is the self-inductance of the charging inductor and C_s the stray capacitance. The total heat dissipated in R is also difficult to calculate exactly but, in practice, it is slightly more than $C V^2 f$, where V is the supply voltage and f the recurrence frequency of the generator. If C is made equal to $4C_s$ then an assumption of a total power loss of $5C_s V^2 f$ watts will be satisfactory. Fig. 4 shows the waveform at point A of Fig. 3, altered by such damping.

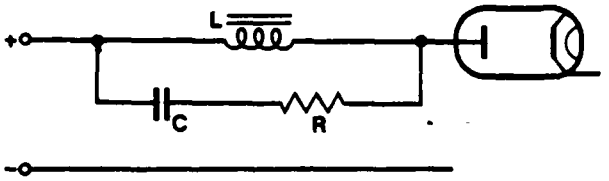

Fig.3

Fig. 4

Reduction by Charge-Sharing. Another approach to this problem is to use rectifiers to switch an extra capacitor in parallel with the stray capacitance, thereby sharing its charge and so reducing the amplitude of any subsequent oscillations. This technique does not by itself introduce any extra losses, as the circuit is such that the shared energy is automatically returned to the power supply. It is preferable to include resistance in series with this extra capacitor in order to limit the peak current which can flow through the rectifiers whenever thyratron T fires. This also reduces any residual oscillations. Fig. 5 shows a charge-sharing circuit of this type and it will be seen that any current flowing through the rectifiers X and Y must reduce the total current supplied to the pulse generator. Assuming that C_1 and the PFN are initially uncharged, no capacitor current can flow until such time as the voltage of point A equals that of the supply. C_1 then charges via rectifier Y and, when the PFN is fully charged, the voltage across C_1 will be equal to the difference between that of the PFN and that of the supply. As soon as point A commences to oscillate in potential, both terminals of C_1 become more and more negative until the potential of point B falls to that of the negative supply terminal. Rectifier X now conducts and this is as C_1 had been directly connected in parallel with the stray capacitance C_s. Any tendency to overswing is therefore reduced in the ratio $\frac{C_s}{C_s+C_1}$ and so, if for example C_1 is made equal to 4 times C_s, it will be seen that any overswing is only 1/5 of what it would have been in the absence of the new circuit. Rectifier X then ceases to conduct and so disconnects C_1 and C_s once more. The subsequent oscillations are thus not affected by C_1 but, once, as explained, their amplitude has been reduced, this is unlikely to affect the rest of the circuit to any appreciable extent. Fig. 6 shows the voltage at point A of Fig. 5.

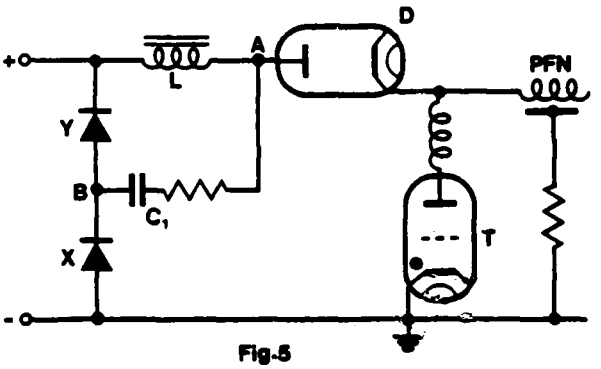

Fig.5

Fig.6

When T fires, any residual charge left in C_1 discharges via X, D and T and this can be used to form an inverse diode circuit. If C_1 is made comparable with the capacitance of the PFN, then any reversal of voltage across T results in sharing of charge between PFN and C_1, the result being similar to that of a normal inverse diode circuit. In such

cases resistance would normally be added in series with C_1 to control the current amplitude but the conventional value would usually be too small to affect the oscillation of the inductor appreciably. In this case, of course, C_1 would be so large that the residual oscillations would be of negligible amplitude. This inverse diode variant has the disadvantage of circulating energy via L and C_1, but, due to the diode-pump action[2] of rectifiers X and Y, it has very little effect on the total power required by the whole circuit.

Internal Self Oscillations

Charging inductors are also liable to generate internal oscillations when used in pulse generating applications and these can often cause internal breakdown due to unsuspected over-stressing of the insulation[3]. Inductors intended for alternative series or parallel operation of two windings are very liable to such oscillation and the author was once faced with the problem of an inductor of this type in which 4-inch arcs were liable to occur between terminals if the windings were connected in series. The mechanism which generates internal oscillations is a simple one but it is probable that many designers of pulse generators are not even aware of their presence. Fig. 7 shows the simple model of the relevant stray capacitances associated with a charging inductor. In Fig. 8 the horizontal line AB represents the length of the winding, whilst the vertical line AC represents an impulse voltage applied to one end. The straight line CB represents the ideal (and final) voltage distribution and the line CDB that which would occur initially if the circuit were actually that shown in Fig. 7. The true distribution is more of the form of the curve CEB and it will be apparent,

(a) that there is considerable departure from the ideal at the middle of the winding and

(b) that those turns of wire adjacent to the "live" terminal are stressed to many times the voltage across those at the other end of the winding.

The effect of (a) is to set up oscillations whose amplitude "envelope" lies between curves CEB and CFB whilst that of (b) can be to cause interturn or interlayer breakdown of the winding. Referring now to Fig. 1, it will be apparent that such a voltage transient occurs whenever thyratron T fires and so a succession of trains of high frequency oscillations will occur at the recurrence frequency of the generator. The oscillation frequency will depend upon the sum of all the stray capacitances as seen from the centre of the winding, in association with the two leakage inductances, in parallel, of the separate halves of the winding. Fig. 9 shows one such train of oscillations.

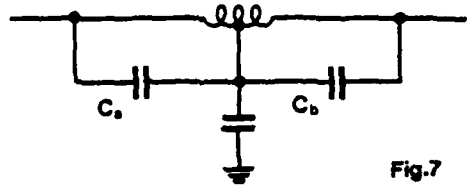

Fig.7

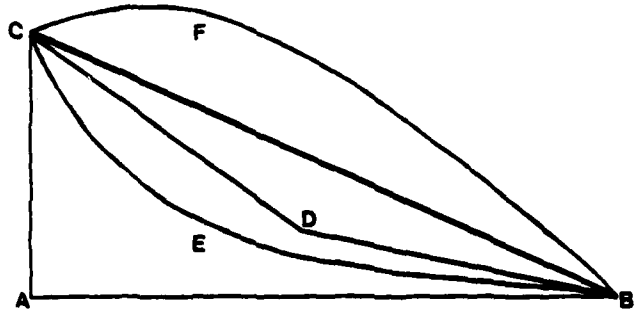

Fig.8

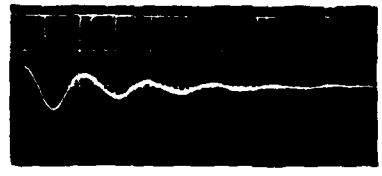
Fig.9

Reduction by Capacitive Potential Divider. From consideration of Figs. 7 and 8 it will be seen that as C_b is made larger, so will the departure from the ideal waveform become less. Thus by adding the correct value of extra capacitance between points G and H (Fig. 10) it is possible to achieve almost perfect voltage distribution at the centre point of a charging inductor. Any residual oscillations elsewhere in the winding are then most likely to be insignificant. Fig. 11 should be compared with Fig. 9 to see how well such an added capacitor removes the oscillations.

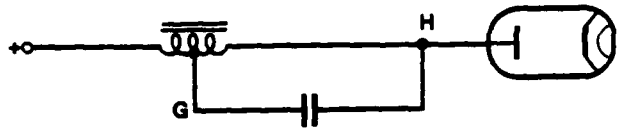

Fig.10

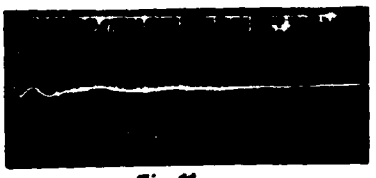

Fig. 11

Reduction by Damping. Conventional damping methods can also be used to reduce internal "ringing" and Fig. 12 shows the optimum orientation of components to achieve this. The correct values of C and R are rather difficult to calculate but they can be found easily by experiment. Consideration of Fig. 12 shows that the centre-tapped charging inductor must also behave as an auto-transformer and hence the damping circuit shown must also act to reduce the oscillations across the windings as well as within them. Figs. 13 and 14 show this and should be compared with Figs. 9 and 2 respectively.

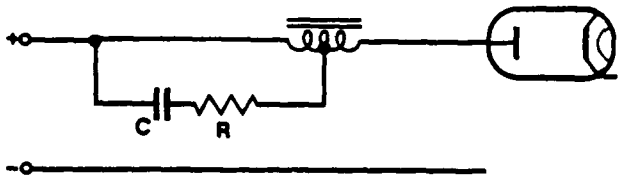

Fig.12

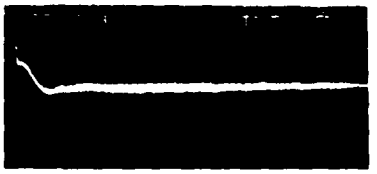

Fig. 13

Fig. 14

Reduction by Clipping. Another technique makes use of rectifiers to clip all negative voltage excursions appearing at the centre point of the inductor which are greater than the value associated with oscillation-free operation. All the "ringing" energy is therefore directed away from the inductor, leaving the latter substantially free from any residual oscillations. Three versions of this method are indicated in Fig. 15, the datum being set, respectively, by

(a) a centre-tapping on the power supply

(b) a capacitive "dump" and

(c) a diode-pump circuit.

Of these the first is the simplest but only if a half way tapping point is available. The second requires experimental adjustment of resistance R, capacitor C being relatively large in value. The third is self-adjusting but it should be noted that if C is large then it can also function as an amplitude - limiter and an inverse diode circuit. Preferably a series resistance of about 100 ohms is connected between the actual clipping circuit and the centre-tapped inductor. This protects the rectifier(s) against risk of damage by current transients and will have little effect on the clipping action. Fig. 16 shows the effect of circuit (c) and should be compared with the waveforms of Fig. 9.

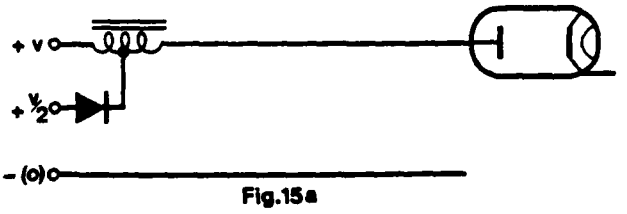

Fig.15a

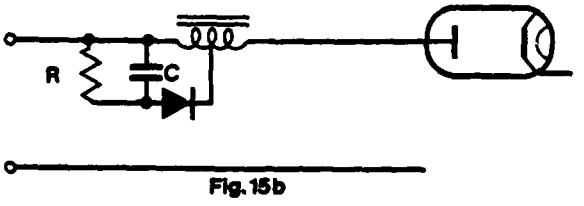

Fig.15b

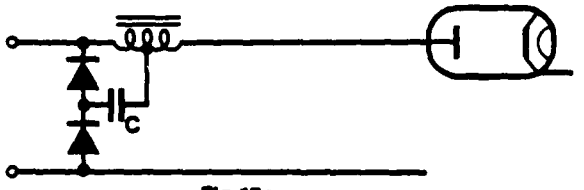

Fig.15c

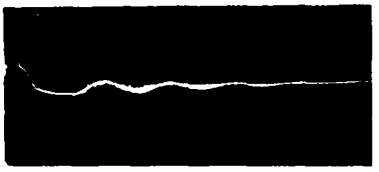

Fig. 16

The "Double Auto-connection"

Inductors are often wound on the two legs of a "core-type" core and if the two windings are then connected in series the arrangement is almost certain to generate excessive internal oscillations whenever one terminal is subjected to a voltage transient. Since the only coupling between the two windings is via the magnetic flux in the core, the leakage inductances are likely to be a much greater proportion of the self-inductance than in other designs. The damping, sharing and clipping techniques already described can obviously be used to reduce such oscillations but it has recently been found that if the two windings are tapped and cross-connected then

(a) the leakage inductances are very much reduced and

(b) a method exists of adjusting the self inductance without at the same time introducing "overhung" windings and further sources of unwanted oscillations.

Fig. 17 (a) shows such a series-connected inductor and Fig. 17 (b) the improved connection as described. The tapping points must be similar on both legs and it will be seen that as the tappings move upwards from the "bottom" to the "top" of the windings, the circuit merges smoothly from a full series to a full parallel connection. The use of the centre tapping points is preferred as in this case circulating coupling currents are small and the coupling itself is relatively good. In such a case, of course, the effective number of turns is ½ of the total and the inductance should be 9/16 of its original value. In practice it may be somewhat different from this, due to imperfections in the coupling.

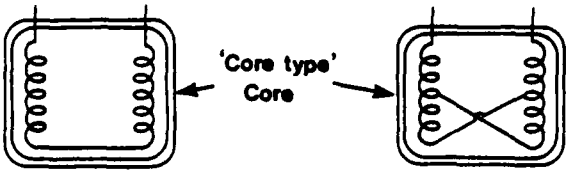

Fig. 17

Double Auto-connected Power Transformers

Fig. 18 (a) shows one winding of a conventionally tapped power transformer and Fig. 18 (b) how it can be improved by the "double-auto" technique. The overhung portions of Fig. 18 (a) will almost certainly oscillate under transient conditions (e.g. switching or lightning) and, as these oscillations will have random phasing, it follows that dangerous voltages can be set up between the adjacent "free" ends. With the arrangement of Fig. 18 (b) there is no overhang and so the equivalent voltages are unlikely to be much in excess of the voltage across the windings due to the mains. The coupling between the two parts of the winding is also increased considerably and it is suggested that these advantages far outweigh the extra complication of double switching.

Fig. 18

Multi-ratio Pulse Transformers

With normal tapping methods it is almost impossible to construct a satisfactory multi-ratio pulse transformer. This is because good design requires the windings to behave as "current sheets" and, obviously, the use of tappings must result in portions of the winding which carry no current[4]. The "double-auto" connection eliminates such unused portions almost entirely but, owing to the load current having to be shared between the parallel-connected portions, a true current sheet is not achieved. Nevertheless, this must result in a much closer approximation to a current sheet than has been achieved hitherto and hence the use of this new technique is likely to result in tapped transformers which handle pulse waveforms more accurately than existing designs.

References

(1) Handbook of Electronic Circuits,
Section 29-2.
G. J. Scoles (John Wiley).

(2) Handbook of Electronic Circuits,
Sections 13-2, 21-1.
G. J. Scoles (John Wiley).

(3) The Effects of Impulse Voltages on
Transformer Windings.
T. E. Allibone, D. B. McKenzie and
F. R. Perry.
IEE Journal, Volume 80, No. 482,
February 1937.

(4) Pulse Generators (MIT Series),
Chapters 12-15.
McGraw Hill/Dover.

Acknowledgements

The author wishes to thank the Directors of English Electric Valve Co. Ltd. for permission to publish this paper.

THE REDUCTION OF EXCESSIVE FORWARD AND INVERSE VOLTAGES IN LINE-TYPE PULSE GENERATING CIRCUITS

G. J. Scoles
English Electric Valve Company Limited
Chelmsford, England.

Summary

Following a brief explanation of how excess voltages can occur as a result of failure or mismatching of the load, a number of ways of removing or reducing such voltages are described. Some, based on inverse diode techniques, have been used since the earliest days of radar and linear accelerators. Others are more fundamental and have not previously been described.

One such family of circuits uses a pair of capacitively or inductively-coupled windings to generate a voltage difference which reverses polarity as the network charging voltage reaches twice that of the high tension supply. A suitably poled diode then serves to divert any remaining charging current back to the supply, thereby preventing further increase of voltage in a substantially loss-free manner.

Another method uses a centre-tapped charging inductor as an auto-transformer, the tapping point of which is then used to energise a diode-pump rectifier circuit. This rectifier is directly connected across the high tension supply terminals and acts to limit over-voltages of either polarity. Any such tendency results in the surplus energy being returned directly to the supply.

Introduction

From the earliest days of radar and of linear accelerators it has been found necessary to provide protective means so as to avoid the generation of excessive forward and/or inverse voltages as a result of malfunctioning of the equipment. Prior to modern gas-filled rectifiers and suitably rated semi-conductor diodes becoming available, this problem was relatively difficult to solve. Either an inverse diode circuit using a larger number of parallel-connected high vacuum diodes or else a protective circuit using a quenched spark gap had to be used and neither of these was as convenient as the modern components.

A number of different techniques can be used: some have been known for a number of years but others are of more recent origin. In two of the latter, excessive voltages cause clipping diodes to conduct and so force the circuit as a whole to operate within predetermined limits. Both are regenerative, so that any tendency to produce overvoltages results in current flowing back to the power supply.

Inverse Diode Methods

Here it will be assumed that the circuit to be protected is one in which a pulse forming network (PFN) is recurrently charged via inductance and a diode and then discharged into a substantially matched and resistive load by triggering a hydrogen thyratron or other switching means. If correctly matched and in the absence of losses, the pulse forming network will charge cosinusoidally[7] to twice the supply voltage and, ideally, will be discharged to exactly zero every time the pulse is generated. In practice, due to mismatching and to losses, some negative overswing is probable and the positive excursion is likely to differ from the voltage doubling mentioned. This will happen for every cycle of the circuit and, in fact, negative overswing is often intentionally used to provide extra time for the switching device to recover.

If such a pulse generator is used to energise a load susceptible to occasional flashing or mismatching (such as a magnetron or a gas laser) then any reduction in load impedance must result in a cumulative build-up of voltage across the charging inductor and hence in the appearance of excessive positive and negative voltages across the switching device and PFN. This can also damage any associated components and so extra circuitry must be introduced to eliminate or at least to reduce the effect. Quite apart from the effects of mismatching, imperfections in the PFN itself can also cause short duration negative voltage spikes immediately following the generation of the output pulse. For all these reasons, some means of controlling excess voltage is needed in almost all cases.

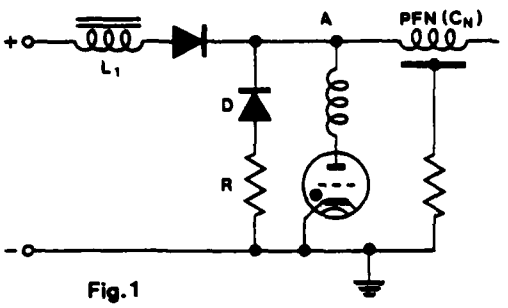

Fig. 1

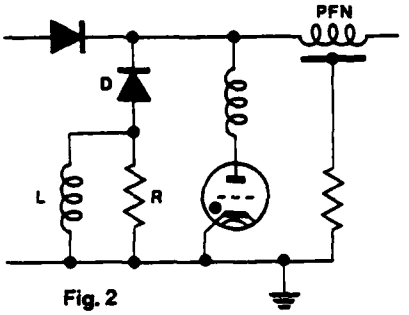

Fig. 2

Fig. 1 shows the arrangement most commonly used and here the inverse diode D conducts whenever the voltage at the point A becomes negative. Resistance R limits the current and it is normal practice to choose R such that the time constant RC_N is between 5 and 10% of the resonant time to charge of $\pi\sqrt{L_1 C_N}$ seconds. (Here C_N is the network capacitance and L_1 the inductance of the charging inductor.) This allows sufficient time for the negative voltage at A to subside before any appreciable recharging of PFN has taken place. Thus the negative voltage is rapidly removed, thereby preventing any appreciable subsequent increase of positive voltage from occurring. Fig. 2 shows a variant in which an inductor L is connected in parallel with R[1]. Here L passes a current which initially increases while that through R is decreasing, thereby enabling more charge to be removed in a given time without at the same time increasing the peak current carried by D. With this circuit PFN is left with a small positive charge at the instant when D ceases to conduct. This is not necessarily bad, so long as the switching device has by then fully recovered. (Series-connected inductance and resistance has also been used[2] in order to obtain a relatively large positive charge but as this version both slows down the rate of removal of charge and also causes the supply voltage to fluctuate, its use is not now recommended.)

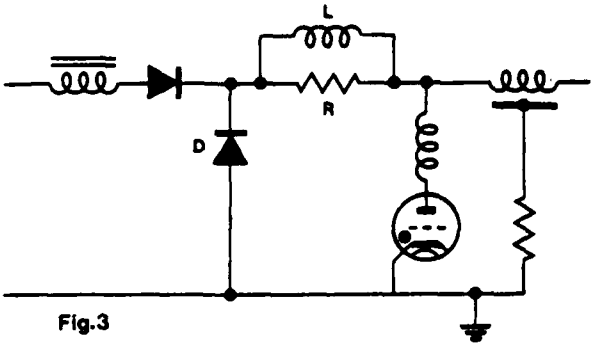

Fig. 3

Fig. 3 shows another variant[3] which has the advantage that because D is directly connected across the output of the charging circuit, it is quite impossible for any build-up of positive voltage to occur as a result of failure of the load. It has the further advantages

(a) of not adding any extra capacitance directly across the switching device and

(b) if d.c. primed thyratrons are used[4] as indicated in Fig. 3, of enabling a single heater transformer to be used to energise the charging diode and the inverse diode simultaneously.

The inductance of L can be as in the Fig. 2 circuit, but normally its function is to permit the network charging current to bypass R, thereby reducing the rating of that component and also the total power dissipated in the equipment. In such a case, of course, the inductance of L is made sufficiently large to prevent the current flowing through it from rising appreciably during the period when D is conducting.

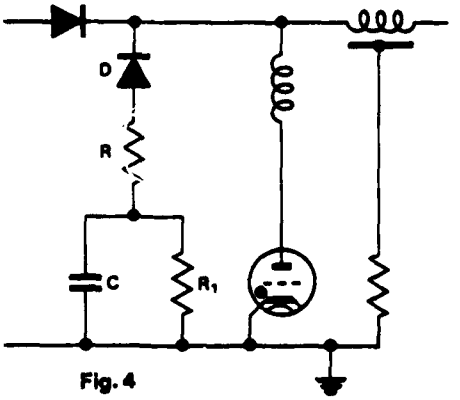

Fig. 4

Fig. 4 shows a circuit[5] in which a conventional inverse diode circuit is connected in series with parallel-connected

resistance and capacitance. The capacitor C becomes negatively charged by the inverse diode current and so behaves as though it were a battery whose voltage can be controlled by means of the resistance R_1. This has the effect of applying a negative voltage datum to the circuit, so that the inverse diode does not conduct until that voltage is reached. This subjects the switching device to a finite negative anode voltage following conduction and so gives it adequate time to recover.

End of Line Clippers

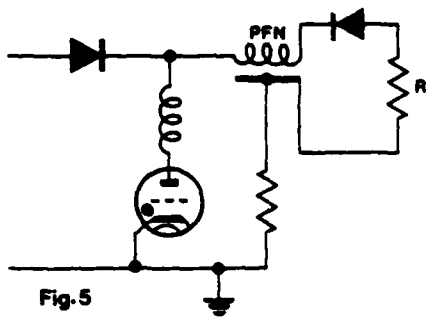

Fig.5

Alternatively, instead of the various inverse diode arrangements of Figs. 1 to 4, a series-connected diode and resistance can be connected across the end of the PFN remote from the switching device (Fig. 5). This does nothing at all so long as the PFN voltage is positive, but should negative voltage appear at that point (due to load mismatching or flashing) the diode immediately conducts. If R is chosen to match the PFN, then the latter is fully discharged in two transits of the network. This does not directly protect the switching device but with PFN fully discharged the only sources of excess voltage are charged stray capacitance and energy stored in a pulse transformer. In practice the method works well, but only, of course, in circuits where intentional slight mismatch is not used to allow time for recovery. (The use of parallel-connected C and R as in Fig. 4 can help in this respect.)

It is worth mentioning in passing that the power supply to a PFN has often been connected to the end remote from the switching device, apparently in the belief that the addition of stray capacitance at the remote end has less effect than at the near end. On investigation it has been found that whilst any added capacitance at the near end can be effectively isolated from the switching device by adding a few microhenrys in series, that at the remote end tends to introduce an unwanted step into the middle of the pulse waveform and also to slow up the tail of the pulse. It is therefore recommended that the near end connection should always be used and the various circuits shown in this paper all show this. (Apart from Fig. 3, any series inductance has been omitted in order to simplify the diagrams.)

In cases where stray capacitance across the load remains charged after the PFN has fully discharged, this can result in the appearance of a negative voltage spike of relatively short duration but often of excessive amplitude across the switching device. Capacitance added at this point can help considerably, as it is initially uncharged and so acts to share the residual charge with the load capacitance and thereby reduces the amplitude of the spike. This is yet another reason why connecting the charging circuit to the near end of the PFN is advantageous.

Prevention of Cumulative Build-up of Voltage following "Fire-Through" of the Switching Device

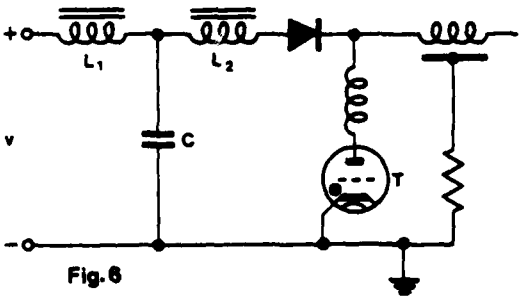

Fig.6

The power supply to a pulse generator of the type here considered often consists of a rectifier circuit followed by a smoothing filter of the "choke-input" (inductance/capacitance) type[8]. It is not always appreciated that such a circuit can generate dangerously high voltages if the component values are wrongly chosen and if the switching device should fail to recover after conduction. Fig. 6 shows such a circuit and so long as the inductance of L_1 is much smaller than that of L_2, then excessive voltage build-up cannot occur. If, however, L_1 is considerably larger than L_2, then failure to recover of thyratron T will cause current to build up in L_2 as the capacitor C discharges through L_2. This is a resonant circuit and, because T is a rectifier, the discharge ends up with C

charged negatively to a voltage approximately equal to that of the supply. The relatively large inductor L_1 will have had little effect during this period, but now it recharges C from -V to about +3V. This overvoltage is likely to cause T to conduct prematurely, or else to cause flashover or breakdown elsewhere in the circuit. If T fires, of course, the original mechanism is repeated to generate even higher voltages than before. This action is cumulative and so sparkover or failure is virtually certain after one or two repetitions of the cycle.

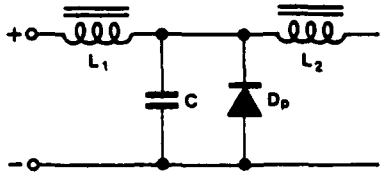

Fig. 7

The solution to the problem is either to ensure that L_2 is larger than L_1 (which is not always practical) or else to provide a protective diode D_p as in Fig. 7[6]. The diode conducts to prevent any voltage reversal across C, and as conduction occurs at a point of current maximum, L_2 then ensures that T will continue to conduct via D_p until the over-current protection[9] operates to switch off the equipment. This entirely eliminates any risk of generating dangerous positive over-voltages. If for any reason L_1 has to have more inductance than L_2, it is good engineering practice not to omit such a simple means of protection.

The Use of Clipping Techniques

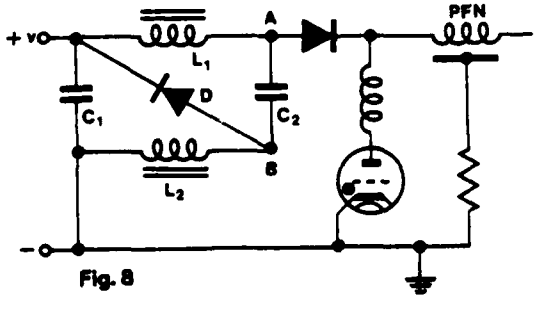

Fig. 8

Coupled Windings

Fig. 8 shows how by splitting the conventional reservoir capacitor and charging inductor into two separate half-circuits, the addition of a single diode not only makes cumulative build-up of voltage impossible, but also returns any surplus energy to the supply. The two half circuits are clearly C_1L_1 and C_2L_2 and it will be apparent that during charging of PFN the two capacitors discharge equally via their associated inductors to supply the necessary current. The waveform at A has the normal cosinusoidal shape[7] and that of B is identical, apart from a shift of datum equal to the voltage of the supply. If the voltage at A does not exceed twice the supply voltage V, then that at B cannot be more positive than the supply terminal. Diode D does not conduct and no clipping action can occur. Any increase in voltage, however, causes both circuits to bypass excess energy via D, thereby preventing the voltage to which PFN is charged from increasing beyond approximately twice the voltage of the supply. The bypassed energy is returned to the two capacitors, thereby reducing the total current drain on the supply.

The practical effect is that if, for example, partial short-circuiting of the load should occur, then a negative overswing will appear across the switching device but no cumulative build-up of positive voltage is possible. This usually means that the equipment will continue to run as though nothing had happened, the only significant symptoms being an increase in any d.c. component of current flowing through L_2 and, obviously, in the observed output of the equipment. The use of separate inductors has been described but if they are also coupled together magnetically, then construction is simplified and one iron core can be dispensed with. Inductor L_1 carries more r.m.s. current than L_2, for the obvious reason that the d.c. component of the charging current can only flow through L_1.

A simplified version of this circuit in which split capacitors are not used and all the couplings are magnetic has been successfully used in commercial equipment manufactured by the Marconi Company. This works very much as explained, but, in the absence of the capacitor C_2, leakage inductance may well make it rather less precise than the split circuit described. This in no way alters its effectiveness as a means of limiting dangerous voltage excursions, but in this case all the charging current flows through winding L_1.

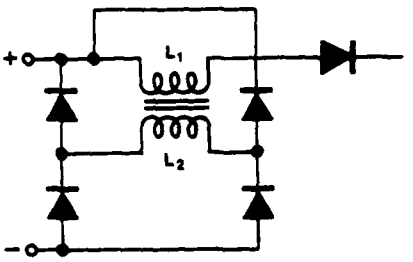

Fig. 9

One disadvantage of this circuit (in either form) is that diode D may have to withstand an inverse voltage of rather more than twice that of the supply. In cases where a suitably rated diode is not available, it so happens that an alternative circuit exists which does not have this voltage limitation. Here the two windings must be magnetically coupled and the capacitors between them omitted. Winding L_2 no longer contributes to the charging of PFN, but with the bridge configuration of Fig. 9 any over-voltage of either polarity is bypassed back to the supply. This has the leakage-inductance effect common to all magnetically-coupled systems, and, clearly, can also be affected by excessive interwinding capacitance. A minor advantage of this bridge circuit is that the two windings need not be in exact 1 : 1 ratio and this can give extra flexibility to the designer.

The Tapped Charging Inductor Method

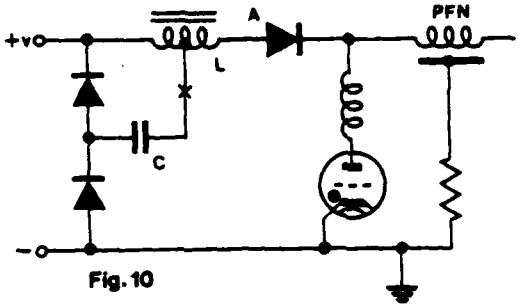

Fig. 10

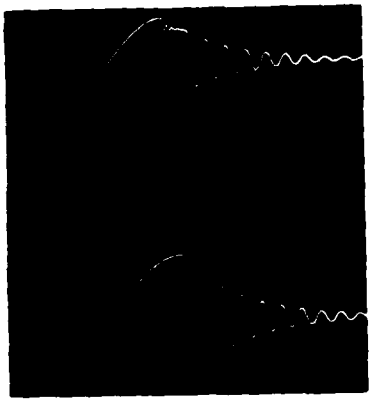
Fig. 11

This is an arrangement, as shown in Fig. 10, in which the charging inductor is tapped and the tapping point connected via a diode-pump circuit[10] to the supply. It is normally preferable for the inductor to be centre-tapped. Assuming the ideal cosinusoidal charging of PFN to twice the supply voltage, it follows that the peak-to-peak excursion of voltage at the centre-tap is exactly equal to the voltage V at the input terminals. Capacitor C rapidly becomes charged to $\frac{V}{2}$, after which neither diode conducts. Immediately the voltage swing increases for any reason, the diodes conduct alternately to return energy to the supply. Assuming that L behaves as a perfect auto-transformer, it follows that this mechanism acts to limit over-voltages of either polarity and, provided C is large enough to store the bypassed energy without appreciable change of voltage, any cumulative build-up of voltage cannot occur. Imperfect interturn couplings within L make this system less precise than that of Fig. 8 but, as Fig. 11 shows, the voltage at point A is still clipped very effectively.

Series resistance should be added (at the point marked X in Fig. 10) to limit any transient currents which might flow. It will be seen that because L behaves as an auto-transformer, the whole circuit must also behave partly as if it included an inverse diode as well as a voltage-limiting clipper. With this in mind, the value of added resistance should be chosen to be one quarter of that used in a conventional inverse diode circuit.

References

(1) British Patent No. 832,122.

(2) Pulse Generators (MIT Series)
Section 10-6
McGraw Hill/Dover.

(3) British Patent No. 1,096,821.

(4) The Use of Hydrogen Thyratrons as High Speed High Voltage Rectifiers
H. Menown and G. J. Scoles
Eleventh Modulator Symposium 1973
(EEV Reprint).

(5) A Compact 70 MW Modulator for Linear Accelerators Using High Voltage Thyratrons
C. Latham, H. Menown and N. S. Nicholls
Ninth Modulator Symposium 1966.

(6) British Patent No. 899,633.

(7) Handbook of Electronic Circuits
Section 29-2
G. J. Scoles (J. Wiley).

(8) Handbook of Electronic Circuits
Section 25-1
G. J. Scoles (J. Wiley).

(9) Handbook of Electronic Circuits
Section 25-7
G. J. Scoles (J. Wiley).

(10) Handbook of Electronic Circuits
Section 13-2 and Section 21-1
G. J. Scoles (J. Wiley).

Acknowledgements

The author wishes to thank the Directors of English Electric Valve Co. Ltd. for permission to publish this paper.

A 100-kA DIRECT DRIVE EMP PULSER

John E. Allen
GTE Sylvania, Incorporated
189 "B" Street
Needham, Massachusetts 02194

Summary

A pulser is described which was built to directly drive 100 kA into a Minuteman silo closure seal. The pulser has a 50-kV charge voltage, a 10-nanosecond rise time and a 50-microsecond fall time. Physical features and performance characteristics are described along with a summary of its successful operation in pulsing the silo cover.

Objectives

The pulser was designed to meet the needs of a Silo Closure Measurement Program. The objective of this program was to simulate the effects of a close-in nuclear burst as manifested in a voltage and resultant current across the seal which the top of the silo makes at the cover. The effects of this simulated pulser were to be measured within the silo.

The objective, then, as it related to the pulser, was to drive the cover seal with a pulse having an open-circuit peak voltage level of 50 kV and a short-circuit current of 100 kA. The e-fold rise time objective was established as 5 nanoseconds with a 10 nanosecond maximum; the fall time objective was 100 microseconds with 50 microseconds minimum.

Pulser Description

In the course of designing the pulser, a number of concepts were considered for developing the pulse and for delivering it to the seal. Since the required impedance of the pulser as a generator was half an ohm (50 kV ÷ 100 kA), the requirement for output connections rapidly narrowed down to 100, 50-ohm cables, matched at the source end. Various numbers of gas switches were considered for developing the pulse, as was the possibility of using peaking switches for obtaining the fast rise time; however, the availability of a very low-inductance switch capable of mounting atop a 3-microfarad storage capacitor offered the promise of a simple, 36-switch pulser meeting the rise time requirements.

The pulser concept is illustrated schematically in Figure 1. Starting from the bottom of the figure are shown the 36 storage capacitors which are charged through individual resistors and discharged through triggered gaps. The discharge current flows through the 50-ohm matching resistors to the 108 output cables.

Each gas switch and its associated 50-ohm load resistors are mounted in a cylindrical assembly whose cross section is sketched in Figure 2. The storage capacitor has coaxial terminals which are connected to the outer shell and lower electrode, respectively. A photograph of these two pieces mounted on the capacitor is shown in Figure 3.

The storage capacitor is an Aerovox PX 240D23 and is identical to the familiar 1.85-microfarad PX 300D26 capacitor except that its capacitance is 3.3 microfarads, it is one inch higher (11 by 14 by 26 inches high), and it is not rated for oscillatory discharge. The characteristic impedance of the coaxial line formed by the lower electrode and the shell, approximately 60 ohms, is about as low as is feasible without incurring the possibility of arcover. What is at least as important as that is that the line length is extremely short and the transitions are smooth.

The upper electrode is also cup-shaped and is inverted as shown in Figure 2. By way of further portrayal, Figure 4 shows the upper electrode set on a spacing jig, with its connection to the three 50-ohm load resistors indicated. When this upper electrode assembly is placed in the position in which it is assembled, the appearance is that shown in Figure 5.

The trigger electrode is a sharp-edged disc as indicated in Figure 2, which is located half way between the upper and lower gap electrodes. Its height is determined by the depth of insertion of its shaft into its mounting bushing as indicated in Figure 6. It is electrically driven via this bushing through trigger isolation resistors in the acrylic tube shown in the center of Figures 2, 4 and 5.

The three output connections and the trigger input connection are made at the top of the switch assembly as shown in Figure 7. The volume inside the whole switch enclosure is pressurized through a gas connection at the bottom of the assembly. This connection, as well as the charge cable connection, are shown in Figures 2 and 5. Figure 8 shows a row of switch assemblies in the pulser trailer.

The 36 switches are grouped into 9 modules for charging purposes. As indicated in Figure 9, any or all of the first six modules can be charged from the first power supply, and any or all of the last four modules can be charged from the other. This allows for portions of the load to be driven uniformly or differentially as required in the Silo Closure Measurement Program.

The power distribution and charging control, shown within the broken line of Figure 9, were contained in an oil-filled tank, shown in the photo of Figure 10. Half of the assembly has been lifted out of the oil bath to show the charging resistors. Most of the cables connected to the top of the link box are the charge cables which go to the individual switch assemblies.

A block diagram of the trigger system is shown in Figure 11. A 5-volt pulse from the synchronization pulse is amplified to a 300-volt level at the control console and then transmitted to the trigger enclosure shown in Figure 12. Here, the trigger generator shown at the front corner raises the pulse level to 50 kV, and that trigger fires two trigger output switches which are oil bathed, which feed the 36 pulser cables. The trigger output switches discharge 36, 15-foot storage cables which loop out of the trigger tank and back into it and account for the large number of cable connections shown in the photo.

Not shown in the diagrams of the link box and the trigger tank (Figures 9 and 11) is the method of biasing the mid-plane trigger electrode in each of the 36 main pulser gaps (Figures 1 and 2). Each trigger element is biased at the half-potential between the main gap electrodes while they are charging; e.g., at +25 kV or -25 kV when the storage capacitor is charged to + or -50 kV respectively. The bias is developed as shown in Figure 13.

As indicated in the figure, the mid-point bias is developed for each module by a 200-megohm potential divider in the link box and transmitted via a cable to the trigger tank. Here, each of the nine bias voltages are distributed to the four trigger output cables associated with the particular module through 200 megohm isolation resistors. Each of these output cables

(36 total) goes to the appropriate switch where, as indicated in Figures 2, 4 and 5, it is connected to the mid-place trigger electrode through a series of four mid-plane trigger isolation resistors.

The trigger isolation resistance in each switch totals 500 ohms and allows the trigger electrode to produce a cascade breakdown of the main gap. Prior to the receipt of the trigger pulse, the mid-plane electrode will ideally produce no field enhancement at its knife edge. When the pulse arrives, however, a very high field is produced at this edge and an arc is formed between it and whichever main electrode is at the farthest potantial from it (depending on whether the associated storage capacitor has been charged positively or negatively; the trigger pulse is always positive). Because of the isolation, the trigger electrode voltage then jumps immediately to approximately that of the main electrode to which it has arced, thus, overvolting the remaining half-gap to much beyond what is required to complete the main arc.

Two power supplies are used for charging the main switch capacitors. They are each housed in an oil-filled drum as shown in Figure 14. The polarity of each one can be changed by reconnecting a submerged jumper panel through the access hole shown in Figure 15.

The control cabinet is shown in Figure 16. It consists of three panels, a power supply control, a trigger and gas control, and a firing indicator panel. The upper panel contains mode indicators, mode controls, and main power supply controls and indicators. The center panel contains a trigger voltage supply motor, trigger controls and the means for gas selection and pressure and flushing control.

The lower panel contains 36 lamps, each of which lights when the corresponding switch has fired and remains lit until either the power is removed or the lamp test/reset button is depressed. The pulse which sets the lamp to the "on" condition is developed by a single-turn current monitor loop, shown at the top of Figure 2, which connects through a small-size coaxial cable from the top of each switch assembly which can be seen in Figure 8.

The equipment is arranged in the pulser trailer as shown in Figure 17. The controls are in the small room at the front of the trailer and the high voltage equipment in the large room. The 36 individual switches making up the nine modules run up and down each side of the trailer with other equipment placed where convenient.

The output cables run overhead to the front of that room and then exit through the floor as indicated in Figures 8 and 18. These figures show the views looking forward along the sides of the room shown at the top and the bottom, respectively, of Figure 17. An external view of the trailer, taken from the front, beside the instrumentation and control van, with which it is normally associated, is shown in Figure 19.

Application To The Silo Closure Test

In the performance of the Silo Closure Test, it was required that the 108 output cables be connected between a replica silo cover and the silo shell itself. (Since it was impractical to drive the real silo cover, it was replaced by a replica cover for this test.) Current probes were attached to every third pulser cable at its point of connection so that the current from each of the 36 switch assemblies could be monitored. A voltage probe was connected from the cover to the silo in each quadrant to allow monitoring of the voltage buildup and, hence, some indication of the condition of the seal. (Additional probes within the silo were used for more conclusive results.)

With no intentional imperfections placed underneath the replica cover, the seal was sufficiently conductive that it appeared as a short circuit to the pulser. Under this condition, the summation of currents flowing in one quadrant of the seal, as indicated by the current probes, was that shown in Figure 20. Part of the figure shows an e-fold rise time of less than 10 nanoseconds and part b indicates a fall time of 55 microseconds.

In the course of the test, some 800 shots were obtained at various charge voltages and polarity combinations. Of these, 500 were deemed successful. The majority of those rejected appeared to have too high a time difference between the two trigger output pulses (Figure 11). Late in the test series, the method of measuring this time difference was improved and the difference subsequently found to be 4 nanoseconds or less. It is now believed that there was a jitter between these two triggers early in the operation of the pulser but that this cleared as a result of burn-in. However, the time at which the erratic operation disappeared is not known due to faults in the method of measurement.

Conclusions

The 100-kA pulser used for the Silo Closure testing has proven itself a reliable pulser consistently delivering a transient-free 1 kA pulse to up to 108 terminals. It has a diversity of polarity which should add to its usefulness in further EMP testing.

Acknowledgments

The writer wishes to acknowledge the work of a large number of contributors to the success of design and application of the silo closure pulser including: Frank G. Albertini, Edward G. Argerake, David L. Fye, C. Peter Garbaczeski, Anthony R. Ingegneri, Charles R. Marchetti, Lawrence J. Marino, Robert R. Norander, Richard R. Perilli, Sumner E. Perlman, Charles N. Rigal and Norman E. Tetreault of GTE Sylvania Incorporated; Harlan K. Aslin, Joe Bailey, Joseph P. Lennon, Donald R. Sink, and Boris Yen of Physics International Company; Dr. Helmut Milde of Ion Physics Corporation; and Robert S. Gordon of Robert S. Gordon Associates. C. Peter Garbaczeski, Anthone R. Ingegneri, Charles R. Marchetti, Lawrence J. Marino, Robert R. Norander, Richard R. Perilli, Sumner E. Perlman, Charles N. Rigal and Norman E. Tetreault of GTE Sylvania Incorporated; Harlan K. Aslin, Joe Bailey, Joseph P. Lennon, Donald R. Sink, and Boris Yen of Physics International Company; Dr. Helmut Milde of Ion Physics Corporation; and Robert S. Gordon of Robert S. Gordon Associates.

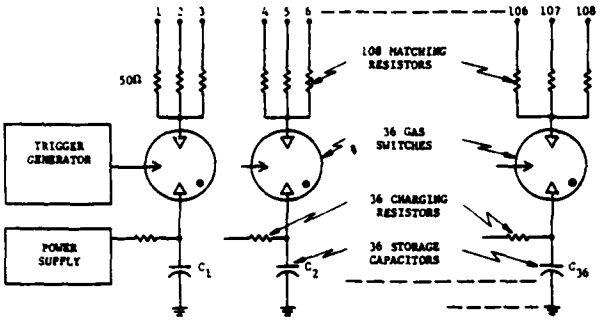

Figure 1. Simplified Pulser Schematic

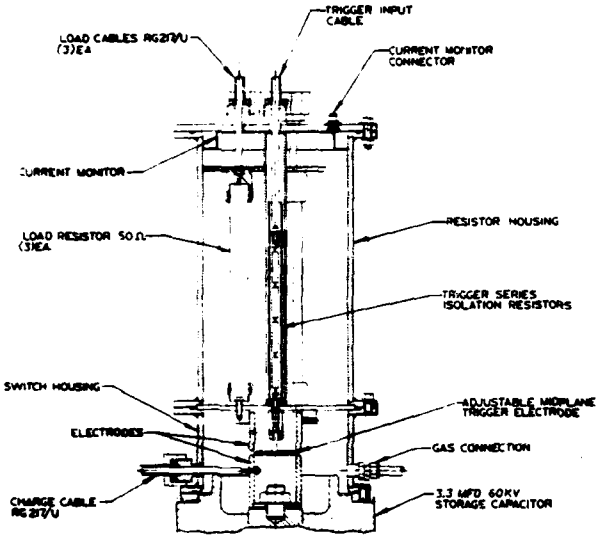

Figure 2. Capacitor/Switch Assembly

Figure 3. Connections to Storage Capacitor

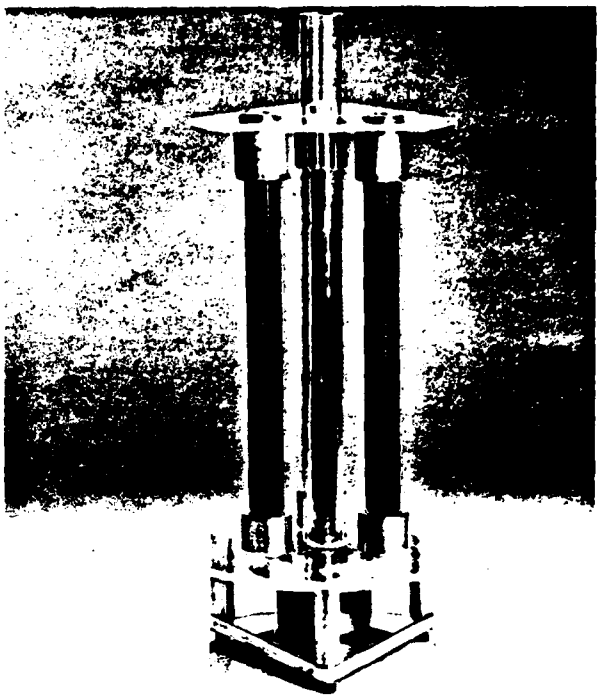

Figure 4. Upper Electrode and Resistor Assembly

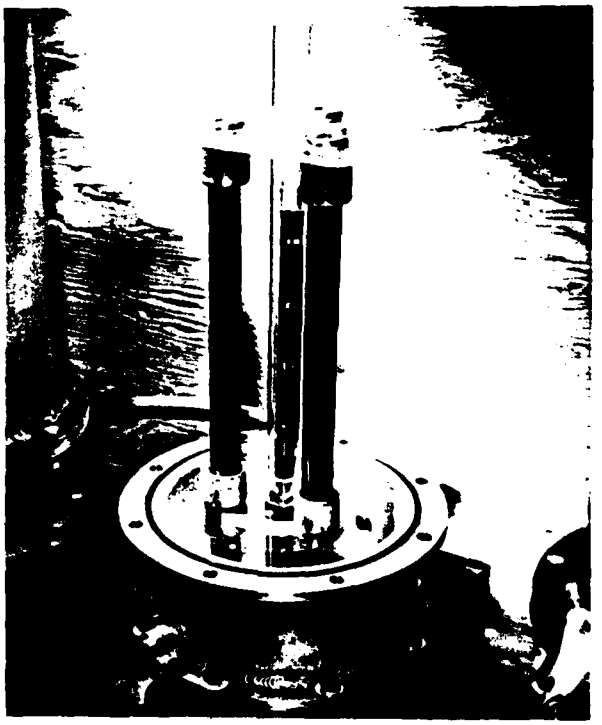

Figure 5. Upper Assembly in Place

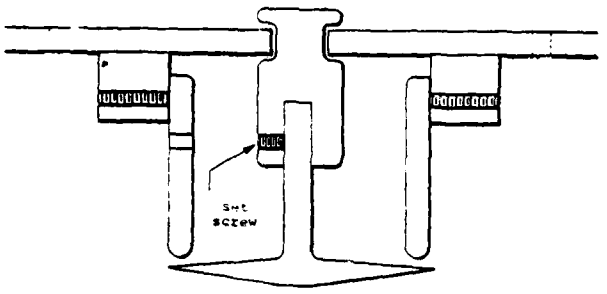

Figure 6. Trigger and Upper Electrode Assembly

Figure 7. Cable Connections to Switch

Figure 8. Switch Assemblies in Trailer

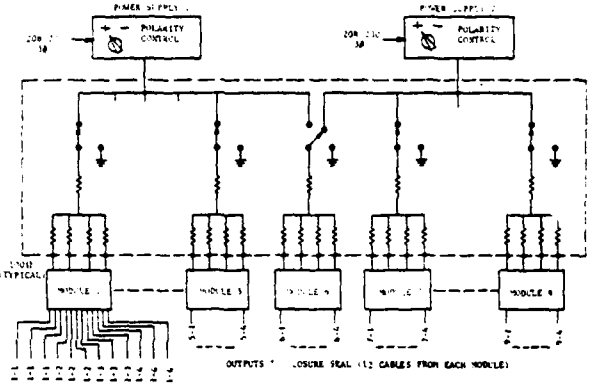

Figure 9. Polarity Control

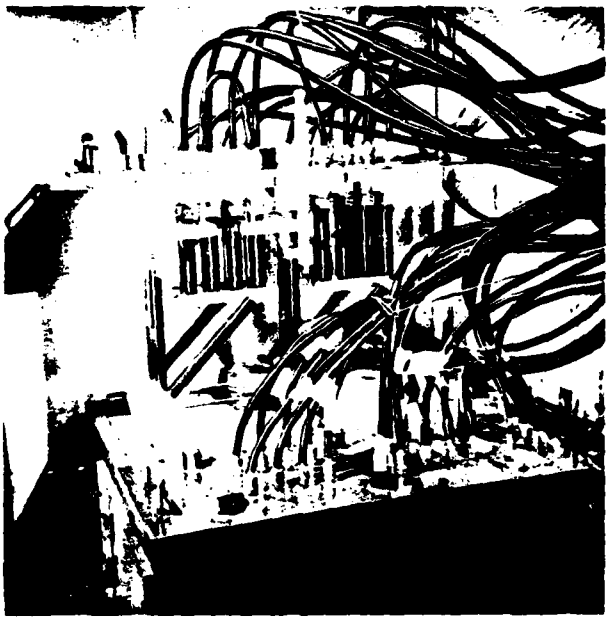

Figure 10. Link Tank, Partially Disassembled

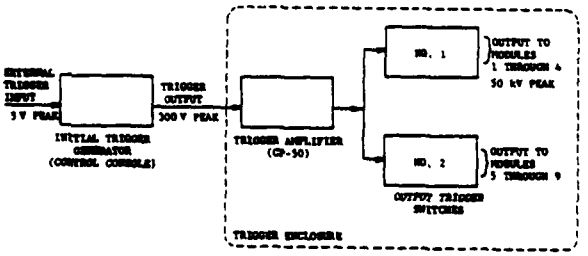

Figure 11. Trigger System

Figure 12. Trigger Tank

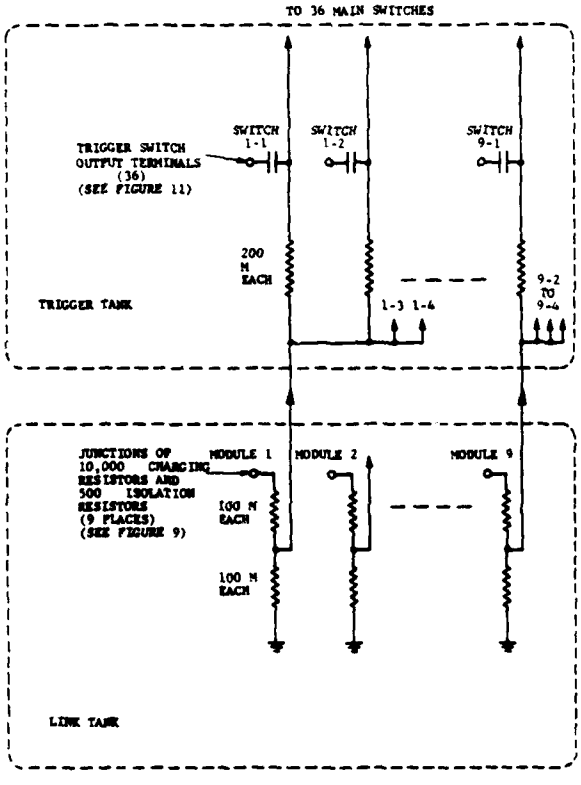

Figure 13. Trigger Bias Distribution

Figure 14. Main Power Supplies

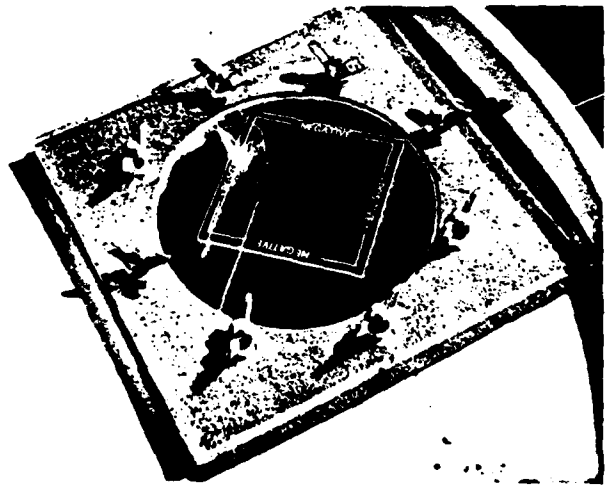

Figure 15. Polarity Access Hole and Cover

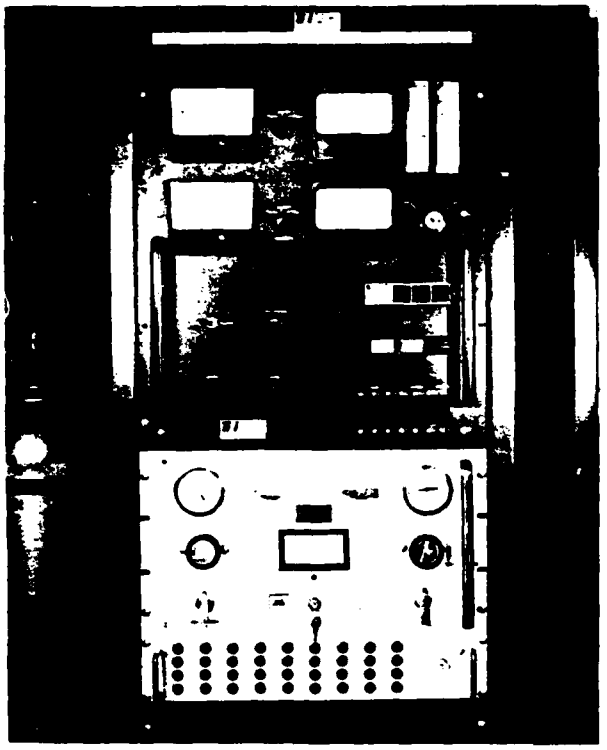

Figure 16. Control Panel

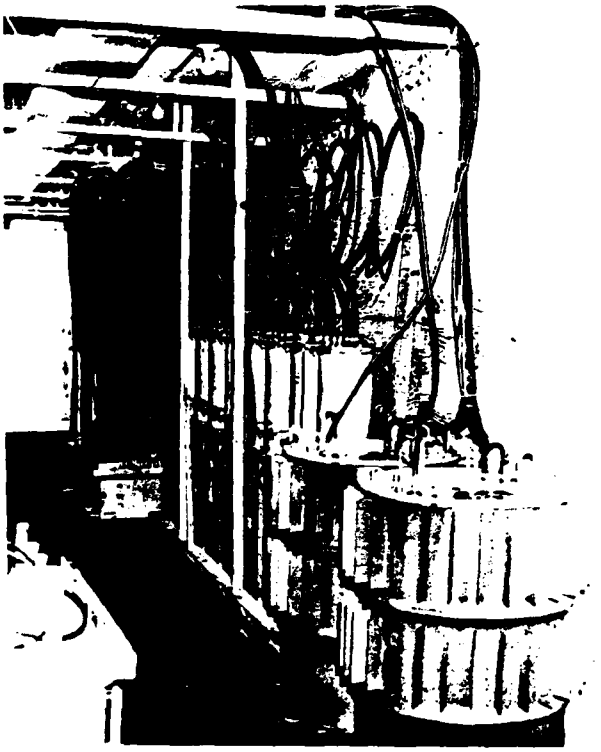

Figure 18. View of One Side of Trailer

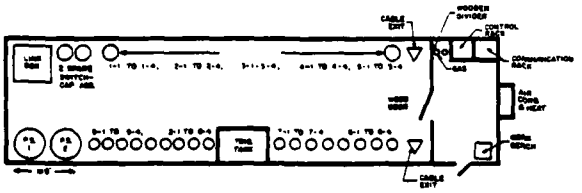

Figure 17. Van Layout

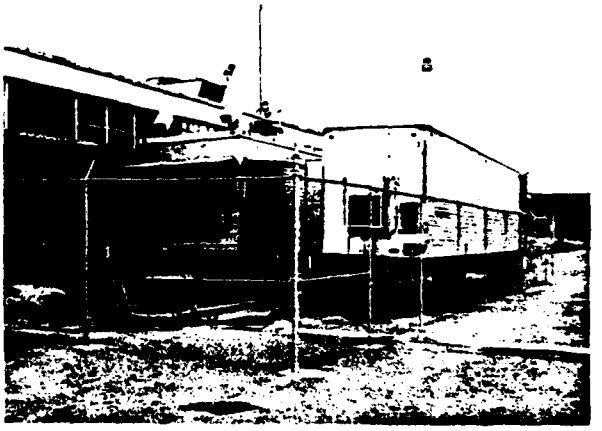

Figure 19. Instrumentation and Control Van and Pulser Van

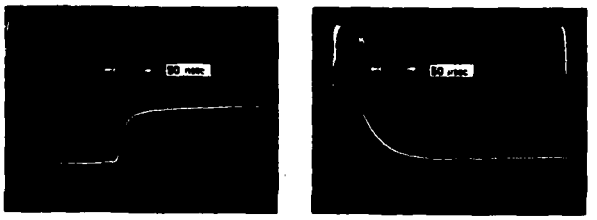

Figure 20. Pulse Output Waveform

CONVERSION OF A MARX GENERATOR TO A TYPE-A PULSE FORMING NETWORK

David B. Cummings
Physics International Company
2700 Merced Street
San Leandro, California 94577

Two systems involving Marx generators have been converted into Type-A pulse forming networks for generating long (>1 μsec) pulses. This was done by adding a parallel L-C filter in series. The Pulserad 1140/1150 can thus be operated in either short or long pulse mode with a rapid conversion. The design procedure and results are described.

Statement of Problem

Recent developments in laser and fusion research have created a need for high voltage (>1 MV) pulsers with pulse lengths of a microsecond or more. Previously the emphasis had been on pulse lengths in the range of 20 nsec to 100 nsec. Many such pulsers have been built for radiography and electron beam work. Most of these units have a Marx generator to charge up a low-impedance output pulse line such as a coaxial line or Blumlein network. This line is then discharged through an output switch into the load.

Two pulsers have been converted into pulse forming networks (PFNs) at Physics International. The first was a portion of a SIEGE II Marx generator which is simpler than the kinds of systems described above. This system, originally built as an EMP simulation pulser, employed 16 parallel Marx generators for a 50-μsec decay time. Each Marx was in a separate oil tank and had 16-1/2 stages consisting of six 1.85-μF, 60-kV capacitors (3 in parallel, 2 in series). The individual Marx generators had no pulse line or output switch. The conversion called for rearranging a 16-1/2-stage Marx into two 6-stage Marxs within the original tank and making them into PFNs. The goal was to produce a 350-kV, 4-μsec pulse into a 4-ohm laser load. One PFN was built.

The second system was the Pulserad 1140 pulser used at the PI plant for a variety of research programs. It consisted of a 40-stage Marx with 0.5-μF, 100-kV capacitors. At the same time the Marx generator was to be upgraded to 50 stages for increased voltage and energy. The nomenclature then became Pulserad 1150. It had a 45-nsec, 35-ohm oil Blumlein network and an output switch. This conversion assumed removal of both Blumlein and switch. Also it was necessary that the conversion be easy and reversible so that the system could be operated in either short or long pulse mode. The goal was a 2-MV, 1.5-μsec output for long pulse diode research.[1]

Both Marx generators were of a folded design to minimize length and volume. Both had hybrid triggering systems though different from each other. Both requirements for risetime and flatness could be satisfied with a 2 section PFN.

The choice of circuit, the design, and conversion of both of these systems will be described in subsequent sections.

Alternative PFNs

Figure 1 shows the three types of PFN circuits which could be considered for such a conversion. Type C has the advantage of employing two higher inductance circuits in parallel and hence is more tolerant of relatively high inductance Marx generators. A Type-C PFN could be formed by putting a second Marx generator in parallel with the existing one. Parallel Marx erection is feasible for these pulse lengths. However this would require doubling the number of switches, trigger circuits, charging circuits, etc., and hence would be costly. Also the layout of the tanks did not favor parallel Marx connections. In addition the inductance of the load is a deviation from the ideal circuit although a small one.

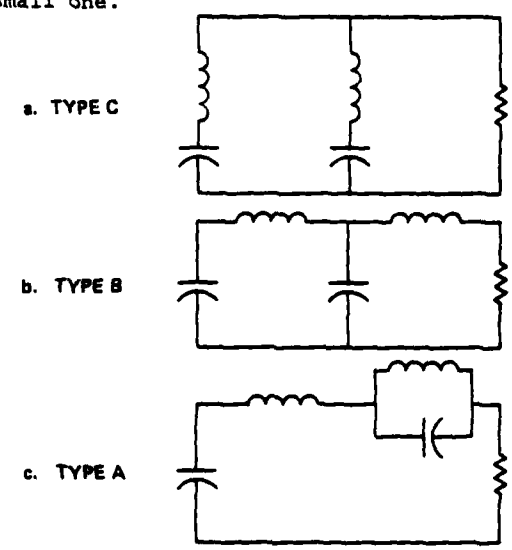

Figure 1 Types of Guilleman voltage-fed networks considered for Marx generator PFN conversion.

Another approach is to convert each stage of the Marx into a PFN by adding a series L-C circuit in parallel with the existing capacitors of the Marx. Since the switches and leads constitute a substantial part of the Marx inductance, an ideal PFN circuit cannot be achieved. However, the deviation is manageable for Type C. Type C also has a much smaller value of capacitance for the add-on circuit than Type B. In addition Type B requires the smaller capacitance be next to the output; therefore, the circuit connections would require change. Type A would also

require a major change to place a parallel L-C circuit in series with each stage of the Marx. Thus, the Type-C PFN is most attractive for conversion within each stage but the conversion would be laborious. Lastly such a conversion would increase the size of the Marx and decrease either the working space or the clearances or both to an unacceptable degree.

A third alternative is to make a Type-A PFN by the addition of a single parallel L-C circuit (filter) in series with the Marx generator. This is the only conversion in which the idealized circuit can be achieved (except for the stray capacitances common to all options). There are no first-order unwanted components or connections as in the other options. No modification of the Marx generator is required. In addition, such a filter could readily be put in the space made available by (a) moving some stages in the SIEGE Marx and (b) removing the Blumlein network and output switch from the Pulserad 1140/1150. A small disadvantage is the uncharged filter capacitance which does not contribute to the initial energy store.

The Type-A circuit was judged the most attractive for the conversion of both Marx generators into PFNs. The more complete circuit with stray capacitance and inductance is shown in Figure 2.

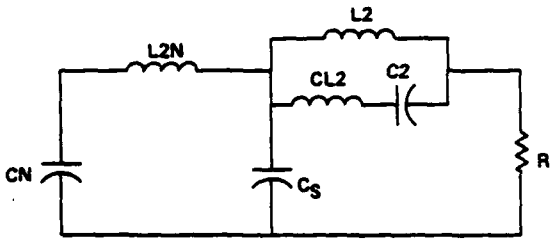

Figure 2 Type-A PFN with stray capacitance and inductance of most importance.

Design Calculation

In both cases a 2-section PFN was sufficient to meet the performance requirements so a single filter stage was needed. There are both theoretic and practical advantages to the simulation of a wave with a parabolic rise and fall, and a flat top. There is more rapid convergence than rectangular or trapezoidal pulses. In addition none of the parameters go negative as with trapezoidal design formulas. The general approach and a few normalized design values are given in Reference 2. The waveshape being synthesized is shown in Figure 3. The pulse width τ is measured at the base line and the rise and fall times a, relative to τ, are measured from 0 to 100%. Design values were computed for up to 5 sections and a wide range of relative risetime a. The normalized design values for a = 1/3, which was used for the SIEGE Marx PFN conversion, are

$$CN(N) = 0.387 \qquad L2N(N) = 0.190$$
$$C2(N) = 0.256 \qquad L2(N) = 0.0606$$

The design equations are

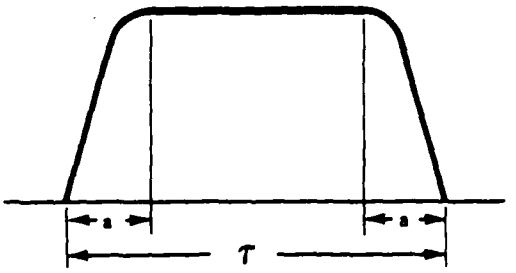

Figure 3 Pulse waveform to be used as goal for synthesis-parabolic rise and fall with flat top.

$$L(A) = L(N)\ Z\ \tau \qquad (1)$$

and

$$C(A) = C(N)\ Z/\tau \qquad (2)$$

where L(A) and C(A) are the actual values of any inductor or capacitor and the L(N) and C(N) are the normalized values for the same parameter. Z is the actual load impedance and τ is the actual pulse length (both are unity for normalized values). From Eqs. (1) and (2) the following equations can be derived in terms of the impedance and pulse length characteristic for a given Marx generator:

$$Z = \sqrt{\frac{L2N(A)\ CN(N)}{L2N(N)\ CN(A)}} \qquad (3)$$

and

$$\tau = \sqrt{\frac{L2N(A)\ CN(A)}{L2N(N)\ CN(N)}} \qquad (4)$$

where L2N(A) includes inductances of the filter and load as well as the Marx generator inductance. From these values of Z and τ the filter capacitance and inductance can readily be calculated. The resulting component values are given in Table I.

TABLE I VALUES FOR SIEGE II MARX PFN CONVERSION

Component	Normalized	Actual
CN	0.387 F	0.463 μF
C2	0.256 F	0.306 μF
L2N	0.190 H	3.63 μH
L2	0.0606 H	1.16 μH
Z	1.0 Ω	4.0 Ω
τ	1 second	4.79 μsec 4.07 μsec (FWHM)

The requirements for the conversion of the Pulserad 1140/1150 were complicated by the need to operate into a diode with an appreciable decrease of impedance during the pulse. However, the values for a constant impedance load and a = 0.28 are given in Table II.

TABLE II VALUE FOR PULSERAD 1140/1150 PFN CONVERSION

Component	Normalized	Actual
CN	0.404 F	10.0 nF
C2	0.245 F	6.07 nF
L2N	0.0680 H	27.7 μH
L2	0.169 H	11.1 μH
Z	1 Ω	81.3 Ω
τ	1 second	2.01 μsec 1.70 μsec (FWHM)

Circuit Design for SIEGE Marx PFN Conversion

The capacitance calculated for this circuit leads naturally to a filter design using 15-nF, 50-kV tubular capacitors. They were connected 4 in series and 77 in parallel. The capacitors were arranged in two concentric circles around the inductor consisting of a straight rod between round discs to which the ends of the capacitors were attached (see Figure 4). Empty holes were left so that capacitors could be added (or removed). The inductor could be removed and cut down (or replaced with a larger rod). This permitted easily calculated and easily performed adjustments to tune the filter.

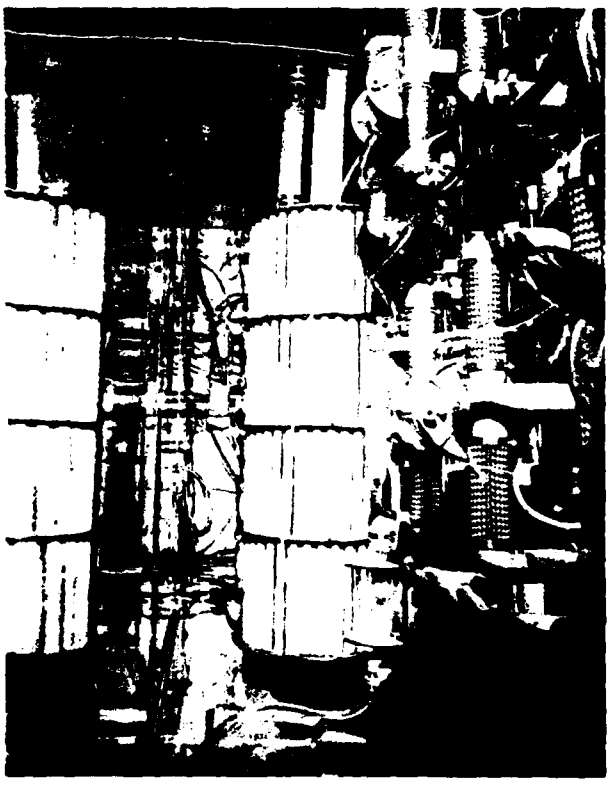

Figure 4 Six-stage SIEGE Marx generator modified to Type-A PFN. Filter section at end with dummy load at top. Note filter at left is reflection by tank wall.

The waveshape is shown in Figure 5. The risetime is 0.55 μsec and the duration is 3.81 μsec (FWHM). It is very much like the computed waveshape giving confirmation of the design. It also established in this low-impedance circuit that the distributed capacitance to ground C_s is negligible. Note the Marx interstage oscillations excited by the erection persisting through the risetime, however, they caused no problems.

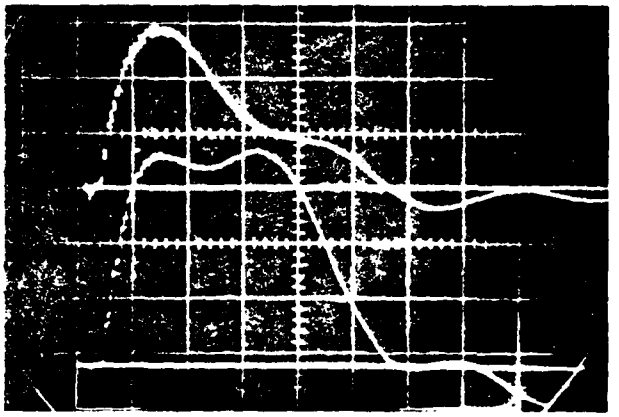

Figure 5 SIEGE Marx PFN waveforms with 4-ohm load. Upper voltage into filter 164 kV/div. Lower voltage into load 72.8 kV/div, 1 μsec/div.

The performance of the circuit is fairly sensitive to LC2 which is the inductance of the filter capacitor C2. It may not be obvious but the definition of LC2 is not simply the total inductance of such an array of capacitors. If magnetic flux links all of the filter capacitors and also the filter inductor, then this is the inductance of the whole filter and becomes part of L2N where it has little effect. It does not appear as an inductance within the filter circuit. For a filter with an ideal capacitor made up of two concentric cylinders separated by dielectric cylinders all magnetic flux which links the capacitor also links the inductor on the centerline (neglecting transit time effects). For this case all flux outside the capacitor becomes part of L2N and all flux within the capacitor becomes part of L2. Therefore, L2 is zero.

For a real filter design with n parallel tubular capacitors the inductance LC2 consists of three terms as follows, the sum of which is then divided by n.

1. The self-inductance of a single capacitor. This results from magnetic flux which links only a single capacitor.

2. Positive mutual inductances from all other capacitors which are closer than the filter inductor (<60° away). These result from magnetic flux which links more than one capacitor but not the filter inductor.

3. Negative mutual inductances from all other capacitors which are farther than the filter inductor (>60° away). These result from magnetic flux which links more than one

capacitor and also the filter inductor. The negative sign is applied since the polarity of the voltage induced in the filter circuit is opposite that induced by the self-inductance. A filter with a circle of many parallel capacitors has many more negative mutual terms than positive ones. Therefore, the inductance LC2 in a real filter can be made quite small. Indeed, simple assumptions for current distributions can lead to unreal negative inductance values. To calculate the exact residual inductance would require the calculation of multiple proximity effects for the flow of current in a tubular capacitor. Since the experimental results confirmed that the value is negligible, the exact value remains undetermined

Circuit Design for Pulserad 1140/1150 PFN Conversion

A diagram of the arrangement of components in the Pulserad 1140/1150 is shown in Figure 6. This shows the position and size of the Blumlein network and output switch, and hence the space available for the filter.

The values computed for the Pulserad 1140/1150 filter likewise permitted the use of the 15-nF, 50-kV tubular capacitors. The design shown in its handling frame in Figure 7 accommodated up to 53 capacitors in series and 14 in parallel. Because of large total length they were folded back and forth between inner 38-inch OD discs and outer 72-inch-diameter corona rings. The filter was 80-inches long. The inductor was a solenoid mounted on the axis of the array between the round end plates. The solenoid also contained the shunt resistors for damping voltage excursions in the events of a fault.

The filter occupied only a portion of space formerly containing the coax line and the output switch. Therefore a transition section of pipe was inserted to make the connection between the filter and the diode. Figure 8 shows the filter and transition section in place in the tank. Some of the Marx can be seen behind the filter. Conversion to or from the PFN mode can be done in a day.

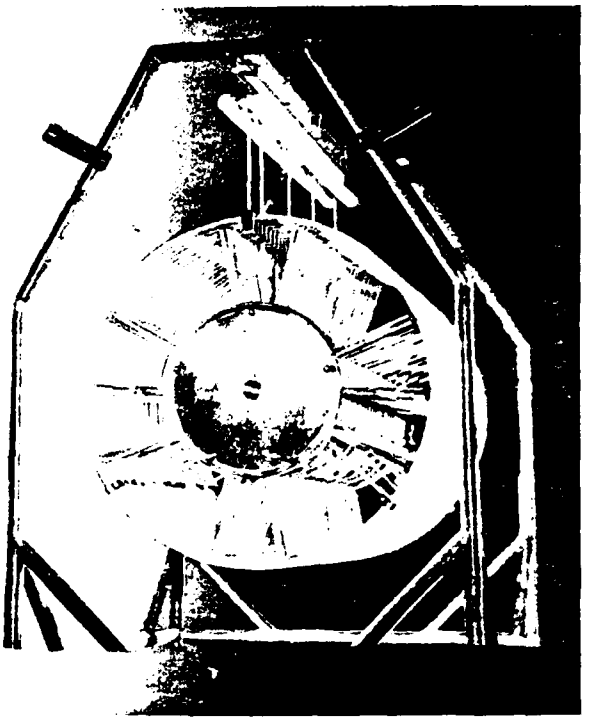

Figure 7 Pulserad 1140/1150 PFN filter in handling frame.

The system was first tested into an 83-ohm constant impedance load. The value of filter capacitance was adjusted to compensate for the distributed capacitance of the filter and transition section. The result is shown in Figure 9.

The effect of diode impedance collapse was simulated. The performance of the circuit was computed using a time-changing load with an average value equal to Z. The result was a pulse with significant droop. The relative heights of the peaks can be corrected by decreasing the value of C2; the greater the decrease in Z, the smaller the value of C2.

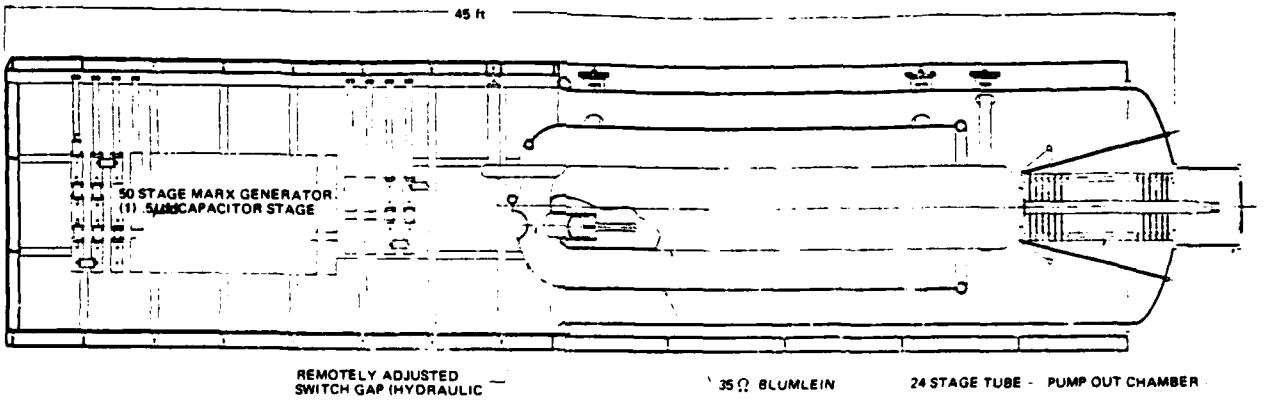

Figure 6 Diagram of Pulserad 1140/1150 with Blumlein network and output switch in place.

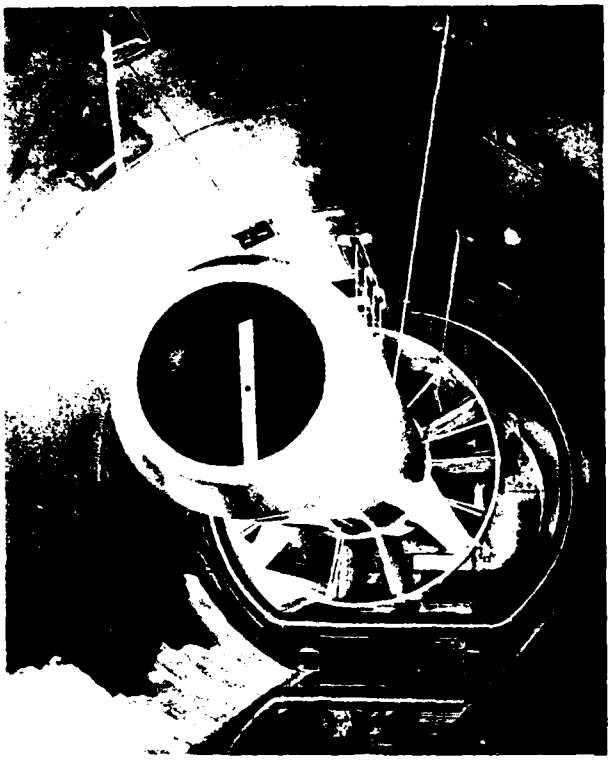

Figure 8 Pulserad 1140/1150 PFN filter and transition section in place in bank. Note Marx generator behind filter.

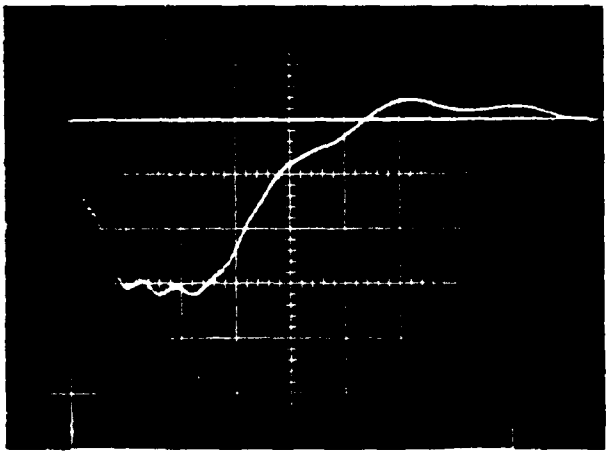

Figure 9 Pulserad 1140/1150 PFN waveform into constant 83-ohm load. 705 kV/div, 500 nsec/div.

The filter was trimmed for operation into the diode load with the results shown in Figure 10. After all of the deviations and corrections from a simple Type-A PFN, the results are necessarily different from the ideal. A low voltage shot is shown since at higher voltages the diode impedance change is less smooth and the diode characteristics tend to mask the performance of the PFN. However the waveshape was satisfactory for the application.

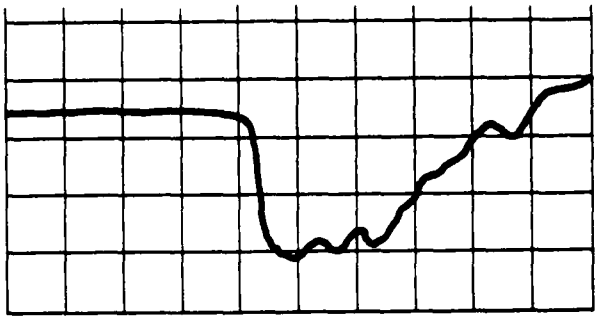

Figure 10 Typical low-voltage Pulserad 1140/1150 PFN waveform into diode load. Tube voltage 282 kV/div, 500 nsec/div.

Summary

Existing Marx generators can most easily be converted into Type-A PFNs. Such circuits have proven to be reliable and give satisfactory waveshapes into both constant impedance and time-changing diode loads. The ease of conversion makes possible operation in both long and short pulse modes.

Acknowledgements

This work was made possible by the support of many fellow workers. In particular, Ian Smith, Bernard Bernstein, Clay Agee, Edward Pereira, Larry Sanders, and James Hauck made many valuable contributions.

References

1. R. Schneider, C. Stallings, and D. Cummings, Generation and Extraction of Microsecond Intense Relativistic Electron Beams, J. Vac, Sci. Technol., 12, 6 1191 (1975).

2. MIT Radiation Laboratory Series, Pulse Generators, Chapter 6, Volume 5, Boston Technical Publishers, Boston, Mass.

THE SPS FAST PULSED MAGNET SYSTEMS

P.E. Faugeras, E. Frick, C.G. Harrison, H. Kuhn,
V. Rödel, G.H. Schröder, J.P. Zanasco

Summary

This paper describes the fast pulsed magnet systems which have been built for the new CERN 400 GeV Proton Synchrotron (SPS). After a short explanation of the principles, the major components of a system are treated in detail. Particular emphasis is put on the H.V. switches which are capable to switch current pulses of 10 kA amplitude, 100 ns rise time and 24 µs duration. Extensive tests have been made on a composite switch called 'thyragnitron' and made of a multigap double ended ceramic thyratron, bypassed by three ignitrons in series. Experimental pulse shapes and results of life tests are presented and discussed.

Introduction

The CERN 400 GeV Proton Synchrotron (SPS)[1] which will shortly be put into operation is equipped with the following fast pulsed magnet systems :

- the injection system, which must bring the beam from its injection trajectory onto the closed orbit of the machine.
- the fast extraction system, which will deflect the beam into the extraction channel after acceleration.
- the beam dumping system, which must dispose the beam onto an absorber block in case of emergency or during tests of the accelerator.
- the Q-measurement system, which generates coherent betatron oscillations in the proton beam to measure some beam characteristics.

In all cases, the pulsed magnetic field must have rise and fall times very short as compared to the proton revolution time of 23.1 µs. Therefore each system has to be split into several identical modules which each consists of a fast pulsed magnet, called kicker, powered by its own pulse generator. In total eleven of these modules are installed. Although peak current, impedance, pulse shape, pulse duration and repetition time are different for every system the module components have been standardized as far as possible. This paper will give at first a general description of the systems for fast extraction and for beam dumping, the first being the most complex and the latter the most powerful one. Thereafter the four main components of a module will be described, i.e. the pulse forming network, the fast switches, the magnet load and the resonant charging power supply.

1. System description

1.1 Fast extraction

The fast extraction of protons out of the accelerator is done through an extraction channel shown in Fig. 1a. The first element is a pair of kicker magnets (MKE), followed by a series of devices, called septa, whose main property is to provide a region of strong deflecting field, to extract the protons, adjacent to a region in which the field vanishes and where the non-extracted beam circulates. The first element after the kicker, the electrostatic septum (ES) generates an electrostatic field between an array of wires (the septum itself) of 0.1 mm thickness at earth potential and an h.t. electrode. The following devices use magnetic fields for deflection and their septa are current conductors, the first being 4 mm thick (MST) the other 16 mm (MSE).

When excited, the first pair of kickers deflects the beam onto the wire array of the electrostatic septum (Fig. 1b). This septum cuts the beam in two parts. The first portion of the beam which has entered the region of electrostatic field is sufficiently strongly deflected to pass through the following septa, where it gets further deflection until the separation between deflected and circulating beam is large enough to use standard beam line elements. [2]

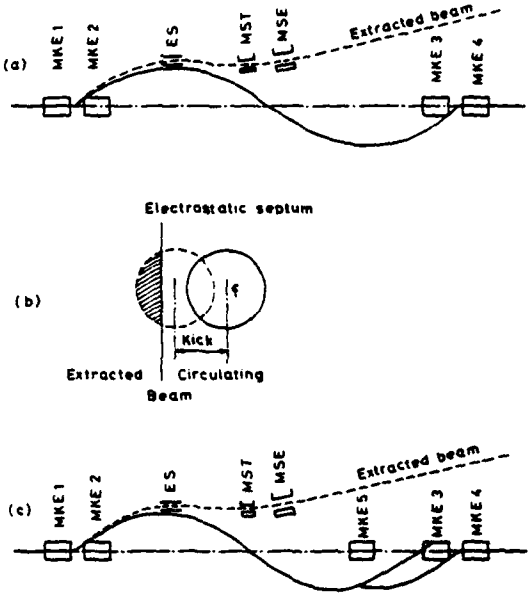

FIG.1 LAYOUT OF EXTRACTION CHANNEL

The other portion of the beam which has not jumped the electrostatic septum remains circulating in the machine. However, as it has been deflected by the first pair of kickers it performs coherent betatron oscillations which are cancelled by a second pair of kickers, installed one betatron wavelength downstreams of the first pair. A fifth kicker is necessary when the betatron wavelength is not equal to the physical distance between the two pairs of kickers (Fig. 1c).

The kicker systems are built in such a way that kick amplitude, pulse length and repetition rate are variable. This configuration allows great operational flexibility as one wants to extract several proton bursts per machine cycle, the duration and the intensity of each of these being adjustable.

The main system parameters emerging from these requirements are summarized in table 1.

1.2 Beam dumping

The SPS accelerator is designed to accelerate at least 10^{13} protons per pulse at 400 GeV, which amounts to a stored energy of 640 KJ.[3] Therefore, in order to prevent uncontrolled beam losses in the accelerator, which can cause thermal and radiation damages to machine components, an internal beam dumping system is necessary.

Table 1

Main system parameters

System	Fast Extraction	Beam Dumping
Number of modules	5	2
Impedance	10 Ω	3.125 Ω
Maximum pulse current	3000 A	10 000 A
Pulse duration	adjustable between 1.0 and 24 μs	fixed 24 μs
Pulse shape	rectangular	rectangular with purposely superimposed oscillations
Kick rise time	0.9 μs	1.0 μs
Kick fall time	0.9 μs	~ 5.0 μs
Flat top ripple	< ± 1%	± 10%
Pulse repetition time	3 pulses 100 ms apart within 4 s	4 s

It consists of fast pulsed magnets which deflect the beam vertically onto a metallic absorber block during one revolution. If one excites the kickers with a rectangular current pulse, the beam would hit the block on one small spot inducing a temperature spike far outside the capability of the block. The thermal and mechanical stresses induced in the block can be sufficiently reduced if the spot size is increased by about a factor 10. This is done in the following way (Fig. 2): an oscillation is deliberately superimposed onto the flat top of the pulse exciting the vertically deflecting kickers (MKDV). At the moment, at which the kickers are triggered a second set of magnets (MKDH), called sweepers, starts to deflect horizontally the beam with a sinusoidal pulse shape reaching its maximum after 23.1 μs. The combined horizontal and vertical fast deflections move the beam out of the aperture hole of the absorber block onto its front face where it thereafter describes a two-dimensional sinusoidal trace. [4]

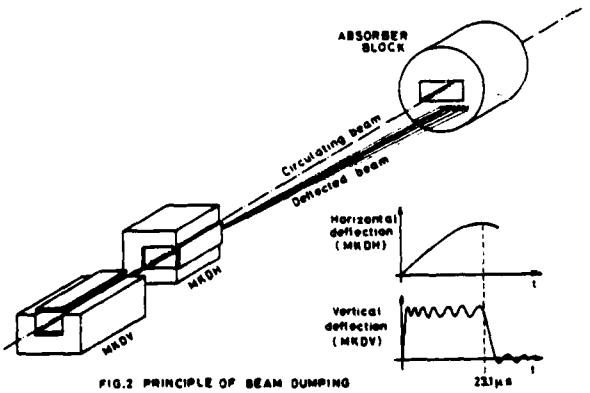

FIG.2 PRINCIPLE OF BEAM DUMPING

Because of the particular pulse shape the sweeper magnets are of a different design as compared to the kicker magnets and will therefore not be described in this paper.

Contrary to the kickers for fast extraction the beam dumping magnets do not need a variable pulse length and short fall time, because the pulse length must always correspond to at least one complete turn of the protons in the machine and the fall time is of no importance, once all protons in the accelerator are dumped.

However, the deflection to be given to the beam is more than 3 times larger. The main parameters of this system are shown in table 1.

1.3 Module circuit

The deflecting power of a kicker magnet is proportional to the current passing through it and to its length. On the other hand, its rise time is mainly determined by the ratio L/Z, where Z is the system impedance and L the overall inductance of the magnet which is also proportional to the magnet length.[5] In order to reduce the kick rise and fall times for a given deflecting power, one must split the magnet in several identical modules, each of which being excited by its own pulse generator.

A block diagram of a module of the fast extraction kicker system is given in figure 3. The rectangular current pulse is generated by means of a pulse forming network (pfn), which is charged by a power supply to a voltage of 60 kV maximum. Then the pfn is discharged by high power fast switches through a matched transmission line into the kicker magnet, which is terminated by a matched resistor.

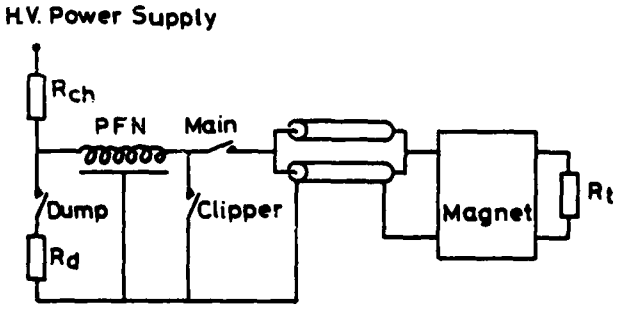

FIG.3 BLOCK DIAGRAM OF MODULE CIRCUIT

It has been shown previously that 3 switches, called main, clipper and dump switches, are necessary in order to get a fast fall time and an adjustable pulse length.[5]

The kicker magnet is installed in the accelerator ring which is in a tunnel up to 60 m below the ground level. As the pulse generators are housed in service buildings on the ground surface, each generator is connected to its magnet by a transmission line of up to 260 m. Each line is made of several high performance coaxial cables in parallel, which have an outer diameter of 30 mm and a characteristic impedance of 50 Ω, type RG 220/U, manufactured by Felten & Guilleaume in Germany. The line is matched to the system by connecting the appropriate number of cables in parallel: for instance, in the beam dumping system 16 cables in parallel are required.

The kicker magnet has an electrical circuit in the form of a lumped delay line with the same characteristic impedance as the pfn. Therefore the pulse travels through the magnet without major deformation and is absorbed in the matched terminating resistor.

2. Pulse forming networks

2.1 Constant cell distribution

Lumped parameter delay lines have been chosen as pulse forming networks (Fig. 4). The reasons for this and the theoretical response of a constant cell LC ladder network have been published previously. [6] The engineering execution will be presented here.

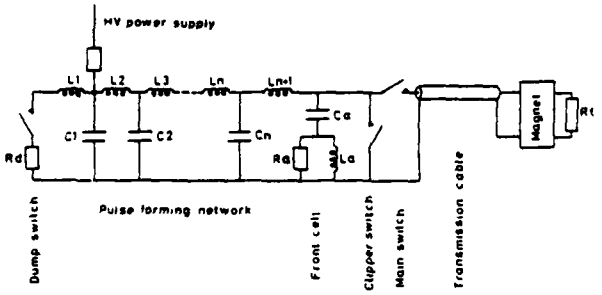

FIG.4 ELECTRICAL CIRCUIT OF THE PFN

For standardization purposes all pfn's use the same type of capacitor made by LCC (France). The capacitor has a paper/polypropylen mixture as dielectric and is impregnated with mineral oil. The active part is mounted in a metallic case of dimensions 200x200x700 mm and equipped on the top with one h.t. bushing, the case being the return conductor. The internal stray inductance is less than 100 nH, the design charging voltage 70 kV and the discharge peak current 12 kA with 65 % voltage reversal for a life time of > $2.5 \cdot 10^7$ pulses.

The pfn of the fast extraction system has 27 equal cells, each cell consists of one capacitor of 50 nF and an inductance of 5 uH giving a characteristic impedance of 10 Ω. The capacitors are fixed on mounting pads upright in a large steel tank. The coils are one layer solenoids wound from copper tube of 8 mm outer diameter. They are fixed to the capacitor bushings with their axes aligned horizontally.

The coil length is adjustable in order to minimize the flat top ripple. The first cell is preceeded by a front cell made of a capacitor of 25 nF in series with a 10 Ω resistor paralleled by an inductance of ∿ 5 uH. The front cell improves greatly the pulse rise time.

Although the best pfn configuration would be to have all cells aligned in one row, the cells have been arranged in a serpentine with 5 rows (Fig. 5) which gives a more suitable shape for the pfn tank (1.7 x 1.4 x 1.1 m^3). As a consequence one has to screen carefully each row against the others, in order to avoid stray coupling between rows, which would disturb the pulse shape. Figure 8a shows the current pulse given by such a pfn.

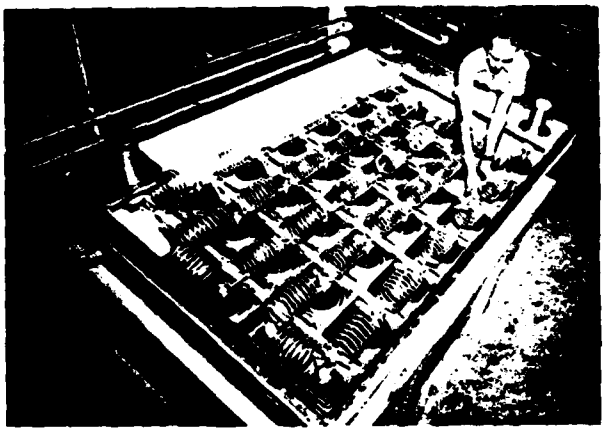

FIG.5 THE PFN WITH CONSTANT CELL DISTRIBUTION

Finally, the pfn is completely filled with silicon oil for its insulation. Mineral oil cannot be used because of fire hazards, and chlorinated diphenyls - askarels - have been excluded as they are poisons and attack insulating materials.

2.2 Progressive distribution

Theoretically, oscillations can be superimposed onto the flat top of the pulse, when the time constant $\tau_n = \sqrt{L_n C_n}$ of each cell is increased with respect to the preceding one, starting with the cell adjacent to the discharge switch. The characteristic impedance $Z_c = \sqrt{L_n/C_n}$ of all cells must be kept constant. [4] Because of the increasing time constant, the frequency of the oscillations decreases during the pulse. Computer calculations gave pulses with oscillations of a constant amplitude of about ± 10% of the mean flat top current, when the time constant of the cells follows the series $\tau, 2\tau, 3\tau, \ldots 14\tau$, where τ is the time constant of the first cell, not taking into account the front cell for faster rise. Although the prototype realization showed some deviation from the calculated pulse shape, probably because the program did not take into account the frequency dependence of the inductance value, it was nevertheless possible to adjust the cells empirically so that regular oscillations are obtained (Fig. 6). This is a complicated process, as in general each oscillation cannot be set directly into relation to the discharge of a particular cell. Most oscillations are rather complex superpositions of the discharge waveform of several cells, all having mutually different phase angles.

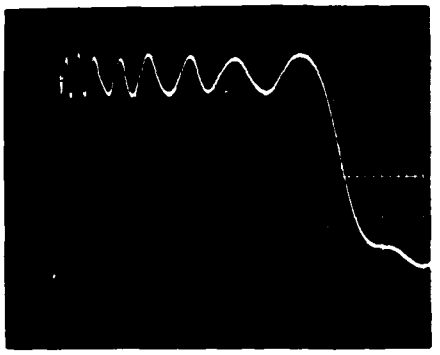

FIG.6 CURRENT PULSE WITH DELIBERATELY SUPERIMPOSED OSCILLATIONS (VERTICAL SCALE 2 kA/CM, HORIZONATAL SCALE 5 µs/CM)

The same engineering execution, as described above for the constant cell pfn's, was applied here. Several capacitors are grouped together by means of copper h.t. plates to form the cells of different size. Due to the low impedance, the steel tanks are the largest of all systems with dimensions of 3.8 x 1.4 x 1.1 m^3 (Fig. 7). Again, insulation is provided by filling the tank with silicon oil.

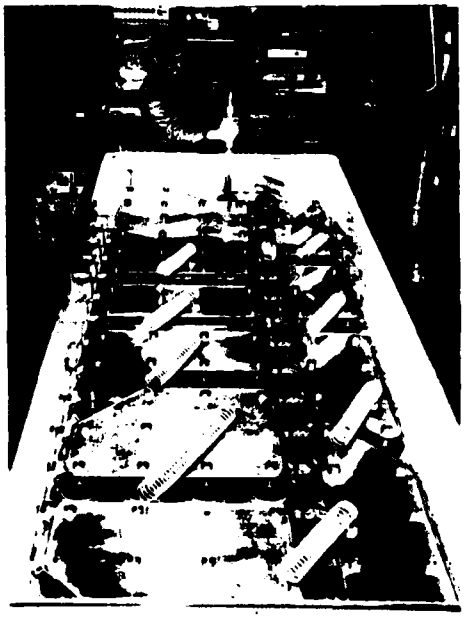

FIG.7 THE PFN WITH PROGRESSIVE CELL DISTRIBUTION

3. The H.V. switches

3.1 Switch type

The fast pulsed magnet systems of the SPS require 20 high power switches capable of fulfilling the following specifications :

- working voltage range 5 kV to 60 kV
- current amplitude 10 kA maximum
- pulse duration 1 to 24 µs (continuously adjustable)
- rate of rise of current > 100 kA/µs
- turn on jitter < 10 ns
- rate of erroneous firing < 10^{-5}
- life time > $2 \cdot 10^7$ pulses.

Possible switches have already been discussed in a previous paper [7], in which it was shown that normal multistage deuterium thyratrons are not suitable. For the required pulse current and duration, they are subject to quenching owing to the depletion of the plasma discharge, and they become very sensitive to voltage reversals, which induces back arcing. Both effects reduce considerably the life time of these switches.

Two ways of overcoming these limitations were presented in this paper :

- the 'thyragnitron' which uses a normal multistage thyratron bypassed by three ignitrons in series. The thyratron provides only the steep current rise and the precise turn on, whereafter the ignitron chain progressively takes over the discharge current and protects the thyratron from quenching and back arcing.
- the double ended thyratron [8], in which the anode of a normal thyratron has been replaced by a second cathode assembly, making it a bidirectional switch. Also quenching of this valve for long pulses is less probable because of the second reservoir in the 'anode' region.

The final arrangement for the main switch is a combination of both solutions, i.e. a 'thyragnitron' circuit made of a double ended thyratron EEV type CX1171B, bypassed by 3 ignitrons EEV type 7703. Apart from being the most promising solution, the reason for this choice is the following: because of the unavoidable stray inductance L_{ign} of the ignitron chain, a negative voltage

$$U = L_{ign} \frac{dI_{ign}}{dt}$$

appears across the thyragnitron during the fall time of the pulse. For very fast pulse fall times, when a clipper switch is used, this voltage may exceed the back arcing threshold of a normal thyratron. With a double ended thyratron, which can pass the current in both directions, this problem no longer exists as it is shown in figure 8: curve a is the overall pulse, i.e. the sum of the thyratron current and of the ignitrons current, which falls to zero in about 200 nsec when the clipper is fired. Curve b shows the ignitrons current which decreases slowly because of the inductance and resistance of the switch loop, while on curve c one can see the negative spike in the thyratron current, which is perfectly conducted through this bidirectional switch.

It must be noted that because of lack of time, it has not been possible to test extensively a double ended thyratron alone as a main switch. It may well be that this type of thyratron would be sufficient to switch the required long pulses without quenching, but to be safe, the ignitrons chain has been kept in the circuit.

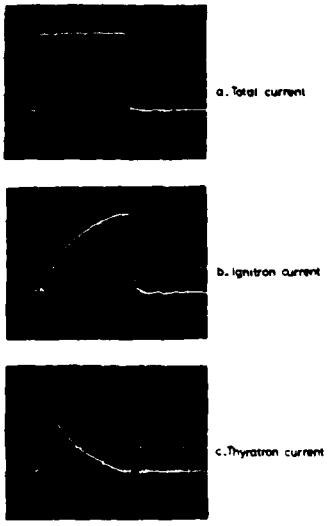

FIG. 8 CURRENT DISTRIBUTION IN THE THYRAGNITRON SWITCH (VERTICAL SCALE 1 kA/cm, HORIZONTAL SCALE 5 µs/cm)

The dump switch is also made of this thyragnitron circuit, as for very short pulses in the magnet load it has to divert most of the stored energy of the pfn into the dump resistor. Also, if the clipper is fired, it has to pass a negative block of current and must then be bidirectional. The clipper switch is a double ended thyratron, without ignitrons in parallel, as the clipper has to pass the current in both directions but only for the tail of the pfn pulse.

The three stages of each thyratron as well as the three ignitrons connected in series are kept at their appropriate potential by means of voltage dividers, which are frequency compensated because of the fast voltage changes.

3.2 Construction

During the earlier life tests it was already found, that dump and clipper switches, which are normally triggered after the main switch, have the tendency to be triggered by spurious signals already at the main switch instant. To overcome this, several measures have been taken :

- As the pfn separates physically the dump switch from the main and clipper switches, they have been housed in two separate tanks. Both tanks, one for the dump, the other for the main and clipper, are connected via short pieces of coaxial cable to the pfn. This measure eliminates the risk of an early dump switch firing.
- To avoid premature triggering of the clipper switch the three switch branches in the main/clipper tank have been carefully screened in separate coaxial tubes. The compensated voltage dividers, built up of 120 carbon mass resistors of 2 Watt and 9 ceramic capacitors surround coaxially each switch branch (Fig. 9) and can therefore be housed inside the coaxial screen.

The heater, reservoir, grid bias and trigger circuitry is grouped in a screened box mounted on a heater transformer. From there heater and trigger leads arrive screened in a coaxial plug and socket system at both ends of the thyratron.

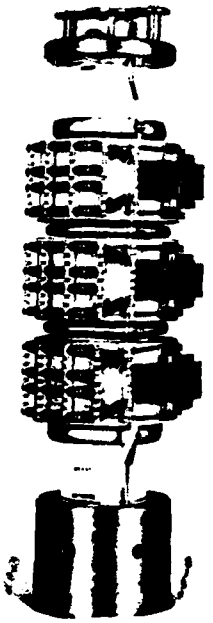

FIG. 9 THYRATRON EEV CX1171B WITH ITS FREQUENCY COMPENSATED VOLTAGE DIVIDER.

These measures proved to be adequate to avoid premature triggering of dump and clipper switches.

Figure 10 shows the final construction of the main/clipper switches. The layout of the dump switch is similar. The central part which is lifted up by the crane, contains the three switch branches, i.e. two thyratrons and one ignitron chain. On the lower part which stands on a support, one sees on each side two heater transformers together with their screening boxes containing the grid and trigger circuitry. Also the screened heater leads with their plugs can be seen. The whole assembly is immersed in a tank filled with silicon fluid for insulation and cooling.

3.3 Switch performance

Extensive life tests have been performed on two prototype systems, a 7.5 Ω system, generating a rectangular current pulse of 4 kA, and a 3 Ω system with an amplitude of 10 kA and superimposed oscillations. The 7.5 kA system was equipped with main, clipper and dump switches and was charged with a resonant charging power supply, delivering 2 pulses 100 ms apart once every 2 s. The 3 Ω system used a d.c. charging supply with a repetition rate of one pulse per 2 s. Both systems were charged to a voltage of 60 kV.

The first CX1171B thyratron tested in the 7.5 Ω system in main thyragnitron position had a life time of 3.9 Million pulses, 1190 filament hours and 632 erratics, of which a portion is probably due to erroneous pickup in the counter electronics. Thereafter it had to be exchanged because of too many erratic firings.

The following thyratron switched 4.1 Million pulses as main switch (4 kA, 25 µs) and 1.7 Million pulse as dump switch (± 4 kA, 2 µs), with an erratic rate of 10^{-5}. Then it had to be demounted, again because of too many erratic firings. The ignitron chain remained always mounted and worked very reliably.

As the prototype system was mainly operating with a 24 µs long pulse, the dump thyratron switched a pair of 4 kA/2 µs pulses, one positive, the other negative, both pulses 12 µs apart. Under these conditions a thyratron switched 4.2 Million pulses of 4 kA and 5.3 Million pulses of 2 kA before the rate of erratic firing increased such that the valve had to be exchanged. The filaments were heated for 3400 h. The rate of erratic firing was about 10^{-5} during the useful life. All these tests were carried out with the prototype resonant charging power supply which worked without any problem.

Best performances of all switches tested so far were obtained with the thyragnitron of the 3 Ω prototype system: It was running for more than 10 months without major incidents and switched 6.7 Million pulses of 10 kA amplitude with the superimposed oscillations. The filaments were heated for 4500 h and the erratic rate of the thyratron was of the order of 10^{-5}. Then it was exchanged because of a too low cathode emission. The ignitron chain worked again very satisfactorily.

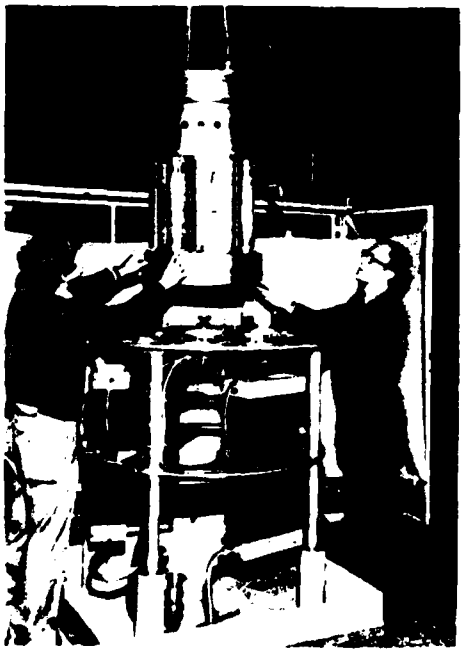

FIG. 10 ENGINEERING EXECUTION OF THE MAIN/CLIPPER SWITCH.

4. The magnet load

4.1 Magnet equivalent circuit

The electrical circuit of the magnet has been optimized by means of a computer program [6] in order to obtain

- a short rise time of the kick strength (the integral of the magnetic field along the orbit of the beam)
- good pulse transmission properties
- a low reflection coefficient.

Best results are obtained when the magnet is split into several LC sections with a front cell connected to the magnet input. The magnet forms then a lumped delay line with the same characteristic impedance as the pfn. The rise time of the kick is determined by the rise time of the pulse arriving from the generator and the travelling time of the pulse through the magnet. The amplitude of the reflections decreases when the number of cells increases, but above a certain number, the improvement per added cell becomes marginal, mainly because the stray inductances in the capacitor branches are no longer small compared to the inductance per magnet cell.

Table 2 gives the main design parameters of both systems :

Table 2

Main parameters of kicker magnets

System	Fast Extraction	Beam Dumping
Maximum kick strength of a module	0.20 Tm	0.41 Tm
Gap width	135 mm (horizontal)	56 mm (vertical)
Gap height	32 mm (vertical)	75 mm (horizontal)
Module length	1.674 m	2.560 m
Magnetic field	0.12 T	0.16 T
Inductance per module	8.9 µH	2.4 µH
Number of cells	7	5
Travelling time	0.89 µsec	0.77 µsec

4.2 Configuration

Owing to the required pulse response of the magnet, ferrite must be used as magnetic material. In addition to the pulse performance, the field distribtuion in the magnet aperture is of great importance. The non uniformity must be less than 1 %. Two different magnet configurations, the window frame and the C-shape have been compared in this respect by means of a computer program. [9] The best field distribution is obtained with a window frame configuration using rectangular conductors which touch the ferrite. This configuration has however two major drawbacks :

- the magnet must be completely insulated from its vacuum tank because both conductors are inductive
- there is a risk of flashover along the ferrite surface between the conductors during the pulse.

Therefore a C-shape configuration has been chosen with the inductive conductor touching the ferrite and a small gap between the ferrite and the conductor at earth potential. Such a configuration avoids both drawbacks. However the field is slightly non-uniform near the outer conductor. This can be partly cured by adding a 1 mm thick shim to the ferrite profile near the outer conductor.

4.3 Magnet construction

A special Ni-Zn ferrite offering high saturation induction, high resistivity and a low coercitive force has been used (Philips, type FXC 8C1C). The induction at 10 Oe and 23°C is higher than 0.3 T and the corres-

ponding coercitive force smaller than 0.25 Oe. This material is especially suitable for application under high vacuum, because the porosity and therefore the outgassing rate are low due to the comparatively high density of 5.1 g/cm^3. This ferrite is delivered in large bricks with flat ground surfaces, typical brick dimensions being 230 x 205 x 60 mm.

In a cross-sectional view the C-shaped magnet circuit is made of three bricks, a central one forming part of the magnetic yoke and two side bricks forming the poles. Ten sets of 3 bricks each for the beam dumping kickers and seven sets for the fast extraction kickers, are put alongside to set up an entire magnet module (Fig. 11). The ferrite bricks are positioned inside a rigid metallic frame by means of small alumina spacers and springs which press the bricks together. One set of 3 bricks in case of the fast extraction kicker and two sets of 3 bricks in case of the beam dumping kicker form an elementary magnet cell. Cells are separated by h.t. plates with the same cross-section as the magnetic material. They are the connection taps for the matching capacitors.

FIG. 11 ASSEMBLY OF THE KICKER MAGNET FOR BEAM DUMPING.

The magnet in its frame is supported at 3 points by a thick stainless steel plate, which forms the base of the vacuum tank. The tank cover has an omega cross-section and flanges for alignment supports and connections for the adjacent vacuum chambers. Only the ferrite, the conductors and the purely metallic supporting structure are put into the accelerator vacuum. In order to minimize the vacuum requirements, the other magnet elements, i.e. the matching capacitors, the terminating resistor and the collection point of the transmission line, are mounted in separate matching boxes filled with silicon fluid for insulation and cooling. Each box is fixed underneath the tank and is connected to the corresponding magnet cell via a coaxial vacuum tight ceramic feedthrough of low inductance. A magnet can have up to 8 boxes.

4.4 The terminating resistor

One of the critical items of the fast pulsed magnet systems is the terminating resistor, which has to accept every machine cycle - in case of the beam dumping system - an energy pulse of 7.5 kJ within 24 us. This corresponds to 300 MW of peak power.

The construction of the resistor is complicated, because

- the stray inductance must be small against the inductance of an elementary magnet cell
- the resistor must withstand pulse voltages of 30 kV
- the resistance value must be controlled to within ± 1 %
- the space to house the resistor under the vacuum tank is very limited.

The resistor body is built with Allen Bradley ceramic resistor disks 1 inch thick with 3 inches outer diameter and a central hole of 1.25 inch. These disks are made from a mixture of clays, alumina and carbon (type BM4), which is fired at high temperatures. Then brass is flame sprayed onto the flat faces of the disks to provide electrical contact and antitrack coating is applied to the periphery of the disk to improve the dielectric rigidity. Due to the high package density of the active resistor material a high rate of instantaneous power can be absorbed and a low inductance construction is possible.

The load is made of a stack of 10 disks mounted in a coaxial housing. The contact from one disk to the adjacent is made via flat metallic spirals, which allow the circulation of cooling fluid between the disks. The fluid is pushed into the central hole and flows between the spirals to the periphery of the disks. The cooling medium is silicon fluid, which provides at the same time dielectric insulation. A water cooled copper spiral, mounted onto the outer coaxial conductor, removes the heat from the silicon. The resistance value and the temperature are controlled by means of a regulation loop (see Fig. 12).

This set-up works perfectly when the rectangular current pulse is applied. When the resistor is subjected to the pulse with superimposed oscillations, an additional thin layer of silver has to be flame-sprayed onto the brass layer of the disks and the spirals have to be gold-plated in order to improve the r.f. contact between the disks and the spirals.

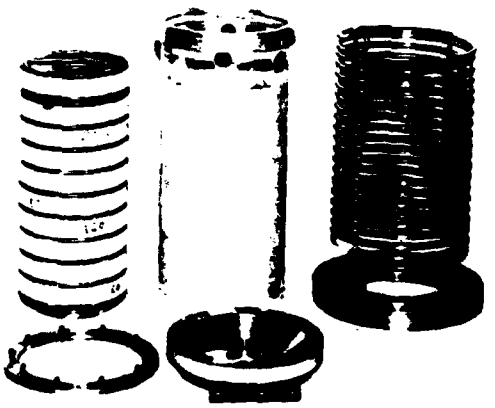

FIG. 12 DISKS OF THE TERMINATION RESISTOR ASSEMBLED WITH THEIR CONTACT SPIRALS (LEFT), THE COAXIAL RETURN CONDUCTOR (MIDDLE) AND THE COOLING SPIRAL (RIGHT).

5. Resonant charging power supplies

The fast extraction system must be able to deliver three pulses per machine cycle of 4 sec duration. The time interval between two successive pulses must be as short as 100 ms. Thyristor controlled H.V. power supplies, which for example, are used for the beam dumping system, need about 1s to charge a pfn to a preset value with an accuracy of ± 0.2 %. A shorter charging time would require a complete redesign of the power supply. On the other hand, resonant charging power supplies have previously been constructed for a similar application and could charge a pfn within less than 10 ms with the required accuracy and reliability. [10] They were therefore chosen as charging supplies for kicker systems with short time intervals between pulses.

5.1 Principle

The basic circuit diagram of a resonant charging power supply is given in figure 13: several capacitor banks are connected in parallel through thyristors to the primary winding of a transformer. Each of the capacitor banks is charged to a preset voltage by its own d.c. power supply. The secondary winding of the transformer is connected via a stack of h.t. diodes to the uncharged pfn capacitance. When a thyristor is triggered, a resonance is excited between the corresponding primary capacitor bank, the pfn capacitance and the leakage inductance of the transformer. Energy is now transferred from the primary capacitor bank to the pfn. When the voltage on the pfn reaches its maximum value, the diodes stop the resonance and disconnect the charged pfn from the transformer. The thyristor stops to conduct and the transformer is recovering from the unidirectional flux swing.

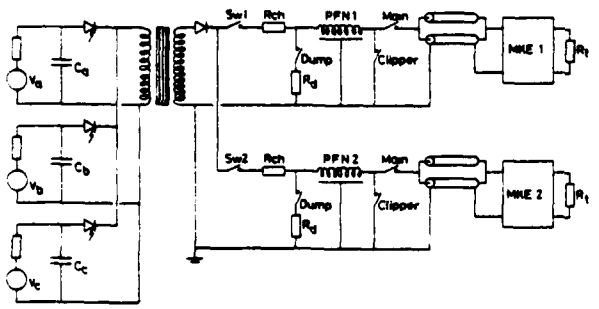

Fig 13. BLOCK DIAGRAM OF THE RESONANT CHARGING POWER SUPPLY WITH ITS PAIR OF FAST EXTRACTION MODULES

After the discharge of the pfn the following charging cycle is initiated by triggering the next thyristor. By means of the auxiliary winding of the transformer a negative premagnetisation can be provided in order to adjust the magnetic working point of the transformer core, and to avoid its saturation.

5.2 Realization

One resonant charging power supply charges two pfn's of the fast extraction system in parallel. Each of the three primary capacitor banks stores an energy of 14 kJ, which is about 3 times the energy of two pfn's.

A primary charging voltage of 2 kV has been chosen because then 2 power thyristors in series can reliably block the voltage, taking into account that overswings are present.

A higher primary voltage would have required gas discharge switches, which are less convenient to use, a lower primary voltage would have resulted in a too high charging current.

The frequency of the charge transfer has been chosen in the power frequency range, so that a transformer with 50 Hz ratings can be used. The transformer is however mechanically reinforced because of the repetitive pulse forces during operation.

Two high power, high voltage thyristors in series (Westinghouse, type 73T30) switch the energy of the primary capacitor bank. Figure 14 shows the charging voltage on the pfn and the charging current in the thyristor. The thyristor size is determined by a fault condition in the thyratron: when a premature firing occurs during the charge transfer period of the charging supply the pfn capacity and the transformer are short-circuited. The $\int i^2 dt$, which determines the thyristor size, increases then by about a factor 10 and reaches 70 000 A^2S.

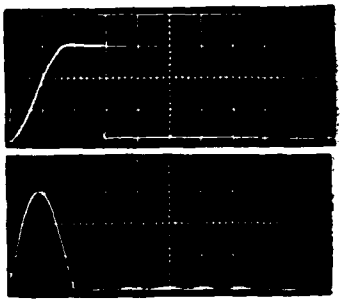

FIG. 14 CHARGING VOLTAGE AND CURRENT OF THE RESONANT CHARGING POWER SUPPLY (VERTICAL SCALE, UPPER TRACE, 20 kV/cm, LOWER TRACE 600 A/cm, HORIZONTAL SCALE 2 ms/cm)

Conclusion

The experimental results obtained on the prototype fast pulsed magnet modules have shown that the bidirectional composite switch chosen is capable to withstand reliably a forward voltage of 60 kV and to conduct a current pulse of 10 kA amplitude, 100 ns rise time and 24 µs duration, with a reasonable life time of 3 to 6 million pulses. The physical separation of the main/clipper switch and the dump switch in two different tanks and the screened coaxial construction have resulted in a reliable operation without premature turn on of the delayed triggered clipper and dump switches.

The standardization of the components of different systems, resulting in only a few standard modules, identical for all systems, has allowed to put all the design and constructional effort in the optimization of a relatively small number of items.

The final systems are now installed in the various auxiliary buildings of the SPS accelerator and are being linked to the SPS control system [11] in such a way that they will be operated completely remotely from the SPS Main Control Room through the SPS computer network. The first tests on the remote operation of one system have been successful: with a set of programmes written in the interactive language NODAL [12], it has been possible to start up the system, to adjust the pulse voltages, pulse duration and repetition rate, to observe the pulse shape and to watch to the correct functioning of the system with surveillance programmes.

Acknowledgements

This work was undertaken as part of the SPS project and has benefitted from the contribution of various persons in the SPS Division, in particular member the BT and ME Groups, who participated in the design, construction and testing of the equipment.

We also acknowledge the various manufacturers for their contributions and close co-operation, in particular H. Menown and R. Snelling of English Electric Valve Co., United Kingdom.

References

1. The 300 GeV programme, CERN/1050.

2. Extraction from the 300 GeV machine, Y. Baconnier, K.H. Kissler, A. Knezovic, W.C. Middelkoop, B. de Raad, CERN LabII/BT/71-4.

3. Beam dumping in the SPS, P.E. Faugeras, W.C. Middelkoop, B. de Raad, G. Schröder, P. Sievers, CERN LabII/BT/Int./72-5.

4. Design study of the SPS beam dumping system, P.E. Faugeras, C.G. Harrison, G.H. Schröder, CERN LabII/BT/Int./73-5.

5. The design of 'fast kicker' magnets, P.G. Innocenti, B. Kuiper, A. Messina and H. Riege, 3rd Int.Conf. on Magnet Technology, Hamburg, 1970.

6. Calculations on the SPS inflector magnet and its pulse generator, P.E. Faugeras, CERN LabII/BT/72-1.

7. Generation of high current, long duration rectangular pulses, P.E. Faugeras, H. Kuhn, J.P. Zanasco, presented at the 11th Modulator Symposium, New York, September, 1973.

8. A multigap, double-ended, hydrogen thyratron, H. Menown, B.P. Newton, 11th Modulator Symposium, New York, September 18-19, 1973.

9. Programme for two-dimensional magnetic fields including saturation, C. Iselin, CERN Computer Program Library T 600.

10. Design and tests of a 5 kJ, 60 kV resonant charging power supply for the ISR beam dumping system, G.H. Schröder, CERN-ISR-PO/72-22.

11. The control system for the SPS, M.C. Crowley-Milling, CERN/LabII-CO/75-3, May, 1975.

12. The NODAL system for the SPS, M.C. Crowley-Milling S.T. Hyman and G.C. Shering, CERN/LabII-CO/74-2, December, 1974.

PFN DESIGN FOR TIME VARYING LOAD

Don Ball and T.R. Burkes
Department of Electrical Engineering
Texas Tech University
Lubbock, Texas 79409

Summary

Some types of nonlinear pulsed loads can be described as time-varying resistances. By using Guillemin's method of PFN design, it is possible to design a voltage fed network that will deliver a constant voltage pulse to a time-varying resistor. The synthesis procedure requires prior knowledge of the load response for a constant voltage pulse.

Basically, the desired current response is assumed to be repeatitive as is the case for the short circuit response of most PFN's. The Fourier components of the desired current response are then determined and the coefficients compared to the short circuit response of series L-C networks. By paralleling the series L-C networks, a type C network is obtained. The derived network will deliver a constant voltage pulse to the time-varying load. For some types of loads, the Fourier coefficients are negative and special attention is required to maintain physical realizability. The L-C networks associated with the negative coefficients can be realized by using the networks only for pulse shaping and not for primary energy storage.

Introduction

High power pulse generation was historically derived for radar modulator supplies.[1] Networks designed for radar systems assume a constant load impedance. Modern technology has increased the number of uses for pulsers. Many of these applications involve different types of gaseous discharges.[2] Most gaseous discharge devices represent current-dependent impedances. The non-linear resistive characteristics of certain gaseous discharges are well known.[3,4] These characteristics depend upon such parameters as gas pressure, temperature, ion density, and mobility. One application of pulser technology is in the area of fusion research.[4,5] Lasers, electron beam sources and other similar devices also make use of electrical pulsers.

The first networks used for line-type pulsers were designed to simulate transmission lines. In an effort to improve PFN design, considerable work on line-type voltage-fed networks was done by Guillemin.[6] Guillemin's theory involved design of passive LC networks to supply constant impedance loads, primarily resistive in character. Guillemin utilized the Fourier transform of the desired current pulse to determine the network values. Guillemin, however, did not consider current dependent loads. When constant voltage pulses are applied to current dependent loads, the load can be assumed to behave like a resistor whose resistance varies with time. This assumption requires that the load current be known for a constant voltage pulse. The time-varying load resistance is also required to remain positive. The purpose of this paper is to develop a procedure for synthesizing passive networks which are capable of producing a rectangular voltage pulse across a time-varying resistive load. Discussion is restricted to line-type, voltage-fed networks.

Guillemin's Theory

Pulses generated by lumped networks that simulate transmission lines often have overshoots and oscillations during the pulse that are usually objectionable. E.A. Guillemin believed that these problems were caused by trying to generate a pulse with an infinite rate of rise and fall by means of a network composed of lumped elements. Guillemin suggested that the theoretical pulse should be chosen to have a finite rate of rise and fall. Several different network configurations have been defined by Guillemin and labeled A through F.

Guillemin's procedure for derivation of the type C network (Figure 1) involves defining the desired short circuit current response and then determining the Fourier coefficients of the desired response.

The short circuit current response of a lossless L-C network is repeative in time.

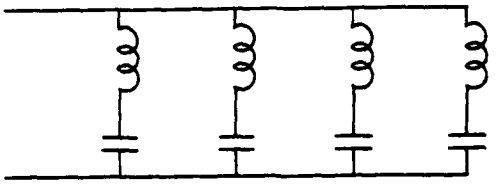

Figure 1

Since the current is an odd function, the Fourier series contains only sine terms. Thus,

$$i(t) = I_L \sum_{k=1}^{\infty} b_k \sin \frac{k\pi t}{\tau} \qquad (1)$$

where

$$b_k = \frac{2}{\tau} \int_0^{\tau} \frac{i(t)}{I_L} \sin \frac{k\pi t}{\tau}\, dt. \qquad (2)$$

Each term of i(t) is composed of a sine wave given by

$$i_k = I_L\, b_k \sin \frac{k\pi t}{\tau} \qquad (3)$$

A series LC circuit will produce a short circuit current given by

$$i_k = V_N\sqrt{C_k/L_k}\ \sin\frac{t}{\sqrt{L_kC_k}}\ . \tag{4}$$

By comparing these values with the coefficients of the Fourier series, the values of L_k and C_k become

$$L_k = \frac{Z_N\tau}{k\pi b_k}$$

and

$$C_k = \frac{\tau b_k}{k\pi Z_N} \tag{5}$$

where $Z_N = V_N/I_L$ is the characteristic impedance of the network.

The entire network needed to produce the desired current wave shape becomes a parallel combination of the LC series sections as shown in Fig. 1. The load current is the sum of the currents produced by each section. For a rectangular current pulse, b_k is zero for even values of k, and the resultant values of L_k and C_k become

$$L_k = \frac{Z_N\tau}{4} \quad \text{for k odd}$$

and

$$C_k = \frac{4}{k^2\pi^2}\ \frac{\tau}{Z_N} \quad \text{for k odd.} \tag{6}$$

The type C network can be transformed to other network configurations which may yield more practical component values.

Pulse-Forming Networks for Time-Varying Loads

The problem of designing a PFN to produce any desired current waveform for an inductive load has been considered by Rigney, Kraus, and Malamud.[7] A method of synthesizing a particular load current for any load has been outlined by Black.[8] Black's method assumes that the actual current pulse deviates from the desired pulse, but it fails to provide any method of determining this error function. This method also requires the solution of a differential equation for which the boundary conditions necessary for a complete solution are not known. Thus, the desired PFN values are not easily determined. A method similar to Guillemin's approach may be utilized to synthesize the proper network. In order to design such a PFN, knowledge of the time-varying current pulse is required. From Ohm's law, the required current pulse is given by

$$i(t) = \frac{V_L}{R_L(t)} \tag{7}$$

where V_L is the amplitude of the desired voltage pulse, and $R_L(t)$ is the time-varying load resistance. If this current pulse is expanded into an alternating current waveform, similar to the one shown in Fig. 2, the Fourier coefficients may be calculated. As may be seen from Fig. 2, the current is an odd function of time. Thus, the Fourier series expansion contains only sine terms and is given by

$$i(t) = \sum_{k=1}^{\infty} b_k \sin\frac{k\pi t}{\tau} \tag{8}$$

where

$$b_k = \frac{2}{\tau}\int_0^{\tau} i(t)\sin\frac{k\pi t}{\tau}\,dt. \tag{9}$$

Since i(t) is given by Eq. (7) for $0 \le t \le \tau$, the Fourier coefficients, b_k, may be expressed as

$$b_k = \frac{2}{\tau}\int_0^{\tau}\frac{V_L}{R_L(t)}\sin\frac{k\pi t}{\tau}\,dt. \tag{10}$$

Modified Fourier coefficients, d_k, may be defined as

$$d_k = \frac{b_k}{V_L} = \frac{2}{\tau}\int_0^{\tau}\frac{1}{R_L(t)}\sin\frac{k\pi t}{\tau}\,dt. \tag{11}$$

Each term of i(t) is now given by

$$i_k = b_k \sin\frac{k\pi t}{\tau} = V_L\, d_k \sin\frac{k\pi t}{\tau}\ . \tag{12}$$

A realizable network capable of generating a sine wave with the magnitude and frequency required by the Fourier coefficients in Eq. (12) is needed. Assume that a series LC circuit, with the capacitor initially charged to a voltage V_N, is discharged into a constant voltage source. The voltage source, V_L, represents the amplitude of the desired load voltage pulse. Applying Kirchhoff's voltage law around the closed loop yields

$$V_L = V_N - L_k\frac{di_k}{dt} - \frac{1}{C_k}\int i_k\,dt.$$

This equation reduces to

$$\frac{di_k}{dt} + \frac{1}{L_kC_k}\int i_k\,dt = V_N - V_L.$$

This differential equation can be solved with the initial conditions

$$i_k(0) = 0$$

and

$$\left.\frac{di_k}{dt}\right|_{t=0} = \frac{V_N - V_L}{L_k}$$

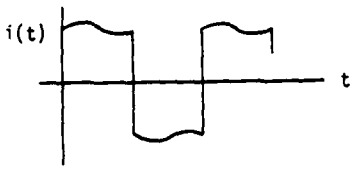

Figure 2

to obtain the solution

$$i_k = (V_N - V_L)\sqrt{C_k/L_k}\,\sin\frac{t}{\sqrt{L_k C_k}}\,. \tag{13}$$

Comparing the amplitude and frequency of Eq. (12) to those of Eq. (13) results in

$$V_L\, d_k = (V_N - V_L)\sqrt{C_k/L_k} \tag{14}$$

and

$$\frac{k\pi}{\tau} = \frac{1}{\sqrt{L_k C_k}}\,. \tag{15}$$

From Eq. (14) and Eq. (15), the values of L_k and C_k become

$$L_k = \frac{(V_N - V_L)\,\tau}{k\,\pi\,V_L\,d_k}$$

and

$$C_k = \frac{\tau\,V_L\,d_k}{(V_N - V_L)\,k\,\pi}\,. \tag{16}$$

Thus, the values of L_k and C_k are determined so as to produce the k^{th} component of the Fourier series of the desired current pulse. Each of the series LC sections are connected in parallel so that the currents are added together. The resulting circuit is the familiar type C network. Adding more sections realizes more terms of the Fourier series, and hence, a closer approximation of the desired current pulse.

In general, a time-varying current pulse may contain both positive and negative Fourier coefficients. The magnitude of the current given in Eq. (13) should always be $V_L\sqrt{C_k/L_k}$. This implies that

$$V_N - V_L = \pm V_L. \tag{17}$$

Any other possibility will not result in the proper Fourier current components and a constant voltage pulse will not occur. Thus, as in the usual networks, the voltage pulse at the load will be half the charge voltage. The correct sign to be used in Eq. (17) is that of the modified Fourier coefficient d_k. If d_k is positive, V_N becomes $2V_L$. If d_k is negative, V_N should be zero in order to produce a negative V_L in Eq. (17), and thus to maintain physical realizability (avoiding negative inductances and capacitances). This implies no initial voltage on the capacitor. Thus, the series LC sections which satisfy the requirements for the negative Fourier coefficients provide pulse shaping, but no energy storage before the pulse.

Since by definition the term $(V_N - V_L)$ in Eq. (14) always reduces to $\pm V_L$, Eq. (14) becomes

$$d_k = \pm\sqrt{C_k/L_k}\,. \tag{18}$$

Since the sign of $(V_N - V_L)$ is always the same as that of d_k, Eq. (16) reduces to

$$L_k = \frac{\pm V_L\,\tau}{k\pi V_L\,d_k} = \frac{\tau}{k\pi|d_k|}$$

and

$$C_k = \frac{\tau V_L d_k}{\pm V_L\, k\pi} = \frac{\tau|d_k|}{k\pi}\,. \tag{19}$$

Thus, L_k and C_k are always positive and are determined from Eq. (19). The initial voltage on C_k is $2V_L$ if d_k is positive and zero if d_k is negative.

It should be noticed that the network of Fig. (1) has a particular driving-point impedance Z(s) as does any passive network. *This driving-point impedance*, however, should not be considered a characteristic impedance as in the case of a time-invariant load. The concept of a PFN having a characteristic impedance is not applicable to the time-varying case since a time-varying load cannot be matched to a constant characteristic impedance.

In order to facilitate investigation of the problems associated with time-varying loads, two particular examples will be discussed. The first case will consider a resistance which increases with time, while the second case studies a decreasing load resistance.

Resistance Increasing With Time

As an example, consider a load resistance that *increases linearly with time* which is described by $R_L(t) = 1 + t$ for $0 \le t \le \tau$. For a rectangular voltage pulse, the current pulse is then given by

$$i(t) = \frac{V_L}{1 + t} \tag{20}$$

where V_L is the desired magnitude of the voltage pulse. Substituting this current into Eq. (11) yields the modified Fourier coefficients

$$d_k = \frac{2}{\tau}\int_0^{\tau}\frac{1}{1 + t}\sin\frac{k\pi t}{\tau}\,dt. \tag{21}$$

The network component values are found from Eq. (19). For a rectangular voltage pulse of one microsecond duration, the values of L_k and C_k and the resultant six-section network are shown in Fig. 3. The calculated voltage is shown in Fig. 4. The output voltage is obtained by utilizing a circuit analysis program (SCEPTRE) on a digital computer.

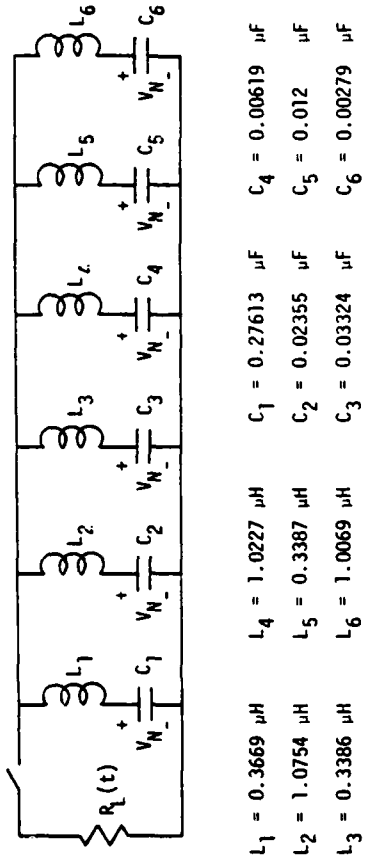

$L_1 = 0.3669\ \mu H$ $L_4 = 1.0227\ \mu H$ $C_1 = 0.27613\ \mu F$ $C_4 = 0.00619\ \mu F$

$L_2 = 1.0754\ \mu H$ $L_5 = 0.3387\ \mu H$ $C_2 = 0.02355\ \mu F$ $C_5 = 0.012\ \mu F$

$L_3 = 0.3386\ \mu H$ $L_6 = 1.0069\ \mu H$ $C_3 = 0.03324\ \mu F$ $C_6 = 0.00279\ \mu F$

Fig. 3. Six-section PFN for $R_L(t) = 1 + t$.

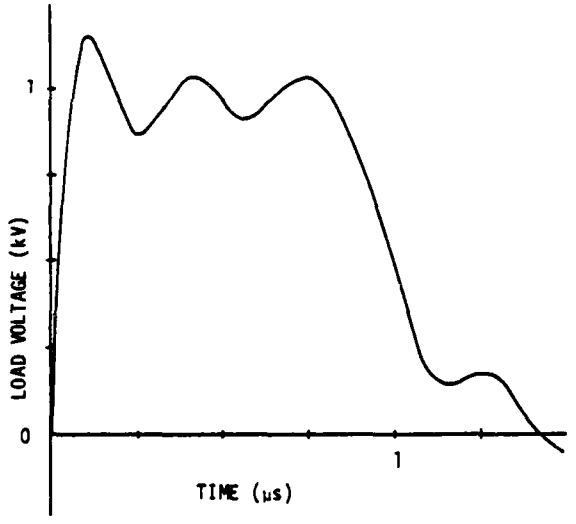

Fig. 4. Response of six-section PFN for $R_L(t) = 1 + t$.

Resistance Decreasing With Time

As an example of a resistance that decreases with time, a load resistance given by $R_L(t) = 2 - t$ for $0 \leq t \leq \tau$ is assumed where $\tau < 2$ μs. For a rectangular voltage pulse, the current pulse should be

$$i(t) = \frac{V_L}{2 - t}$$

where V_L is again the desired magnitude of the voltage pulse. The modified Fourier coefficients of this current are found from Eq. (11) to be

$$d_k = \frac{2}{\tau} \int_0^{\tau} \frac{1}{2 - t} \sin \frac{k\pi t}{\tau} \, dt. \qquad (20)$$

The component values are again determined from Eq. (19). For a six-section PFN, the values of L_k and C_k for a rectangular voltage pulse of one microsecond duration and the resulting network are shown in Fig. 5. Because some of the Fourier coefficients are negative, two networks are necessary. Thus, there is no initial voltage on C_k for even values of k. For odd values of k, the initial voltage on C_k should be twice the desired output voltage. These conditions may be easily implemented by placing the LC sections with no initial stored energy in parallel with the load resistance. The LC sections with initial voltage on the capacitors are connected together and switched across the load after they are all charged to the same voltage, $2V_L$, as shown in Fig. 5. The sections with no initial voltage are necessary for pulse shaping although they do not store energy before the pulse. The response of the six-section network of Fig. 5 is shown in Fig. 6. It is easily seen that the output voltage is a near rectangular pulse with some oscillation during the main part of the pulse.

To illustrate the effect of the shaping portion of the network shown in Fig. 5, a six-section network derived using only the positive Fourier coefficients is shown in Fig. 7 and its response in Fig. 8. Also, a twelve-section network and response is shown in Figs. 9 and 10 for comparison.

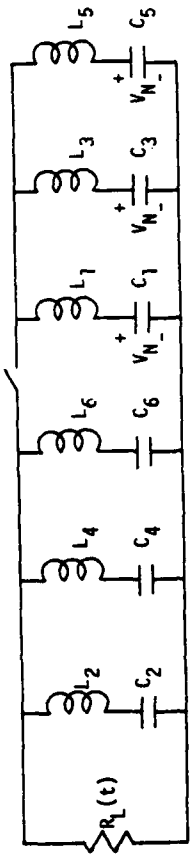

L_1 = 0.3669 μH L_4 = 1.0221 μH C_1 = 0.27613 μF C_4 = 0.0062 μF

L_2 = 1.0761 μH L_5 = 0.3387 μH C_2 = 0.02354 μF C_5 = 0.012 μF

L_3 = 0.3385 μH L_6 = 1.012 μH C_3 = 0.03325 μF C_6 = 0.00278 μF

Fig. 5. Six-section PFN for $R_L(t) = 2 - t$.

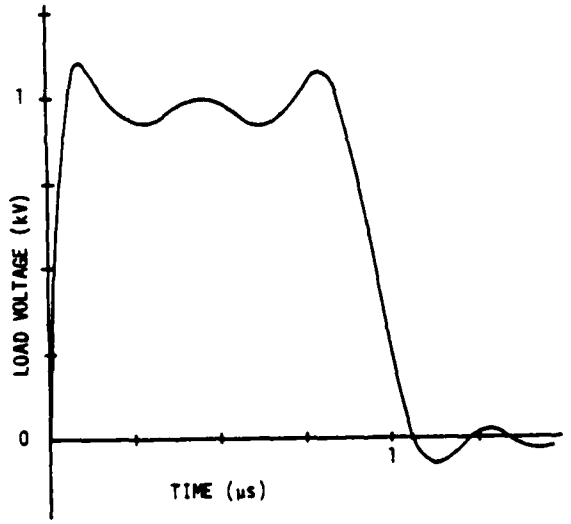

Fig. 6. Response of six-section PFN for $R_L(t) = 2 - t$.

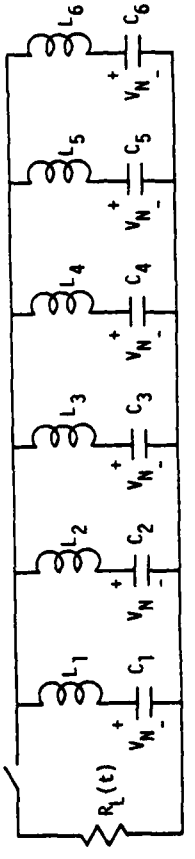

L_1 = 0.3669 μH L_4 = 0.3348 μH C_1 = 0.27613 μF C_4 = 0.00618 μF

L_2 = 0.3385 μH L_5 = 0.3347 μH C_2 = 0.03325 μF C_5 = 0.00374 μF

L_3 = 0.338[illegible] μH L_6 = 0.3349 μH C_3 = 0.0012 μF C_6 = 0.0025 μF

Fig. 7. Six-section PFN with no uncharged sections for $R_L(t) = 2 - t$.

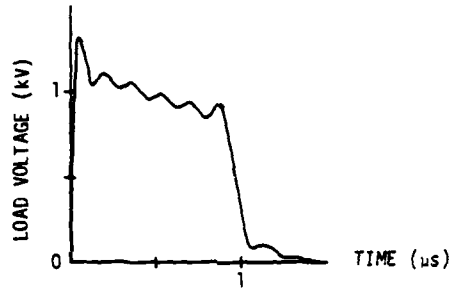

Fig. 8. Response of six-section PFN with no uncharged sections for $R_L(t) = 2 - t$.

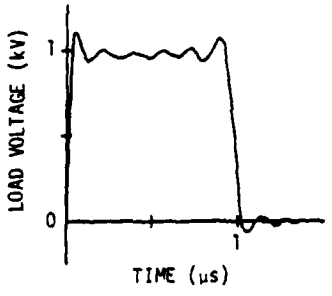

Fig. 10. Response of twelve-section PFN for $R_L(t) = 2 - t$.

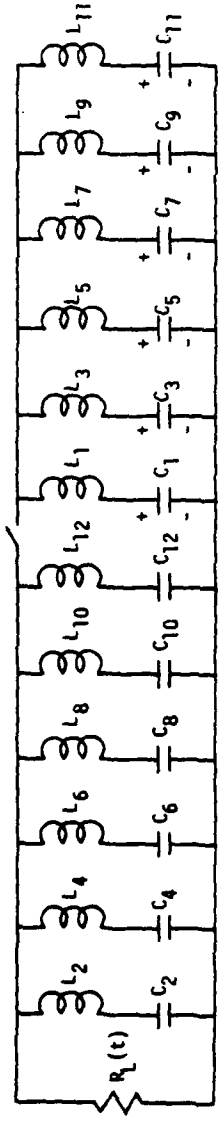

$C_{1,3,5,7,9,11}$ charged to V_N with polarity as shown.

$L_1 = 0.3669$ μH	$L_7 = 0.3348$ μH	$C_1 = 0.27613$ μF	$C_7 = 0.00618$ μF
$L_2 = 1.0761$ μH	$L_8 = 1.0064$ μH	$C_2 = 0.02354$ μF	$C_8 = 0.00157$ μF
$L_3 = 0.3385$ μH	$L_9 = 0.3347$ μH	$C_3 = 0.03325$ μF	$C_9 = 0.00374$ μF
$L_4 = 1.0221$ μH	$L_{10} = 1.0105$ μH	$C_4 = 0.0062$ μF	$C_{10} = 0.001$ μF
$L_5 = 0.3387$ μH	$L_{11} = 0.3349$ μH	$C_5 = 0.012$ μF	$C_{11} = 0.0025$ μF
$L_6 = 1.012$ μH	$L_{12} = 1.0041$ μH	$C_6 = 0.00278$ μF	$C_{12} = 0.0007$ μF

Fig. 9. Twelve-section PFN for $R_L(t) = 2 - t$.

Conclusions

It has been demonstrated on a theoretical basis that a PFN composed entirely of passive elements can be designed to drive time-varying loads. Although no laboratory experiments have been performed there is little doubt that the networks will perform as predicted.

The type C network is only one example of many possible networks that can be derived. One method for deriving alternate networks is to find the driving point impedance of the synthesized type C network and then use the usual synthesis techniques to derive the alternate forms. For instance, a rational fraction expansion of the driving point impedance function will yield a type B network.

Much more work is yet to be performed, and a more detailed procedure is required so that economical networks can be synthesized, such as a variation of the type E network. Also, more work is required in load characterization than has been the case. However, a good ground work has been laid for the solution of pulser design for nonlinear loads.

References

1. G.N. Glasoe and J.V. Lebacqz, eds., Pulse Generators, New York: McGraw-Hill Book Company, Inc., 1948.

2. Gordon Francis, Ionization Phenomena in Gases, New York: Academic Press Inc., 1960, pp. 128-130.

3. J.J. Thomson and G.P. Thomson, Conduction of Electricity Through Gases, 3rd ed., Vol. 1, London: Cambridge University Press, 1928, pp. 16-19.

4. J.M. Somerville, The Electric Arc, New York: John Wiley and Sons, Inc., 1959.

5. I.V. Kurchatov, "On the Possibility of Producing Thermonuclear Reactions in a Gas Discharge", Journal of Nuclear Energy, Vol. 4, No. 2, February 1957, pp. 193-202.

6. E.A. Guillemin, "A Historical Account of the Development of a Design Procedure for Pulse-forming Networks," RL Report No. 43, October 16, 1944.

7. D. Rigney, L. Kraus, and H. Malamud, "Synthesis of Current Waveforms by Type C Networks," Plasma Propulsion Laboratory, Republic Aviation Corporation, Farmingdale, L.I., New York, Report No. PPL-TR-61-4(258), January 30, 1961.

8. Neville A. Black, "Dynamics of a Pinch Discharge Driven by a High Current Pulse-forming Network," Guggenheim Laboratories for the Aerospace Propulsion Sciences, Department of Aerospace and Mechanical Sciences, Princeton University, Princeton, New Jersey, Report No. 778, May 1966.

A BLUMLEIN MODULATOR FOR A TIME-VARYING LOAD

William H. Wright, Anthony J. Buffa, Sol Schneider
US Army Electronics Technology and Devices Laboratory (ECOM)
Fort Monmouth, New Jersey 07703

Summary. The Blumlein circuit uses two identical charged PFN's and a switch to short across one PFN to invert it. After inversion, the two PFN's and the load are in series with an effective loop voltage twice the charging voltage. With a mismatched load there are multiple reflections through the PFN's, the switch, and the load. In the present application, the time-varying load (a ramp current in response to a constant voltage pulse) is inherently mismatched. A dissipative clamper circuit was devised which, when connected in parallel with the load, draws a decreasing ramp current. The sum of the clamper and load currents approximates a constant amplitude pulse, and the parallel connection approximates a constant impedance which can be matched to the modulator impedance. Protective circuits included are a clipper diode across the thyratron and an end-of-line clipper circuit to dissipate the stored energy in the event of a load arc. The thyratron used is a 10 section iterative cavity grid tube designed for 250 kV and 20 kVA peak current. Two such modulators have been built. One is at ECOM with a 2.5 μs pulse length, resistive load, and a megawatt of average power available. The other is at MICOM with 5 μs, time-varying E-Beam gun load, and to date only single shot operation. Both have operated at 210 kV single shot, and the one at ECOM at 175 kV and 10 Hz.

INTRODUCTION

The drive requirements for a cold cathode electron beam gun of current interest in high energy pulsed lasers are a flat 250 kV, 5 μs pulse with a rising ramp current of 10000 amperes at a pulse repetition rate of 50 Hz. Consideration of the problems in designing switches, charging chokes, power supplies, and pulse transformers for this requirement led to the decision to build a transformerless modulator using a Blumlein circuit and developing a 250 kV switch.

DISCUSSION

E-Beam Modulator Circuit

The Blumlein circuit is the two network case of a Darlington circuit. A schematic diagram of the circuit is shown in Figure 1. The circuit works in the following manner. The thyratron short circuits the front end of the network on the left. This is equivalent to reversing the potential of this network, thus putting it in series with the network on the right. If the gun has an impedance equal to the series rearrangement of the networks, voltage equal to the original dc charging voltage appears across the gun. The reversal process results in a fixed time delay equal to half the pulse width between the firing of the switch and the application of voltage to the gun.

The charging diode, the front end clipper, and the end-of-line clipper are primarily for protective purposes. The charging diode serves a double function. Since the network on the right is isolated from ground, it provides a charging path for this network. In addition, it acts as a clipper diode for the E-Beam gun, removing any inverse voltage that may appear across the load caused by mismatches between the gun and the network. The front-end clipper serves the same function for the thyratron. Excess inverse voltage on the thyratron may cause it to fire in the inverse direction thus limiting its ability to deionize before application of recharge voltage. The end-of-line clipper with its matching resistor of 12.5 ohms is required in the event of a gun fault. If a gun fault occurs the circuit essentially behaves as a conventional line type modulator with twice the pulse length and zero load impedance. Full inverse voltage appears at the back end of the network on the right. The end-of-line clipper with its resistance matched to the network acts as a load, dissipates the energy and removes the inverse voltage, permitting the modulator to act normally on the next pulse providing the fault in the gun has cleared.

Since the gun has a variable impedance with its resistance varying from essentially infinity at the beginning of the pulse to the effective network impedance of 25 ohms at the end of the pulse, the positive mismatch at the beginning of the pulse causes the full voltage of the networks in series, 500 kV, to appear on the gun causing it to arc. Therefore a clamper circuit is required to limit the voltage. The conventional clamper circuit consists of a large capacitor charged to the operating voltage of the load with a diode in series to prevent discharge into the load. The size of the capacitance is determined by the degree of variability in the load and the percentage regulation required. Since the specific gun uses only half the available charge, approximately half of the 10000 joules stored in the network would have to be diverted to the clamper capacitor. In addition, the voltage on the gun is not to rise more than 10 percent during the pulse. Therefore the additional 5000 joules on the clamper capacitor should not raise the voltage beyond 275 kV. The minimum size capacitor is 0.76 μF and stores 29000 joules at the maximum voltage. If the negative end of the gun is grounded the power supply filter bank could be used as the clamper capacitor with the energy conserved. Since the positive side of the gun is grounded, the clamper circuit is now the opposite polarity and a separate capacitor bank and a 250 kV power supply are required. In addition, a bleeder resistor across the clamper capacitor is required to discharge the capacitor back to 250 kV between pulses. A potential problem could occur if the clamper diode were to short and the stored energy dissipated in the gun.

Considering the problem in the use of a conventional clamper circuit, a clamper circuit was devised to eliminate the need for large energy storage and an additional power supply. The basis for the new circuit is that the parallel combination of the E-beam gun and the clamper circuit should effectively appear as a constant 25 ohm load impedance to the modulator. The circuit devised is shown on the diagram. It consists of a capacitor in series with a 25 ohm resistor and diode with a bleeder resistor across the capacitor. When the initial voltage pulse appears across the combined load it sees a 25 ohm impedance. The gun dissipates only half of the stored 10000 joules in the network. Since about half of the diverted energy is dissipated by the series resistor in charging the clamper capacitor the size of the clamper capacitor is chosen to charge to 250 kV with the remaining energy. The size of the required clamper capacitor is reduced to 0.08 μF, one-tenth of the size of capacitor

required in a conventional clamper circuit. The bleeder resistor must now during the interpulse interval, dissipate the 2500 joules stored in the capacitor. The time constant of the bleeder resistor in combination with the clamper capacitor must be less than one-fifth the interpulse interval. This clamper circuit permits single-shot operation, varying repetition rates, eliminates the additional power supply and reduces the danger if the clamper diode shorts because of the low energy storage and the series resistor.

The Blumlein circuit and the clamper circuit were tested in a low voltage circuit at 5000 volts. Figure 2 shows the results. In this circuit a Blumlein circuit consisting of two 45 ohm, 2 us networks and an L-R load to simulate the gun characteristic were used. The clamper circuit consisted of an 0.02 μF capacitor in series with an 88 ohm resistor and a 58000 ohm bleeder resistor in parallel with the capacitor. Figure 2 (a) shows the waveforms without a clamper. The initial voltage on the load is nearly doubled and various voltages, both positive and negative, appear across the load after the main pulse. Also an additional current pulse appears in the thyratron circuit. Figure 2 (b) shows the effect of the clamper circuit. The load voltage is constant and the various voltage excursions after the pulse disappear. The slow decay in load current at the end of the pulse is due to the inductance used to simulate the time varying gun impedance. The I-t characteristic of the actual E-Beam gun load is shown in Figure 3, increasing approximately linearly for 3.5 us and slowly thereafter. The gun impedance at the knee is 17.0 ohms.

Two full-scale modulators at 250 kV have been built and will be described later. Because of malfunctions in the clamper and EOL clipper diodes, additional simulation was done to determine the transients during load-open (gun not conducting) and load-short conditions. This was done at 100 volts with two 5 us, 25 ohm PFN's and a microswitch in place of the thyratron. The circuit has a matched EOL clipper, charging diode, and clamper circuit. The load resistor was omitted to simulate a non-firing gun, but the normal operation waveforms, Figure 4, were obtained by shorting the clamper capacitor, C_c, using the clamper resistor as a dummy load. The values of the clamper components, R_c and C_c, were chosen so that R_c equalled the sum of the characteristic impedances of the PFN's, 50 ohms, and C_c 0.05 μF, equalled 1/4 the total PFN capacitance. The factor of 1/4 comes from the fact that with a linear ramp current and constant voltage, 1/2 the stored energy goes into the load and 1/2 into the clamper circuit. One-half the clamper energy goes into the clamper resistor, R_s, the rest is stored in the clamper capacitor to be bled off in the interpulse interval. In practice, the size of C_c will be adjusted for the best pulse shapes and least reflections throughout the circuit. As C_c is decreased the amplitude of the voltages in the clamper circuit increases, and Figure 5 shows the waveforms for C_c = 0.05 and C_c = 0.025 μF. To have flexibility in varying the clamper circuit for best matching, the clamper components must be chosen conservatively. With C_c = 0.025 μF, the clamper voltage goes to 165 percent of the dc charging voltage. For other load current pulse shapes, more complex clamper circuits, or even multiple paralleled clamper circuits, with R's, L's, C's, PFN's, and initial bias could be used. If the gun or load shorts at the beginning of the load pulse, the switch current pulse is its normal amplitude and double its normal length, and both PFN's invert, forward biasing the EOL diode and driving a double length current pulse through the EOL resistor, as in Figure 6. The EOL resistance is half that of the load resistor because, with both PFN's inverted, the PFN's are in cascade rather than in series as they are in normal operation. With an open load and C_c = 0.025 μF, Figure 7, the EOL diode voltage rises 26 percent over the charging voltage, but there is no current in the EOL circuit. An SCR across the clamper, which could be triggered at various times with respect to the switch current, was used to simulate a gun short at some time during the load pulse with the load open and the load voltage higher than normal. Figure 8 shows the clipper diode voltage and current when the open load is shorted near the end of the load pulse; Figure 9 is an expansion in amplitude and time showing oscillations which are shock excited by the high di/dt in the clamper circuit. Figure 10 shows the difference in clipper diode current for a fast- and slow-recovery diode. The high frequency ringing is 3.5 times less with the fast diode.

The effect of a short after part of the load voltage pulse into an open is shown in Figure 11, along with the difference between a slow-and-fast-recovery clamper diode. The slow diode contains more stored charge which must be swept out by reverse current before conduction stops. The very large dV/dt across the clmaper diode, even though in the direction of decreasing voltage, and the fast ringing in the clipper diode, together with the lack of R-C compensation may account for the diode failures. The replacement diodes will be compensated.

Two similar Blumlein modulators have been built to operate at 250 kV. One, at ECOM, shown in Figure 12, uses two 12.5 ohm,2.5μs PFN's, energy storage of 5000 joules, a resistive load, no end-of-line clipper, no clamper circuit, and no charging diode. This modulator is used for developing the iterative cavity-grid thyratrons and has a megawatt of average power available - 4 amperes at 250 kV. The other at MICOM, has two 12.5 ohm 5 us PFN's, clamper, EOL clipper, charging diode, and the cold cathode electron beam gun load. To date, only single shot testing has been done on this modulator because of power supply limitations. The series resistor in the clamper circuit can be connected as a dummy load for testing. All resistors used are copper sulfate-sulfuric acid-water electrolytes in glass pipes and are cooled by circulating through heat exchangers. The EOL resistor, because its use is intermittent, is uncooled. The switch in both modulators is a 10-gap iterative cavity-grid deuterium thyratron built by EG&G. The tube development is not yet complete, especially with regard to grid baffling and external voltage-division circuits, but both modulators have operated up to 210 kV single shot and the one at ECOM at 175 kV at 10 Hz. The thyratrons and voltage dividers in both modulators are enclosed in plastic boxes to enable surrounding these components with a high-dielectric-strength gas. Figure 13 is an 8-gap version of the thyratron with a graphical cutaway showing the inner structure. Figure 14 is another view of the same tube.

After running the MICOM modulator for several thousand shots into a resistive load at voltages between 100 and 210 kV, the E-Beam gun load was connected to the modulator with four coax cables,

each 50 feet long. The gun was pulsed between 150 and 200 kV for several hundred shots, after which it stopped drawing current, probably because of the clean-up of the light oxide layers which acted as electron sources during the start of gun conduction. A circuit change by Dezenberg at MICOM separating the clamper from the gun with coax cable delayed the clamping effect by 100 ns, putting a voltage spike on the gun to act as a "tickler" and draw electrons from the gun electrodes by field emission. With this change the gun fired satisfactorily, but the diodes had already been heavily damaged.

In addition to clamper and EOL clipper repair, the gun impedance is 17.0 ohms, which presents a basic mismatch to the 25 ohm Blumlein impedance for which the clamper can't compensate. Either the gun impedance will be increased by changing the electrode spacings, or the PFN impedance will be decreased by decreasing inductance.

CONCLUSIONS

A passive, dissipative clamper circuit can improve the matching and reduce transients caused by a time-varying load. Although applicable to any type of modulator, it has been demonstrated here with a Blumlein circuit. When using a load which occasionally may not conduct, such as a field emission E-Beam gun, safety factors must be included when choosing the clamper and clipper diodes, particularly if flexibility is desired in the clamper circuit to optimize waveforms. For the conditions used in the simulation, the clamper capacitor one-eighth the PFN capacitance and shorting the load near the end of the load voltage pulse with the load open, the clamper voltage was 165 percent and the clipper voltage 126 percent of the dc charging voltage. The large dV/dt and ringing currents indicated that R-C compensated diodes should be used.

If it is unlikely that the load will not conduct, the load fault during the pulse is less severe and the safety factors can be reduced accordingly.

ACKNOWLEDGEMENTS

The authors would like to thank Dr. Dezenberg of MICOM, both for financial support and technical suggestions; D. Turnquist and S. Merz of EG&G for their continuing help in the development of the iterative thyratron; and J. Creedon of ECOM for technical assistance in all phases of the modulator program.

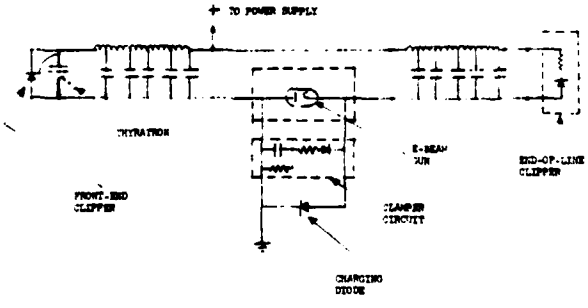

Figure 1. Schematic Of Blumlein Modulator

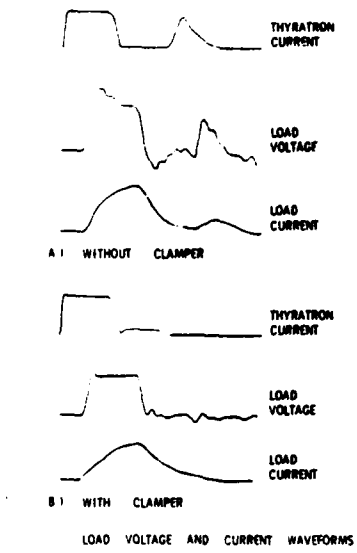

Figure 2. Effect of Clamper Circuit on Modulator Waveforms - Blumlein Simulation

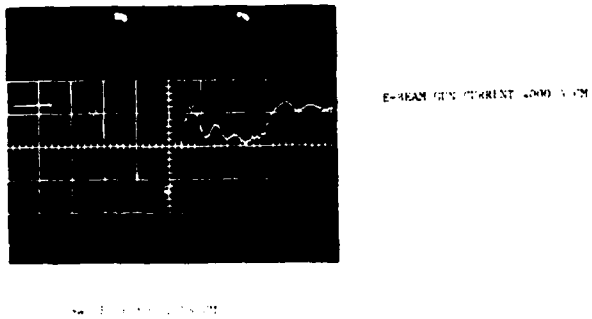

Figure 3. Load Current Pulse In E-Beam Gun

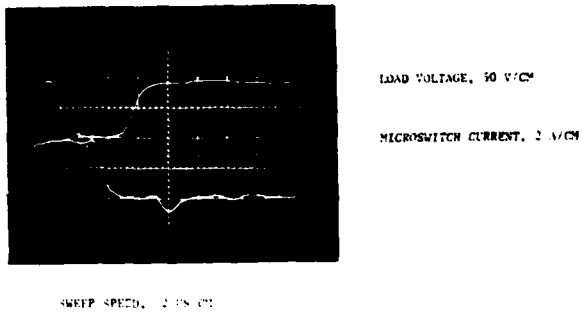

Figure 4. Blumlein Simulation Circuit. Normal Waveforms

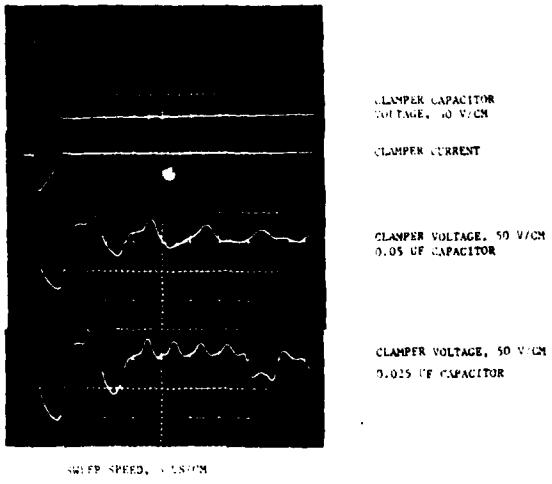

Figure 5. Clamper Circuit Waveforms, Open Load

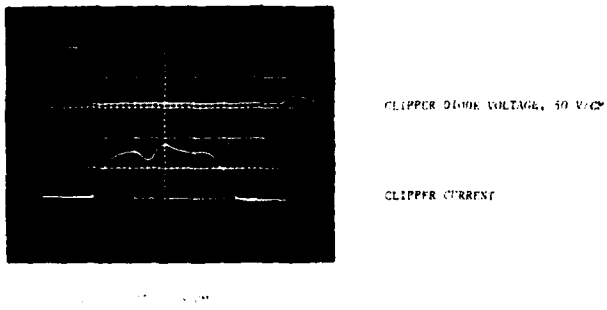

Figure 6. End-Of-Line Clipper Waveforms, Load Shorted

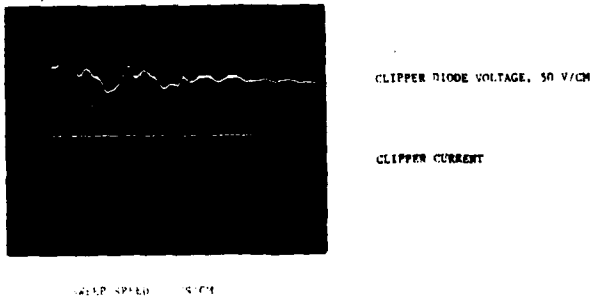

Figure 7. End-Of-Line Clipper Waveforms, Open Load

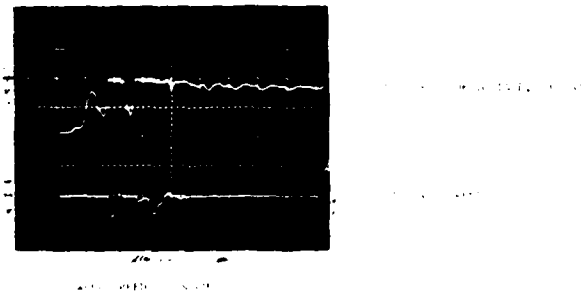

Figure 8. End-Of-Line Clipper Waveforms, Load Initially Open, Shorted Near End Of Pulse

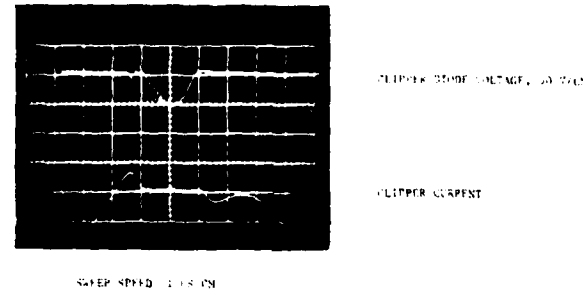

Figure 9, *Oscillations In End-Of-Line Clipper*, Load Initially Open, Shorted Near End Of Pulse

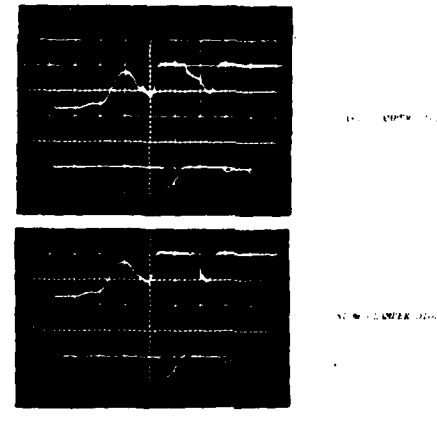

Figure 10. Effect Of Clamper Diode Recovery Time On EOL Clipper Waveforms, Load Initially Open, Shorted Near End Of Pulse

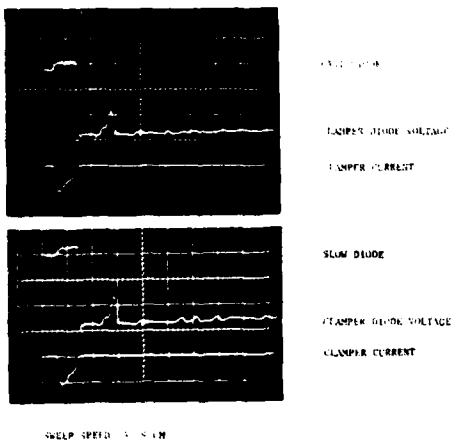

Figure 11. Effect Of Clamper Diode Recovery Time On Clamper Waveforms, Load Initially Open, Shorted Near End Of Pulse

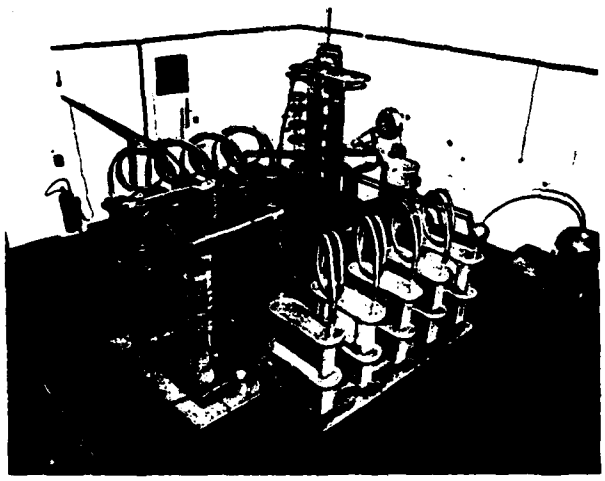

Figure 12. ECOM 250 kv Blumlein Modulator

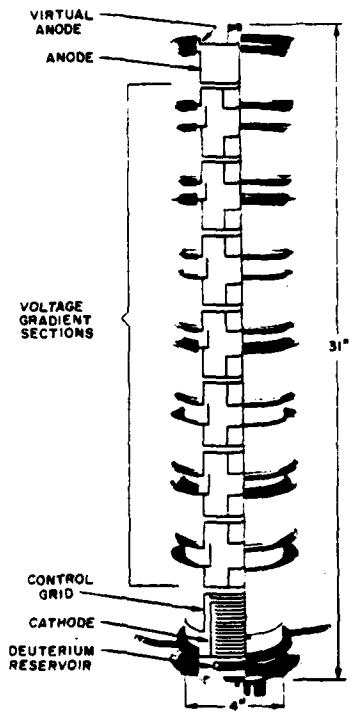

HIGH VOLTAGE DEUTERIUM THYRATRON

Figure 13

Figure 14. 250 kv Iterative Gap - Cavity Thyration

A PASSIVE ASSIST FOR HARD TUBE MODULATORS

Thomas A. Weil
Raytheon Company
Wayland, Massachusetts

Summary

One limitation in switch tube selection (or in maximum modulator PRF) for a hard-tube modulator is the switch tube dissipation resulting from charging and discharging of the total stray capacitance across the load. This limit occurs especially in modulators for a linear-beam tube with a modulating anode; because such a load draws very little current during the pulse, a small high-voltage switch tube may suffice except for dissipation capability.

Passive networks are described that can be used in series with the switch tube anode to divert a major fraction of the dissipation from the switch tube anode to external resistors. These networks must divert the energy during the high-dissipation switching period without introducing excessive voltage drop or ringing at other times. Precautions are discussed to prevent undesirable stretching of the pulse rise and settling times when these networks are added.

A system application incorporating this passive assist, now operational, will be described.

Switching Dissipation

A classic limitation in the design of hard-tube modulators is the amount of power dissipation that occurs in the switch tubes in the process of charging and discharging stray capacitance across the load. In high-voltage applications, even very small amounts of stray capacitance across the load can result in significant switch-tube dissipation, especially at high PRF's. This switching dissipation occurs because of the well-known rule that charging a capacitance from a fixed voltage source through a resistance results in 50% charging efficiency, regardless of how the resistance (such as that of a switch tube) may vary during the charging time. I.E., for each joule of energy that ends up in the charged capacitor, two joules are drawn from the source, and the extra joule is dissipated in the resistance of the charging path. (If the charging path has inductance, the energy drawn from the source is still exactly twice the capacitive energy at the time when the capacitor voltage just reaches the supply voltage, but some of the excess energy may have become stored in the inductive elements instead of having been dissipated. If the stored energy is allowed to cause the capacitor voltage to continue charging beyond the supply voltage, as in resonant charging, the stored inductive energy may be at least partially recovered; but if the requirement is to charge the capacitance just to the supply voltage, the stored energy is not readily recovered, and, if dissipated, results in exactly the same 50% charging efficiency as in the resistive-charging case.)

The amount of dissipated energy per pulse is thus the same as the energy delivered to the capacitive load. The power dissipation is then:

$$P_D = \frac{1}{2} CV^2 \times PRF$$

where C is the total load capacitance, including the stray capacitances of all circuits and wiring connected to the load, including the stray capacitance of the switch tube or tubes themselves. Whatever discharges the capacitance at the end of each pulse must, of course, dissipate an equal amount of power.

Switch Tube Power Ratings

Switch tubes are available in many sizes and combinations of ratings, but, in general, rated plate power dissipation is far less than the product of average-current rating and peak-voltage rating. This is not surprising, because many switch tubes were developed for applications where maximum voltage and maximum current generally are not present at the same time, except perhaps very briefly. As a result, switch tube dissipation may readily be exceeded if the tube is operated at high PRF, even though the tube may otherwise be within its ratings. This problem is especially true in floating-deck modulators for linear-beam tubes with modulating anodes (ref. 1, p. 7-81). In such applications, the required intrapulse current and dissipation are small, and since modulating-anode RF tubes are primarily used at low PRF, the switching dissipation usually is also small. As a result, switch tubes have been developed for modulating-anode modulator service with high voltage ratings, high peak current ratings to provide short modulator rise times, but relatively low plate power dissipation ratings. The Eimac Y354, a version of the 4PR250 specially processed and tested to 65 kV, is an example of such devices, with ratings of:

Maximum DC working voltage:	50 kV
Peak pulse current:	6 amperes
Maximum plate dissipation:	250 watts.

Tube designs of this type are attractive because they are relatively small and require relatively little heater power and grid drive power.

Modulator Example

In a recent case, a transmitter had been designed around a linear-beam tube with a modulating anode to permit use of a small, efficient modulator and to provide long pulses free of modulator ringing. As shown in Fig. 1, a pair of Y354 switch tubes is used to pulse the modulating anode alternately on and off. Fig. 2 shows the modulating anode pulse waveform. Of particular interest are the voltage rise and fall time. With a total capacitance at the modulating anode of 250 pf, the theoretical minimum rise time (if a constant 6 amperes peak current were maintained by the switch tube even as its plate voltage fell to zero) would be 2.1 microseconds; as shown, the actual rise time is 2.6 microseconds to 45 kV, with slower settling after that. In this system, for reasons related to time jitter and phase stability interactions, the useful beam pulse time is considered to start when the modulating-anode rate-of-change of voltage settles to less than 0.1 kV per microsecond, and this point is reached in 3.5 microseconds. In operation at a maximum PRF of 600 pps, dissipation in each switch tube is 175 watts, which is a comfortable 70% of maximum rated plate dissipation.

It then became desirable to add a higher-PRF mode to the system for improved MTI performance. 1200 pps, as requested, would have resulted in doubling the dissipation in each switch tube to 350 watts, which would be an intolerable 140% of maximum rating. There appeared to be no reasonable way to reduce load capacitance or operating voltage without major redesign. Larger switch tubes were considered, or pairs of Y354's; such a change would also have required costly changes in heater power and in

grid drive circuits. Although feasible in principle, this approach was extremely unattractive because it would have required major redesign, together with major repackaging to provide room for the new and larger parts.

Passive Assist

To avoid major redesign, attention was given to finding a passive network that could be placed in series with the switch tube to divert some of the dissipation away from the switch tube without otherwise interfering with normal modulator operation. To be successful, this network would have to:

1) have high voltage drop during the early portion of the switching time so it would absorb a significant fraction of the switching dissipation, but

2) have gradually falling voltage drop, so as to allow adequate plate voltage always to remain available to the switch tube to let it operate at full peak current to keep the rise time short, and

3) have very low and constant drop during the flat portion of the pulse, in order not to disturb the desired flat-topped long pulse shape, and

4) be able to dissipate safely the losses thus diverted from the switch tube.

Because this technique is reminiscent (in some ways) of C. Eichenauer's "Magnetic Assist" for hydrogen thyratrons[2], it was decided to call this passive dissipation-diverting network a "Passive Assist" for hard-tube modulators.

Ideal network characteristics to meet requirements 1 and 2 can readily be seen from the circuit waveforms; Fig. 3 shows waveforms of interest during the pulse rise time. The instantaneous switch tube dissipation is, of course, the product of its instantaneous plate voltage and plate current. The plate current must exist to charge the load capacitance, but only 2.0 kV of plate voltage is necessary to permit the switch tube to conduct its maximum rated peak current of 6 amperes. An ideal network would be one that would absorb all the excess voltage above the minimum when excited with the 6 ampere pulse of current. This ideal network would lower the average plate voltage during the rise time to 2.0 kV instead of an average of 25 kV and would thus divert over 90% of the dissipation from the switch tube. The ideal network can only be approximated, of course; and since too much network voltage drop will lower tube current and cause the rise time to be lengthened, all tolerances must be on the side of allowing more plate voltage, which results in less diversion of dissipation. However, since only 50% diversion was needed, there was considerable room for compromise.

Finding a suitable network was made difficult by the conflict between the third requirement and the first two. The first two require the network to behave in a rapidly changing manner during the pulse rise time, while the third requires it to "keep still" for a relatively long period immediately following the rise time. Requirement 4 is readily met in any passive network by proper component selection.

A simple resistor would meet requirement 1 but not 2 or 3. If used, a resistor would cause excessive wasted beam duty (ref. 1, p. 7-82). It might also cause excess loss of modulating anode voltage if there is appreciable modulating anode current during the intrapulse period.

A resistor shunted by an inductor would meet requirements 1 and 2 but would have severe voltage backswing or overshoot following the rise time, and thus would not meet 3.

A resistor shunted by an inductor, also shunted by a diode, can be made to meet requirements 1, 2, and 3, as well as 4. Fig. 4 shows the resulting circuit, and Fig. 5 shows the waveforms. At the start of the rise time, there is a large voltage drop in R1, which minimizes dissipation in the ON switch tube. During the rise time, current builds up in L1, gradually "shorting out" R1 as the rise time proceeds. At the end of the rise time, the current in L1 remains flowing and would tend to cause a large overshoot in modulating anode voltage, but CR1 clamps the voltage across L1 at a voltage equal to its diode voltage drop, essentially removing the extra network from the circuit. By proper choice of component values, including diode drop and the resistance of L1, the current in L1 can be made to continue flowing through CR1 for the full duration of the modulator pulse, so that the passive network remains shorted out for the whole pulse. This approach ensures that the flat-topped pulse will not be disturbed in any way and that it will not vary from pulse to pulse and affect transmitter stability.

Results

The rise time of the circuit with the Passive Assist included is shown in Fig. 5. Although the time to reach 45 kV is slightly increased (from 2.6 to 2.8 microseconds), the time to reach less than 0.1 kV per microsecond is still 3.5 microseconds. As a result, even though 64% of the anode dissipation is diverted from the ON switch tube by the network, wasted beam time is not increased. On the other hand, if more wasted beam time were permissible, the network values could be chosen to divert an even larger fraction of the switching dissipation. Optimization for our particular set of system requirements was readily handled by a computer simulation.

As shown in Fig. 4, only a simple resistor is used in the OFF tube circuit. Stretching of the completion of the voltage fall time is much less critical than the completion of the rise time, because completion of the fall time does not result in significant wasted beam power (i.e., the beam is nearly off anyway). The 3/2 power law also helps during the fall time; when the modulating anode voltage is down to 10% of full voltage, the beam current is down to 3%. As long as noise from the residual beam current in the linear-beam tube does not compete with close-in target returns, completion of the voltage fall time can be allowed to be gradual, so the simple resistor meets the requirements well enough in diverting dissipation from the OFF tube.

The values shown have permitted modulator PRF to be doubled while actually reducing switch tube dissipation. At 1200 pps, dissipation in each switch tube is 125 watts, or just 50% of rated maximum. An incidental advantage is that X-ray generation is also reduced by the energy-diverting network, because plate voltage is reduced during the current-conduction period.

Problems

During operation of the Passive Assist, one problem appeared. If the linear-beam tube arcs from modulating anode to cathode during the pulse, and if this arc is followed by an arc in the ON switch tube, the network diode fails. Since the diode is normally

conducting forward current at that time, it was theorized that the arcs resulted in excessive reverse current surges in the diode before it could recover. This problem was solved by revising the circuit as shown in Fig. 6 to ensure that peak currents occuring during arcing are limited to safe values by adequate resistance in the fault path. Since that revision, there have been no problems with the circuit. The circuit has been operating for 3 years, and one system has been operational for over a year.

Better Networks

Higher-order networks than a simple resistor and inductor could be considered in other applications to reduce switch tube dissipation even further. However, the limitation is expected to be the complexity required to prevent disturbances of the flat-topped intra-pulse period following the rise time, without having to add active clamping circuits.

Other Applications

Passive-Assist networks are expected also to be useful with solid-state switching devices, but such applications are beyond the scope of this paper.

Conclusion

In summary, the passive assist allows using switch tubes at higher PRFs or at reduced plate dissipation, or both, by diverting some of the plate dissipation, to passive elements that can safely dissipate the power. Modulator efficiency is unchanged; the same switching power is dissipated, but the Passive Assist allows the designer to exercise more control over where the dissipation occurs.

References

1. Radar Handbook, ed. by M. I. Skolnik, McGraw-Hill, 1970.

2. "A Magnetic Assist to Hydrogen Thyratron Switch Tubes", C. J. Eichenauer, 4th Hydrogen Thyratron Symposium, Ft. Monmouth, Nov. 17, 1955. (Proceedings not available; see related paper: "A Magnetic Assist for High-Power Hydrogen Thyratrons", J. E. Creedon and S. Schneider, Proceedings of Fifth Symposium on Hydrogen Thyratrons and Modulators, Ft. Monmouth, May 20, 1958, AD650889, pp. 145-158.)

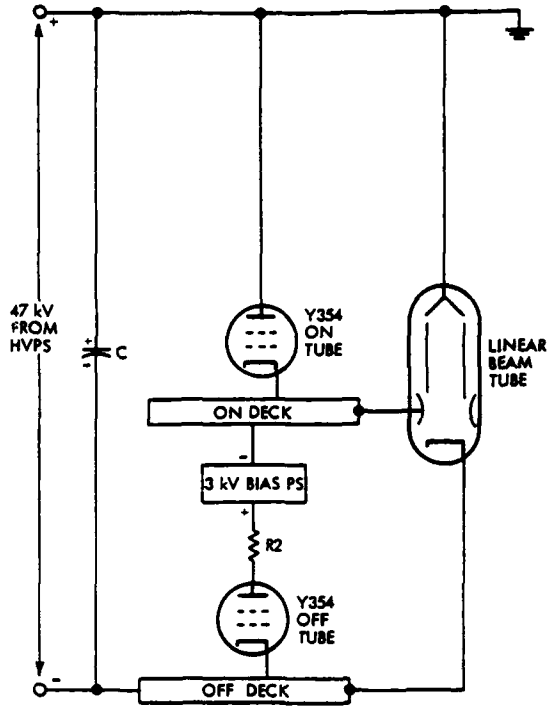

FIG. 1. MODULATOR FOR MODULATING ANODE LINEAR BEAM

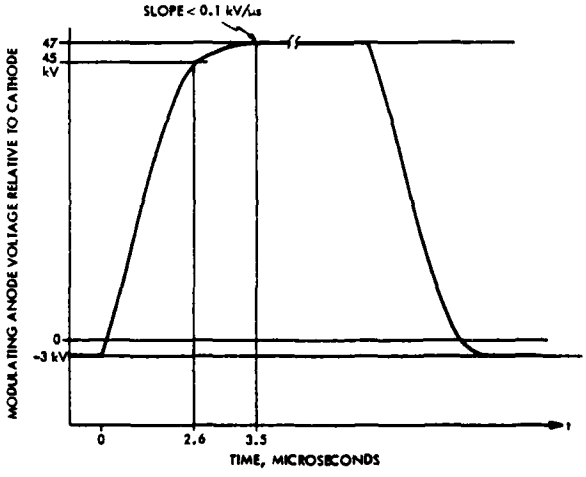

FIG. 2. MODULATOR WAVEFORM

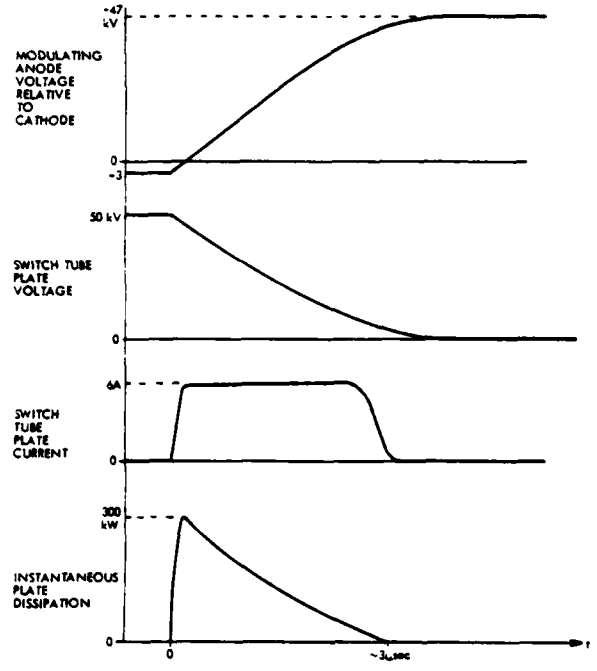

FIG. 3. RISE TIME WAVEFORMS

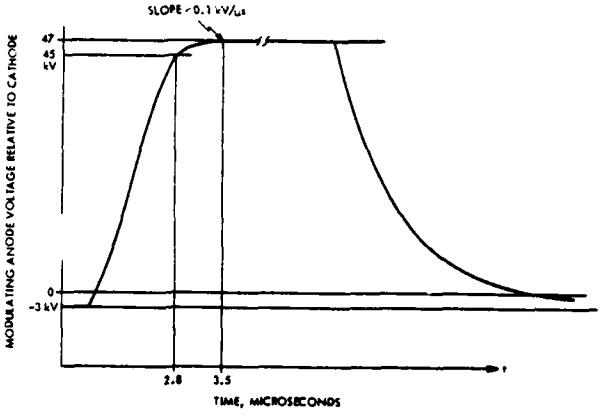

FIG. 5. MODULATOR WAVEFORM WITH PASSIVE ASSIST

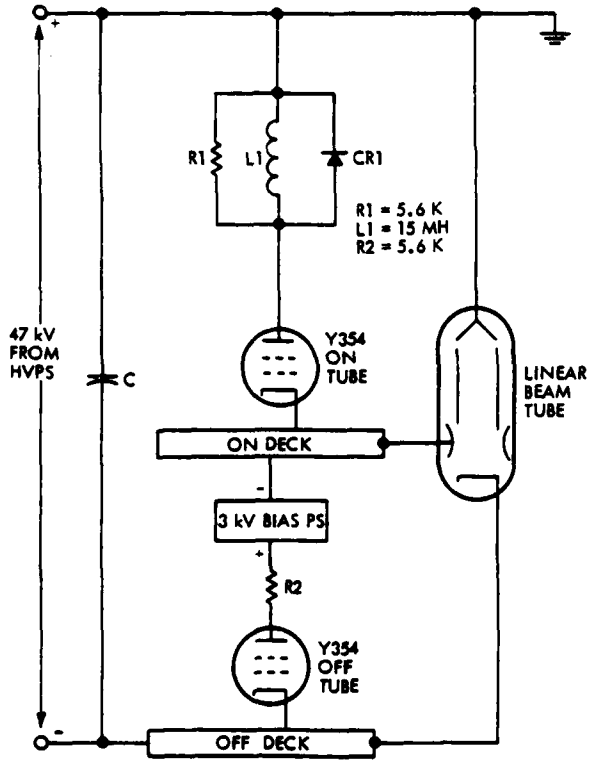

FIG. 4. MODULATOR WITH PASSIVE ASSIST NETWORKS

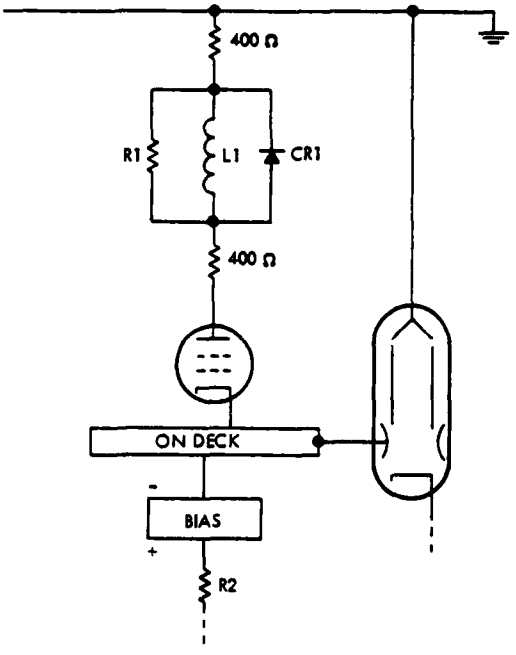

FIG. 6. PORTION OF MODULATOR, SHOWING MODIFICATIONS TO PROTECT CR1 DURING ARCING.

LONG PULSE SWITCHING OF HIGH POWER TETRODES

Bobby R. Gray
High Power Component & Effects Section
Techniques Branch
Surveillance Division
Griffiss Air Force Base, New York

Summary

The Energy Research and Development Administration in conjunction with its several participating contractor operated laboratories is presently performing research in thermonuclear fusion using toroidal confinement techniques. This process, sometimes called the Tokomak process, attempts to confine a toroidal shaped plasma for further compression and heating by various methods to achieve the 100 million degrees thought necessary for fusion to occur. Ohmic heating of the plasma by high induced currents in the plasma, heating by RF power at selected frequencies, and neutral beam heating are some of the main ways presently being investigated. This paper reports on a test at Rome Air Development Center, in support of the neutral beam technique. Information on the capability of the Eimac X2170 high power tetrode to conduct 2 second long pulses at currents up to 65 amperes and 65 KVDC hold off was needed by Oak Ridge National Labs. Purpose of this pulse is to pulse a beam of neutral particles into the toroidal plasma itself.

Important features of a pulser for this program:

1. Output pulse polarity - positive.
2. Have a well regulated pulse output.
3. Be interruptible in event of a shorted load.
4. Be able to withstand a load current break or cut-off.

Introduction

High power pulsers for radar transmitters, accelerators, and communication purposes have generally operated within rather narrow confines of pulse length and pulse repetition rates. Duty factors tended to fall within a range of 0.001 to .06 typically. Within this duty range, the pulse length rarely, if ever, exceeds 10 milliseconds. The peak current switched by any single device might be several thousand amperes peak but at an average current of much less. Thermal stability of the device is hardly achieved on a single pulse and many pulses are required for the system components to become temperature stable. Switch tubes can be designed to have a fairly low average current capability but have a peak emission of several times greater. In most cases the achievable peak current is limited by factors other than the filament. Space charge current limiting, dissipation in the grids, or anode are usually of greater concern. Line type modulators are practically limited to less than 50 microsecond pulse length although it is conceivable to think of pulse lengths much longer. The component values in this case become excessively large and losses become more critical.

There are now requirements in thermonuclear fusion research that require a new look at the past way of designing pulsers and consider some additional constraints. In these requirements, pulse lengths could extend up to several seconds. Duty factor can go as high as 0.1 or greater. Pulse voltage on the load are presently in the 40 KV range but 150 KV pulses at pulse lengths to 1 second are projected in the near future. Current at this voltage level is a nominal 65 amperes although in the future greater levels are possibilities.[1,2]

These parameters should indicate that a system designed for this application would differ from the more conventional one with shorter pulse. The loading factor on power supplies would be reversed in that the average current capability of the supply must be near the peak current requirements while the actual demand is reduced by the duty ratio. Switch tubes must average current ratings equal to the peak ratings. At these long pulse lengths, a capacitor bank becomes unreasonably large to depend on for flat pulse tops. Utilizing capacitive energy storage for a one second 60 ampere pulse with a nominal 10% voltage droop would require a capacitor bank in excess of one farad possibly at the 150-200 KVDC voltage level. A series switch tube between the supply and the load would be required to better regulate the pulse output and switch the load current.

X2170 Tetrode Test

The remainder of this paper is concerned with the testing of an Eimac X2170 tetrode which is to be used in a neutral beam injector system as part of the Tokomak process for controlled thermonuclear reaction. The X2170 Tetrode shown in outline form in Figure 1 with 1000 volt screen voltage characteristic curve in Figure 2 was initially designed for RF service. Average anode dissipation of 625 kilowatts with the proper amount of cooling water is very impressive from the standpoint of switch tube applications where low tube drop is expected.

Objectives were to evaluate the tube for these conditions:

a. Hold-off voltage - 65 KVDC max
b. Anode current - 50-60 amperes
c. Pulse length - up to 2 seconds
d. PRF - one per 10 seconds
e. Load impedance - 800 - 1000 ohms
f. Shorted load - 10-15 ohms

It is a fairly common practice to use tubes designed for RF service in a high power video pulse application but the pulse length is usually much shorter than two seconds and the peak current is generally higher than the average DC rating of the tube. Note from the characteristic curves that the proposed anode current can be easily reached with the grid still at negative voltage and with screen at modest levels (i.e. 1000 volts).

Experimental Results

This test produced some interesting results. It was proven that the X2170 is capable of producing the desired 2 second pulse length and is able to hold off the high voltage under the right circuit conditions. The following table gives some data points taken for several values of screen voltage. Note the dual readings under the power supply voltage and currents. This is the reading taken at the beginning and end of the two seconds pulse and is the result of supply voltage regulation and its effect on anode current.

P.S. Volt KV	Plate Amperes	Tube Drop	Grid Voltage KV	Anode Power KW	Screen Voltage
41	49/35	2.85	-20	99	650
51	58/44	2.85	0	125	650
57	68.5/51	2.8	0	145	650
46	54.5/41	1.95	0	79	700
58	64/40.9	2.5	0	116.8	700
44/35	28.8	2.74	-60	78	750
44/35	36	3.32	-35	118	750
48	24	13.2	-60	316*	750
54/42	42/40	12.4	-50	532*	750
54/42	44.9	3.5	-35	118	750
56	58/46	1.5	-10	69.5	750
35/28	15.6	21.7	-190	338*	1000
40/34	27.4	17.4	-200	476*	1000
42	32.7	2	-20	65.4	1000
51	49/40	2.38	-10	97.3	1000

*-points where anode spot heating occurs.

Observations

In conducting the test certain observations were made of the performance. Some of these are noted in the following section and some comments on how certain problems were overcome are included.

a. High Voltage Conditioning

Prior to pulsing the tube, it was high voltage conditioned several hours to insure that maximum voltage could be achieved during operation. Initially most tubes, after being out of service for some period of time, do require some degree of conditioning before the supply voltage levels can be held off reliably. This particular tube would hold-off the high voltage, while the filaments were cold, up to about 40 KVDC anode voltage. Continued application of voltage, with the limited energy discharge into the tube allowed gradual conditioning of the tube up to 80 KVDC. Flashover across the anode-screen terminal occurred at voltages much above 80 KV.

b. Audible Noise

During one test excercise of the tube an audible high pitched noise was clearly heard. The normal level of audible noise in the immediate area of the control console makes conversation difficult. To be able to discern this additional sound was somewhat of a surprise. The noise began at the beginning of the pulse and ended with the pulse. The normal amount of light from the filament that glows through the tube ceramic extends up about two inches from the screen terminal. When the audible noise appeared however, this glowing area increased by a factor of 2.

Tube parameters which tended to produce the squeeling were a high screen voltage and a negative grid voltage that limited the anode current along with a high tube drop. With screen voltage at 1500 volts the squeeling sound would appear if the grid voltage were more negative than about 100 volts. The tube drop under these conditions was about 20 KVDC and tube current 20 amperes. Lowering the screen voltages and/or making the grid more positive either reduced or stopped the squeeling sound. The only logical explanation for the effect is a focusing of the electron stream into very narrow beams that cause spot heating of the anode. accompanied with a higher than normal anode voltage drop. The lowest point where audible squeeling was still apparent was with about 317 kilowatts dissipation.

As the screen voltage increases, the grid voltage must be made more negative to keep the tube turned off during the interpulse period and also to control the pulse current during the pulse. This increasing negative grid voltage tends to cause squeezing or focusing of the electron stream as it passes through the grid region as shown in a simplified sketch in Figure 3 . Although the changes in the focusing effect tended to follow grid voltage changes the exact cause of the focusing might not be merely a squeezing of the electron stream by the negative grid but an effect of the higher anode voltage drop. The equal potential lines of the anode to grid voltage could be bent or distorted by the presence of the screen grids to form an electrostatic lens. As the plate drop increases and the screen voltage is greater the lens focusing effect increases. If the tube operated with grid at values near zero volts or even if it were at some positive value, the electron stream is not quite so dense and is more evenly deposited on the anode surface. This phenomena is generally not of importance because either the pulses are of short duration or tube operating conditons are such that it cannot exist, as in the case of positive grid voltages. Also, it should be pointed out that this phenomena is not unique to this tube type. Any electron tube that has sufficient emission current can produce a similar effect i.e. focused heating if operated under similar circumstances.

c. Oscillations or Instabilities

This test as is usual for most pulse amplifiers utilizing high gain circuits encountered oscillations. These were easily controlled by usual suppression techniques of:

1. Screen suppressor resistor.
2. Screen bypass capacitor.
3. Filament center tapping transformer bypass capacitor.
4. Grid suppressor.

During a shorted load test some oscillation was observed on the anode current and voltage pulse. This was probably caused by high velocity electrons impacting on the anode and causing secondary electrons which interact with the screen to produce a Dynatron type oscillation.

d. Ripple Voltage Effects

Long pulse operation makes control of ripple voltages difficult when simple power supplies with no electronic regulation are used. Filtering of the supplies through simple inductive and capacitive filters is difficult because of the extremely high amount of capacitance required. The leading edge of the pulse is apt to have a spike on it, which represents the discharge of the stored energy in the filter capacitors down to the RMS level of the supply output under loaded conditions. On more usual pulsers this spike would be equivalent to a slight voltage droop on the pulse. The importance of this point is that the ripple voltage of the power supplies tends to modulate the pulser output after the capacitor bank voltage droops to the power supply level. This effect was quite noticeable in our tests. In general, the harder the tube was driven, the more noticeable the ripple voltage. Ripple voltage is here defined as those components related to the residual line frequencies or harmonics being imposed on the DC level of the power supplies.

The grids, screen, or filament are also elements through which ripple voltage can be introduced to the pulser output. To alleviate some of the 60 Hz from the filament a center tapped filament transformer with RF bypass capacitor was used. Very little could be done for the ripple voltage caused by 60 Hz components on the grid, screen, and anode supplies. Electronic regulation was used where possible to reduce the 60 Hz but the anode supply had a basic 4 percent ripple voltage on it after the capacitor bank voltage drooped down to the rectifier output level.

e. Current Shut-off Induced Voltage Spike

As has been mentioned, the leading edge of the pulse has a current spike that follows the droop of the capacitor bank voltage, and regulation of the supply voltage because of internal impedance. As current flows through the supply an IR drop develops. This drop in voltage adds to the voltage drop from the capacitor droop for the tube anode voltage and current. After the capacitor bank voltage has drooped to the rectifier output voltage level the load current is derived from the rectifier directly. This variation in voltage and current is intolerable in both testing and in the actual final application. While trying to remove the spike current on the leading edge of the pulse, it seemed reasonable to simply remove the capacitor bank since most of the pulse current came directly from the power supply. However, when this was done some spectacular fireworks resulted. The tube, which had operated satisfactorily at 60 KVDC before, could not operate with 20 KVDC without arcing. Other effects such as a high voltage capacitive divider exploding and high voltage bus work arcing to ground occurred. Pulsing the tube with a low anode voltage and current revealed that the anode current was practically a rectangular pulse with no spike on the leading edge, which is what we desired. The anode voltage, however, with only a few amperes flowing through the tube, had a spike at the trailing edge of the pulse that added to the DC level by several times and the spike level was directly dependent on the current level.

As described earlier the supply transformers have built-in certain inductance, partly through normal transformer leakage reactions and magnetizing inductance, but also an additional inductor in each phase of the HV transformer secondary. High current thus flows through this inductance during the pulse. For continuous conduction this causes no problem but when current flow in the circuit inductance is terminated, a voltage is developed equal to product of the circuit inductance and the time rate of change of current. From measurements of the voltage spike generated at low level tests, the calculated inductance of the system is about 4-5 henries. The shut-off of anode current occurs in less than 100×10^{-6} seconds thus the theoretical value of voltage could be as high as:

$$L \frac{dI}{dt} = \frac{(4)\ (50)}{100\ 10^{-6}} = 1 \times 10^{6} \text{ volts}$$

assuming the tube was pulsing the desired pulse current of 50 amperes. This kind of voltage spike of course would cause breakdown before it reached the theoretical value.

Solution of the problem requires either reducing the inductance or increasing the current shut-off fall time. An alternate scheme would be put a snubbing capacitor across the switch tube, which is where the voltage spike appears mostly. Clipping this inductive spike with a diode could not be employed here because the inductance is in the supply itself and not across the load. It was found that a 1.6 ufd capacitor would limit the voltage surge across the tube and that the anode voltage spike did not rise above the DC level. In Figure 4a , we see the effect of this on the tube anode voltage and current as compared to the condition with 54 ufd in the capacitor bank at the supply side of the load shown in Figure 4b.

The final solution for the test was to put 54 ufd capacitor bank back on the supply in order to prevent damage to the supply diodes from any high peak inverse voltages.

Fault Current Interrupt Test

The tetrode tends to have fairly constant current features depending on where the operating point of the tube is. Variations in anode voltage, grid or screen voltage causing changes in anode current can be minimized by selecting the operating point either above or below the knee of the characteristic curve. For most systems, this feature is evaluated on the basis of power supply ripple, regulation, or other small changes. A different situation occurs when load shorts are a possibility. The load impedance in a shorted state is reduced from a relatively high impedance to nearly zero ohms depending on the load arc itself. Most power supplies used for high power pulsers are designed as constant voltage sources and when the load shorts, the anode voltage of the switch tube is raised to power supply level or greater in the event the system becomes oscillatory. If the tube was operating above the knee of the curve before the load faulted, current increase may be on the order of 10%-20%. However, if the operating point is below the knee of the curve, current could increase 200-300% typically. The greatly increased plate voltage may cause

difficulties with the tube stability. If the grid voltage was negative before the plate voltage changed, a condition is set up for possible etching of the anode by the intense electron streams. Even if there were no etching or burning of the anode wall secondary electrons are likely to be emitted to cause circuit instabilities.

These points have been raised to show that the constant current features of the tetrode are not always totally dependable and additional protection to a load fault is necessary. The fault current must be shut off to prevent excessive damage to the fault load and to protect the switch tube itself In an extreme case such as the switch tube arcing or failing to block the fault current, the power supply must be crowbarred.

This evaluation of the X2170 included a faulted load test. For this SI shown in the test circuit Figure 5 was used. At some point within the two second pulse the vacuum switch shunted across load was closed which reduced the load resistance to a simulated faulted load level of about 20 ohms. The resulting current level was then detected and a trigger pulse was initiated to trigger a thyratron in the grid circuit of the switch tube which returned cutoff bias back onto the tube. An adjustable delay was provided to see the effects of the rapidly increasing plate current.

Photographs in Figure 6 show the increases in current after the load short and dropping off of the faulted current after a delay. The test indicated that the tetrode could interrupt the fault current reliably but if the delay were too long the supply would overload first. An important point to remember in the shut off of the tube under fault conditions is that a higher than normal plate voltage on the switch tube is possible unless it is clamped someway or the shut off speed is adjusted properly. Figure 7 shows effect on plate current from slight load impedance change.

Circuit Details

Circuit for testing the tube is shown in Figure 5. The power supply used to provide power for this test was designed as a fairly flexible system consisting of 6 power supplies operated in tandem for AC input voltage and paralleled for DC output. See Figure 8 for a simplified sketch of this supply. Regulation of the input voltage is by a tap changing General Electric Indutrol regulator. Built into each of the supplies are three inductors which limit the fault current from the supply. In addition to these added inductors there is the internal inductance and impedance of the transformers. The estimated inductance of the supply network is 4 or 5 henries. Output of the rectifiers connects to the load and energy storage filter bank through a 10 ohm resistor. Each supply connects to a 9 ufd capacitor bank and for all supplies in parallel a total capacity of 54 ufd is available. In general, the supply was built for high PRF operation with short pulse lengths.

The screen power supply is a conventional system with one exception. Regulation against screen voltage caused by negative screen currents is achieved by both fixed resistance and an electronic shunt regulator. Without this, the anode current would tend to rise during the pulse if the screen regulates to higher levels.

Figure 9 is a scope photograph of increasing plate current for two anode voltages when the screen supply voltage was less than the regulating level. Note that the plate current leveled off after the regulating level was reached.

Crowbar protection to prevent unwanted dissipation of energy into the tube in event of failure is provided by two spark gap crowbars. These crowbar units, one a two ball spark gap with needle point triggering and the other a 20 gap device provide energy diversion within 2-5 microseconds after trigger signal is applied. Signals to trigger the crowbar and open the main PS circuit breaker are obtained from various sensors which determine the tube operating condition. These are the:

1. Main DC overload relay.
2. Loss of bias after the pulse.
3. Too high negative voltage on grid during pulse.
4. Anode fault to ground or screen.
5. Screen current overload.

The grid voltage pulse is a positive going signal rising from the cutoff grid bias level up to a maximum of zero volts grid cathode voltage. Grid voltage for the tube consists of V_{01} and V_{02}. V_{01} and V_{02} in series keep the tube cut off during the interpulse period. V_{02} acting alone establishes the grid level to produce required anode current. The grid voltage pulse is produced by shutting off the bias control tube V2 which removes the cutoff bias voltage established across the resistor R2. Diode CR1 is used to prevent positive excursion of the grid in event of faults within tube or load. Drive required for the Wx4101 tube is obtained from a direct coupled transistorized pulser. The basic variable pulse length is generated in a 74122 integrated circuit timer and amplified up to about 180 volts peak at the grid of V2 through several stages of amplification. One advantage this system has is that arcs within the main switch tube do not cause catastrophic failure to the solid state driver stages because the control tube acts as a buffer stage between the high and low voltage stages.

It turns out that monitoring these long pulses creates some minor difficulty. Normal pulse current viewing transformers and capacitance dividers are of little use except for the leading edges or trailing edge of the pulse. We used high power non-inductive resistors for monitoring the anode voltage pulse and the anode current. The tube grid protection was provided by fast acting contact making meters and a RC discharge circuit which produced a pulse output when the trip-out point was reached which fired the crowbar. With the meter and a multiplier resistor connected across the grid circuit it could follow the grid pulse as long as the pulse rate were low and pulse length long.

In order to ease the difficulty of making consistent measurements from the scope trace, the pulse repetition rate was synchronized to the line frequency with a Tektronix 555 scope operating from line Synch and the scope adjusted for 1 second per centimeter sweep speed a delayed

trigger was taken from the scope to in turn trigger the pulser for the switch tube.

Cooling of the tube is primarily by water flow through the anode, the filament, connectors, and screen connectors. Air is also required for cooling the grid area and the deep well inside the filament terminal area. Since the tube was originally designed for RF service applications it seemed less water flow would be necessary since the tube would be driven hard for pulse service to have much less average dissipation in order to maintain low voltage drop.

Due to the long puise however, it was uncertain whether or not to consider the peak power as if it were an average power rating. Flow was initially set at 100 gpm. Tests showed this to be adequate when the tube was operated properly. However, under the condition where spot heating was taking place (discussed earlier) additional flow may have helped the problem. Since this was considered an abnormal condition, the flow was maintained at 100 gpm and operation where the spot heating could occur was avoided.

Load Resistance

The simulated load for the X2170 is a sodium nitrite liquid load rated for about 500 KW. This rating is somewhat arbitrary however because electrolyte liquid resistors have a fairly strong conductivity dependence on the temperature of the solution and adequate cooling must be provided to maintain constant resistance. Certain electrolytes however tend to have a fairly flat conductivity-concentration response curve and can have a saturated conductivity where increased concentration levels and/or high temperature has little effect on overall resistance. These electrolytes, called weak electrolytes, also tend to have less corrosive effects than the strong electrolytes such as sodium chloride and copper sulphate. We have used all three electrolytes at RADC in attempting to build loads. In general, if a relatively high value is desired i.e. several hundred ohms, we would use sodium nitrite and a series of glass tubing with a fairly large length to cross-section ratio. Low values of resistance, less than one hundred and as low as 1 ohm to date, have been achieved with copper sulphate and a small length to cross-section ratio.

For the X2170 test, we used a sodium nitrite liquid load that serves as a combination surge current limiting resistor and/or load resistor in our high power test stand. The load itself floats at high voltage and is cooled by a high volume flow of air through a heat exchanger, floating also at high voltage. The liquid of the resistor itself is pumped by a hydraulic driven motor.

Conclusion

This series of tests show the X2170 tube is capable of operating at long pulses under the limitation of the average DC plate current ratings and is capable of holding off up to 65 KVDC plate voltage. It is also able to reliably block a fault current when the load shorts. The test showed some of the problems encountered when the tube is operated with a long pulse up to two seconds in length. Certain insights in methods to maintain stable operation under these conditions were obtained.

References

1. "Modulators for High Power Neutral Beam Systems", N. S. Ponte and G. Schilling, Proceeding Symposium Eng., Probl. of Fusion Research, San Diego, California, Nov 1975.

2. "High Intensity Ion Sources for Thermonuclear Research and Development", D. B. Morgan, Second Symposium on Ion Sources and Formation of Beams", Berkely, California, Oct 1974.

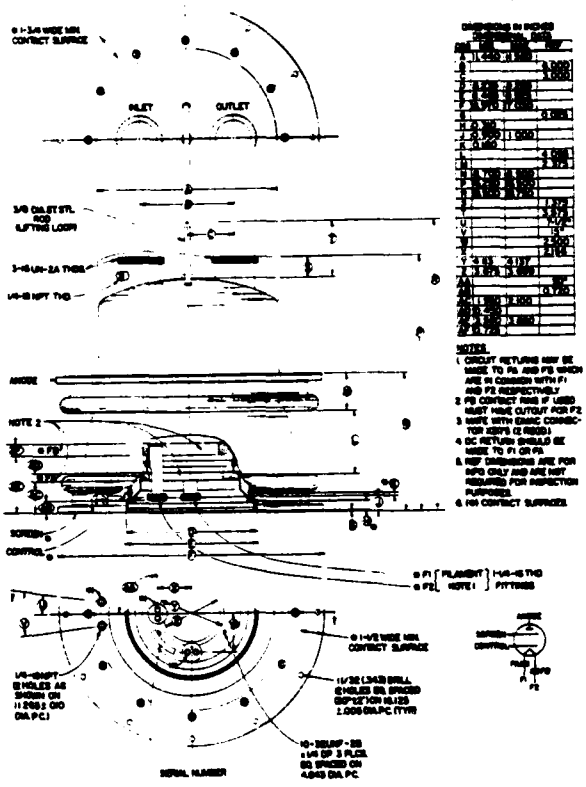

Figure 1. Outline of Eimac X2170 Tetrode

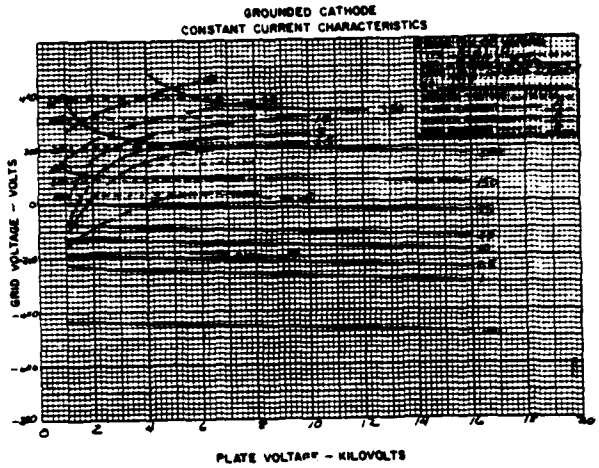

Figure 2. Characterisitic Curve for X2170 Tube

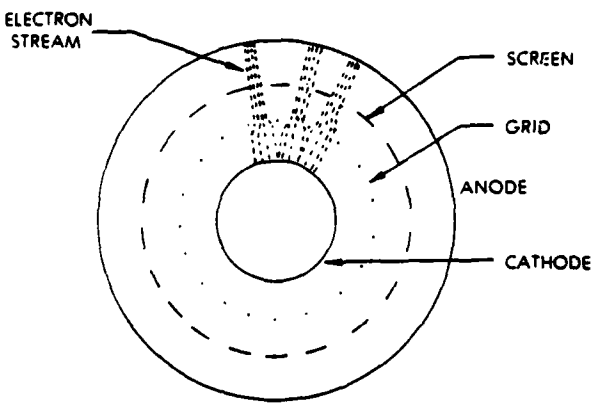

Figure 3. Illustration of Focusing of Electrons on Anode Surface.

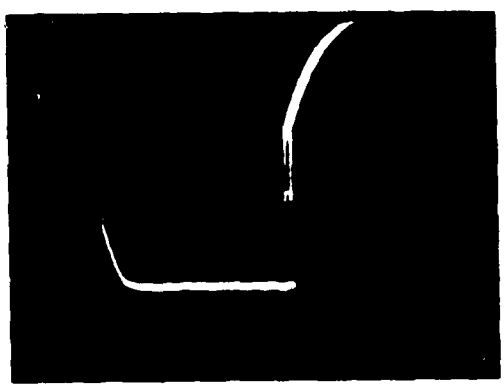

Figure 4a. Anode Voltage Pulse with 54 ufd Capacitor Bank in Circuit.
Ebb = 50 KVDC
Vert-20 V/cm x 476
Horiz - .5 sec/cm

Figure 4b. Anode Voltage and Current Pulse with only 1.67 ufd Capacitor Bank
Voltage Pulse - Ebb- 50 KVDC
Vert- 20V/cm x 4176:1
Horiz - 20msec/cm
Current Pulse - Vert - 20 V/cm: 1.467
Horiz - 20 msec/cm

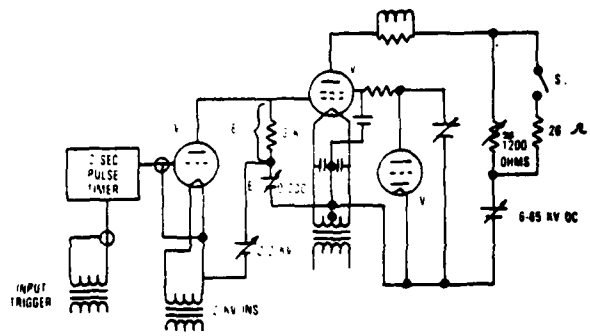

Figure 5. Simplified Schematic of Basic Test Circuit.

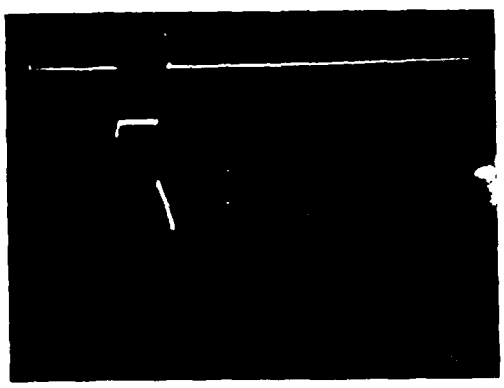

Figure 6. Photo of Anode Current Change when Load Value changes from 1200 ohms to 26 ohms.

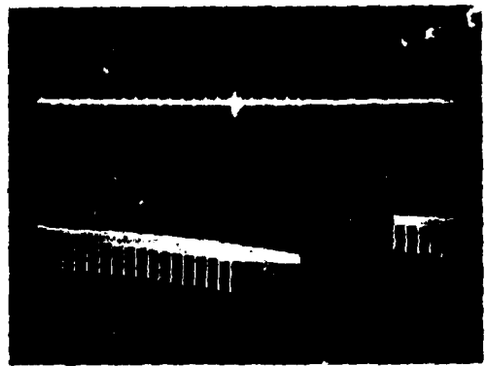

Figure 7. Series of Anode Current Pulses showing effect of load heating

Pulse length = 1.5 sec
Vertical Scale - 20V/cm x 1.467 amp/volt

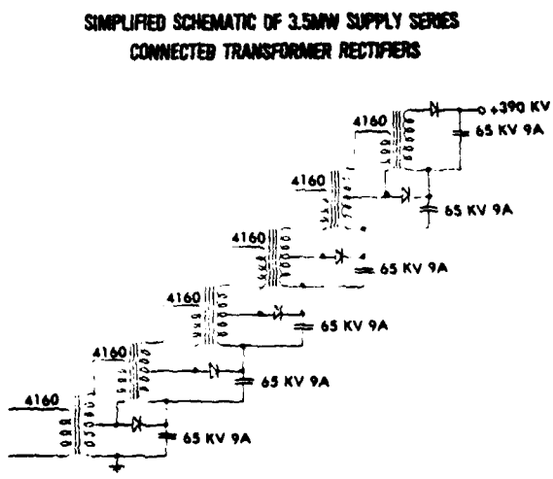

Figure 8. Simplified Schematic of HV Power Supply used in Test.

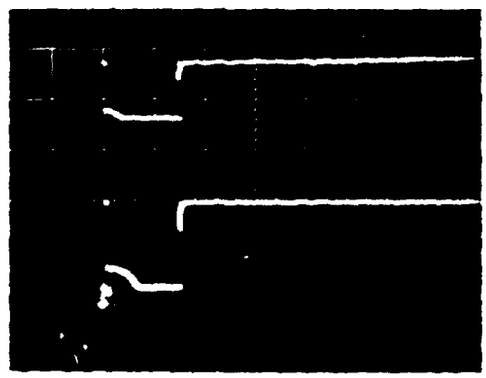

Figure 9. Photo of Anode Current Showing Effect of having an Unregulated Screen Supply.

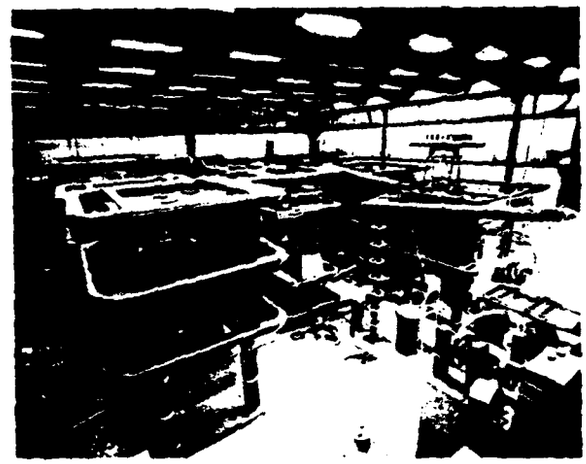

Figure 10. Photo of Test Power Supply

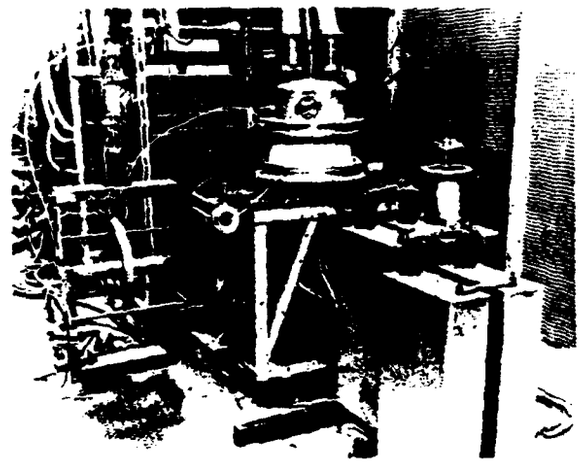

Figure 11. Photo of Tube in Test Stand

Figure 12. Photo of Sodium Nitrite Load and Air Plenum Chamber

A SOLID-STATE TWT MODULATOR

M. J. Feil
The Johns Hopkins University
Applied Physics Laboratory
Laurel, Maryland

Summary

A solid-state modulator that will pulse a 1-kilowatt traveling wave tube (TWT) of a repeater amplifier has been developed. This pulse repeater amplifier is required to minimize the propagation delay plus the rise time of the radio frequency (rf) output as opposed to radar pulse amplifiers that require specific pulse shapes. The propagation delay of the modulator is 38 nanoseconds (ns) from 10 percent of the input trigger to 90 percent of the output pulse, while the rise time is 18 ns from 10 to 90 percent of the output pulse.

Discussion

The modulator is a solid-state device that is built in two parts: the solid-state modulator and the modulator driver. The solid-state modulator (Figure 1) is of a floating deck configuration. The modulator driver is coupled to the floating deck by a transformer. Transformer coupling, as opposed to capacitive coupling, reduces the energy in the high voltage deck so that the modulator will survive if a rapid shutdown of the high voltage occurs. The solid-state modulator uses two transistors, each of which switches one-half the voltage of the modulator pulse, thus allowing the design to utilize faster transistors. The modulator is triggered on and off by the leading and trailing edges, respectively, of the trigger pulse. The trigger pulse can be generated by a TTL Schottky driver, such as an SN74S20.

Solid-State Modulator

Operation

There are four operating states of the solid-state modulator:

1. The quiescent state when the TWT is biased off.
2. The turn-on condition.
3. The active state when the TWT is biased on.
4. The recovery condition.

In the quiescent state, both transistors of the solid-state modulator are biased off with a base-to-emitter voltage equal to zero volt. The effect of this condition is that the TWT cathode is connected to the positive side of power supply PS_2, while the TWT grid is connected to the negative side of PS_2. PS_2 is set to 150 volts; thus, the TWT is biased off and draws no current, causing the current draining from PS_1 and PS_2 to be equal to the bleeder resistor current plus any leakage current.

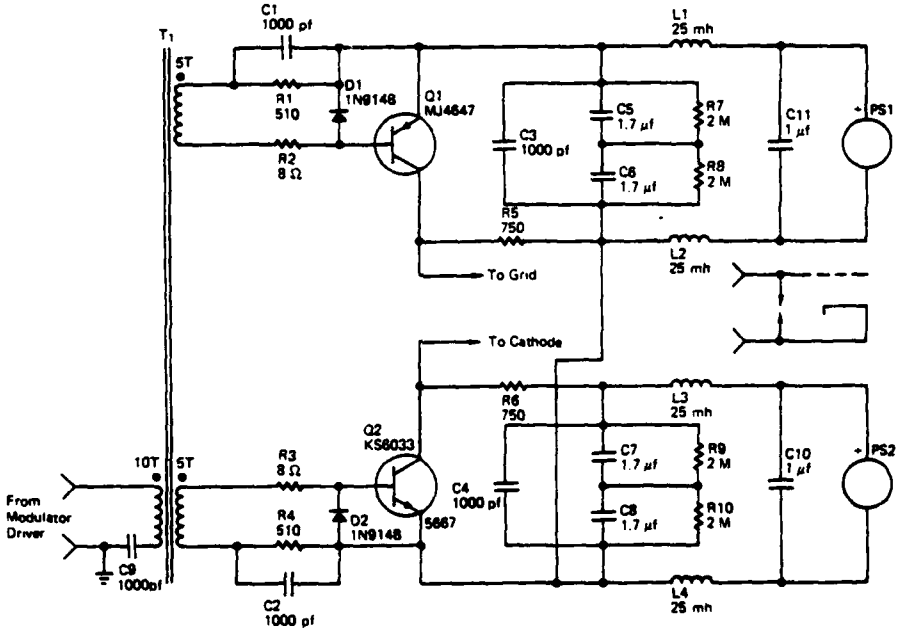

Figure 1 The Solid State Modulator Schematic

The turn-on condition of the solid-state modulator is initiated when a positive pulse excites transformer T_1, causing both transistors to turn on with an initial base current of 0.5 ampere. The base current will exponentially decay to 15 milliamperes with a time constant of 8 ns. During the pulse rise time, the TWT grid cathode load can be modeled as a 50 picofarad load to the modulator, and the modulator can be considered a

constant current source of 0.8 ampere. Thus, the initial collector current to base current ratio is less than 2. This causes the very rapid turn-on condition of the solid-state modulator.

In the active state, both transistors are biased to saturation. The transistor's base current is 15 milliamperes, and the collector current equals the sum of the TWT grid current plus the current in resistor R_5 for transistor Q_1 or in resistor R_6 for transistor Q_2. The collector current is approximately 0.3 ampere. The effect of this condition is that the TWT grid is connected to the positive side of PS_1, while the cathode is connected to the negative side of PS_1. Thus, the TWT grid to cathode On condition is set by the power supply potential of PS_1.

The recovery condition is initiated by the trailing edge of the input drive pulse to transformer T_1. The output of T_1 will back bias the base-to-emitter junction of both transistors by 0.7 volt. To reduce the storage time of the transistors, the collector current to base current ratio was increased to 20 in the active region. The recovery time has been measured at 70 to 250 ns, 90 to 10 percent of pulse output, depending upon the transistors used. The modulator has no active devices to restore the TWT to its quiescent state, which allows the modulator to be retriggered during the recovery time. The TWT grid to cathode potential exponentially decays to the quiescent state.

Power Supplies

The solid-state modulator requires two power supplies that are not referenced to the TWT grid, cathode, or system ground. Any stray capacitance of the power supplies to the TWT grid, cathode, or ground will add to the load of the modulator, which will slow down the modulator response. To minimize these stray capacitance effects, inductors L_1 through L_4 were used in the solid-state modulator. Capacitors C_3 through C_8 make up the final filter for PS_1 and PS_2. PS_2 sets the TWT Off condition, and PS_1 sets the TWT On condition.

Modulator Driver

The modulator driver (Figure 2) is a monostable multibrator with an emitter follower output. Under normal operating conditions, the modulator driver is triggered on and off by the leading and trailing edges, respectively, of the input trigger pulses. The monostable multivibrator is used to limit the maximum pulse width and to ensure the state of the modulator driver.

Operation

In the quiescent state (modulator Off state), transistor Q_2 is biased in the active region rather than in the saturation region, while Q_1 is biased off. Biasing transistor Q_2 to the active region reduces the delay of Q_2 when the transistor is switched to the Off state. The modulator driver is triggered on by the leading edge of a negative trigger pulse, which switches transistor Q_2 off and transistor Q_1 into saturation.

The modulator driver is triggered off by either the trailing edge of the trigger pulse or the decay of the voltage stored in capacitor C_2, whichever occurs first.

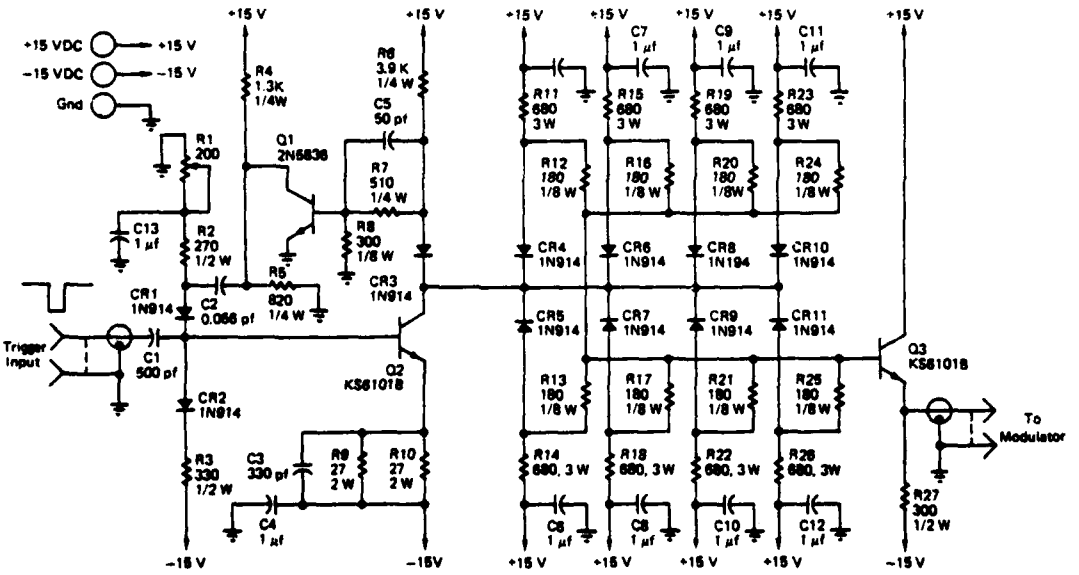

Figure 2 The Modulator Driver Schematic

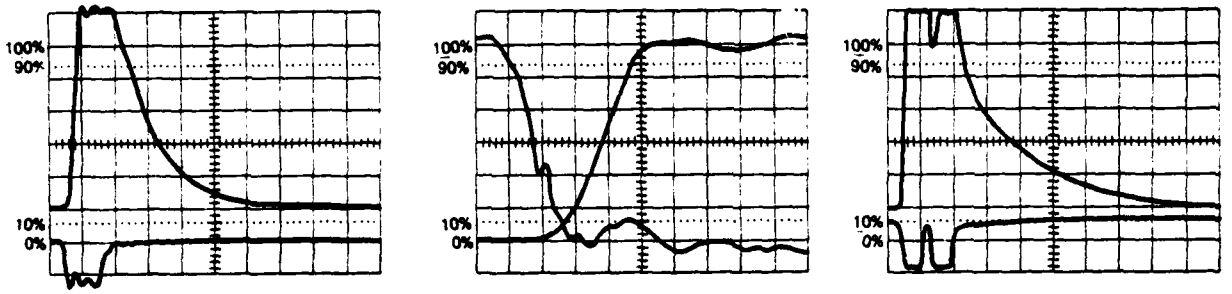

A. General response of the modulator. Upper trace is the modulator output 50 volts/div., lower trace is input to the modulator driver 5 volts/div., X axis is 100 ns/div.

B. Propagation delay and rise time response. X axis is 10 ns/div., negative going slope is input to modulator driver, positive going slope is output of modulator.

C. Modulator being retriggered during the recovery time of the modulator. Upper trace is modulator output 50 volts/div., lower trace is input to modulator driver, X axis is 100 ns/div.

Figure 3 Modulator Output Response as Compared to the Input of the Modulator Driver

Conclusion

The solid-state modulator has been built and installed in several repeater amplifiers. The primary features of this modulator are the reduction of the propagation delay plus the rise time, which is 50 ns from 10 percent of the trigger pulse leading edge to 90 percent of the rf output pulse leading edge and the ability to retrigger the TWT when the modulator is recovering to its quiescent state. Figure 3 illustrates the modulator output compared with the input trigger. Figure 3A shows the general response of the modulator output as compared with the trigger input; Figure 3B shows the propagation delay and rise time of the modulator; and Figure 3C shows the modulator when it is retriggered in the recovery condition. The modulator specifications are listed in Table 1.

TABLE I

OPERATING PARAMETERS OF THE SOLID-STATE TWT MODULATOR

Propagation delay plus rise time of the modulation pulse	38 ns
Propagation delay plus rise time of the detected rf signal	48 ns
Propagation delay of modulation pulse	20 ns
Rise time of modulation pulse	18 ns
Rise time of the detected rf signal	5 ns
Recovery Time	less than 100 nsec
Pulse width (variable)	100 to 1000 ns
Modulator Pulse amplitude	150 to 350 volts

DEFINITION OF TERMS

Propagation delay pulse rise time - 10% of input to 90% of output

Propagation delay - 50% of input to 50% of output

Rise time - 10% of pulse to 90% of pulse

Recovery time - 90% of pulse to 50% of pulse

A MODULAR MODULATOR FOR AN AIR DEFENSE RADAR

Charles A. Corson
Westinghouse Electric Corporation
Baltimore, Maryland

SUMMARY

A high power, solid state modulator which uses twenty identical plug-in solid state modules in parallel is currently in production as part of a high performance Air Defense Radar. Sixteen of thirty-two transmitters have been tested and shipped to date. This transmitter represents the transition of technology from the laboratory to production.

INTRODUCTION

The Air Defense Radar System uses two different transmitters which operate at L-band and S-band. The modulator load in the L-band transmitter is a tuneable klystron and in the S-band system is a wideband twystron. These amplifier tubes were selected because their perveances are identical and are operated at similar levels so that they could be powered by the same modulator. Both amplifiers operate at 112 kV at about 80 amps. Therefore, by using the same PRF and pulse width for each system it was possible to use the identical modulator for both transmitters. The table below summarizes the modulator and transmitter parameters:

- Peak Video Power ..... 9 MW
- Peak RF Power ..... 4 MW
- Video Pulse Width ..... 9 µSec
- RF Pulse Width ..... 6 µSec
- Pulse Repetition Rate ..... 275 PPS (Avg)
- Average Video Power ..... 22 kW
- RF Frequency ..... 1250-1350 MHz and 2900-3100 MHz
- PFN Voltage ..... 2800 Volts
- Pulse Transformer Input ..... 6500 Amps
- Total PFN Impedance ..... 0.22 Ω
- PFN Impedance per Module .... 4.38 Ω
- Pulse to Pulse Voltage Regulation ..... Better than 0.02%

The modulator was designed so that it could be operated with two of the twenty modules removed and still perform satisfactorily. By using plug-in modules, a failed module can be unplugged for repair while the transmitter is placed back on line. The modulator can be run satisfactorily at lower power levels with up to half of the modules removed.

MODULATOR CIRCUIT DESCRIPTION

Figure 1 is a block diagram/schematic of the modulator system. Three phase AC power is controlled by a motor driven variac and fed to a step up transformer whose output is rectified and fed into an LC filter for use by the modulator. This 1500 VDC power supply is automatically regulated to ± 1% accuracy with the variac. When the transmitter is in standby, the input line voltage is sensed by the regulator which continuously adjusts the variac so that the proper power supply voltage is produced at turn on. This eliminates the slow manual run up present in many other power supply systems.

A command charge trigger is amplified and applied to four series SCR's which feed power supply voltage into the charging diode and charging choke. This allows a delay so that the solid state switches can recover after the main discharge. The PFN and switch section consist of 20 PFN modules connected in parallel. The charging input to each module is fused to disconnect any module that might fault during charging. Thus, the front end of all the PFN's are connected in parallel. The back end of each PFN is connected to a series string of four RSR's (reverse switching rectifiers) which are grounded at the pulse transformer. The capacitive terminal of each PFN is connected to one of the twenty identical primaries on the pulse transformer. Figure 2 shows the schematic of a PFN module and Figure 3 shows an actual module.

After the PFN modules are charged, there is a period of time before the "main bang" discharge during which a shunt regulator bleeds down the PFN voltage to a precise value. The minimum interpulse period (2700 µS) is divided up as follows:

900 µS for solid state switch recovery
1000 µS for charging
800 µS for precision regulating

The midpoint of the RSR stack in each of the twenty modules are capacitively coupled to a single pair of trigger RSR's that are biased to one half the PFN voltage. The main discharge trigger is amplified onto the trigger RSR's which in turn trigger all twenty stacks when they ground the coupling capacitors.

An 85:1 step-up pulse transformer combines the outputs of all the modules and cathode pulses the klystrons and twystrons to -122 kV.

The use of many PFN's improves the video pulse waveshape as it averages out the PFN ripple and provides a flatter top pulse to the load.

The Reverse Switching Rectifier used is the T40R which is manufactured by the Westinghouse Semiconductor Division in Youngwood, Pennsylvania. This device has a blocking voltage of 800 volts and a peak current rating of 2000 amps, with a di/dt capability of 3000 amps/microsecond. The RSR has a long history of successful development modulators which have been previously discussed in other papers.[1-8]

PFN CHARGER REGULATOR

One of the most significant contributors to the high performance of these transmitters is the shunt regulator which controls the pulse to pulse voltage on the PFN's to better than 0.02%. This allows the transmitters to provide exceptionally stable phase performance. The MTI Improvement Factor Limitation is well over 50 dB. Figure 4 shows the regulator. The shunt regulator is a high voltage triode connected across the charging input terminals to ground. A solid state amplifier compares a sample of the PFN voltage to a reference and drives the grid of the triode to bleed the PFN's down to the desired voltage. Because the staggered PRF rate varies by as much as ± 25%, the pulse to pulse PFN voltage variations would be 1.7% without the regulator.

By using a heavily filtered sample of the high voltage power supply as the reference, the modulator output level is then easily varied by adjusting the high voltage control. This permits the charger regulator to operate efficiently at all output levels. The regulator dissipates less than 4% of the total video power in the modulator.

PROTECTION AND MONITORING

Several modulator parameters are sensed and fed into protective shut down circuits which are displayed on the front of the control panel. They are:

- High voltage power supply overload
- High peak charging current
- PFN voltage too low
- Power supply voltage too high
- Modulator output pulse current too high
- Modulator backswing excessive
- Shunt regulator current too high
- Non-operating module (module either removed or not triggering)

Except for the last, each of these faults stops either the command charge trigger or the modulator discharge trigger before the next pulse, whichever is appropriate, and in some cases, the high voltage power supply is turned off.

Test jacks are provided for viewing the individual output currents from each module, as well as charging current, PFN voltage and modulator pulse voltage. Also displayed is the 112 kV pulse voltage.

Figure 5 is a picture of one of the transmitters with the doors open. Controls and displays are at the top of the center cabinet and test jacks for viewing various waveforms are lined up along the top of the right hand cabinet. Figures 6, 7, and 8 show the left, center, and right hand cabinets respectively, with their access doors open. The PFN modules are in the right hand cabinet and slots are provided beside them for storing spare modules if needed. The command charging circuits and charging choke are above the PFN modules and the high voltage power supply is spread across the bottom of the middle and left hand cabinet. The PFN shunt regulator is in the middle of the center cabinet.

CONCLUSION

The results of testing have proved that a high performance radar using a high powered solid state modulator is very reliable and can be manufactured in quantity without any need for "hand tuning". Plug-in solid state modules can be combined to provide a high power modulator, and the basic building blocks used in this modulator can easily be combined to provide various pulse widths, repetition rates and power levels for almost any application.

REFERENCES

1. E. H. Hooper and B. L. Jordan, "Advanced Reverse Switching Rectifier (RSR) Modulator," Final Technical Report, Air Force Weapons Laboratory, Kirtland Air Force Base, New Mexico.

2. R. A. Hill and W. R. Olson, "Lightweight High Power Modulator Uses RSR Switch Devices, Tenth Modulator Symposium, May, 1968, New York, New York.

3. J. B. Brewster and P. F. Pittman, "A New Solid State Switch for Power Pulse Modulator Applications, the Reverse Switching Rectifier, IEEE Conference Record of 1973 Eleventh Modulator Symposium, September, 1973, New York, p. 6-9.

4. R. A. Hill and R. A. Smith, "Application of the RSR Switch," IEEE Conference Record of 1973 Eleventh Modulator Symposium, September, 1973, New York, New York, pp. 95-105.

5. R. A. Smith and H. S. Fledmesser, "Lightweight Modulator Pulser," Final Technical Report RADC-TR-69-33, Rome Air Development Center, Griffiss Air Force Base, New York, March, 1969.

6. Final Development Report for Modular Solid State Modulator Development (Contract N00039-70-C-1506), U.S. Navy Department, Bureau of Ships, Electronics Division, November, 1970.

7. R. A. Gardenghi, E. H. Hooper and F. S. Zimmerman, "A New High Power RSR Solid State Switch", IEEE Conference Record of 1975 Power Electronic Specialists Conference, June, 1975, Culver City, California, pp. 313-317.

8. R. A. Gardenghi, "A Super Power RSR". Twelfth Modulator Symposium, February 1976, New York, New York.

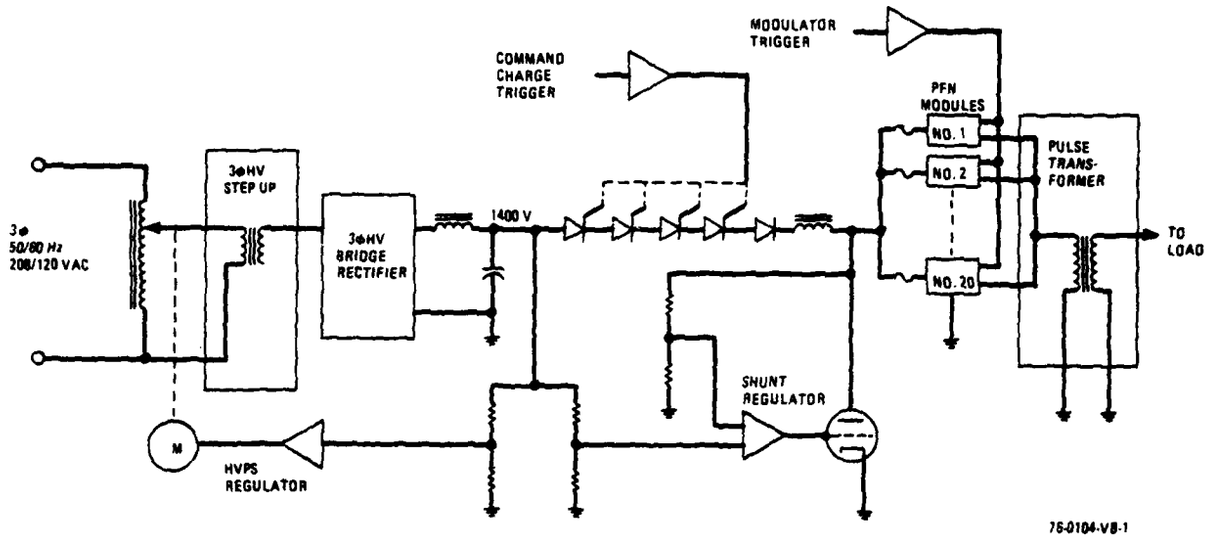

Figure 1. Modulator Diagram

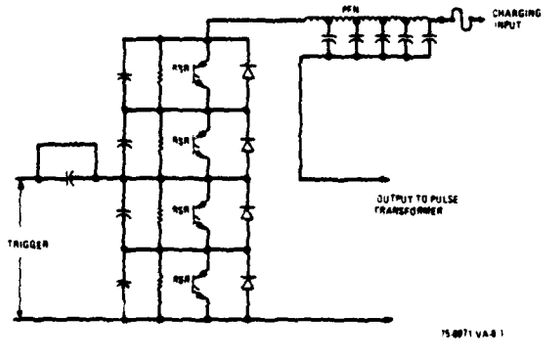

Figure 2. PFN Module Schematic

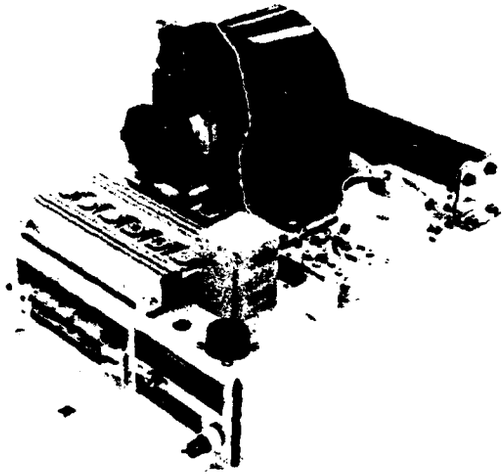

Figure 4. PFN Shunt Regulator

Figure 3. PFN Module

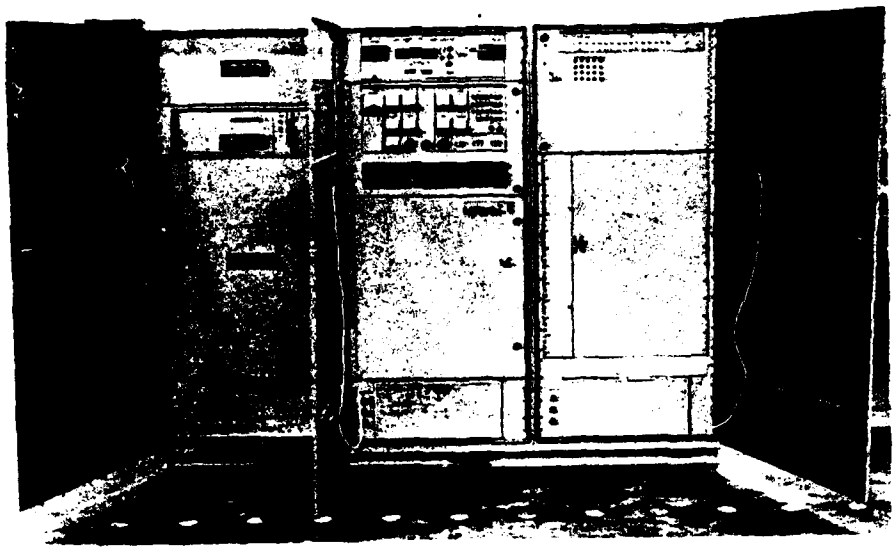

Figure 5. Air Defense Radar Transmitter

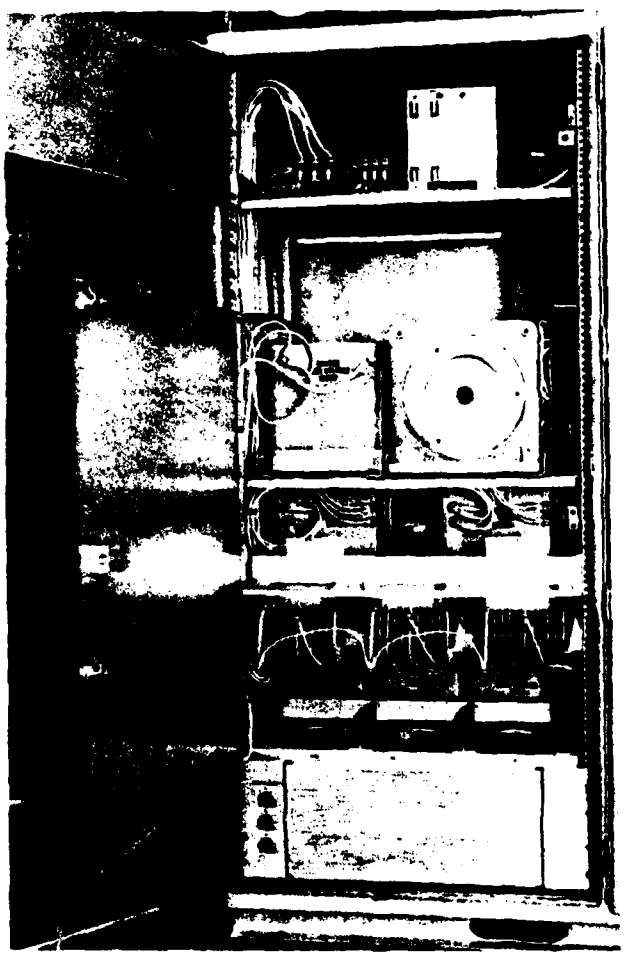

Figure 6. Left Cabinet

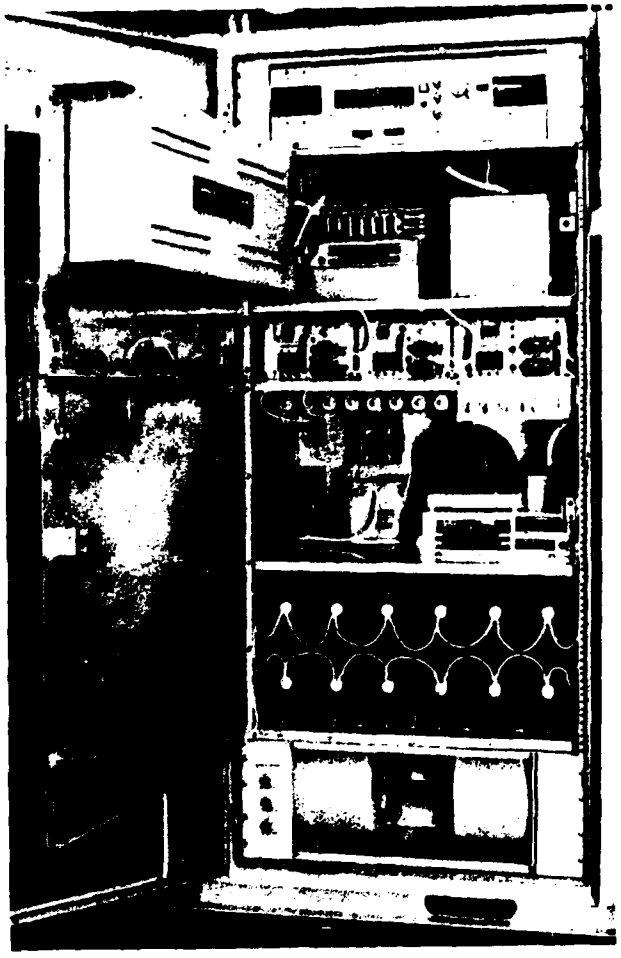

Figure 7. Center Cabinet

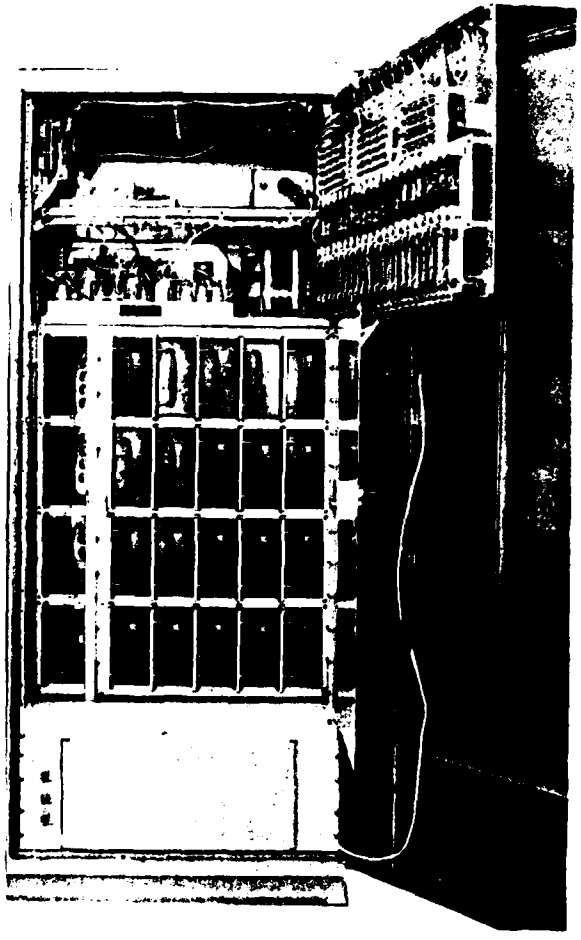

Figure 8. Right Cabinet

AD-A119 661 PALISADES INST FOR RESEARCH SERVICES INC NEW YORK F/G 9/5
IEEE CONFERENCE RECORD OF 1976 TWELFTH MODULATOR SYMPOSIUM, NEW--ETC(U)
1976
UNCLASSIFIED 76-CH-1045-4-ED NL

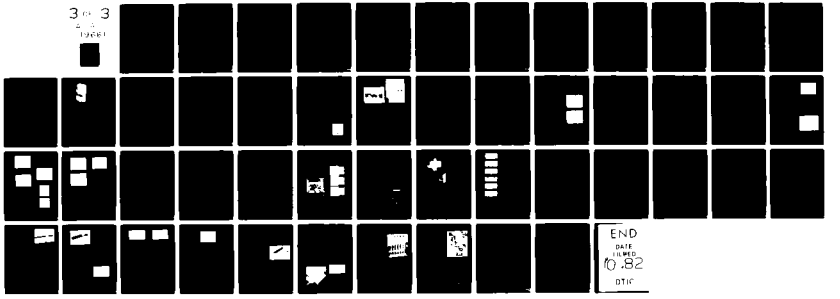

MAGNETIC SWITCH MODULATOR

Raffee Mgrdechian

Axel Electronics, Inc.
A Unit of General Signal Corp.
134-20 Jamaica Ave.
Jamaica, N.Y. 11418

A Modulator is presented which is switched by the saturation of a saturable reactor. The output of the Modulator pulses a coaxial magnetron.

The specifications for the Modulator are:

1. Input Peak Charge: +10KV @ 0.045 joules max.
2. Output Voltage: 14.5KV PK
3. Output Current: 17A PK
4. Pulse Width: 3DB points of detected RF (50% Current Pulse Amplitude), 0.12US ±.02US
5. Maximum PRF: 6350PPS
6. Pulse Transformer Reset Current 100MA.D.C.
7. Maximum Saturated Inductance of Saturable Reactor: 7.9uhy (stipulated)

Figure I shows the components of the Modulator within their housing.

Figure II indicates the additional circuitry external to the housing to complete the pulse modulator.

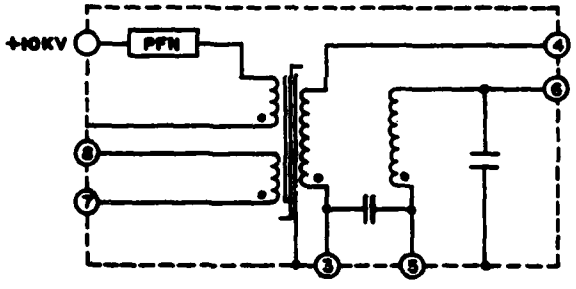

FIGURE I
Pulse Modulator Components

The Modulator

The load to the Modulator is a coaxial magnetron. Coaxial magnetrons require a controlled voltage rate of rise (Vrr). The Vrr control is usually achieved by adding a capacitor between the magnetron cathode and ground. This capacitor, called a despiker, is in addition to the magnetron tube capacitance and the stray capacitance of the pulse transformer. At high repetition rates the losses due to these capacitances must be considered in determining stored energy required at the PFN, otherwise pulse widths below specification limits are likely to appear at the output. The sequence of operation after the low voltage storage capacitors are charged (Figure II), is, with the application of a trigger to the SCR, the transfer of energy from the low voltage storage capacitors to the high voltage PFN capacitor takes place through SR-1. The saturable switch (SR-1) then saturates and its saturated inductance plus the pulse transformer leakage inductance are considered part of the PFN. More than one section for the PFN is impractical for narrow pulse widths due to the diminishing value of the inductance required. The pulse transformer at the start of the

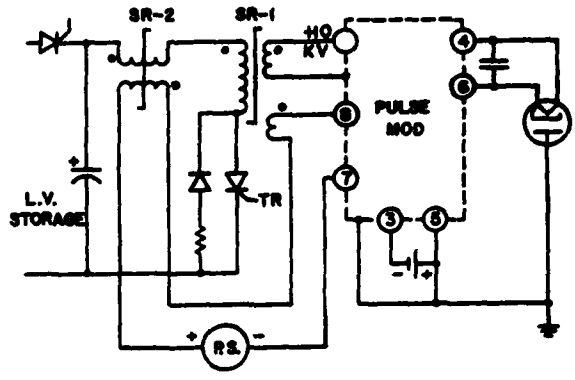

FIGURE II
Pulse Modulator

pulse discharge is biased in the negative region of its hysteresis loop, Figure III. After the pulse discharge is complete, the pulse transformer is reset through its reset winding preparatory to repeat of the charge-discharge cycle.

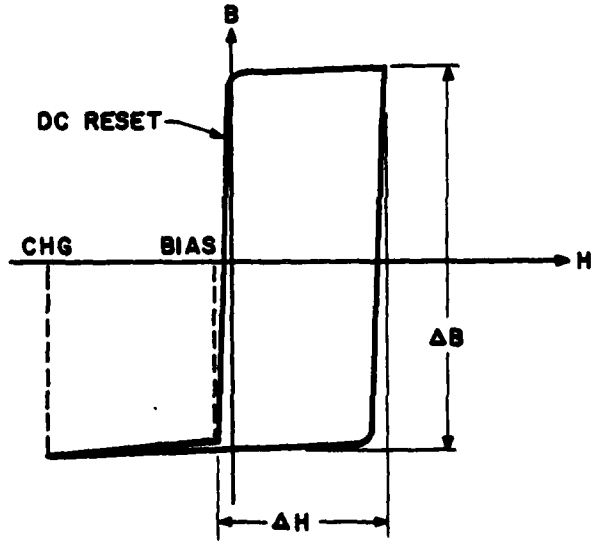

FIGURE III
Pulse Transformer Hysteresis Loop

The Pulse Transformer

The core selected is .001 mo-permalloy specified with a minimum hysteresis loop squareness of 85%. To

achieve maximum hysteresis loop squareness (for high pulse permeability), an uncut, unimpregnated core is selected to be cased at Axel Electronics, with provision for dielectric cooling oil to freely circulate around the core. For narrow pulse widths the volts per turn are high to keep leakage inductance low. The high volts per turn generate higher core losses whose heating effects must be controlled by the circulating cooling oil. The net area of the core is 0.0963 square inches and the magnetic length is 5.73 inches. A turns ratio of 3/1 step up is selected.

The static load to the PT is:

$$R_L = \frac{14500}{17} = 853 \text{ ohms}$$

Reflected to the primary of the PT:

$$R_{PRI} = \frac{853}{9} = 94.78 \text{ ohms}$$

The pertinent data of the PT is:

1. L_{KPRI} = 0.64uhy
2. Open circuit inductance primary = 109uhy
3. Distributed capacitance = 28pf
4. Total losses = 29 watts

The Pulse Forming Network

The specification limits the maximum energy to be stored in the PFN to .045 joules. The maximum PFN capacitance at 10KV charging voltage is,

$$C_{PFN} = \frac{\text{Joules } x2}{V^2} = \frac{(.045)(2)}{100 \times 10^6}$$

$$C_{PFN} = .0009\text{ufd (Maximum)}$$

To determine the actual value of capacitance to be selected, the power delivered to the load plus all the losses must be considered.

$$P_L = E \cdot I \cdot du = 14500 \times 17 \times .12 \times 10^{-6} \times 6350 = 187.83W$$

$$P(\text{Stray Capacity})^* = \tfrac{1}{2}(80)(10^{-12})(14.5)^2(10^{-6})(6350) = 53.4W$$

PFN losses (2% of stored power) = 5.72W

PT losses = 29.00W

Total Input Power = 275.95 watts

Converting the input power required to joules we get,

$$\text{Joules} = \frac{275.95}{6350} = .0435$$

which meets the requirement of .045 joules maximum. Converting to capacitance

$$C_{PFN} = \frac{2(.0435)}{100 \times 10^6} = .00087\text{ufd}$$

This value of capacitance is taken as a nominal value with the maximum capacitance limit of .0009uf, reflecting the maximum required by specification.

The impedance of the PFN is set at:

$$Z_{PFN} = 1.05 \times R_{PRI(PT)} = 1.05 \times 94.78 = 99.52 \text{ ohms}$$

*Stray capacitance is the sum of PT, Tube, Despiker.

The PFN inductance must be:

$$L = Z_{PFN}^2 \times C_{PFN} = 8.62\text{uhy}$$

The saturable reactor saturated inductance must be less than:

$$L_{S.R.} \leq L_{PFN} - L_{KPT}$$
$$\leq 8.62 - 0.64$$
$$\leq 7.98\text{uhy}$$

7.9uhy was stipulated for $L_{S.R.}$

The PFN at discharge appears as in Figure IV.

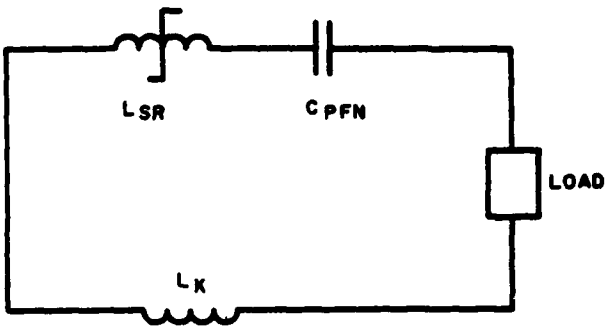

FIGURE IV
PFN Equivalent Circuit At PFN Discharge

Circuit Components

The SCR

The di/dt and peak current specifications are limiting factors in the allowable discharge time of the low voltage capacitor. The faster the charging time of the PFN capacitor, the less severe the volt-second requirement for SR-1. The charging time of the PFN capacitor is controlled with the inductor SR-2 (Figure II). If the di/dt requirement of the SCR require a delay before discharge of the low voltage capacitor then a saturable delay reactor is required with specifications established for,

1. Delay Time
2. Saturated Inductance
3. Open Circuit Inductance

Magnetic Switch (SR-1)

The saturated inductance of SR-1 was determined when the PFN was designed. The charging time was established in the SCR evaluation. The volt-second requirement is known for SR-1. The turns ratio is established by relating the peak charging voltage of the PFN to the low voltage capacitor voltage, less the SCR voltage drop. The SR-1 specifications would list,

1. Turns Ratio
2. Volt-Second requirement
3. Saturated Inductance
4. Core Reset requirement

Circuit Performance

The charge and discharge of the PFN capacitor is shown in Figure V.

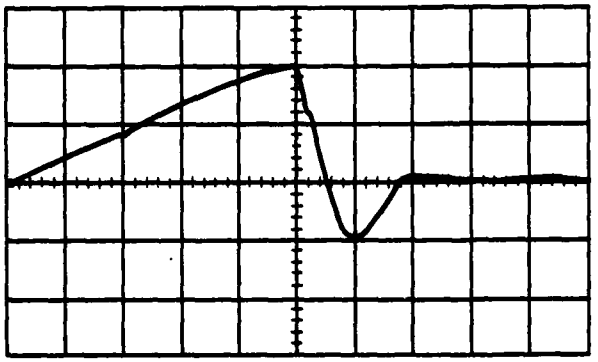

FIGURE V
Charge - Discharge PFN
Vertical - 5KV/Div; Horizontal - 0.2US/Div

The voltage at the magnetron cathode is shown in Figure VI.

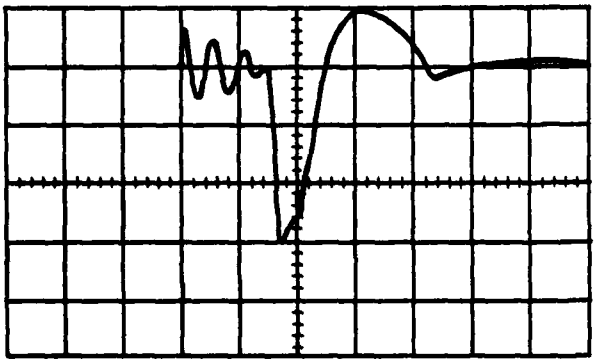

FIGURE VI
Magnetron Cathode Voltage
Vertical - 5KV/Div; Horizontal - .5US/cm

The magnetron current pulse is shown in Figure VII.

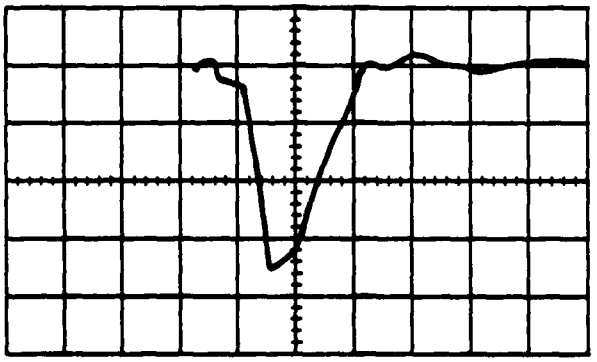

FIGURE VII
Magnetron Current
Vertical - 5A/Div; Horizontal - .1US/Div

The Detected RF is shown in Figure VIII.

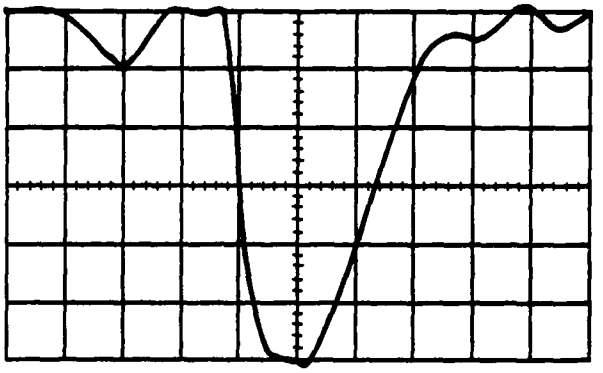

FIGURE VIII
Detected RF
3DB Center - Horizontal .1US/Div

Figure IX shows the unit.

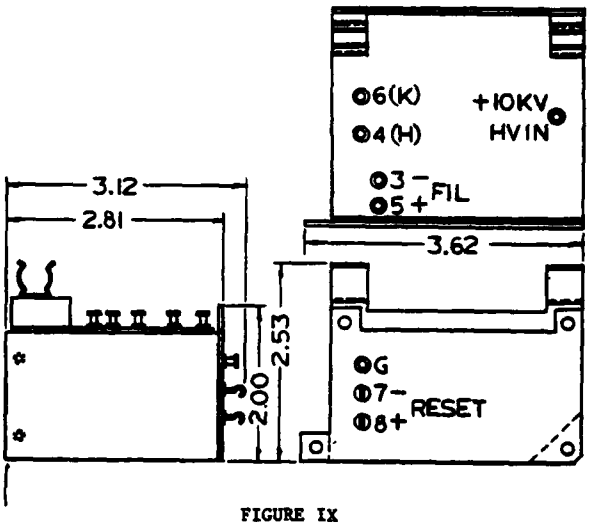

FIGURE IX
Pulse Modulator Housing

Conclusion

A narrow pulse has been produced with a "solid state" modulator. The dificulties usually encountered in high step up pulse transformer modulator is overcome by using a magnetic switch, properly specified, at higher impedance levels. At higher impedance levels for the PFN, circuit inductance can be tolerated. The high step up type modulator does not adapt itself to narrow pulses because of the limiting factors of the SCR di/dt ratings. To introduce a saturable delay reactor at low impedance levels for di/dt control would be satisfactory if also the saturated inductance and loop inductances can be reduced to disappearing values. Both types of modulators have their specific usefulness and must be properly evaluated for a given requirement.

SOLID-STATE SWITCHING DEVICES ADAPTED TO THYRATRON PULSE CIRCUITS

V. Nicholas Martin

Sanders Associates, Inc.
Nashua, New Hampshire

Summary

This paper reports the early, often forgotten, works of engineers whose novel circuits employed spark gaps and thyratrons with their inherent limitations. These limitations are often overcome by substituting contemporary solid-state switching devices, thereby providing very useful circuits to meet current needs for the generation of high power video and RF pulses.

Introduction

For engineers specialized in the development of high power pulse generating equipment, the Proceedings of the Modulator Symposia are priceless documents revealing the achievements of engineers here and abroad. When confronted with a new radar transmitter design or when an existing modulator equipment problem arises, after exhausting one's mind from past experience, one falls back upon the Modulator Symposium Proceedings.

Frequently, one reverts to basics as expounded in "Pulse Generators" - Volume V[1] and Früngel's "High Speed Pulse Generators" - Volumes I and II.

Aside from IEEE technical publications and trade journals, there are buried within the annals of high power switching and pulse generation circuit developments a frequently forgotten source of information, i.e., patent literature. This becomes very apparent to the engineer who files for a patent for his newly-developed circuit, often only to find that someone else not only developed a similar circuit in the past, but had it patented with claims for half a dozen or more applications and variations. Such has been the case of the author, who in the past presented papers[6, 14] of original work only to find out later that several people had received patents for similar circuits.

The disappointment is overcome, somewhat, when reprints are ordered of the referenced patents cited on the one in conflict with his own disclosure. In turn, a review of each of the referenced modulator circuit patents leads to obtaining reprints of the additional patent references; thereby pyramiding to a formidable library of information.

1. Line-Type Modulator Producing Output Pulses With An Amplitude Equal to the DC Input Voltage

The study of H. Anger's patent[2] discloses certain limitations that are not revealed in the detailed analysis and discussion of the revised Anger Circuit in Volume . - Pulse Generators. These limitations are not applicable to SCR's if they were directly substituted in place of the original thyratrons. The revised Anger circuit, however, is applicable for operation with a single SCR as discussed below.

One version of the Anger circuit, in a contemporary embodiment using SCR's is shown in Figure 1A. Neglecting circuit losses, it theoretically provides output pulses having an amplitude equal to the DC source voltage if the network impedance is equal to that of the load impedance. For the network polarity shown for Condition 1, SCR-1 has 2V across it comprising the battery and network voltages. After SCR-1 is fired, the resulting current produces a voltage of amplitude V across the load. Immediately after the output pulse has been generated, the network voltage reverses the polarity to Condition 2, or that of the power supply in the forward direction. At a later instant, SCR-2 is fired and the resulting mismatch of network discharge into inductor L causes a reverse in voltage to the polarity shown for Condition 1. This process of alternately firing SCR's to provide a reverse voltage at the network which adds to the power supply voltage is evident from the accompanying waveforms.

In order to eliminate the need for the second SCR:SCR-2, H. Anger substituted the choke L, which is shown in Figure 1B. It's value is designed such that it resonates with the total network capacitance at a frequency, which is one-half the modulator pulse repetition rate . order for the potential in the transmission line to reverse properly.

As before, if one initially assumes a reverse voltage on the pfn, equal to the supply voltage, when the SCR is fired the output voltage equals the supply voltage for a matched condition between the pfn and load. At the termination of pulse, the open-ended transmission line is charged to V and current begins to flow through the series circuit composed of the choke and pfn. The current flows

until the pfn is charged in the oposite direction from the former condition at which time the potential across the SCR is equal to 2E.

With a slightly negative impedance mismatch between load and pfn and through the use of fast recovery SCR's, this circuit would be applicable in contemporary solid-state modulators.

2. Generation of Coded Pulse Trains of Closely Spaced Pulses

In his original disclosure filed in 1945/awarded in 1952, D. F. Winter[3] employed two thyratrons and two pulse transformers to provide closely spaced pulses to drive a magnetron. In an updated circuit revision as shown in Figure 2A, by combining the pulse transformers into a single transformer and providing a DC forward bias on SCR-2 to preclude the effects of dV/dt turn-on[4], the circuit allows alternate pulses to be generated by charging the pfn through SCR-1 and discharging it through SCR-2.

The idealized waveforms neglect SCR losses and impedance mismatches by assuming that the network impedance is matched to the load impedance. Circuit logic would program the SCR gates for codes to be transmitted by sonobuoys, radar beacons and IFF transponders.

D. F. Winter references J. A. Rado's patent[5]: "High Frequency Generator" also filed in 1943 and awarded in 1946. Rado used two thyratrons for the generation of a coded pulse train, from a single series of triggers utilizing the shift in anode potential of the discharge thyratron to enhance the alternate acceptance of triggers to fire it.

In an improvement on this circuit, Rado employed two alternately fired thyratrons whose SCR equivalent is shown in Figure 2B. In considering the operation, assume SCR1 and 2 to be nonconducting. Then capacitor C is charged to power supply voltage V and through voltage divider action capacitors A and B are charged to ½V. When SCR1 is triggered, the A capacitors are discharged and a pulse is delivered to the output winding. The discharge of the A capacitors acts like an effective short so that the alternate capacitors B charge to +V. When SCR2 is fired, the B capacitors discharge resulting in another output pulse and capacitors A charge to +V.

3. Variable Pulse Width Generation System

The generation of variable pulse width pulses in a line type modulator was reported at the Sixth Thyratron and Modulator Symposium[6] by me. This was a report on original work done in order to meet the needs for a proposed lightweight radar transmitter/modulator. A preliminary patent search disclosed several patents[7,8,9] awarded for the same circuit techniques.

An embodiment of this technique is shown shown in Figure 3. Here it can be seen that SCR's are connected at both ends of the pulse forming network. If only one SCR is fired, the output pulse would have a time duration of $2T_o$. Simultaneous firing of both SCR's results in two pulses in the same time phase with equal time durations. If on the other hand, t_2 lags t_1, then the output of SCR-1 is $T_o+(t_2-t_1)$.

For more effective operation, the otherwise wasted energy fed to the dummy load could be fed back by T_2 to the power supply.

It is interesting to note that in the reference cited, the variable time delay between incoming triggers is controlled by means of varying the resistance of an RC integrator at the grid of the second thyratron. In each disclosure, a single incoming trigger is discussed with thyratron grid bias lines, slopes of RC integration voltage, and difference in firing points being emphasized. The disclosure of W. S. Ivans, Jr.[9] refers to the Rado patent for close pulse generation and employs four thyratrons; a pair to charge the network, the second of which is delayed in firing to produce a variable output pulse. The second pair discharges the networks, the second of which is delayed in firing to produce a variable output pulse.

4. An Accurate Current Regulator for a Sin^2 Pulse Modulator

The present circuit was originally disclosed in two patents [10, 11] by A. F. Standing employing a thyratron as a modulator switch. The circuit comprises a line-type modulator with a center-tapped pulse transformer secondary winding. An LC circuit is connected between the center-tap and thyratron anode.

Figure 4 shows an embodiment of this circuit employing an SCR. The coupling between coils L1 and L2 is mechanically controlled by means of varying the distance between them along a common dielectric bar. The sin^2 pulses are produced by the use of two exponentially decaying discharge circuits. These two decaying currents are rendered 180° out of phase by passing them through the primary and secondary of the pulse transformer.

Since the initial discharge currents have been found to be excessively high for most thyratrons, the author wound the inductors L1 and L2 on mandrels and varied the mutual inductance of the oppositely wound coils to provide positive mutual inductance. This limits or regulates the current in the modulator switch and very accurately controls the shape of the sin^2 output pulses.

5. Pulse Voltage Multiplication Through The Use of Multiple Delay Lines and One SCR

The use of a pair of delay lines for parallel charging and series discharging is employed in the well-known Blumlein circuit. An increase in the number of delay lines, however, requires a commensurate increase in the number of modulator switches.

A basic circuit improvement utilizing a plurality of delay lines and a single ignitron or thyratron is disclosed by L. Greenwald in his patent [12]. The invention discloses a line pulse modulator capable of generating a voltage nE with the use of a single electronic switch, wherein n corresponds to the number of delay lines used in the modulator and E is the power source voltage connected to the modulator.

Figure 5A shows an embodiment of this circuit employing an SCR or series SCR's as the modulator switch. The circuit incorporates four pfn's having equal impedances and a load having an impedance equal to four times that of the individual network impedance. The pfn's comprise two 2-terminal and two 4-terminal networks. Prior to SCR firing the distribution of voltages is as shown in Figure 5B. The voltage across each pfn is $2V_{DC}$ due to the voltage doubling action resulting from the DC resonant charging of the total pfn capacitance with the charging choke. After the firing of the SCR, an effective [illegible] is placed across the 4-terminal networks resulting in a reversal polarity after the wavefront reaches the end of the line. The resulting equivalent circuit is shown in Figure 5C. Here it can be seen that the four networks are now connected in series-aiding across the magnetron load, and through DC resonant charging with the resulting doubling, providing four times the DC voltage feeding the modulator.

Figure 5D illustrates how additional pairs of networks may be added for higher multiplication factors without the use of a pulse transformer.

6. Line-Type Modulator Impervious to High Load Impedances

Greatest efficiency and maximum energy transfer result in a line-type modulator when the characteristic impedance of its pulse forming network is equal to the load impedance. Conventionally, the load impedance is made slightly lower than that of the network to produce a negative mismatch resulting in a negative voltage across the pulse forming network immediately after pulse discharge. This negative voltage assists in hydrogen thyratron gas deionization or SCR recovery, depending upon the type of modulator switch being used.

When the load impedance is higher than the pfn impedance, the resulting positive mismatch inhibits modulator switch recovery, thereby producing a short circuit across the DC power supply.

J. Grabowski[13] employed a second thyratron to clamp the output voltage of a lightly loaded pulse to the DC power supply output capacitor. Figure 6A illustrates an embodiment of this circuit using a silicon diode, D, whose cathode is connected to the output capacitor of the power supply.

Through a suitable choice of turns ratios, the tertiary or clamp winding may be so designed that if the load impedance increases or becomes open-circuited, the commensurate build-up of voltage across the main output winding and clamp winding will cause the clamp winding voltage to exceed that of the power supply voltage. At this time, the diode will conduct, return part of the unused energy to the power supply, and present a near matched condition of reflected load and network impedances, to enhance SCR recovery.

One additional feature of the clamp circuit is that it provides a substantial improvement in rise-time in high load impedance circuits. This is explained from the fact that when a pulse transformer is unloaded or open circuited, its output voltage could theoretically approach four times that of its normally loaded value into a matched load. When the clamp voltage is attained, the fast voltage rise-time, associated with the unloaded case, is attained at this level, with a net result of a faster rise time.

Application of the circuit shown in Figure 6A could be used to provide parallel pulsed anode power to a succession of cascaded RF amplifiers. Previously, when using a line-type modulator to plate-pulse an RF amplifier chain, during the RF tuning/tweaking or adjustment of bias, positive mismatches would result causing overloads. The present circuit eliminates this problem by clamping to the power supply voltage.

A variation of this circuit was employed by the author in a high duty cycle hard-tube modulator. The ferrite core pulse transformer design produced a very large backswing voltage. Conventional backswing diode/resistor circuitry would have dissipated excessive power. Figure 6B shows how the energy released from the pulse transformer during the post pulse period is clamped by the diode to the power supply, thereby limiting the magnitude of inverse voltage applied to the klystron tube and returning the stored energy released by the transformer back to the power supply.

7. Generation of High Voltage Pulses from a Low Voltage DC Source Without a Pulse Transformer

This circuit was developed by the author through the use of SCR's and reported at the Eighth Symposium on Hydrogen Thyratrons and Modulators in 1968[14]. Prior to publication,

an application for patent was made and a similar approach using thyratrons was cited in a patent of A. A. Nims, Jr. of Westinghouse in 1954[15].

A mathematical treatise is presented in the technical paper. For reference purposes, however, the circuit using SCR's is shown here in Figure 7. Here it can be seen that triggers are simultaneously fed to SCR1 and SCR2, such that there is a reverse voltage reflected to the network due to the shorting action of SCR2. During each recharge cycle, the progressively higher inverse voltage adds to the supply voltage for increased voltage doubling. As shown in the waveforms at the time t_c only, the main SCR1 is triggered, thereby releasing a large pulse of voltage to the load.

A modification of this circuit would be to substitute a step-up pulse transformer in place of the load resistance in order to obtain a further increase in voltage.

References

1) "Pulse Generators" - G. N. Glasoe and J. V. Labacqz, Volume V, M.I.T., Radiation Laboratory Series.

2) Patent No. 2,698,900 dated 4 January 1955, "Delay Line Pulse Generator" - H. O. Anger.

3) U. S. Patent No. 2 603,752 dated 15 July 1952 - "Voltage Pulse Generator" - D. F. Winter.

4) "Tail-Biter Circuit Techniques Employing Solid-State Switches to Promote Fast Fall Times" - V. N. Martin, Presented at I.E.E.E. - IGA Group Annual Meeting, Detroit, Michigan, October 1969.

5) U. S. Patent No. 2,409,897 dated 22 October 1946 - "High Frequency Pulse Generator" - J. A. Rado.

6) "Generation of Output Pulses Having a Continuously Variable Pulse Width in a Line-Type Modulator" - V. N. Martin, Presented at the Sixth Hydrogen Thyratron and Modulator Symposium, Fort Monmouth, N. H. 1960.

7) U. S. Patent 2,605,449 dated 29 July 1952 - "Pulse Generator" - G. F. Schrader.

8) U. S. Patent 2,869,038 dated 13 January 1959 - "Thyratron Variable Pulse-Width Generator" - H. L. McCord.

9) U. S. Patent 2,575,961 dated 20 November 1951 - "Variable Width Pulse Generating System" - W. S. Ivans, Jr.

10) U. S. Patent 2,990,481 dated 27 June 1961 - "Shaped Pulse Modulator" - A. F. Standing and C. J. Miller.

11) U. S. Patent 3,110,822 dated 12 November 1963 - "Pulse Generator" - A. F. Standing.

12) U. S. Patent 2,474,243 dated 28 June 1949 - "Line Pulse Modulator" - L. Greenwald.

13) "Output Voltage Clamper with Regulating Action for Line-Type Modulators" - S. J. Grabowski, Presented at the Fifth Hydrogen Thyratron and Modulator Symposium, Fort Monmouth, N. J., May 1958.

14) "High-Efficiency Solid-State Line-Type Modulator and Active Tail-Biter Adaptable to Pulsing Capacitive Loads" - V. N. Martin, Presented at the Eighth Symposium on Hydrogen Thyratron and Modulators, Fort Monmouth, N.J. May 1964.

15) U. S. Patent 2,677,053 dated 27 April 1954 - "Pulse Generator" - A. A. Nims, Jr.

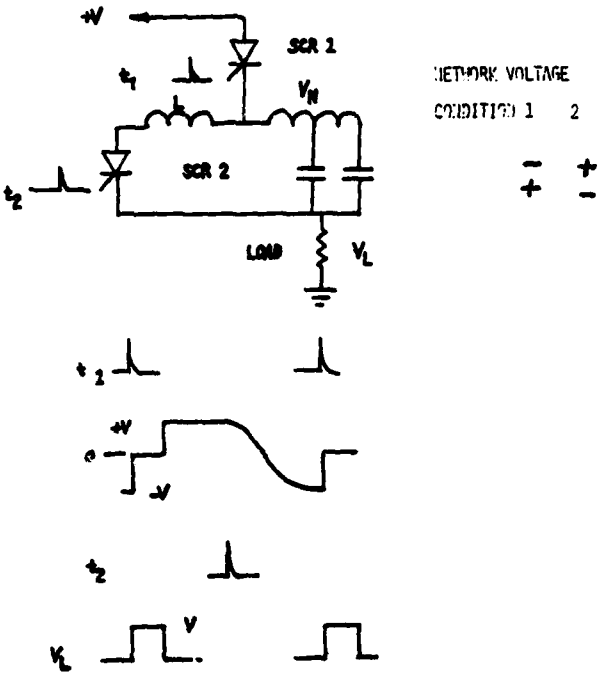

FIGURE 1A PULSE GENERATOR WHOSE OUTPUT PULSE VOLTAGE EQUALS SUPPLY VOLTAGE USING TWO SCR'S.

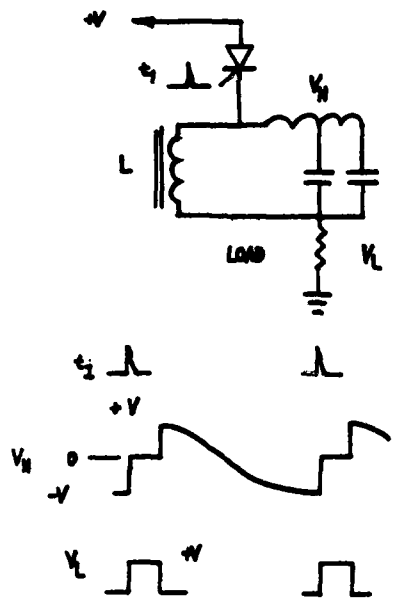

FIGURE 1B PULSE GENERATOR WHOSE OUTPUT PULSE VOLTAGE EQUALS SUPPLY VOLTAGE USING A SINGLE SCR

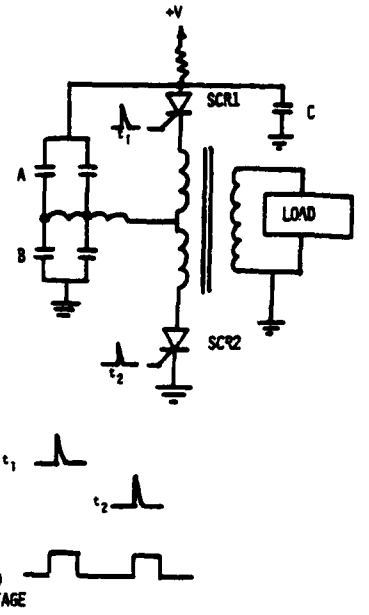

Figure 2B - GENERATION OF CLOSELY SPACED PULSES BY ALTERNATELY FIRING SCR's

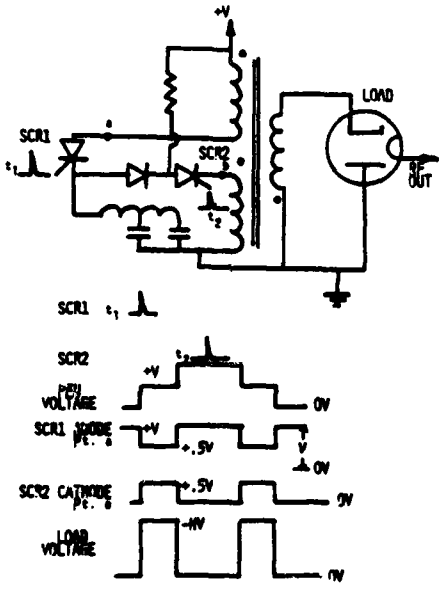

Figure 2A - GENERATION OF PULSE TRAINS OF CLOSELY SPACED PULSES

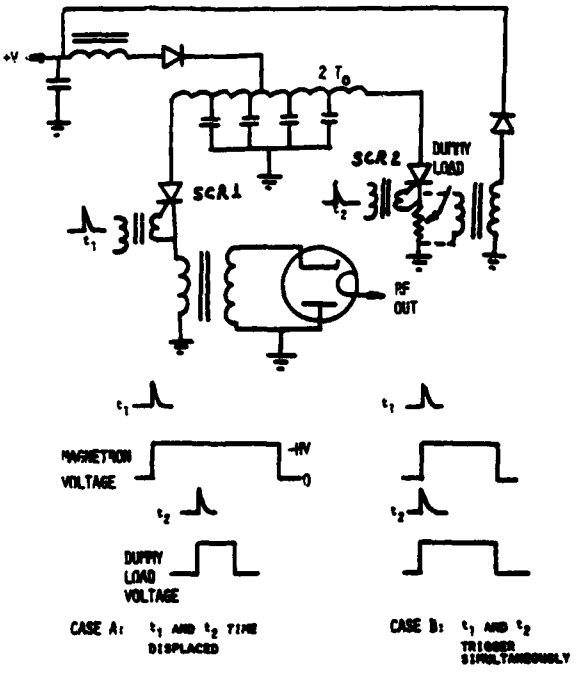

Figure 3 - VARIABLE PULSE WIDTH GENERATION IN A LINE-TYPE MODULATOR

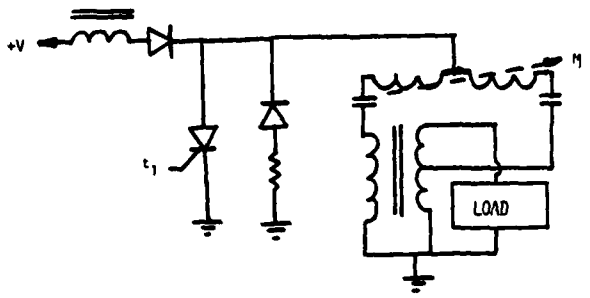

FIGURE 4 - AN ACCURATE CURRENT REGULATOR FOR SIN² PULSE GENERATION

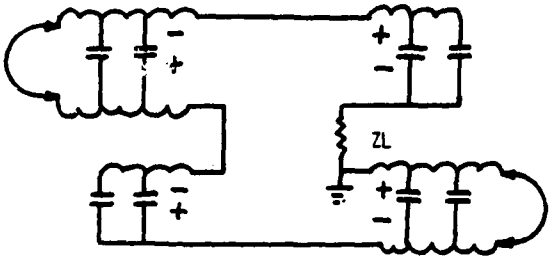

FIGURE 5C - EQUIVALENT CIRCUIT AFTER SCR FIRING AND VOLTAGE REVERSAL FROM END OF LINE SHORTING

$$V_N = 2\,V_{DC}$$

$$Z_L = 4\,Z_N$$

$$I_L = \frac{4\,V_N}{4\,Z_N + Z_L} = \frac{V_N}{2Z_N}$$

$$V_L = I_L Z_L = \frac{V_N}{2Z_N} \times 4Z_N$$

$$V_L = 2\,V_N$$

$$V_L = 4\,V_{DC}$$

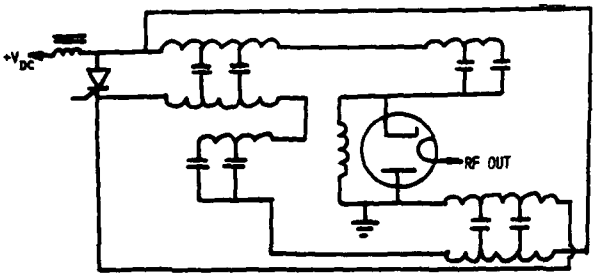

FIGURE 5A - PULSE VOLTAGE MULTIPLICATION CIRCUIT EMPLOYING MULTIPLE DELAY LINES AND ONE SCR

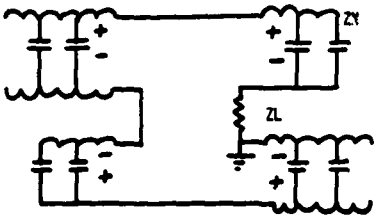

FIGURE 5B - EQUIVALENT CIRCUIT BEFORE SCR FIRING.

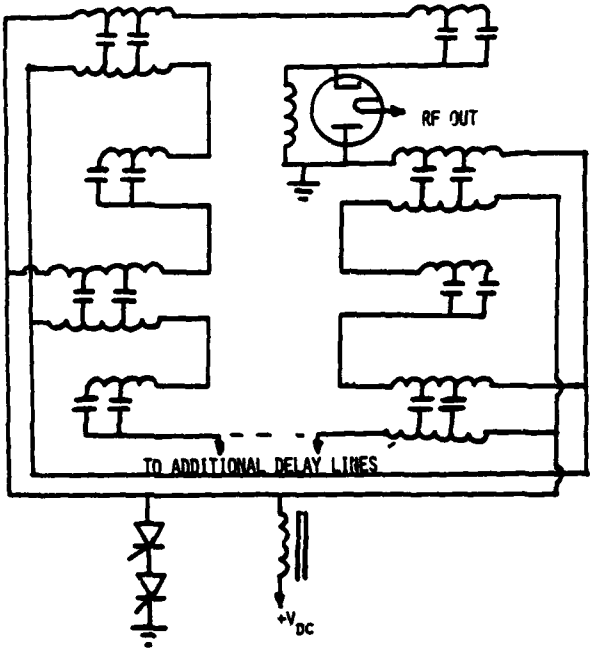

FIGURE 5D - HIGH VOLTAGE PULSE MULTIPLIER USING MULTIPLE NETWORKS

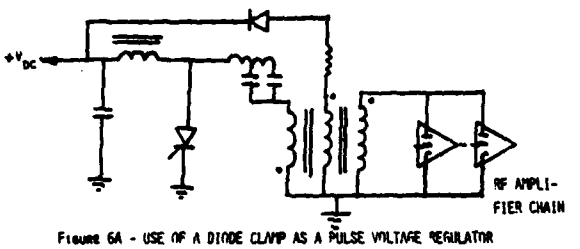

Figure 6A - USE OF A DIODE CLAMP AS A PULSE VOLTAGE REGULATOR

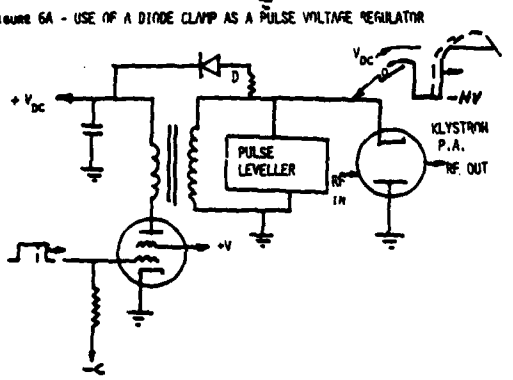

Figure 6B - USE OF A HIGH VOLTAGE DIODE TO CLAMP BACKSWING VOLTAGE TO POWER SUPPLY LEVEL

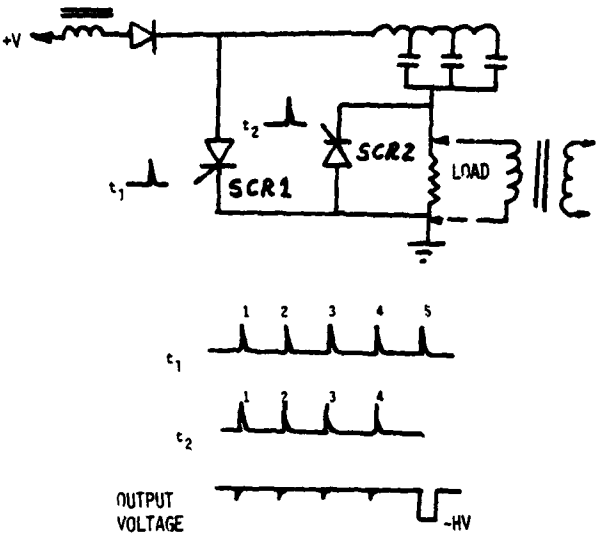

Figure 7 - HIGH VOLTAGE PULSE GENERATOR FROM A LOW VOLTAGE DC SOURCE

COMPACT, ULTRA HIGH DENSITY, RADAR POWER AMPLIFIER

by Giovanni Scerch and Paolo Porzio

Selenia S.p.A. - Rome - Italy

1. Summary

This paper describes the main solutions that have allowed the realization of an ultra compact solid state modulator for a MTI frequency agile medium power TWT amplifier.

This paper will be concerned primarily with a general description of the modulator placing special emphasis on two important items of its design: the TWT solid state grid driving circuit, employing SCR, and the cooling and insulating system realized by FC liquid.

2. Amplifier Characteristics

The tube used in this amplifier is a gridded electron gun PPM TWT and it is driven directly by a solid state amplifier due to its high gain (50 db).

The output peak power is about 15 KW and the average power is about 200W at C frequency band. Due to MTI requirements all cathode HVPS and grid modulator circuits have been designed to be extremely stable in voltage to allow high phase and amplitude stability for the output r.f. The high voltage path, which supplies cathode and collector voltages is a convention al one.

The cathode is fixed at -25 KV by a very stable power supply while a second HVPS between cathode and collector depresses this one at -12.5 KV respect to ground level.

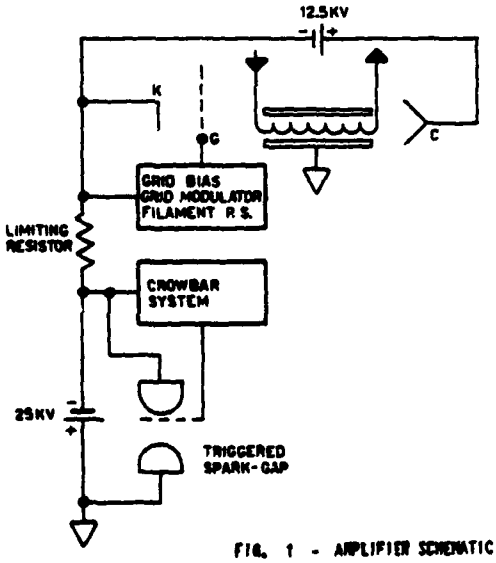

FIG. 1 - AMPLIFIER SCHEMATIC DIAGRAM

A crowbar system[1] prevents the discharge of H.V. capacitor energy into TWT in case of malfunction, thus avoiding its destruction.

Fig. 1 shows the complete amplifier schematic diagram.

3. Grid Modulator Circuit

The TWT grid modulator has been realized using solid state techniques.

The swing that it supplies to the grid is about 500V and its length can be adjusted between 2 and 5 μs. Pulse repetition rate can be as high as 5.000 pulses/s.

This modulator schematic, which is a particular modification of the conventional line type modulator, is shown in fig. 2.

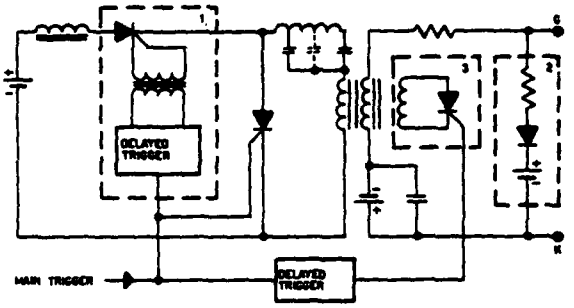

FIG. 2 - GRID MODULATOR SCHEMATIC

Modifications are pointed out in the dotted line squares 1, 2, 3 of this figure. A S.C.R. has been used as switching element. It is designed for pulse operation with controlled current and recovery time (about 10 mA, 20 μs). It is necessary to limit the current in the S.C.R. immediately after the pulse to a value and for the time said above to be sure of its recovery.

When the pulse generator works at high repetition rate, this condition can be achieved only by delaying the onset of the pulse forming network, being the charging inductance normally limited to mH value by the necessity to have a very short charging period[2]. Its minimum value is normally limited only by the allowed rate of rise of voltage on the S.C.R. switching element during the charge.

In the described modulator the aforementioned condition has been reached by replacing the conventional charging diode with a S.C.R. switched device. It is triggered on, starting the charging period, about 20 μs after the main pulse (square 1 fig. 2). The modificat-

ions in the discharging circuit have the scope to have a flat top of the grid pulse (square 2) and to control its width (square 3).

A clipper fast switching diode polarized with a very stable power supply cuts the pulse to some very stable value, thus avoiding any oscillations and decay on the top of the pulse (square 2). This condition is necessary to achieve a very stable phase and amplitude modulation in the r.f. pulse during the transmitted pulse and from pulse to pulse.

It is to be noted that in case of a short circuit of the clipper diode a positive D.C. voltage can remain on the grid tube causing the grid destruction. In this case a very fast protection (/us time) short circuits clipper polarization power supply fixing a negative bias grid voltage.

The square 3 shows the circuits realized to control the pulse width. A S.C.R. coupled to the transformer through a third winding short circuits the pulse at some adjustable pulse length. The stop of the pulse is realized by a trigger delayed with respect to the S.C.R. switch one, from 2 and 5 /us. The third winding is realized to match the primary impedence to S.C.R. characteristics.

It is matter of course that the short circuits, and in consequence the decay time of time of the pulse, is limited by the leakage inductance of the transformer. Also the law of decay depends on transformer parameters. It has been necessary to minimize this leakage inductance and to optimize the transformer parameters to have a minimum of pulse decay time.

A computer simulation and optimization of grid modulator has been made. Computer analysis of waveshape shows close agreement to actual test results on the realized modulator. The characteristics are: pulse rise time 0.1 /us, pulse decay time 0.15 /us. As mentioned at the beginning; pulse amplitude is about 500 V, pulse length 2-5 /us and pulse repetition rate up to 5000 pulses/s.

4. Technological Solution

One of the main requirements of the amplifier was to minimize the size of the complete modulator.

As mentioned above, the microwave tube has a gridded electron gun. This allows the possibility of controlling the electron beam by a relatively low voltage pulse applied between grid and cathode, keeping constant cathode to ground D.C. power supply. However, as it is possible to see from fig. 1, this solution implies the necessity to have many amplifier circuits at a high voltage level.

This is the situation on one hand for grid bias power supply, grid modulator and regulated filament power supply, and, on the other hand, for all those circuits needed to bias and trig ger the hydrogen thyratron used, as, switch in the crowbar circuit.

It follows that there is necessity to spa ce all these circuits referred to high voltage from ground level, and therefore to increase the transmitter size. On the other hand, the dimensions of dissipative components can be re duced increasing their heat transferring capability. One of the most effective ways to transfer heat from electronic components is to keep them in direct contact with a cooling liquid at boiling temperature. In this way, it is possible to obtain very high transfer of heat at relatively low difference of temperature between components and liquid surfaces.

Both these conditions can be reached by putting the amplifier circuits in a liquid system, which provides high voltage insulation as well as cooling for modulator components.

The liquid used is FC75 (a Fluorochemical liquid) that ensures both insulating and cooling characteristics. Its boiling temperature is about 100 degrees centigrade at normal pressure, and its electric strength about 33 KV/mm. All the transmitter circuits are immersed in this liquid. Owing to its high electric strength with respect to the air, it is possible to minimize the space between high voltage circuits and ground.

Owing to its cooling capability, it is possible to reduce size and weight of dissipative components, especially to magnetic ones. From this point of view, it is useful to present the results of some tests performed on a typical power supply transformer to investigate the possibility of strongly reducing its dimensions and weight, within the limits of regulation allowed, core and winding increase of temperature.

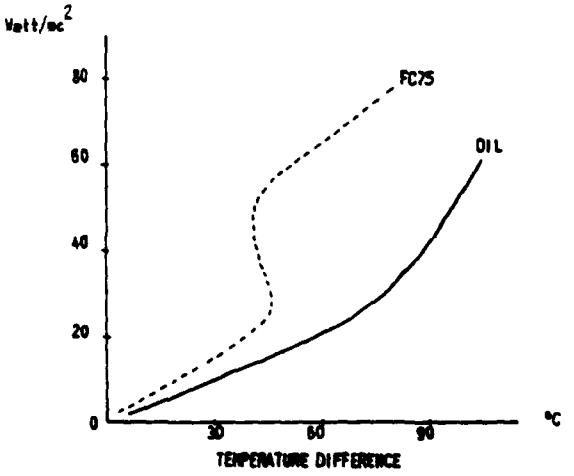

FIG. 3

Fig. 3 shows the trend of the temperature increase versus power dissipation for the same transformer immersed in silicon mineral oil or in FC75.

As it is known, the core dissipation in a transformer increases with increasing magnetic flux density and, at the same flux, with increasing of the main line frequency.

In 400 Hz transformers, as in our case, the limitation in reducing core size is normally due to the maximum allowed core and winding losses related to maximum operating temperature of core, winding, insulating parts and to the heat transferring capability of the component. This sets a limit to the maximum operating flux density of the core that is normally, at 400 Hz, well below saturating point.

By increasing heat transferring capability, it is possible to reduce the dimensions of the core, thus increasing its operating flux density. In the same way, for the same current, it is possible to reduce the cupper size, increasing the losses. Both these conditions strongly reduce transformer dimensions and weight (naturally making the transformer regulation worse).

A comparison of the improvement achieved in size and weight by using FC75 instead of silicon oil is reported in the following table, which shows the characteristics of two transformers with the same input/output characteristics realized by FC75 (transformer A) and silicon oil (transformer B).

	A	B
Main Line	400 Hz	400 Hz
Input Voltage	3ø 200 Vac	3ø 200 Vac
Output Voltage	9500 Vac	9500 Vac
Output Current	0.10 Amp	0.10 Amp
Insulation	40 KV	40 KV
Core Loss (watt)	80	35
Cupper Loss (watt)	90	33
Core Weight (Kg)	1.8	8
Total Weight (Kg)	2.6	13
Overall Volume (lt)	1.3	6.4

Some other tests have been performed to fix the power rating at which it is possible to operate the other electronic components for this particular environment. Some tests have shown that for components such as resistors, it is possible to reach even ten times the power ratings suggested by manufactors in air; however, for a conservative design and also to increase the reliability of the component, a factor of about five has been chosen.

Some problems also arise because of the use of solid state components immersed in boiling liquid at high temperature, very close to the maximum permissible junction temperature of transistors, diodes and S.C.R.

This problem has arisen very seriously for the S.C.R. used in the grid modulator. In fact, the junction temperature has a very effective influence on the recovery time and holding current of an S.C.R. particularly when the operating temperature becomes very close to the maximum junction temperature permissible for this element. Because the turn off time increases with increasing operating temperature, in order to assure a correct operation of switch S.C.R. it has been necessary, as mentioned before, to replace the conventional charging diode with another S.C.R. which delays the onset of recharge. It has also been necessary to make a considerable investigation in order to select a class of S.C.R. which could operate satisfactorily at the above conditions. Another parameter that is strongly affected by high operating temperature is the life of solid state devices.

Besides the effect of thermal stress, the design of grid modulator has been performed in order to minimize S.C.R. loss during its switching time. In this way we obtain a smaller rise of junction temperature and then an improvement of life of the component.

5. Realization

The first prototype of this amplifier has been realized and checked for many hundred hours.

As mentioned before, main line is 400 Hz, 3 phase, 200 V. The electronic circuits have been divided into three functional parts. Each of these subunits is located in a container. The mechanical distribution of electronic components with high dissipation avoids strong differences of liquid temperature inside the container.

The three containers (among which is included the heat exchanger), have the following dimensions:

260 x 460 x 180 mm.

In addition to the circuits realized in FC75, the amplifier consists of microwave TWT, high voltage capacitor and BITE circuits.

The circuits inside one of three containers is shown in fig. 4; its weight is about 40 Kg.

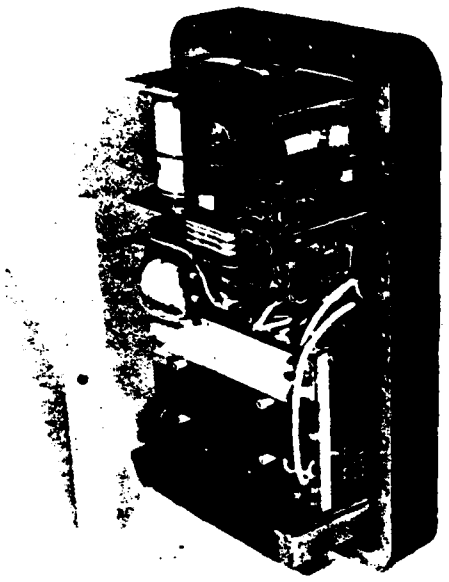

Fig. 4

6. References

1. G. SCERCH

   Microseconds electronic protections for radar transmitters

   ALTA FREQUENZA Vol. XXXIX - N. 7 - 1970

2. G. SCERCH

   The use of S.C.R. in pulse modulation of radar modulator

   ALTA FREQUENZA Vol. XXXVIII - N. 12 - 1969

SOLID STATE PULSE MODULATOR

Raffee Mgrdechian

Axel Electronics, Inc.
A Unit of General Signal Corp.
134-20 Jamaica Ave.
Jamaica, N.Y. 11418

A Pulse Modulator is presented which can be triggered by an external SCR to provide an output capable of driving the grid of a large High Voltage Thyratron, i.e. those requiring trigger voltages up to 2000V at source impedances as low as 15 ohms with plate voltage capability to 33KV PK.

Typical Specifications

Input: 225VDC, 500M.A.D.C. Max.
Output: No Load; 2000V PK
Full Load; 1000V PK @ 15 ohms
Pulse Width; 2usec
P.R.F.; 450 P.P.S.
Physical: 5 in. x 5 in. x 5-3/4 inc.
Weight; 14 lbs.

The Modulator contains the following components within its housing:

1. Pulse Transformer (PT)
2. Discharge Delay Saturable Reactor (L3)
3. Pulse Forming Network (PFN)
4. Charging Delay Saturable Reactor (L2)
5. Charging Reactor (L1)

Figure I shows the components of the Modulator within their housing.

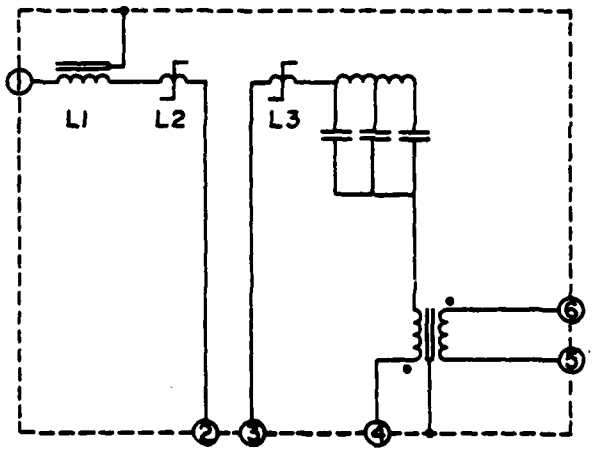

FIGURE I
Pulse Modulator Components

Figure II indicates the additional components external to the housing to complete the Pulse Modulator. The power supply is rated at 225V.D.C. at 500 M.A.D.C.

The Modulator

The load to the Modulator is to be the grid of a thyratron. Initially the Modulator sees an open circuit, until conduction starts, then the current to the thyratron will be limited by the internal impedance of the Modulator. For evaluation purposes two conditions of operation are considered,

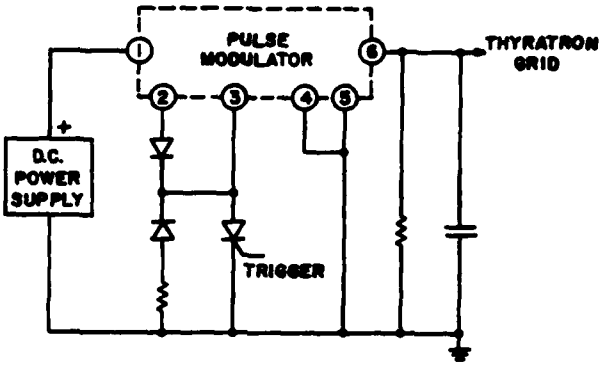

FIGURE II
Pulse Modulator

1. Open Circuit (150 ohms, 2000V PK, output)
2. Full Load (15 ohms, 1000V PK, output)

During open circuit the PFN full voltage less SCR voltage drop will appear across the PT primary for transformation. At full load the PFN and the PT reflected impedances are closely matched causing approximately one-half the no load voltage to appear across the pulse transformer primary.

The Pulse Transformer

To establish the PT step up ratio, estimates of voltage drops are made at the time of discharge of the PFN, then verified by the data sheets of the SCR or by bench testing to establish the dynamic voltage drop of the SCR at the discharge peak current.

The peak charging voltage at the PFN is estimated at 440 volts. After the discharge delay saturable reactor (L3) saturates, the voltage drop across it is small and negligible. However the SCR voltage drop will be a major drop, it is estimated at 35 volts. With a slight PFN, PT mismatch to allow for a small negative anode voltage at the end of the discharge, helping to turn off SCR, the PT primary voltage is calculated to be

$$E_{PT} = \frac{(E_{PFN} - E_{SCR})R_{PT}}{R_{PT} + 1.03\,R_{PT}} = \frac{405}{2.03}$$

$$E_{PT} = 200 \text{ Volts}$$

The PT ratio is established as

$$\frac{E_{out}}{E_{in}} = \frac{1000V}{200V} = \frac{5}{1}$$

Reflecting the PT secondary load, 15 ohms, to the PT primary

$$R_{PT(PRI)} = \left(\frac{1}{5}\right)^2 \times 15 = \frac{15}{25} = 0.6 \text{ ohm}$$

$$\text{PFN } Z = 1.03 \times 0.6 = .618 \text{ ohm}$$

$$I_{PK \text{ Discharge}} = \frac{405}{1.218} = 332.5 \text{ A. PK.}$$

To verify the estimated SCR voltage drop, the SCR peak current and the delay time are required. The delay required for an SCR with a di/dt rating of 400A/usec will be

$$\Delta T = \frac{332.5}{400} = .83 \text{ US}$$

The SCR voltage drop determined from manufacturers data (Fig. III) indicates between 35 and 36 volts. The voltage drop is close to the estimated value therefore a pulse transformer ratio of 5/1 stepup is acceptable.

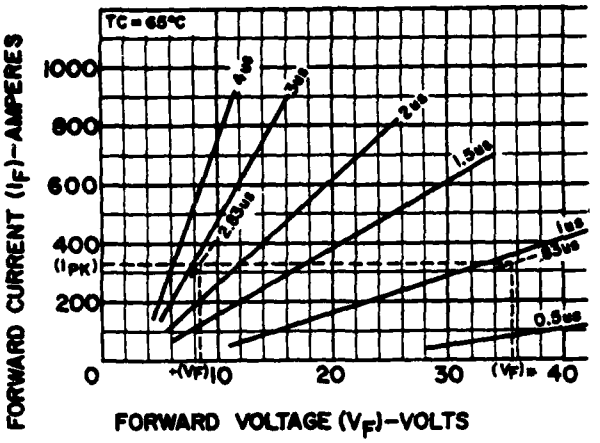

FIGURE III
Forward Voltage - Current Characteristics
As a Function of Time

The pulse transformer was designed on a core having an area of 1/2 square inches, a magnetic length of 5.62 inches. The losses of the pulse transformer are 1.5 watts, the open circuit inductance 23uhy (primary), the leakage inductance referred to the primary is 0.077uhy. The stray capacitance losses are negligible (.09W).

The SCR

Choice of the SCR is critical to proper operation of the Modulator. In general Pulse Modulator SCR's should have high di/dt capabilities and a fast turn off time. The turn on loss and the losses during conduction must be considered to achieve correct pulse width and for heat sink considerations. The small amount of loss at turn off is usually negligible.

*Voltage Drop at Start of Conduction
+Voltage Drop at End of Conduction Period

Fig. IV depicts the instantaneous forward dissipation versus instantaneous forward current as a function of time.

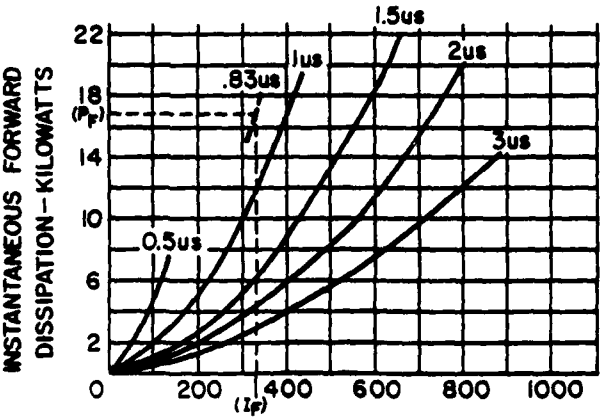

FIGURE IV

Instantaneous Forward Dissipation
vs Instantaneous Forward Current

Utilizing the curves of Figure III and Figure IV the average losses of the SCR are calculated,

"Turn on" = $\frac{15000}{2} \times .83(10^{-6}) \times 450 = 2.8$ watts

"Conduction" = $8 \times 332.5 \times 2\ (10^{-6}) \times 450 = 2.4$ watts

"Conduction" = $\frac{35-8}{2} \times 332.5 \times 2(10^{-6}) \times 450 = 4.04$ watts

"Off" = $\frac{8 \times 332.5}{2} \times .67(10^{-6}) \times 450 = 0.4$ watts

Total -- 9.64 watts

In an ambient of 50°C a case temperature rise of 15°C to 65°C case temperature is allowed. A modest heat sink will be required and its design is available in the literature.

It should be noted that the dynamic losses could be reduced if a longer discharge delay could be used. To increase the discharge delay period one of two alternatives are available:

1. Increase the physical size so that the saturated inductance of the discharge delay saturable reactor may be kept low and the unsaturated inductance high. The volume of the core goes up.

2. In the same physical size more turns may be added, increasing the saturated inductance and reducing the fidelity of the wave shape.

The Pulse Forming Network

The PFN stored energy must be enough to allow for the SCR, PFN, PT losses and the power to the load. Totaling up the power:

Output = $\frac{E^2}{R}$ x du = $\frac{10^6}{15}$ x.0009 = 60 watts

SCR losses = 9.64 watts
PT losses = 1.5 watts
PFN losses = 1.5 watts (estimated)

Total = 72.64 watts

The PFN voltage will be 440 volts, therefore:

$$C_{PFN} = \frac{(\text{watts output})(2)}{V_{PFN}^2 \times PRF} = 1.67\text{ufd}$$

Total coil inductance of PFN,

$$L = Z^2C = (.618)^2(1.67)(10^{-6})$$

$$L = .638\text{uhy}$$

Utilizing a three section PFN the L of each section will be .638/3 = .213uhy the rise time will be

$$T_R = \frac{PW}{2N} = \frac{2.0}{6} = .333US$$

The saturated inductance of the discharge delay saturable reactor plus the PT leakage inductance must not exceed 0.213uhy, the PFN first section inductance requirement.

The Discharge Delay Reactor

Specifications for the discharge delay reactor are:

1. Saturated L $\leq$ 0.213 - L_{KPT}
2. Delay + Tr_{PFN} $\geq$ 0.83US
3. Unsaturated inductance > 10 x (PT OCL)

The PT had the following parameters:

1. L_{KPT} = 0.077uhy
2. PT OCL = 23uhy

The PFN parameter Tr_{PFN} = .333US

The discharge delay reactor parameters are:

1. Saturated L $\leq$ 0.213 - .077 = .136uhy
2. Delay $\geq$ 0.83 - .333 = .497US
3. Unsaturated inductance >10(23) = 230uhy

The delay reactor core material chosen is Orthonol, area of core = .05 cm^2, l_c = 6.18 cm, turns equal 17. The saturated permeability is taken as 3, and the unsaturated permeability has been experimentally determined to be 25000.

Saturated L = $\frac{4\pi N^2 A_c U_s (10^{-9})}{l_c}$ = .088uhy

Unsaturated L = $\frac{4\pi N^2 A_c U (10^{-9})}{l_c}$ = 734uhy

Delay (T) = $\frac{\Delta B A_c N}{E \times 100} = \frac{(29000)(.05)(17)}{440 \times 100}$ = .56US

The discharge delay reactor is reset after each discharge by the charging current.

The Charge Delay Reactor

The minimum interpulse period is taken as 2000US, allowing for approximately 10% increase in PRF to 500PPS. It is stipulated that an 80US hold off period before pulse discharge is required. The minimum hold off period before initiation of charge is to be 40US, the SCR maximum turn off time. The sum of (80 + 40) x 1.1 = 132US is not available for charging. The actual maximum charging time is 2000 - 132 = 1868US.

The maximum charging inductance required is:

$$L = \frac{(T_{CHG})^2}{\pi^2 C_{PFN}} = \frac{(1.868)^2(10^{-6})}{\pi^2 (1.754)(10^{-6})} = .202\text{hy}$$

The PFN capacitance of 1.67ufd was increased by 5% to allow for capacitance tolerances.

The specifications for the charging delay saturable reactor will be:

1. Saturated inductance $\leq$ 0.1 (.202) $\leq$.02hy
2. Unsaturated inductance $\geq$10 (.202) $\geq$ 2hy
3. Delay $\geq$ 40US

A round hysteresis loop material (supermalloy) is selected so that it will not require external resetting, Figure V.

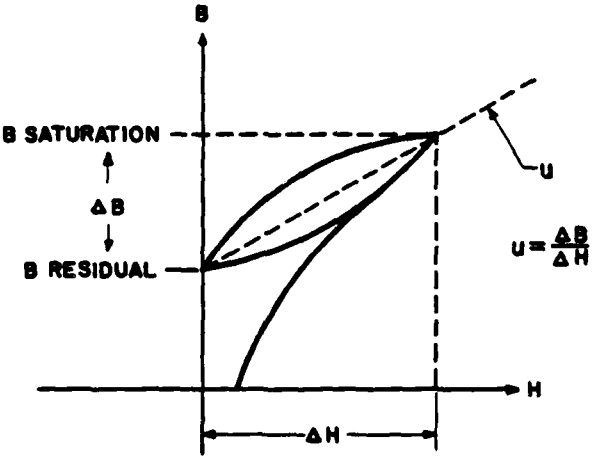

FIGURE V
B-H Hysteresis Loop
Charging Delay Saturable Reactor

The saturated permeability is taken as 6 and the unsaturated permeability has been determined to be 14000. The reactor has 510 turns. The ΔB is 2700 gauss. The core area is .726 cm^2, l_c = 10.97 cm. In the same manner as calculated for the discharge delay reactor, for the charge delay reactor:

1. Saturated L = 1.3mhy
2. Unsaturated L = 3.03h
3. Delay = 44.4US

The voltage being delayed is 225V for the charging delay reactor calculation.

The Charging Reactor

The saturated inductance of the charge delay saturable reactor is negligible in determining the inductance value for the charging reactor. Taking into

account manufacturing tolerances, the specification for the charging reactor is:

1. Inductance: .18 to .19hy
2. Peak current = .66A
3. RMS current = .42A
4. Average current = .331A
5. Q >20

The charging choke is designed using a core area of .141 sq. in., l_c = 5.47 inches, 1000 turns and gapped for inductance. The copper losses of the charging reactor and the saturable delay reactor total 1.37 watts, core loss .86 watts giving a total charging circuit loss of 2.24 watts. The power delivered to the PFN is 72.64 watts at 450PPS. The charging circuit efficiency is 97%.

The Q of the charging circuit is:

$$Q = \frac{\text{watts delivered}}{\text{watts loss}} = \frac{72.64}{2.24}$$

$$Q = 32.45$$

Performance Results

The voltage viewed at the anode of the SCR is shown in Figure VI.

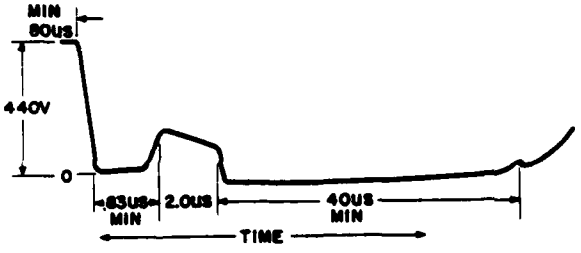

Figure VI
SCR Anode Voltage vs Time

The no load output voltage is shown in Figure VII.

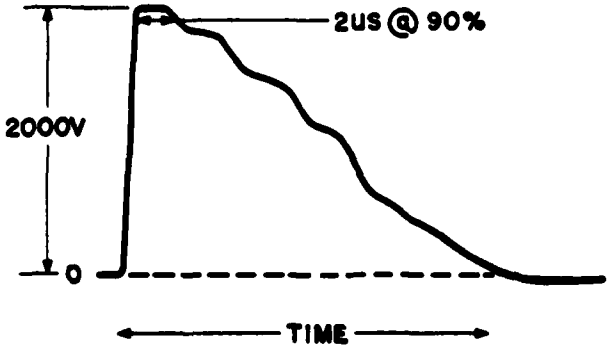

Figure VII
No Load Output Voltage vs Time

The full load output voltage is shown in Figure VIII.

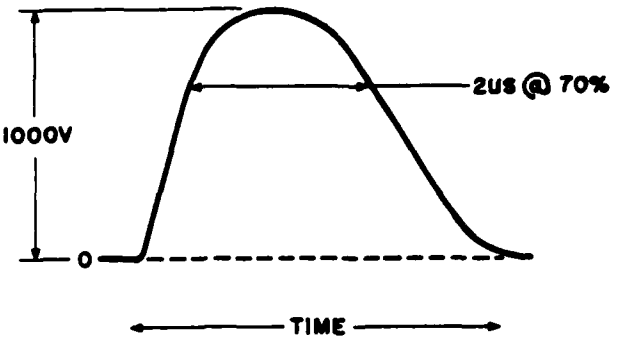

Figure VIII
Full Load Output Voltage vs Time

Conclusion

An efficient Pulse Modulator, small in size and reliable has been developed by proper component selection. Overall efficiency is 80.6% from output to d.c. power input. The small size, Figure IX, compared to

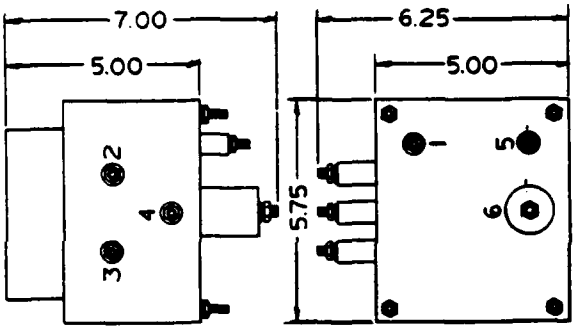

Figure IX
Pulse Modulator Component Housing

tube type triggers, allows for equipment miniaturization. Axel Electronics has extended the principles discussed to design a trigger pulse modulator which operates to 10KHZ. Figure X is a picture of the test set modulator. Figure XI compares the test set modulator to a tube type in present use.

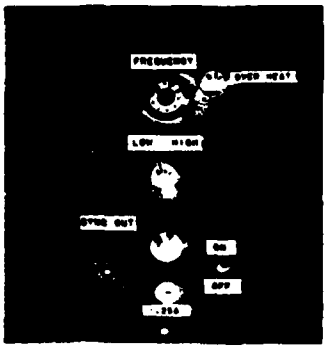

Figure X
Test Set Pulse Modulator

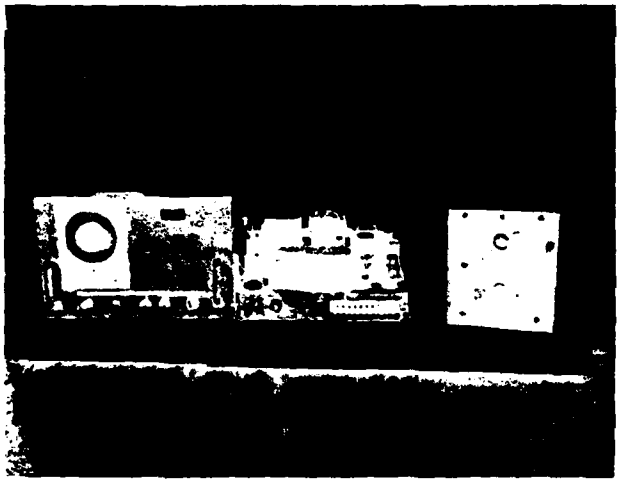

Figure XI
Comparison
Test Set Modulator to Tube Type Modulator

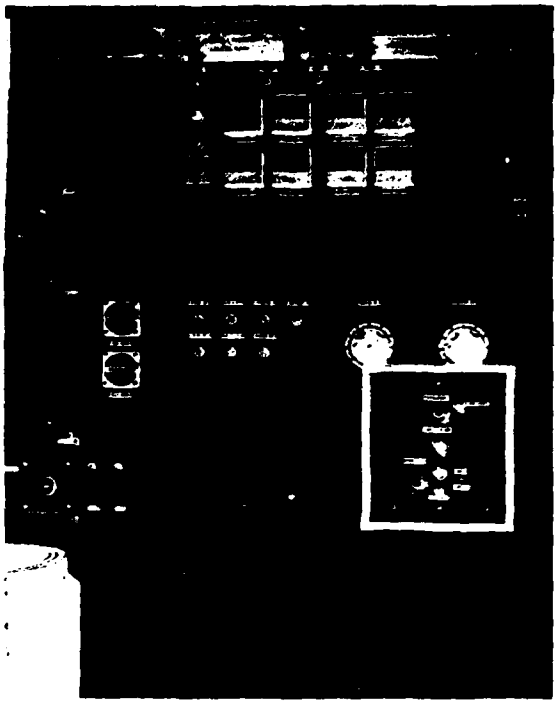

Figure XII

HIGH ENERGY TRANSIENT SIMULATOR AND IT'S EFFECTS ON SOLID STATE CIRCUITRY

Joseph J. Polniaszek
Rome Air Development Center
High Power Component & Effects Section
Techniques Branch
Surveillance Division
Griffiss Air Force Base, New York

Summary

A device was designed and fabricated that generates pulses of energy with exponential waveshape. It utilized high power silicon control rectifiers in a configuration similar to a line type pulser. By direct coupling the output to a telecommunication line, the effects of a lightning storm in the vicinity could be simulated and system failures analyzed.

Introduction

The Air Force System's Command discovered a need to design, develop and fabricate a device that simulated the effects of an electrical storm in the vicinity of telecommunication systems. This was a response to the low mean time between failure (MTBF) of the AN/GRN-27 solid state landing system. System failure occurred mainly in line driver and receiver equipment and a correlation was put forth associating failures and electrical storms in the vicinity. The mechanism was presumed to be a ground current induced by a lightning strike between earth grounds of the system. Therefore, the lightning simulator became a key component in firstly proving the hypothesis and secondly testing and evaluating the method of solution.

Simulator Criterion

Due to the highly erratic nature of lightning phenomenon; it was necessary to construct a device that would be a repeatable source of transients similar to what the AN/GRN-27 was experiencing in the field. Based on data obtained in a textbook on "Protection of Transmission Systems Against Lightning"[1] and a technical memo obtained from Bell Canada, certain representative characteristics of lightning were listed. Principally, these characteristics are:

1. Repetition Waveshape.- In a report by Schonland and assoc[2], it is documented that a single lightning bolt has up to 27 discharges. Undocumented reports list up to 40.

2. Ground Currents.- According to Lewis[1], instantaneous ground currents can be up to 200,000 AMPS with a lower bound of less than 100 AMPS.

3. Voltage and Current Waveshape.- A single discharge would have a current waveshape as indicated in Figure 1.

4. Time Duration.- Ground currents have been measured for times greater than 10,000 usec with greater than 50% of all cloud to earth strikes of duration of at least 600 usec.

The high powers involved in lightning are hard to simulate in a portable device. However, the desired device needed only to simulate a lightning strike in the vicinity, i.e., a high ground current between devices of the system. Therefore, the scaling of parameters was not a liability as long as the method of coupling to the system was not lossy. Consequently, the following characteristics were chosen as sufficient:

1. A device of single pulse or multiple pulse capability. The maximum number of pulses per burst was chosen to be 40 pulses.

2. A continuously adjustable peak voltage output from 0 to 1000 V.

3. A pulse duration defined by the 50% power points that ranged from 100 usec to 10 ms.

4. A pulse repetition frequency from .1 Hz to 100 Hz where .1Hz synthesized a storm passing at a distance from the equipment and the 100 Hz synthesized a near strike with multiple discharges.

5. A exponential waveshape as indicated in Figure 2 into a resistive load.

6. An energy content of from 4 joules to 28 joules per pulse.

7. DC coupling between the simulator and telecommunication lines.

Again, these characteristics by no means simulate the optimum characteristics of lightning but, for the use intended, i.e., indirect lightning strikes, they were considered to be sufficient.

Theor, of Operation

The lightning simulator, tenatively nomenclatured AN/GRM( )XW is a solid state power switching device that creates a pulse or pulse train as illustrated in Figure 2. This pulse has an exponential decay of variable pulse width and pulse repetition rate. The primary circuit of the lightning simulator is illustrated in Figure 3. It's operation is as follows: First, SCR1 (the charging SCR) is triggered as in Figure 4a, the capacitor bank C is charged as in Figure 4b to the power supply voltage. The current drops to the holding current and SCR1 turns off. The circuit is now ready to fire. SCR3 (the load SCR) is then triggered at time T as illustrated in Figure 4d and a resistive load experiences a voltage as indicated in Figure 4e. This waveshape is determined by the equation:

$$V_{out} = V_{supply} \text{ EXP } (-t/_{RC})$$

where:

V_{out} is the load voltage

V_{supply} is the supply voltage

R is the load impedance

C is the capacitance in the circuit

t is time

If the load impedance does not dissipate all the energy within the desired pulse width, i.e, the load impedance is higher than anticipated, SCR2 (the Tail Clipper SCR) fires and "clips" the pulse as shown in Figure 4f and 4G.

The SCR's utilized for this switching system were General Electric type C150 PC. Although the SCR's had a typical turn on time of 8 usec, and a di/dt of 50-75 AMPS/usec, this was not considered a constraining factor since actual lightning has an exponential rise. The units were used conservatively with a peak current of 40 amps and voltage of 1000 V when compared with maximum values of 110 AMPS (RMS) and 1300 V.

The second major building block of the lightning simulator is the trigger generator and logic control subsystem. A block diagram of the system is shown in Figure 5. The subsystem operates as follows: the oscillator is operating astably at a frequency of 1 to 10 KHz. When the initiate cycle switch is depressed, the flip flop's (JKFF) Q output is raised to +5 V. The output of the NOR gate therefore follows the oscillator input and the divide by 10's begin counting. The output of the divide by 10 selected by the switch then triggers monostable 1 on the leading edge of the pulse and a pulse that is the prescribed pulse width and repetition rate is produced. This output triggers SCR3 (Output SCR). This opposite output (Q not) triggers the BCD countdown circuits and the "borrow" signal from this circuit resets the counters, inhibits the monostable multivibrator and resets the JKFF. Monostable 2 is triggered by the falling edge of the monostable 1 signal and it triggers SCR2 (Tail Clipper SCR). The delay monostable is triggered on the falling edge of monostable 2 and establishes the amount of time between the tailclipper and charging signals generated by monostable 4.

The remainder of the circuitry is a simple rectifier bridge type power supply whose voltage is controlled by a variac. In addition, there is interlock system disabling high voltage until all subsystems are operational.

After approximately 1000 hours of testing, only one problem arose with the device. When the simulator was connected to highly inductive loads, for example, an alarm bell coil, the load SCR would fail to return to a non-conducting state. This was due to a power factor problem that could only be alleviated by the addition of a compensation network in the switching circuit. Unfortunately, such a network would have to be switched out of the circuit when testing resistive loads. It was found that such a network was unnecessary for the majority of the tests done on the AN/GRN-27, because all control lines had a power factor near the value of 1.

Failure Mechanisms and Experimental Results

The basic failure mechanism involved in lightning induced failures is described by Klewe[3]. He terms the mechanism as conductive coupling. This mechanism is illustrated pictorially and schematically in Figure 6. V_1 is the signal source needed for operation of the system. Z_1 is the load impedance of the system and Z_2 is the ground impedance between points A and B. V_2 is the voltage of the strike and Z_3 is the impedance between points C and B. It is obvious that when a strike occurs, current will flow through all branches of the circuit. Considering the high currents involved, even a small amount of this power will be sufficient to cause a failure of solid state equipment that is not properly protected. There are two ways that protection can be effected. First and most simply, impedance Z_2 can be eliminated by adequate groundings. However, due to local soil and seasonal conditions, this method is both cost and time prohibitive. The second method is to devise a protective circuit that will short out Z_1 when lightning occurs. Figure 7 illustrates a simple circuit of this type.

The values in the protective circuit are adjusted so that normal control signals are only slightly attenuated thereby not affecting system operation. When a strike does occur, however; the spark gap SG conducts at it's ionization voltage dissipating the majority of the power and zener diode D_1, in conjunction with the network of R_1 and R_2 dissipate the remaining power until it is of a tolerable power level. A circuit such as this will not allow wanted signals to pass during a transient.

In the AN/GRN-27 system, this did not create a problem because data was of a static nature and was in the form of a DC level on the line. Therefore addition of a 10 ms delay circuit allowed the system to never sense a change in level that was of such a short duration. This slowed reaction time of the system; however, speed was not essential in this application. If digital information was to be transmitted; however, the only cost effective approach to transient suppression would be individual return lines for each communication line. Therefore only electromagnetic coupling could occur and would probably be within tolerable limits of the system.

Results obtained in the field utilizing the transient simulator and protective circuits verify the results hypothesized. No component failures were noted on signal or control lines utilizing the protectors and 100% failure was noted without protectors. The principal failure mode on solid state components being base-emitter junction failures and resultant beam lead melting.

Conclusions

Solid State equipment is finding numerous applications in hostile environments. Due to the low power needed for operation, it is vulnerable to natural phenomena such as lightning. As these applications increase, without adequate consideration by both system designers and circuit designers, situations such as the AN/GRN-27 experienced will continue to occur. The Air Force System Command is attempting to insure that such situations do not occur on future systems by including a transient vulnerability specification on all new procurements.

References

1. W. W. Lewis, "The Protection of Transmission Systems Against Lightning,", John Wiley and Sons, 1950.

2. B. F. J. Schonland, "Progressive Lightning-IV: The Discharge Mechanism", Proceedings of the Royal Society, Series A, Vol 165, Feb 18, 1938, pp 132-150.

3. H. R. J. Kleve, "Interference Between Power Systems and Telecommunication Lines", Edward Arnold (Publishers) LTD., 1958.

Figure 1 Typical Waveform of Lightning Discharge

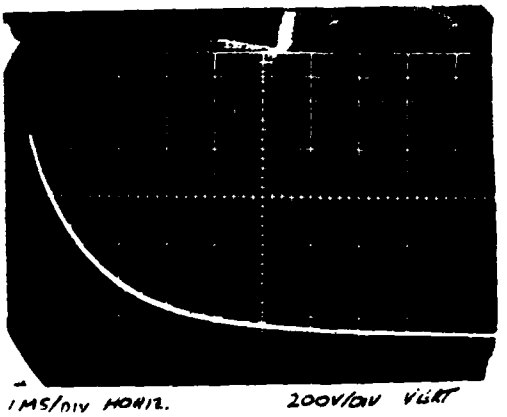

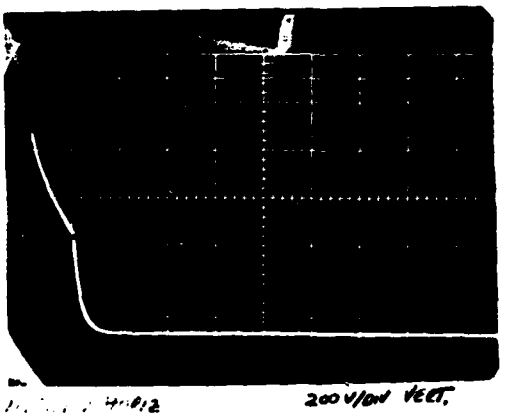

Figure 2 Output Waveform of Transient Simulator

(a) Waveform with R=25 OHM, C = 56 MFD
(b) With "Tail Clipper" at Half Power Point

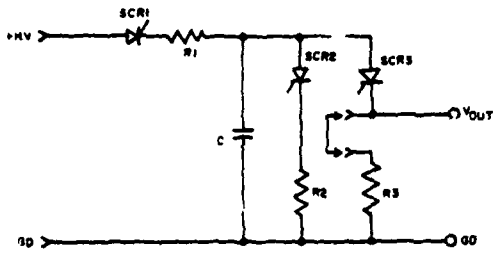

Figure 3 High Power Switching Circuit

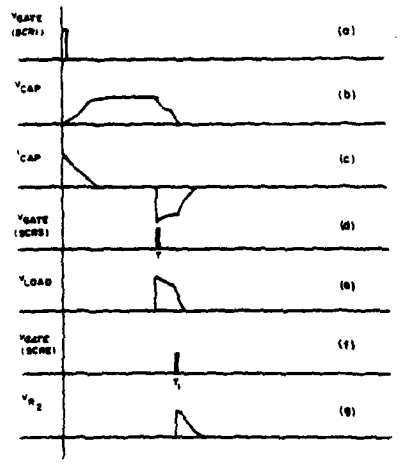

Figure 4 Waveforms of High Power Switching Circuit

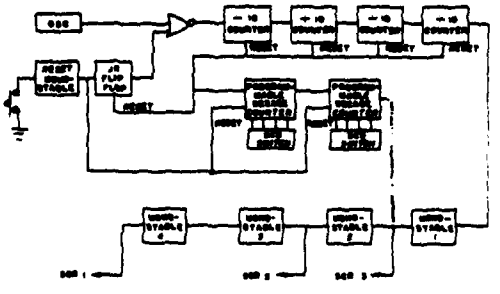

Figure 5 Block Diagram of Logic Control and Pulse Generation

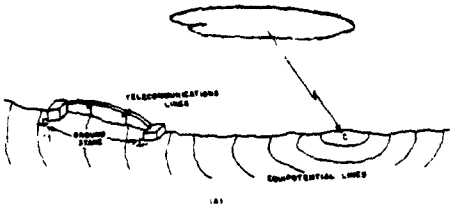

Figure 6 (a) Pictorial of Lightning Strike Mechanism

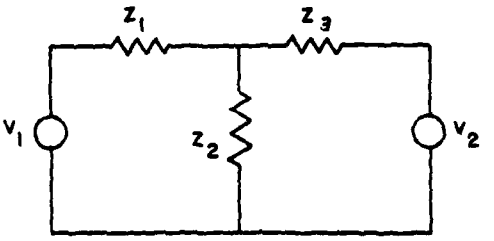

(B)

Figure 6 (b) Schematic

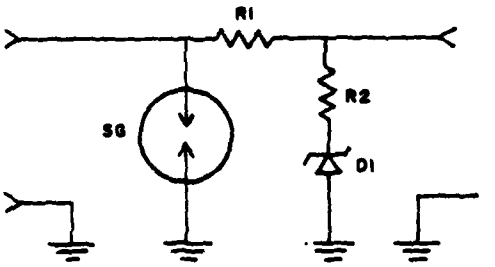

Figure 7 Schematic of a Typical Protector Circuit

MEGAWATT NANOSECOND SWITCHING OF HIGH POWER LASER ACTIVATED SILICON SWITCHES *

O. S. Zucker, J. R. Long, V. L. Smith
Lawrence Livermore Laboratory
Livermore, California

D. J. Page and J. S. Roberts
Westinghouse Research Laboratory
Pittsburgh, Pennsylvania

Light activated multilayered silicon semiconductor devices have been used to switch at Megawatt power levels with nanosecond turnon time. Current rate of rise of 750 kA/μs at 10 KAMP, with 1 kV across the load have been achieved.

Introduction

To achieve high-power, energy compression devices depend on switches as the primary nonlinear element required for time compression.[1]

The most important characteristics of a switch required for energy compression applications are: Power handling capacity, impedance, rise time, repetition rate capability and life time. Another consideration for large systems is the ability of many switches to function simultaneously.

The light activated silicon switch (LASS) represents a combination of switch parameters which is unique and potentially better than currently available switches. The LASS meets all the switch requirements for energy compression. Solid dielectric switches currently handle the highest power and have good rise time. However, they are single shot devices and have simultaneity problems. The best currently available repetitive device is the high pressure spark gap. It can carry up to 1 MA per channel (.1 μsec), hold off 500 kV/cm (100 psi), the inductance is around .05 nH/kV (25 nH at 500 kV), and the simultaneity is in the nanosecond regime.[2] The LASS device has the potential of lower inductance, higher repetition rate, longer life, and improved simultaneity over the high pressure spark gap.

This report describes the results of initial tests with research silicon devices which demonstrate significant improvements in current rate of rise over existing silicon switches (thyristor).

The Device

Semiconductor switches come in many forms such as transistors, thyristors, triacs, and several modified forms of these. However, the same principle of switching is common to all. In the blocking or open circuit state a region within the device, usually a p-n junction, is depleted of mobile charge and acts as an insulator. The voltage applied to this insulating region sweeps out the mobile charge and preserves the insulating state.

To convert this region to the conducting state, charge is injected into this depleted region, usually from a second p-n junction as in a transistor or from two p-n junctions, one on each side, in the case of a thyristor. The injected charge is made large enough ($\approx 10^{18}/cm^3$) to reduce the impedance of the depleted region so that a substantial amount of current can flow. Usually the voltage drop of the device in conduction is less than two volts.

There is a limit to the speed that such devices can switch. The injection of charge from the p-n junction is a relatively slow process and is limited by the transit-time for the carriers to traverse the space between the injecting p-n junction and the depleted junction. This time varies with the device design, but for high power transistors and thyristors is about a microsecond. If the current is allowed to rise within the device before sufficient charge has been injected, the impedance will be high enough to either cause a substantial loss of efficiency or will result in the thermal destruction of the device.

The current method of transforming the depleted region into the conducting state is by photon absorption. In this case the mobile charge, electrons and holes, is created in-situ and can be accomplished as fast as the light enters the device. A suitable laser having an output photon energy closely matched to the band-gap of silicon can be used to efficiently accomplish this process.

A typical power device has a volume of silicon in the active region of $10^{-2}cm^3$. If this volume is to be filled with carriers to the normal on-state density of $10^{18}/cm^3$ and each electron hole pair requires an energy of 1.1 eV, the total energy required will be:

$$E = \text{volume} \times \text{density} \times \text{photon energy (1.09 eV)}$$
$$= 10^{-2} \times 10^{18} \times 1.09 \times 1.6 \times 10^{-19}$$
$$= 1.75 \text{ mJ.}$$

This amount of energy is readily obtained by available lasers. The calculation assumes complete conversion of photons to electron hole pairs and no recombination during the illumination time. The choice of wavelength, such as using a Nd^{+++} doped YAG laser having an output of 1.06 μ, which is closely matched to the band gap of silicon, ensures efficient conversion of photons to electron-hole pairs. The carrier lifetime in power devices is usually longer than 10 microseconds, so negligible recombination will take place during illumination, which usually occurs for a few nanoseconds. Turning off such devices is accomplished in single junction (back biased diode) or dual junction (transistor) by sweeping out the carriers in the reverse direction to allow the development of a depletion region.

The Experiment

The experiments performed with the LASS were to determine first if the device would respond with rise-time in the nanosecond regime, and second to attempt to achieve high rates of current rise. The first experiment utilized a 50 Ω charged line. The line was switched with the LASS into another 50 line. A "Q-Switched" Nd doped YAG laser (1.06 μ) was used to illuminate the switch wafer. A photograph of the laser output on a S-1 cathode photo diode is shown in Figure 1. The laser output was approximately 3-5 mJ/pulse. The fixture used to mount the switch wafer in a 50 Ω structure is shown in Figure 2, along with an electrical schematic of the test. Typical results are shown in Figure 3. The line was charged to 1500 volts (near avalanche) and

*Work performed under the auspices of the U.S. Energy Research & Development Administration under Contract No. W-7405-Eng. 48.

the output pulse was approximately 750 volts with a rise time of 4 ns (10-90%). This output represents 15 amps in 4 ns or 3.75 kA/μsec. However, the important point is the switch turned completely on in nanoseconds.

In an additional experiment two 50 Ω cables were connected in parallel to obtain a 25 Ω circuit. The result is shown in Figure 4. The output is essentially the same as the 50 Ω case but at twice the current.

In order to obtain significantly higher rates of current rise and current, a fixture was designed which would accommodate several strip transmission lines in parallel. The LASS in this case is designed to short the transmission line at one end. The fixture design and test schematic are shown in Figure 5. When the switch closes a pulse propagates down the line and a current flows in the switch equal to the voltage of the pulse across the characteristic impedance of the transmission line.

The strip transmission line used in the experiment is three flat conductors separated by insulation. The characteristic impedance calculated from the geometry and presumed dielectric constant was 1.4 Ω. Due to the uncertainties in this calculation (and the close spacing which made the skin effect potentially important) a measurement of the impedance was made. The experimental schematic is shown in Figure 6, and the result in Figure 7. From this experiment, a value of 1.25 Ω was used as the characteristic impedance of the strip transmission lines.

The experimental results for eight strip lines in parallel are shown in Figure 8. The voltage pulse shown is the pulse on the transmission line. The voltage at the switch end of the line does not go to zero implying the existance of some impedance in the switch and/or connections to the switch. We believe this impedance is resistance in the LASS due to the very small area of the device we can illuminate the present experiment. The interpretation of the amount of current flowing is independent of these considerations since it is determined simply by a measured voltage pulse on a known impedance transmission line.

With eight transmission lines in parallel charged to 1300 volts a pulse of 1110 volts was measured on the transmission line. The rise time was 12 ns. The eight lines in parallel represents an impedance of .156 Ω. Therefore, 1110 volts across .156 Ω in 12 ns yields a current rate of rise of 640 kA/μs and a peak current of 7100 amperes. The same experiment with 12 lines in parallel gave the result 760 kA/μsec at 9800 amps peak current. Figure 9. The results of all experiments are shown in Table 1.

For comparison purposes two copper washers separated by mylar were inserted in place of the LASS in the test fixture. A nail was driven through the washers to short circuit the transmission lines. This is an example of the classic "hammer switch" and can be taken as a basis of comparison. The result is shown in Figure 10 and the waveshape is seen to be poorer to the previous results.

To review the demonstrated results of the LASS:

1. Power - 10 MW
2. Impedance - .1 Ω
3. Risetime - 3-14 ns
4. Repetition rate - not tested but line is recharged in approximately 1 millisecond.

The other switch requirements for high power applications were long life and simultaneity. Silicon switches have demonstrated long life in similar service where only the speed of response is slower. The nature of the triggering (or turning on) mechanism makes it possible to predict that perfect simultaneity can be achieved by insuring that the light pulse reaches all switches at the same time.

Conclusions and Potential Applications

Immediate Applications

There are several applications of the LASS device which can be immediately pursued. The device used in the above experiments utilized a total area of .1 cm^2 out of a total available area of 2.5 cm^2. The reason is that during the time of our experiment diffusion does not take place and thus only the area illuminated can conduct. Thus with only 50% efficiency our experimental device could conduct 125 kA if fully illuminated. These devices have been fabricated in diameters of 5 or 7.5 cm so that area extrapolation to mega-ampere devices should be straightforward.

The device should lend itself very easily to the design of improved MARX Generators. The inductance of the device is arbitrarily low (.1 nH/kV or less) since practically all the magnetic flux can be external to the device. Triggering arrays of switches is particularly easy since laser triggering provides both high voltage isolation and perfect simultaneity (sub-nanosecond laser pulses are readily available). Thus the erection and discharge times of MARX Generators can be substantially reduced providing higher fields and higher power densities in liquid dielectric transmission line or blumlein applications.

The discharge of megajoule megaampere capacitor banks on a repetitive basis can now be considered feasible. The coulomb transfer of the LASS is in excess of 10 coulombs which is adequate. The primary limitation to high repetition rate is cooling of the devices. The flat large area geometry and the dissipation rate of between .1 and 1% of transferred energy make these devices particularly promising. For example a 1 kV - 100 kA switch can deliver 10^8 watts instantaneous power. If the dissipation is 1 MW (1%) and we can cool the device by convection or heat sinking at a 1 kW rate then the duty cycle could be 10^{-3}. This result implies a 1 kHz repetition rate for 100 MW - 1 μs pulse or a 100 kHz rate for a 100 MW - 10 ns pulse. Currently available silicon switches typically have junction cooling rates of 100 W/cm^2.

There are many more conventional applications (e.g. Radar Modulators) for which the LASS would be useful.

Potential Applications

One interesting potential development would be to modify the geometry of the device to improve the coupling of the device to the circuit. The self inductance associated with the switch could be significantly reduced. Another possibility of geometrical modification is to integrate either a GaAs Laser or Amplifier intimately coupled optically to the device to supply the light pulse. The device could then be triggered electrically or by a relatively weak light pulse which would maintain electrical isolation of the trigger.

Another possibility is the generation of megawatt wide-band microwave power.

Picosecond turn on in intrinsic silicon has been demonstrated by Auston of Bell Laboratories.[3,4] There

is no reason to suspect that turn on in junction devices would be slower than in bulk intrinsic material. A crude estimate of the turn on time is the light transit time in the depletion layer which is about 1-2 ps.

The turn off characteristics in single and dual junction devices should be similar to performance of the storage or snapoff diode. These diodes generate gigahertz harmonics when the charge in the depletion layer is swept out and the diode snaps off. In a typical application such a bulk biased junction biased at 1 kV, would be turned on with a picosecond rise time laser pulse. Depending on the waveguide impedance amperes to kiloamperes could be conducted. When the light turns off the carriers are swept out and the device snaps off. This snap off can be timed extremely accurately since both the number of carriers and the recombination rates are known. Thus a resonant cavity could be excited with precise phasing. This phasing could be controlled by varying the spacing between the laser pulses. This can be done quite easily with electrooptic techniques. Thus megawatts per device of microwave power can be generated at extremely broad bandwidth. We could construct phased array radar sources of very high powers.

Finally, the use of these devices as programmed nonlinear elements in waveguides would make possible energy compression of microwave energy at unprecedented powers.

Acknowledgement

We would like to thank Henry Chau for his help with the laser and Al Myers for his technical assistance.

References

1. O. S. F. Zucker and W. H. Bostick, "Theoretical and Practical Aspects of Energy Storage and Compression", Proc. of the Int'l. Conf. on Energy Storage, Compression, and Switching, Torino, Italy, 11/5 - 7/74.

2. Private communication with Philip Champney, Physics International Corp. (1975).

3. A. M. Johnson and D. H. Auston, "Microwave Switching by Picosecond Photoconductivity", IEEE Journal of Quantum Electronics, Vol. QE-11, No. 6, June, 1975.

4. P. LeFur and D. H. Auston, "A Kilovolt Picosecond Optoelectronic Switch and Pockel's Cell", Applied Physics Letters, Vol. 28, No.1, January 1976.

Figure 1: Oscilloscope trace of laser pulse used to trigger the LASS.

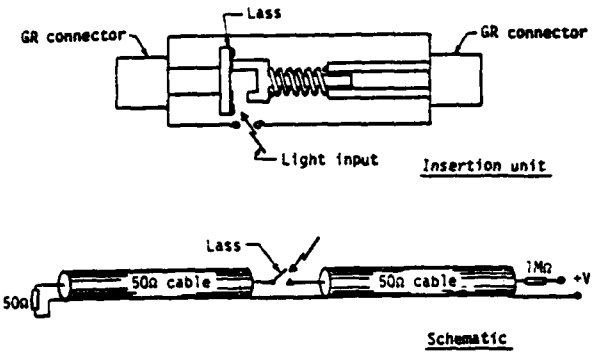

Figure 2: Fixture diagram and schematic for 50 Ω experiment.

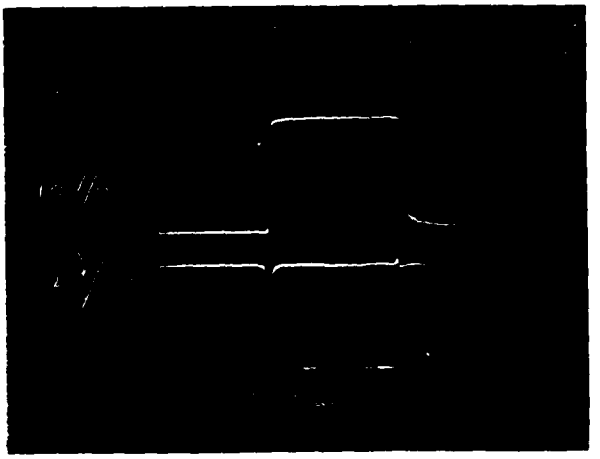

Figure 3: Pulse output of 50 Ω experiment

a) 50 ns/div sweep-bottom trace laser pulse

FIGURE 3B
b) Rise time at 2 nd/div

Figure 4: Pulse output of 25 Ω experiment - rise time - 2 ns/div

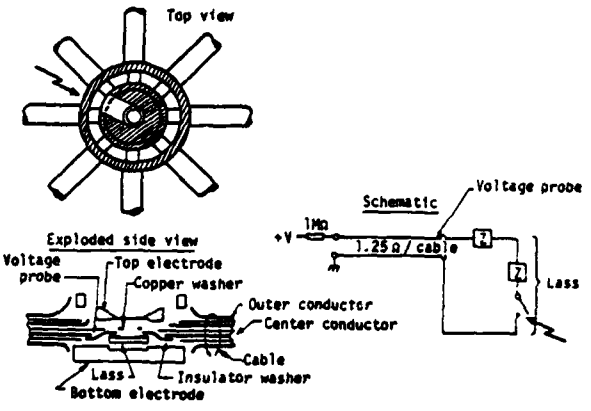

Figure 5: Shorting fixture diagram and schematic of strip line experiment

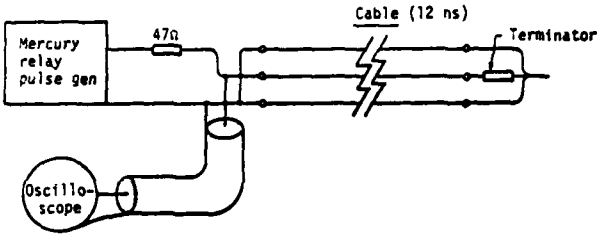

Figure 6: Cable characterization circuit

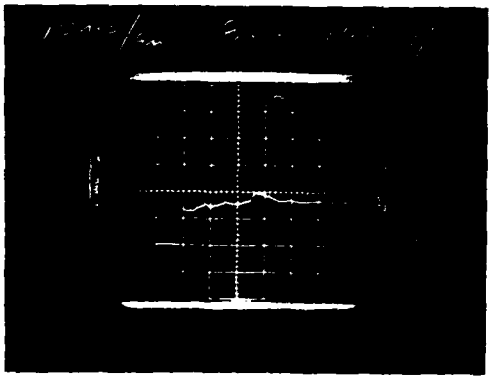

Figure 7: Result of cable characterization test showing minimum reflected pulse

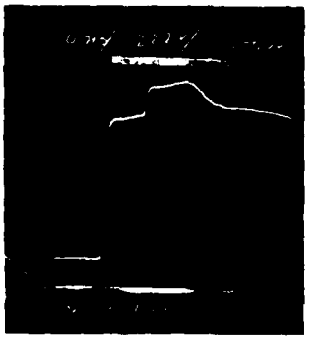

Figure 8: Transmission line pulse with 8 parallel lines
a) 50 ns/div sweep
b) 5 ns/div sweep

Figure 10: Transmission line pulse with dielectric switch in place of LASS.

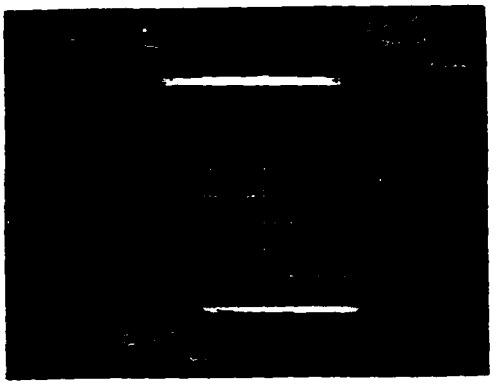

Figure 9: Transmission line pulse with 12 parallel lines

a) 50 ns/div sweep

b) 2 ns/div sweep

Z (Ω)	V (volts)	I = V/Z (amps)	τ $\times 10^{-9}$ sec	I = I/τ $\times 10^{9}$ (kA/μs)	P = VI (MW)
50	750	15	4	3.75	0.011
25	750	30	4	7.5	0.022
0.156	1110	7115	11	647	7.9
0.104	1020	9820	13	755	10

On line

Z = Line impedance
V = Pulse voltage
I = Peak current
τ = Rise time
I = Rate of current rise
P = Power, load

Table 1: Summary of results

SUB-CYCLIC SOLID STATE INTERRUPTION OF PRIME LINE CURRENTS IN FAULTED PHASED ARRAY POWER SUPPLIES

C. J. Eichenauer, Jr.
General Electric Co., HMED
Court Street
Syracuse, NY 13201

Summary

Since in theory, electronic interruption devices can provide more rapid interruption of the prime line currents of a faulted d-c power supply than conventional electro-mechanical interruption devices, their use was investigated in connection with several high power phased array radar power system problems. A computer model of one such system was evaluated initially in order to establish the electrical requirements for the interrupter. The subsequent design and successful evaluation of the system's solid state interrupter are described.

Introduction

The principles of sub-cyclic electronic line current interruptions are not new—in fact, practical systems which used ignitrons for this purpose were implemented in the 1930s. Strangely, these systems were initiated for virtually the same purpose as are today's systems—to provide protection for the multiple power amplifier tube configurations associated with the super power radio transmitters of that era. In the intervening years sub-cyclic interrupting techniques have apparently not been very extensively used. This is possibly due to the fact that modern high speed mechanical circuit breakers—capable of providing interruption of ac line fault currents with several cycles—have proved adequate for most situations.

Some recent multiple channel high power phased array radar system requirements have necessitated a re-examination of the line interruption situation. Problems with insufficiently fast a-c line interrupting devices largely came about as a result of the crowbar fault diverters used with multiple channel phased array systems. Typically, insufficiently fast interruption of a faulted channel could result in line voltage draw down on the common a-c bus supplying a number of other channels, for a sufficient period of time, to cause radar system malfunctions in the non-crowbarred channels.

This paper describes the results of an investigation into the line interruption problems associated with a multichannel system to this type which was necessitated because of a proposed change in the prime power source capabilities. Initially, separate three phase generators (connected to a common drive shaft) were to be utilized for each channel, hence, the equipment design was provided with the ultimate degree of isolation between channels insofar as power faults were concerned. For reasons of radar site cost effectiveness, the common bus system was proposed at a later date, and it was then necessary to establish to what degree the transmitter performance capabilities might be compromised if the original equipment design remained unchanged.

System Configuration

The elements of the common bus phased array power system investigated are shown in figure 1. Each of the channels had four R-F power amplifier tubes energized from the output of its unregulated high voltage d-c power supply. An arc fault in any of the power amplifier tubes would cause the crowbar fault diverter to close, thus diverting most of the energy of the storage element away from the tube fault path in the conventional manner. The resultant short circuit across the output of the d-c power supply, of course, results in the build up of abnormally high currents in the three phase power lines of the faulted channel and in the power source. It is then inevitable that a voltage draw down will occur on the common bus. The d-c voltage outputs of the unregulated d-c power supplies of the other channels will likewise draw down until the interrupter of the faulted channel opens. The degree of performance degradation on the other channels will obviously be minimized as the speed of operation of the interrupter on the faulted channel is increased.

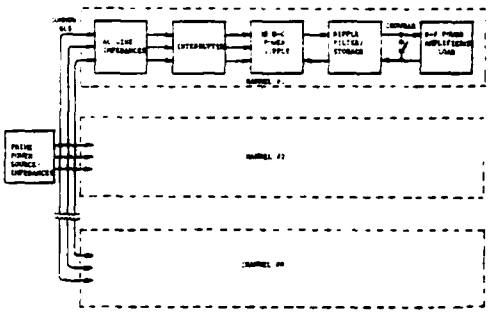

Figure 1. Common Bus Transmitter Block Diagram

Figure 2 tabulates a number of capabilities the a-c line interrupter should ideally possess. The rationale for the first two points has just been described. With regard to the third point, voltage transients, circuit inductance and nonlinear elements (e.g. rectifiers) inherent in the interrupter's paths make portions of the overall circuit vulnerable to quite high transient voltages when fault currents are being handled by the interrupter, but these effects can be minimized by more rapid fault removal. With regard to the reliability/maintainability implications of the next two points, the ideal interrupter should provide a significant improvement over the relatively limited number of operations between overhauls typically associated with devices utilizing the mechanical motion of metalic contacts as the interrupting means. Finally, the capability of rapid reclosure of the interrupter should be inherent in the device if minimum system down time is a consideration. Solid state interruption techniques were selected as the means of achieving all of these objectives.

- MINIMIZE VOLTAGE DIP ON COMMON BUS
- MINIMIZE AC FAULT CURRENT AMPLITUDES
- MINIMIZE CIRCUIT TRANSIENT VOLTAGES
- POSSESS HIGH RELIABILITY
- POSSESS CAPABILITY OF MILLIONS OF OPERATIONS
- POSSESS RAPID RECYCLE CAPABILITY

Figure 2 Capabilities of Ideal Line Interrupter

System Modeling

An accurate prediction of the behavior of a large phased array power system necessitates the preparation of a detailed model comprised of all significant elements in the system. Since the resulting system model is typically both non linear and of a mathematically complex nature, the use of an appropriate non-linear digital computer circuit analysis program is usually necessary. Figure 3 shows the key elements of the model used for analysis.

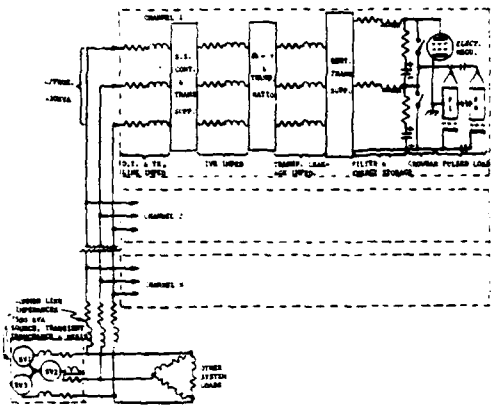

Figure 3 Simplified Computer Simulation Schematic

In brief explanation, starting from the pulsed load, the power amplifier tubes were programmed as two constant current generators (connected in reverse polarity) to simulate the body and collector currents drawn by the traveling wave tubes from the high voltage power supply and energy storage capacitors. These generators were also programmed in terms of amplitude and time to simulate the pulse templets of the radar system. Next the two crowbars were simulated simply as open switches, and these likewise were programmed to close at a prescribed point in time. The filter inductor and the energy storage capacitor banks were simulated exactly as shown. If a higher degree of accuracy is required the filter reactors may be programmed as non-linear elements. The dual three phase full wave rectifier block was programmed as twelve independent diodes which present either a very high reverse resistance or a low forward voltage drop in accordance with the polarity of the voltage applied to their anodes. This block also includes the R-C transient despiker circuits necessitated because of severe rectification commutation transients. Next appropriate inductance and resistance values, referred to the secondary, were inserted to simulate the leakage inductance and resistance of the high voltage transformers. The delta to wye block shown simulated the turns ratio of each of the six single phase transformers elements, (by means of their exciting inductance ratios and coefficients of coupling) and in addition, connected the primary and secondarys in delta and wye respectively. Then, each primary line of each channel had series impedances inserted consisting of the leakage inductance and resistance values of the distribution transformer and the induction voltage regulator respectively, plus the channel distribution transmission line inductance and resistance. Finally, the channel solid state interrupter was programmed as a pair of back to back controlled rectifiers which had the same action as the power supply diodes described previously in their normal mode of operation. When interruption was to be affected, the controlled rectifiers were programmed so that after the turn-off command took place, each diode remained in its high resistance state when its anode voltage became negative for the first time. Transient suppression networks were included at the input and output of each back to back pair.

The other three channels of the power system were programmed in an identical manner, however, their crowbar elements were eliminated. Each channel had a full load rating of approximately 420 kVA.

The 7500 kVA common bus power system was simulated as three ideal sine wave generators, wye connected, for the source. Each phase had the machine's specified transient inductance and winding resistance values inserted to represent the generator's short term regulation characteristic. Since a reasonably long transmission line connected the power house to the radar site, the effective value of this line's inductance and resistance was then included in each phase. Finally, to completely define the overall power system's regulation characteristics, the effective value of all other attached generator loads were simulated in lumped three phase fashion.

The model just described was then programmed in CIRCUS 2 format. This digital computer analysis program is widely available throughout the country and it is particularly useful for the analysis of systems such as this one where semi-sinusoidal and transient effects are superimposed. Following initial program de-bugging and several accuracy confirmation runs, a number of detailed system performance runs were conducted. These are briefly described in the next section.

Results of Analysis

The consequences of two system operating modes were of concern; first, what was the effect on the three operating channels when the fourth channel crowbarred; second, what was the effect on the three operating channels when the fourth channel snapped on again (i.e., the snap-on mode is one where the ac line voltage to the channel is instantaneously applied without recourse to any run up cycle). A third condition of concern existed regarding the effect on the three operating channels when a line to neutral fault occurred on the affected channel's power lines (e.g., on the output side of the interrupter but not isolated by the transmitter's iron core component impedances).

Figure 4 presents a summary of worst case results observed from a number of computer runs which simulated the above conditions. A comparison is made in this figure between the baseline (separate bus) system and the proposed common bus system. Columns (1) and (2) demonstrate that if a crowbar or a snap-on takes place on a single channel, the other three channels will experience a worst case common bus dip of about 3%. Columns (3) and (4) illustrate the effect on the bus voltage of the channel under test for the conditions of snap-on and crowbar, while the columns (5) and (6) illustrate the maximum amplitude of the line currents for the same two conditions. Of greater significance from a system performance point of view, columns (7) and (8) show the maximum excursion in the dc collector voltage power supply output when the snap-on and crowbar occur. Since this voltage is one of the factors influencing the r-f amplifier tube's stability, it has overall radar system impact. Column (9) describes the voltage overshoot on snap-on (i.e., above its steady state level). Column (10) shows the consequence of a line to line neutral fault on a channels's supply line. This value determines the worst case interrupting requirement for the a-c line circuit breaker while column (11) indicates the absolute worst case voltage dip on

the common bus. With regard to the crowbar fault conditions it should be noted that the worst case results in all of the above situations were those which would occur without benefit of a solid state interrupter circuit (i.e., the controlled rectifier turn off feature noted previously was not activated in these computer runs).

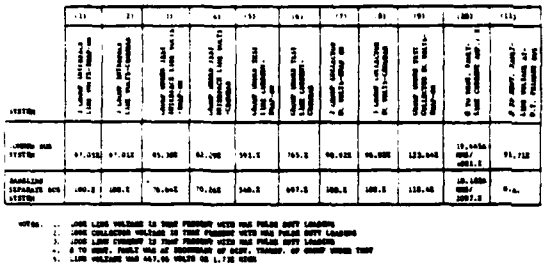

Figure 4 Worst Case Summary

Figure 5 is a transient presentation of the worst case common bus data presented in column (9), and as such, it allows a more meaningful assessment of the capabilities of a solid state interrupter to be made. At zero on the time scale the crowbar has just fired following the completion of a radar pulse. Tho horizontal arrow indicates the level at which the storage capacitor bank was providing collector voltage (at the leading edge of a pulse) during steady state operation. Because of power supply filter delay times, several pulses elapse before the voltage decayed significantly, however, once started the draw down is quite rapid. Since the longest opening time of a solid state interrupter would be about 2/3 of a cycle it can be seen that the average voltage draw down after this period of time would be equivalent to only about 400 volts in 30 kilovolts, or about 1.3%, as compared to slightly over 3% in the worst case analysis of column (8) in figure 4. It should be noted that the worst case in figure 4 assumed a conventional interrupter could clear the fault in slightly less than two cycles (including all sensing time). It is probable that mechanical circuit breakers could not do this well, and if not, the draw down reduction provided by the solid state circuit breaker would be even more significant.

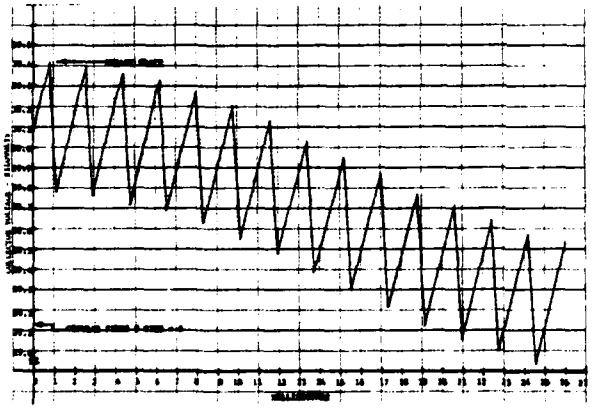

Figure 5 Collector Voltage on Un-Faulted Channels

For the common bus system under consideration in this case, the collector voltage draw down was within radar system r-f phase and amplitude tolerances when solid state interruption was used. Fortunately, the original transmitter design had incorporated a solid state contactor primarily because of some of the other advantages indicated in figure 2. Since sufficient overload capability margin was inherent in the original solid state interrupter design to accommodate the much higher a-c line fault currents of the common bus power system, this power system proved to be an acceptable alternate without the need of transmitter equipment modifications.

Solid State Contactor Design

Figure 6 shows, in simplified schematic form, the solid state contactor used to control the normal turn-on and turn-off of the 460 volt ac three phase lines to the high voltage power supply of each channel. The circuit also provides the means to rapidly interrupt the 460 volt lines under the load fault conditions just described.

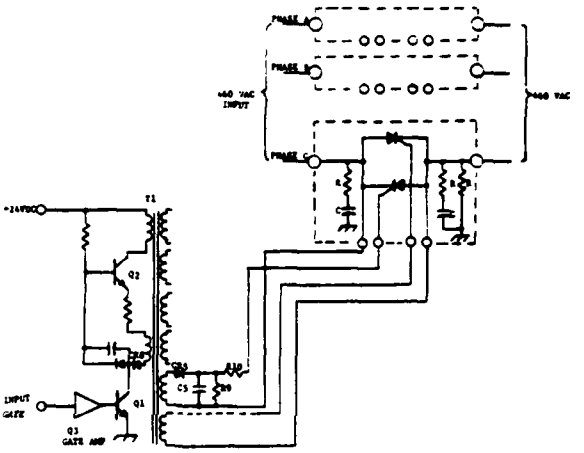

Figure 6 Simplified Schematic of Solid State Contactor

Each line uses an inverse parallel connected set of thyristors as detailed in phase C. Since both the input and output circuits attached to the SCR's are inductive, the RC despiking circuits shown were necessary to attenuate transients which would otherwise be destructive to the SCR's and possibly to other overall circuit components.

Gate triggers for the SCR's are coupled to all six units by means of six secondary windings on transformer T1 in order to obtain electrical isolation of the low level control circuits from the 460 volt lines. The output signal from each winding is half wave rectified by means of CR5 to provide unidirectional gate signals. The operating frequency applied to the primary of T1 is a CW wave of approximately 18 kHz. This frequency is sufficiently high so as to insure the SCR's trigger early in each cycle of the 60 Hz prime line voltage wave. Also, since 18 kHz is above the typical audible range, an annoying sound source is avoided.

Transistor Q2 functions as the driver oscillator with positive feedback obtained from an appropriate winding of transformer T1. The driver oscillator is turned on by the application of a +15 volt d-c gate to transistor Q3. This gate functions to turn on transistors Q3 and Q1. Q1 provides a ground return

for the +24 volt source of oscillator Q2 thus initiating oscillator action and the resulting triggering of all six SCR's. When the 15 volt gate to Q3 is removed, the oscillator ceases operation within 100 microseconds, thereby providing interruption of the 460 volt three phase prime lines. On an ideal waveform basis, all three lines would always be interrupted within 1/2 cycle of the line voltage waveform. In actual operation, due to the rather severe waveform distortion introduced as a result of rectifier commutation of the high currents associated with a d-c power supply fault, somewhat longer interrupting times, possibly as great as 2/3 cycle may result under worst case conditions. On the other hand, many faults are interrupted in less than 1/2 cycle if the fault occurs at a more favorable point in time with respect to the line voltage waveform crossovers.

Figure 7 shows the physical configuration of the solid state contactor. The basic SCR units are similar to the General Electric C600 series which carry 1200 repetitive inverse voltage and 900 ampere average current ratings. The units shown utilize a special packaging format, however. They are packaged by the semiconductor manufacturer as type G10 liquid cooled switches, and as such, are supplied with back to back SCR pairs, input and output bus bar connections, gate terminal strip connections, and liquid coolant fittings.

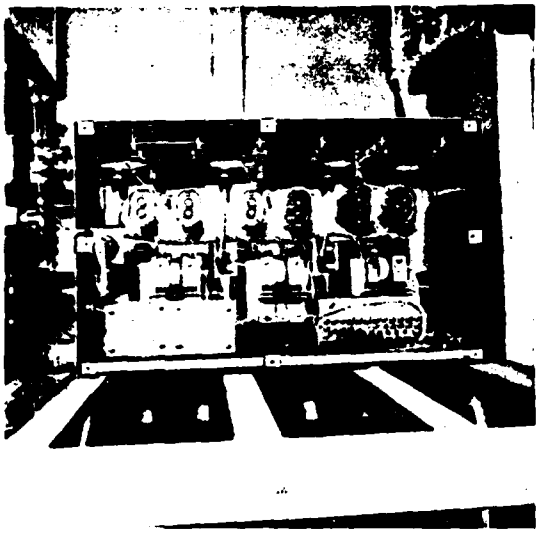

Figure 7 Solid State Interrupter Assembly

The overall solid state contactor package has dimensions of 32" X 19" X 12" and weighs approximately 70 pounds. It has a calculated MTBF of 114,000 hours and a MTTR not greater than 1 hour.

Test Results and Conclusions

While final site installation of the system discussed here has not been completed, a prototype channel of the transmitter has been fabricated and tested extensively. A power source having substantially the same stiffness as that of the final power system was used during the evaluation phase. The performance of the solid state contactor was essentially identical with the results predicted from the computer aided analysis.

Some typical waveforms are shown in figure 8. The upper waveform shows the nature of one of the line currents when the system was running at maximum pulse duty factor. The center waveform was the result of about 12 trial crowbar shots taken to establish a worst case negative current interruption while the lower waveform represents the same situation for a positive current interruption. In both cases the scope sweep was triggered by the firing of the crowbar, and in both cases the interruption was complete in approximately 1/2 cycle. The transient near the top of each waveform coincides with the time at which the first phase was interrupted.

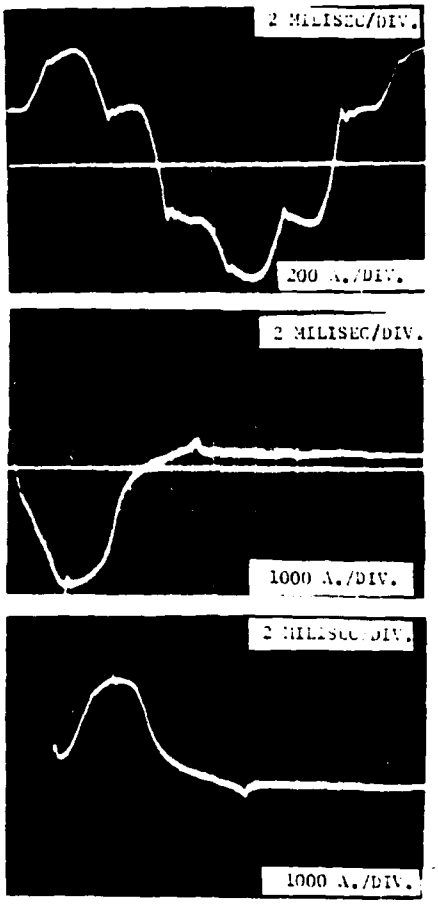

Figure 8 Interrupter Performance Waveforms

Where rapid interruption of prime line currents in multiple channel d-c power supply systems is a requisite, the use of electronic line interrupters appears to be extremely beneficial from the points of view of maximum speed of operation and high reliability. Possible limitations of the electronic interruption approach lie in the availability of the back to back switch elements for use in higher voltage and/or higher current systems. For such systems, the use of ignitrons could overcome both the voltage and current limitations. Similarly, series and parallel connected SCR's could perhaps also overcome both voltage and current limitations. Either approach would probably result in considerably more circuit complexity than the extremely simple approach employed for this application.

A THYRATRON WITH MAGNETIC INTERRUPTION

R. J. Wheldon
English Electric Valve Company Limited
Chelmsford, Essex.

Summary

It is not possible to interrupt the current flowing through a hydrogen thyratron by applying a negative control grid potential as in a hard tube; it can only be turned off by reducing the anode voltage to near zero. This paper describes a multi-grid thyratron where the discharge can be extinguished within a few microseconds by the application of a pulsed magnetic field. The fast recovery capability of the multi-grid thyratron enables interruption to be achieved by means of a short magnetic pulse applied to the grid region of the tube.

Such a tube can be used as a protective device in series with a high voltage power supply unit, the magnetic field rapidly turning off the current in the event of a fault occurring in the load circuit. The voltage would remain on the power supply and hence the load current can be restarted immediately the fault has cleared by triggering the thyratron interrupter. Other applications include use as a triggered charging tube with magnetic protection or for forming long current pulses by alternately triggering the control grid and magnetically switching off.

Introduction

Thyratrons are rapid acting switches operating at present up to 240 kV, peak currents up to 10 kA and average currents up to 50 A and there is little doubt that all these parameters could be exceeded should the demand arise. Conduction is normally established by application of a positive trigger pulse to the control grid; thereafter the grid loses control until the circuit causes the anode voltage to fall below the arc voltage of the device. It is not normally possible to switch off a thyratron by applying a negative voltage to the grid because once conduction has started the grid is immersed in a plasma of ions and electrons. A negative voltage on the grid results in the formation of a thin sheath around the grid aperture across which all the volts are dropped and thus the effect of grid potential on plasma potential is very small. The discharge can only be extinguished if the sheaths grow large enough to block the grid aperture. This normally only occurs during the recovery period as the plasma dies away.

It has been found possible to interrupt the discharge in a hydrogen thyratron by means of a pulsed magnetic field. Two approaches have recently been made to this development; one has been to apply the magnetic field to a post-anode discharge[1] and the other to apply the field to the grid region of the tube[2]. The present paper describes the latter approach. It has the advantage that the thyratron design is simpler and involves far lower power loss in the actual switching device during the "on" period.

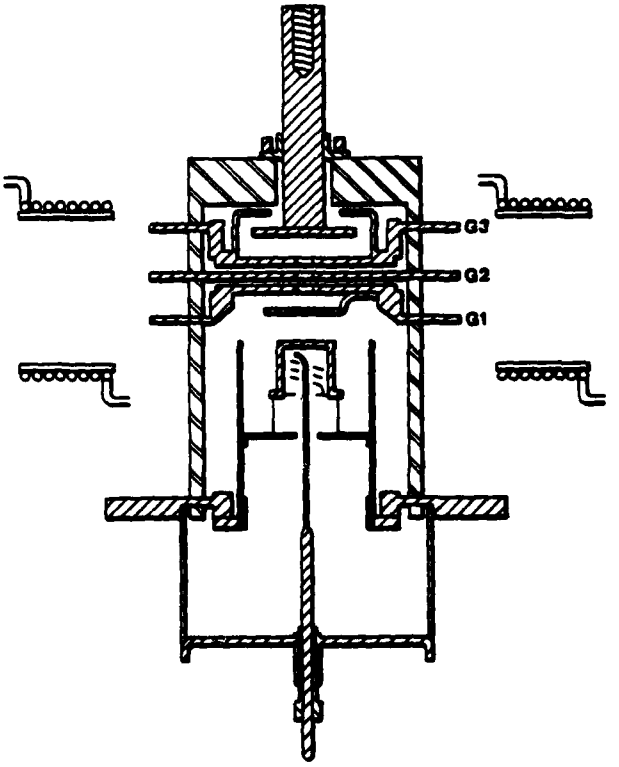

Fig.1
Diagram of Triple Grid Thyratron with Magnetic Field Coils

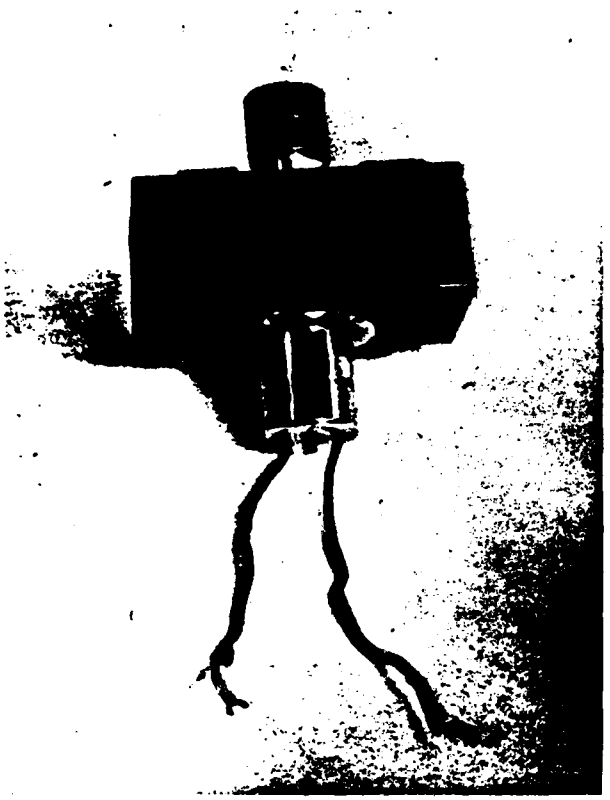

Fig.2

The Thyratron Interrupter

Fig. 1 is a diagram of the tube and its associated magnetic field coils. Fig. 2 is a photograph of this arrangement.

The tube construction is basically that of a multi-grid thyratron with grid 2 shielded from the anode and with close spacings to produce fast recovery characteristics. This ensures that on interruption the tube recovers within a few microseconds, minimising the pulse length requirements of the magnetic field. Because of the low anode to G2 capacitance, the rapid build up of high anode voltage across the tube after interruption does not cause the tube to refire. The grid slot configuration and its relation to the magnetic field is an important factor in optimising the field-discharge interaction.

Fig. 3 shows one circuit which has been used to investigate magnetic current interruption.

A d.c. power supply (P1) charges the reservoir capacitor C_1 to a voltage V (typically 5 - 10 kV) whilst a second supply (P2) charges the 3 μF capacitor C_2 in the magnetic circuit to 10 kV. On initiating the prime trigger the thyratron interrupter is fired immediately causing a current controlled by R (typically 0.1 to 150 A) to flow from C_1. The same trigger pulse after passing through a variable delay unit fires the 8503 thyratron in the magnetic circuit, discharging the 3 μF capacitor through the magnetic field coils.

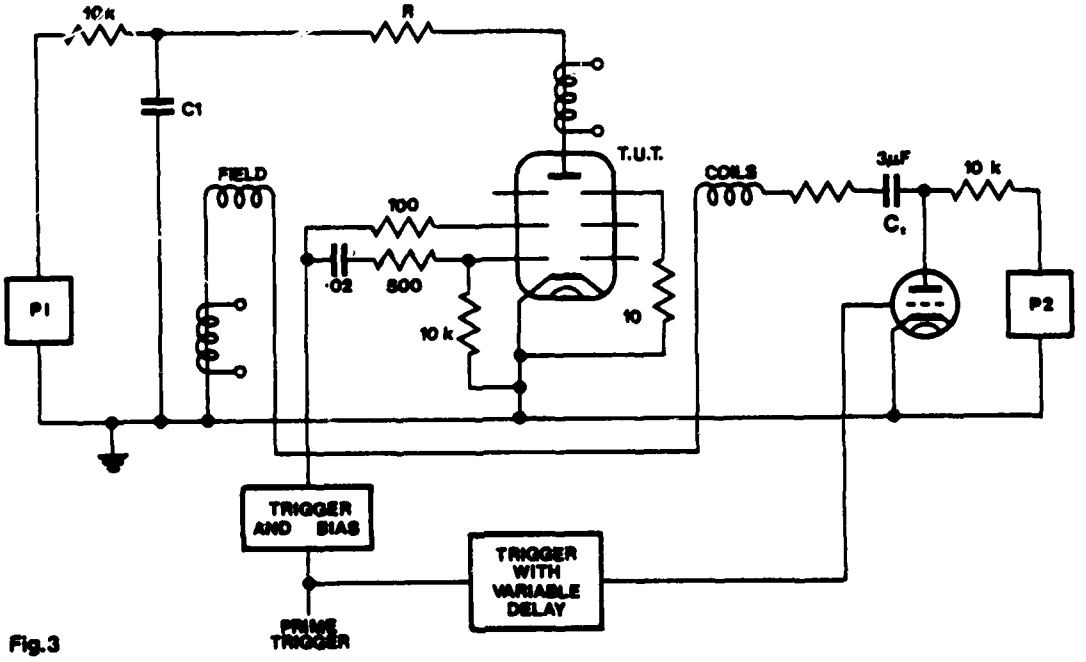

Fig.3

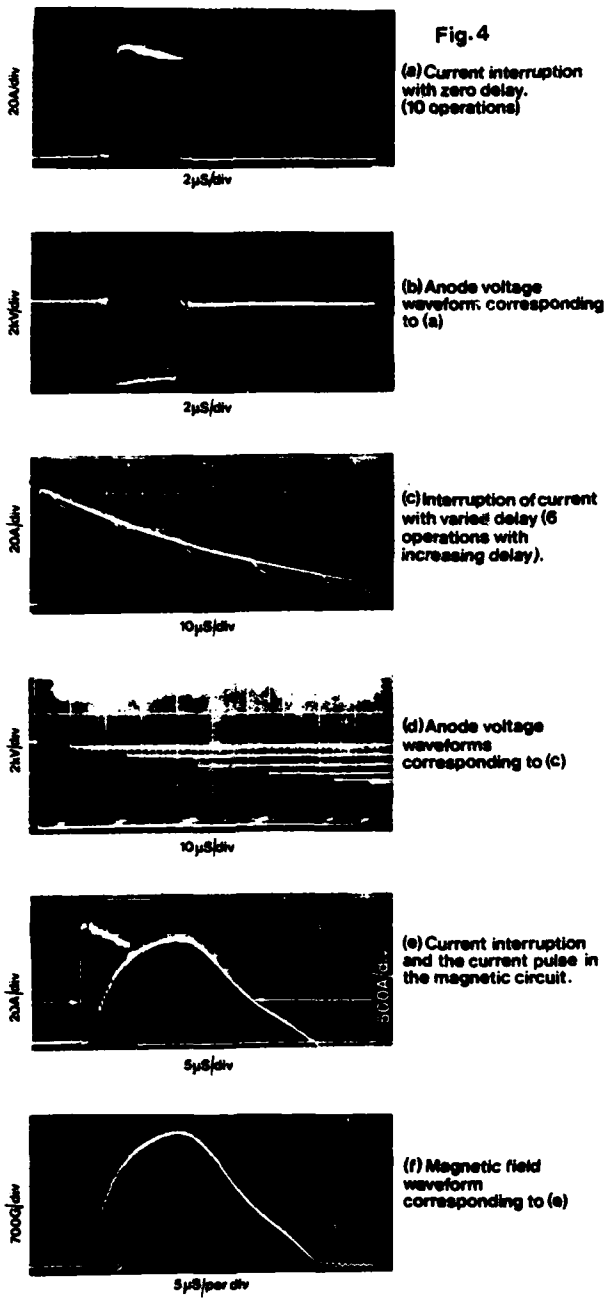

Fig. 4

Fig. 4 shows photographs of current and voltage waveforms observed with this circuit.

(a) Interruption of current with zero delay. (10 superimposed shots).

(b) Anode voltage waveforms corresponding to (a).

(c) Interruption of current with varied delay.

(d) Anode voltage waveform corresponding to (c).

(e) Current interruption and the current pulse in the magnetic circuit.

(f) Magnetic field waveforms corresponding to (e).

Fig. 4 (e) shows the delay associated with the interruption process. This is comprised of the risetime of the magnetic pulse together with any delay due to the interruption process. Fig. 4 (a) shows 10 superimposed shots indicating that the jitter is small and of the order of 0.5 μs. Fig. 4 (b) shows the anode voltage recovering rapidly without any tendency to retrigger the thyratron.

Figs. 4 (c) and 4 (d) show how the time interval between triggering and recovery can be controlled, producing current pulses of any desired duration. In these waveforms the pulse length was increased successively from one pulse to the next at 1 p.p.s.

Fig. 4 (d) shows that with the particular arrangement under investigation, the minimum duration of conduction was of the order of 4 μs.

Fig. 4 (e) shows the relatively slow build-up of current in the coils and Fig. 4 (f) how closely magnetic field is associated with that current build-up.

Coil Design Considerations

Whereas the mechanism of current extinction is not fully understood, it would seem probable that the highly conductive plasma is moved bodily by the interaction between the current and the magnetic field, thus behaving very similarly to a conductor in a magnetic field. The coil should be designed to produce the maximum uniform field strength in the vicinity of the grids and its inductance should be as low as practical so as to improve the rate of build-up of the magnetic field and hence reduce the time which must elapse before the current is interrupted.

Since inductance is proportional to the square of the number of turns whilst the field depends only on that number, it would seem preferable to use the minimum number of turns and the maximum current if rapid interruption is required. This, requires high voltages to be used and hence, a thyratron must be used to switch the magnetic field. High voltages

introduce inter-turn insulation problems and so the optimum design becomes a compromise between these various factors.

The magnetic field must persist, for as long as it takes the thyratron (a) to interrupt the current and (b) to recover sufficiently to avoid any risk of subsequent re-firing as the anode voltage rises after the interruption.

Experimental Results

In addition to the results given in the various oscillograms of Fig. 4, an investigation has been made of the inter-relation between the current interrupted and the maximum voltage at which reliable interruption can be obtained. The tests were carried out with the peak magnetic field of 2.5 kGauss and which exceeded 1.6 kGauss for 15 μs and Fig. 5 shows how one particular thyratron behaved. With 5 kV or less on the anode reliable interruption was obtained of currents up to 150 A. With 10 kV on the anode the current level fell to a few amps. These results appear typical for the small thyratron used. The energy in the magnetic pulse was 135 joules.

Applications of the Thyratron Interrupter

Two obvious applications for a thyratron interrupter are:-

(a) To protect delicate equipment, such as, a travelling wave tube or a gridded klystron against damage due to flash arcs.

(b) As an efficient means of generating long current pulses.

In application (a) the device is directly interposed between the device to be protected and its source of power. The thyratron is triggered in order to initiate conduction and, in the absence of any fault, then carries the full load current for as long as is necessary. The voltage drop across the device is typically less than 100 V. Should a fault occur the field-generating circuit is triggered. This then interrupts the current flow within a few microseconds. As soon as the fault has been cleared, it is possible to re-trigger the thyratron and so revert to normal operation more rapidly than by means of electro-

Fig. 5 Limit of Reliable Interruption

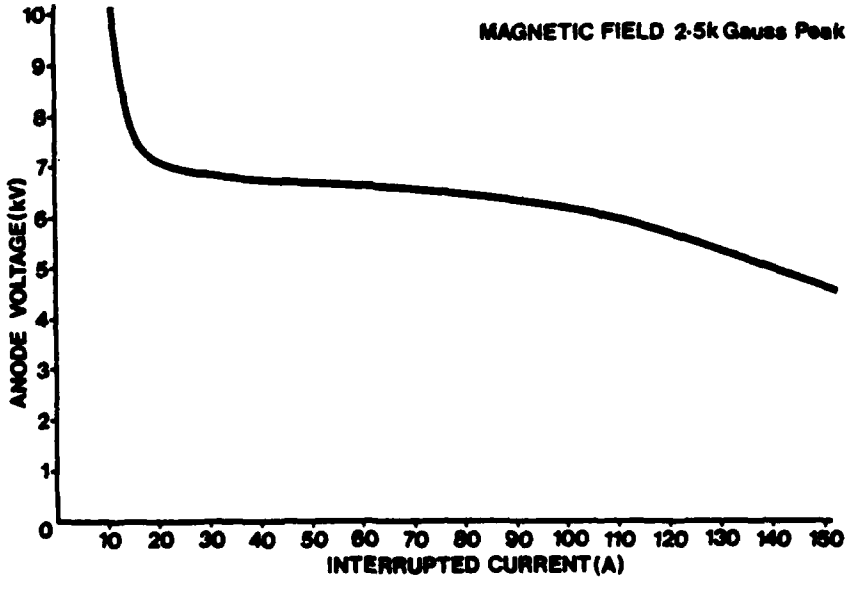

mechanical switching or electronic control of the power supply. Fig. 6 illustrates such an application. Here the pulser can be triggered in the event of a fault and this starts to act as a crowbar.

For application (b) the thyratron is triggered to initiate the pulse then, after a suitable delay, the magnetic circuit is triggered to terminate it. This enables pulses to be generated of almost any duration over the minimum shown in Fig. 4 (a) and, apart from practical considerations such as heating of the thyratron and allowing enough time for recovery of the magnetic switching circuit, there would seem to be few limitations to the system.

For pulse lengths approaching the minimum the interruption time jitter may be a significant factor (say 0.5 μs) but for substantially longer pulses this amount of jitter may be found acceptable.

Conclusion

The results described were obtained by using standard parts readily available. They indicate that a fast interruption process appears possible but whether or not optimum conditions existed is a fact open to doubt.. Nor is it certain whether or not the result obtained can be substantially extended to higher voltages and currents.

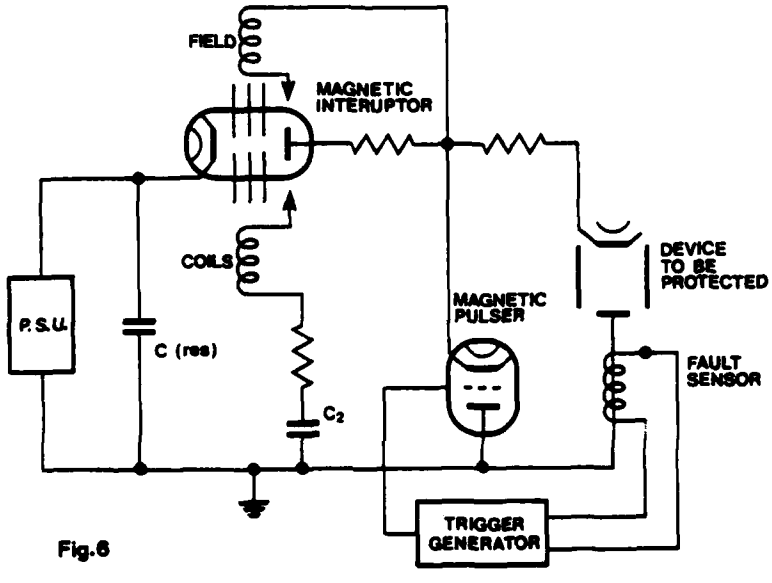

Fig.6

References

(1) Magnetic Field Control of a Gas Discharge Switch.
D. V. Turnquist.
Modulator Symposium 1966.

(2) A High Speed Thyratron D.C. Circuit Breaker.
B. O. Baker.
IEE Conference on Gas Discharges 1970.

Acknowledgements

The author wishes to thank the Directors English Electric Valve Company Limited permission to publish this paper.

REPETITIVE SERIES INTERRUPTER

Maurice Weiner
US Army Electronics Technology and Devices Laboratory (ECOM)
Fort Monmouth, New Jersey 07703

Summary. Self modulated high power microwave tubes may be protected against arcs in at least two ways. One technique involves the use of a crowbar to divert the energy. Another approach is a high voltage fuse. In both cases a great deal of down time is involved. This work describes a third approach wherein a normally closed series device is placed in the discharge circuit. Upon the sensing of an arc the device interrupts the current until the arc clears. This permits operation on the next pulse. The device is basically a thyratron with a long discharge region in series with a perforated anode. Operation of the device depends on the application of a pulsed magnetic field in the interaction region to vary the impedance of the discharge. The interrupter device is described and measurement results of voltage tube drop, pulse shape, and magnetic fields needed for current interruption are given. The physical mechanisms underlying the current interruption are discussed. Results of the study demonstrate overall feasibility and point out areas requiring further development.

INTRODUCTION

High power, self-modulated microwave tubes may be protected against arcs in two ways. One means for tube protection is the use of a high voltage fuse. When a tube arc occurs the increased current causes the fuse to open, thereby preventing further damage to the tube. The second technique involves a crowbar switch shunting the microwave tube. In the event of an occasional tube arc the switch is closed and energy is diverted from the tube to the crowbar circuit. In both these techniques the system shuts down and time is required to return the system to operation.

This paper discusses a protective device, the repetitive series interrupter (RSI), which is basically an electronically resettable fuse and therefore does not require system shut down. The RSI is placed in series with the microwave tube in the discharge circuit (Fig. 1). The RSI is normally closed. In the event of an occasional tube arc, however, a current sensor causes the RSI to temporarily interrupt the current allowing the tube arc to clear. The RSI then returns to its normally closed position during the interpulse time, allowing the next pulse to occur. As a result a continuous tracking capability may be maintained for a radar system. In the event of continual arcing, the logic for the RSI can be programmed to permanently open up the circuit after a specified number of consecutive interruptions (typically 5). This can be of particular importance in a radar using multiple microwave generators since the system can continue operation with diminished rf output. An RSI can also be used to immediately turn on a stand-by microwave generator if continuous full power operation is required.

The same basic device may be used in two other protective modes of operation, as shown in Figs. 2a and 2b. As in the previous mode of operation, these two modes serve to protect against the occasional arc without resorting to system shut-down. Figure 2A shows an RSI in the charging circuit. In the event of an arc a current sensor causes the RSI to interrupt the charging current. The advantage of this technique is that no pulse jitter, distortion or delay is introduced because the protective device is not located in the discharge circuit. This mode assumes the microwave tube is capable of dissipating the stored energy in the capacitor without suffering permanent damage. This mode of operation also eliminates the necessity of resistively charging the secondary capacitor, thus enhancing the efficiency.[1] In Fig. 2b the device operates in a crowbar mode; the normally open protective device shunts the microwave tube. When arcing occurs the device is triggered into conduction, diverting the arc current from the tube and allowing the arc to clear. The protective device is then triggered back into the non-conducting state. The power supply need not be shut down unless the arc does not clear. Longer life may be attained since the device does not operate continuously. The disadvantages are: (1) resistance in the capacitor circuit is required, thereby lowering efficiency, and (2) the device must be designed to handle higher currents.

In this paper experimental results will be presented on the RSI operating exclusively in the discharge circuit, as shown in Fig. 1. No experimental results were obtained on the protective modes of Figs. 2a and 2b. Previous experimental work, however, has been performed on the RSI device in the charging circuit.[2]

The principle of operation, the design, and measurements of tube drop, pulse wave form, and parameters necessary to interrupt the current are discussed.

DISCUSSION

Device Concept

The RSI is shown schematically in Fig. 3. The device consists of a thyratron section coupled, via a perforated anode, to a relatively long magnetic interaction column. The final anode is located at the end of the column. Current interruption is achieved by the application of a pulsed magnetic field directed transverse to the axis of the interaction column. The magnetic field effectively increases the impedance of the interaction region eventually causing complete interruption of the current. The magnetic field is removed before the start of the next pulse, thus preparing the RSI for conduction on the next pulse.

The thyratron section may be operated in either a keep-alive or triggered grid mode for a pulse system. The keep-alive mode is necessary for a CW system. In a pulse system, the advantage of the keep-alive is the elimination of a trigger for each rf pulse. The use of the grid mode on the other hand, allows for possibly a simpler way to permanently interrupt the current.

Experimental Designs

Two designs of the RSI device were tested. The type A design is shown in Fig. 4 together with a photograph of the finished device in Fig. 5. The device was fabricated by C. Shackelford of ITT under Contract DAAB07-73-C-0320. The thyratron is an 8613 model

capable of 15 kV peak and 0.5 amps average current, and a peak current rating of 500 amps. The grid structure is modified to allow for the introduction of a separate keep-alive, which requires 140 volts and runs at 100 mA. The reservoir is set for a pressure of 0.45 torr hydrogen. The thyratron section is coupled to the magnetic interaction section by means of a wire mesh. The interaction region is folded back to reduce device length and facilitate magnetic field design. The length of the inner column is approximately 14" and that of the folded region is 10". The ID of the inner column is 3/8" and the folded annular region has an ID of 1/2" and an OD of 1.0". The design A model is discussed in more detail in Reference 2 where the device was developed for use in the charging line.

Design B is shown in Fig. 6 together with a photograph of the completed device in Fig. 7. The device was built by D. Turnquist of EG&G under Contract DAAB07-73-C-0274. The thyratron is a 7665 model capable of 16 kV peak, 0.5 amps average, and 350 amps peak. The grid element was operated as a keep-alive, running at 75 volts and 30 mA. The pressure is 0.4-25 torr hydrogen. The thyratron is coupled to the interaction region by means of a circular aperture. The interaction region is folded 3 times, thus providing 4 sections, each approximately 5 1/2" long. An electrode is provided at the end of each section, so that the effect of interaction length on the device behavior could be investigated. The ID of the interaction region is 0.181". The design criteria leading to the construction of the type B device is given in Reference 3.

Test Set-Up

The set-up is shown in Fig. 8. Tube drop, waveforms and magnetic fields to interrupt normal conduction currents were measured. The microwave tube is simulated by a combined hard tube, the Machlett 6544, and a 500 ohm low inductance load resistor. The RSI is in series with the load. The pulse current is supplied by a 0.5 μf capacitor charged to 15 kV. The pulse current was measured with a wide band transformer and pulse voltages were measured with a Tektronix P6015 probe. Measurements were obtained using a keep-alive mode of operation in the thyratron.

A 17 turn bifilar coil, ten inches long, produced approximately 1.64 gauss/amp. A single current pulse for the coil was supplied by a 75 μf capacitor charged to 4 kV. Switching was accomplished by a triggered spark gap. The triggering of the spark gap was done after the start of the normal current pulse.

The test set-up for measuring the interruption behavior under fault current conditions (Fig. 9) is similar except for the addition of a thyratron switch, which shunts the load resistor and the hard tube. After the start of the normal conduction pulse the thyratron is triggered into conduction, effectively shorting the load and hard tube and providing a fault current to the RSI. The level of fault current thru the thyratron is varied by adjusting the tap on the series resistance of the hard tube.

Measurement Results

a. Tube Drop. Tube drop measurements are shown in Figs. 10 and 11 for both designs. The hard tube was operated in the linear range. The conduction current increased with source voltage, reaching about 20 amps at 15 kV. It is noted that the tube drop decreases slightly as the source voltage and peak current are increased. The voltage drop in the thyratron section accounts for only a small part of the total tube drop; the thyratron voltage drop in type A tube is 150 volts and in the type B tube it is 75 volts. The increase in tube drop as the interaction length increases is evident from Fig. 11. The tube drop is approximately proportional to the interaction length.

b. Magnetic Fields Required for Interruption. Figure 12a shows, for the type A device, the interrupted fault current superimposed on the uninterrupted fault current (upper traces). The bottom trace shows the magnetic field current pulse. Because of the large coil inductance the field current reaches its peak (corresponding to 5000 gauss) at about 100 μs. Figure 12b shows the results when interrupting normal conduction pulse under non-fault conditions. Based on previous work (Reference 3) the plasma reacts to turn-off fields in less than a microsecond. The turn-off times observed are not representative of those that can be achieved with magnetic field generators having smaller risetimes.

Figure 13 shows the variation of turn-off field as a function of the fault current for the type A model. The source voltage is fixed at 8.6 kV. The fault current was changed by varying the value of resistance shunted by the thyratron switch. The field was measured by noting the current flowing in the magnet coils at the time the fault current goes to zero. It is seen that the turn-off field changes little as the fault current increases.

Figure 14 shows the variation of the turn-off field, interrupting normal conduction currents, as a function of the source voltage. As noted from the figure the turn-off field increases linearly with source voltage. Comparison of Figs. 13 and 14 shows that the turn-off field is largely dependent on the source voltage, rather than the peak current.

Figure 15 shows typical waveforms, for the type B tube, of the interrupted and non-interrupted discharge currents (lower traces) and the magnetic field current pulse (upper traces). The current pulses interrupted here are for normal conduction pulses, i.e., no fault current was introduced. The magnetic field coil used was the one designated for the type A tube geometry.

Figure 16 shows the variation of the turn-off field as a function of the interaction length for the type B tube. The turn-off field decreases as the interaction length is increased. The tube drop, on the other hand, increases with interaction length. Comparison of Figs. 16 and 11 shows the kind of trade-off which may be made between the tube drop and turn-off magnetic field as the interaction length is varied.

c. Current Waveform. Figure 17 shows the current pulse in the cathode leg of the 6544 at 10.8 kV operated in series with the type B tube using 4 interaction lengths. The initial spike is the 6544 capacitance discharging. This is followed by a 1.0 μs delay before full current conduction occurs, corresponding to full RSI conduction. The results are complicated by feedback to grid drive producing oscillation. Jitter, if present, is hidden in these oscillations. The observed delay decreases several tenths of a microsecond when the voltage is increased from 7 to 15 kV. No delay is observed when the magnetic interaction region is not used. The reduction in delay by using one instead of four sections, is approximately 15%. The delay therefore can be attributed primarily to a formative time lag which involves the coupling aperture connecting the thyratron section and the magnetic interaction region.

Physical Mechanisms of Current Interruption

Two possible mechanisms which explain current interruption, caused by the magnetic field, are: (a) an increase in the transverse electron mobility, thereby increasing the discharge impedance, and (b) motion of the discharge against the tube wall, caused by $\vec{J} \times \vec{B}$ forces, where $\vec{J}$ is the current density and $\vec{B}$ is the magnetic field. The proximity of the wall to the discharge enhances electron diffusion to the wall, as well as recombination, so that the discharge impedance is again increased.

The increase in the transverse mobility qualitatively explains certain features of the current interruption. In particular, for the type B tube, the change in turn-off field as a function of the interaction length, as well as the variation in discharge current with field (Fig. 15), may be qualitatively explained. However, wall effects arising from $\vec{J} \times \vec{B}$ forces cannot be ruled out as a contributing factor, or even a predominant factor, to the current interruption, since (a) selective "scorching" of the tube walls have been observed in agreement with the $\vec{J} \times \vec{B}$ direction, (b) the calculated time for the motion of the discharge against the wall is of the order of 1.0 μs, which is much less than the time frames used in the measurements of current interruption, and (c) a complete model describing wall effects arising from $\vec{J} \times \vec{B}$ force is not yet available, but may presumably explain the observed current interruption.

An observation concerning the current interruption is worth mentioning since it may provide a clue to the underlying physical mechanisms. From Figs. 12a and 12b, which apply to the type A tube, it may be seen that the current decreases rapidly at first, but at the end of 20 μs or so the current decline becomes oscillatory and apparently more gradual. This behavoir barely appears in the type B tube, and at that only for the single interaction length, and not in the cases where the interaction length is longer. In any event the change in the current decline, as the field increases, is probably indicative of a change in the mechanism controlling the current interruption.

CONCLUSIONS AND RECOMMENDATIONS

Test results of an RSI device operating in the discharge circuit have been presented. The device consists of a thyratron coupled to a magnetic interaction region. Current interruption is achieved when a pulsed magnetic field is directed perpendicular to the current flow. Measurements of tube drop, turn-off magnetic field, and pulse wave form were obtained. Measurements showing the trade-off between tube drop and turn-off magnetic field amplitude, as a function of interaction length, are given. The measurements also show the strong dependence of the turn-off field on the applied voltage, in contrast to the weak dependence on discharge current.

The results obtained show that the RSI is a feasible concept. Additional studies have to be conducted at full average power to determine reliability and life. The various types of circuit applications have to be investigated more thoroughly. Because of system requirements the magnetic field generator must be compact. In this regard the use of ferromagnetic material for producing the field may be applicable.

ACKNOWLEDGEMENTS

Useful discussions with S. Schneider and J. Creedon, US Army Electronics Technology and Devices Laboratory (ECOM), are acknowledged.

REFERENCES

1. G. Taylor, S. Schneider, "Energy Control for Microwave Amplifier Arrays," IEEE Transactions on Aerospace and Electronic Systems, Vol. AES-4, No. 5, pp. 659-664, September 1968.

2. C. Shackelford, "Repetitive Series Interrupter," Final Report, ECOM Contract DAAB07-73-C-0320, September 1974.

3. J. Thomas, H. Vanden Brink, D. Turnquist, "New Switching Concepts," Final Report, ECOM Contract DA28-043 AMC-00123CE, October 1967.

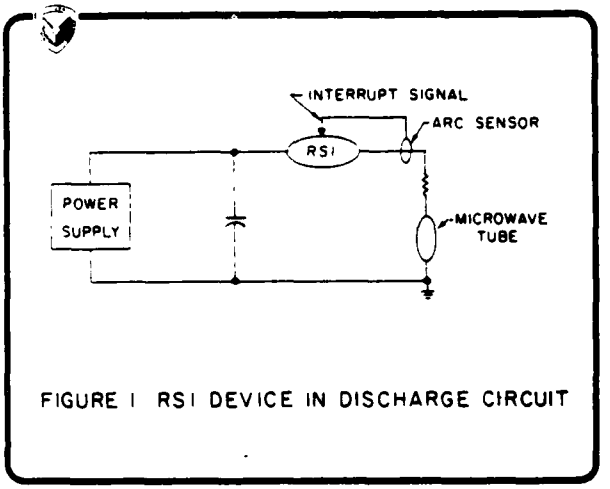

FIGURE 1 RSI DEVICE IN DISCHARGE CIRCUIT

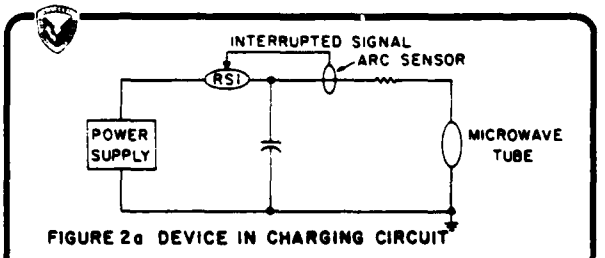

FIGURE 2a DEVICE IN CHARGING CIRCUIT

FIGURE 2b. RESETTABLE CROWBAR

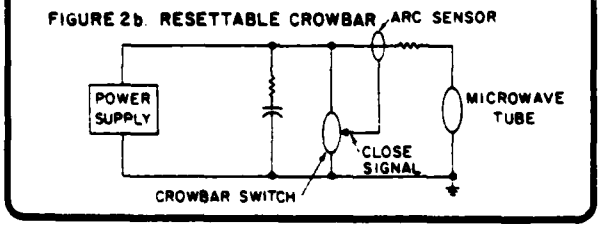

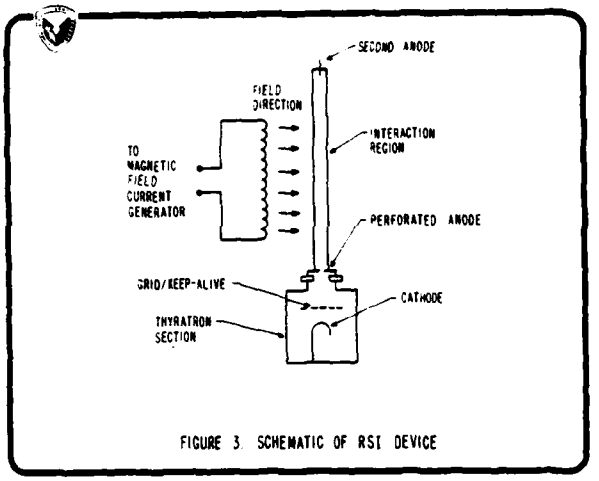

FIGURE 3. SCHEMATIC OF RSI DEVICE

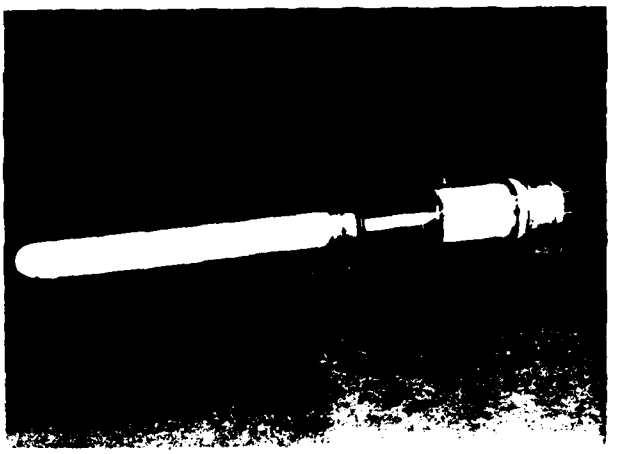

FIGURE 5. RSI DEVICE TYPE A

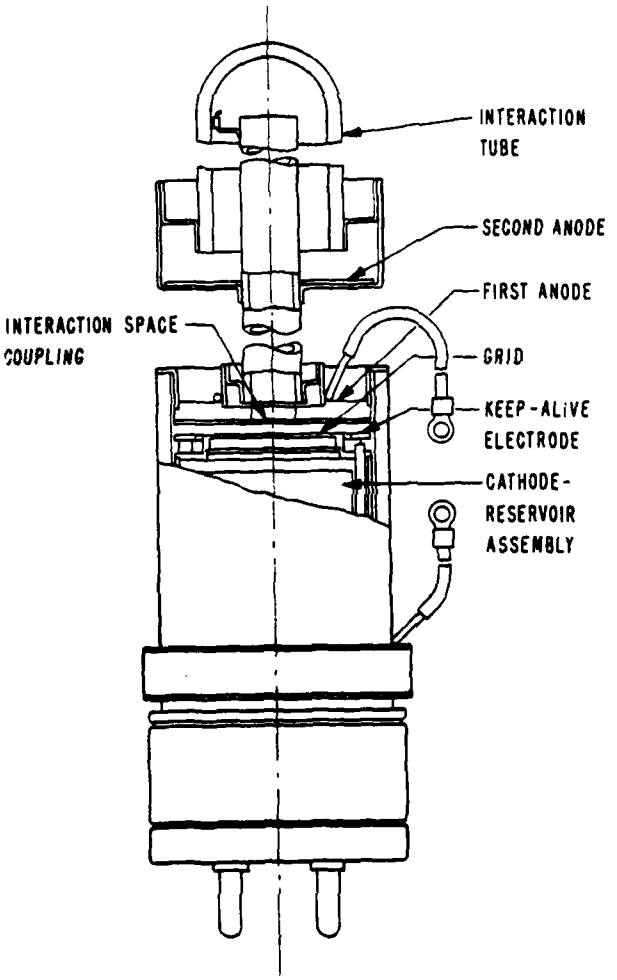

FIGURE 4: RSI DEVICE: DESIGN A

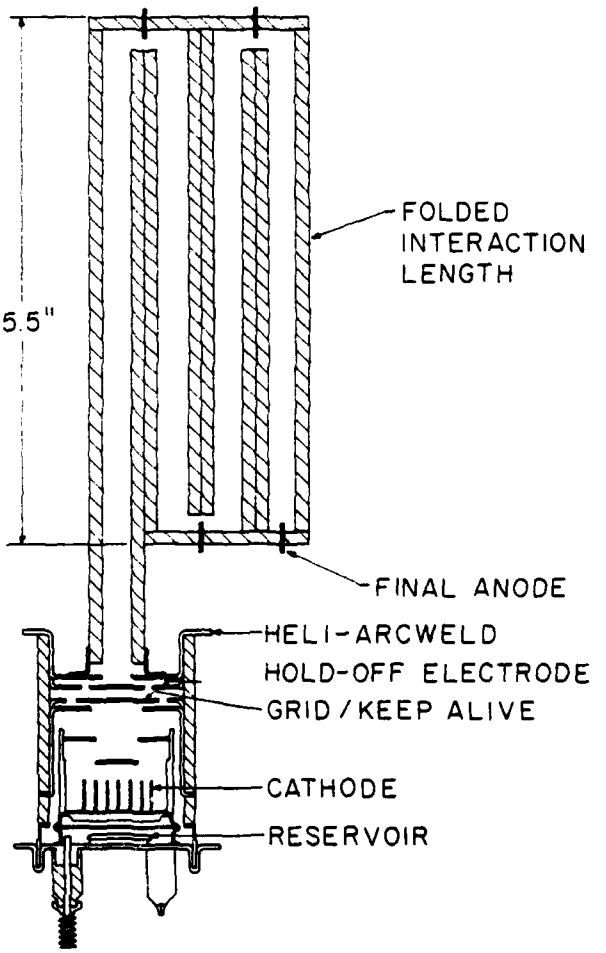

FIGURE 6. RSI DEVICE TYPE B

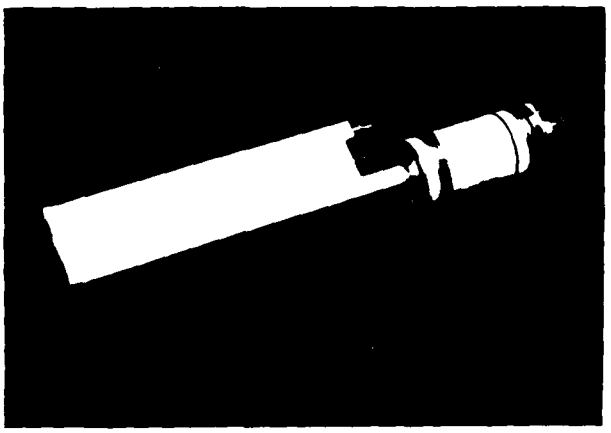

FIGURE 7 RSI DEVICE: TYPE B

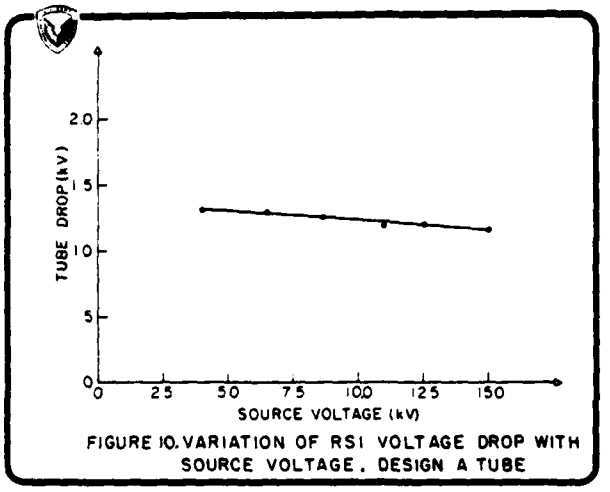

FIGURE 10. VARIATION OF RSI VOLTAGE DROP WITH SOURCE VOLTAGE, DESIGN A TUBE

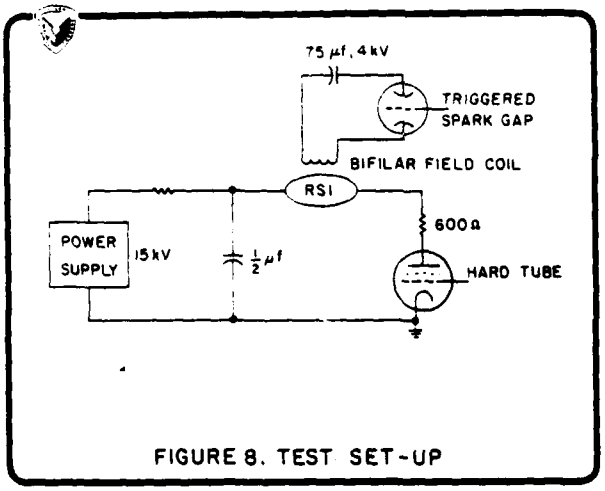

FIGURE 8. TEST SET-UP

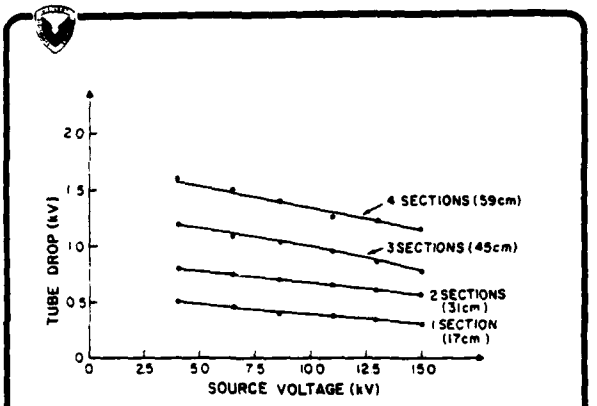

FIGURE 11. VARIATION OF RSI VOLTAGE DROP WITH SOURCE VOLTAGE, DESIGN B TUBE

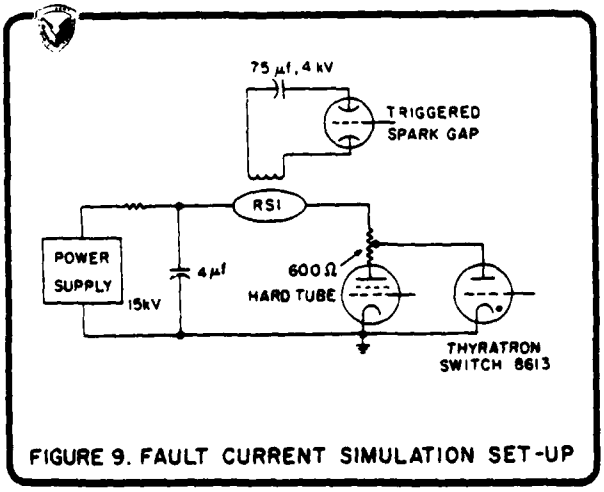

FIGURE 9. FAULT CURRENT SIMULATION SET-UP

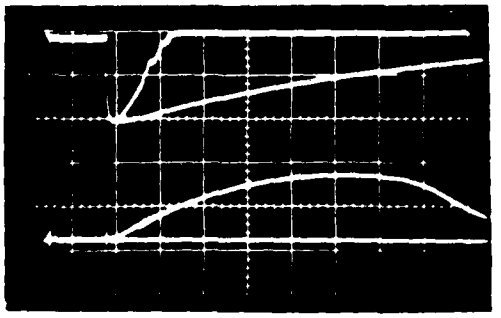

F'gure 12a
Interrupted Fault Current and Field Current Waveforms in Type A Device

Upper Traces: Interrupted current superimposed on the uninterrupted current at 6.4 kV
Horizontal = 20 μs/cm
Vertical = 50 amps/cm

Lower Trace: Field Current
Horizontal = 20 μs/cm
Vertical = 2000 amps/cm

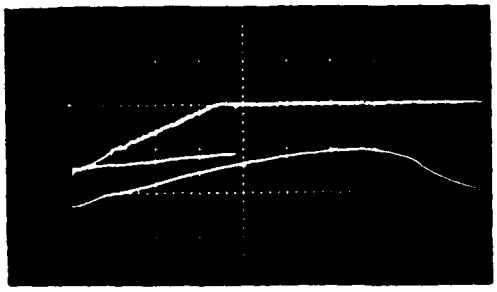

Figure 12b

Interrupted Normal Conduction Current and Field Current Waveforms in Type A Device

Upper Traces: Interrupted normal current superimposed on uninterrupted current at 12.8 kV
Horizontal = 20 μs/cm
Vertical = 10 amps/cm

Lower Trace; Field Current
Horizontal = 20 μs/cm
Vertical = 2000 amps/cm

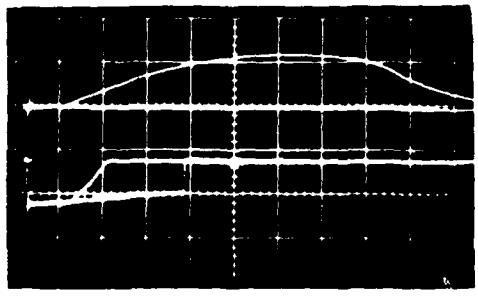

Figure 15

Interrupted Normal Conduction Current and Field Current Waveforms in Type B Device

Lower Traces: Interrupted normal current superimposed on uninterrupted current at 7.6 kV
Horizontal = 20 μs/cm
Vertical = 10 amps/cm

Upper Trace: Field Current
Horizontal = 20 μs/cm
Vertical = 2000 amps/cm

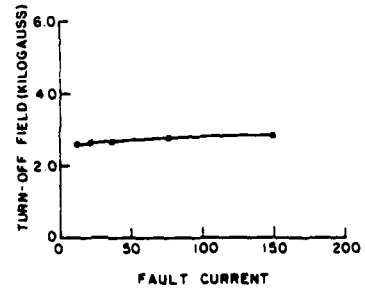

FIGURE 13. VARIATION OF TURN-OFF FIELD WITH FAULT CURRENT. DESIGN A TUBE, SOURCE AT 8.6kV

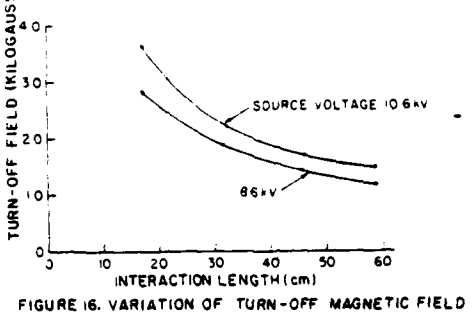

FIGURE 16. VARIATION OF TURN-OFF MAGNETIC FIELD WITH INTERACTION LENGTH DESIGN B TUBE

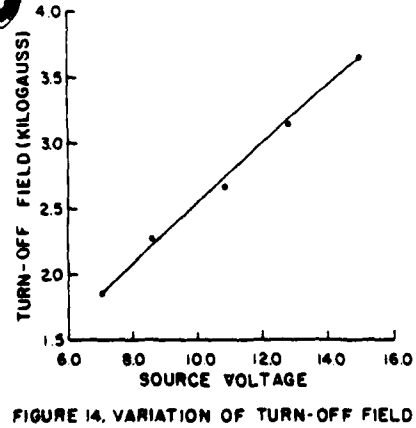

FIGURE 14. VARIATION OF TURN-OFF FIELD WITH SOURCE VOLTAGE. DESIGN A TUBE

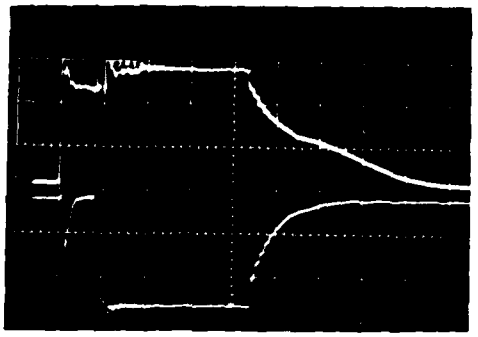

Figure 17

Current Waveform at 10.8 kV. Type B Tube.
Maximum Interaction Length.

Upper Trace: Grid Pulse to Hard Tube
Horizontal: 1 μs/cm
Vertical: 250 V/cm

Lower Trace: Discharge Current Pulse.
Initial Current Spike is
from Hard Tube Capacitance.
Horizontal: 1 μs/cm
Vertical: 5 amps/cm

THE USE OF A DOUBLE-ENDED HYDROGEN THYRATRON FOR CROWBAR APPLICATIONS

W. E. Hannant & C. Rowe
Radiation Dynamics Limited
Swindon, Wilts.

H. Menown
English Electric Valve Company Limited
Chelmsford, England.

Summary

Hydrogen thyratrons have been successfully used for many years as energy diverter switches for the protection of high power tubes of various kinds but in applications which involve current reversal or extra long conduction periods they may act as rectifiers or else "quench" before all the energy has been removed. Double-ended hydrogen thyratrons[1] are capable of carrying current in either direction once they have been triggered and also, due to the relatively large volumes of gas associated with the grid/cathode spaces at each end, any risk of quenching is virtually eliminated.

A new application for a double-ended thyratron has arisen for protecting a grid switched klystron supplied from a large capacitor charged to 90 kV. Overload currents in excess of twice the normal full-load value are detected by applying the voltage across a non-inductive shunt to an electronic comparator circuit. The crowbar thyratron is then triggered after minimal delay.

The equipment has been made as rugged and as compact as possible and is capable of being used in mobile as well as static applications. The whole equipment is housed in two oil-filled tanks: the power supply and crowbar thyratron are in one and the klystron and its ancillaries in the other. The state of readiness of the thyratron is continuously checked by relays and provision is also made for the crowbar to be "fired" manually for test purposes.

Introduction

When a new high power gridded gun klystron power supply was under consideration, the double ended multigap tetrode thyratron, EEV type CX1171B, (Fig. 1) was selected for its ability to conduct current in either direction, so that in the event of circuit "ringing" it would remain in conduction until virtually all the stored energy had been dissipated in the crowbar load, and the supply removed, without any necessity for re-triggering.

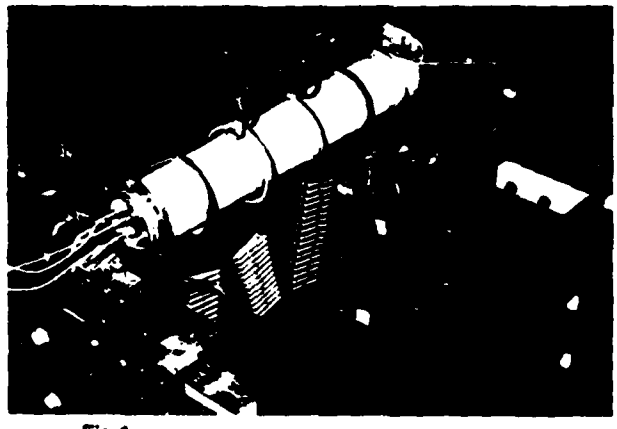

Fig.1

In the system the thyratron grid 1 is d.c. primed at both ends and the priming current is continuously monitored within specified limits to ensure that the equipment cannot be operated at high voltage without the crowbar tube being in a state of readiness. The energy stored in the high voltage reservoir capacitor C1 is very rapidly dumped into load resistors R1 (Fig. 2) whenever the crowbar thyratron is fired.

Removal of the high voltage power supply is initiated by current passing in the crowbar load circuit and backed up by a fully duplicated overload circuit, capable of removing the power input from the high voltage supply in less than 25 msecs. This limits the total dissipation of energy within the system per crowbar firing to an acceptable value. Subsequent to a crowbar firing and/or overload the high voltage supply is latched out for a period of approximately 10 secs, which is determined by the controls and the regulation time of the 400 Hz supply system.

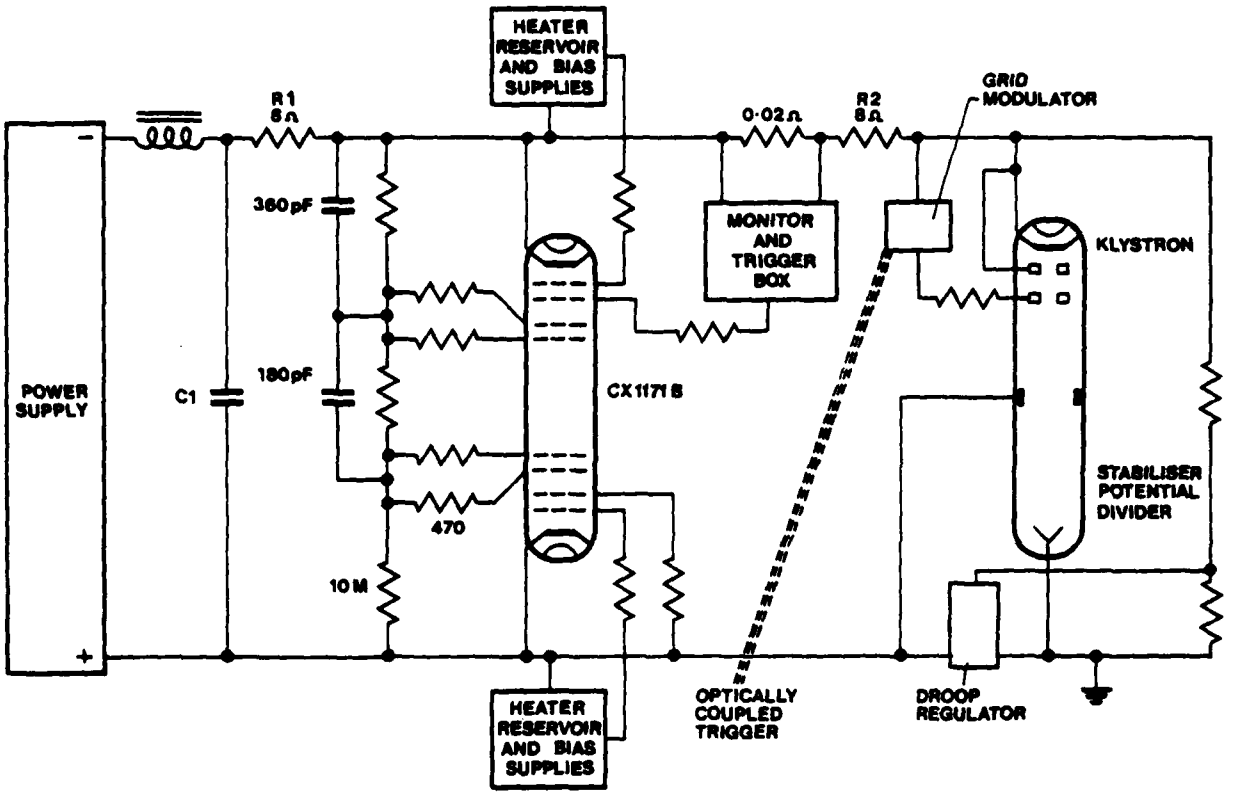

Fig. 2

Crowbar initiation is sensed from a shunt of minimal inductance in the load circuit. For pulsed loads some compensation is required for the non-resistive component of the shunt, the criticality of this depending on the normal rise time of the load pulse. Detector circuit sensitivity can initiate crowbar firing for load currents in excess of twice the normal pulse current of 45 A and a setting of 3 times the normal pulse current has been found reasonable in practice.

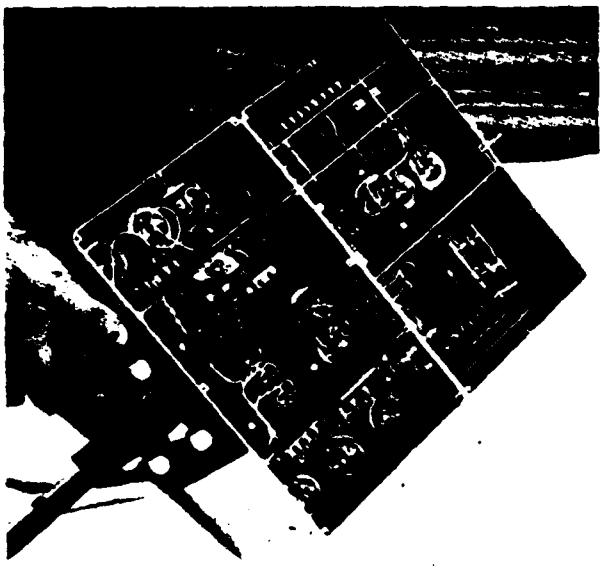

Fig. 3

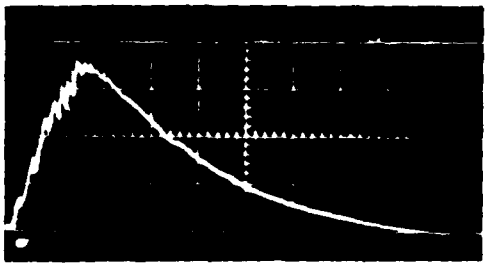

Fig. 4

The sensing and trigger circuitry for detecting the presence of excess current in the normal load circuit and processing this to the point at which the crowbar tube is triggered (via its grid 2 at what is effectively its cathode end) is contained in a heavily screened enclosure which is solidly bonded at cathode potential (Fig. 3).

The elapsed time from the load current exceeding the pre-set level to the crowbar load circuit reaching its peak current is 5 μsec in the case where the current rises slowly to an excess level. This falls to less than 1.5 μsec when the excess current rises rapidly to greater than twice the pre-set value. The delay in the logic for the detect circuit and the thyristor is around 700 nsec and the crowbar thyratron has reached its peak current less than 1 μsec later, (Fig. 4). The stored energy, a maximum of 3.3 kJ at the maximum working voltage of 90 kV, is dissipated in a relatively small, low inductance, resistor bank.

The effectiveness of the crowbar depends to a large extent upon keeping stray inductance to a minimum, both for rapidly detecting a potentially dangerous rise in klystron current and also for rapidly removing all high voltage from the system. Therefore, the crowbar is built as a closely integrated part of the equipment. It is equally necessary that the high voltage power supply be capable of withstanding without damage the very high peak currents involved in crowbar discharge. In the system under review crowbar currents in excess of 11,000 A can be reached in 100 nsec.

Summary of Design Requirements

Maximum Working d.c. Voltage at Klystron Socket	90 kV
Maximum d.c. Average Current	500 mA
Maximum Stored Energy at 90 kV	3.3 kJ
Pulse Current	45 A
Pulse Length	35 μsec
Maximum P.R.F.	250 p.p.s.
Rise Time of Normal Load Current	30 A/μsec
Time Constant of Crowbar Discharge Current	7 μsec
Ripple at 330 mA Average d.c. Current	30 V (peak to peak) 2.4 kHz
D.C. Source Impedance	25 kΩ
Voltage Stabilisation	Feedback control of 400 Hz Alternator
Pulse Voltage Droop Compensation (For Klystron Cathode/Body Voltage Regulation)	2 kV over 35 μsec pulse

Table 1

Power Supply and Crowbar

The above table shows the basic design parameters of the equipment. The transformer rectifier circuit operates from a 3-phase 400 Hz supply with a transformer reactance of 9% to limit the short circuit current to 11 times normal full load current. Conventional L.C. smoothing at 2.4 kHz employs the storage capacitor in its combined duty of smoothing and discharge for the pulse current of the klystron.

The crowbar diverter circuit is shown in simplified form in Fig. 2. Maximum energy diversion is achieved using equal value 8 Ω resistors on either side of the crowbar thyratron. (Fig. 5).

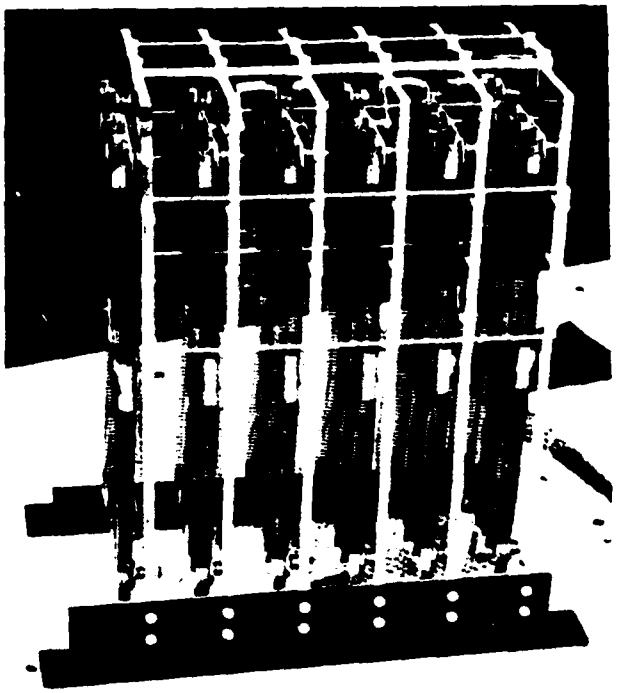

Fig.5

This resistor bank comprises a number of standard expanded metal nichrome elements spaced in the oil to provide voltage clearance and connected to minimise inductance. This form of resistor is ideally suited to withstand the surge power when the crowbar is fired. Sensing of greater than normal pulse current is derived from a monitor resistance in the klystron circuit and variable sensitivity is provided in the logic input circuit by adjustment of the reference voltage of the comparator.

Triggering is achieved from a thyristor switched modulator, pulse transformer coupled to the grid 2 of the thyratron.

Grid 1 at each end of the crowbar thyratron is d.c. primed[2] and is continuously monitored and interlocked to the ready condition of the control system.

Capacitors are connected to the resistor divider chain between the gradient grids to ensure current build-up in the thyratron under conditions of rapidly falling potential between "anode" and cathode.

Protection

The following automatic devices protect the klystron and power supply from damage.

Crowbar Diverter	Discharge time constant:- 7 μsec. Sensitivity:- typically set to operate at 135 A pulse current discharge, and fired in a time of less than 2 μsec. Removes 400 Hz 3-phase supply in 25 msec maximum.
D.C. Overload	Sensitivity:- adjustable but typically set for 650 mA maximum. Removes 400 Hz 3-phase supply in 35 msec maximum.
A.C. Overload (2 phases measured for 3-phase protection)	Sensitivity:- adjustable but typically set at 80 A line current. Removes 400 Hz 3-phase supply in 150 msec maximum.
Oil Flow and Temperature	Monitored continuously and interlocked to the ready state of the control system.

Table 2

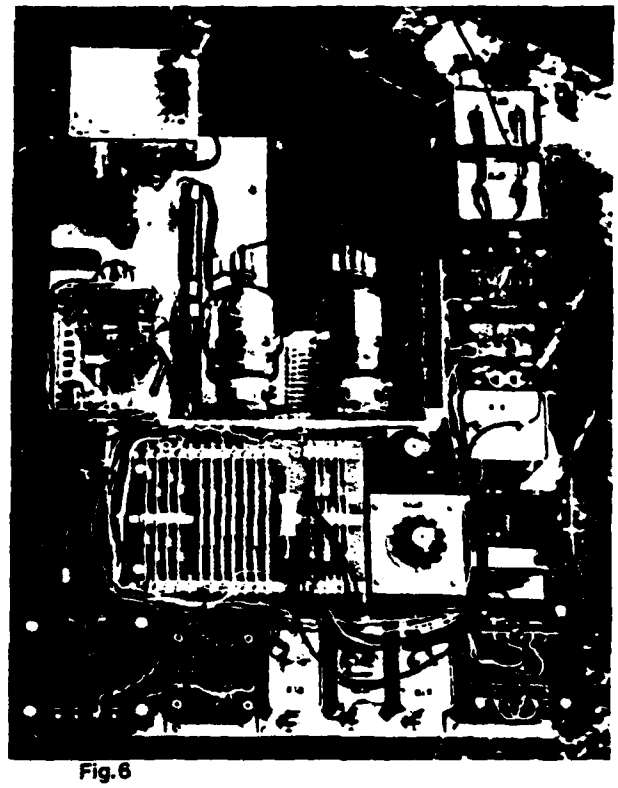

Fig.6

Pulse Droop Compensation

The klystron, together with its grid modulator and a droop compensator, is housed in a separate adjacent oil filled tank. This is connected to the power supply tank by a double-screened high voltage cable.

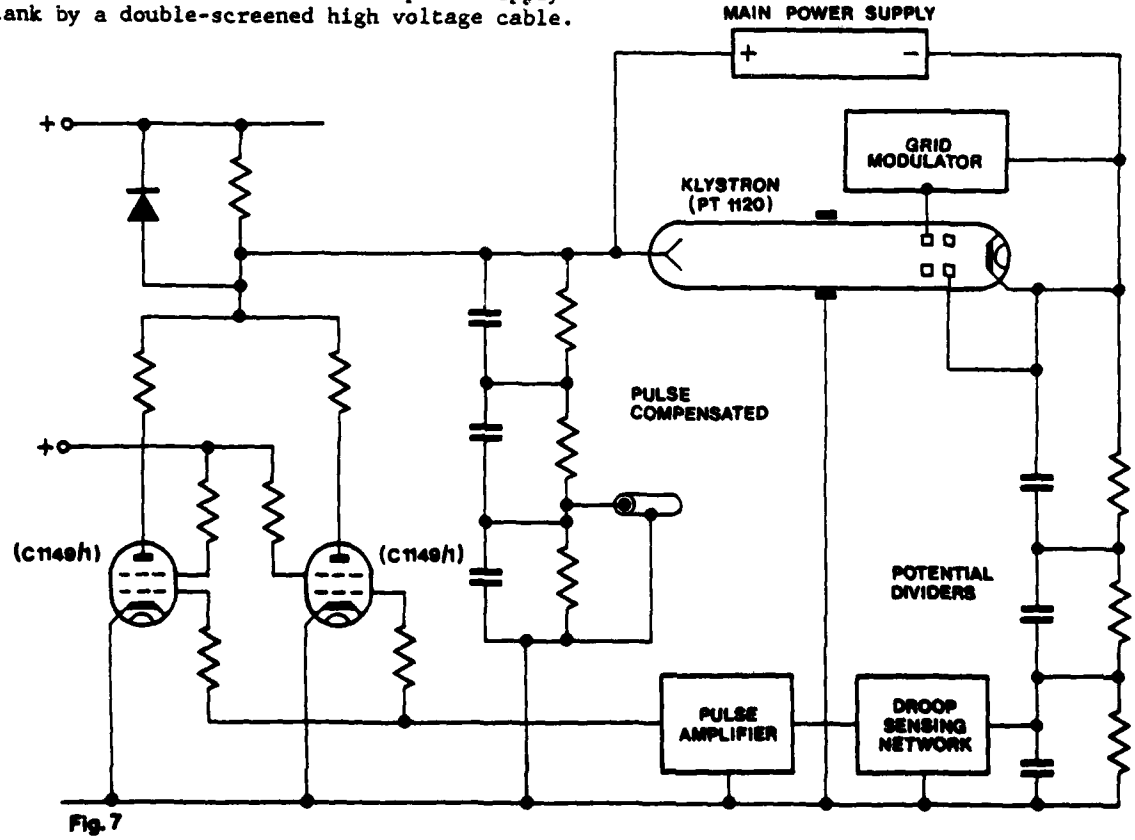

Fig. 7

Regulation of the voltage between klystron cathode and body is achieved by biasing the positive rail of the main power supply (and hence the entire supply) positive with respect to the earthed klystron body by approximately 2.5 kV during the inter-pulse interval (43 msec). This bias is then discharged during the pulse approximately linearly by two radial beam tetrodes in parallel which simultaneously carry the body current. This effectively swings the body positive with respect to the main power supply, matching the fall of negative cathode potential. (Fig. 6).

Because the charging rate of the droop regulator bias and the main H.T. are similar, this maintains a body to cathode voltage which is independent of p.r.f. variations.

Control of the discharge tetrodes (E.E.V. type C1149/1) is by means of an all hard valve amplifier, sensing the cathode to body potential via the compensated potential divider chain in the klystron tank. (Fig. 7).

Preliminary Test Results

D.C. Load	
1. Short circuit (metalfoil) induced crowbar firings between 50 and 90 kV - majority at 80 kV.	250 shots
Including a continuous run of 24 hours, interspersed with crowbar firings.	
Total H.T. time 100 hours	
Total L.T. time 150 hours	
Pulse Load - (Triode Gun)	
2. Load induced firings during ageing at voltages between 60 and 80 kV.	11 shots
Total H.T. time 32 hours	
Total L.T. time 92 hours	
3. (a) Klystron load (Klystron previously aged and tested to full R.F. duty)	10 shots
Operation at 75 kV	
Total H.T. time 50 hours	
Total L.T. time 120 hours	
(b) (Klystron not previously aged)	2 shots
Operation at 65 kV	
Total H.T. time 16 hours	
Total L.T. time 40 hours	

Table 3

The 2.5 kV bias supply is controlled by a variable auto-transformer giving full adjustment of bias from zero to maximum, thereby allowing for variations of characteristics of individual klystrons.

No deterioration in performance of triode gun, klystrons or crowbar thyratron has been observed to date.

References

(1) A Multigap, Double Ended Hydrogen Thyratron
H. Menown, B. P. Newton
Eleventh Modulator Symposium, 1973
p. 232.

(2) Hydrogen Thyratron Premable, pp 32 and 41.
Hydrogen Thyratrons and Pulse Amplifier Tetrodes
English Electric Valve Co. Ltd.,
Chelmsford, U.K.

Acknowledgements

The authors wish to thank the Directors of English Electric Valve Co. Ltd. and Radiation Dynamics Ltd. for permission to publish this paper.

AUTHORS INDEX


DATE
ILME
8